Dissertation zur Erlangung des Doktorgrades
der Fakultät für Chemie und Pharmazie
der Ludwig-Maximilians-Universität München

# Mouse models for aberrant NF-κB activation in B-cell development and lymphomagenesis

Valeria Rosa Lucia Soberon

aus

Lima, Peru

2018

Erklärung

Diese Dissertation wurde im Sinne von §7 der Promotionsordnung vom 28. November 2011 von Herrn Prof. Dr. Marc Schmidt-Supprian betreut und von Herrn Prof. Dr. Matthias Mann von der Fakultät für Chemie und Pharmazie vertreten.

Eidesstattliche Versicherung

Diese Dissertation wurde eigenständig und ohne unerlaubte Hilfe erarbeitet.

München, 02.11.2018

_____

Valeria Rosa Lucia Soberon

| | |
|---|---|
| Dissertation eingereicht am: | 06.09.2018 |
| 1. Gutachter: | Prof. Dr. Matthias Mann |
| 2. Gutachter: | Prof. Dr. Marc Schmidt-Supprian |
| Mündliche Prüfung am: | 02.11.2018 |

**SUMMARY**

The NF-κB family of transcription factors promotes the expression of survival, proliferation, inflammation, and differentiation programs in B-cells as well as in other cells of the immune system. Additionally, its aberrant constitutive activation is a hallmark of several B-cell neoplasms. Moreover, recurrent genetic lesions targeting the NF-κB activation pathways have been identified in patient samples from different B-cell neoplasms. For instance, genetic abnormalities in A20, the negative regulator of the canonical NF-κB pathway, and the alternative NF-κB arm TRAF3/NIK have been reported in splenic marginal zone lymphoma (sMZL). In contrast, few genetic lesions affecting NF-κB activation have been detected in chronic lymphocytic leukaemia (CLL), albeit the observed constitutive NF-κB activation in CLL. It has been proposed that signals from the microenvironment might promote NF-κB activation in CLL. Taken together, the recurrent observation of enhanced or constitutive NF-κB activation and the broad spectrum of genetic lesions targeting NF-κB in B-cell neoplasm, strongly suggest that NF-κB activation could act as a general mechanism in B-cell transformation. To date, there is little evidence linking activation of the NF-κB pathways directly to B-cell transformation and there are few available *in vivo* models addressing the role of NF-κB activation in B-cell lymphomagenesis that bring a better understanding of the disease development, progression and therapeutic strategies. Therefore, the objective of this thesis was to investigate the role of aberrant NF-κB activation in B-cell transformation and lymphomagenesis using available mouse models. First, the potential cooperation between canonical and alternative NF-κB activation in predisposing mice to sMZL was investigated by making use of the published mouse strains mimicking the chromosomal gains in NIK and deletions in A20 observed in human sMZL patients. Second, the direct effect of constitutive canonical NF-κB activation in B-cell transformation was investigated by conditionally expressing an IKK2 constitutive active mutant (IKK2ca) in B-cells, and in the Eμ-TCL1tg mouse model for human CLL.

As expected, the hemizygous ablation of A20 cooperated with NIK overexpression in expanding the marginal zone B-cell (MZB) pool in mice. However, homozygous ablation of A20 in combination with NIK overexpression resulted in an unexpected impaired mature B-cell homeostasis that was evident by a systemic depletion of mature B-cells in secondary lymphoid organs and recirculating B-cells in the bone marrow. Moreover, loss of A20 aggravated the previously reported block in adaptive immunity imposed by the overexpression of NIK in B-cells. Aberrant NF-κB activation by ablation of A20 and

NIK overexpression resulted in an abnormal pre-activated antigen presenting cell phenotype in B-cells that was accompanied by the altered expression of integrins, important for retaining cells in the MZ. Furthermore, the impairment in B-cell homeostasis was accompanied by the expansion of regulatory $CD25^+$ CD4 T-cells in addition to effector-like CD4 and CD8 T-cells. This T-cell hyperplasia was maintained in aged mice that developed an expansion of myeloid cells with age. The concomitant effector T-cell hyperplasia and later expansion of myeloid cells, suggest a possible involvement of these cells in the observed reduced B-cell numbers. It seems that aberrant canonical and alternative NF-κB activation in B-cells affect the terminal differentiation of mature B-cells forcing cells into a stage that fails to terminally differentiate into follicular B-cells and MZB-cells. Moreover, their aberrant phenotype possibly triggered a T-cell dependent immune response that may be involved in the elimination of these aberrant B-cells.

On the other hand, constitutive canonical NF-κB activation by expression of the IKK2ca mutant in B-cells resulted in the expansion of B1a-cells that with age developed into a disease reminiscent of human small lymphocytic lymphoma - a form of human CLL - where CD5+ B-cells infiltrated and accumulated in different lymphoid compartments. Moreover, constitutive NF-κB activation in B-cells shortened mice life span in an IKK2ca dose dependent manner. Furthermore, expression of IKK2ca in B-cells cooperated with the TCL1tg oncogene in accelerating the disease progression in Eμ-TCL1tg CLL mouse model also in a dose dependent manner. Strikingly, similar survival dynamics were observed when the conditional IKK2ca allele was activated during early B-cell development (CD19cre) or in a small percentage of mature B-cells (Cγ1cre or AIDcre). Finally, adoptive transplant experiments demonstrated that constitutive NF-κB activation failed to compensate for microenvironment dependent-signals required for the proper support of CLL-cells *in vivo*.

In conclusion, aberrant NF-κB activation in B-cells had different effects that were dependent on the mechanism of NF-κB activation and transcriptional programs this regulated. While ablation of A20 in combination with NIK overexpression in B-cells impaired mature B-cell homeostasis; IKK2ca-dependent constitutive NF-κB activation promoted the development of B-cell neoplasms in mice and collaborated with the TCL1 oncogene accelerating CLL progression in mice.

# I INTRODUCTION

In the recent decade, the advances made in DNA sequencing technologies have facilitated the analysis of diverse tumour samples generating an increasing amount of data regarding the mutations and genetic aberrations present in diverse lymphoid malignancies. However, further studies are needed to evaluate the biological significance of these genomic lesions and further validate them as potential drivers. One pathway particularly affected in B-cell lymphoid cancers activates the family of nuclear factor kappa-light-chain-enhancer of activated B-cells (NF-κB) transcription factors. Importantly, the NF-κB transcription factors are indispensable for the development of the immune system and regulate several steps during B-cell differentiation. This family of transcription factors regulates the expression of genes involved in proliferation, cell survival, adhesion, inflammation and other processes. There are two tightly regulated pathways that lead to the activation of NF-κB: the canonical and alternative pathway. Alterations in these pathways can lead to constitutive activation of NF-κB and as a result the aberrant expression of survival and proliferation genes. To date, several reports identified mutations in cancer affecting both canonical and alternative pathways. Particularly, enhanced or constitutive NF-κB activation is a hallmark of several lymphoid cancers [1-9], suggesting that these genetic aberrations might influence the regulation of NF-κB target genes. However, there is little evidence linking activation of the NF-κB pathways directly to B-cell transformation and there are few available *in vivo* models addressing the role of NF-κB activation in B-cell lymphomagenesis that bring a better understanding of the disease development, progression and therapeutic strategies. Therefore, taking advantage of available conditional mouse models I want to address the effect of deregulated NF-κB activation in B-cells lymphomagenesis *in vivo* as a first step towards understating the role of NF-κB activation in B-cell cancer.

## I.1 THE NF-κB FAMILY OF TRANSCRIPTION FACTORS

The nuclear factor-κB (NF-κB) proteins constitute a family of inducible transcription factors that bind the κB sequences in the DNA. The NF-κB family of transcription factors regulates different transcriptional programs involved in B-cell development, inflammation, cell adhesion, cell survival and proliferation. Deregulation in the tight control of these transcriptional programs can result in severe immune deficiencies leading to autoimmunity and inflammatory diseases.

There are 5 different NF-κB subunits, namely p105/p50 (NF-κB1), p100/p52 (NF-κB2), RelA (p65), RelB and c-Rel, all of which have a N-terminal Rel homology domain (RHD) required for dimerization and DNA binding [10-12]. The different NF-κB subunits can act as homo- or heterodimers regulating the expression of different target genes. There are two pathways that promote their activation. Primarily, the classical pathway promotes the activation of p50, RelA and c-Rel (Figure 1A) while the alternative pathway activates p52 and RelB (Figure 1B) [11, 13].

In their inactive states the RelA, RelB and c-Rel containing dimers are retained in the cytoplasm bound to inhibitory proteins belonging to the classic inhibitory of κ-B (I-κB) family (Figure 1). The NF-κb subunits p50 and p52 are a result of signal-induced processing of their inactive precursors proteins p105 and p100, respectively, containing an I-κB homologous domain at their C-terminus. Additionally, both p50 and p52 lack the C-terminal transcription activation domain (TAD) and require binding to other subunits to promote gene expression [10, 13, 14]. While p105 undergoes mostly continued processing into p50, cell stimulation promotes phosphorylation of p100 targeting it for proteosomal processing to p52 (Figure 1B) [13]. The IκB-like domain in p100 allows to function also as member of the I-κB inhibitory proteins [13]. Cell stimulation induces phosphorylation of I-κB proteins, which promotes their Lysine-48-linked (K48) polyubiquitination targeting them for proteosomal degradation. The release of the previously bound NF-κB dimers unmasks the nuclear localization signal of the RelA, RelB and c-Rel subunits; thus allowing their translocation to the nucleus (Figure 1A) [10, 11, 15].

Both NF-κB activation pathways are tightly regulated and following particular stimuli promote NF-κB nuclear translocation and activation of transcriptional programs. Key interactions are generated by post-translational modifications where Lysine-63-linked

(K63) and linear (M1) polyubiquitin chains provide binding sites for interaction partners containing adequate ubiquitin binding domains. Following activation, proper signal termination is important particularly in immune cells where prolonged activation can result in inflammation, autoimmunity and even cancer. Therefore, there are several mechanisms for terminating canonical as well as the alternative NF-κB activation.

### I.1.1 ACTIVATION OF THE CANONICAL NF-κB PATHWAY

The canonical NF-κB activation is triggered by cytokines including Tumour necrosis factor-α (TNF-α) and Interleukin-β1 (IL-β1), by microbial products binding to Toll-like receptors (TLR) and antigen binding to the B-cell receptor (BCR) [10, 11]. Receptor triggering initiates signalling promoting the interaction of E2 and E3 ubiquitin ligases and scaffolding proteins involved in K63/M1 polyubiquitination of downstream signalling partners. These signalling pathways converge in the activation of the trimeric I-κB kinase complex (IKK) by the transforming growth factor-β (TGF-β) activated protein kinase 1 (TAK1) (Figure 1A) [10, 11]. The IKK complex is composed of a non-catalytic regulatory subunit NF-κB essential modulator (NEMO, also called IKK-γ) and two catalytic subunits IKK1 and IKK2 (also called IKK-α and IKK-β, respectively). Activation of the IKK complex requires post-translations modification of NEMO consisting in linear polyubiquitination by the Linear Ubiquitin Chain Assembly Complex (LUBAC) [15, 16], and phosphorylation of IKK2 by TAK1 [11]. Although the main catalytic subunit in the canonical NF-κB activation is IKK2, in the absence of IKK2, IKK1 can also activate canonical NF-κB. After IKK activation, IKK2 phosphorylates I-κB inhibitors bound to NF-κB dimers, marking them for K48 polyubiquitin-dependent proteosomal degradation. After degradation of the I-κB inhibitor the NF-κB dimers can translocate to the nucleus and promote gene transcription [10, 11].

#### Distal signals activating canonical NF-κB activation

First, TNF-α receptor 1 (TNFR1) binding promotes its oligomerization, followed by the recruitment of the TNFR1-associated DEATH domain protein (TRADD) and Receptor-interacting protein 1 (RIP1) to its cytosolic tail. TRADD then recruits the TNFR associated factor (TRAF) 2 to form a complex with the E3 ubiquitin ligases Inhibitor of apoptosis proteins 1 (IAP1) and 2 (IAP2), where TRAF5 might also play a role. Although TRAF2 and TRAF5 are also E3 ubiquitin ligases, they mainly act as adaptors mediating the interaction between IAP1/2 and their substrate. The TRAF2/5-IAP1/2 complex adds

K63-polyubiquitin chains to RIP1, which provides a binding site for the TAK1 complex and NEMO ubiquitin-binding domains (UBD). The TRAF2/5-RIP1-IAP1/2 complex interaction with the IKK complex is further stabilized by the linear ubiquitination of NEMO through LUBAC. TAK1 can then phosphorylate IKK1 and IKK2 in its activation loop activating the canonical NF-κB pathway (Figure 1A) [10, 11, 16].

Second, the canonical NF-κB activation following IL-1β and LPS stimulation partakes in similar mechanisms. The IL-1β receptor 1 (IL-1βR1) and TLR4 have a common intracellular homology domain Toll/IL-1R (TIR) that recruits the Myeloid differentiation factor 88 (MyD88) adaptor following activation (Figure 1A). MyD88 in turn recruits the IL-1 receptor-associated kinase 1 (IRAK1) and IRAK4 adaptor proteins. IRAK1 is phosphorylated by IRAK4 and can recruit TRAF6 to MyD88 promoting its oligomerization and activation (Figure 1A). Activated TRAF6 undergoes auto-K63-polyubiquitination and ubiquitinates IRAK1 generating a K63-polyubiquitin chain scaffolding platform for the binding of the TAK1 complex and NEMO. TRAF6 then proceeds to activate TAK1, which can now phosphorylate the IKK complex and activate the canonical NF-κB pathway [10, 11, 17, 18].

Finally, canonical NF-κB activation following B-cell receptor antigen recognition is more complex and requires more intermediate activation steps. Following antigen binding and oligomerization, the BCR complex composed of the membrane-bound IgM (mIgM) and its co-stimulatory molecules Igα and Igβ will transduce the signal into the cytoplasm (Figure 1A). The molecules involved in proximal BCR signalling are the protein tyrosine kinases Spleen tyrosine kinase (Syk), Lyn and Burton's tyrosine kinase (BTK) in addition to the protein adaptor (BLNK) [19-21]. These kinases will activate a signalling cascade that will trigger distal effector enzymes involved in the production of key second messengers in BCR signalling. The phosphorylated phosphoinositide-3-kinase (PI3K) phosphorylates phosphatidyl-inositol-4,5-biphosphate ($PIP_2$) into phosphatidyl-inositol-3,4,5-triphosphate ($PIP_3$), which acts as a docking site for the phospholipase Cγ2 (PLCγ2), among other enzymes. PLCγ2 in turn will convert $PIP_3$ to the second messengers inositol-1,4,5-triphospate ($IP_3$) and diacylglycerol (DAG) [19-21]. $IP_3$ is an important second messenger for the intracellular release of calcium following BCR activation [22]. The accumulation of intracellular calcium and the presence of DAG will activate the Protein kinase C-β (PKC-β) that links BCR signalling with canonical NF-κB activation [19, 20, 23]. Active PKC–β proceeds to phosphorylate the scaffolding protein

CARD11 (also know as CARMA1). This phosphorylation promotes the binding of BCL10 and MALT1 to make the CARD11-BCL10-MATL1 (CBM) complex (Figure 1A). This complex can interact with TRAF2/6 and activate the canonical NF-κB pathway via K63 polyubiquitination of TAK1 and possibly NEMO [23, 24].

### I.1.2 ACTIVATION OF THE ALTERNATIVE NF-κB PATHWAY

The alternative NF-κB pathway is activated following stimulation of TNFRs for the B-cell activation factor belonging to the TNF family (BAFF), CD40 ligand (CD40L), lymphotoxin-α/β (LT–α/β), receptor activator of NF-κB ligand (RANKL) and the TNF related weak inducer of apoptosis (TWEAK) [10]. The first step in the activation of the alternative pathway promotes the stabilization and accumulation of NF-κB inducing kinase (NIK) levels. In un-stimulated cells NIK is constantly K48 polyubiquitinated and targeted for proteosomal degradation by an E3 ubiquitin-ligase complex composed of IAP1/2, and TRAF2/3 proteins (Figure 1B) [10, 13, 25]. When cells are stimulated TRAF2 binds the receptors cytosolic tail, where it recruits and K63-polyubiquitinates IAP1/IAP2. These modifications alter IAP1/2 specificity promoting K48-polyubiquitination of TRAF3, targeting TRAF3 for proteosomal degradation. In the absence of TRAF3, stabilized levels of NIK in the cytosol can phosphorylate and activate IKK1 dimers [10, 13]. Active IKK1 dimers will in turn phosphorylate p100 in p100:RelB dimers promoting its partial ubiquitin-mediated proteolysis to active p52:RelB dimers, which can translocate to the nucleus (Figure 1B) [13].

### I.1.3 NEGATIVE REGULATION OF NF-κB ACTIVATION

The canonical NF-κB activation results in a rapid but transient activation. Several negative regulatory loops are required to terminate the signal in a timely manner. First, the I-κB inhibitors are canonical NF-κB target genes. Therefore, in response to NF-κB activation I-κB inhibitors are *de novo* synthesized and bind to canonical NF-κB dimers to extract them from the nucleus and sequester them in the cytosol, thereby terminating the response. Ablation of I-κBα, for instance, results in prolonged activation that can have deleterious effects [11, 26]. Therefore, a proper and timely regulation is required.

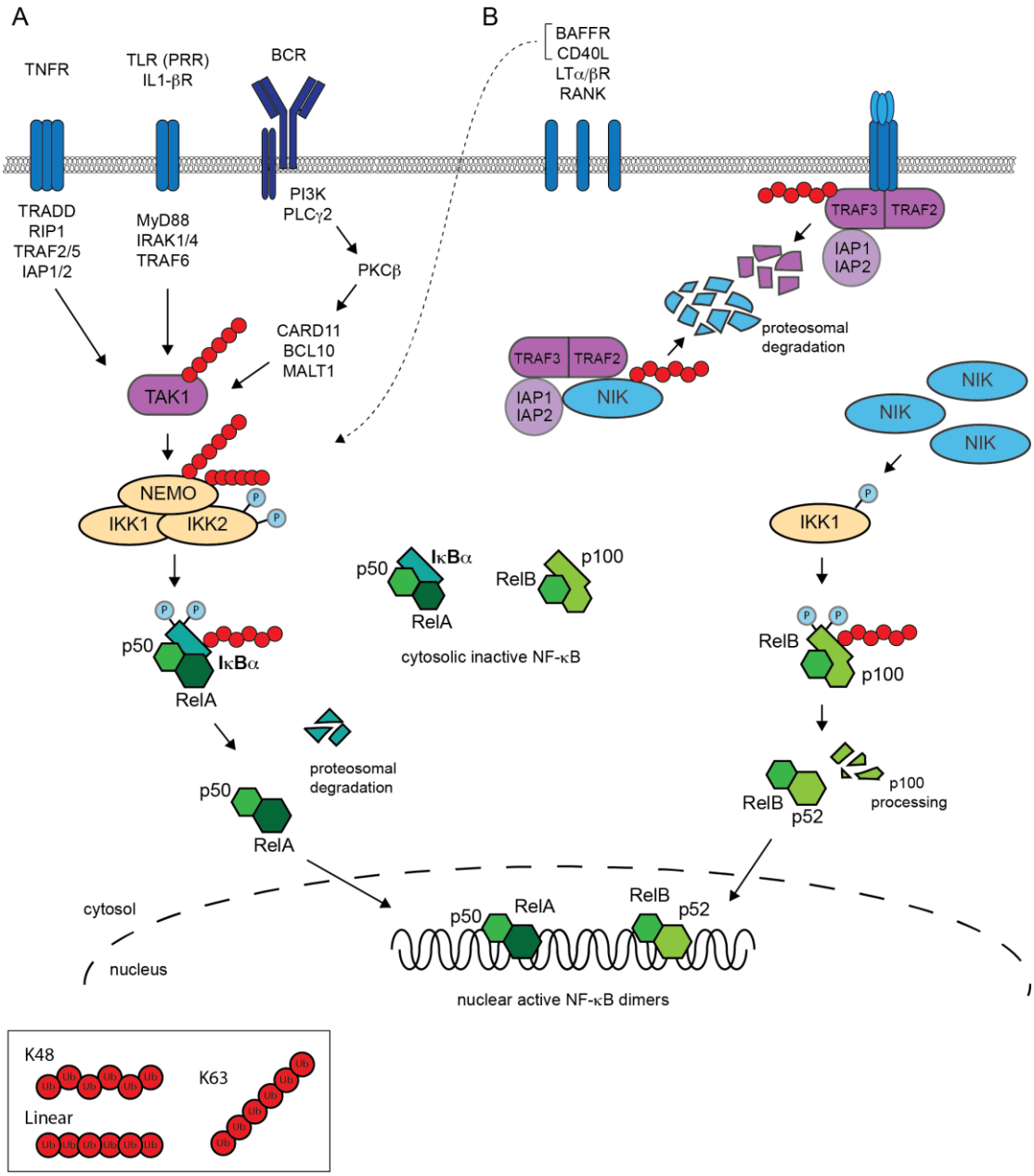


**Figure 1. Simplified illustration depicts NF-κB activation pathways.**

(A) Canonical NF-κB activation following TNF-α, IL-1β, LPS and antigen stimulation result in the activation of TAK1. Active TAK1 phosphorylates and activates the IKK complex that in turn marks the I-κB inhibitory protein for proteosomal degradation. Released NF-κB dimers can translocate to the nucleus and drive gene expression. (B) Alternative NF-κB in resting cells promotes NIK kinase proteosomal degradation by the TRAF2/3-IAP1/2 complex. Following stimulation, the TRAF2/3-IAP1/2 complex is relocated to the receptor intracellular tail where TRAF3 is targeted for proteosomal degradation by TRAF2-IAP1/2 complex. NIK protein levels stabilize and the protein can phosphorylate and activate IKK1. Activated IKK1 will target p100-containing dimers for proteosomal processing to p52, which can now translocate to the nucleus and drive gene expression. BAFFR and CD40 signalling activate the canonical and alternative NF-κB pathway.

TNF-α (tumour necrosis factor α), IL-1β (interleukin-1β), LPS (lipopolysaccharides), BAFFR (B-cell activation factor receptor)

Second, the tumour necrosis factor-alpha-inducible gene (TNFAIP3) encodes A20, a negative regulator of the canonical NF-κB activation [26]. Similar to the I-κB inhibitors, A20 is also a canonical NF-κB target and its expression is induced after TNF-α, IL-1β, LPS and BCR stimulation [11, 26]. A20 is characterized by presenting an Ovarian Tumour domain (OTD) and 7 Zinc finger (ZnF) domains. A20 can have a dual ubiquitin editing enzyme activity *in vitro*, acting as a deubiquitinase (DUB) that removes K63-polyubiquitin chains and as a E3 ubiquitin ligase coupling K48-polyubiquitin chains [27]. However, whether this dual activity is relevant *in vivo* remains unclear. A20 removes K63-polyubiquitin chains from RIP1, RIP2, TRAF6 and MALT1 [28, 29]; and adding K48-polyubiquitin chains to RIP1 marking it for proteosomal degradation [11, 27] Additionally, it has been reported that A20 inhibits IKK2 in a non-enzymatic way [30]. Therefore, A20 is involved in inhibiting distal signalling effects by destabilizing the interaction of complexes.

A20 acts as part of the 'A20 ubiquitin editing complex' composed of TAXBP1 and the E3 ligases Itch and RNF11, which are indispensable for A20 negative regulatory role in TNF-α–, IL-1β– and LPS-induced NF-κB activation [10, 11, 31]. Given that *in vitro* A20 deubiquitinates K48-polyubiqutin chains [11] and that TAXBP1 interacts with TRAF6 and other A20 substrates, it is most likely that TAXBP1 is involved in determining substrate specificity [11, 29, 32]. A20 also interacts with A20 binding inhibitor of NF-κB1 (ABIN), and it is likely that ABIN also serves as adaptor molecule to particular substrates such as NEMO [11]. Interestingly, A20 activity is positively regulated by phosphorylation through IKK2, while A20 itself is a proteolytic target of MALT1 [11]. Therefore, at least in the BCR signalling pathway MALT1 and A20 tightly regulate the threshold of canonical NF-κB activation.

Third, the tumour suppressor CYLD (cylindromatosis) is involved in terminating canonical NF-κB activation by removing K63 polyubiquitin chains from NEMO, TRAF2, TRAF6, TAK1, BCL3 and RIP1 [10, 11, 33]. Similarly to A20, CYLD is phosphorylated by IKK2, however this phosphorylation inhibits CYLDs DUB activity [11]. Although A20 and CYLD have overlapping substrates, their functions are non redundant in B-cell activation [34]. It has been suggested that CYLD plays a role in regulating basal NF-κB activation, while A20 acts in a negative regulatory loop that inactivates NF-κB [11].

In contrast to the canonical NF-κB pathway, the activation of the alternative NF-κB pathway requires the translational accumulation of NIK, therefore requiring a longer activation period. In order to terminate the accumulation of NIK, the alternative NF-κB has several negative regulatory loops that ensure a proper signal termination. First, the deubiquitinase Cezanne removes TRAF3 K48-polyubiquitin chains required for its proteosomal degradation following LTβ or CD40L signals [13]. Second, phosphorylation of NIK by IKK1 and other kinases results in NIK destabilization and alternative NF-κB signal termination. Third, receptor trafficking and degradation also play a role in alternative NF-κB signal termination [13].

### I.1.4 CROSS-TALK AND DUAL NF-κB SIGNALLING

The current understanding of how NF-κB signals are activated and regulated by different stimuli is not completely understood. Most of the current knowledge comes from *in vitro*, *in vivo* and genetic studies from knockout and conditional knockout mice. In the recent decade, it has become evident that certain signals such as CD40 and BAFF have the ability to activate both the canonical and alternative NF-κB pathways [35-37], pointing to a more complex system that requires further studies (Figure 1).

Certain components of the individual activation pathways have been reported to modulate their partner NF-κB pathway. First, weak antigen-independent BCR signalling regulates the expression of p100 and the BAFF receptor (BAFFR) by c-Rel, thereby modulating the alternative NF-κB response to BAFF [38]. Second, although the main NF-κB subunits activated by the canonical pathway are p50, RelA and c-Rel, RelA can interact with p100 and therefore be regulated by the proteosomal processing of p100 triggered by the alternative pathway [10, 39]. Similarly, RelB can bind to I-κBα and this portion of cellular RelB translocates to the nucleus only following canonical NF-κB activation [13]. Second, following antigen stimulation, canonical NF-κB activation will regulate the expression of p100 NF-κB subunit, modulating the alternative NF-κB response [38, 40]. Third, previous evidence suggest that both CD40 stimulation as well as BAFFR activation can also activate the canonical NF-κB pathway [36, 41]. Finally, two reports have implicated TRAF3-NIK in activation of the canonical NF-κB pathway [42, 43]. Gray et al. (2014) identified constitutive accumulation of NIK accompanied by basal activation of the alternative NF-κB pathway in NEMO-deficient peripheral blood lymphocytes from patients with NEMO immunodeficiency (NEMO-ID) [43]. The

regulation of NIK was restored by expression of full-length NEMO [43]. In line with this finding, Zarnegar et al. (2008) provided evidence that TRAF3 also negatively regulates the canonical NF-κB pathway. In the absence of TRAF3, the IKK complex was activated in a NIK dependent manner [42]. Particularly, in case of TNFR1 and LTβR synergy, NIK could acts as an amplifier of the canonical NF-κB pathway [42].

Taken together, although the distinct pathways leading to the activation of NF-κB respond to distinct stimuli, there is a potential for crosstalk between the canonical and alternative pathways.

## I.2 THE IMMUNE SYSTEM

The immune system has evolved to protect complex organisms from foreign pathogens. In higher organisms, the immune system is comprised of two arms fighting against infections and foreign invaders: the innate and the adaptive immunity [44, 45]. The innate immunity is the first line of defence against foreign pathogens. It mounts an immediate response as soon as the infection or foreign pathogen has been detected. It is composed from a series of specialized cells - myeloid cells, natural killer cells, and marginal zone B-cells (MZB) and B1-cells - that will control de infection until the adaptive immunity has time to develop and clear the remaining pathogens. The adaptive immune response, as it name suggests, is a response that needs to adapt to the particular pathogen that has entered the organism. A complex series of events leads to pathogen recognition, the presentation of the antigens to cognate T- and B-cells with the final aim of producing high affinity antigen-specific antibodies that help clear the infection. NF-κB activation plays an important role in T- and B-cell development and additionally is required to mount an appropriate immune response against pathogens.

The process of generating antigen specific antibody producing cells is highly complex. It requires B-cells to undergo several rounds of proliferation and of genomic DNA editing where the cell is in a state of genomic instability [46]. It is during this process that many chromosomal translocations and genetic alterations take place that will later lead to the development of non-Hodgkin mature B-cell lymphomas and leukaemia [47].

## I.3 B-LYMPHOCYTES

B-cells are lymphocytes specialized in the production of antibodies. In addition to their humoral immune response, B-cells can also act as antigen presenting cells activating T-cells and produce cytokines that can modulate immune responses [48]. There are two main subsets of mature naïve B-cells: B1-cells and B2-cells, which can be further subdivided into MZB- and follicular B-cells (FOB). B1- and MZB-cells are mainly involved in T-cell independent (TI) and innate-like immune responses, while FOB-cells are key players in T-cell dependent (TD) immune responses in adaptive immunity.

### I.3.1 EARLY B-CELL DEVELOPMENT

B-cells develop from pluripotent hematopoietic stem cells (pHSC) in the foetal liver during embryonic development and in the bone marrow from the embryonic day E17.5 onwards[49]. Following very tight specific cues, pHSC give rise to multipotent myeloid/lymphoid progenitors (MMP) that further differentiate into a common lymphoid progenitor (CLP), which give rise to the first B-cell committed stage: the pro-B cell stage (Figure 2A) [49-51].

The early B-cell differentiation in the bone marrow consist on the progression from the pro-B cell stage to the large and later small pre-B cell, terminating in the immature B-cell stage (Figure 2A). Pro-B cells are characterized by the expression of c-kit and IL-7 receptor alpha (IL-7Rα) required for cell proliferation and survival [49-51]. When cells differentiate to pre-B cells, they down regulate the expression of c-kit and IL-7 receptor alpha (IL-7Rα) while they up regulate the expression of IL-2 receptor alpha (IL-2Rα or CD25) [49, 51]. The transition through these stages is tightly linked to survival signals produced by the efficient rearrangement of the immunoglobulin heavy-chain (IgH) and light-chain (IgL) loci to produce a functional non-self reactive BCR (Figure 2A) [49, 52]. Moreover, two major checkpoints involved in the development of central tolerance take place during early B-cell development. The first involves the recognition of self-antigens by the rearranged IgH within the pre B-cell receptor (pre-BCR). The second checkpoint involves the recognition of self-antigens by the fully formed BCR, after rearrangement of both IgH and IgL [53].

The development of early B-cells is regulated by the expression of a network of transcription factors that proceed to commit the cell to the B-cell lineage, and the majority of published evidence suggests that NF-κB does not play a role. Low levels of

the transcription factor PU.1 at the MPP stage promote the transition to the CLP stage and they are associated with ensuing B-cell lineage commitment [50, 51]. A tight sequential expression of the transcription factors E2A, EBF and PAX5 among others drives the B-cell differentiation program. First, the transcription factor E2A is expressed at the pro-B cell stage and is involved in the expression of the recombination-activating-genes (RAG) proteins [49, 54]. Second, the transcription factor EBF is expressed from the pro-B to the pre-B cell stage and in mature B-cells. Importantly, EBF regulates the expression of the Igα and Igβ co-receptors required for the transduction of signals of the pre-BCR and the BCR, as well as the VpreB and λ5 subunits of the surrogate light chain (SLC), and the transcription factor PAX5 [49, 51]. Finally, the transcription factor PAX5, expressed at the pre-B cell stage, commits the cell to the B-cell lineage and is required for the rearrangement of the IgH [49, 51].

#### I.3.1.1 V(D)J recombination

Part of the early B-cell development requires the expression of a functional BCR. The assembly of the IgH and IgL chains requires a series of site-specific somatic recombination events that will join the germline variability- (VH), diversity- (DH) and joining-gene segments (JH) or VL and JL gene segments, respectively. Upon successful completion, the process of V(D)J recombination of the immunoglobulin loci will generate a diverse BCR repertoire.

In mice, the IgH is encoded on chromosome 12, while the IgL is encoded by two loci: immunoglobulin kappa (Igκ) on chromosome 6 and immunoglobulin lambda (Igλ) on chromosome 16 [52, 55]. Structurally, both IgH and IgL have N-terminal variable region specialized in antigen recognition, while only the IgH has a C-terminal constant region, which can be exchanged for other forms during class-switch recombination [52]. The IgH variable-region is formed by the rearranged VH-DH-JH while the IgL variable-region is formed by the VL-JL rearrangement [52]. The site-specific somatic recombination is directed by the endonucleases RAG1 and RAG2 [52, 56, 57]. In mice, the absence of one of these enzymes and other enzymes related to V(D)J recombination results in severe combined immune deficiency (SCID) due to an early block in B- and T-cell development [50, 57], indicating the importance of the BCR and TCR for the development of both cell types respectively.

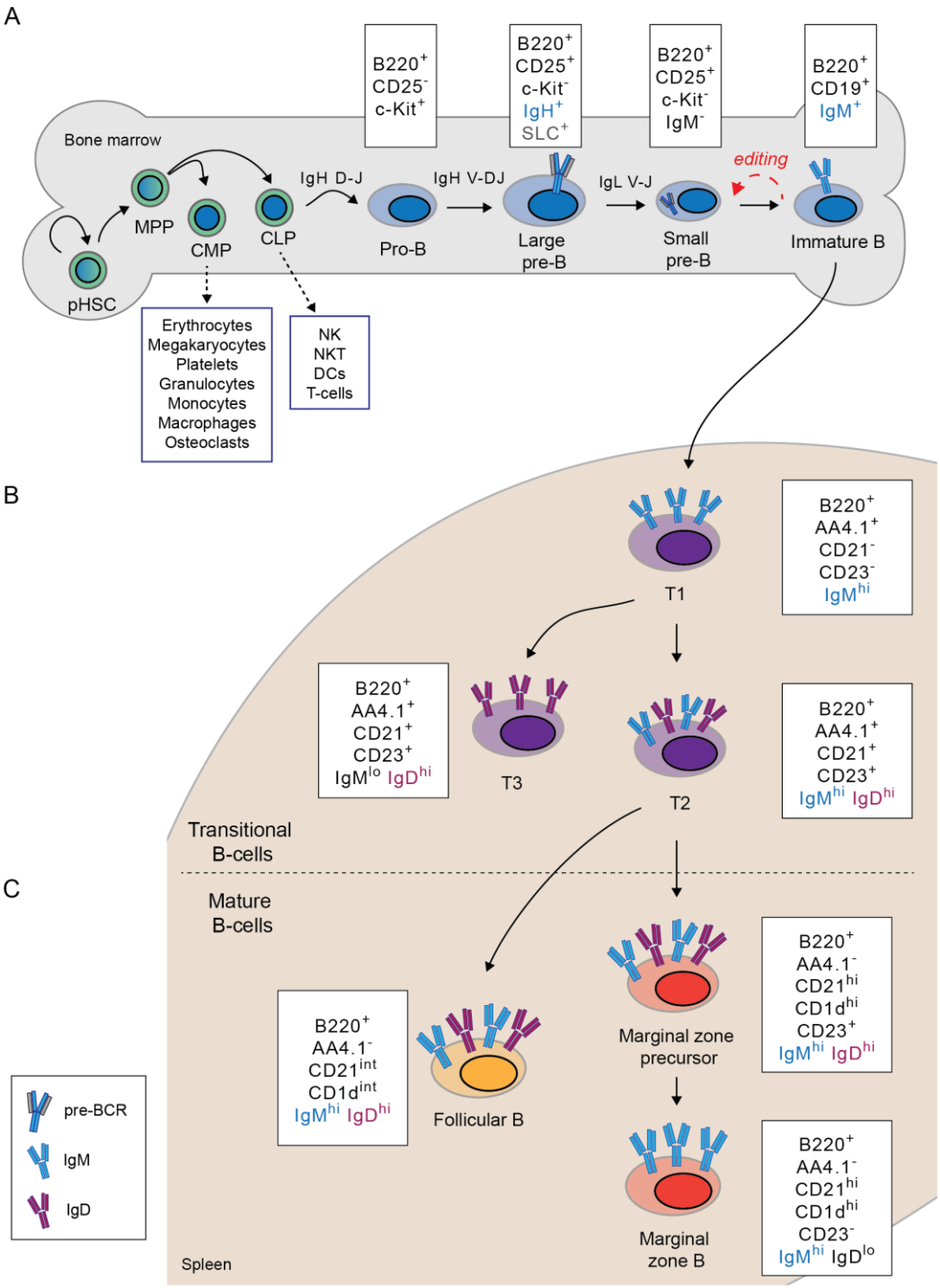


**Figure 2. Simplified illustration depicts the different developmental stages in B-cell development.**

(A) Early B-cell development in the bone marrow depends on the recombination of VH, DH, and JH gene segments to produce a functional pre-BCR and later VL and JL, for a functional BCR. (B) Immature B-cells can migrate to the spleen and differentiate to T2 cells by tonic BCR signals and survival signals provided by BAFF, or become anergic T3 cells by aberrant BCR activation signals. (C) Mature B-cell differentiation in the spleen depends on chronic BCR signals that promote the follicular B-cell fate or the combination of BAFF and chronic BCR signals that promote the marginal zone B-cell fate.

pHSC (pluripotent hematopoietic stem cell), MPP (myeloid/lymphoid multipotent precursor), CMP (common myeloid progenitor), CLP (common lymphoid progenitor), and T (transitional).

The V(D)J recombination starts at the pro-B cell stage. First, during transition from CLP to pro-B cell, the RAG1 and RAG2 enzymes are expressed and both IgH alleles open to undergo the DH-to-JH recombination (Figure 2A) resulting in the rearrangement of both alleles [49, 52, 58, 59]. Second, during the differentiation to the large pre-B cell stage, the one DHJH rearrangement can recombine to the VH in the same allele (Figure 2A) [49, 51].

If the VHDHJH rearrangement in the first allele is in frame and results in the productive expression of a functional IgH, downstream signals from the membrane-bound IgH on the surface promote the closing of the second IgH allele and down regulate expression of the RAG proteins, a process referred to as allelic exclusion [49, 52, 59] In this way, the cell avoid the recombination of the second allele and only expresses one IgH allele. Moreover, the functionality of the newly rearranged IgH is tested by pairing it to the SLC - formed by λ5 and VpreB - to form the pre-BCR (Figure 2A) [49-51]. This is the initial checkpoint involved in B-cell tolerance [49, 51, 53]. First, signalling through the pre-BCR will activate canonical NF-κB and the expression of pro-survival genes rescuing cells from apoptosis [49, 60, 61]. Second, pre-BCR signalling will down regulate the expression of the SLC thereby limiting the pre-BCR amount present at the surface, so that after a couple of cell divisions the amount of SLC becomes limiting and the cells becomes a resting small pre B-cell [49].

The last V(D)J recombination step takes place during the small pre-B cell stage (Figure 2A) [49] where the RAG proteins are expressed and the IgL loci open up, both prerequisites for the JL-to-VL recombination [49]. The Igκ locus is initially recombined. However, if the recombination is not productive, the cell can proceed to recombine the Igλ locus [62]. The recombination into the Igλ is dependent on NF-κB signals [63].

Rearranged IgH and IgL will combine to produce the BCR. The expression of a fully rearranged BCR on the cell surface is the second crucial checkpoint in B-cell development and central tolerance. Downstream signals from a functional not self-reactive BCR will terminate the expression of the RAG proteins and close the IgL loci [49]. However, if the BCR is self-reactive, the expression of the RAG proteins is maintained and the IgL loci remain open to allow receptor editing by further recombination of the IgL loci to produce a non-self-reactive BCR [19, 49, 53, 57]. Alternatively, self-reactive B-cells are eliminated by apoptosis or are inactivated and become anergic [51].

Finally, Pre-B cells differentiate into immature B-cells, which express the mIgM BCR that has undergone a negative selection process [19]. The immature B-cell can enter the circulation and migrate to the spleen where it will differentiate to naïve mature B-cells (Figure 2).

V(D)J recombination gives rise to a diverse repertoire of variable-regions in the BCR. Additionally, the expression of the enzyme terminal deoxynucleotidyl transferase (TdT) adds random nucleotides in the sequence between the DH-to-JH and VH-to-DHJH junctions, called N-regions, adding another layer of diversity [49, 62]. Of importance, the major 5' part of VH encodes the first and second constant determining regions (CDR1 and CDR2) involved in antigen recognition of the IgH which confer germline diversity [62]. While the VHDHJH junction sequence encodes the third complementary-determining region (CDR3) that confers somatic diversity to the IgH and plays a major role in antigen recognition and repertoire diversity [62]. In humans and mice, problems with V(D)J recombination can result in SCID and cancer [57, 64]. Humans with mutations in the V(D)J recombination enzymes develop T-cell and T-cell and B-cell related SCID [57, 64].

### I.3.2 TRANSITIONAL IMMATURE B-CELLS

Immature B-cells in the bone marrow can enter the peripheral circulation and migrate to the spleen where they differentiate to transitional B-cells. The differentiation of immature to mature FO or MZ naïve B-cells is thought to follow linear developmental stages. A small proportion of immature B-cells remain in the bone marrow where they can differentiate into FOB-cells as well {Pillai:2009bs}. Transitional B-cells can be differentiated by their characteristic expression of different surface proteins (Figure 2B), differential response to BCR signalling as well as to T-cell help and defined anatomical localization in the spleen [19, 65].

Three developmental stages of transitional B-cells have been described (Figure 2B). Transitional 1 (T1) cells are the most immature cells and are characterized by expressing the AA4.1 surface marker as well the membrane bound IgM (Figure 2B: T1 AA4.1$^{+}$ CD21$^{-}$ CD23$^{-}$ IgM$^{high}$ IgD$^{-}$) [48, 51, 65]. Transitional 2 (T2) cells are late immature cells characterized by the additional expression of membrane bound IgD and the surface markers CD21 and CD23 (Figure 2B: T2 AA4.1$^{+}$ CD21$^{+}$ CD23$^{+}$ IgM$^{high}$ IgD$^{+}$) [48, 51, 65]. This transitional B-cell subset will differentiate to the mature naive B-cells. There is an

additional transitional 3 (T3) developmental stage, with lower IgM levels, otherwise similar to T2 [48, 51, 65]. It has been suggested that cells in the T3 subgroup correspond to self-reactive clones that have become anergic (Figure 2B) [48]. Transitional cells that mature in the spleen have a specific physical location. Early transitional cells locate to the outer periarteriolar lymphoid sheath (PALS), while later transitional cells migrate towards the B-cell follicle [65].

Immature T1 B-cells are prone to apoptosis and require survival signals to rescue them from cell death and promote their differentiation [48]. Two main signals coordinate the expression of anti-apoptotic proteins and promote differentiation: (1) signals downstream of the BCR, and (2) signals from the pro-survival factor BAFF [19, 23, 53, 66].

Studies with genetically modified mice demonstrated the requirement of NF-κB activation during the differentiation from T1 to T2 cells. Ablation of NEMO or both IKK1/2 in B-cells results in a developmental block at the T1 stage [63]. Similarly, ablation of c-Rel/RelA, NF-κB1/NF-κB2, c-Rel/RelB [36] or expression of the NF-κB2 dominant negative mutant (unable to be processed to p52) in B-cells also results in a T1 developmental block (Reviewed in [67]). The fact that both canonical and alternative NF-κB activation are indispensible for the transition of immature B-cells supports the requirement for both BCR and BAFF signals driving B-cell differentiation at this stage.

#### I.3.2.1 BCR signalling and transitional B-cell differentiation

Signals from the BCR are required for transition from T1 to T2 B-cells. The BCR signalosome is composed of a complex network of proximal and distal signalling molecules that culminates in the activation of the mitogen activated protein kinases (MAPK) in manner dependent on Ras, NF-κB transcription factors (Figure 1A) and nuclear factor of activated T-cells (NFAT) that will coordinate the expression of genes required for proliferation and survival [19, 23].

During the T1 developmental stage, weak tonic antigen-independent BCR signalling activates proximal PI3K and AKT that promote B-cell survival, rescuing cells from apoptosis [23, 53]. Progression to T2 developmental stage requires activation of distal BCR signalling resulting in canonical NF-κB activation [67].

It has been suggested that early transitional cells remain sensitive to negative selection and can undergo receptor editing or deletion depending on the BCR signal strength[65]. First, strong BCR signals can lead to re-expression of RAG enzymes [65] required for auto-reactive B-cells to continue the IgL editing process to recombine the Igλ locus to produce a non-self reactive BCR [50, 53]. Weak tonic BCR signals down regulate the expression of the RAG proteins and other proteins involved in V(D)J recombination, thus terminating the BCR editing process [23, 53]. Second, T1 cells are sensitive to BCR-mediated apoptosis via BIM [53, 65]. Recognition of a cognate-self antigen by auto-reactive B-cells that results in strong BCR signalling leads to the expression of the pro-apoptotic protein BIM [53], while tonic BCR signalling decreases BIM expression in an AKT-dependent manner promoting cell survival [53].

Studies with genetically modified mice demonstrated the importance of BCR proximal signalling events in T1 development and distal ones in the T1-to-T2 transition [19, 65]. First, ablation of proximal BCR signalling molecules, such as the Syk kinase or the cytoplasmic tail of Igα, results in a developmental block at the T1 stage; while ablation of distal BCR signalling molecules results in a T2 developmental block (reviewed in [67], [65] and [19]). Therefore, T1 differentiation into T2 involves the development of a complete network of BCR signals [65]. Likewise, as they transition from T1 to T2 they become more responsive to T-cell-derived signals including IL-4 and CD40-ligand (CD40L) [19, 65].

#### I.3.2.2 BAFF and transitional B-cell differentiation

Transitional B-cell differentiation requires survival signals that rescue cells from apoptosis and promote differentiation. Additionally to weak tonic BCR signals, the differentiation of T2 cells requires the cytokine BAFF and signalling through its receptor [66]. BAFF is expressed as a membrane bound protein that is proteolytically cleaved and released to the circulation. There are three different receptors that can bind BAFF: the BAFF-receptor (BAFFR) [68], B-cell maturation antigen (BCMA) and the transmembrane activator and calcium modulator and cyclophilin ligand interactor (TACI) [66]. BAFFR expression increases as B-cells mature.

Genetic studies in mice suggest that the major role of BAFF is to provide T1 cells with survival signals required for the differentiation into the T2 and later differentiation stages [19, 66, 69, 70]. Mice deficient in BAFF [69] or BAFFR [70] suffer from a B-cell

developmental block at the T1 stage [66], which can be partially rescued by the enforced overexpression of the pro-survival protein BCL-XL at least in the absence of BAFFR [70]. In contrast, mice expressing a BAFF transgene develop a T2 cell hyperplasia, suggesting that excess of BAFF prolongs the survival of transitional cells [66]. BAFF promotes B-cell survival first by promoting the expression of the anti-apoptotic protein B-cell lymphoma 2 (BCL2) and second by reducing the expression of pro-apoptotic proteins BIM and BCL2 modifying factor (Bmf) in an NF-κB dependent manner (Figure 1B) [40, 71, 72]. BAFF-dependent NF-κB activation is indispensable for the T1-to-T2 transition. Both canonical and alternative NF-κB activation pathways seem to have a complementary role in controlling transcriptional programs required for this transition [36, 37, 61, 65]. Interestingly, enforced BCL2 expression does not compensate for the absence of NFκB activation during B-cell maturation [40]. Additionally, it has been suggested that elevated BAFF levels, independently of T-cell help, can enhance the survival of low affinity auto-reactive B-cells in mice [53, 66, 73].

Taken together, the transition from immature T1 to T2 cells requires survival signals provided by tonic BCR signalling and the BAFF cytokine. As cells mature towards the T2 developmental stage, the BCR downstream signalling reaches a higher activation threshold, probably by a proper localization and organization of signalling complexes.

### I.3.3 MATURE NAÏVE B-CELLS

Late transitional T2 cells can differentiate into FOB- or MZB-cells (Figure 2C). FOB-cells are characterized by expressing intermediate levels of CD21 and CD1d; high levels of CD23; and high membrane-bound IgD with reduced IgM expression. In contrast, MZB-cells are characterized by expressing high levels of CD21 and CD1d; absence of CD23; and high membrane bound IgM with reduced IgD expression. The differentiation to MZB-cells includes an intermediate precursor stage: marginal zone precursor (MZP), during the differentiation from the MZP to MZB-cell the expression of CD23 is lost (Figure 2C).

FOB-cells are involved in TD immune responses, as they can present antigens and participate in T-cell activation additionally to become activated, differentiate into germinal centre B-cells that will give rise to memory or antigen secreting plasma cells [47, 48]. Activated FOB-cells can become short-lived plasma cells in the spleen, but cannot migrate to different organs [46, 48]. Moreover, FOB-cells can circulate in the

periphery into secondary lymphoid organs as well as recirculate to the spleen and bone marrow [48]. In the bone marrow, recirculating mature B-cells can also be involved in TI immune response to blood-borne pathogens [48, 74].

MZB-cells on the other hand are mainly involved in TI immune responses to blood-borne pathogens and mainly reside in the outer area of the B-cell follicle in the spleen [48]. MZB-cells are pre-activated B-cells, expressing high levels of the major histocompatibility complex class-II (MHC-II) and the co-stimulatory molecules CD80 and CD86, and have the ability to self-renew [74]. Additionally, MZB-cells also express high levels of the integrin heterodimers alpha-L beta-2 leukocyte function-associated antigen 1 (LFA-1) and alpha-4 beta1 [75]. MZB-cells can become activated by antigens and differentiate into antibody producing plasma cells [48]. Moreover, they can act as antigen presenting cells (APC) as they (1) shuttle between the marginal zone and the follicle [76], (2) can carry antigens and immune complexes [77], and (3) express high levels of MHC-II, CD80 and CD86 required for the immunological synapse [48, 74]. It has been proposed that B-cell recognition of LPS or other bacterial products might decrease integrin activation rendering MZB-cells less static [48]. MZB-cells have also been implicated in TD immune responses to protein and lipid antigens [48].

The development of FOB- and MZB-cells is regulated by NF-κB signals, however it is even more critical for MZB-cell development. Ablation of NF-κB1, NF-κB1/c-Rel [78], NF-κB2/BCL3, or NIK/BCL3 results in an impairment in FOB-cell development [67]; while ablation of the individual NF-κB subunits NF-κB1 or NF-κB2 results in the absence of MZB-cells (Reviewed in [67]). Similarly, B-cells deficient in the components of the CBM complex, TRAF6, TAK1 or IKK2 fail to differentiate to MZB-cells [67]. Interestingly, the canonical NF-κB negative regulator A20 is also required for normal differentiation of MZB-cells [79, 80]. Loss of A20 leads to the accumulation of MZP that cannot differentiate into functionally mature MZB-cells [79]. All the evidence suggests that there is stringent requirement for NF-κB signals in the differentiation of FOB- and MZB-cells.

#### I.3.3.1 Follicular versus marginal zone B-cell fate decision

Late immature B-cells need particular cues to differentiate into FOB- or MZB-cells. The current model for cell fate decision involves BCR chronic signalling, where signal strength and specificity will tip the balance towards either FOB- or MZB-cell

differentiation [19, 48, 81]. In addition, BAFF as well as Notch2 and most likely integrin or cytokine dependent signals will influence MZB-cell fate decisions.

First, evidence from mouse experiments supports the notion that intermediate strength BCR signalling will promote FOB-cell differentiation, while weak BCR signalling will favour the generation of MZB-cells [19, 74, 81]. Cariappa *et al.* (2001) have shown that relatively strong BCR signals induced by ablation of the transcription factor Aiolos in B-cells results in FOB-cell expansion at the expense of MZB-cell development [82]. Similarly, absence of negative regulators of the BCR, SHP1 and PTEN, result in enhanced BCR signalling and defects in MZB-cell development [74]. In contrast, ablation of BTK, PLCγ2 or BCL10, which abrogate BCR downstream signalling (Figure 1A), or constitutive inhibition of canonical NF-κB block FOB- and MZB-cell differentiation [60, 74, 83]. Recently, Shinohara et al. (2016) reported that the ablation of the kinase TAK1 (Figure 1A) in B-cells results in aberrantly activated alternative NF-κB and marginal zone B-cell expansion [84]. Taking into consideration that ablation of upstream BCR signals and downstream NEMO and IKK2 result reduced MZB-cells [40], TAK1 activation downstream BCR signalling could be involved in FOB- versus MZB-cell fate decisions.

Second, experiments with genetically modified mouse strains expressing BCRs specific for self antigens (DNA) or microbial lipids (phosphoryl-choline) preferentially give rise to MZB-cells [48]. On the other hand, enforced expression of BCRs specific for the hen egg lysozyme (HEL) in the absence of selection results in FOB-cell differentiation [74]. Therefore, it is likely that self-reactive immature B-cells that have escaped negative selection can differentiate into the MZB-cell subset by BCR signalling.

Third, the pro-survival factor BAFF plays a critical role in MZB-cells differentiation. While BAFF promotes the survival of both, FOB- and MZB-cells [85], distinct downstream NF-κB transcriptional programs, independent of survival, are required for MZB-cell differentiation [40, 74]. The mechanism of BAFF-driven MZB-cell differentiation is not fully understood. However, activation of canonical and alternative NF-κB pathways coordinates MZB-cell differentiation [36, 37, 40, 84, 86-89].

Fourth, conditional mouse knockout experiments demonstrated the requirement for Notch2 signals for MZB-cell differentiation [48, 74]. Ablation of Notch2, its ligand Delta like canonical Notch ligand 1 (DLL1) or downstream effectors blocks MZB-cell development while Notch2 signalling overactivation results in strongly enhanced MZB-

cell formation [48, 74, 90]. Given the complex spleen architecture and that the expression of DLL1 takes place in the red pup venules and also in the follicle {Fasnacht:2014hm}, MZB-cell differentiation requires the recirculation of the cells in the spleen. The migration of future MZB-cells requires the reorganization of the actin cytoskeleton, which is associated to integrin activation. It is therefore likely that chemokine or BCR signals might influence MZB-cell homeostasis via integrin interactions [19, 20].

Taken together, FOB-cell differentiation requires BCR signals of intermediate strength accompanied by BAFF-induced survival signals. MZB-cell differentiation is a more complex process where weak BCR signals synergize with Notch2- and BAFF-mediated signalling.

### I.3.4 B-CELLS IN ADAPTIVE IMMUNITY

After naïve B2-cells encounter an antigen, they can experience three different fates. First, they can migrate to the outside of the follicle and mature into short-lived extra-follicular plasmablasts that produce low-affinity antigen specific antibodies. Second, they can migrate to the border of the T-cell zone, and become memory B-cells [91, 92]. Third, they can migrate to the follicle where with the help of follicular helper T-cells ($T_{FH}$) they develop into germinal centre (GC) B-cells and mature to long-term high-affinity memory B-cells or antibody secreting plasma cells (PC) [46, 47, 92].

Upon activation by antigen, B-cells require a set of additional cues that promote their migration towards the T-cell zone interface in the secondary lymphoid organs where further direct interactions with cognate T-cells will result in additional activation [47, 92]. Although it is still not satisfactorily clarified what determinates the extra-follicular versus the germinal centre cell-fate decision, it is likely influenced by positive antigen selection, as extra-follicular PC produce low affinity antibodies [46, 92]. Additionally, the responsiveness to the cytokine CXCL13 may play an important role, as GC B-cells are characterized by the expression of the CXCL13 receptor CXCR5, while extra-follicular B-cell have lost its expression [46].

### I.3.4.1 Germinal centre reaction

GC B-cells are defined by expressing high levels of the death receptor FAS (also know as CD95), and binding to peanut agglutinin (PNA) and the epitope bound by the GL7 monoclonal antibody [46, 91]. Murine GC B-cells are additionally characterized by down regulating the expression of CD38 [91].

Cognate $T_{FH}$ provide co-stimulatory cell-to-cell signals and cytokines that will drive activated B-cells to form GC B-cells. $T_{FH}$ are characterized by the expression of CXCR5, Programmed cell death 1 (PD1), Inducible T-cell co-stimulator (ICOS) and CD40L, among others [46]. Several signals required for GC formation have already been identified: TCR binding to cognate peptide presented by the Major histocompatibility complex class II (MHC-II) in B-cells, CD40L binding to CD40 and CD28 binding to the co-stimulatory molecules CD80 and CD86 on the B-cells [46]. Additionally $T_{FH}$ cells secrete IL-4 and IL-21 that are required for proper GC development [46, 92].

At the beginning of the GC reaction, activated B-cells are highly proliferative. After 7 days, the GC starts polarizing into distinct zones, termed dark zone (DZ) and light zone (LZ) for their appearance in histological sections {Zhang:2016ks}. The formation of the DZ and the LZ depend on the CXCL12 chemokine and its receptor CXCR4, while the proper DZ/LZ polarization depends on the chemokine CXCL13 and its receptor CXCR5 {Allen:2004bi}. The current model for antibody affinity maturation involves the re-cycling of GC B-cells through the DZ and LZ, which is influenced by the expression of CXCR4 in GC B-cells and the high CXCL12 gradient in the DZ, and a high CXCL13 gradient in the LZ [47, 92]. In the DZ highly proliferating B-cells, called centroblasts, reduce their BCR expression and undergo affinity maturation of their BCR via the process of somatic hyper-mutation (SHM) [46, 47, 92]. The cells stop proliferating, down regulate the expression of CXCR4 and migrate towards the high CXCL13 gradient in the LZ, facilitated by their expression of CXCR5 [47, 92]. In the LZ, GC B-cells up-regulate their BCR expression and compete for the interaction with cognate $T_{FH}$ and follicular dendritic cells. Through interactions with $T_{FH}$ and most likely follicular dendritic cells, GC B-cells carrying high affinity BCRs are recued from apoptosis to become centrocytes [46]. $T_{FH}$ cells may positively select GC B-cells that efficiently present the cognate antigen via MHC-II. It is likely that high affinity BCRs are more efficient at antigen capture and allowing centrocytes a higher antigen presentation through their MHC-II [46, 92]. In the LZ, the affinity of the BCR is tested and the cell can have one of three fates: (1) it can die in the absence of survival signals from the $T_{FH}$, (2) the cell can recycle to the DZ to

undergo another round of BCR affinity maturation, or (3) terminally differentiate into a memory B-cell or high affinity antibody secreting PC [46, 47]. Positively selected centrocytes in the LZ up-regulate the expression of CXCR4 and migrate to the DZ to further modify their BCR affinity [92].

As mentioned before, SHM in the DZ is responsible for antibody affinity maturation. This process introduces single nucleotide exchanges into the immunoglobulin variable region. The process is initiated by the Activation-induced deaminase (AID) enzyme that deaminates cytidines converting C:G base pairs into U:G base pairs that need to be fixed by the cells DNA-repair machinery [47]. Therefore, GC experienced B-cells can be identified by mutations in their immunoglobulin variable region acquired during their transition through the GC.

Once the B-cells have been positively selected for high affinity antibodies in the LZ, they undergo an additional process termed class switch recombination (CSR), where they change their immunoglobulin heavy chain mu (IgM) and delta (IgD) constant regions for a different class, in an AID-dependent mechanism. The different classes of heavy chains have different functions and different cytokines and co-stimulatory molecules determine to which class the recombination takes place. Known signals that coordinate the CSR process include CD40-CD40L, ICOS-ICOSL and stimulation of the TACI and BAFFR [47].

The development and function of the GC reaction are regulated by the transcriptional repressor B-cell lymphoma 6 (BCL6) [93] and the transcription factor Interferon regulatory factor 4 (IRF4) [94-96]. In the DZ, BCL6 blocks transcriptional programs involved in cell cycle arrest and differentiation [97], thus generating a permissive environment for the genetic instability caused by high proliferation and DNA-damage associated with SHM [47]. Exit of the DZ and migration to the LZ requires the repression of BCL6. In the LZ, CD40 signalling rescues cells from apoptosis and promotes the NF-κB dependent expression of the transcription factor IRF4. High IRF4 levels repress Bcl6, promote the expression of AID for CSR, and promote the expression of transcription factor B lymphocyte-induced maturation protein 1 (Blimp1) required for commitment to the PC state [46, 47, 98]. IL-4 is indispensible for DZ proliferation, SHM and production of memory B-cells. IL-21 is involved in early plasma cell formation and is required for the generation of antibody secreting PC [46, 99].

Recent evidence demonstrates the requirement for a tight control of NF-κB activation in GC maintenance and plasma cell differentiation [35, 100-103]. During positive selection, CD40 and BCR downstream signals in the LZ coordinate the activation of both canonical and alternative NF-κB. Canonical NF-κB activation via c-Rel and alternative NF-κB activation of both RelB and p52 are both independently required for GC maintenance, regulating different transcriptional programs. The evidence suggests that while the canonical NF-κB pathway regulates the metabolic requirements for centrocyte recycling from the LZ to the DZ [100], the alternative NF-κB pathway regulates the expression of ICOSL required for $T_{FH}$ help in the LZ and for the re-entry of cells into the cell cycle required for further affinity maturation in the DZ [101]. Moreover, RelA-dependent canonical NF-κB activation and alternative p52 activation are independently required for terminal differentiation into plasma cells [100, 101].

The B-cells then egress the follicle and differentiate into long-lived plasma cell and memory B-cell. There is a tight transcriptional regulation at the germinal centre stage in B-cells during differentiation into plasma cells. Pax5, Bcl6 and Bach2 drive the B-cell transcriptional program, while Blimp1 and Xbp1 control plasma cell differentiation [98]. Long lived plasma cells can migrate to the bone marrow, where their survival is supported by BAFF- and APRIL-induced signals via BCMA [48].

### I.3.5 B1-CELL DEVELOPMENT

In mice, B1-cells are a well-defined B-cell subset that is involved in innate-like and T-cell independent immunity [104]. B1-cells are mainly located in the pleural and peritoneal cavities, with a small population also present in the spleen and few cells observed in the peripheral blood, bone marrow and draining lymph nodes [104]. B1-cells are characterized by a surface phenotype of $CD19^{hi}$ $B220^{lo}$ $IgM^{+}$ $IgD^{variable}$ $CD23^{-}$ $CD43^{+}$ [104, 105] and can be subdivided into B1a- and B1b-cell subsets by the presence or absence of the inhibitory protein CD5, respectively.

It has been suggested that splenic and peritoneal B1-cells are phenotypically and functionally different [106]. First, B1a-cells from the peritoneal cavity have constitutively active STAT3, while splenic B1a-cells do not [105]. Second, B1a-cells from the spleen are able to mobilize calcium after BCR crosslinking compared to B1a-cells from the peritoneal cavity [105]. Finally, B1a-cells in the spleen secrete the majority of

natural antibodies, while the secretion of natural antibodies from B1a-cells in the peritoneum is negligible [107].

In humans, the identification of a counterpart to murine B1a-cells has been challenging since human activated B-cells also express CD5 [108]. Several efforts of strictly sorted pure human B-cells have identified a human counterpart for B1-cells, with similar functions [109]. This finding underscores the relevance of studying B1-cell biology in suitable mouse models.

To date, the best fitted model explaining B1-cell development in mice is the two-pathway model [104]: During embryonic development in the mouse foetal pHSC give rise to self-renewable B1a- and B1b-cells with a restricted VH repertoire [49], while in the adult bone marrow early lymphoid progenitors (ELP) and to a lesser extent CLPs have the ability to differentiate into B1a- but mainly B1b-cells with a broader VH repertoire [110]. In the steady state the B1-cell pool in the adult mouse is maintained by the self-renewal capacity of foetal liver-derived B1a- and B1b-cells and the bone marrow-derived B1-cells have only a minor contribution [104]. It is in particular cases after B1-cell depletion that the bone marrow-derived B1-cells replenish the pool [104]. One report described the transformation of B2-cells into cells with a B1a phenotype by conditional expression of B1a-cell-derived anti-phosphatidyl-choline specific BCR [111]. This suggests the potential of B2-derived B1-cells, nonetheless it is unclear if these transformed B1a-cells behave physiologically as B1a-cells. Therefore, the mature B1 cell pool in the adult mouse consists mainly of self-renewable foetal liver-derived B1-cells with a small contribution of bone marrow-derived B1-cells.

In mice, B1a-cells are the main source of natural antibodies [107, 108, 112]. These natural antibodies have low antigen-affinity, represent a skewed BCR repertoire, and are poly-reactive recognizing self-antigens, apoptotic cells and microbes [104, 105, 112]. The presence of stereotyped BCRs in B1-cells and evidence for a requirement of natural antigens engaging their cognate BCRs for B1-cell development support the model for positive antigen selection in B1-cell development [49, 104, 105, 112]. Genetic studies in mice demonstrated the requirement for the BCR signalling complex for the development and/or survival of B1-cells [105, 112-115]. Moreover, it appears that the strength of BCR signalling and not the affinity strength of the antibody to its cognate antigen plays a role in B1-cell development. Strong BCR signalling is required for B1-cell development while intermediate BCR signalling is associated with the development of FOB- and MZB-

cells [81]. Therefore, it is likely that both models are not mutually exclusive and play a role during the development of B1-cells.

Additionally to producing natural antibodies, B1-cells can migrate into tissues and partially differentiate into antibody secreting cells: IgA-secreting cells in the gut-associated lymphoid tissue (GALT), in particular lamina propia and mesenteric lymph nodes [116].

The B1b-cell subset is somewhat less well studied. However, it is clear that B1b-cells are also involved in the production of natural antibodies [117]. Moreover, B1b-cells are responsible for producing an adaptive antibody response against pneumococcal polysaccharides [116].

The BCR crosslinking in B1-cells seems to have a different effect compared to B2-cells [118]. After BCR crosslinking *in vitro*, calcium mobilization is minimal in B1-cells and they fail to proliferate [118]. Nonetheless, B1-cells are not anergic as AKT is activated in a phosphoinositide-3-kinase (PI3K)-dependent manner and MHC-II expression is up regulated after BCR crosslinking in B1-cells [104]. In contrast, other stimuli such as phorbol myristate acetate (PMA), CD40 and TLR ligands result in B1-cell proliferation *in vitro* [105, 112]. In response to TLR stimulation, B1-cells can produce IL-6 and IL-10 and thus modulate the immune response [119].

Genetic experiments in mice demonstrated that NF-κB activation plays an important role in B1-cell development and differentiation. Ablation of the NF-κB subunits NF-κB2, c-Rel/NF-κB2 [78], NF-κB1/NF-κB2 as well as of NEMO or IKK2 [40] result in reduced numbers or a complete absence of B1-cells [67]. Additionally, LUBAC deficient B-cell cannot differentiate to B1-cells [35]. Moreover, ablation of components of the CBM complex in B-cells also results in impaired B1-cell development [67, 120]. Taken together, these studies demonstrate the requirement for canonical and alternative NF-κB signals in B1-cell development.

Similarly, genetic experiment in mice demonstrated that B1-cell activation is tightly controlled by negative regulators of BCR signalling such as CD5 and the member of the CD22 family of sialic acid binding proteins Siglec-G. First, CD5 is a pan T-cell marker that is associated with decreased TCR sensitivity [105]. In B1a-cells, CD5 is associated with mIgM, therefore constantly modulating BCR activation. In CD5 knockout mice, B1-cells

respond to BCR crosslinking by higher calcium mobilization, activation of NF-κB and proliferation [105, 108]. It has been proposed that the CD5-SHP1 binding/association to mIgM lowers its sensitivity to antigen activation [105]. Second, ablation of Siglec-G in two different mouse models resulted in the abnormal expansion of B1a-cells associated with higher calcium mobilization post BCR-crosslinking [121] or NF-κB activation [122] [123]. Therefore, these inhibitory signals may play a role at limiting B-cell self reactivity [108].

B1-cells have also been implicated in autoimmune diseases by the fact that B1-cell numbers are expanded in Sjoegren's syndrome, systemic lupus erythematosus, and rheumatoid arthritis in humans as well as in mouse models for systemic autoimmunity [105, 116]. There are several different mechanisms how B1-cells can modulate the immune response and trigger autoimmune diseases. First, the production of natural antibodies [107] can lead to the production of pathogenic antibodies that results in the deposit of immune-complexes that trigger autoimmune disease [105, 116]. Second, B1-cells have the potential to act as antigen presenting cells to T-cells [119]. Therefore, if a self antigen is presented by a B1-cell it could trigger an immune response [105, 116]. Finally, the evidence suggests that activated B1-cells can produce and secrete cytokines such as IL-10 and affect surrounding cells [119]. Genetic experiments in mice have implicated B1a-cells in systemic autoimmune disease [114], collagen-induced arthritis model [124], haemolytic anaemia and lupus erythematosus [105, 116] amongst others. Therefore, a better understanding of B1-cell biology will help understanding the aetiology of and ultimately treating these autoimmune diseases.

## I.4 MALIGNANT TRANSFORMATION LEADING TO B-CELL NEOPLASMS

During normal B-cell development, B-cells transition through several stages of genomic instability where single and double strand DNA breaks are tolerated for the generation of functional high-affinity BCRs: (1) V(D)J recombination during IgH and IgL assembly in early B-cell development, (2) SHM required for BCR affinity maturation, and (3) CSR for production of different classes of antibodies [47]. The nature of these processes predisposes B-cells for chromosomal translocations, amplifications and deletions, as well as somatic mutations that can activate oncogenes, generate fusion proteins, or inactivate tumour suppressor and thereby drive lymphomagenesis.

Several chromosomal translocations implicating the immunoglobulin locus have been identified in many B-cell neoplasms: BCL2 translocations are common in follicular lymphoma (FL), translocation involving the oncogene Myc are common in Burkitt's lymphoma (BL), translocations with the GC repressor BCL6 are common in diffuse-large B-cell lymphomas (DLBCL) [47], and translocations involving the MALT1 and BCL10 proteins of the CBM complex downstream of BCR signalling are common in splenic marginal zone lymphoma (sMZL) [125]. Moreover, chromosomal translocations can also result in fusion proteins that drive lymphomagenesis. For instance, the chromosomal translocation t(11;18) produces IAP2-MALT1, a fusion protein implicated in sMZL. This fusion protein promotes the aberrant cleavage of RelB leading to its constitutive activation [125].

The process of SHM also affects non-immunoglobulin genes. SHM hot spots have been identified for the GC repressor BCL6, where aberrant SHM introduces mutations in the 5' regulatory sequence of the gene affecting its expression [47]. Additionally, aberrant SHM can introduce mutations that affect the function or regulation proteins controlling cell survival and proliferation.

### I.4.1 CONSTITUTIVE ACTIVATION OF NF-κB IN B-CELL MALIGNANCIES

Several human B-cell neoplasms are characterized by the constitutive activation of NF-κB [1-9]. Aberrant NF-κB activation can result in the enhanced expression of genes involved in (1) proliferation, including Cyclin D1, Cyclin D2, c-Myc and c-Myb; (2) survival, including BCL2 and BCL-XL; (3) cytokines, such as IL-2 and IL6; and (4) CD40L [10]. Moreover, a higher expression of these NF-κB targets has been identified in different B-cell neoplasms, linked to nuclear NF-κB [126-130], suggesting a role for NF-

κB activation in B-cell transformation. Therefore, further studies are required to address its pathological role as a potential driver in B-cell transformation.

In the past 15 years novel somatic mutations, chromosomal number alterations and translocations with the potential to deregulate NF-κB activation have been identified in B-cell malignancies (summarized in Table 1), further supporting the involvement of NF-κB activation in lymphomagenesis. Novel mutations involved in innate immunity targeting TLR downstream proximal signalling partners MyD88 or TRAF6 (Table 1, Figure 1A) have been identified in chronic lymphocytic leukaemia (CLL) [131], FL [132], activated B-cell (ABC)-DLBCL [132-135] and sMZL (Table 3). Similarly, novel genomic alterations associated with antigen signalling targeting the BCR complex protein Igβ or the downstream CBM complex (Table 1, Figure 1A) have been identified in mantel cell lymphoma (MCL) [136], FL [137], DLBCL [6, 134, 135, 138, 139], primary mediastinal B-cell lymphoma (PMBL) [139], mucosa-associated lymphoid tissue (MALT) lymphoma [10] and sMZL (Table 3). The recurrent targets in diverse types of B-cell lymphomas (Table 1) suggest a potential role in NF-κB activation as a common mechanism in B-cell neoplasm.

Particular attention has been given in the past years to A20, a central negative regulator of canonical NF-κB activation. The TNFAIP3/A20 locus maps to the recurrent chromosomal deletion 6q23.3-24 found in various types of B-cell neoplasms (Table 2). Additionally, several somatic mutations with a predicted loss-of-function phenotype have been reported for A20 (Table 2). Finally, the promoter of A20 is also recurrently silenced by methylation in lymphoma [140]. The combination of these genomic lesions results in A20 inactivation, where both alleles have been deleted or silenced [140]. This has prompted the idea of A20 acting as a classical two hit tumour suppressor in B-cell lymphomagenesis. However, genetic studies in mice found that ablation of A20 in B-cells results only in sporadic B-cell lymphomas in aged mice [79] Chu unpublished, suggesting that ablation of A20 alone is insufficient to efficiently transform B-cells, and additional genetic lesions are required.

**Table 1. Constitutive NF-κB activation in B-cell neoplasms**

| Tumour | NF-κB activating mechanism | NF-κB pathway or subunit | Citation |
|---|---|---|---|
| **CLL** | Tumour microenvironment interactions | RelA | [141] |
| | MyD88 somatic mutations | Canonical | [131] |
| | Notch1 somatic mutations | RelA | [142] |
| | I-κBε somatic mutations | RelA | [143] |
| **MCL** | Tumour microenvironment interactions | RelA | [1] |
| | Chromosome 18q21 gains containing MALT1 and BCL2 (12%, 4/33) | | [136] |
| | TRAF2 somatic mutations | Canonical | [144] |
| **FL** | Locus amplification c-Rel (28.8%, 5/52), TRAF6 (9.6%, 5/52) | Canonical | [132] |
| **and tFL** | Somatic mutations in A20, CARD11 and Igβ; and chromosomal deletions in A20 | Canonical | [137] |
| **DLBCL** | RelA deregulation (8.4% $RelA^{hi}$, 50% $RelA^{+}$) | RelA | [2] |
| | Somatic mutations in A20, CAR11 (11%), TRAF2 (3%), TRAF5 (5%), TAK1 (5%), RANK (8.1%) | p50, p52 and p50+p52 | [6] |
| | Locus amplification of c-Rel (29%,18/62), TRAF6 (11.3%, 7/62) | Canonical | [132] |
| | BAFFR-TRAF3-NIK constitutive activation | Canonical Alternative | [145] |
| | BCL3 expression (46.2%, 36/78) BCL3 gains (5.1%, 4/78) | | [146] |
| | Somatic mutations affecting A20, Igβ, MyD88, CARD11. Chromosomal gains in c-Rel or deletions in A20 and TRAF3 | Canonical | [138] |
| | Somatic mutations in A20, CARD11, MyD88 (ABC type) and Igβ□□□□□□□□□□□ | Canonical | [133] |
| | Somatic mutations in MyD88 (24.3%, 43/177) and Igβ□□□□□□□□□□ only 12.2%) | Canonical | [134] |
| **ABC-DLBCL** | Somatic mutations in Igβ, BCL10, MyD88 A20 somatic mutations and chromosomal deletions | Canonical | [135] |

CLL (Chronic lymphocytic leukaemia/lymphoma), MCL (Mantel cell lymphoma), FL (Follicular lymphoma), tFL (transformed follicular lymphoma), DCBCL (diffuse large B-cell lymphoma), ABC-DLBCL (Activated B-cell like DLBCL).

**Table 1 (continued). Constitutive NF-κB activation in B-cell neoplasm**

| Tumour | NF-κB activating mechanism | NF-κB pathway or subunit | Citation |
|---|---|---|---|
| **GCB-DLBCL** | Somatic mutations in CARD11, I-κBα and I-κBε | Canonical | [135] |
| | c-Rel locus amplification | Canonical | Reviewed in [10] |
| | 3' deletions in NF-κB2 (constitutive active p52) | Alternative | Reviewed in [10] |
| **PMBL** | A20 chromosomal deletions and Rel, BCL10 and MALT1 chromosomal amplifications | Canonical | Reviewed in [139] |
| | I-κBε somatic mutations | Canonical | [147] |
| **MALT lymphoma** | BCR-CBM complex translocations (IAP-MALT1 fusion protein, IgH-MALT1, IgH-BCL10) | Canonical | Reviewed in [10] |
| **HL** | 40-50% Rel locus amplification<br>15-20% somatic inactivating mutations in I-κBα<br>30-40% somatic inactivating mutations in A20 | Canonical | Reviewed in [148] |
| | RelB and NIK activation | Alternative | [149] |
| **Classical HL** | TRAF3 deletions and NIK amplifications | Alternative | [150] |
| **MM** | NF-κB1, A20, CYLD, TACI mutations | Canonical | [151]<br>[152] |
| | NF-κB2, NIK, TRAF2/3, IAP1/2 mutants | Alternative | [151]<br>Reviewed in [7] |
| **EBV** | LMP1 c-Rel dependent activation<br>LMP1 NIK p52 activation | Canonical<br>Alternative | Reviewed in [10] |
| **Kaposi sarcoma-associated herpes virus (KSHV)** | vFLIP activation of IKK2 | Canonical | Reviewed in [10] |
| **HCV induced BCL (DLBCL)** | Reduced A20 expression, nuclear RelA and p50 | Canonical<br>Alternative | [153] |

GCB-DLBCL (Germinal centre B-cell like DLBCL), PMBL (primary mediastinal B-cell lymphoma), MALT (mucosa-associated lymphoid tissue), HL (Hodgkin's lymphoma), MM (multiple myeloma), EBV (Epstein-Barr virus), HCV (Hepatitis C Virus)

**Table 2. Inactivation of A20 as a current event in B-cell neoplasms**

| Tumour entity | A20 inactivation mechanism | Incidence | Citation |
|---|---|---|---|
| **MZL**[1] | Somatic mutations | 19% | [154] |
| | 6q23.3-24 chromosomal deletions | 37.5% | [155, 156] |
| **MALT lymphoma**[2,3,4] | Somatic mutations | 28.6% | [157] |
| | 6q23.3-24 chromosomal deletion | 7-17.2% | [157-159] |
| | Biallelic inactivation by 6q23.3-24 chromosomal deletions and somatic mutations | 21.8% | [132] |
| **Classical HL**[5] | Somatic mutations | 33.3-44% | [132, 160] |
| | 6q23.3-24 chromosomal hemizygous or homozygous deletion | 32%<br>11% | [161] |
| **MCL** | 6q23.3-24 chromosomal deletion | 31% | [158] |
| **DLBCL** | 6q23.3-24 chromosomal hemizygous or homozygous deletion | 21.6%<br>1.5% | [162] |
| **ABC-type** | Somatic mutations | 24.3% | [6] |
| | 6q23.3-24 chromosomal deletion | 48-50% | [6, 158] |
| **GCB-type** | Somatic mutations | 2.3% | [6] |
| | 6q23.3-24 chromosomal deletion | 22% | [158] |
| **PMBL-type** | Somatic mutations | 36% | [160] |
| **FL** | 6q23.3-24 chromosomal deletion | 26% | [158] |
| **MM** | 6q23.3-24 chromosomal deletion | 17.7% | [152] |
| **CLL** | 6q23.3-24 chromosomal hemizygous deletion | 25% | [163] |

[1] Cohort in Novak et al. (2009) includes splenic (1/8), nodal (3/9) and extranodal (2/11) MZL. [2]Chromosomal deletions in cohort in Chanudet et al. (2009) were only identified in ocular adnexa (8/42), salivary glands (2/28), thyroid (1/11) and liver (1/2) MZL. [3,5]Cohorts in Kato et al. (2009) includes stomach (3/23), ocular (13/43) and lung (2/12) extranodal MZL and HL of the nodular sclerosis type. [4] Cohort in Bi et al. (2012) analysed ocular adnexal extranodal MZL.
MZL (Marginal zone lymphoma), MALT (mucosa-associated lymphoid tissue), HL (Hodgkin's lymphoma), MCL (Mantel cell lymphoma), DCBCL (diffuse large B-cell lymphoma), ABC- (Activated B-cell like DLBCL), GCB (Germinal centre B-cell like DLBCL), PMBL (primary mediastinal B-cell lymphoma), FL (Follicular lymphoma), MM (multiple myeloma), and CLL (Chronic lymphocytic leukaemia/lymphoma)

To date, the role of the mutations associated with NF-κB activation are still incompletely understood. Two independent studies demonstrated the cooperation of NF-κB activation with other oncogenic events in the development of DLBCL in mice. First, Calado et al. (2010) showed that constitutive canonical NF-κB activation collaborates with Blimp1 deletions in B-cells in the development of ABC-DLBCL in mice [164]. Second, Zhang et al. (2015) found that alternative NF-κB activation cooperates with overexpression of BCL6 in B-cells in the development of GC-DLBCL in mice [165]. Moreover, Calado et al. (2010) also found that constitutive canonical NF-κB expression in GC B-cells resulted in plasma cell hyperplasia [164]. Thus, the evidence supports the involvement of NF-κB activation in cooperation with oncogenic events in B-cell transformation.

Moreover, it has been proposed that signals from the microenvironment might play a role in NF-κB activation in cases were no evident genetic lesions affecting NF-κB activation have been detected. Evidence for this hypothesis has been put forward in CLL [141, 166, 167] and in MCL[1]. Additionally, a subset of DLBCL is characterized by high expression of RelA accompanied by nuclear translocation of RelA, in the absence of any known genomic aberration that could promote RelA activation [2], which may also imply a role of the microenvironment in NF-κB activation.

Taken together, the recurrent observation of enhanced or constitutive NF-κB activation and the broad spectrum of genetic lesions targeting NF-κB in B-cell neoplasm, suggest that NF-κB activation could act as a general mechanism in B-cell transformation. Therefore, further studies are required to investigate the roles of canonical and alternative NF-κB activation in different B-cell malignancies.

### I.4.2 SPLENIC MARGINAL ZONE LYMPHOMA AND NF-κB ACTIVATION

MZLs are an indolent type of lymphoma that can be subdivided into three different subtypes: sMZL, nodal marginal zone lymphoma (nMZL) and extra-nodal marginal zone lymphoma of the MALT type (also known as MALT lymphoma) [125]. sMZL accounts for 2-5% of lymphoid neoplasms [168]. The disease is characterized by splenomegaly accompanied by bone marrow, peripheral blood and in some cases liver infiltration [169]. It is likely that the cell of origin is a pre- or post-GC B-cell [168]. Although the disease patho-mechanism are unknown, the biased IGHV gene usage [170, 171], high

incidence of hepatitis C virus infections among patients [171, 172] and association with chronic inflammation or autoimmune diseases suggest that antigen stimulation plays a role [125, 168, 169]. Moreover, 30% of the sMZL cases are of the aggressive form with worst prognosis and out of those, 5-10% can transform into diffuse large B-cell lymphoma (DLBCL) [20, 173]. Therefore, a better understanding of the disease pathogenesis could lead to improved treatment options, for example through preventing transformation into a more aggressive form.

The most common genetic abnormalities found in sMZL are deletions of 7q21-32 present in about 30% of the patients [171, 173] and chromosomal translocations involving the immunoglobulin heavy and light chain loci such as t(11;18), t(1;14) and t(14;18) [125, 154].

Advances in whole genome sequencing (WGS) and whole exome sequencing (WES) in the past decade have identified a variety of novel mutations related to sMZL (Table 3). The most commonly affected pathways include the NF-κB [154, 171, 174-177] and the Notch2 [178-181] pathways, required for normal MZB-cell differentiation [90, 182].

Analysis of sMZL patient biopsies demonstrated the constitutive activation of NF-κB in 50% of the samples analysed [176, 183]. In addition, several genomic alterations resulting in potential NF-κB activation have been reported in sMZL patient samples (summarised in Table 3). First, the NF-κB genomic alteration in sMZL affect both the canonical NF-κB arm (IKK2/A20, Table 3) and alternative NF-κB arm (TRAF3/IAP1/NIK, Table 3) and have the potential to promote stronger or constitutive NF-κB activation [154, 179, 183]{Kai:2014iw}. Genetic lesions affecting canonical NF-κB signalling have been identified in IKK2 and A20 (Table 3). The positions of the somatic mutations in IKK2 suggest that they are gain-of-function mutations. While somatic mutations in A20 most likely result in loss-of-function. Therefore, they would both result in enhanced and/or prolonged activation of NF-κB. The alternative NF-κB pathway has been affected by somatic mutations resulting in loss-of-function or chromosomal deletions affecting TRAF3 and IAP proteins, as well as chromosomal gains affecting the NIK locus (Table 3). TRAF3 mutations putatively affect NIK binding and recruitment for ubiquitination, while IAP1 mutations affect ubiquitination of NIK required for its proteosomal degradation [125, 179, 183].

**Table 3. Most common genetic abnormalities identified in sMZL**

| Pathway Gene/Protein | Somatic mutations | Chromosomal aberrations [a] | Citation |
|---|---|---|---|
| *NF-κB pathway* | 34-36% | | [174, 183] |
| *Canonical arm* | | | |
| TNFAIP3/A20 | 6-21% | 7-9% | [154, 171, 174, 177, 183] |
| IKBKB/IKK2 | 1-7% | | [174, 177, 183] |
| *Alternative arm* | | | |
| BIRC3/IAP1 | 4-6% | 5-6% | [174, 177, 183] |
| TRAF3 | 3-15% | 5-7% | [174, 177, 183] |
| MAPK14/NIK | 1% | 6-7% [b] | [174, 183] |
| *TLR and BCR* | | | |
| MyD88 | 5-15% | | [171, 174, 177, 180] |
| CARD11 | 6-10% | | [171, 174, 177] |
| BCL10 | 3% | | [177] |
| KLF2 | 17-40% | | [177, 181] |
| *Notch Pathway* | 32% | | [174] |
| Notch2 | 10-25% | | [174, 177, 178, 180, 181] |

[a] Chromosomal deletions and gains
[b] Chromosomal gains

Second, the most prevalent genetic alternation observed in sMZL patients was the loss-of-function of the transcription factor Kruppel-like factor 2 (KLF2, Table 3) activated downstream BCR and Toll-like receptor (TLR) stimulation and associated with NF-κB repression that resulted in NF-κB hyper-activation [125, 177, 180, 181].

Third, additional genetic alterations potentially resulting in constitutive NF-κB activation were reported for the B-cell receptor downstream activators CARD11 [171, 174, 177] and BCL10 [177], and the TLR associated protein MyD88 mutation L256P [171, 174, 177, 180]. While mutations in CARD11 and BCL10 would promote the spontaneous formation of the BCM complex, the L256P MyD88 mutation affects its interaction with IRAK1 and IRAK4 promoting a spontaneous complex formation [125].

Finally, methylation changes have also been implicated with silencing and overexpression of genes involved in NF-κB activation [125]. Therefore, all the evidence suggests that constitutive canonical and alternative NF-κB activation could play a prominent role in sMZL development and pathogenesis.

Importantly, the studies of Rossi et al (2011) and Rossi et al (2012) claimed that the genetic lesions affecting NF-κB activation seem to be mutually exclusive where 11-15% of the samples analysed had lesions affecting the canonical NF-κB arm, while 21% of the samples presented lesions in the alternative NF-κB arm (Figure 3). However a further analysis of their results revealed that 4-7% of the patients presented with lesions involving both A20 and the alternative NF-κB arm [179, 183].

Genetically modified mice provided evidence for the role of alternative NF-κB TRAF3/IAP1/NIK arm in MZB-cell development and lymphomagenesis. Activation of the alternative NF-κB transcription factor pathway in B-cells by the conditional overexpression of NIK leads to the expansion of MZB-cells in mice [89]. Ablation of the adaptor TRAF3 in B-cells leads to development of clonal sMZL and B1a lymphomas in 18 months old mice [184].

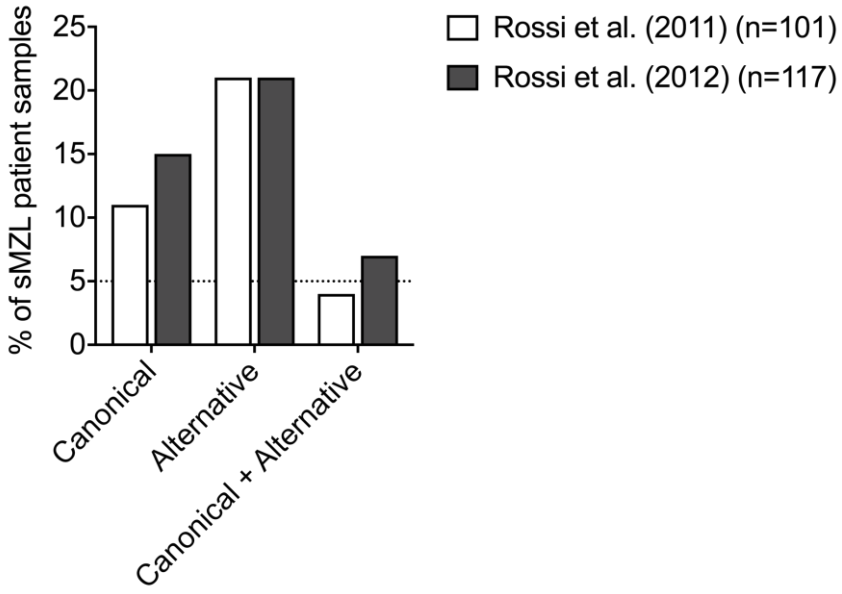


**Figure 3. Genomic alterations affecting the canonical and alternative NF-κB activation arms in splenic marginal zone lymphoma patients. (Data analysed from [179, 183])**

Similarly, genetic mouse models provided direct and indirect evidence for the role of canonical NF-κB activation in MZB-cell development and lymphomagenesis. The conditional expression of the constitutive active mutant IKK2 in B-cells results in enlarged pool of MZB-cells [37]. Transgenic mice overexpressing the BCL10 protein in B-cells have increased MZB-cell numbers and can develop features of human MZL [185]. Moreover, BCL10 overexpression is accompanied by canonical and alternative NF-κB activation [185]. Ablation of BCL10 in mice affects the development of mature B-cells, resulting in reduced MZB-cell numbers with reduced functionality [83]. Supporting the role of KLF2 mutations in sMZL, ablation of KLF2 transcription factor in mice results in increased MZB-cell numbers and splenic marginal zone hyperplasia [186, 187]. However, ablation of the NF-κB negative regulator A20 in B-cells results in the accumulation of MZP with impaired migration to the MZ and terminal differentiation into MZB-cell [79, 80].

In summary, sMZL is a very heterogeneous disease and the pathological mechanisms resulting in sMZL are poorly understood. The identification of genetic alterations in sMZL activating NF-κB, in addition to the fact that NF-κB signals are indispensible in MZB-cell development, suggest that constitutive activation of the canonical and alternative pathway are involved in sMZL transformation. Therefore, the potential involvement of canonical and alternative NF-κB activation as pathogenic mechanism in sMZL needs to be investigated.

### I.4.3 CHRONIC LYMPHOCYTIC LEUKAEMIA

Chronic lymphocytic leukaemia (CLL) is an indolent type B-cell neoplasm, characterized by the slow accumulation of small $CD5^+$ $IgM^+$ B-cells. CLL is the most common Western World B-cell neoplasm and to date there is no cure. Treatment often results in relapse due to the selection of resistant clones [188, 189]. Moreover, about 10% of CLL patients develop Richter syndrome (RS), a transformation to a more aggressive disease, usually DLBCL [190, 191]. CLL can be divided by the presence or absence of somatic mutations in the immunoglobulin gene in a more indolent mutated-CLL type or an aggressive unmutated-CLL type, respectively. It has been speculated that the cell of origin for the mutated-CLL is a germinal centre experienced cell, while the origin of the unmutated-CLL is pre-GC B-cell [192].

CLL is a very genetically heterogeneous disease [193] with several genetic aberrations targeting different pathways (Table 4), suggesting that different pathogenic insults can converge in the development of CLL. To date, the most recurrently mutated genes in CLL identified by WGS and WES are Notch1, SF3B1, I-κBε, IAP1 (BIRC3) and MyD88 [147, 191, 194] (summarized in Table 4). Their involvement in CLL development and pathogenesis is partially understood. First, Notch1 deletions in CLL target the C-terminal PEST domain. The predicted effect of these mutations result in impaired degradation and accumulation of the active Notch1. Notch1 activates different transcriptional programs, and a potential effect of Notch1 mutations is the expression of NF-κB molecules [191]. Second, the SF3B1 protein is involved in splicing and mRNA metabolism, however the predicted role of these mutations and its involvement in CLL is unknown. Third, I-κBε mutations result in decreased NF-κB inhibition, increased p65 phosphorylation and nuclear translocation [143]. Fourth, the mutations and chromosomal deletions affecting IAP seem to constitutively activate the alternative NF-κB pathway [191]. Moreover, the IAP locus maps to the commonly deleted region 11q22-q23, previously associated with ATM deletion in CLL. Finally, the MyD88 protein activates TLR downstream signals leading to canonical NF-κB activation (Figure 1A). The most prevalent MyD88 mutation L256P, found in 3% of CLL patients and present in other types of B-cell neoplasms, results in the constitutive activation of canonical NF-κB downstream of the TLR [191].

CLL is characterized by canonical NF-κB activation, with patients samples exhibiting different levels of activation [166, 195, 196], that is required for the survival of CLL-cells

[197] [198]. Moreover, canonical NF-κB activation, particularly RelA, have been suggested as a prognostic marker and potential therapeutic target [199, 200].

The mechanism by which canonical NF-κB is activated in CLL is poorly understood. First, it has been suggested that signals from the microenvironment activate canonical NF-κB [141] and regulate the expression of anti-apoptotic proteins such as BCL-xL [201-203]. It has been reported that the cytokines BAFF and APRIL induce canonical NF-κB activation in cultured CLL-cells [203]. Similarly, cell-to-cell contact possibly via CD40 or other interactions results in NF-κB activation [167, 201, 202]. Additionally, Lutzny et al. (2013) found that CLL-cells remodel their microenvironment, in a cell-to-cell contact-dependent fashion. This microenvironment remodelling, that induces the expression of the PKC-βII splice-variant in stromal cells of the microenvironments, is indispensable for CLL survival [167].

Second, it has been suggested that BCR signals activate NF-κB in CLL-cells and promote their survival [204]. There is strong evidence supporting the role of BCR activation in CLL pathogenesis. Several inhibitors targeting the downstream BCR kinase BTK inhibit BCR signals, reduce NF-κB activation and reduce proliferation of CLL-cells [205-207]. Interestingly, 30% of all CLL patients express stereotyped BCRs, suggesting a positive antigen selection process during lymphomagenesis [208].

Finally, somatic mutations or chromosomal deletions targeting NF-κB related genes have been identified in CLL in a small percentage of patients (Tables 1 and 4).

Various mouse models have been made to investigate the role of recurrent genetic lesions or oncogenes in the development of CLL [228]. The overexpression of the human oncogene TCL1 in B-cells results in the development of a CLL-like disease in mice [229]. Several mechanisms have been associated with TCL1 overexpression and CLL development, one being activation of canonical NF-κB, but further studies are required to validate their pathogenic role in CLL [230-233].

**Table 4. Most common genetic abnormalities identified in CLL**

| Targeted pathway or gene | Mechanism | Incidence | Citation |
|---|---|---|---|
| Cell cycle, survival (BCL2 regulation) | 13q14 deletion: lncRNAs (Dleu1 and Dleu2) and miRNAs (miR15-16) | 60-70% | [209-212] |
| ATM, IAP | 11q22.3 deletion | 27% | [211, 213] |
| Cell cycle? | Trisomy 12 | 29% | [214] |
| Cell cycle and proliferation | Chromosomal deletions 17q13: TP53 | 7-37% | [215, 216] |
| IRF4 | 6p25.3 deletion | 7% | [211, 217] |
| MYC | 8q24.21 gains | 5% | [211] |
| Pre-mRNA processing | Somatic mutations in the splicing factor SF3B1 | 10-26% | [194, 212, 213, 216, 218-220] |
| Notch, canonical NF-κB | Somatic mutations in Notch1 | 6-15% | [131, 194, 212, 213, 216, 219-223] |
| TLR, canonical NF-κB | Somatic mutations in MyD88 | 1-3% | [131, 194, 212, 213] |
| mRNA export | Somatic mutations in XPO1 | 2-8% | [131, 194] |
| BCR signalling | Somatic mutations in EGR2 | 8% | [194] |
| Canonical NF-κB | I-κBε mutations | 7-11% | [147, 194] |
| Alternative NF-κB | IAP mutations | 6.5% | [219] |
| Cell cycle and proliferation | Mutations in TP53 | 6-30% | [194, 212, 213, 220, 221, 223] |
| Genomic abnormalities | Somatic mutations in POT1 (Protection of telomeres 1) | 3.5% | [224] |
| GC B-cell related | Somatic mutations in KLHL6 | 1.8% | [131] |
| IRF4 | Somatic mutations | 1.5% | [225] |
| NF-κB activation? | CYLD downregulation | | [226] |
| Canonical NF-κB (IKK2) | miR708 promoter and enhancer methylation | | [227] |

lncRNA (long non-coding RNA).

Two individual studies have modelled the role of the recurrent 13q14 chromosomal deletion in CLL in mice [234, 235]. Klein et al. (2010) targeted the two loci mapped to the minimal deleted region (MDR) 13q14: miR25/16 and Dleu2. They found that ablation of mRI15/16 in B-cells resulted in the development of human CLL-like disease in 21% of the animals, while ablation of the MDR resulted in a similar disease in 27% of the animals [234]. Lia et al. (2012) targeted the common deleted region 13q4 that included the Dleu1 locus. They observed a similar incidence of 24-25% of the animals developing human CLL-like disease between the heterozygous deletion of the MDR and the common deleted region [235].

The role APRIL produced by the microenvironment and BCR signals in the development of CLL have also been investigated using mouse models. First, the transgenic expression of APRIL promotes B1-cell neoplasms in mice [236]. Moreover, the transgenic expression of APRIL accelerated the disease progression in APRIL-tg TCL1-tg compound mice [237]. Second, overexpression of human BTK in the murine mouse model for CLL IgH.ETmu accelerated the disease progression [238]. Thus, supporting the role of both cytokines present in the microenvironment and BCR signals in CLL development.

In summary, diverse pathogenic mechanisms converge in the development of a disease similar to human CLL in mice. However, the role of canonical NF-κB activation by the microenvironment in CLL pathogenesis remains to be elucidated.

# II AIM OF THE THESIS

Constitutive NF-κB activation is a hallmark of several B-cell neoplasms [1-9], however to date there is no direct evidence linking NF-κB activation to B-cell transformation. Taken into consideration the stringent requirement for NF-κB regulated transcriptional programs in B-cell development and activation, and the presence of diverse recurrent genetic lesions targeting both canonical and alternative NF-κB pathways in different B-cell neoplasms; it is of outmost importance to investigate participation of NF-κB activation in the development of B-cell neoplasms. Thus, the aim of this thesis was to investigate the direct role of NF-κB activation in B-cell transformation and lymphomagenesis using genetic mouse models.

First, I wanted to investigate the potential cooperation of canonical and alternative NF-κB activation in predisposing mice to splenic marginal zone lymphoma (sMZL) using already available mouse strains mimicking the chromosomal gains in NIK [89] and deletions in A20 [239] observed in human sMZL patients (Table 3).

Second, I wanted to investigate if constitutive canonical NF-κB activation in B-cells could promote B-cell neoplasms in mice using the already available mouse strain that allows conditional expression of a constitutive active IKK2 mutant (IKK2ca)[37]. In addition, I wanted to investigate the effect of the observed constitutive canonical NF-κB activation in human chronic lymphocytic leukaemia (CLL) in the disease development and progression by constitutively activating canonical NF-κB in the Eμ-hTCL1 mouse model for human CLL [229].

# III MATERIALS AND METHODS

## GENETICALLY MODIFIED MOUSE STRAINS

All mouse lines used in this study have been previously published. All mice used for this study were backcrossed to or generated in the C57BL/6 background. All mice were bred and kept in specific pathogen-free (SPF) conditions following the guidelines of the Region of Upper Bavaria (Regierun von Oberbayern) and the European Union.

Mice were housed at the mouse facilities of the Max-Planck Institute of Biochemistry in Munich, the Centre for Preclinical Research of the MRI (Zentrum für Präklinisches Forschung, ZPF) in Munich, Harlan in Milan and Charles River in Calco, Italy.

To model potential splenic marginal zone lymphoma (sMZL) I bred the $A20^{FL}$ mouse strain[240] to the R26-$Stop^{FL}$Nik (NIK-tg) mouse strain [89] in combination with the CD19cre mouse strain[113, 241].

To model aspects of chronic lymphocytic leukaemia I bred the Eμ-hTCL1tg (TCL1tg) mouse strain[229] to the R26-$Stop^{FL}$ikk2ca (R26-IKK2ca) mouse strain[37] in combination with the CD19cre strain [113, 241]. Additionally, I bred the Eμ-hTCL1tg mouse strain to the R26-$Stop^{FL}$ikk2ca or to the R26/CAG-CARΔ$1^{StopF}$[242] (R26-CAR) in combination with the Cγ1cre[243] strain or the AIDcre strain[244]. Moreover, the PKC-β knockout mouse strain $Prkcb^{tm1Tara}$ [245] was back crossed to the C57BL/6 genetic background and breed heterozygous or homozygous as recipients for transplantation experiments.

Mouse lines were genotyped for the different mutations combinations by polymerase chain reaction (PCR). Genomic DNA was extracted from tail or ear biopsy by Proteinase K treatment, followed by isopropanol precipitation. The PCR protocols are included in the supplementary material. Primers were produced by Metabion International AG (Munich, Germany) or Eurofins Genomics (Munich, Germany) and sequences are shown in Table 5.

**Table 5. PCR primers used for genotyping mouse strains**

| Targeted allele | Primer name | Sequence (5´-3' orientation) | Amplicon size |
|---|---|---|---|
| CD19cre | Cre8 | CCCAGAAATGCCAGATTA | Wild type allele: 452bp |
| | CD19c | AACCAGTCAACACCCTTCC | Knock-in allele: 500bp |
| | CD19d | CCAGACTAGATACAGACCAG | |
| Cγ1cre | Cg1Cre A | TGTTGGGACAAACGAGCAATC | Wild type allele: 250bp |
| | Cg1Cre B | GGTGGCTGGACCAATGTAAATA | Knock-in allele: 470bp |
| | Cg1Cre C | GTCATGGCAATGCCAAGGTCGCTAG | |
| Rosa26-Knock-in* | 790 rosa fw | AAAGTCGCTCTGAGTTGTTATC | Wild type allele: 570bp |
| | 791 rosa rev | GATATGAAGTACTGGGCTCTT | Knock-in allele: 450bp |
| | 792 Neo rev | GCATCGCCTTCTATCGCCT | |
| Rosa26-CAR | CARIIonly fw | CCTGCTGTGCTTCGTGCTCC | Wild type allele: N.P. |
| | CARIIonly RV | CGTAACATCTCGCACCTGAAGGC | Knock-in allele: 435bp |
| Eμ-TCL1tg | Tcl1 fw | AGTGGTAAATATAGGGTTGTCTACACG | Wild type allele: N.P. |
| | Tcl1 rv | CCCGTAACTGTAACCTATCCTTTA | Transgene allele: 250bp |
| A20 | A20_28 Fw | CACAGAGCCTCAGTATCATGT | Wild type allele: 150bp |
| | A20_31Rv | CCTGTCAACATCTCAGAAGG | Floxed allele: 230bp |
| | A20_30Fw | GCAGCTGGAATCTCTGAAATC | Deleted allele: 370bp |
| PKC-β KO | PKCbeta-fw | CAGGGTCGAATTGCCATCCTCCA | Wild type allele: 391bp |
| | PKC-MO13-fw | CTTGGGTGGAGAGGCTATTC | Knock out allele: 800bp |
| | PKCbeta_rv new | AGCCACTCTCGGTGCTGTG | |

* Used to genotype both R26-IKK2ca or R26-CAR
N.P. not possible

## MOUSE EXPERIMENTS

Animals were analysed at 2-3 months of age to assess effects of combining different genomic alteration in the immune development. Furthermore, mice were aged to monitor for disease development and progression. Animals were closely monitored for signs of cancer development: splenomegaly, hepatomegaly, enlarged lymph nodes or anaemia. When modelling for chronic lymphocytic leukaemia (CLL) in mice, blood samples were taken monthly to monitor for the development of malignant cells in peripheral blood. Animals were considered to be sick when the CLL-like cell burden in peripheral blood reach over 50% of total living cells, or there was visible lymphoid organ enlargement. In the absence of disease mice were analysed at 12-18 months of age. All animal experiments were approved by the Regierun of Oberbayern.

## PERIPHERAL BLOOD BLEEDING

Blood samples were collected by pouch bleeding into 1.5mL tubes with 50ul of heparin (20U/ml, Sigma-Aldrich). For serum collection, heparin treated Microvette® (Cat. No.

16.443, Sarstedt) or clotting activator treated Microvette® (Cat. No. 20.1343, Sarstedt) were used. If peripheral blood sample was to be furthered processed, red blood cell lysis of erythrocytes was done using ACK lysis buffer. Cells were later washed with cell buffer solution containing 2% foetal bovine serum (FBS), penicillin/streptomycin in phosphate buffered saline (PBS) (all Gibco). Cells were further processed for FACS staining.

## ADOPTIVE TRANSPLANT INTO PKC-β KNOCK-OUT MICE

Splenic CLL-like cells from either (1) TCL1tg CD19cre or (2) TCL1 R26-IKK2ca CD19cre donor mice were enriched by depleting for lineage positive cells and intra-peritoneally injected into non-irradiated PKC-beta KO heterozygous and homozygous recipients.

Magnetic assorted cell sorting (MACS): Single cell suspension of splenic CLL-like cells were labelled with biotinylated antibodies against CD3e, F4/80, CD11c, Ter119, IL7Rα, Gr1 and IgD to deplete for T-cells, myeloid cells and IgD+ B-cells (Table 2). Labelled cells were later incubated with anti-biotin magnetic beads (130-090-485, Miltenyi Biotec) and manually separated through a magnetic LS column (130-042-401, Miltenyi Biotec). Cell enrichment purity was assessed by Flow Cytometry, with a minimal threshold of 95%.

**Table 6. Biotinylated antibodies used for MACS negative selection**

| Antigen | Clone | Vendor | Catalogue Nr. |
|---|---|---|---|
| CD3e | eBio500A2 | eBioscience | 13-0033-81 |
| F4/80 | CI:A3-1 | AbD serotec | MCA497B |
| CD11c | N418 | eBioscience | 13-0114-81 |
| Ter119 | Ter119 | eBioscience | 13-5921-81 |
| IL7Rα (□□□□□) | A7R34 | eBioscience | 13-1271-82 |
| Gr1 (Ly-6G) | RB6-8C5 | eBioscience | 13-5931-81 |
| IgD | 11-26 | eBioscience | 13-5993-81 |

Enriched $CD5^+$ B1a-like cells were washed and resuspended to a density of 20 million cells in 200ul in PBS (Gibco). Each paired aged matched recipient, PKC-β heterozygous and homozygous, was injected intra-peritoneally with 20 million donor cells. Recipient mice weight was monitored after transplant, and peripheral blood was collected weekly to monitor for disease development and progression.

Mice were followed up for a period of 6 months after transplant. If after the 6 months no CLL-like symptoms had been observed, animals were analysed.

## ORGAN PROCESSING

Cells from the peritoneal cavity were extracted by lavage with 5ml cell buffer solution. Liver and spleen masses were weight before processing. Total mesenteric lymph nodes were harvested, as well as all visible Payer's Patches structures. Draining lymph nodes (inguinal, axillary brachial and superficial cervical) were collected and pooled as indicated. A single cell suspension was obtained from spleen, lymph nodes and payer's patches by crushing organs with glass slides and resuspending cells in cell buffer. Bone marrow was collected from one tibia and femur. Cells were obtained by crushing bones in a mortar.

Erythrocytes were removed from spleen and bone marrow samples using the Gey's solution for red blood cell lysis. Single cell suspensions were filtered and viable total cell numbers were calculated using a Neubauer counting chamber with Trypan Blue (Gibco) exclusion dye.

## FLOW CYTOMETRY

Two to 3 million cells were stained for flow cytometry. Cells were pre-stained with the anti-mouse CD16/CD32 (clone 93, eBioscience, 14-0161-81), to block Fc receptor binding and prevent any unspecific binding. Cells were then stained with different fluorescently labelled antibodies to identify defined immune populations. Surface extracellular labelling was done using FACS buffer (0.5% Azide, 2μM EDTA, 2% FBS in PBS). Cell viability was assessed using the non-fixable dye eBioscience™ 7-AAD Viability Staining Solution (Thermo Fisher Scientific, 00-5523-00) or the LIVE/DEAD™ Fixable Near-IR Dead Cell Staining Kit (Thermo Fisher Scientific, L10119) for 633/635nm excitation. For intracellular labelling with antibodies, cells were previously fixated in 2% paraformaldehyde (PFA) solution followed by a methanol permeabilization, or alternatively using the eBioscience™ Foxp3/Transcription Factor Staining Buffer Set (eBioscience, 00-5523-00). Tables 3 and 4 shows a list of all fluorescently couples antibodies used.

Single staining for compensation were done using splenocytes, eGFP expressing splenocytes or with UltraComp eBeads™ Compensation Beads (Thermo Fisher Scientific, 01-2222-42).

Flow cytometry measurements were done in a BD FACS Canto™ II System (BD Bioscience, Cat. No. 338962) or BD FACS Canto™ (BD Bioscience, Cat. No. 657338). Flow cytometry sorting was performed in a BD FACS Aria™ II Flow Cytometer and BD FACS Aria™ III Flow Cytometer (BD Bioscience, 643180). Flow cell analysis was done using the software FlowJo version 9 and FlowJo version X (Tree Star Inc.).

## APOPTOSIS ASSAY – CASPASE 3 ACTIVATION

Cell death by apoptosis was assessed via flow cytometry by staining for pan-Caspases. Cells were stained using the CaspGLOW™ Red Active Caspase Staining Kit (BioVision, K190-25) following the manufacturers instructions. Briefly, cells were incubated with the pan-Caspase inhibitor Red-DEDV-FMK that binds irreversibly to active Caspases.

## PRIMARY MOUSE CELL CULTURE

Sorted or MACS purified B-cells were cultured in RPMI 1640 medium supplemented with 10% heat inactivated FBS, non-essential amino acids, HEPES, sodium-pyruvate, β-mercaptoethanol, penicillin/streptomycin and L-glutamine (all Gibco).

*In vitro* proliferation assay

Sorted B1a-like cells ($CD19^+$ $B220^{lo}$ $CD5^+$ and $eGFP^+$ for the samples expressing the IKK2ca knock-in) or B2-like cells ($CD19^+$ $B220^{hi}$ and $eGFP^+$ for the samples expressing the IKK2ca knock-in) were pre-labelled with the eBioscience™ Cell Proliferation Dye eFluor™ 450 (Thermo Fisher Scientific, Cat. No. 65-0842-85) following manufacturers instructions. *Ex vivo* cell proliferation was evaluated under resting conditions or in the presence of different concentrations of anti-IgM (Jackson ImmunoRe- search Laboratories) or the soluble B-cell activating factor (BAFF).

Cell viability was assed by flow cytometry using Annexin-V (BD Bioscience) and 7AAD to identify viable (Annexin-$V^-$ $7AAD^-$), apoptotic (early apoptotic Annexin-$V^+$ $7AAD^-$ and late apoptotic Annexin-$V^+$ $7AAD^+$) and dead cells (Annexin-$V^-$ $7AAD^+$). Additionally, 123count eBeads counting beads (Thermo Fisher Scientific, Cat. No. 01-1234-42) were used calculate the total cell numbers using flow cytometry, following the manufacturer instructions. Cell proliferation was assessed using the FlowJo Proliferation analysis Package (Tree Star Inc.).

**Table 7. Fluorescently coupled antibodies used for flow cytometry**

| Antigen | Clone | Manufacturer |
|---|---|---|
| AA4.1 | AA4.1 | eBioscience™ |
| B220 | RA3-6B2 | BioLegends |
| CD138 | 281-2 | BD Bioscience |
| CD19 | MB19-1 | eBioscience™ |
| CD1d | 1B1 | eBioscience™ |
| CD21/CD35 | eBio8D9 | eBioscience™ |
| CD23 | B3B4 | eBioscience™ |
| CD25 | PC61.5 | eBioscience™ |
| CD38 | 90 | BioLegend |
| CD4 | RM4-5 | BioLegend |
| CD44 | IM7 | eBioscience™ |
| CD5 | 53-7.3 | eBioscience™ |
| CD62L | MEL-14 | eBioscience™ |
| CD62L | MEL-14 | BioLegend |
| CD69 | H1-2F3 | eBioscience™ |
| CD8-alpha | 53-6.7 | eBioscience™ |
| CD80 | 16-10A1 | eBioscience™ |
| CD86 | GL1 | eBioscience™ |
| CD95 | Jo2 | BD Bioscience |
| cKIT | 2B8 | eBioscience™ |
| CXCR5 | 2G8 | BD Bioscience |
| CXCR5 | 2B11/CXCR4 | BD Bioscience |
| F4/80 | CI:A3-1 | AbD serotec |
| GL7 | GL7 | eBioscience™ |
| Gr-1 | RB6-8C5 | eBioscience™ |
| Icos | 7E.17G9 | eBioscience™ |
| Ig-kappa | 187.1 | BD Bioscience |
| Ig-lambda | R26-46 | BD Bioscience |
| Ig-lambda5 | LM34 | BD Bioscience |
| IgA | 11-44-2 | eBioscience™ |
| IgD | 11-26c/11-26 | eBioscience™ |
| IgG1 | X56 | eBioscience™ |
| IgG1 | 10.9 | BD Bioscience |
| IgG2a | m2a-15F8 | eBioscience™ |
| IgM | II/41 | eBioscience™ |
| Integrin alpha-4 (CD49d) | 9C10 | BD Bioscience |
| Integrin alpha-5 (CD49e) | 5H10-27 | PharMingen |
| Integrin alpha-L (CD11a) | M17/4 | eBioscience |
| Integrin alpha-M (CD11b) | M1/70 | eBioscience™ |
| Integrin alpha-X (CD11c) | N418 | eBioscience™ |
| Integrin beta-1 (CD29) | HMbeta1-1 | BioLegend |
| Integrin beta-2 (CD18) | C71/16 | BD Bioscience |
| Integrin beta-3 (CD61) | 2C9.G3 | eBioscience |
| Integrin beta-7 | FIB504 | eBioscience™ |

**Table 7 (continued). Fluorescently coupled antibodies used for flow cytometry**

| Antigen | Clone | Vendor |
|---|---|---|
| MHC-II | M5/114.15.2 | eBioscience™ |
| PD-1 | J43 | eBioscience™ |
| Siglec-F | E50-2440 | BD Bioscience |
| TCR-beta | H57-597 | eBioscience™ |

**Table 8. Fluorescently couples antibodies used for intracellular flow cytometry**

| Antigen | Clone | Vendor |
|---|---|---|
| BCL6 | K112-91 | BD Bioscience |
| Blimp1 | 5E7 | BD Bioscience |
| IRF4 | 3E4 | eBioscience™ |
| human TCL1 | eBio1-21 | eBioscience™ |
| human TCL1 | 27D6/20 | MBL |
| Zap70 | 1E7.2 | eBioscience™ |

## IMMUNOGLOBULIN HEAVY-CHAIN JOINING-GENE SEGMENT USAGE

As an initial step to determine the clonality of the $CD5^+$ B1a-like cells, the usage of the BCR JH-gene segment was assessed. A PCR was designed to amplify the recombined variable (VH)-, diversity (DH)- and JH-gene segments (VDJ) of the IgH.

A degenerate forward primer binds up-stream of the VH-gene segments and reverse primer binds at the 3´ end of the JH4-gene segment (See Table 5 for BCR amplification primer sequences). The different amplified PCR VDJ IgH rearrangements can be visualized by separating them by size by agarose electrophoresis: rearrangements into JH1 will produce amplicon of 1.6 Kb size, while rearrangements into JH2, JH3 and JH4 will have a size of 1.3 Kb, 1 Kb and 500 bp, respectively (Figure S 31, lane 5).

The PCR reaction was done using Phusion Taq (2U/µL, Thermo Scientific F-530S, Germany), the 5X Phusion GC Buffer, 3% DMSO, 0.2mM dNTPs (Takara, US), 1.5mM $MgCl_2$, 0.16µM of each primer, Ampuwa water and 150ng of genomic DNA. Thermal cycling conditions were:

| | | |
|---|---|---|
| Initial denaturation | 98° C x 10 min | |
| Denaturation | 98° C x 10 s | |
| Annealing | ***69° C x 20 s*** | X 35 cycles |
| Extension | 72° C x 60 s | |
| Final extension | 72° C x 10min | |

All PCRs were performed in a thermal cycler Biometra TProfessional Trio (Analytik Jena, Germany).

## IMMUNOGLOBULIN HEAVY-CHAIN VDJ CLONING

To further assess $CD5^+$ B1a-like tumours clonality, the IgH VDJ rearrangements were amplified, subsequently cloned into destination vectors, and finally sequenced using Sanger sequencing.

The IgH VDJ rearrangement was amplified using a forward primer that binds up-stream the most commonly used VH-gene segments. Rearrangements into JH1 and JH4-gene segments were amplified using a the reverse primer $J_H1/4$ Arnaout, while rearrangements into JH2 and JH3-gene segments were amplified using primers $J_H2/3$ Arnaout and $J_H2$ Arnaout (modified from [246]) (Figure S 32A) [247].

**Table 9. Primers used for amplifying the B-cell receptor**

| Primer name | Sequence (5´-3' orientation) | Amplicon size |
|---|---|---|
| MsVhE AH | TCGAGTTTTTCAGCAAGATGAGGTGCAGCTGCAGGAGTCTGG | |
| $J_H1/4$ Arnaout | CTTACCTGAGGAGACGGTGAC | 350bp |
| $J_H2/3$ Arnaout | AGGACTCACCTGAGGAGAC | 350bp |
| $J_H2$ Arnaout | AGGACTCACCTGCAGAGAC | 350bp |
| JH4rev | CTGAGGAGACGGTGACTGAGG | JH1 1.6kb<br>JH2 1.3kb<br>JH3 1.0kb<br>JH4 0.5kb |

For each PCR reaction, 100ng of genomic DNA were amplified using 1 U of Phusion® High-Fidelity DNA Polymerase (2U/μL, Thermo Scientific F-530S) with the 5X Phusion HF Buffer (Thermo Scientific), 1.5mM $MgCl_2$, 0.2mM dNTPs (Takara), 0.16μM of each primer in PCR-grade water (Ampuwa). Thermal cycling conditions were as follows:

| | | |
|---|---|---|
| Initial denaturation | 98° C x 10 min | |
| Denaturation | 98° C x 10 s | |
| Annealing | ***69° C x 20 s*** | X 35 cycles |
| Extension | 72° C x 60 s | |
| Final extension | 72° C x 10min | |

A small sample of the PCR product was run in an agarose gel to qualitatively determine the success of the reaction. The rest of the sample was column purified using the

QIAquick PCR purification kit (Qiagen, 28106) to remove for any primer dimers or excess dNTPs following manufacturers instructions. Samples were eluted in Qiagen elution buffer. Purified PCR samples were later quantified using the Quibit dsDNA High Sensibility (HS) kit (Thermo Fisher Scientific).

## QUICK AND CLEAN CLONING (QC CLONING) OF THE B-CELL RECEPTOR

Quick and clean cloning (QC cloning) was used to clone the amplified VDJ rearrangements into JH1, JH2, JH3 or JH4 catch sequence (CS) specific destination vectors [248].

All vectors had similar structure: A CS for the specific JH-gene segments. The lacZ-α gene flanked by binding sites for the type-II restriction enzyme BsmBI, used for blue/white screening. The cDNA of the eco47IR enzyme divided in two parts: the 5`sequence (part 1) and the 3`sequence (part 2) divided by the insert targeting site and Lac-Zα screening marker. In the absence of this insert, the cDNA of the enzyme would be reconstituted and function as a suicide gene. The ampicillin resistance gene that allows for positive selection of transfected bacteria (Vector maps and sequences can be found in the Supplementary material).

Destination vectors (see Supplemental methods) were digested with the type-II restriction enzyme BsmBI (New England BioLabs Inc., R0580S) to remove the lacZ-α sequence. Fragments were separated by agarose electrophoresis. The linearized backbone was purified using the QIAquick Gel Extraction Kit (Qiagen, 28706), and later quantified using the Quibit dsDNA High Sensibility (HS) kit (Thermo Fisher Scientific).

For the QC cloning, 15ng of the linearized backbone and 25ng of the corresponding purified amplicon were mixed in a 0.2mL PCR tube in a final volume of 20µL. The DNA Polymerase I Large (Klenow) Fragment (New England BioLabs Inc., M0210S) was used as the 3' to 5' exonuclease in combination with the NEB2 buffer. The mix was incubated 2 hours at 37° C in a Biometra Tprofessional Trio (Analytik Jena, Germany) thermal cycler.

Five µl of the reaction were transformed into 100µl of commercial chemically competent NEB® 10-beta Competent E. coli (High Efficiency), DH10β (New England BioLabs Inc., C3019I). Either 10% and 90% or 100% of the transformation was plated

on LB agar plates with ampicillin and X-gal (all Sigma-Aldrich) agar plates and incubated over night at 37° C and blue/white colonies were counted. An average of 10 colonies per JH-gene segment were picked, grown overnight in 2ml 96-well plate with LB media with ampicillin and sent for processing and Sanger sequencing (BigDye 3.1 chemistry, Applied Biosystems) to Eurofins MWG Operon in Martinsried, Munich.

Sequencing results were analysed with SeqMan Pro (DNASTAR V15.0). Backbone sequences were trimmed, sequences were aligned using the Pro Assembler (Match size 250bp, minimum match percentage 99) and contigs with identical sequences were annotated. The VDJ insert sequence was later analysed with IMGT/HighV-QUEST (Immuno Genetics) [249]. CDR3 sequences of productive rearrangements were compared between the different clones from the same sample. VH-gene segments were also compared to germ-line. If the sequence differed > 5% from the germ-line, the samples were considered to have undergone somatic hypermutation.

## III.1 STATISTICAL ANALYSIS

Total cell numbers and other calculations were performed using Excel (Microsoft Office 2011). Flow cytometry contour plots were generated using FlowJo version 9 or version 10 (Tree Start Inc.). Bar charts and heatmaps were generated with GraphPad Prism version 7 (GraphPad Software). Statistical analysis was calculated using GraphPad Prism. Normal distribution of the samples was assessed using the D'Angostino and Pearson normality test. Statistical analysis for normally distributed populations was calculated using T-test or One-way ANOVA (Holm-Sidak's multiple comparisons test), while the Kurskal-Wallis non-parametric test (Dunn's multiple comparison test) was calculated for samples without a normal distribution. Significance lower than $p<0.05$ was is indicated in figures and legends.

Illustrations and figures where prepared using Adobe Illustrator (Adobe Systems).

# IV RESULTS

## IV.1 LOSS OF A20 IN COMBINATION WITH ENHANCED EXPRESSION OF THE ALTERNATIVE NF-κB REGULATOR NIK IN B-CELL BIOLOGY

Initially, I wanted to combine two different genetic alterations, loss of A20/Tnfaip3 and activation of alternative NF-κB pathway, to model aspects of splenic marginal zone (sMZL) lymphoma in mice. Genetic abnormalities in both NF-κB related pathways have been observed in sMZL patient samples [183]. Moreover, loss of A20 and deregulation of the alternative NF-κB pathway have been proposed as candidates in sMZL. By combining them in an *in vivo* model, I wanted to address the question of whether mutations in A20 and the TRAF3/NIK arm can cooperate in sMZL development.

I made use of the available conditional mouse strain lines $A20^{FL}$, R26-$Stop^{FL}$Nik and CD19cre to generate mice with B-cells that mimic the genetic alterations that have been identified in sMZL patients. Using the $A20^{FL}$ mouse line I could inactivate one ($A20^{F/wt}$) or both alleles of A20 ($A20^{F/F}$) in B-cells *in vivo* [240]. Activation of the alternative NF-κB pathway, by loss of BIRC3 and TRAF3 or gain of MAP3K14, could be mimicked with the gain of one allele of a conditional NIK transgene (NIK-tg) knocked into the ROSA26 locus [89]. For that purpose, I used the R26-$Stop^{FL}$Nik mouse strain that expresses NIK after Cre-mediated excision of a loxP-flanked STOP cassette, always heterozygously (NIK-tg: R26-$Stop^{FL}Nik^{I/wt}$). B-cells that express the NIK-tg after Cre-mediated recombination also express the enhanced green fluorescent protein (eGFP) as a reporter, located after an internal ribosomal entry site (IRES) sequence 3' from the NIK cDNA, thus allowing the tracking of the recombined cells. To conditionally inactivate or activate my genes of interest, I used the CD19cre mouse strain [241]. The Cre recombinase is expressed as knock-in under control of the endogenous CD19 promoter instead of endogenous CD19, thus $CD19cre^{I/wt}$ mice are heterozygous for CD19cre. In the CD19cre mice, the Cre recombinase expression starts as early as the pro-B cell stage and recombination can be observed from the pre-B cell stage onwards.

### IV.1.1 HOMOZYGOUS LOSS OF A20 IN COMBINATION WITH ALTERNATIVE NF-κB ACTIVATION LEADS TO MASSIVE REDUCTION OF B-CELLS IN SPLEENS OF YOUNG MICE

The constitutive expression in B-cells of an additional allele of NIK (NIK-tg$^{l/wt}$ CD19cre$^{l/wt}$, from now on referred to as NIK-tg CD19cre) leads to slightly bigger spleens and a tendency for increased B-cell numbers (Figure 4A and B) [89]. The additional loss of one allele of A20 (A20$^{F/wt}$ NIK-tg$^{l/wt}$ CD19cre$^{l/wt}$, from now on referred to as A20F/wt NIK-tg CD19cre) leads to a higher splenic cellularity, accompanied by a 10% increase in B-cell percentage and increase in total cell numbers (Figure 4A and B). However, loss of the second allele of A20 (A20$^{F/F}$ NIK-tg$^{l/wt}$ CD19cre$^{l/wt}$, from now on referred to as A20F/F NIK-tg CD19cre) surprisingly results in a significant reduction of B-cell percentage and B-cell numbers (Figure 4B), although spleen mass and cellularity are increased compared to wild type and NIK-tg CD19cre controls (Figure 4A).

Interestingly, the percentage and cell numbers of *ex vivo* isolated B-cells expressing the eGFP transgene reporter are also significantly reduced in the A20-/-;NIK+ B-cells compared to the NIK+ alone or A20+/-;NIK+ *ex vivo* B-cells (Figure 4C). Moreover, the number of *ex vivo* eGFP negative B-cells in the A20F/F NIK-tg CD19cre mice is higher than that observed in the NIK-tg CD19cre or A20F/wt NIK-tg CD19cre age matched controls (Figure 4C) suggesting a negative selection of the eGFP+;A20-/-;NIK+ cells.

Given the strong *ex vivo* phenotype observed on B-cells when the absence of A20 is combined with activation of the alternative NF-κB pathway, I decided to focus my attention on the diminished *ex vivo* B-cell numbers observed.

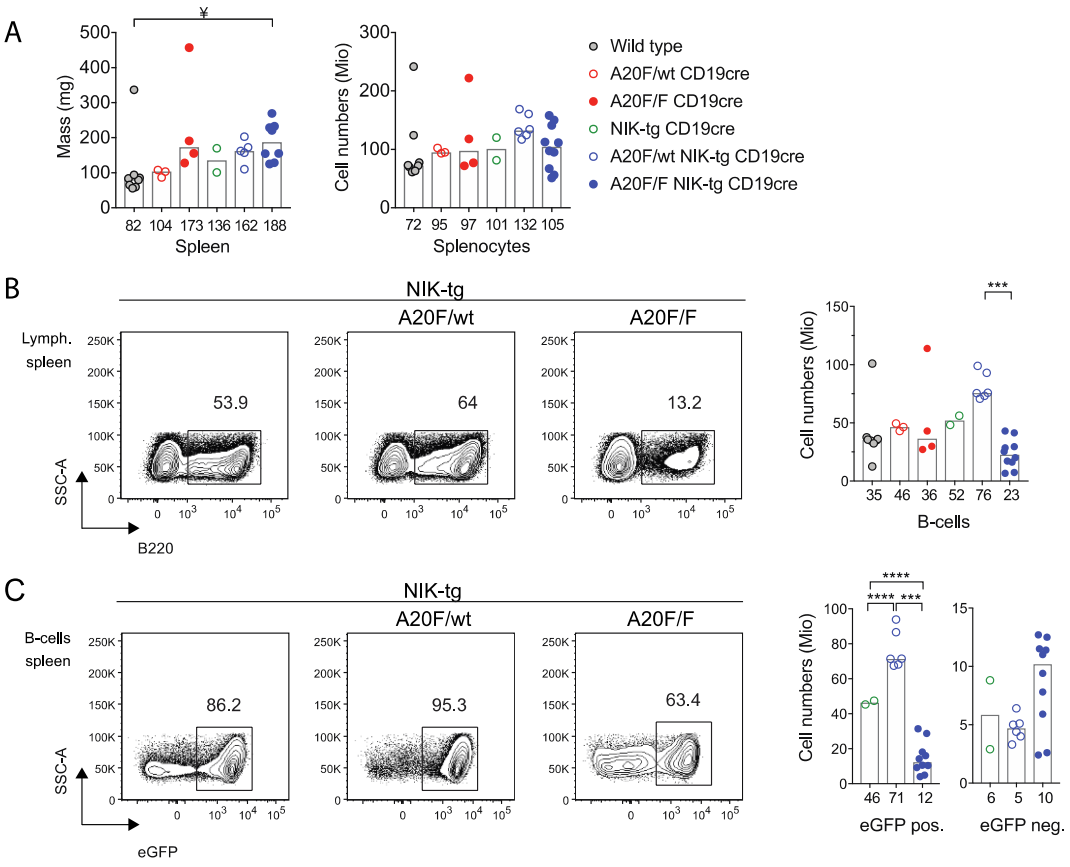


**Figure 4. Reduced A20-/-;NIK+ B-cell numbers in spleen of young mice**

*Ex vivo* analysis of B-cells from spleens of young mice using flow cytometry. (A) Spleen mass in milligrams and splenocytes cell numbers. Contour plots depict percentages and bar charts indicate cell numbers for (B) B-cells and (C) eGFP reporter expressing B-cells. All flow cytometry plots are representative of at least 2 experiments. Bar charts depict medians and the values are indicated below each histogram. Statistical analysis was done using One-way ANOVA (*** $p<0.001$, **** $p<0.0001$) or Kruskal-Wallis (¥ $p<0.05$).
eGFP (enhanced green fluorescent protein), pos. (positive), neg. (negative), B-cells ($B220^+$), eGFP pos. ($B220^+$ $eGFP^+$), eGFP neg. ($B220^+$ $eGFP^-$).

### IV.1.2 HOMOZYGOUS LOSS OF A20 IN COMBINATION WITH ALTERNATIVE NF-κB ACTIVATION LEADS TO SYSTEMIC DEPLETION OF B-CELLS IN SECONDARY LYMPHOID ORGANS OF YOUNG MICE

Since the spleens of young A20F/F NIK-tg CD19cre mice present a significant loss of B-cells, I proceeded to analyse other secondary lymphoid organs to determine whether the observed loss of B-cells was a general phenomenon in these mice.

The lymph nodes (LN) cellularity, normalized to 1 LN, presented a tendency for higher numbers in the A20F/F NIK-tg CD19cre animals, compared to the other genotypes analysed (Figure 5A). The loss of one allele of A20 in a NIK-tg CD19cre background led to an increase in B-cell percentages, but the cell numbers remained constant. However, the percentages and total cell number of B-cells when the second allele of A20 was lost were significantly reduced (Figure 5B). The percentage and number of *ex vivo* eGFP expressing B-cells were also significantly reduced in the A20F/F NIK-tg CD19cre mice.

Similarly, the *ex vivo* analysis of the mesenteric lymph nodes (mLN) revealed a massive reduction in B-cell percentages and numbers in A20F/F NIK-tg CD19cre mice (Figure S 1B). The loss of the second allele of A20 lead to almost absent B-cells in the mLN, decreasing from 12.3 million A20+/-;NIK+ B-cells to less than 1 million B-cells in the A20F/F NIK-tg CD19cre mice (Figure S 1B). The eGFP expressing cells were almost completely absent in the A20F/F NIK-tg CD19cre mice (Figure S 1C).

Likewise, the *ex vivo* analysis of B-cells in the Peyer's patches (PP) also revealed a drastic reduction in B-cell percentages and cell numbers in the A20F/F NIK-tg CD19cre compared to the other mice analysed (Figure S 2B). Of the few B-cells observed in these mice, only 20-30% expressed the eGFP reporter (Figure S 2C). Moreover, the total number of cells in the PP of the A20F/F NIK-tg CD19cre mice was significantly lower than the observed for A20F/wt NIK-tg CD19cre mice (Figure S 2A).

Finally, the *ex vivo* analysis after the lavage of the peritoneal cavity of the A20F/F NIK-tg CD19cre mice also revealed a significant reduction in B-cell percentages and total cell numbers compared to A20F/wt NIK-tg CD19cre and the wild type controls (Figure 6B). It is remarkable that the increase in B-cell numbers, and cellularity of the lavage, observed from the NIK-tg CD19cre to the A20F/wt NIK-tg CD19cre is lost when the second allele of A20 is ablated (Figure 6A and B). Moreover, the percentage and thereof

number of *ex vivo* B-cells expressing the eGFP reporter in the peritoneal cavity of the A20F/F NIK-tg CD19cre mice is extremely low, 10%, compared to other organs (Figure 6C).

Interestingly, the negative effect observed in *ex vivo* A20-/-;NIK+ B-cells in the peritoneal cavity affects all different B-cell subsets but to different extents. The *ex vivo* analysis of the NIK-tg CD19cre mice showed that 50% of the B-cells belong to the B2 subset, and the other 50% to the B1 subset, but it only reflects in a one-fold increase in cell numbers compared to wild type control ( Figure 7A). The additional loss of one allele of A20, favoured the B1 subset and in particular the B1b subset ( Figure 7A and B).

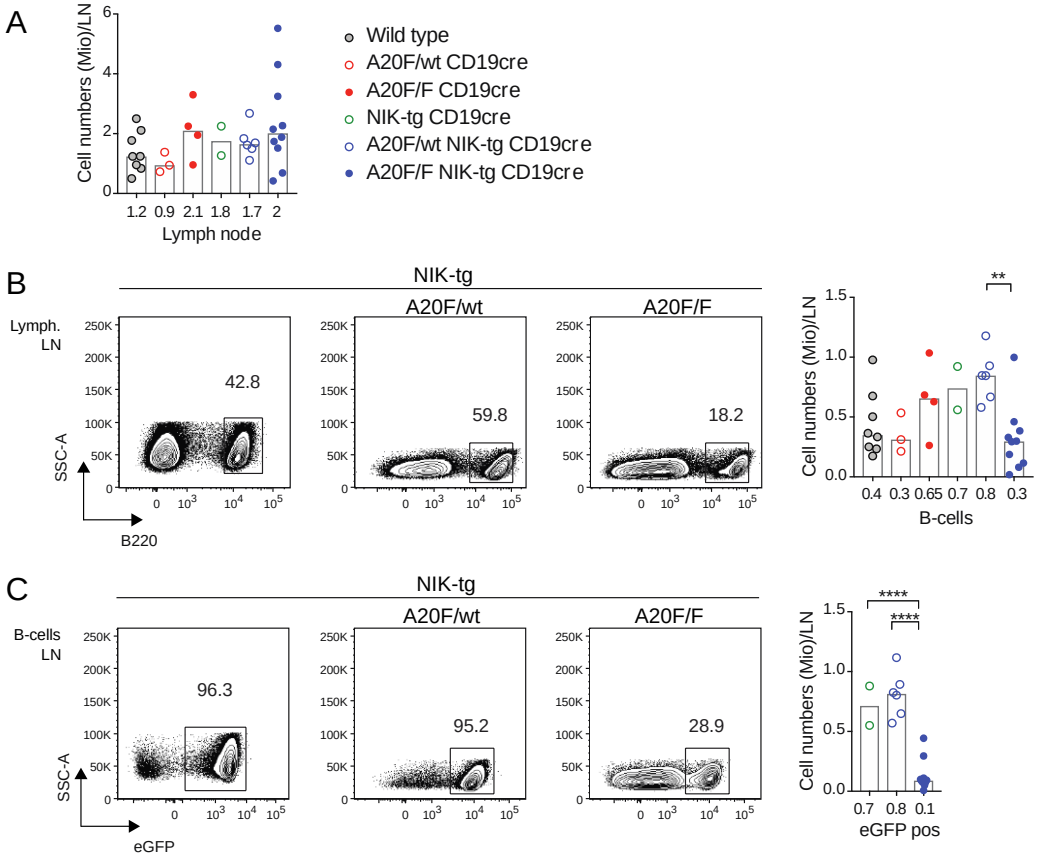


**Figure 5. Reduced A20-/-;NIK+ B-cell numbers in lymph nodes of young mice**

*Ex vivo* analysis of B-cells from lymph nodes of young mice using flow cytometry, normalized to one lymph node. (A) Cell numbers for one lymph node. Contour plots depict percentages and bar charts indicate cell numbers for (B) B-cell and (C) eGFP positive B-cell. All flow cytometry plots are representative of at least 2 experiments. The NIK-tg CD19cre contour plots do not belong to the same experiment as A20-deficient NIK-tg CD19cre plots. Bar charts depict medians and the values are indicated below each histogram. Statistical analysis was done using One-way ANOVA (** $p<0.01$, **** $p<0.0001$).
LN (lymph node), eGFP (enhanced green fluorescent protein), pos (positive), B-cells ($B220^+$) and eGFP pos ($B220^+$ $eGFP^+$).

The loss of the second allele of A20 in B-cells in the peritoneal cavity affects drastically the B1 subset, and specially the B1b subset ( Figure 7B). Although the B2 subset is also massively reduced in A20F/F NIK-tg CD19cre mice, it corresponds to the majority of B-cells found in this compartment. However, the near absence of B1-cells in the A20F/F NIK-tg CD19cre mice is interesting, since they are self-replenishing population and have a different developmental origin than the B2-cells [250]. This phenomenon could point to a negative cooperation between A20 and activation of NIK in alternative NF-κB pathway in B1-cells proliferation and or survival.

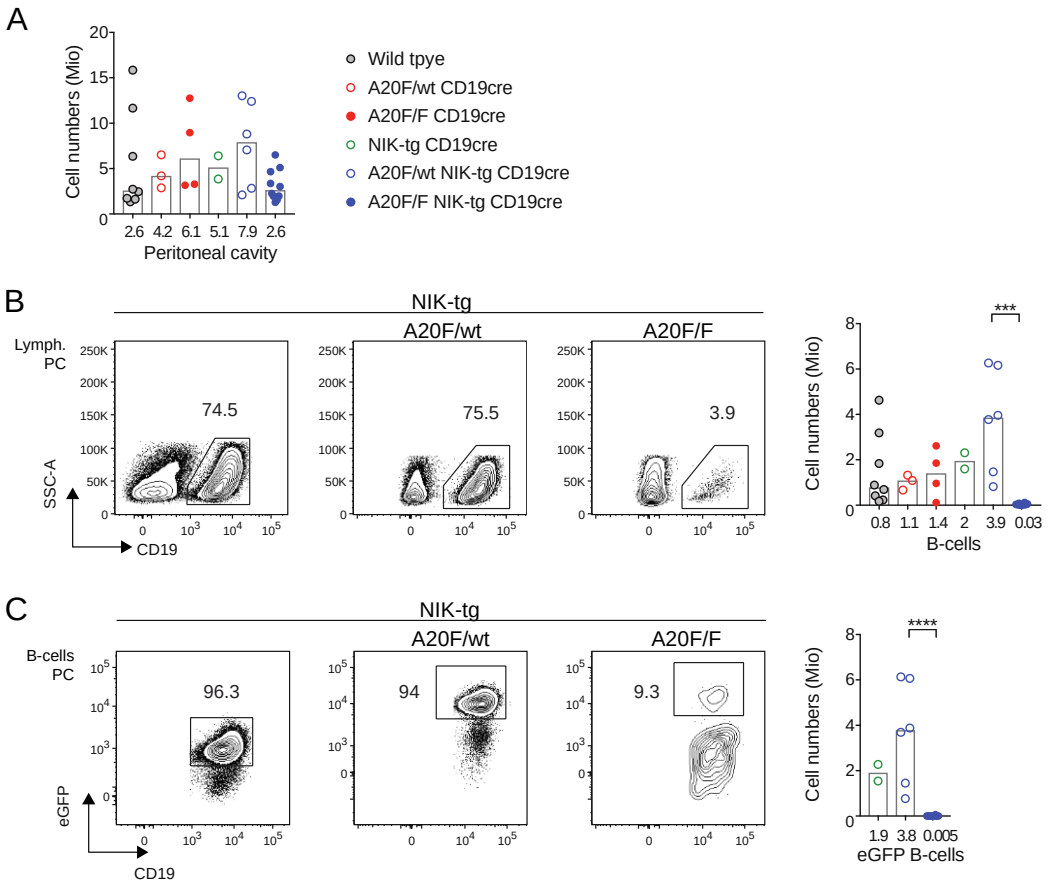


**Figure 6. Reduced A20-/-;NIK+ B-cell numbers in peritoneal cavity of young mice**

*Ex vivo* analysis of B-cells in peritoneal cavity of young mice using flow cytometry, after lavage. (A) Peritoneal cavity cell numbers. Contour plots depict percentages and bar charts indicate total cell numbers for (B) B-cells and (C) eGFP positive B-cells. The NIK-tg CD19cre contour plots do not belong to the same experiment as A20-deficient NIK-tg CD19cre plots. Bar charts depict medians and the values are indicated below each histogram. Statistical analysis was done using One-way ANOVA (*** p<0.001, **** p<0.0001) and statistical significance when P<0.5 is indicated.
PC (peritoneal cavity), eGFP (enhanced green fluorescent protein), B-cells ($CD19^+$) and eGFP B-cells ($CD19^+$ $eGFP^+$).

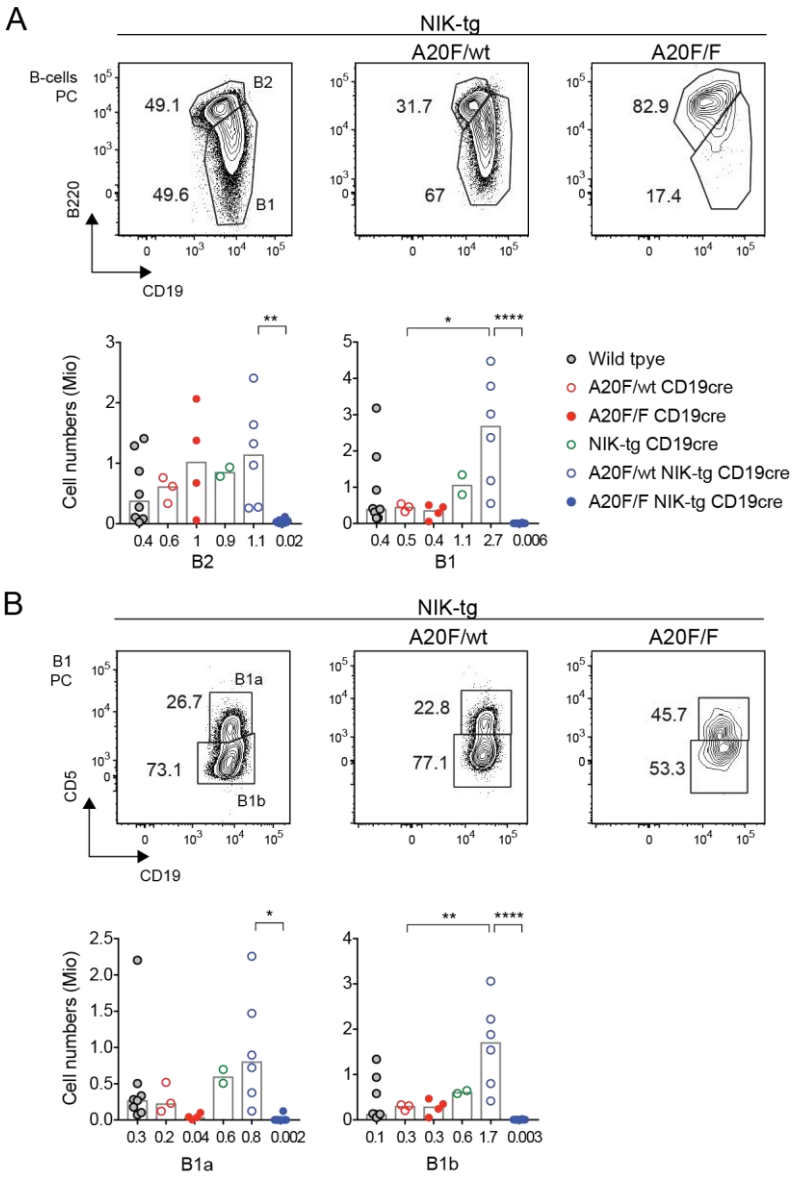


**Figure 7. Reduced A20-/-;NIK+ B1 population in peritoneal cavity of young mice**

*Ex vivo* analysis of B-cells subsets in peritoneal cavity of young mice using flow cytometry. Contour plots depict the percentages and bar charts indicate total cell numbers for (A) B2 and B1 B-cell subsets, and (B) B1a and B1b B1 subsets. All flow cytometry contour plots are representative of at least 2 experiments. The NIK-tg CD19cre contour plots do not belong to the same experiment as A20-deficient NIK-tg CD19cre plots. Bar charts depict medians and the values are indicated below each histogram. Statistical analysis was done using One-way ANOVA (* $p<0.05$, ** $p<0.01$, **** $p<0.0001$).

PC (peritoneal cavity), B-cells ($CD19^+$), B2 ($CD19^+$ $B220^{hi}$), B1 ($CD19^+$ $B220^{lo}$), B1a ($CD19^+$ $B220^{lo}$ $CD5^+$) and B1b ($CD19^+$ $B220^{lo}$ $CD5^-$),.

The percentage of *ex vivo* B-cells observed in lymph nodes (Figure 5), mesenteric lymph nodes (Figure S 1), Peyer's patches (Figure S 2) and peritoneal cavity (Figure 6 and Figure 7) for the A20F/F NIK-tg CD19cre mice was significantly lower compared that of A20F/wt NIK-tg and NIK-tg alone. Furthermore, the low percentages of *ex vivo* eGFP+;A20-/-;NIK+ B-cells observed suggests a systemic negative effect of combining loss of A20 with gain of NIK in B-cells.

To determine whether the detrimental effect of strong NF-κB activation by the loss of the second allele of A20 in cooperation with an extra copy of NIK-tg in B-cells was due to a developmental block in B-cell development, as it appears to be for the B1-subset, I first proceeded to characterize the different stages of B-cell development.

## IV.1.3 ROLE OF LOSS OF A20 IN COMBINATION WITH ACTIVATION OF THE ALTERNATIVE NF-κB PATHWAY IN B-CELL DEVELOPMENT

### IV.1.3.1 Homozygous loss of A20 in combination with alternative NF-κB activation leads to a loss of mature B-cells in spleen of young mice

In spleens of young mice, there is an increase in the percentage and numbers of *ex vivo* A20+/-;NIK+ mature B-cells compared to NIK+ only mature B-cells (Figure 8A and B). This B-cell expansion in the A20F/wt NIK-tg CD19cre mice is more pronounced in the MZB population (two-fold increase in MZB-cell numbers compared to the NIK-tg CD19cre mice, Figure 8C and E). Nonetheless, there is also a clear follicular B-cell (FOB) expansion (Figure 8D). The combination of both heterozygous loss of A20 in combination with the activation of the alternative NF-κB pathway by overexpression of NIK-tg cooperate in expanding the MZB pool up to 10 million cells (three-fold compared to wild type), as originally hypothesized (Figure 8C and E).

Loss of the second A20 allele in NIK+ B-cells leads to lower *ex vivo* mature B-cell percentages and a significant reduction in *ex vivo* cell numbers (Figure 8A and B) compared to the A20+/-;NIK+ mature B-cells. Both FOB and MZB populations are strongly affected. Interestingly, almost all A20-/-;NIK+ MZB-cells ($CD21^{hi}$ $CD1d^{hi}$) express the eGFP reporter, were as only 8 out of the 11 million of FOB-cells express the eGFP reporter (Figure 8D and E).

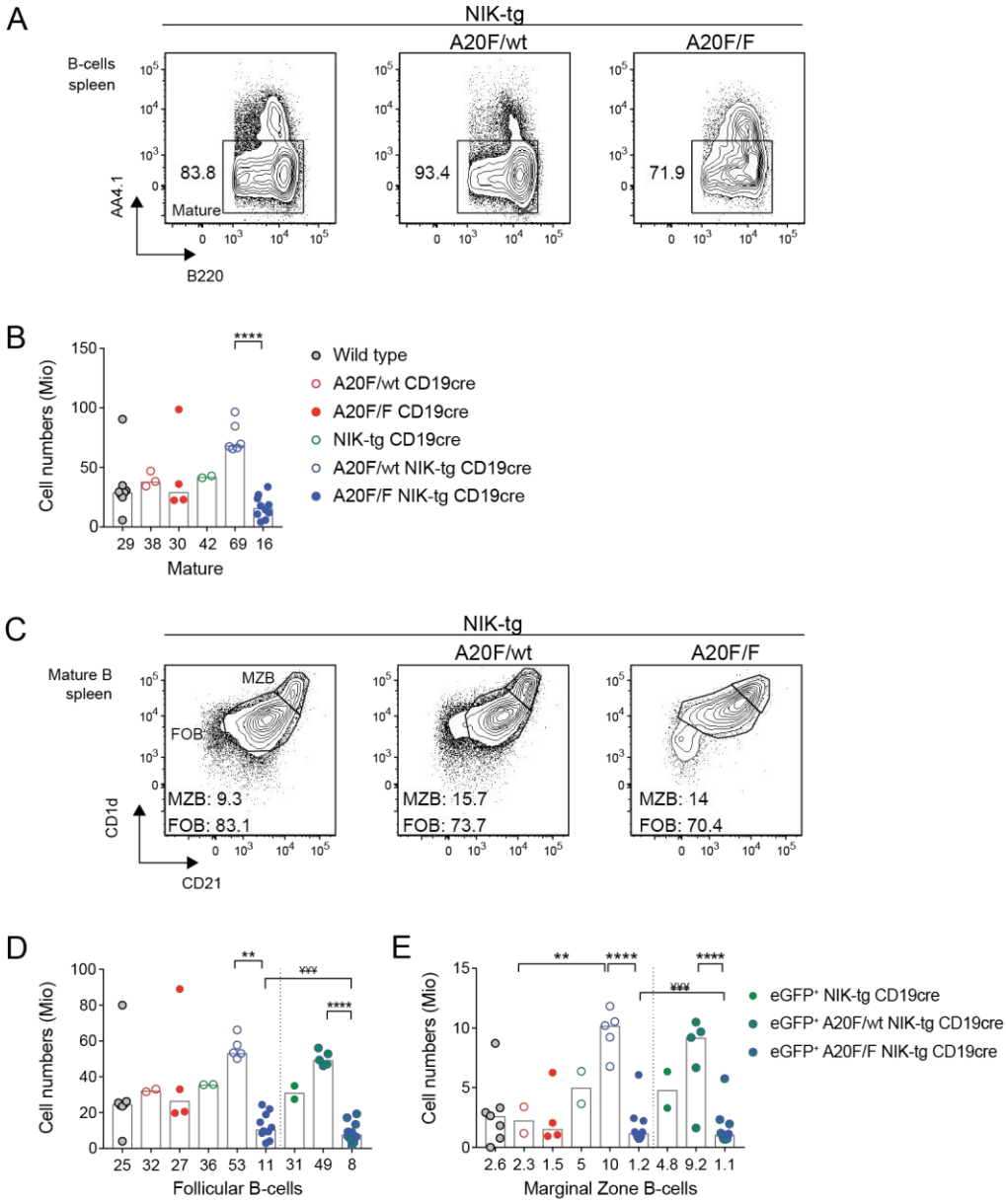


**Figure 8. Reduced mature B-cells in spleens from A20F/F NIK-tg CD19cre mice**

*Ex vivo* analysis of B-cells from spleens of young mice using flow cytometry. Contour plots depict percentages and bar chart indicate total cell numbers for (A, B) immature and mature B-cell, and (C, D, E) follicular B-cells, marginal zone B-cells and eGFP positive cells. All flow cytometry plots are representative of at least 2 experiments. Bar charts depict medians and the values are indicated below each histogram. Statistical analysis was done using One-way ANOVA (** p<0.01, **** p<0.0001) or Two-tailed paired T-test (¥¥¥ p<0.001).
eGFP (enhanced green fluorescent protein), B-cells ($B220^+$), Mature ($B220^+$ $AA4.1^-$), FOB (Follicular B-cell, $B220^+$ $AA4.1^-$ $CD21^{int}$ $CD1d^{int}$), and MZB (Marginal Zone B-cell, $B220^+$ $AA4.1^-$ $CD21^{hi}$ $CD1d^{hi}$).

It is important to keep in mind that the *ex vivo* expression of the markers used to define the mature B-cell population (ie. CD21, CD1d and CD23), especially in A20-/-;NIK+ B-cells, is directly or indirectly modified by NF-κB activation (Figure 8C and Figure S 3A).

*Ex vivo* eGFP+;A20-/-;NIK+ mature B-cells have intermediate expression levels of CD21 accompanied with higher levels of CD1d compared to eGFP+;NIK+ or eGFP+;A20+/-;NIK+ mature B-cells (Figure S 3A). On the other hand, the expression of the surface marker CD23, a known NF-κB target gene, is lower in *ex vivo* eGFP+;A20-deficient;NIK+ mature B-cells than in eGFP+;NIK+ or eGFP+;A20+/-;NIK+ mature B-cells (Figure S 3A).

MZB-cells are characterized for having a higher expression of CD1d and CD21, and lacking the expression of CD23 [251]. The altered expression patter of CD23 and CD1d in *ex vivo* A20-deficient NIK-expressing mature B-cells could be therefore representative of MZ-like phenotype (Figure S 3A). However, using alternative MZB-cell gating strategies the MZB population seems to be absent in A20-deficient NIK-expressing mature B-cells (Figure S 3B), making it difficult to properly define this population.

The loss of the second allele of A20 in combination with the expression of an extra copy of NIK leads to a clear failure to produce or maintain mature B-cells in A20F/F NIK-tg CD19cre mice and it affects both the FOB and the MZB compartment. To further understand if the reduced *ex vivo* B-cell numbers are result of a developmental block I analysed the immature B-cell compartment in the spleen of young mice.

#### IV.1.3.2 Homozygous loss of A20 in combination with alternative NF-κB activation drives a faster transition through the immature B-cell stages in the spleen of young mice

The expression of a NIK transgene specifically in B-cells leads to an increase of mature B-cell numbers that is further enlarged by the additional loss of one allele of A20. However, the further loss of the second allele of A20 leads to a completely different scenario, where B-cells are negatively affected. To identify whether this negative effect is due to a developmental block in B-cells, I further characterized the immature B-cell subsets in the spleen of young mice.

The number of *ex vivo* immature B-cells and eGFP expressing immature B-cells in the different NIK-tg and A20 compound mice are all similar (Figure 9B). However, the loss of A20 affects the transitional 1 (T1) B-cells subset by lowering the percentage and total cell numbers in an A20 dose dependent manner (Figure 9C and D) in a NIK-tg background.

In particularly, there is a significant reduction of the T1 subset of *ex vivo* A20-/-;NIK+ immature B-cells compared to wild type controls, accompanied by a slight increase in the transitional 2 (T2) subset cell numbers (Figure 9D). Moreover, this is accompanied by a significant reduction in eGFP positive T1 B-cells compared to A20F/wt NIK-tg CD19cre mice (Figure 9E). Only 20% of A20-/-;NIK+ T1 B-cells (0.2 million / 1 million cells) actually expresses eGFP where as about 66% of the T2 B-cells (1.8 million / 2.9 million cells) expresses the eGFP reporter (Figure 9E).

Although the expression of surface protein CD23 is also used for defining the different transitional stages of immature B-cells, the *ex vivo* expression levels of CD23 are relatively similar between NIK+ alone, A20+/-;NIK+ or A20-/-;NIK+;eGFP+ immature B-cells (Figure S 4A). Interestingly, when defining immature B-cells by CD23 expression alone, CD23 low transitional 1 ($T1_{CD23}$) and CD23 high transitional 2 ($T2_{CD23}$) [252], there is a increase in the percentage of $T2_{CD23}$ B-cells in an A20-loss dependent manner (Figure S 4B). This translates into significantly lower $T1_{CD23}$ B-cell numbers in the A20F/F NIK-tg CD19cre mice compared to wild type controls, accompanied by significantly lower eGFP positive $T1_{CD23}$ B-cells compared to NIK-tg CD19cre mice (Figure S 4E).

Alternatively, immature B-cells could be defined by the expression of the CD21 protein alone into CD21 low transitional 1 ($T1_{CD21}$) and CD21 high transitional 2 ($T2_{CD21}$) B-cells [252]. Although it has been reported that CD21 is also an NF-κB target gene, the *ex vivo* expression levels of CD21 are also relatively similar between NIK+ alone, A20+/-;NIK+ or A20-/-;NIK+;eGFP+ immature B-cells (Figure S 4A). In this case there is also an increase in the percentage of $T2_{CD21}$ B-cells in an A20-loss dependent manner (Figure S 4C). Moreover, this is accompanied by significantly lower fraction of eGFP positive cells for the A20-/-;NIK+ $T2_{CD21}$ B-cells (Figure S 4C). However, the observed $T1_{CD21}$ and $T2_{CD21}$ B-cell numbers are similar for all the genotypes analysed.

Finally, the combination of both CD21 and CD23 expression to define the transitional immature B-cells leads to similar increased transitional 2 (T2) percentages in an A20-loss dependent manner (Figure S 4D). Although this translates into similar T1 and T2 B-cell numbers for all the genotypes analysed, there is a significant decrease in eGFP positive cell percentages and cell numbers in the T1 population for the A20F/F NIK-tg CD19cre mice compared to the A20F/wt NIK-tg CD19cre mice (Figure S 4D and G).

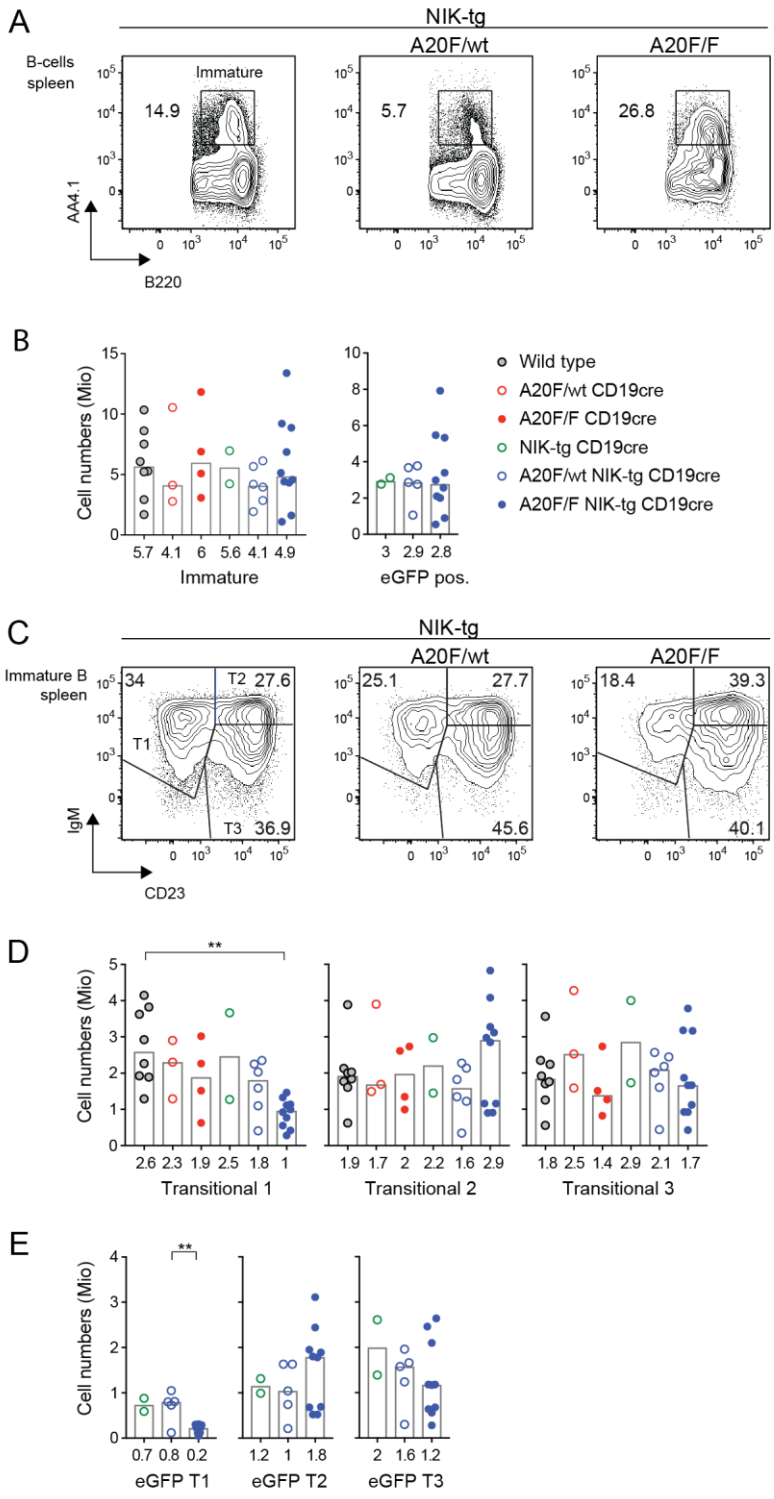


**Figure 9. Reduced Transitional 1 immature B-cells in A20F/F NIK-tg CD19cre mice during B-cell development in the spleen**

*Ex vivo* analysis of immature B-cells from spleen of young mice using flow cytometry. Contour plots depict percentages and bar charts indicate total cell numbers for (A) immature and eGFP positive immature B-cells, (B, C) transitional B-cells and (D) eGFP positive transitional B-cells. All flow cytometry plots are representative of at least 2 experiments. Bar charts depict medians and the values are indicated below each histogram. Statistical analysis was done using One-way ANOVA ($p < 0.05$, ** $p<0.01$).

Figure 9 **(continued)** Immature ($B220^+$ $AA4.1^+$), eGFP (enhanced green fluorescent protein), T1 (Transitional 1, $B220^+$ $AA4.1^+$ $IgM^+$ $CD23^-$), T2 (Transitional 2, $B220^+$ $AA4.1^+$ $IgM^+$ $CD23^+$), T3 (Transitional 3, $B220^+$ $AA4.1^+$ $IgM^{int}$ $CD23^+$) and eGFP pos ($eGFP^+$).

Although the total immature B-cells numbers seem not affected by the combination of NIK overexpression and loss of A20, when A20 is homozygously inactivated the transition from T1 to T2 immature B-cells balance shifts towards the T2 subset. Taking together the classical and all the alternative transitional immature B-cell definitions it is clear that homozygous loss of A20 in combination with overexpression of NIK leads to a significant reduction of eGFP expressing T1 B-cells (Figure 9and Figure S 4).

### IV.1.3.3 Homozygous loss of A20 in combination with alternative NF-κB activation reduces the recirculating/mature B-cell pool in the bone marrow of young mice

To further address if the negative effect of A20 ablation in combination with gain of NIK transcends to the early B-cell development in the bone marrow, I proceeded to analyse the different early B-cell stages in the bone marrow of young animals. Following to the Hardy classification, B-cells development in the bone marrow starts from a CLP that after receiving the proper stimuli and activating the right transcription program commits to the B-cell lineage [50]. B-cell development starts with the pro-B cell, where it undergoes the immunoglobulin heavy locus rearrangement, followed by pre-BCR expression during the pre-B cell stages. The final stage in the bone marrow terminates with the immature B-cell where the BCR is tested for autoreactivity. Some immature B-cell can mature in the bone marrow, but most migrate to peripheral secondary lymphoid organs, such as the spleen, where they mature to MZB- and FOB-cells. B-cells enter the circulation, scan the entire organism for foreign antigens and can migrate back to the bone marrow as mature/recirculating B-cells [51].

The *ex vivo* bone marrow cell numbers for the different genotypes analysed are all similar (Figure 10A). There is a trend for slightly lower percentages and cell numbers of B-cells in the bone marrow from A20F/wt NIK-tg CD19cre to A20F/F NIK-tg CD19cre mice, although not statistically significant (Figure 10B and C). The proportion of *ex vivo* eGFP expressing B-cells in the bone marrow was reduced from 45% in the A20F/wt NIK-tg CD19cre mice to 18% in the A20F/F NIK-tg CD19cre mice (Figure 10D). Accordingly, there was a significant reduction in *ex vivo* eGFP expressing B-cell numbers

although the number of *ex vivo* eGFP negative B-cells remained constant among the NIK-tg compound mice (Figure 10E).

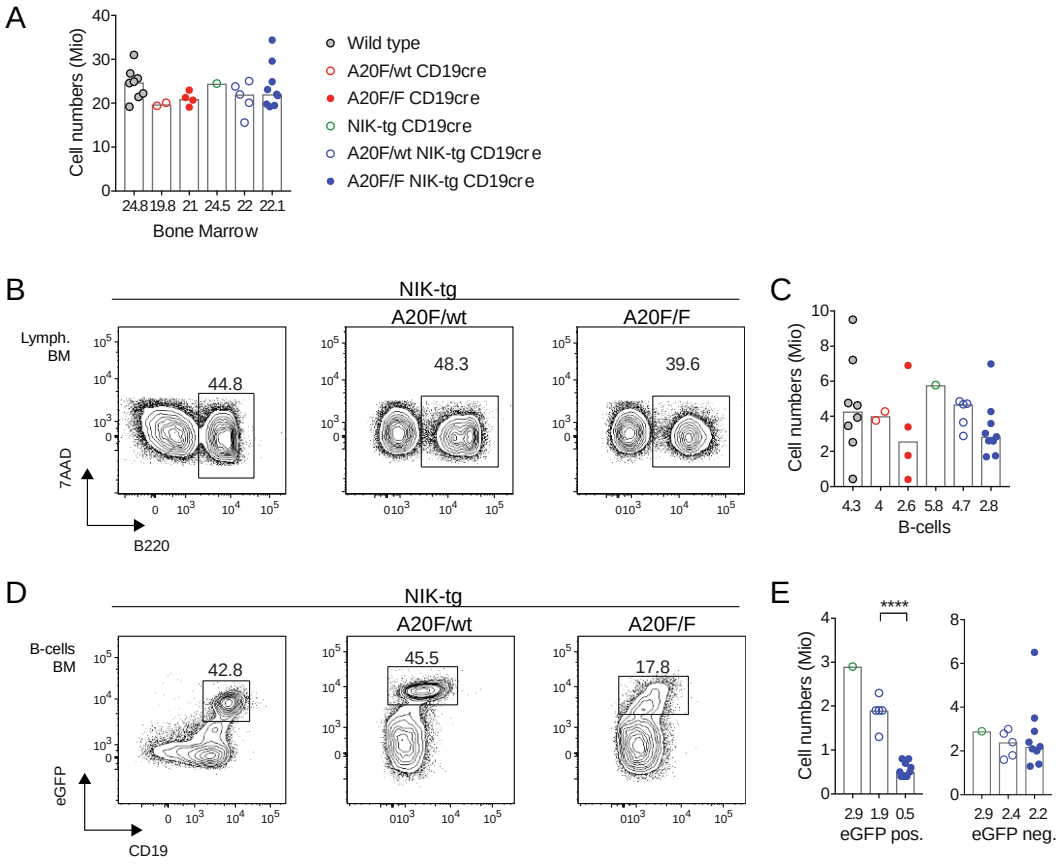


**Figure 10. Reduced eGFP+;A20-/-;NIK+ B-cells in bone marrow from young mice**

*Ex vivo* analysis of B-cells from bone marrow of young animals using flow cytometry. (A) Bone marrow cell numbers for one leg after red blood cell lysis. Flow cytometry contour plots depict percentages and bar charts indicate total cell numbers for (B, C) B-cells and (D, E) eGFP expressing B-cells ($B220^+$ $eGFP^+$). Flow cytometry plots are representative of at least 2 experiments, except for NIK-tg CD19cre mice. The NIK-tg CD19cre contour plots do not belong to the same experiment as A20-deficient NIK-tg CD19cre plots. Bar charts depict medians and the values are indicated below each histogram. Statistical analysis was done using One-way ANOVA (**** $p<0.0001$).
BM (bone marrow), eGFP (green fluorescent protein), B-cells ($B220^+$), eGFP pos. (eGFP positive B-cells, $B220^+$ $eGFP^+$) and eGFP neg. (eGFP negative B-cells, $B220^+$ $eGFP^-$).

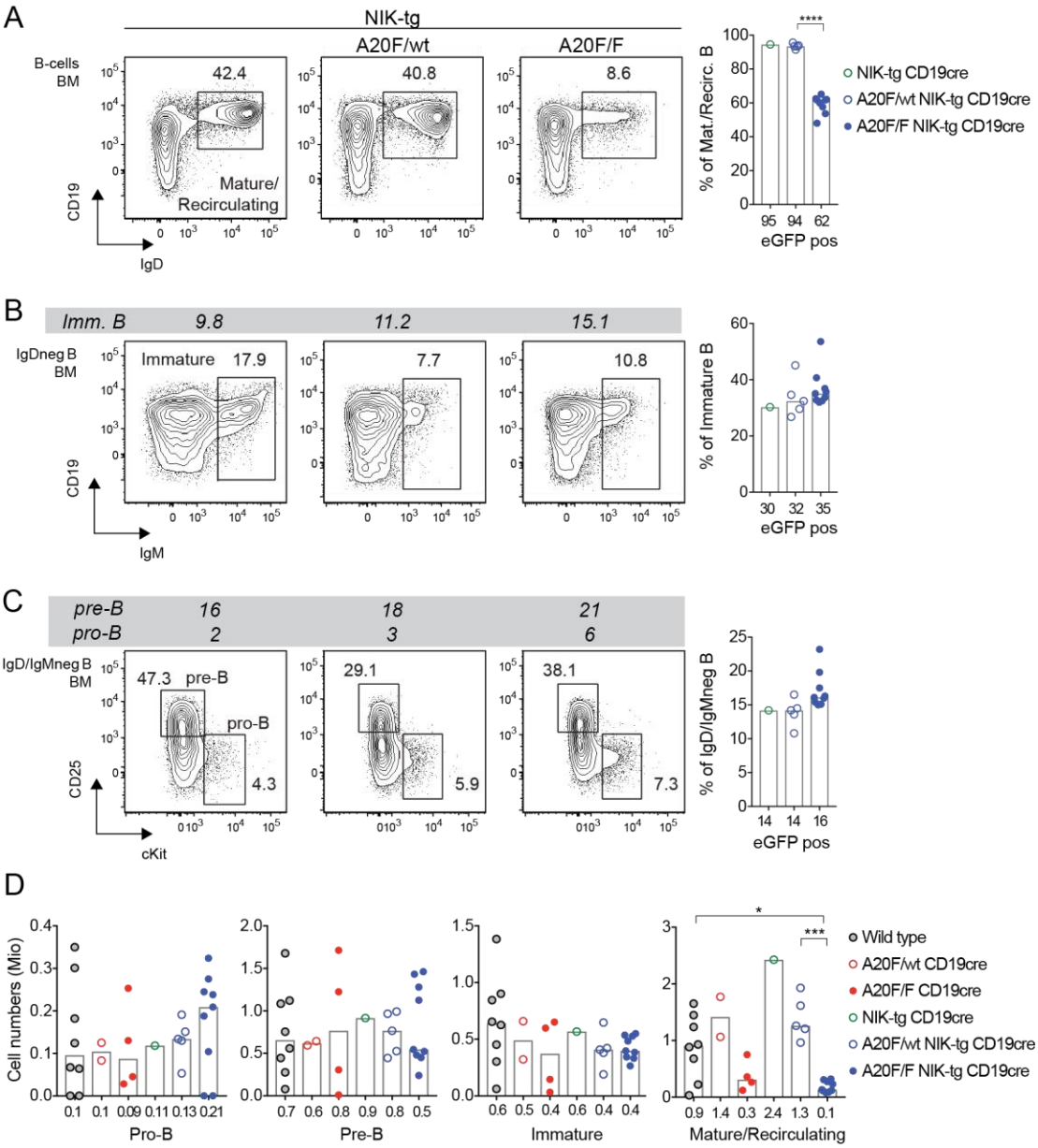


**Figure 11. Reduced mature/recirculating A20-/-;NIK+ B-cells in bone marrow**

*Ex vivo* analysis of B-cells from bone marrow of young animals using flow cytometry. Flow cytometry contour plots depict percentages and bar chart indicate percentages of eGFP positive cells for (A) mature/recirculating B-cells, (B) immature B-cells and (C) pro-B cells and pre-B cell. (D) Bar charts indicate cell numbers for pro-B, pre-B, immature and mature/recirculating B-cells. The median percentage values of immature, pre-B and pro-B are indicated on top of each contour plot. Flow cytometry plots are representative of at least 2 experiments, except for NIK-tg CD19cre mice. The NIK-tg CD19cre contour plots do not belong to the same experiment as A20-deficient NIK-tg CD19cre plots. Bar charts depict medians and the values are indicated below each histogram. Statistical analysis was done using One-way ANOVA (* $p<0.05$, *** $p<0.001$, **** $p<0.0001$).

BM (bone marrow), eGFP (enhanced green fluorescent protein), mature/recirculating ($B220^+$ $IgD^+$), eGFP pos ($eGFP^+$), immature ($B220^+$ $IgM^+$ $IgD^-$), pro-B ($B220^+$ $IgD/IgM^-$ $CD25^+$ $cKIt^-$) and pre-B ($B220^+$ $IgD/IgM^-$ $CD25^-$ $cKit^+$).

The *ex vivo* bone marrow analysis revealed that the *ex vivo* mature/recirculating B-cells are the main population affected by the loss of A20 in combination with the overexpression of NIK.

First, there is a significant reduction in the percentage of mature/recirculating B-cells from 40% in the NIK-tg CD19cre alone or A20F/wt NIK-tg CD19cre to 9% in the A20F/F NIK-tg CD19cre mice (Figure 11A). Moreover, the percentage of *ex vivo* eGFP-expressing mature/recirculating cells in the A20F/F NIK-tg CD19cre mice is reduced to 62%. The total number of A20-/-;NIK+ mature/recirculating B-cells is also significantly reduced compared to the wild type control, and the A20F/wt NIK-tg CD19cre aged matched mice (Figure 11D). As observed before (Chu et al., Blood Supplement), the number of recirculating/mature B-cells in the A20F/F CD19cre mice are also reduced compared to control (Figure 11D).

Second, the *ex vivo* immature B-cell numbers in the bone marrow are not affected by the combination of loss of A20 and gain of the NIK-tg (Figure 11B). There is a slight increase in the percentage of the A20-/-;NIK+ immature B-cells, but that is due to the low percentage of mature/recirculating B-cells. Moreover, the percentage of immature cell expressing the eGFP reporter is similar among all NIK-tg compound mice (Figure 11B).

Third, in the earlier stages of B-cell development there is a small trend for higher pro-B cell and lower pre-B cell numbers in an A20-loss dependent manner in NIK-tg compound mice (Figure 11D). Moreover, there is a small increase in the percentage of pre-B and pro-B cells as more alleles of A20 are inactivated, but again it accounts to missing mature/recirculating B-cells in the bone marrow (Figure 11A and C).

Taking into account the similar cell numbers of pro-B, pre-B and immature B-cells in the bone marrow of young mice, the loss of A20 in combination with the gain of one copy of NIK does not significantly affect early B-cell development in the bone marrow.

#### IV.1.3.4 Immunoglobulin light chain ratios vary from immature to mature B-cells in A20-/-;NIK+ B-cells

Given that the negative effect of combining loss of A20 with overexpression of NIK becomes evident after the immature B-cell stage, I decided to look for an additional control point in normal B-cell development: the proportions of kappa and lambda

immunoglobulin light chain expressing B-cells. During B-cell development, there is a tight control for the rearrangement and expression of a functional BCR. After the heavy chain locus has been rearranged and the pre-BCR has been expressed, the cell proceeds to rearrange the immunoglobulin light chain locus to produce a functional BCR. If rearrangements in the kappa locus lead to the inactivation of the locus, the cell will subsequently rearrange the lambda locus. It has been proposed that although the generation of kappa-chain positive cells is independent of NF-κB activation, the generation of lambda-chain positive cells depends on NF-κB signals [63]. Therefore, strong activation of NF-κB by overexpression of NIK in combination with loss of A20, could lead to the selection of lambda-chain positive cells.

In the bone marrow of young mice, although there is tendency for higher lambda light chain positive immature B-cells in the A20F/wt NIK-tg CD19cre mice compared to wild type mice (Figure 12A and C), the overall levels of kappa light chain positive cells are similar for all NIK-tg compound mice. Interestingly, in the lambda light chain positive immature B-cells, there is a higher percentage of eGFP positive cells as each allele of A20 is deleted in the NIK-tg CD19cre compound mice, although not statistically significant (Figure 12A). On the other hand, the percentage of eGFP positive B-cells in the kappa light chain positive cells are all similar.

At the mature/recirculating B-cell stage in the bone marrow, there is a significant increase in the percentage of lambda light chain positive A20-/-;NIK+ cells compared to the wild type controls (Figure 12B). This is accompanied by a significant decrease in the percentage of kappa light chain positive cells compared to wild type and A20-/- controls. Moreover, the percentage of kappa light chain positive cells expressing eGFP is significantly reduced in A20F/F NIK-tg CD19cre mice compared to the A20F/wt NIK-tg CD19cre mice. However, this is not the case for the lambda light chain positive cells, were all NIK-tg CD19cre background mice have similar percentages of eGFP expressing cells (Figure 12B).

At the immature B-cell stage in the bone marrow the percentage and cell numbers of kappa and lambda light chain are similar between the A20F/wt NIK-tg CD19cre and the A20F/F NIK-tg CD19cre mice (Figure 12A, C and D). However, at the mature/recirculating B-cell stage, the loss of the second allele of A20 in combination of NIK overexpression drastically reduces the cell numbers of both kappa and lambda light chain expressing cells (Figure 12C). Interestingly, although there are similar

percentages of kappa and lambda light chain cells, the fractions that actually express eGFP within each group is lower in the A20F/F NIK-tg CD19cre mice compared to the A20F/wt NIK-tg CD19cre mice (Figure 12C).

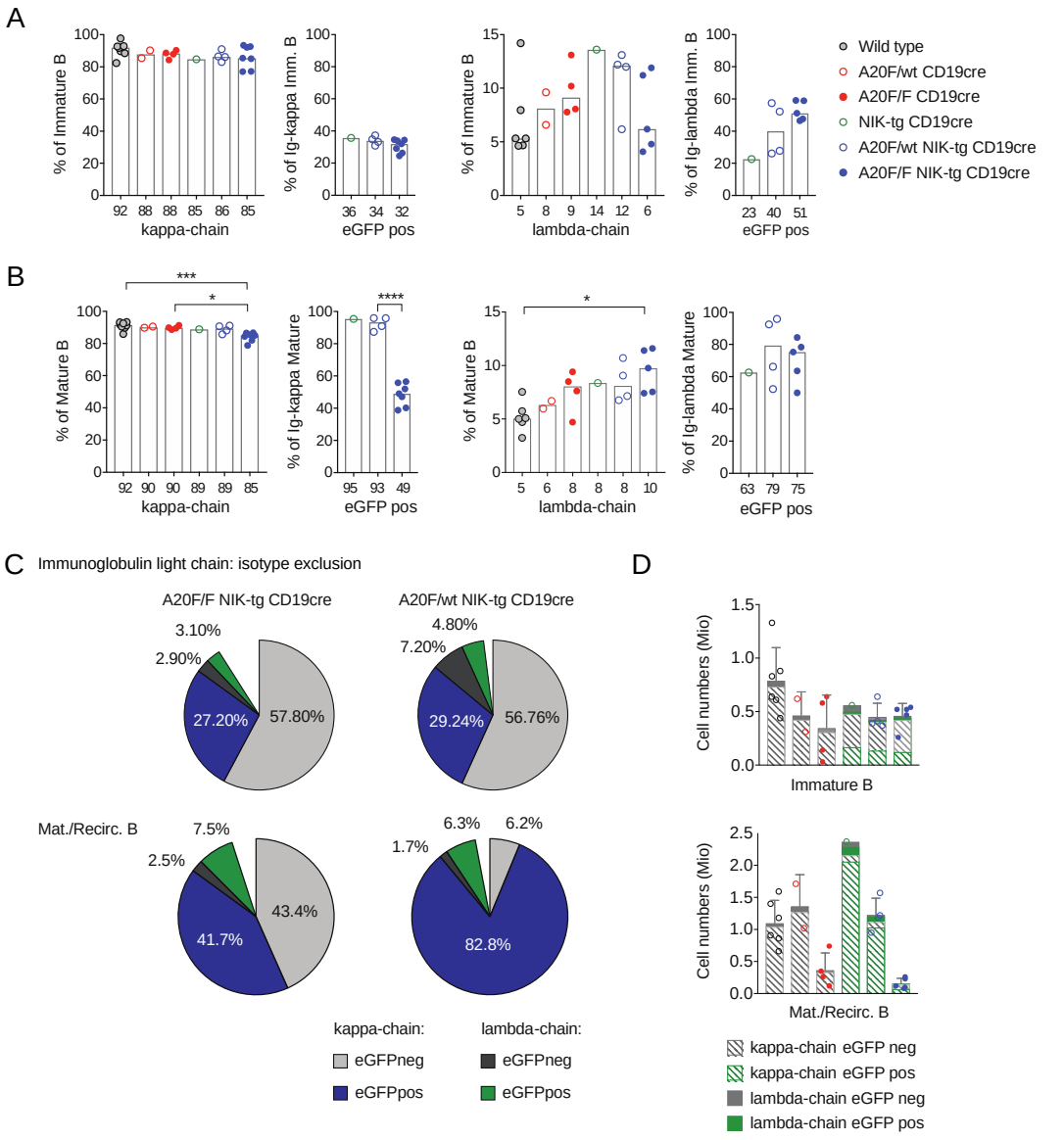


**Figure 12. B-cell receptor light chain isotype in the bone marrow.**

*Ex vivo* analysis of the immunoglobulin light-chain in B-cells from bone marrow of young animals. Bar charts indicate the percentage of (A) immature and (B) mature B-cells expressing the immunoglobulin light chain isotype Ig-*kappa* or Ig-*lambda*, and the percentage of eGFP expressing cells for each isotype. (C) Pie charts depict the mean percentage of Ig-*kappa* and *lambda* cells expressing or not eGFP for the A20-/-;NIK+ and A20+/-;NIK+ immature and mature/recirculating B-cells. (D) Bar charts depict the mean number and standard error of the mean of kappa light chain and lambda light chain expressing immature and recirculating B-cells. Data is representative of at least 2 experiments, except for NIK-tg CD19cre mice. Bar charts depict medians and the values are indicated below each histogram. Statistical analysis was done using One-way ANOVA (* $p<0.05$, *** $p<0.001$, **** $p<0.0001$).

Figure 12 **(continued)**. Ig-*kappa* (immunoglobulin *kappa* light chain), Ig-*lambda* (immunoglobulin *lambda* light chain), immature B-cells ($B220^+$ $IgM^+$ $IgD^-$) and mature/recirculating ($B220^+$ $IgD^+$).

The normal ratios of kappa and lambda light chain immature A20-/-;NIK+ B-cells indicate that the loss of A20 in combination with the overexpression of NIK does not affect the early B-cell development in the bone marrow into the immature B-cell stage. Second, the lambda light chain positive pool is not favoured by the combination of these mutations. It is in the secondary lymphoid organs, starting in the spleen that impairment in homeostasis can be observed. It is interesting that the mature recirculating pool in the bone marrow of the A20F/F NIK-tg CD19cre mice is reduced to 50% of that observed for the A20F/wt NIK-tg CD19cre mice, unlike the increase observed in the spleen.

### IV.1.4 REDUCED POOL OF MATURE B-CELLS IN A20F/F NIK-TG CD19CRE MICE IS NOT DUE TO INCREASED APOPTOSIS

Mice with homozygous loss of A20 in combination with a transgenic copy of NIK in B-cells have a clear reduction in mature B-cell numbers, specifically affecting the eGFP positive population. In order to determine if apoptosis had a role in the B-cell reduction observed, I assessed pan-Caspase *ex vivo* activation, by incubating cells with the irreversible pan-Caspase inhibitor Red-VAD-FMK for 1 hour followed by flow cytometry analysis.

In the bone marrow as well as in the spleen, the percentages of *ex vivo* activated pan-Caspases in either eGFP positive A20+/-;NIK+ or A20-/-;NIK+ total B-cells is similar to or lower compared to wild type controls (Figure 13A and B). Interestingly, eGFP+;A20+/-;NIK+ B-cells have a lower percentage of *ex vivo* pan-Caspase activation compared to their eGFP+;A20-/-;NIK+ counterparts (Figure 13A). Furthermore, while eGFP positive A20+/-;NIK+ B-cells in the spleen display a reduction in *ex vivo* pan-Caspase activation compared to wild type control (8.8% to 2.3%), loss of the second allele of A20 leads to reduced Caspase activation compared to wild type (8.8% to 3.7%) and increased Caspase activation compared to A20+/-;NIK+ counterparts (Figure 13B). Additionally, both *ex vivo* eGFP negative A20+/-;NIK+ and A20-/-;NIK+ B-cells from the spleen show a four- and two-fold increase in the *ex vivo* pan-Caspases activation compared to wild type, respectively (Figure 13B) likely due to the absence of one allele of the CD19 signal transduction molecule involved in B-cell survival{Otero:2003wk} or the Cre-recombinase dependent toxicity {Sharma:2001ch}. Alternatively, the higher

percentage of eGFP negative apoptotic B-cells in the A20F/wt NIK-tg CD19cre and the A20F/F NIK-tg CD19cre mice could indicate a pro-apoptotic effect triggered by the eGFP positive B-cells in these mice. Throughout the B-cell development, eGFP+;A20+/-;NIK+ immature B-cells in the bone marrow and spleen have relative higher *ex vivo* pan-Caspase activation compared to wild type control (Figure 13C). The loss of the second allele of A20 further increases the *ex vivo* pan-Caspases activation in immature B-cells from the bone marrow, however it leads to reduced *ex vivo* pan-Caspase activation in the spleen compared to the A20F/wt NIK-tg CD19cre mice (Figure 13C).

The drop in B-cell numbers in A20F/F NIK-tgCD19cre mice is observed at the mature B-cell stage. The percentage of *ex vivo* activated pan-Caspases in eGFP positive A20-/-;NIK+ B-cells in spleen is lower to that observed for the wild type control (Figure 13C). Interestingly, although the eGFP negative mature B-cells have a similar percentage of early apoptotic cells, a much higher percentage are at the late apoptotic stage. This same phenotype is observed for the mature A20+/-;NIK+ B-cells, where the eGFP positive cells have an even lower percentage of activated pan-Caspase, and the eGFP negative cells have a higher percentage of early and late apoptotic cells, compared to wild type control (Figure 13C).

In the mature/recirculating B-cell stage, both the eGFP positive A20+/-;NIK+ and A20-/-;NIK+ B-cells showed similar *ex vivo* Caspase activation levels compared to the wild type controls (Figure 13C). Surprisingly, the eGFP negative A20+/-;NIK+ B-cells showed an elevated percentage of late apoptotic cells, compared to the other genotypes analysed.

The reduced eGFP positive B-cell numbers observed in A20F/F NIK-tg CD19cre mice are not a result of enhanced programmed cell death due to increased Caspase activation. Furthermore, in the presence of the NIK-tg, which is co-expressed with eGFP from the same mRNA, there is lower activation of pan-Caspases observed. Thus, the presence of the NIK-tg provides an anti-apoptotic advantage, as observed for both the A20+/-;NIK+ and the A20-/-;NIK+ mature B-cells.

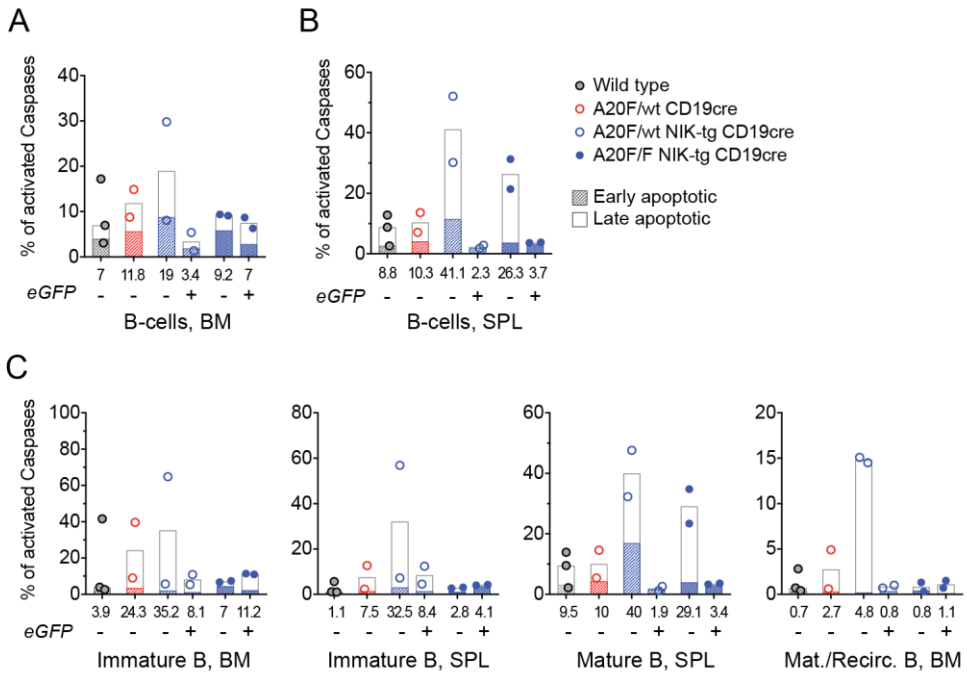


**Figure 13. Reduced A20-/-;NIK+ B-cell numbers are not related to increased apoptosis**

*Ex vivo* programmed cell death analysis. Apoptotic cells were incubated with the irreversible pan-Caspases inhibitor Red-VAD-FMK for one hour, and followed by flow cytometry analysis. Percentage of *ex vivo* activated pan-Caspases in B-cells from (A) bone marrow and (B) spleen. (C) Percentage of *ex vivo* activated pan-Caspases through B-cell development: immature B-cells in the bone marrow and spleen, mature B-cells in the spleen and mature/recirculating B-cells in bone marrow. Bar charts depict medians and the values are indicated below each histogram.
BM (bone marrow), SPL (spleen), early apoptotic (Red-VAD-FMK$^+$ 7AAD$^-$), late apoptotic (Red-VAD-FMK$^+$ 7AAD$^+$), B-cells (B220$^+$), immature B-cells (BM: B220$^+$ IgM$^+$ IgD$^-$ or SPL: B220$^+$ AA4.1$^+$), mature B-cells (BM: B220$^+$ IgD$^+$ or SPL: B220$^+$ AA4.1$^-$).

### IV.1.5 Loss of A20 accentuates the reduced germinal centre B-cells and plasma cells observed in the presence of enhanced alternative NF-κB activation

Germinal centres (GC) are physiological structures in secondary lymphoid organs where antigen-activated B-cells mature to plasma cells or memory B-cell to produce high affinity antigen specific antibodies [47, 92]. In gut associated lymphoid tissues (GALT), including mLN and PP, constant antigen presentation derived from the gut microflora drives GC B-cells to produce an adaptive immune response to the microorganisms found in the gut. It has been reported that the loss of A20 in B-cells affects germinal centre B-cells and results in autoimmunity {Chu:2011dz}, the GC reaction in unimmunized mice was characterised to assess the role of the combination of A20 with enhanced expression of NIK.

In unimmunized mice, spleens and LNs from NIK-tg compound mice show a reduction in the percentage of spontaneous *ex vivo* GC B-cells in comparison with wild type and A20-deficient compound mice (Figure 14A and C, respectively). Spleens of NIK-tg CD19cre mice have similar numbers of e*x vivo* GC B-cells as wild type controls (Figure 14B). However, the additional loss of one allele of A20, instead of increasing the number of GC B-cells as observed in the A20F/wt CD19cre mice [79], leads to lower *ex vivo* GC B-cell numbers compared to the NIK-tg CD19cre mice (Figure 14D). Moreover, the loss of the second allele of A20 in combination with overexpression of NIK leads to almost complete absence of *ex vivo* GC B-cells (Figure 14A and B). Interestingly, almost no eGFP positive *ex vivo* A20-/-;NIK+ GC B-cells are observed (Figure 14B).

Similarly, the number of *ex vivo* GC B-cells in LNs from the NIK-tg compound mice are reduced compared to their NIK-tg negative counterparts (i.e. A20F/wt NIK-tg CD19cre vs. A20F/wt CD19cre) (Figure 14C and D). There is a trend for higher number of *ex vivo* GC B-cells as each allele of A20 is lost in the NIK-tg CD19cre background (Figure 14D), but only a small fraction of the GC B-cells express eGFP, which reports for NIK expression (Figure 14D).

In the GALT, a similar phenotype can be observed in both the mLN and the PP. The few *ex vivo* GC B-cells observed in the NIK-tg CD19cre mice are reduced as A20 is ablated (Figure 14E-H). There is a significant reduction in the number of *ex vivo* GC B-cells in the A20F/F NIK-tg CD19cre mice compared to the wild type control especially in the PP (Figure 14H). Interestingly, although the number of GC B-cells for the A20F/wt NIK-tg CD19cre mice is similar to the one for the A20F/F NIK-tg CD19cre mice, there is a significant reduction of eGFP (≈ NIK) expressing cells when the second allele of A20 is lost (Figure 14H).

Additionally, the overexpression of NIK in B-cells leads to cells with higher expression of the death receptor protein CD95 (FAS) (Figure 16A, Figure S 5A and Figure S 6A). Surprisingly, the higher expression of CD95 does not lead to a higher percentage of apoptosis. In fact, the eGFP positive A20+/-;NIK+ and eGFP positive and negative A20-/-;NIK+ GC B-cells have lower *ex vivo* activation of pan-Caspases compared to wild type controls (Figure S 5B).

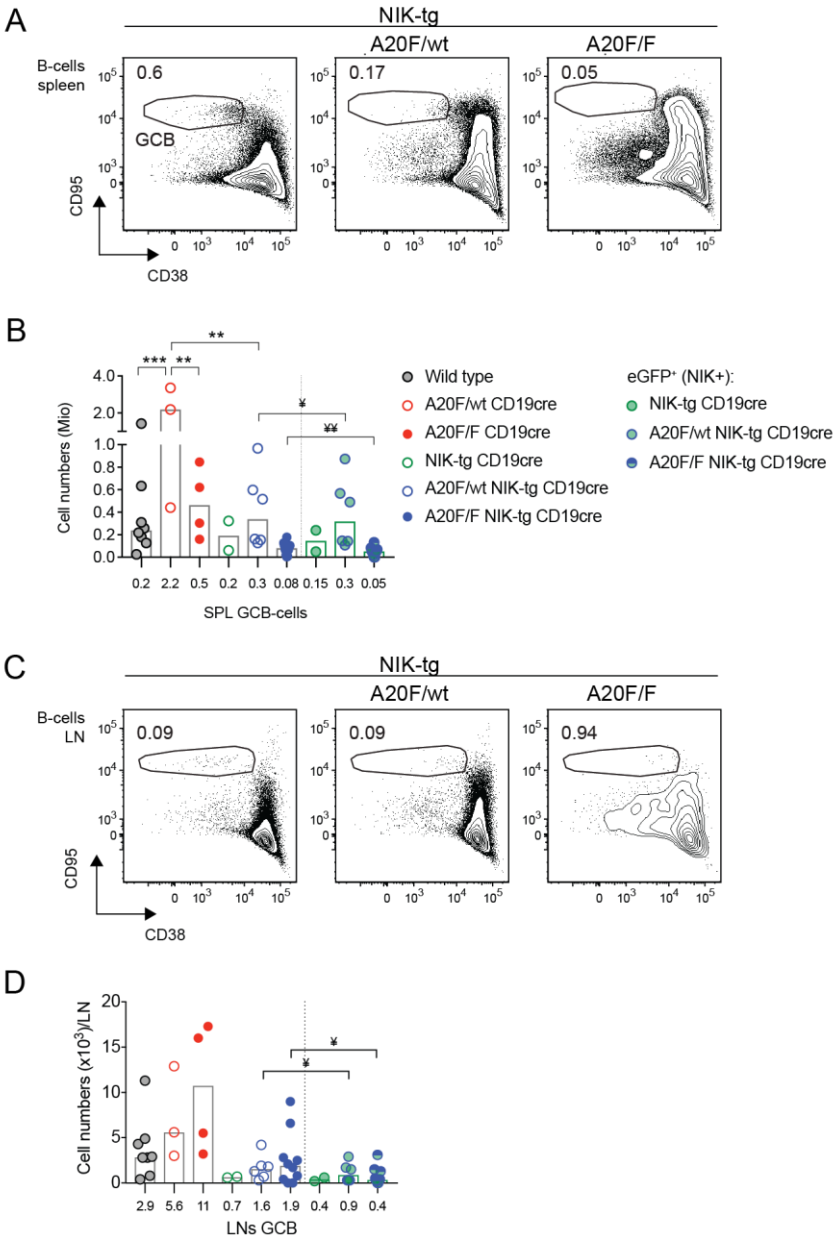


**Figure 14. Diminished germinal centre B-cells in unimmunized NIK-tg compound mice**

*Ex vivo* analysis of germinal centre B-cells in secondary lymphoid organs from unimmunized young mice using flow cytometry. Contour plots depict percentages of germinal centre B-cells from (A) spleens and (C) draining lymph nodes,. Bar charts show germinal centre B-cells and eGFP positive cells numbers for (B) spleens, (D) lymph nodes Draining inguinal, axillary and superficial cervical lymph nodes were pooled and data was normalized to one lymph node. All flow cytometry plots are representative of at least 2 experiments. Bar charts depict medians and values are indicated below each histogram. Statistical analysis was done using Kruskal-Wallis (* $p<0.05$, ** $p<0.01$, *** $p<0.001$) or Two-tailed paired T-test (¥ $p<0.05$, ¥¥ $p<0.01$).

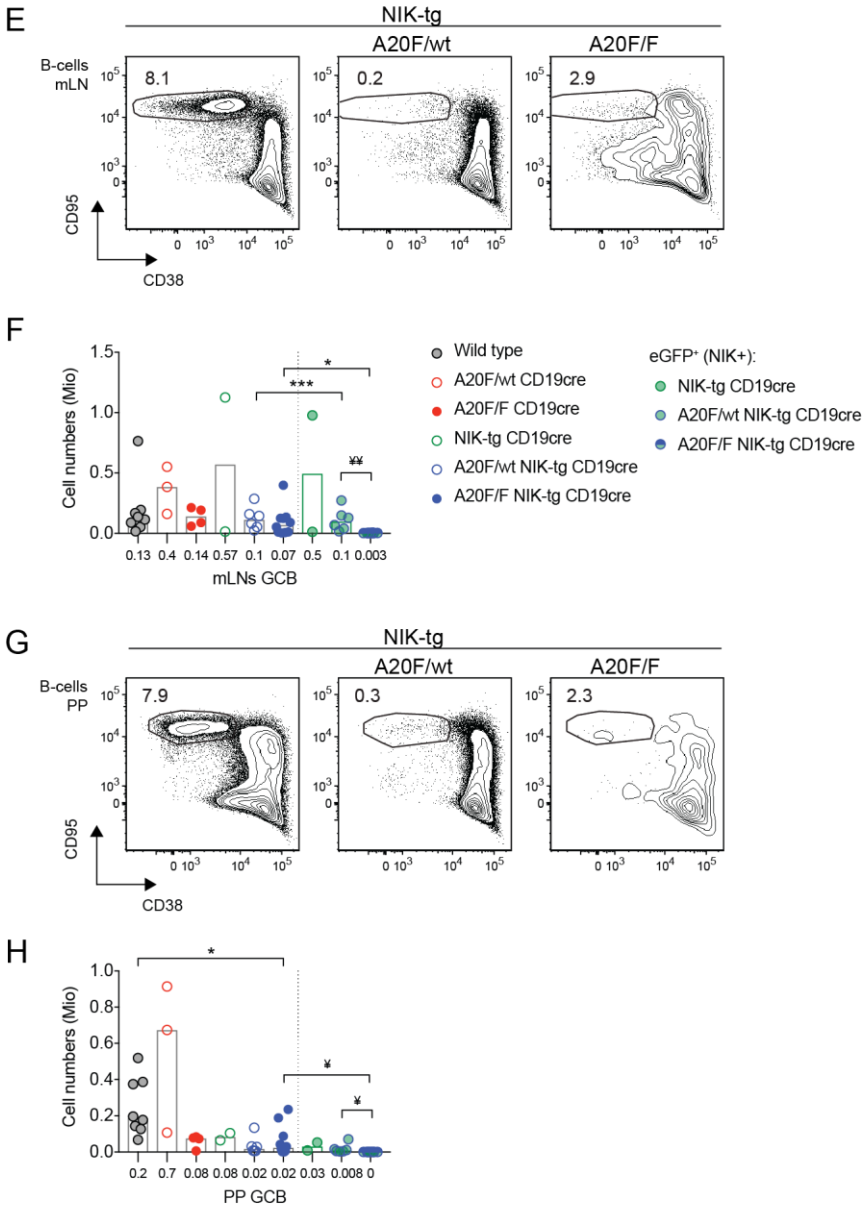


**Figure 14 (continued). Diminished germinal centre B-cells in unimmunized NIK-tg compound mice**

*Ex vivo* analysis of germinal centre B-cells in secondary lymphoid organs from unimmunized young mice using flow cytometry. Contour plots depict percentages of germinal centre B-cells from (E) mesenteric lymph nodes, and (G) Peyer's patches. Bar charts show germinal centre B-cells and eGFP positive cells numbers for (F) mesenteric lymph nodes, and (H) Peyer's patches. All flow cytometry plots are representative of at least 2 experiments. Bar charts depict medians and values are indicated below each histogram. Statistical analysis was done using Kruskal-Wallis (* $p<0.05$, ** $p<0.01$, *** $p<0.001$) or Two-tailed paired T-test (¥ $p<0.05$, ¥¥ $p<0.01$).

SPL (spleen), LN (lymph node), mLN (mesenteric lymph nodes), PP (Peyer's patches), GCB (germinal centre B-cells, $B220^+$ $CD38^-$ $CD95^+$), eGFP (enhanced green fluorescent protein) and eGFP pos ($eGFP^+$).

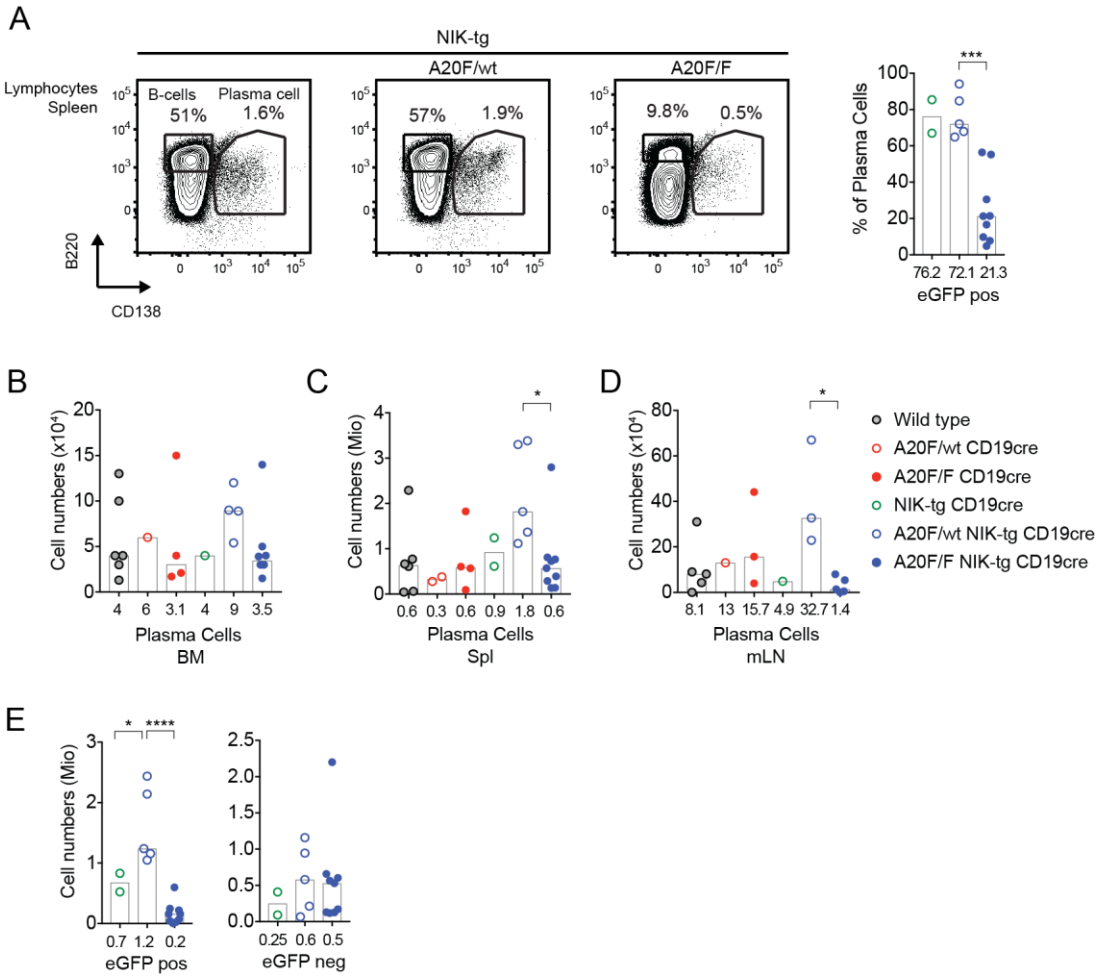


**Figure 15. Decreased plasma cell numbers in unimmunized A20F/F NIK-tg CD19cre mice**

*Ex vivo* analysis of plasma cells from bone marrow, spleen and mesenteric lymph nodes of unimmunized young mice, by flow cytometry. (A) Flow cytometry contour plots depict the percentage of plasma cells and B-cells in spleen. Bar chart indicates the percentage of eGFP positive NIK expressing plasma cells in the NIK-tg CD19cre compound mice. Bar charts indicate numbers for plasma cells in (B) bone marrow, (C) spleen and (D) mesenteric lymph nodes. (E) Bar charts indicate the number of eGFP positive NIK expressing plasma cells and eGFP negative plasma cells in spleen. Data is representative of at least 2 experiments, except for NIK-tg CD19cre mice. Bar charts depict medians and the values are indicated below each histogram. Statistical analysis was done using One-way ANOVA (* $p<0.05$, *** $p<0.001$, **** $p<0.0001$).
BM (bone marrow), Spl (spleen), mLN (mesenteric lymph nodes), eGFP (enhanced green fluorescent protein), Plasma Cells ($B220^{-}$ $CD138^{+}$), eGFP pos ($eGFP^{+}$) and eGFP neg ($eGFP^{-}$).

The end product of the germinal centre reaction is the generation of high affinity specific plasma cells. The loss of one allele of A20 results in the increase in percentage and cell numbers of total ex vivo plasma cells in A20F/wt NIK-tg CD19cre mice compared to NIK-tg CD19cre mice (Figure 15). Interestingly, the number of *ex vivo* plasma cells observed in the spleen of the A20F/F NIK-tg CD19cre mice is similar to the wild type controls, but significantly reduced compared to the A20F/wt NIK-tg CD19cre mice

(Figure 15C). Moreover, only 20% of the plasma cells in the A20F/F NIK-tg CD19cre mice express the eGFP NIK-reporter (Figure 15A and E). Similarly, the loss of the second allele of A20 in the NIK-tg CD19cre background results in reduced plasma cells numbers in the BM and more drastically in the mLN compared to the A20F/wt NIK-tg CD19cre mice (Figure 15A and C).

Taking into account the low GC B-cell numbers and few plasma cells observed in the unimmunized A20F/F NIK-tg CD19cre mice, and the fact that most of these cells are actually eGFP negative, my data point towards the idea that alternative NF-κB signalling is sufficient to hinder the GC reaction. The additional homozygous loss of A20, a negative regulator of the canonical NF-κB signalling, blocks further the GC fate of these cells and additionally prevents general plasma cell differentiation.

### IV.1.6 Loss of A20 in combination with alternative NF-κB activation drives aberrant expression of co-receptor molecules that leads to a pre-activated antigen presenting cell phenotype

The overexpression of NIK in combination with the loss of one allele of A20 (A20+/-;NIK+) leads to an expansion of B-cells that have a MZ-like phenotype. Furthermore, A20F/wt NIK-tg CD19cre mice (Figure 15) have reduced GC B-cells (Figure 14), but slightly increased plasma cell numbers compared to wild type mice. However, the loss of the second allele of A20 (A20-/-;NIK+) leads to massive reduction of mature B-cells as well as inefficient GC B-cell and plasma cell formation. Given the already observed altered expression of different surface proteins such as CD23 and CD95, I decided to take a closer look at the combined effect of loss of A20 and overexpression of NIK in the expression of B-cell activation markers, B to T-cell collaboration proteins, and transcription factors that are essential for B-cell fate and function.

B-cells interact with T-cell through several surface proteins and are modulated by the production of several cytokines produced by T-cells. First, B-cells express ICOS-L that binds the ICOS protein in the T-cell. Second, B-cells also express the activations markers CD80 and CD86 that are required to bind CD28 on T-cells during the presentation of antigens. Third, the MHC-II in B-cells binds the TCR to present antigens. Fourth, the cytokines IL-25 and interferon-γ (IFN-γ) are important signals for B-cell activation and survival. Moreover, the surface protein CD44 functions as a marker of cell activation in T-cell lymphocytes.

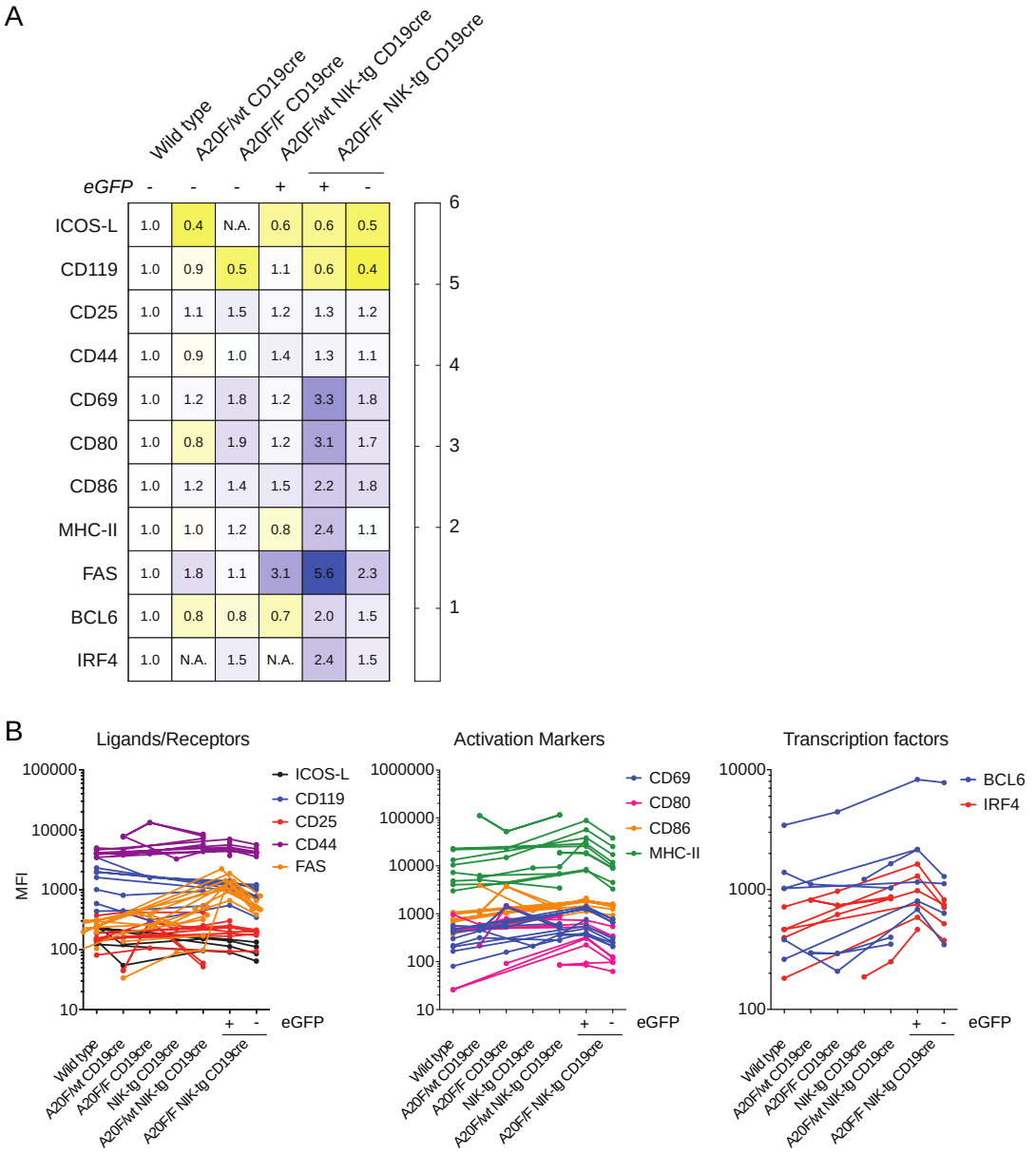


**Figure 16. Aberrant expression of activation makers, receptors and transcription factors in A20-/-;NIK+ B-cells from spleens of young mice.**

*Ex vivo* analysis of B-cells from spleen of young mice using flow cytometry. (A) Heat maps depict the geometric mean of the MFI in B-cells relative to the wild type control. (B) Scatter plots show the absolute MFIs of receptors and ligands (ICOS-L, CD119, CD25, CD44 and FAS/CD95), activation markers (CD69, CD80, CD86 and MHC-II) and transcription factors (BCL6 and IRF4).
N.A. (not available), eGFP (enhanced green fluorescent protein), MFI (Median Fluorescent Intensity)

A20 deficiency in B-cells (A20+/- and A20-/-) leads to lower *ex vivo* expression levels of both ICOS-L and CD119 (IFN-γ receptor) compared to wild type controls (Figure 16 and Figure S 6A). The additional gain of one allele of the NIK-tg does not rescue the expression of ICOS-L nor CD119 in eGFP+;A20-/-;NIK+ B-cells. Moreover, the relative

expression of ICOS-L and CD119 is also reduced in eGFP negative B-cells, to levels observed in the A20-/- B-cells (Figure 16A and Figure S 6A). On the other hand, the *ex vivo* expression of the surface marker proteins CD25 and CD44 is mildly increased by the loss of A20, and the further gain of an extra copy of NIK does not alter their expression (Figure 16 and Figure S 6A).

The relative *ex vivo* expression of the activation makers CD69, CD80 and CD86 is increased in A20-/- B-cells [79]. This is further reinforced by the expression of the NIK-tg as seen in the eGFP+;A20+/-;NIK+ B-cells (Figure 16 and Figure S 6B). The same cannot be said for the A20+/- B-cells, where the gain of NIK transgene does not have the same effect. Interestingly, only the combination of loss of both alleles of A20 with gain of the NIK transgene, leads to an up regulation of the MHC-II molecule (Figure 16 and Figure S 6B). Again, the eGFP-;A20-/-;NIK- B-cells have a similar expression to the A20-/- B-cells.

As mentioned in the previous section, the expression of the NIK transgene drives higher expression of the FAS/CD95 death receptor in B-cells (Figure S 5A). The heterozygous loss of A20 already leads to a higher number of GC B-cells, partly explaining the relative higher expression observed for the A20+/- B-cells. The further activation of the alternative NF-κB pathway by expressing the NIK transgene further increases CD95 expression, reaching a maximum level when the second allele of A20 is inactivated in B-cells. Interestingly, the eGFP-;A20-/-;NIK+ B-cells have an increase of two-fold, compared to the A20-/- B-cells, which could be indicative of a B-cell extrinsic phenotype (Figure 16 and Figure S 6A).

Finally, the BCL6 and IRF4 are major players deciding B-cell differentiation. Loss of A20 in B-cells leads to a relative small decrease in *ex vivo* BCL6 expression. The presence of the NIK transgene in B-cells also decreases the relative expression of BCL6 (Figure 16B and Figure S 6C). However, A20-/-;NIK+ B-cells have a two-fold increase of BCL6 compared to wild type control. On the other hand, loss of A20 in B-cells leads to an increase in the relative *ex vivo* expression of IRF4. The additional gain of NIK further potentiates that expression.

Taken all together, eGFP+;A20-/-;NIK+ B-cells have a surface protein signature reminiscent of an antigen presenting cells, have an aberrant expression T-cell co-

stimulatory proteins required for the GC reaction and elevated BCL6 and IRF4 expression levels.

### IV.1.7 ALTERNATIVE NF-κB ACTIVATION COMBINED WITH LOSS OF A20 LEADS TO ALTERED INTEGRIN EXPRESSION PATTERNS IN B-CELLS

The loss of A20 in combination with overexpression of NIK in B-cells leads to an antigen presenting cell-like phenotype in eGFP (NIK) positive B-cells. Therefore, I decided to analyse the expression of particular integrins that are important for the immune system. During B-cell development and inflammation, B-cells need to migrate through circulation to secondary lymphoid organs where they populate particular niches. The expression of integrins and their activation at particular time points is essential for normal B-cell physiology. Therefore, inappropriate or altered expression of integrins could partly explain the reduced B-cell numbers in the secondary lymphoid organs.

The *ex vivo* expression of alpha-4, alpha-5, alpha-V, alpha-L, alpha-M and alpha-X integrins in B-cells was analysed using flow cytometry. Similarly, the *ex vivo* expression of beta-1, beta-2, beta-3 and beta-7 integrins was analysed in B-cells. Overall, three different *ex vivo* expression patterns were observed in B-cells when A20 was ablated alone or in combination with the expression of the NIK transgene.

The *ex vivo* expression of alpha-4, alpha-L, alpha-5 and alpha-V integrins is affected by both loss of A20 and overexpression of NIK. First, the relative expression of alpha-4 and alpha-L integrins is already reduced in A20 deficient B-cells compared to wild type controls. Interestingly, the *ex vivo* alpha-4 expression returns to normal levels in eGFP+;A20-/-;NIK+ B-cells (**Fehler! Verweisquelle konnte nicht gefunden werden.** and Figure S 5A), while the expression of alpha-L increases two-fold. Second, the relative expression of alpha-5 integrin is reduced in A20+/- B-cells, but normal in A20-/- B-cells. Third, the relative expression of alpha-V integrin is increased when A20 is inactivated, independently of NIK expression.

The relative *ex vivo* expressions of alpha-M is increased in A20+/- B-cells. Additional expression of NIK leads to a slight increase. However, the relative expression in A20-/- B-cells, independent of the expression of NIK, is similar to that of wild type (**Fehler! Verweisquelle konnte nicht gefunden werden.**A and Figure S 7A).

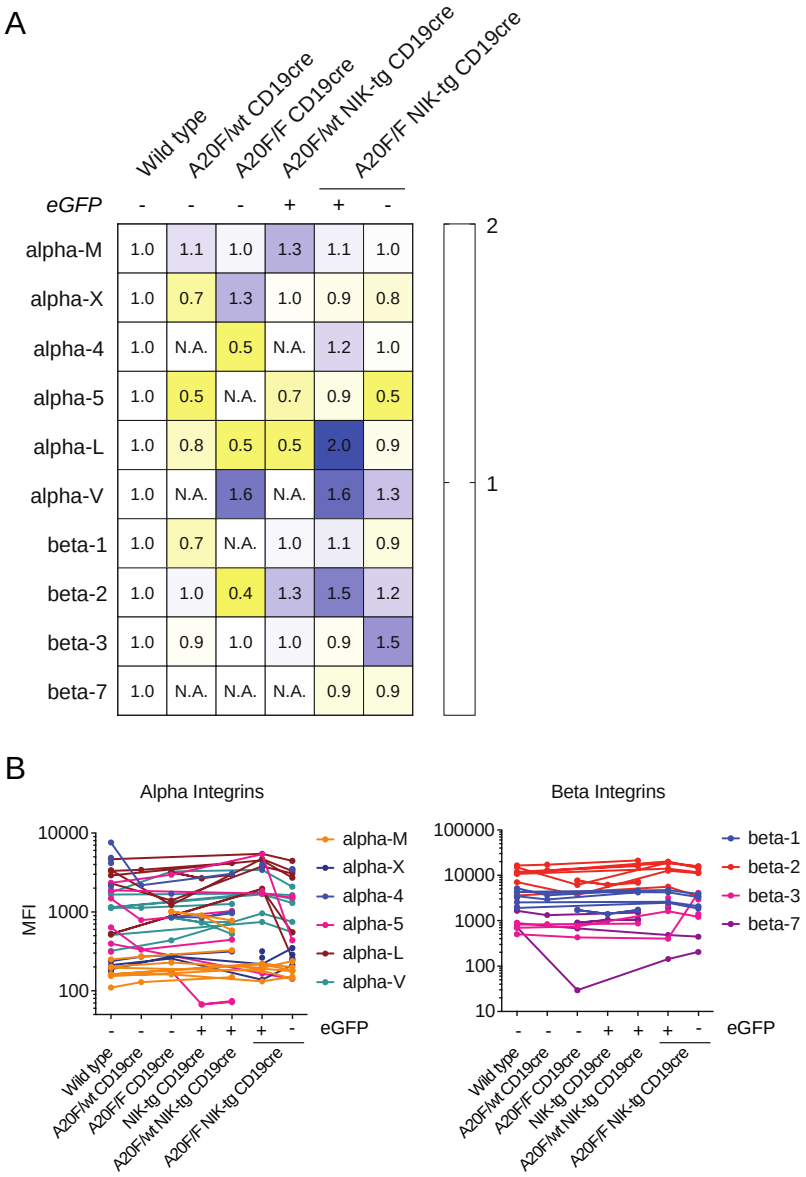


**Figure 17. A20-/-;NIK+ B-cells have altered integrin expression**

*Ex vivo* analysis of B-cells from spleen of young mice using flow cytometry. (A) Heat maps depicting the geometric mean of the MFI for alpha- and beta-integrins in B-cells relative to wild type. (B) Scatter plot show the absolute MFIs of alpha- and beta-integrins in B-cells.
N.A. (not available), eGFP (enhanced green fluorescent protein), MFI (Median Fluorescent Intensity)

The relative *ex vivo* expression of beta-2 integrins in A20-/- B-cells is significantly reduced to 50%. However, the overexpression of NIK leads to a significant increase that not only rescues but also overcomes the effect of A20 loss.

The relative *ex vivo* expression of beta-1 integrins was reduced in A20+/- B-cells, and expression of NIK restored the expression to normal levels. Although the relative *ex vivo*

expression for A20-/- B-cells was not done, the relative expression in A20-/-;NIK+ B-cells was similar to wild type control.

Interestingly, alpha-L and beta-2 integrins, the only two integrins with significantly changed expression levels in eGFP+;A20-/-;NIK+ B-cells, had similar expression patterns. They bind ICAM-I and are important for marginal zone B-cells.

### IV.1.8 ROLE OF B-CELL EXTRINSIC FACTORS IN THE NEGATIVE EFFECT OF LOSS OF A20 IN COMBINATION WITH OVEREXPRESSION OF NIK IN B-CELLS

The loss of A20 in combination with the overexpression of NIK leads to significantly lower mature B-cell numbers in secondary lymphoid organs. The B-cell intrinsic factors analysed, such as a block in development, an increase in apoptosis, enhanced antigen presenting cell-like phenotype, or altered integrin expression profile alone do not necessarily explain the observed phenotype in A20F/F NIK-tg CD19cre mice. I therefore, proceeded to analyse the T-cell and myeloid compartments in these animals.

#### IV.1.8.1 Expansion of CD25$^+$ CD4 regulatory, effector-like CD4 and effector-like CD8 T-cells in spleens of A20F/F NIK-tg CD19cre mice

The loss of A20 in combination with the overexpression of NIK leads to significant lower B-cell numbers in secondary lymphoid organs, affecting particularly the eGFP+;A20-/-;NIK+ B-cell population. Since T-cells are the central players in adaptive immune response and can modulate B-cells in different ways, I decided to analyse the T-cell compartment using flow cytometry.

In spleens of young A20F/F NIK-tg CD19cre mice, there is an evident increment in *ex vivo* T-cell percentages compared to A20F/wt NIK-tg CD19cre and NIK-tg CD19cre mice (Figure 18A). This increment translates to a significant increase in T-cell numbers compared to the wild type controls (Figure 18C). Interestingly, the A20F/wt NIK-tg CD19cre mice already display a trend for increased T-cell numbers compared to wild type mice (Figure 18C).

The increase in *ex vivo* T-cell numbers in A20F/F NIK-tg CD19cre mice affects all T-cells subsets. First, there is an increase in *ex vivo* CD8 T-cell numbers in A20F/F NIK-tg CD19cre mice (Figure 18D), although the percentage of CD8 T-cells in spleen of young mice is similar among the NIK-tg compound mice (Figure 18B). The *ex vivo* CD8 T-cells

numbers in the other compound mice analysed are constant (Figure 18D). Second, there is a significant increase in *ex vivo* conventional CD4 (cCD4) T-cell numbers in A20F/F NIK-tg CD19cre mice compared to WT controls (Figure 18D), even though the cCD4 T-cell subset percentages are also similar among NIK-tg compound mice (Figure 18B). Finally, the percentage of $CD25^+$ CD4 T-cells increases in an A20-loss dependent manner in NIK-tg compound mice (Figure 18B). This translates to significantly higher *ex vivo* number of $CD25^+$ CD4 T-cells in A20F/F NIK-tg CD19cre mice compared to A20F/wt NIK-tg CD19cre and wild type controls (Figure 18D). These CD25+ CD4 T-cells express higher levels of the FoxP3 transcription factor compared to their cCD4 counterparts (Figure S 8), indicating a regulatory effector function in these cells. Interestingly, there is also an expansion of $CD25^+$ CD4 regulatory T-cells in the A20F/F CD19cre mice comparable to the A20F/wt NIK-tg CD19cre mice (Figure 18D).

*Ex vivo* flow cytometry analysis of cCD4 T-cells in the spleens of young mice showed reduced percentages of memory-like T-cells accompanied by increased percentages of effector-like T-cells in mice that were either A20F/F NIK-tg CD19cre or A20F/wt NIK-tg CD19cre compared to NIK-tg CD19cre controls (Figure 19A). Mice with A20+/-;NIK+ B-cells had 45% of effector-like cCD4 T-cells, where as A20-/-;NIK+ B-cells resulted in 31,2% of effector like cCD4 T-cells, compared to 19% in NIK-tg CD19cre controls (Figure 19A). The increase observed in effector-like cells percentage translates into significant higher cell numbers in A20F/F NIK-tg CD19cre mice compared to WT control ($p<0.05$), and similar numbers compared to the A20F/wt NIK-tg CD19cre mice (Figure 19B). The A20F/F NIK-tg CD19cre mice have a trend for higher naïve-like and lower memory-like CD4 T-cell percentage and numbers (Figure 19B).

E*x vivo* characterization of CD8 T-cell activation in spleens of young mice revealed significant lower percentage of naïve-like T-cells accompanied by a significant increase in effector-like T-cells (Figure 19C). This naïve- to effector-like activation is A20-loss dependent, being stronger in the A20F/F NIK-tg CD19cre mice. The elevated effector-like cell percentage observed translates into a significant five-fold increase in effector-like CD8 T-cell numbers in A20F/F NIK-tg CD19cre mice compared to the A20F/wt NIK-tg CD19cre (Figure 19D).

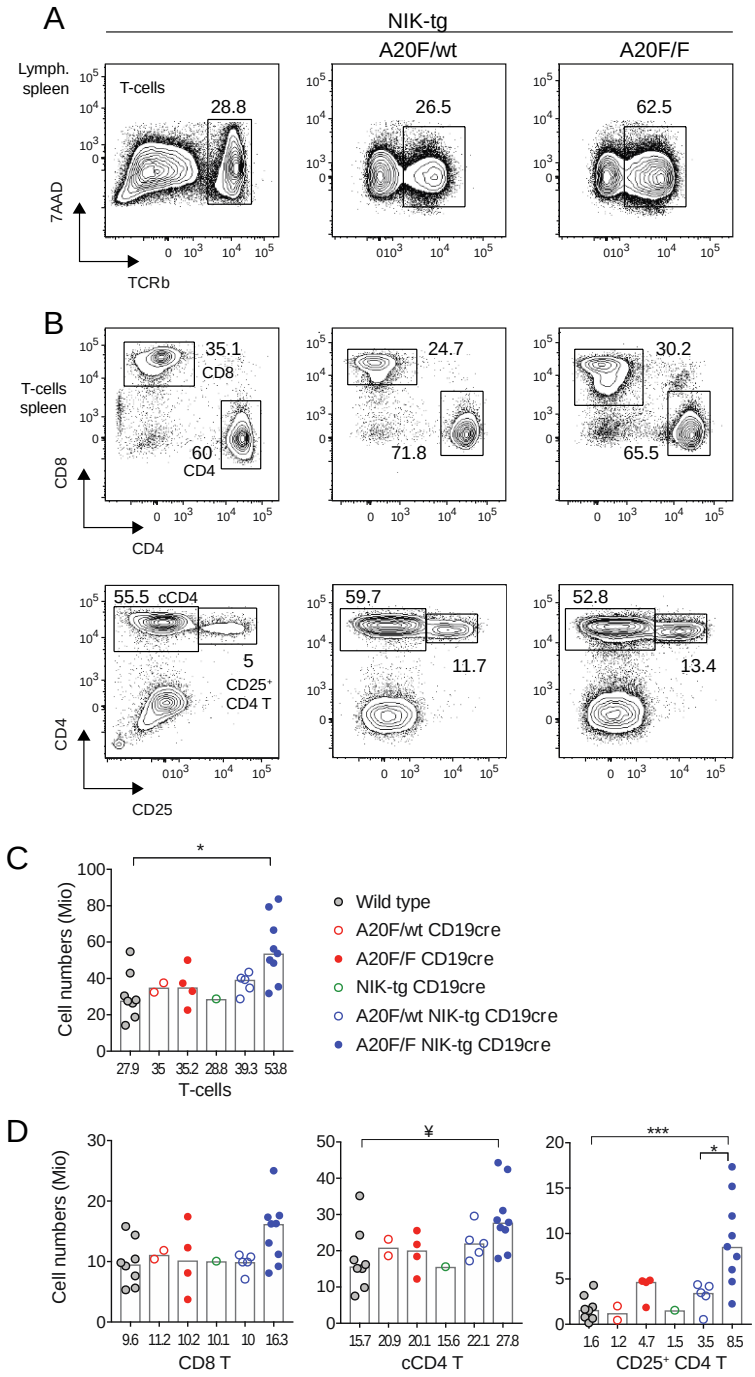


**Figure 18. A20F/F NIK-tg CD19cre mice develop T-cell hyperplasia**

*Ex vivo* analysis of T-cell populations in spleen of young mice using flow cytometry. Contour plots depict percentages and bar charts indicate cell numbers for (A, C) T-cells, and (B, D) conventional CD4, CD8, and CD25$^+$ CD4 T-cells. All flow cytometry plots are representative of at least 2 experiments, except for NIK-tg CD19cre mice. The NIK-tg CD19cre contour plots do not belong to the same experiment as A20-deficient NIK-tg CD19cre plots. Bar charts depict medians and the values are indicated below each histogram. Statistical analysis was done using One-way ANOVA (* $p<0.05$, *** $p<0.001$) or Kruskal-Wallis (¥ $p<0.05$), and statistical significance when $P<0.5$ is indicated.

T-cells (TCR$\beta^+$), CD8 (TCR$\beta^+$ CD4$^-$ CD8$^+$), CD4 (TCR$\beta^+$ CD4$^+$ CD8$^-$), cCD4 (conventional CD4, TCR$\beta^+$ CD4$^+$ CD25$^-$) and CD25$^+$ CD4 T-cells (TCR$\beta^+$ CD4$^+$ CD25$^+$).

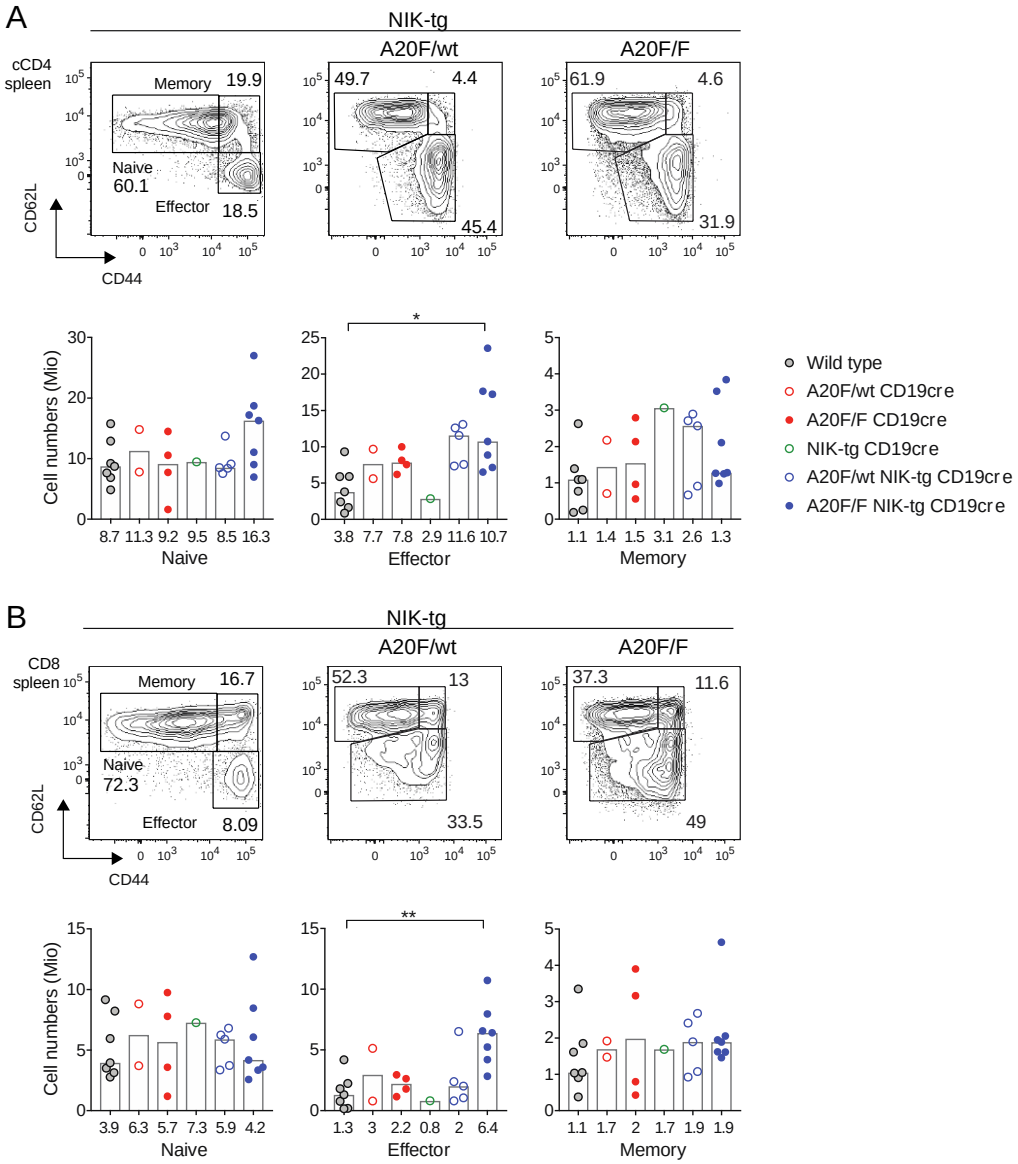


**Figure 19. A20F/F NIK-tg CD19cre mice have an effector-like T-cell phenotype**

*Ex vivo* analysis of T-cell activation in spleen of young mice using flow cytometry. Contour plots depict percentages and bar charts indicate total cell numbers for naïve-like, effector-like and memory-like activation status in (A) conventional CD4 and (B) CD8 T-cells. All flow cytometry plots are representative of at least 2 experiments, except for the NIK-tg CD19cre mice. The NIK-tg CD19cre contour plots do not belong to the same experiment as A20-deficient NIK-tg CD19cre plots. Bar charts depict medians and the values are indicated below each histogram. Statistical analysis was done using One-way ANOVA (* $p<0.05$, ** $p<0.01$).
cCD4 (conventional CD4, TCR$\beta^+$ $CD4^+$ $CD25^-$), CD8 (TCR$\beta^+$ $CD8^+$), naïve ($CD62L^+$ $CD44^-$), effector ($CD62L^-$ $CD44^+$) and memory ($CD62L^+$ $CD44^+$).

There is another CD4 T-cell subset that is required for the GC reaction. Follicular helper T-cells ($T_{FH}$), defined by a high expression of CXCR5, PD1 and BCL6, as their name suggest help B-cells by secreting IL-6 and IL-21. In spleens of young mice, the

percentage of PD1$^{high}$ CXCR5$^{high}$ CD4 T-cells, reminiscent of $T_{FH}$ cells, increases in an A20 loss dependent manner in NIK-tg compound mice (Figure 20A), in spite of the few GC B-cells present in these mice (Figure 11A and C). Moreover, the total number of PD1$^{high}$ CXCR5$^{high}$ CD4 T-cells in spleen of A20F/F NIK-tg CD19cre mice is significantly higher than in wild type ($p<0.01$) and A20F/wt NIK-tg CD19cre mice (Figure 20B). Preliminary results show that these PD1$^{high}$ CXCR5$^{high}$ CD4 T-cells present a higher expression of the transcription factor BCL6 (Figure S 9) suggesting that they are actually $T_{FH}$ and not simply T-cells that have up-regulated PD1 expression. However, further experiments need to be performed to confirm their $T_{FH}$ phenotype.

Taken all together, loss of A20 and overexpression of NIK in B-cells leads to an activated T-cell phenotype in cCD4 and particularly in CD8 T-cells. Moreover, there is an expansion of CD25$^{+}$ CD4 regulatory T-cells and potentially $T_{FH}$ in these mice. Given the strong antigen presenting cell-like phenotype observed in eGFP+;A20-/-;NIK+ B-cells (Figure 16), the observed reduced B-cell numbers could be a result of T-cell dependent clearance of these cells.

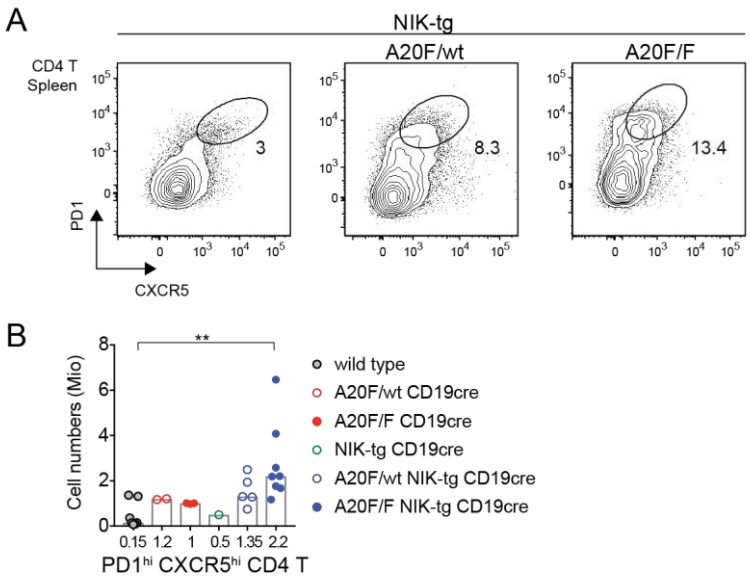


**Figure 20. PD1$^{hi}$ CXCR5$^{hi}$ CD4 T cells reminiscent of $T_{FH}$ cells are expanded in A20F/F NIK-tg CD19cre mice**

*Ex vivo* analysis of follicular helper T-cells in spleens of young mice using flow cytometry. (A) Flow cytometry contour plots depict the percentage and (B) bar chart show the number of PD1$^{hi}$ CXCR5$^{hi}$ CD4 T-cells. All flow cytometry plots are representative of at least 2 experiments, except for the NIK-tg CD19cre mice. Bar charts depict medians and the values are indicated below each histogram. Statistical analysis was done using Kruskal-Wallis (¥¥ $p<0.01$).
$T_{FH}$ (follicular helper T-cells, TCRb$^{+}$ CD4$^{+}$ PD1$^{hi}$ CXCR5$^{hi}$).

### IV.1.8.2 PD1 positive exhausted-like phenotype in CD8 T-cells in spleens of A20F/F NIK-tg CD19cre mice

To further characterize the activation of cCD4 and CD8 T-cells in spleens of A20F/F NIK-tg CD19cre animals, I decided to analyse the expression of the proteins ICOS and PD1, both markers for T-cell activation and exhaustion. In spleens of young mice the additional expression of the NIK-tg in A20+/- B-cells leads to a subpopulation of CD4 T-cells with a higher ICOS and PD1 surface expression levels (Figure 21A, upper panels). On the other hand, the additional expression of NIK-tg in A20-/- B-cells results in CD4 T-cells with similar ICOS expression while a higher PD1 expression (Figure 21A, lower panels). However, the higher percentage of PD1 positive CD4 T-cells in A20F/F NIK-tg CD19cre mice partially corresponds to the higher $T_{FH}$ numbers observed in these animals (Figure 20).

The *ex vivo* flow cytometry analysis of CD8 T-cells in spleens from young mice showed an increase in PD1 expression in response to biallelic loss of A20 in B-cells, which is intensified in the presence of NIK expression (Figure 21B, lower panel) but absent in the A20F/wt compound mice. The percentage of PD1 high CD8 T-cells is significantly higher for A20F/F NIK-tg CD19cre mice compared to the A20F/wt and A20F/F CD19cre controls. This translates into a significant 19-fold increase in PD1 positive CD8 T-cell numbers in A20F/F NIK-tg CD19cre mice compared to wild type and A20F/wt NIK-tg CD19cre mice (Figure 21B). Moreover, there is a small increase in the expression of ICOS in CD8 T-cells in response to A20-/- or A20-/-;NIK+ B-cells, absent in A20F/wt compound mice.

Mice with A20-deficient;NIK+ B-cells have a higher activation in T-cells. In A20F/F NIK-tg CD19cre mice, both CD4 and CD8 T-cells show higher PD1 *ex vivo* expression levels compared to the other compound mice analysed. The expression of PD1 in CD8 T-cells has been reported as a marker for T-cell exhaustion[253], pointing to a possible exhausted phenotype in the effector-like CD8 T-cells expansion observed in the A20F/F NIK-tg CD19cre mice.

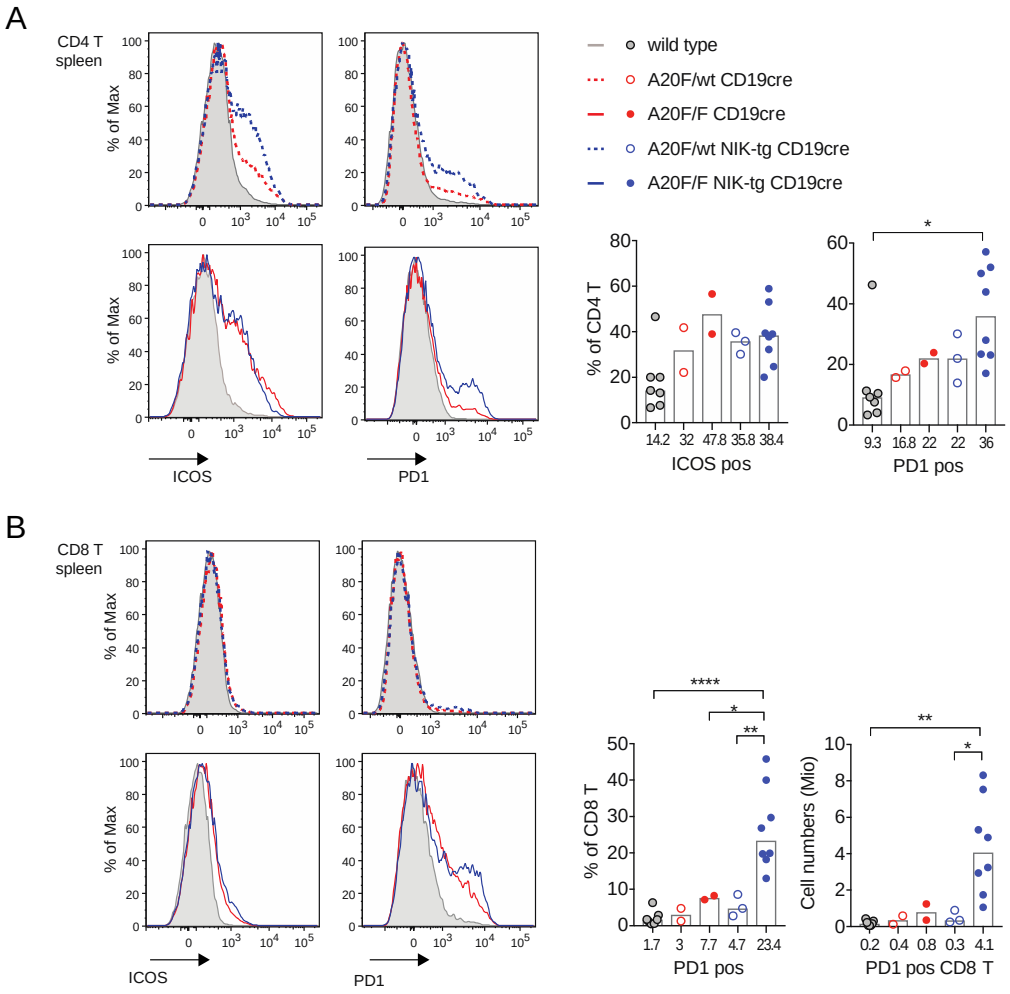


**Figure 21. CD8 T-cells in A20F/F NIK-tg CD19cre mice have an exhausted phenotype**

Flow cytometry analysis of ICOS and PD1 *ex vivo* expression in T-cells from spleen of young mice. Histograms depict the expression of ICOS and PD1 and bar charts indicate the percentage or cell numbers of positive cells in (A) CD4 and (B) CD8 T-cells. Flow cytometry histograms are representative of at least 2 experiments. Bar charts depict medians and the values are indicated below each histogram. Statistical analysis was done using One-way ANOVA (* p<0.05, ** p<0.01, **** p<0.0001).
CD4 T (TCRb$^+$ CD4$^+$ CD8$^-$) and CD8 T (TCRb$^+$ CD4$^-$ CD8$^+$).

### IV.1.8.3 The expansion of CD25$^+$ CD4, effector-like CD4 and effector-like CD8 T-cells is systemic in A20F/F NIK-tg CD19cre mice

After identifying the expansion of several T-cell populations in A20F/F NIK-tg CD19cre mice, I proceeded to investigate the different T-cell populations in the bone marrow and the LN, to determine if this T-cell phenotype was systemic or localized to the spleen.

In the bone marrow of young mice, there is a significant two-fold increase in *ex vivo* T-cell numbers in the A20F/F NIK-tg CD19cre mice compared to both A20F/wt NIK-tg

CD19cre mice and wild type aged matched controls (Figure S 10A). Additionally, the total number of *ex vivo* cCD4 T-cells as well as CD8 and $CD25^+$ CD4 T-cells are increased in the A20F/F NIK-tg CD19cre mice compared to controls (Figure S 10B). First, there is a two-fold increase in the number of cCD4 T-cells in A20F/F NIK-tg CD19cre mice compared to wild type control and A20F/wt NIK-tg CD19cre mice. Second, there is a small increase in the number of CD8 T-cells, although not statistically significant (Figure S 10B). Finally, there is a significant three-fold increase in $CD25^+$ CD4 T-cells as consequence of the loss of the second allele of A20 in NIK-tg B-cells (Figure S 10B).

*Ex vivo* flow cytometry analysis of cCD4 T-cells in the bone marrow, revealed that the number of effector-like CD4 T-cell numbers in A20F/F NIK-tg CD19cre mice is significantly higher compared to controls (Figure S 10C). However, the number of naïve- and memory-like cCD4 T-cells is similar to that of A20F/wt NIK-tg CD19cre animals, and lower than that observed for the wild type controls (Figure S 10C).

Similarly, the number of effector-like CD8 T-cells in A20F/F NIK-tg CD19cre mice is significantly increased compared to controls (Figure S 10D). Moreover, the numbers of naïve- and memory-like CD8 T-cells are also similar to that of A20F/wt NIK-tg CD19cre mice and lower that wild type controls (Figure S 10D).

In the LN of young mice, there is also a significant two-fold increase in total *ex vivo* T-cell numbers in A20F/F NIK-tg CD19cre mice compared to wild type controls (Figure S 11A). This increase is accompanied by a significant increase in CD4 T-cells and to a lesser extent in CD8 T-cells (Figure S 11B). Additionally, the *ex vivo* flow cytometry analysis of CD4 T-cells in the lymph nodes revealed a significant increase in $CD25^+$ T-cells in the A20F/F NIK-tg CD19cre mice compared to the A20F/wt NIK-tg CD19cre mice (Figure S 12A). Moreover, although the majority of cCD4 and CD8 T-cells were in a naïve-like state, there was a significant increase in the number of effector-like cCD4 and CD8 T-cells in the A20F/F NIK-tg CD19cre mice (Figure S 12B and C).

Therefore, compared to NIK-tg and A20wt/- NIK-tg B-cells, the loss of two alleles of A20 in NIK-tg expressing B-cells leads to an expansion of $CD25^+$ CD4 T-cells and effector-like cCD4 and CD8 T-cells in the bone marrow, accompanied by a similar phenotype in the LN.

#### IV.1.8.4 The myeloid compartment is not affected by the combination of loss of A20 and overexpression of NIK-tg in B-cells

Given the expanded T-cells populations observed in the different lymphoid organs, I proceeded to analyse the myeloid populations in these mice. Myeloid cells are antigen presenting cells and produce cytokines that can modulate B- and T-cells responses. It is already known ablation of A20 in B-cells leads to an expansion of myeloid cells [79].

The *ex vivo* analysis of myeloid cells in the spleens of young mice revealed a significant increase in the percentage of monocytes in spleens of A20F/F NIK-tg CD19cre mice compared to the A20F/wt NIK-tg CD19cre mice (Figure S 13A). Furthermore, there was a small increase in the percentage of neutrophils and dendritic cells in A20F/F NIK-tg CD19cre mice compared to wild type control (Figure S 13A). While the percentage of eosinophils was similar for all mice analysed.

The slightly increased percentage of myeloid cells in spleens of A20F/F NIK-tg CD19cre mice, however, was not reflected by the number of myeloid cells. In the A20F/F NIK-tg CD19cre mice there was a tendency for slightly higher numbers of dendritic cells, monocytes and neutrophils compared to controls (Figure S 13B), but this increase did not reach statistical significance. Moreover, the loss of A20 alone in B-cells is sufficient to elicit a similar phenotype ([79] and Figure S 13B). Thus in the bone marrow of young mice the total numbers of the different myeloid cells are constant for all the different genotypes analysed (Figure S 13C).

In young mice, the reduced B-cell numbers and exhausted T-cell phenotype observed A20F/F NIK-tg CD19cre mice seems to be independent of the myeloid compartment. The small increase observed in neutrophils and monocytes in these mice phenocopies the increase in neutrophils and monocytes observed in A20F/F CD19cre mice, therefore most likely is A20 dependent.

### IV.1.9 EFFECT OF LOSS OF A20 IN COMBINATION WITH ALTERNATIVE NF-κB ACTIVATION IN B-CELLS IN AGED MICE

Initially the basis of this project was to combine loss of A20 and activation of the alternative NF-κB pathway, by overexpressing NIK, in B-cells, to evaluate whether this predisposes them to splenic marginal zone lymphoma in mice. For that purpose, a

cohort of mice was aged over 400 days and monitored for any signs or symptoms of disease. After the animals reached 400 days they were analysed by flow cytometry.

#### IV.1.9.1 Reduced A20-/-;NIK+ B-cell pool is maintained in aged animals

In young mice, the combination of homozygous loss of A20 with activation of the alternative NF-κB pathway, by over expression of NIK, in B-cells leads to reduced B-cell numbers in spleen and other secondary lymphoid organs.

In aged mice, the homozygous loss of A20 in B-cells leads to larger spleens compared to CD19cre controls (Figure 19A). On the other hand, the over expression of NIK in B-cells leads to spleens similar in size as controls. Combining loss of A20 and overexpression of NIK in B-cells leads to an A20-loss dose dependent increase in both spleen mass and cellularity (Figure 22A).

The *ex vivo* analysis of spleens of aged mice revealed that the observed reduced B-cell numbers in young A20F/F NIK-tg CD19cre mice are maintained in old age (Figure 22B). Both the over expression of NIK in B-cells, as well as the loss of A20 in B-cells, leads to a two-fold increase in B-cell numbers in spleens of aged mice compared to CD19cre controls (Figure 22C). Combining the heterozygous loss of A20 with overexpression of NIK in B-cells leads to a two-fold increase in B-cell numbers compared to the NIK-tg CD19cre mice (over three-fold increase from CD19cre controls) (Figure 22C). However, the additional inactivation of the second allele of A20 leads to reduced B-cell percentages (Figure 22B) and numbers similar to the CD19cre control mice (Figure 22C).

The expression of the NIK-tg can be followed through expression of the eGFP reporter. The e*x vivo* flow cytometry analysis splenic B-cells shows that 90 to 95% of NIK+ and A20+/-;NIK+ B-cells express eGFP, compared to only 60% of the GFP positive A20-/-;NIK+ B-cells (Figure 22D). In spleens of aged mice, there is a two-fold increase in eGFP+;A20+/-;NIK+ B-cell numbers compared to eGFP+;NIK+ B-cells. While the loss of the second allele of A20 leads to significant 75% reduction in eGFP positive B-cell numbers compared to the eGFP+;A20+/-;NIK+ B-cells (Figure 22E). At the same time, the number of eGFP-;A20-/-;NIK+ B-cells is significantly increased in spleens of A20F/F NIK-tg CD19cre aged mice compared to other NIK compound mice (Figure 22E).

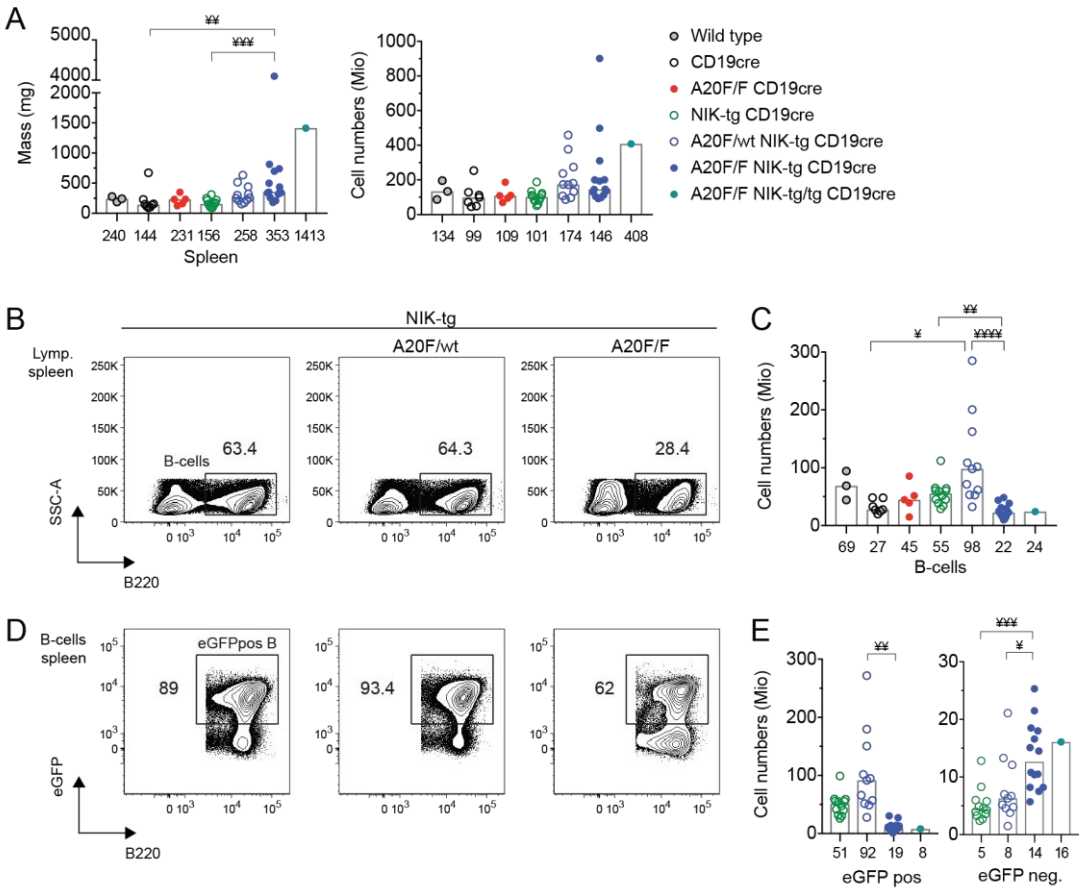


**Figure 22. Reduced B-cell numbers are maintained in A20F/F NIK-tg CD19cre mice**

*Ex vivo* analysis of B-cells in spleens from aged mice using flow cytometry. (A) Spleen mass and splenocytes numbers. Flow cytometry contour plots depict the percentages and bar charts indicate the numbers for (B, C) B-cells and (D, E) eGFP reporter expression in B-cells. All flow cytometry plots are representative of at least 2 experiments, except for the A20F/F NIK-tg/tg CD19cre mice. Bar charts depict medians and the values are indicated below each histogram. Statistical analysis was done using Kruskal-Wallis (¥ $p<0.05$, ¥¥ $p<0.01$, ¥¥¥ $p<0.001$, ¥¥¥¥ $p<0.0001$).
eGFP (enhanced green fluorescent protein), pos. (positive), neg. (negative), B-cells ($B220^+$), eGFP pos ($B220^+$ $eGFP^+$), eGFP neg ($B220^+$ $eGFP^-$)

Loss of A20 combined with activation of the alternative NF-κB signalling leads to a more aggressive B-cell phenotype. Although I only aged and analysed one $A20^{F/F}$ $NIK\text{-}tg^{I/I}$ $CD19cre^{I/wt}$ (from now on referred to as A20F/F NIK-tg/tg CD19cre) mouse, the B-cell phenotype observed is magnified. This one animal had a larger spleen than the median spleen mass for the A20F/F NIK-tg CD19cre mice and presented high cellularity (Figure 22A). Moreover, this mouse presented reduced B-cell numbers comparable to that of the A20F/F NIK-tg CD19cre mice (Figure 22C). Finally, the total number of eGFP positive B-cells was 50% lower than the median value observed in eGFP+;A20-/-;NIK+ B-cells, and

the total number of eGFP negative B-cells was similar to that of eGFP-;A20-/-;NIK+ B-cells (Figure 22E).

In summary, strong activation of the alternative NF-κB pathway in B-cells leads to B-cell hyperplasia in young and old age. Similarly, activation of the canonical NF-κB pathway in B-cells by inactivation of A20, a negative regulator, also leads to B-cell hyperplasia in aged mice. Moreover, the combination of heterozygous loss of A20 with over expression of NIK, leads to exacerbated B-cell hyperplasia in young and old mice. However, the additional inactivation of the second allele of A20 leads to reduced B-cell numbers in young and aged animals.

#### IV.1.9.2 The T-cell activated phenotype is maintained in aged A20F/F NIK-tg CD19cre mice

In young mice, the loss of A20 combined with the overexpression of NIK in B-cells leads to a T-cell hyperplasia that affects mainly $CD25^+$ CD4 regulatory T-cells, as well as effector-like CD4 and CD8 T-cells.

In spleen of aged mice, there is a clear increase in the percentages of *ex vivo* T-cells in A20F/F NIK-tg CD19cre mice compared to other NIK compound mice (Figure 23A). Moreover, this translates in significant higher T-cell numbers in the spleen compared to NIK-tg CD19cre control mice (Figure 23C).

The analysis of the different T-cells subpopulations in the spleen of aged mice was consistent with the phenotype observed in young mice. The $CD25^+$ CD4 regulatory T-cells in A20F/F NIK-tg CD19cre mice are present in higher percentages and higher cell numbers than in A20F/wt NIK-tg CD19cre or NIK-tg CD19cre mice (Figure 23B and D). The increase in CD25+ CD4 regulatory T-cells is accompanied by a reduction in cCD4 T-cell percentages (Figure 23B), however this is not reflected in the cCD4 T-cell numbers. Although the differences are not statistically significant, the A20F/F NIK-tg CD19cre mice have higher cCD4 T-cell numbers compared to the NIK-tg CD19cre mice, while the A20 F/wt NIK-tg CD19cre have intermediate numbers (Figure 23D).

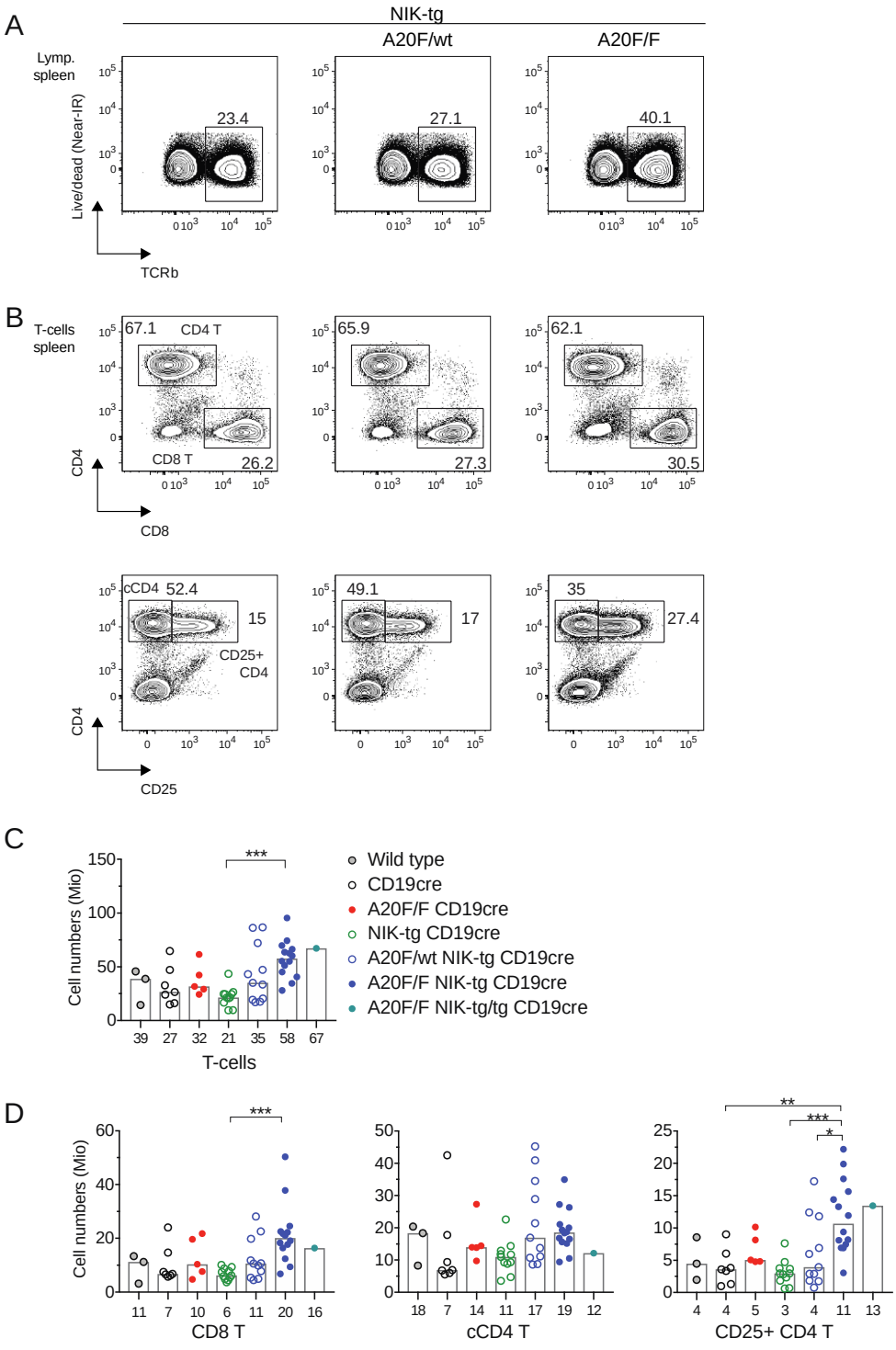


**Figure 23. T-cell hyperplasia is maintained in aged A20F/F NIK-tg CD19cre mice**

*Ex vivo* analysis of T-cells from spleens of aged mice using flow cytometry. Contour plots depict percentages and bar charts indicate cell numbers for (A, C) T-cells and (B, D) CD8 T, cCD4 T and CD25$^{+}$ CD4 T-cell subsets. All flow cytometry plots are representative of at least 2 experiments, except for the A20F/F NIK-tg/tg CD19cre mice. Bar charts depict medians and the values are indicated below each histogram. Statistical analysis was done using One-way ANOVA (* $p<0.05$, ** $p<0.01$, *** $p<0.001$).

Figure 23 **(continued).** T-cells (TCRβ$^+$), CD8 T (TCRβ$^+$ CD8$^+$), CD4 T (TCRβ$^+$ CD4$^+$), cCD4 T (conventional CD4, TCRβ$^+$ CD4$^+$ CD25$^-$) and CD25$^+$ CD4 T (TCRβ$^+$ CD4$^+$ CD25$^-$).

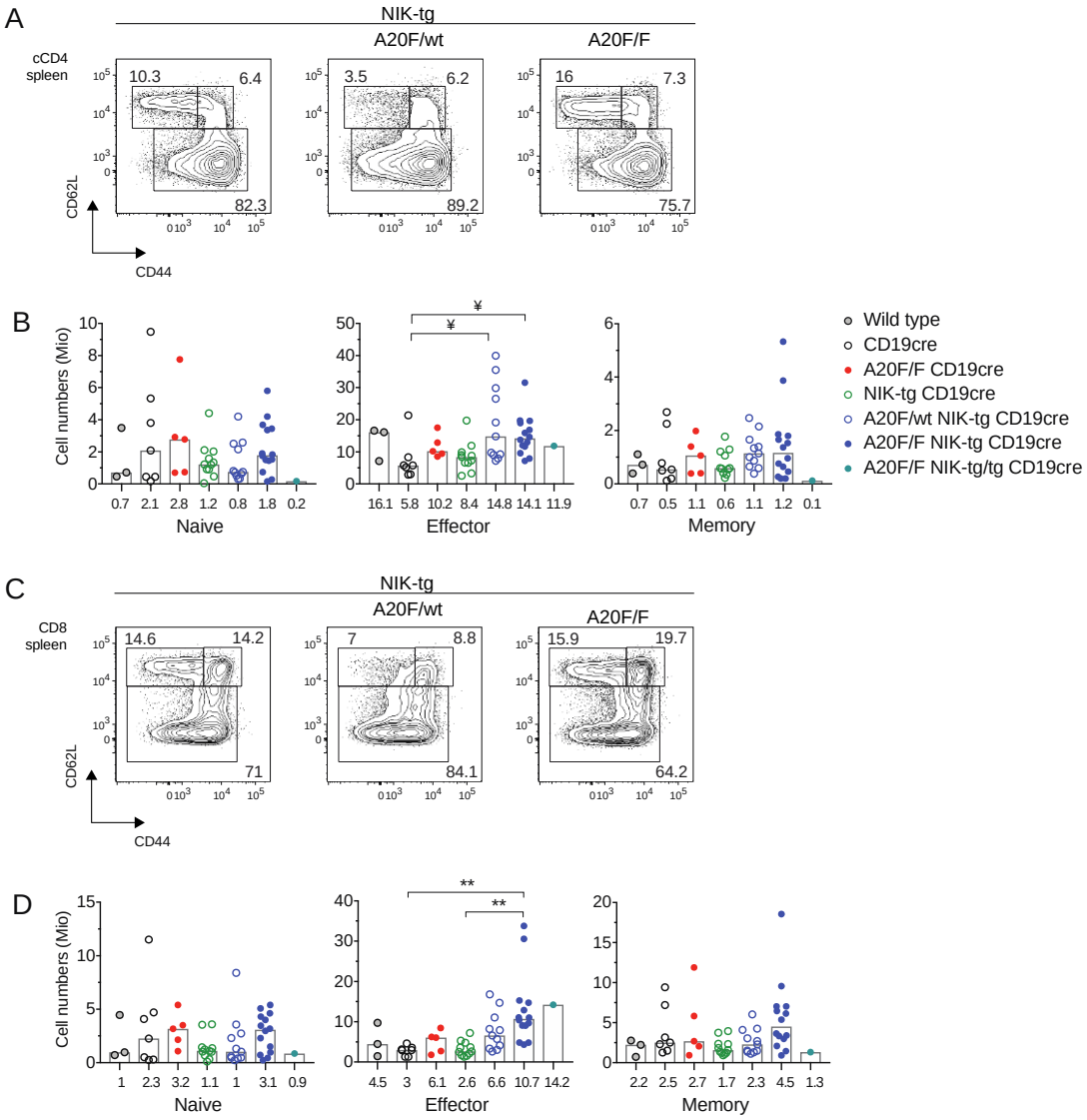


**Figure 24. Effector-like T-cells are expanded in aged A20F/F NIK-tg CD19cre mice**

*Ex vivo* analysis of T-cell activation in spleens from aged mice using flow cytometry. Contour plots depict the percentage of naïve-like, effector-like and memory-like cells and bar charts indicate cell numbers for (A) cCD4 and (B) CD8 T-cells. All flow cytometry plots are representative of at least 2 experiments, except for the A20F/F NIK-tg/tg CD19cre mice. Bar charts depict medians and the values are indicated below each histogram. Statistical analysis was done using One-way ANOVA (** p<0.01) or Kruskal-Wallis (¥ p<0.05).

cCD4 (conventional CD4, TCRβ$^+$ CD4$^+$ CD25$^-$), CD8 (TCRβ$^+$ CD8$^+$), Naïve (CD62L$^+$ CD44$^-$), Effector (CD62L$^-$ CD44$^+$) and Memory (CD62L$^+$ CD44$^+$).

In spleens of aged mice the percentages of CD8 T-cells increased slightly as A20 is lost in NIK-tg CD19cre compound mice (Figure 23B). However this translates into a clear expansion of CD8 T-cells in the A20F/F NIK-tg CD19cre mice (Figure 23D), while the NIK-tg CD19cre have similar CD8 T-cell numbers as the CD19cre controls. Interestingly, the additional loss of one allele of A20 leads to an intermediate phenotype in CD8 T-cell numbers (Figure 23D).

*Ex vivo* flow cytometry analysis of cCD4 T-cells in the spleen of aged mice revealed a similar increase in effector-like CD4 T-cells in A20F/F NIK-tg CD19cre and A20F/wt NIK-tg CD19cre mice compared to controls (Figure 24A and B). Even though not significant, these mice also presented with higher numbers of memory-like CD4 T-cells than the NIK-tg CD19cre controls (Figure 24B).

Likewise, the number of *ex vivo* effector-like CD8 T-cells in A20F/F NIK-tg CD19cre aged mice is significantly increased compared to NIK-tg CD19cre controls (Figure 24D). Again, in mice with A20+/-;NIK+ B-cells, the numbers of CD8 effector-like T-cells are intermediate between the A20F/F NIK-tg CD19cre and the NIK-tg CD19cre mice. Finally, there is an increase in naïve- and memory-like CD8 T-cells numbers in A20F/F NIK-tg CD19cre mice compared to controls (Figure 24D).

Additionally, the one A20F/F NIK-tg/tg CD19cre mouse analysed presented with a similar T-cell phenotype to the A20F/F NIK-tg CD19cre mice. This mouse presented increased T-cell numbers and increased $CD25^+$ CD4 regulatory T-cell numbers comparable to the A20F/F NIK-tg CD19cre mice (Figure 23C and D). Furthermore, most of the cCD4 and CD8 T-cells had an effector-like phenotype (Figure 24B and E).

Therefore, in aged mice the presence of A20-deficient;NIK+ B-cells is accompanied by T-cell hyperplasia that affects all T-cell subsets, similarly to young mice. The elevated *ex vivo* effector-like cCD4 and CD8 T-cell numbers present in these mice suggest a sustained activation of these T-cells during the mouse life.

### IV.1.9.3 Myeloid expansion in aged A20F/F NIK-tg CD19cre mice

In young mice the loss of A20 in combination with the overexpression of NIK has no evident effect on the myeloid populations. Nonetheless, it is in aged the A20F/F CD19cre mice that the myeloid expansion is stronger.[79, 254] Therefore, I decided to characterise myeloid cells in the spleen of aged mice.

The *ex vivo* flow cytometry analysis of spleens from aged mice revealed an expansion of myeloid cells in A20F/F NIK-tg CD19cre mice. There is a tendency for higher myeloid percentages and cell numbers correlating with increasing loss of A20 alleles. The main myeloid population that is affected are the neutrophils. There is a significant four-fold expansion of neutrophil percentages in the A20F/F NIK-tg CD19cre mice compared to both the A20F/wt NIK-tg CD19cre and NIK-tg CD19cre mice (Figure 25B). This expansion translates into a significant five-fold increase of neutrophil cell numbers compared to A20F/wt NIK-tg CD19cre mice (Figure 25A). Second, there is a significant two to three-fold increase in monocyte percentages and a three to four-fold increase in cell numbers in the A20F/F NIK-tg CD19cre mice compared to other NIK-tg mice (Figure 25A and B). Third, there is an increase in eosinophil percentages that translates into a significant two-fold expansion of eosinophils in A20F/F NIK-tg CD19cre mice compared to compound NIK-tg mice. Fourth, there is also a significant increase in the percentage of dendritic cells that translates into a four-fold expansion in cell numbers in the A20F/F NIK-tg CD19cre mice compared to NIK-tg CD19cre aged mice. Moreover, the A20F/wt NIK-tg CD19cre mice already had a significant increase in dendritic cell numbers compared to NIK-tg CD19cre controls (Figure 25A).

Interestingly, the only A20F/F NIK-tg/tg CD19cre mouse analysed has higher dendritic and eosinophil cell numbers compared to the A20F/F NIK-tg CD19cre aged mice. Therefore, this late onset of myeloid expansion could be a long term phenotype arising from B-cell signals with strong aberrant NF-κB activation.

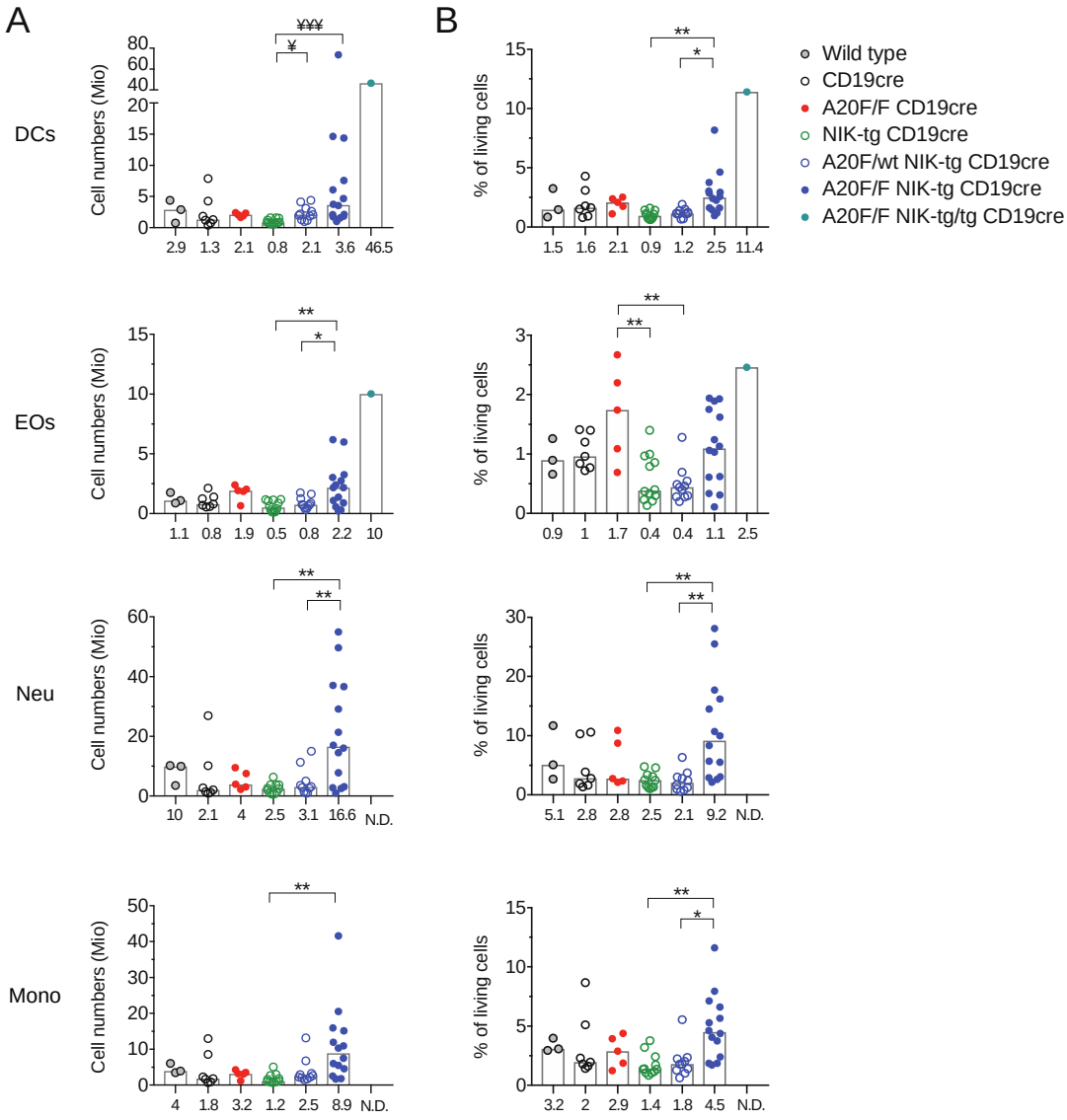


**Figure 25. Myeloid cell expansion in aged A20F/F NIK-tg CD19cre mice**

*Ex vivo* analysis of myeloid cells in spleens from aged mice using flow cytometry. Bar charts show (A) cell numbers and (B) percentages of the different myeloid cells. Bar charts depict medians and the values are indicated below each histogram. Statistical analysis was done using One-way ANOVA (* $p<0.05$, ** $p<0.01$) or Kruskal-Wallis (¥ $p<0.05$, ¥¥¥ $p<0.001$).
DC (dendritic cells, $CD11c^+$), EOs (eosinophils, $CD11c^+$ $CD11b^+$ $SiglecF^{hi}$ $F4/80^{hi}$); Mono (monocytes, $CD11c^+$ $CD11b^+$ $SiglecF^{lo}$ $F4/80^{hi}$ $Gr1^{int}$) and Neu (neutrophils, $CD11c^+$ $CD11b^+$ $SiglecF^{lo}$ $F4/80^{lo}$ $Gr1^{hi}$).

#### IV.1.9.4 NK and NKT cells in aged mice

The presence of B-cells that have activated both the canonical and the alternative NF-κB pathways in aged mice leads to the development of T-cell hyperplasia that is accompanied by a myeloid expansion. In some instances, the aged A20F/F NIK-tg CD19cre mice develop gut inflammation that results in bleeding. To exclude the possibility of an autoimmune phenotype, I analysed a small cohort of aged mice for the presence of natural killer cells (NK) and natural killer T-cells (NKT).

In spleen of aged mice, the percentage of *ex vivo* NK cells in A20F/F NIK-tg CD19cre mice did not differ from that of control mice (Figure S 14A-C). The total number of NK cells observed is similar for all mice except the A20F/F CD19cre animals (Figure S 14D). Additionally, the percentage of *ex vivo* NKT cells observed in A20F/F NIK-tg CD19cre mice is higher than that of the A20F/wt NIK-tg CD19cre mice, but not significantly different from the controls (Figure S 14C). Moreover, the number of NKT cells in the A20F/F NIK-tg CD19cre animals was two-fold higher than that of the A20F/wt NIK-tg CD19cre mice, but similar to the controls. The A20F/F CD19cre mouse also had lower numbers of NKT cells.

Therefore, the reduced B-cell numbers observed in young and aged A20F/F NIK-tg CD19cre mice are not a consequence of an innate immune response associated with NK or NKT cells.

## IV.2 ROLE OF CANONICAL NF-κB IN B-CELL TRANSFORMATION

Canonical NF-κB target genes are involved in proliferation and cell survival, however to date there is no clear evidence that canonical NF-κB activation alone results in B-cell lymphomagenesis [37]. Therefore, I wanted to address the role of canonical NF-κB signalling in driving B-cell lymphomagenesis.

In order to constitutively activate the canonical NF-κB pathway specifically in B-cells I made use of the available conditional mouse strain $R26^{LSL}$-Ikk2ca and the CD19cre mouse strain. The constitutive activation of the canonical NF-κB pathway can be induced by the gain of one or two alleles of a conditional constitutive active mutant of the IKK2/IKK-β subunit (IKK2ca) knocked into ROSA26 locus [37]. For that purpose I used the $R26^{LSL}$-Ikk2ca mouse strain that expresses IKK2ca after Cre-mediated excision of the loxP-flanked STOP cassette either heterozygously ($R26^{LSL}$-$Ikk2ca^{I/wt}$) or homozygously ($R26^{LSL}$-$Ikk2ca^{I/I}$). B-cells that express the IKK2ca knock-in after Cre-mediated recombination will also express the eGFP reporter, located after an IRES sequence 3' of the IKK2ca cDNA, thus allowing the identification of recombined cells by flow cytometry. To conditionally activate my gene of interest specifically in B-cells, I used the CD19cre mouse strain heterozygously ($CD19cre^{I/wt}$) [241]. As mentioned before, this mouse strain expresses the Cre recombinase as a knock-in under the control of the CD19 promoter instead of the endogenous CD19; the resulting $CD19cre^{I/wt}$ mice are heterozygous knockout for CD19 and express the Cre recombinase.

### IV.2.1 CANONICAL NF-κB PROMOTES B1A CELL DEVELOPMENT

It has already been described in young mice that constitutive canonical NF-κB activation in B-cells by the conditional expression of one copy ($R26^{LSL}$-$Ikk2ca^{I/wt}$ $CD19cre^{I/wt}$, from now on referred to as R26-IKK2ca CD19cre) or two copies of the knock-in IKK2ca ($R26^{LSL}$-$Ikk2ca^{I/I}$ $CD19cre^{I/wt}$ from now on referred to as R26-IKK2ca/ca CD19cre) present enlarged spleens and B-cell hyperplasia [37] in a dose dependent manner (Figure S 16). Additionally, constitutive canonical NF-κB activation promotes expansion of the B1 lineage in these mice, affecting mainly the B1a subset but B1b subset in same cases (Figure S 17). This B1a expansion is not limited to the peritoneum, but can also be observed in the spleen of young mice, where the R26-IKK2ca/ca CD19cre mice present a significant 15-fold increase in B1a cell numbers compared to CD19cre controls and R26-

IKK2ca CD19cre mice (Figure S 18). Therefore, constitutive canonical NF-κB activation leads to B-cell hyperplasia and to the expansion of B1a-cells.

### IV.2.2 CONSTITUTIVE CANONICAL NF-κB ACTIVATION IN B-CELLS DRIVES B-CELL EXPANSION RESEMBLING SMALL LYMPHOCYTIC LYMPHOMA IN AGED MICE

In young mice, constitutive canonical NF-κB activation leads to the expansion of the B1a subset. In order to study the role of constitutive NF-κB activation in B-cell lymphomagenesis, mice were aged and monitored for the development of B-cell malignancies. With age, constitutive canonical NF-κB activation leads to the progressive accumulation of B1a cells in the lymphoid organs in mice reminiscent of chronic lymphocytic leukaemia in mice. To further characterize this B1a expansion, aged mice conditionally expressing the IKK2ca knock in in B-cells were compared to the already established model for murine CLL, Eμ-TCL1tg {Bichi:2002fc}. In this part of the results I will first describe the role of constitutive canonical activation in B-cell lymphomagenesis. Second, I will compare the results from the aged IKK2ca cohort with the TCL1tg mice.

#### IV.2.2.1 Constitutive canonical NF-κB activation in B-cells drives a CD5$^+$ B-cell expansion in aged mice

In order to address the role of constitutive NF-κB activation in B-cell lymphomagenesis a cohort of mice was aged in order to monitor development of disease. Interestingly, expression of IKK2ca in B-cells led to a dose-dependent reduction in life-span in mice: R26-IKK2ca CD19cre mice presented a median survival of 476 days, compared to 351 days for the R26-IKK2ca/ca CD19cre mice (Figure 26A). Therefore, the constitutive activation of NF-κB in B-cells leads to a reduced median survival in aged mice compared to CD19cre control mice (Figure 26A), linking the activation of NF-κB in B-cells with a shorter life-span.

The analysis of nine-months or older R26-IKK2ca compound mice revealed slightly enlarged livers that were infiltrated with lymphocytes (Figure 26B and data not shown). Similarly, spleens were significantly enlarged in an IKK2ca dose dependent manner with a two-fold and four-fold mass increase in the R26-IKK2ca CD19cre and R26-IKK2ca/ca CD19cre mice, respectively (Figure 26B).

*Ex vivo* flow cytometry analysis of spleens from aged mice showed that the B-cell hyperplasia observed at young age is maintained throughout the life of the animal (Figure 26C). Interestingly, a substantial percentage of B-cells in the spleens of R26-IKK2ca/ca CD19cre mice is phenotypically similar to the B1a subset (Figure 26D and Figure S 19). While R26-IKK2ca CD19cre spleens showed a two-fold increase in B1a-like cells compared to CD19cre controls, R26-IKK2ca/ca CD19cre spleens had a significant 19-fold and 59-fold increase in B1a-like cell numbers compared to R26-IKK2ca CD19cre and CD19cre control mice respectively (Figure 26C, D and Figure S 19). On the other hand, there was a significant two-fold increase in B2-cells in both R26-IKK2ca/ca CD19cre and R26-IKK2ca CD19cre mice compared to CD19cre controls in spleen (Figure S 19).

Similarly, the long term effect of constitutive canonical NF-κB activation in B-cells resulted in a significant dose dependent increase in cellularity in the peritoneal cavity in aged mice compared to CD19cre controls (Figure 27A). Moreover, a small number of cases additionally presented with fluid in the peritoneal cavity (4 out of 14). Finally, the expression of the IKK2ca knock-in in B-cells resulted in a significant dose dependent increase of total B-cell and B1a cell numbers in the peritoneum of aged mice (Figure 27).

Moreover, in 10-12 months aged R26-IKK2ca/ca CD19cre mice B1a-like cells can be detected in the draining inguinal, axillary, and superficial cervical lymph nodes (Figure 28 and Figure S 20) and to a lesser extent in the mesenteric lymph nodes (Figure S 21). The expression of the IKK2ca knock-in specifically in B-cells leads to aged mice with enlarged lymph nodes accompanied by a significant increase in cellularity and B-cell numbers in a dose dependent manner compared to CD19cre control mice (Figure 28A). There is a significant four-fold and 13-fold increase in B-cell numbers in the lymph nodes of the R26-IKK2ca CD19cre and R26-IKK2ca/ca CD19cre mice (Figure 28B and C). Moreover, constitutive canonical NF-κB in B-cells leads to a dose dependent increase in B2-cell numbers. Additionally, there is an infiltration of B1a-like cells and to a lesser extent B1b-cells in the draining lymph nodes (Figure 28D, E and Figure S 20).

Likewise, constitutive canonical NF-κB activation in B-cells leads to significantly enlarged mLN with higher number of B-cells, particularly in the R26-IKK2ca/ca CD19cre mice (Figure S 21A and B). Moreover, although a few R26-IKK2ca CD19cre mice present an infiltration of B1a-like cells in the mLN, in the R26-IKK2ca/ca CD19cre aged mice this infiltration is more prominent (Figure S 21D and E).

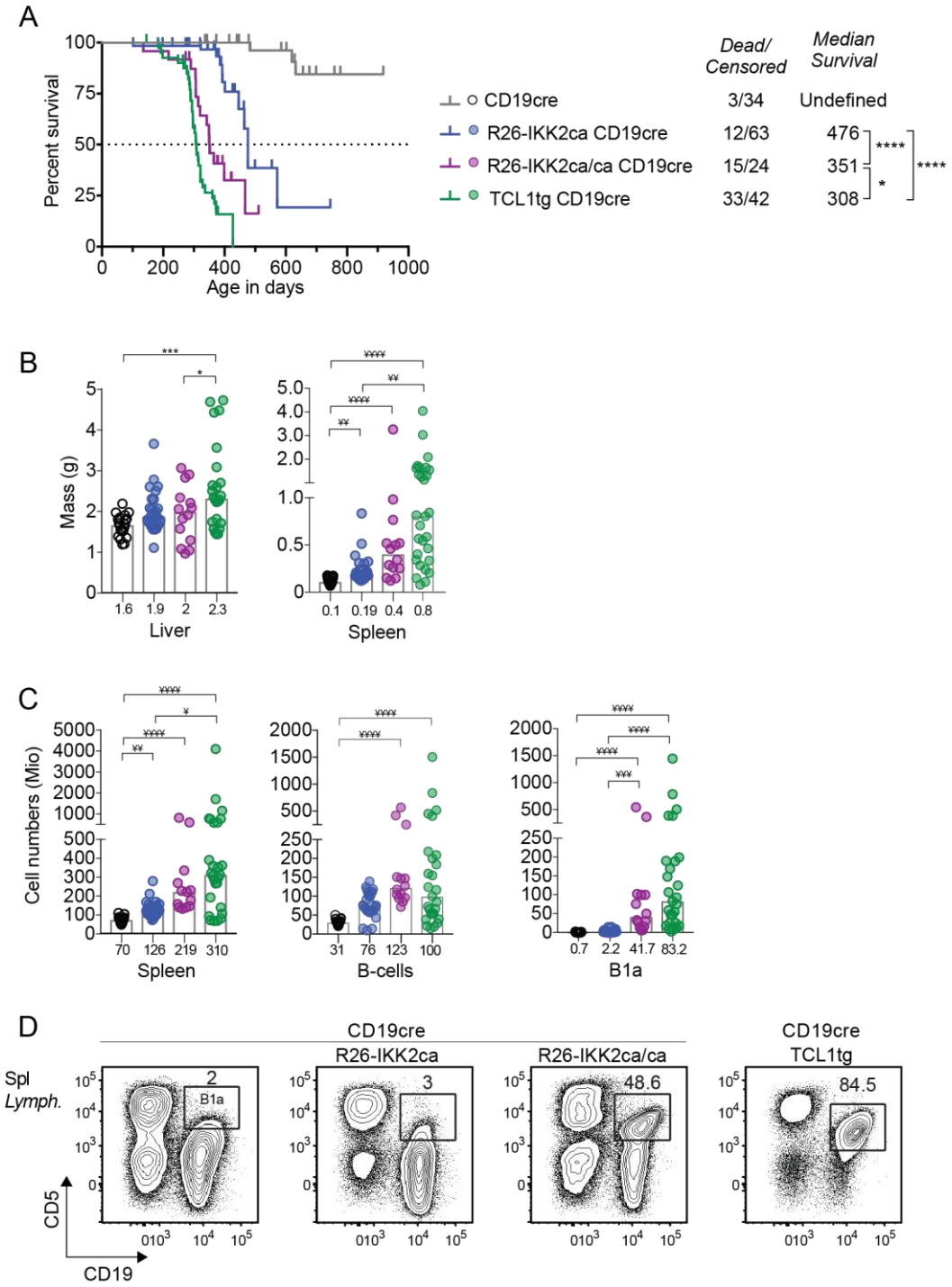


**Figure 26. Canonical NF-κB activation causes splenic B1a cell expansion in aged mice**

E*x vivo* analysis of B-cells in spleens of aged mice (> 9 months) using flow cytometry. (A) Kaplan-Meier survival curve analysis for R26-IKK2ca CD19cre compound mice and TCL1tg CD19cre mice, number of deceased and censored animals is indicated, as well as the median survival age in days. (B) Bar charts show the liver and spleen mass. (C) Bar charts show the number of splenocytes, B-cells and B1a-cells in spleen. (D) Flow cytometry contour plots depict the percentage of B1a-like cells. All flow cytometry contour plots are representative of at least 2 experiments. Histograms depict medians, and values are indicated below each histogram. Statistical analysis was done using One-way ANOVA (* $p<0.05$, *** $p<0.001$) or Kruskal-Wallis (¥ $p<0.05$, ¥¥ $p<0.01$, ¥¥¥ $p<0.001$, ¥¥¥¥ $p<0.0001$).
Spl (spleen), Lymph. (lymphocytes), B-cells ($CD19^+$), and B1a ($CD19^+$ $B220^{lo}$ $CD5^+$ or $CD19^+$ $CD5^+$).

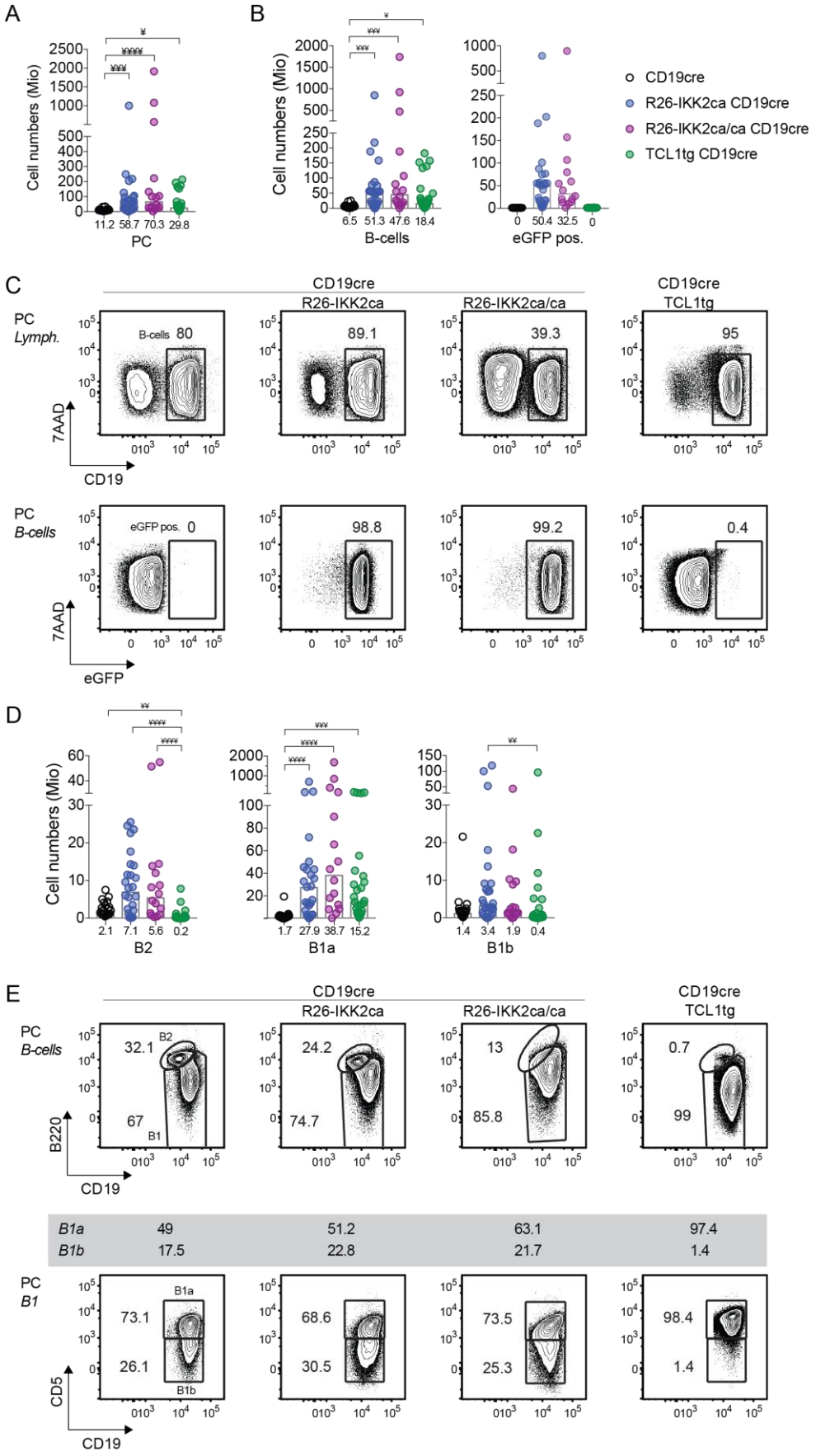


**Figure 27. Canonical NF-κB activation causes B1a cell expansion in the peritoneal cavity of aged mice**

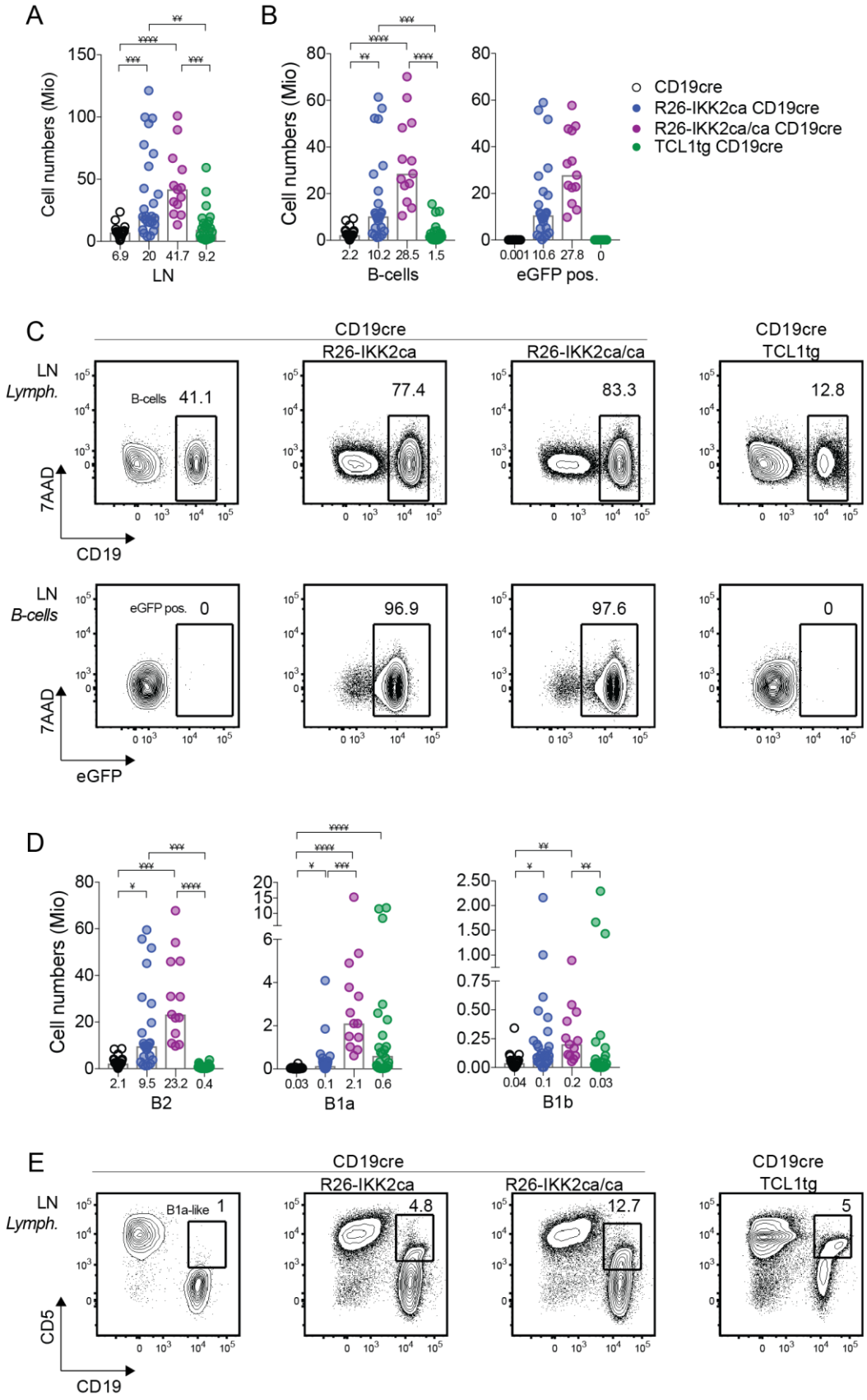


**Figure 28. Canonical NF-κB activation causes B1a cell expansion in the lymph nodes of aged mice**

**Figure 27 (continued). Canonical NF-κB activation causes B1a cell expansion in the peritoneal cavity of aged mice**

*Ex vivo* analysis of B-cells in peritoneal cavity of aged mice using flow cytometry. (A) Peritoneal cavity cell numbers after lavage. (B) Bar charts show total cell numbers and (C) flow cytometry contour plots depict percentages for B-cells and eGFP positive B-cells. (D) Bar charts show B-cell subset B2, B1a and B1b numbers after lavage. (E) Flow cytometry contour plots depict percentages of B2, B1, B1a and B1b-cells. All flow cytometry contour plots are representative of at least 2 experiments. Histograms depict medians, and values are indicated below each histogram. Statistical analysis was done using Kruskal-Wallis (¥ p<0.05, ¥¥ p<0.01, ¥¥¥ p<0.001, ¥¥¥¥ p<0.0001).
PC (peritoneal cavity), Lymph. (lymphocytes), B-cells ($CD19^+$), eGFP pos. ($CD19^+$ $eGFP^+$), B2 ($CD19^+$ $B220^{hi}$), B1 ($CD19^+$ $B220^{lo}$), B1a ($CD19^+$ $B220^{lo}$ $CD5^{hi}$) and B1b ($CD19^+$ $B220^{lo}$ $CD5^-$).

**Figure 28 (continued). Canonical NF-κB activation causes B1a cell expansion in the lymph nodes of aged mice**

*Ex vivo* analysis of B-cell in lymph nodes of aged mice using flow cytometry. Draining inguinal, axillary, and superficial cervical lymph nodes were pooled and analysed together. (A) Bar charts show cell numbers for pooled lymph nodes. (B) Bar charts show cell numbers and (C) flow cytometry contour plots depict percentages for B-cell and eGFP positive B-cells. (D) Bar charts show the number of B2, B1a and B1b subsets in lymph nodes of aged mice. (E) Flow cytometry contour plots depict percentage of B1a-like cells in lymph nodes. All flow cytometry contour plots are representative of at least 2 experiments. Histograms depict medians, and values are indicated below each histogram. Statistical analysis was done using Kruskal-Wallis (¥p<0.05, ¥¥ p<0.01, ¥¥¥ p<0.001, ¥¥¥¥ p<0.0001).
LN (lymph nodes), Lymph. (lymphocytes), B-cells ($CD19^+$), eGFP pos. ($CD19^+$ $eGFP^+$), B2 ($CD19^+$ $B220^{hi}$), B1a ($CD19^+$ $CD5^{hi}$ or $CD19^+$ $B220^{lo}$ $CD5^{hi}$) and B1b ($CD19^+$ $B220^{lo}$ $CD5^-$).

Finally, the *ex vivo* analysis of the bone marrow in aged mice shows slightly reduced median B-cell numbers in the R26-IKK2ca CD19cre compound mice compared to the CD19cre control (Figure S 22B). Reduced B2-like median cell numbers caused this reduction in an R26-IKK2ca knock-in dose dependent manner. Additionally, the R26-IKK2ca/ca CD19cre mice presented with a small B1a-like population (Figure S 22C).

Together, I show here that the constitutive activation of NF-κB in B-cells leads to a significant accumulation of B1a-like cells with age that can migrate to different lymphoid compartments, such as draining lymph nodes (Figure 28). Of the $CD5^+$ B-cell lymphoproliferative disorders described in humans, the novel phenotype described for aged R26-IKK2ca/ca CD19cre mice is reminiscent of a variant of human chronic lymphocytic leukaemia (CLL): human small lymphocytic leukaemia (SLL). Human SLL/CLL is characterized by the expansion of small $CD5^+$ $IgM^+$ B-cells that accumulate with age. The main difference between SLL and CLL is that in the former the spleen and lymph nodes are compromised, while in the latter the $CD5^+$ cells are also detected in the circulation.

### IV.2.2.2 Comparison of the CD5$^{+}$ B-cell expansion in R26-IKK2ca/ca CD19cre mice with TCL1tg-driven CLL-like murine disease

Given the reduced survival and CD5$^{+}$ B220$^{lo}$ B-cell expansion observed in aged R26-IKK2ca/ca CD19cre mice, it is likely that constitutive canonical NF-κB activation leads to a disease similar to SLL/CLL in mice. There are several mouse strain lines available that model different aspects of CLL in mice with different penetrance levels [228]. One of the most used and best validated lines is the Eμ-TCL1 transgenic (Eμ-TCL1tg) line that expresses the human TCL1 oncogene under control of the Eμ enhancer element in B-cells [229]. Mice carrying Eμ-TCL1tg develop a disease similar to human CLL, where there is a gradual accumulation of CD5$^{+}$ CLL-like cells in the mice that infiltrate lymphoid niches and cause a reduced median survival of 12-14 months [229].

Given the SLL-like phenotype observed in aged R26-IKK2ca/ca CD19cre mice, I aged a cohort of Eμ-TCL1tg$^{pos}$ CD19cre$^{I/+}$ (from now on referred to as TCL1tg CD19cre) mice to compare this murine CLL model to the R26-IKK2ca/ca CD19cre diseased mice. The CD19cre knock-in transgene was added to TCL1 to control for the effects of Cre expression and heterozygous knockout of CD19. Aged TCL1tg CD19cre mice have a media survival of 308 days, that although significantly shorter than the R26-IKK2ca/ca (351 days) shows relative similar dynamics (Figure 26A).

The *ex vivo* analysis of terminally sick mice revealed that both the R26-IKK2ca/ca CD19cre and TCL1tg CD19cre aged mice had significant B1a-like population present in the spleen and other lymphoid organs (see below). The two main differences between the TCL1tg CD19cre mice and the R26-IKK2ca/ca CD19cre mice were: first, the TCL1tg CD19cre driven CLL-like disease in mice has a stronger B1a-like cell burden than the R26-IKK2ca/ca CD19cre SLL-like disease described here; second, while there was a clear B1a-like cell expansion in both compound mice, there was a severe reduction of B2-like cells in the TCL1tg CD19cre mice while the B2- and B1b-cells subsets were expanded in the aged R26-IKK2ca/ca CD19cre mice.

The *ex vivo* analysis of aged TCL1tg CD19cre mice revealed, similarly to the R26-IKK2ca/ca CD19cre mice, the presence of enlarged livers and spleens compared to the CD19cre aged matched controls ([229] and Figure 26B). Moreover, the median number of CD5$^{+}$ CLL-like cells in the spleens of burdened TCL1tg CD19cre mice was only two-fold bigger than in the R26-IKK2ca/ca CD19cre mice (Figure 26C and D). Interestingly,

the constitutive canonical NF-κB activation in B-cells allowed for the persistence of B2-cells in R26-IKK2ca/ca CD19cre mice, whereas in the TCL1tg CD19cre mice was reduced to 17% of the CD19cre control (median value of 5 million cells compared to 29 million cells) ([229], Figure 26D and Figure S 19).

Furthermore, in the *ex vivo* analysis of the peritoneal cavity of burdened TCL1tg CD19cre mice showed a significant increase in total, B-cell and B1a-cell numbers compared to the CD19cre control mice, however not as drastic as observed in the R26-IKK2ca or R26-IKK2ca/ca CD19cre compound mice (Figure 27A, B and D). Additionally, the B-cell compartment in the peritoneum was mainly consistent of B1a-like cells in the TCL1tg CD19cre mice, while there were also B2- and B1b-cells in the R26-IKK2ca/ca CD19cre mice (Figure 27D and E).

Similarly to the R26-IKK2ca/ca CD19cre mice, the TCL1tg CD19cre mice also presented with $CD5^+$ CLL-like cells in lymph nodes and in some instances in the mesenteric lymph nodes (Figure 28 and Figure S 21). In the lymph nodes particularly, there were two-folds higher B1a-like cells in the aged R26-IKK2ca/ca CD19cre aged mice compared to the burdened TCL1tg CD19cre mice (Figure 28D). Moreover, in the R26-IKK2ca/ca CD19cre the $CD5^+$ B-cells corresponds only to 6% of all B-cells, whilst it represents 34% in the TCl1tg CD19cre mice (Figure S 20B). Additionally, the TCL1tg CD19cre mice had significantly lower B-cell numbers compared to the R26-IKK2ca CD19cre compound mice (Figure 28B), which corresponded mainly to the reduced B2- cell numbers in the lymph nodes (Figure 28D).

Finally, the burdened TCL1tg CD19cre mice had an infiltration of 0.2 million $CD5^+$ CLL-like cells in the bone marrow, which was two-fold higher than that observed in the aged R26-IKK2ca/ca CD19cre mice. The TCL1tg CD19cre mice had significantly lower cellularity, a tendency for less B-cells and significantly lower B2-cells in the bone marrow compared to aged R26-IKK2ca/ca CD19cre mice (Figure S 22).

The similar phenotypes observed in R26-IKK2ca/ca CD19cre and TCL1tg CD19cre mice suggest a role in constitutive canonical NF-κB signalling in the development of an SLL/CLL-like disease in mice. The slight differences observed in the latency periods are mirrored by the lower burden and infiltration of $CD5^+$ B1a-like cells in the R26-IKK2ca/ca CD19cre compared to the TCL1tg CD19cre mice.

### IV.2.3 EFFECT OF CONSTITUTIVE CANONICAL NF-κB ACTIVATION IN THE TCL1 CHRONIC LYMPHOCYTIC LEUKAEMIA MOUSE MODEL

Strong canonical NF-κB activation in B-cells leads with age to the development of a SLL/CLL-like disease in mice, where there is a steady accumulation of $CD5^+$ B1a-like cells in different lymphoid organs. To further understand the involvement of canonical NF-κB activity in SLL/CLL development I generated compound mice that expressed both the IKK2ca knock-in allele and the Eμ-TCL1tg in B-cells using the CD19cre mouse strain. Mice were aged and monitored for the development of disease.

Blood monitoring allowed to determinate the time point when the animal had reached a burdened phenotype. The humane end point was set to the presence of over 50% of $CD5^+$ B-cells of all living nucleated peripheral blood cells or the development of splenomegaly, hepatomegaly and/or anaemia. The control for disease development was the TCL1tg CD19cre mouse model. As already mentioned above, the median survival for the TCL1tg CD19cre mice was 308 days (Figure 26A and Figure 29A). In the TCL1tg CD19cre compound mice the $CD5^+$ CLL-like B-cells can be detected in the peripheral blood from two months of age onwards (geometric mean 1.5% of living cells). There is a slow progressive accumulation of these cells with time reaching 5% at 5 months and 29% of living cells within 9 months of age (Figure 29B and Figure S 23A).

#### IV.2.3.1 Constitutive NF-κB activation in B-cell cooperates with the TCL1 oncogene by accelerating the disease progression

The survival analysis and blood monitoring shows that constitutive NF-κB activation in B-cells cooperates with the TCL1 oncogene in promoting a CLL-like disease in mice in a shorter time frame in an IKK2ca dose dependent manner (Figure 29). The Eμ-TCL1tg$^{pos}$ R26$^{LSL}$-Ikk2ca$^{l/l}$ CD19cre$^{l/+}$ compound mice (from now on referred to as TCL1tg R26-IKK2ca/ca CD19cre) show the strongest phenotype. These mice have the shortest median survival, 121 days (Figure 29A), and show the most aggressive accumulation of $CD5^+$ B-cells in peripheral blood in the fastest time frame (Figure 29B and Figure S 23C). At 2 months of age 9% of all living cells in the peripheral blood are $CD5^+$ B1a-like cells, rising to 37% at 3 months of age and reaching 72% within 4 months of age (Figure 29B and Figure S 23C).

In contrast, the Eμ-TCL1tg$^{pos}$ R26$^{LSL}$-Ikk2ca$^{l/+}$ CD19cre$^{l/+}$ mice (from now on referred to as TCL1tg R26-IKK2ca CD19cre) showed an intermediate phenotype. The TCL1tg R26-IKK2ca CD19cre mice had a median survival of 186 days, 65 days significantly longer than the TCL1tg R26-IKK2ca/ca CD19cre and 122 days significantly shorter than the TCL1tg CD19cre mice (Figure 29A). There was an intermediate progression in the accumulation of CD5$^+$ B1a-like cells in the peripheral blood, reaching 32% of all living nucleated cells in the peripheral blood at 6 months of age (Figure 29B and Figure S 23B).

*Ex vivo* analysis of the spleen of burdened TCL1tg compound mice further supports the cooperation of constitutive canonical NF-κB activation with the TCL1tg oncogene in promoting the CLL-like disease in mice. Expression of the IKK2ca knock-in in B-cells in combination with the TCL1tg oncogene resulted in enlarged spleens with higher B-cell and CD5$^+$ B1a-cell numbers in a shorter time frame in an IKK2ca dose dependent manner (Figure 30).

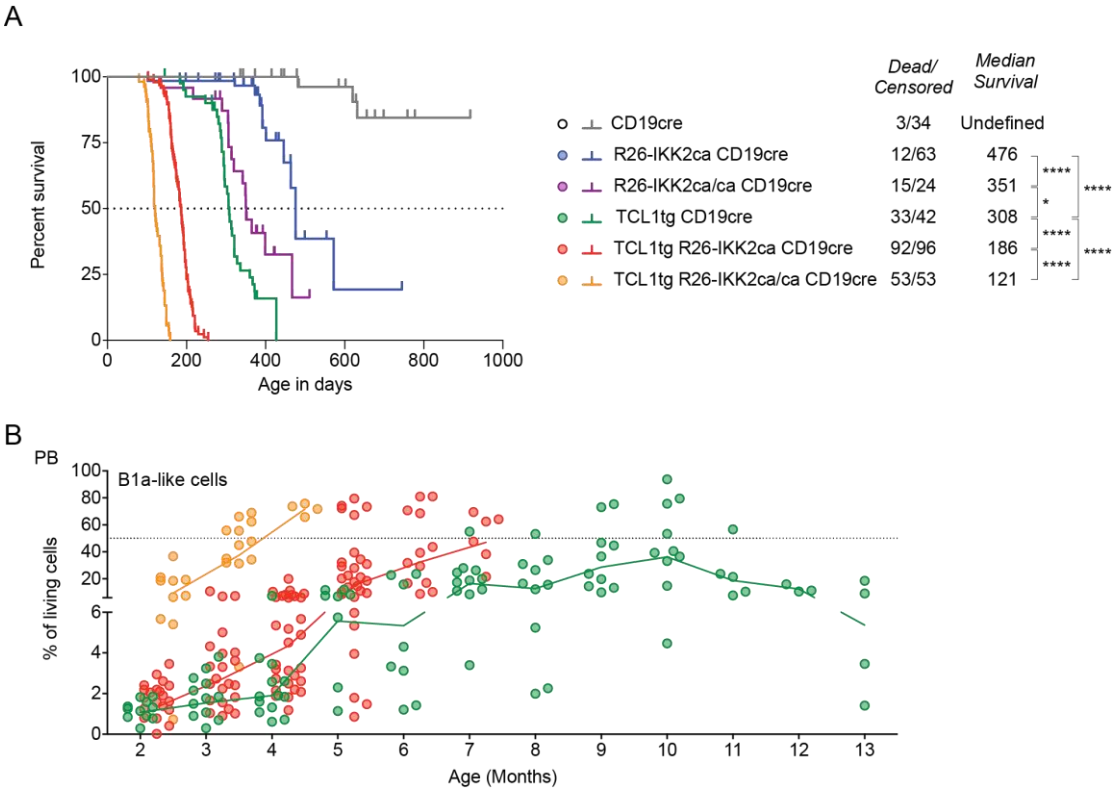


**Figure 29. Co-operation between IKK2ca and TCL1 in CLL-like disease**

Monitoring of TCL1tg CLL-dependent development in the presence of canonical NF-κB activation. (A) Kaplan-Meier survival curve analysis for TCL1tg and R26-IKK2ca compound mice. Number of deceased and censored animals is indicated, as well as the median survival age in days. (B) Scatter plot shows the percentage of B1a-like cells present in peripheral blood after red blood cell lysis, over a period of 13 months. The connecting line represents the mean for each time point.

First, both 3-months-old TCL1tg R26-IKK2ca/ca CD19cre and 5-months-old TCL1tg R26-IKK2ca CD19cre mice had a two-fold increase in spleen size compared to 9-month-old TCL1tg CD19cre mice (Figure 30A). Second, the constitutive canonical NF-κB activation resulted in a small increase in B-cell percentages in the spleen (Figure S 24A). Moreover, there was a significant increase in B-cell numbers caused by the combination of IKK2ca and TCL1 compared to the individual transgene. While the addition of one copy of the IKK2ca knock-in to the TCL1tg resulted in a significant five-fold increase in B-cells numbers at 5 months of age, two copies led to a significant eight-fold increase at 3 months of age compared to 9-month-old TCL1tg CD19cre controls (Figure 30B). The B-cell expansion observed is associated to IKK2ca-mediated canonical NF-κB activation since more than 92% of the B-cells expressed the eGFP reporter (Figure S 24B).

Finally, the *ex vivo* analysis of the spleens revealed that 80-90% of all B-cells present were $CD5^+$ B1a-like cells (Figure 30C, D, E and Figure S 24). There was a significant increase in $CD5^+$ B1a-like cell numbers in the R26-IKK2ca TCL1tg compound mice compared to the aged R26-IKK2ca compound mice. Moreover, the canonical NF-κB activation in B-cells when combined with the TCL1tg oncogene resulted in a 190-fold or 18-fold increase of $CD5^+$ B1a-like cell numbers in the presence of one or two IKK2ca alleles respectively (Figure 30E).

Interestingly, the additional constitutive NF-κB activation in B-cells rescued the diminished B2 population observed in the TCL1tg CD19cre mice, were most of the B2-cells where drastically reduced in burdened mice (Figure 30D and E). The increase in B2-cell numbers in the TCL1tg CD19cre compound mice happens in an IKK2ca dose dependent manner. Nonetheless, the TCL1tg R26-IKK2ca CD19cre mice had significantly lower B2-cell numbers compared to the R26-IKK2ca CD19cre mice.

The $CD5^+$ B1a-like expansion in burdened mice is also observed in the peritoneum (Figure 31 and Figure S 27), the draining inguinal, axillary, and superficial cervical (Figure 32 and Figure S 28) and to a lesser extent the mesenteric lymph nodes (Figure S 29) and in the bone marrow (Figure S 30). There was a significant increase in cell infiltration in the TCL1tg R26-IKK2ca/ca CD19cre mice in all organs analysed compared to the TCL1tg CD19cre control.

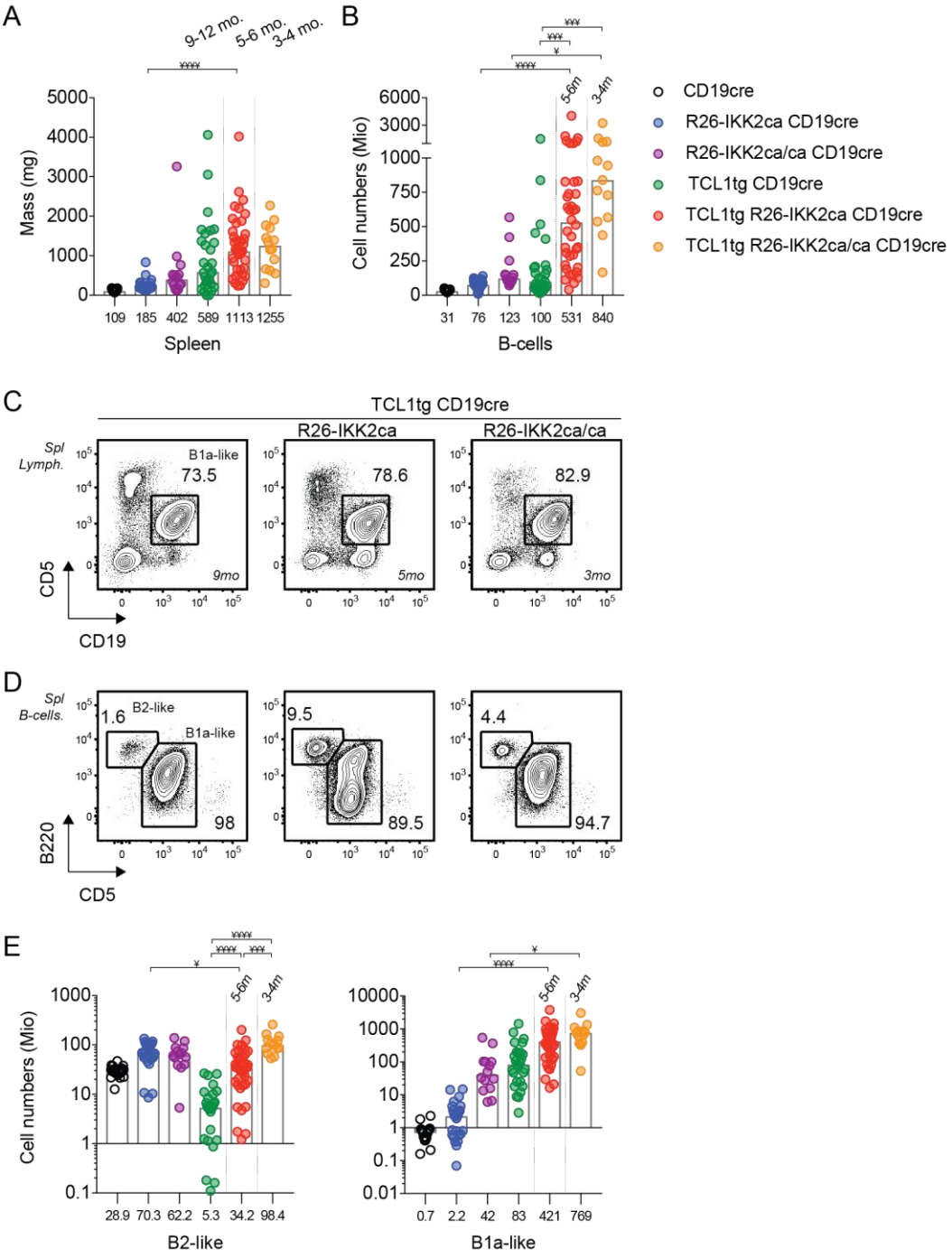


**Figure 30. Co-operation between IKK2ca and TCL1 in splenic B-cells**

*Ex vivo* analysis of spleen from burdened TCL1 compound mice using flow cytometry. Bar charts show (A) spleen mass and (B) B-cell numbers. Flow cytometry contour plots depict the percentage of $CD5^+$ B1a-like cells from (C) lymphocytes and (D) B-cells in spleens from sick mice. (E) Bar charts show B2- and $CD5^+$ B1a-like cell numbers in spleen from burdened mice. As indicated, burdened TCL1tg R26-IKK2ca CD19cre and TCL1tg R26-IKK2ca/ca CD19cre cohorts were analysed between 3-4 months and 5-6 months of age, respectively. TCL1tg CD19cre mice and aged matched controls were analysed between 9-12 months of age. All flow cytometry contour plots are representative of at least 2 experiments. Histograms depict medians, and values are indicated below each histogram. Statistical analysis was done using Kruskal-Wallis (¥p<0.05, ¥¥ p<0.01, ¥¥¥ p<0.001, ¥¥¥¥ p<0.0001).
mo./m (months of aged), Spl. (spleen), Lymph. (lymphocytes), B-cells ($CD19^+$), B1a ($CD19^+$ $CD5^{hi}$ or $CD19^+$ $B220^{lo}$ $CD5^{hi}$), B2-like ($CD19^+$ $B220^{hi}$ $CD5^-$).

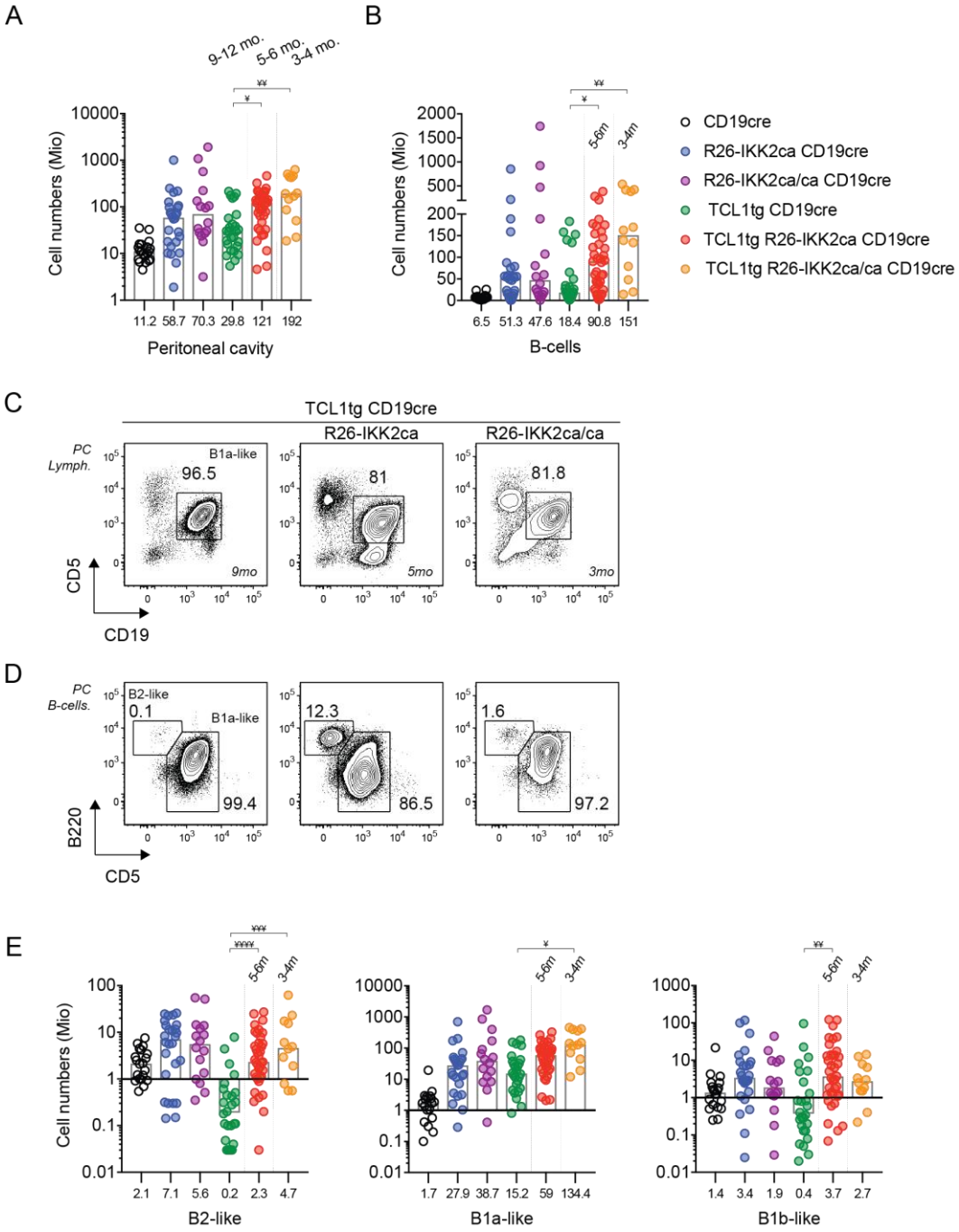


**Figure 31. Co-operation between IKK2ca and TCL1 in peritoneal B-cells**

*Ex vivo* analysis of B-cells in the peritoneal cavity of burdened mice using flow cytometry. Bar chart shows (A) total and (B) B-cell cell numbers after lavage. Flow cytometry contour plots depict the percentage of $CD5^+$ B1a-like cells from (C) lymphocytes and (D) B-cells in the peritoneum of burdened mice. (E) Bar charts show B2- and $CD5^+$ B1a-like cell numbers in PC from burdened mice. As indicated, TCL1tg R26-IKK2ca CD19cre and TCL1tg R26-IKK2ca/ca CD19cre mice cohorts were analysed between 3-4 months and 5-6 months of age, respectively. TCL1tg CD19cre mice and aged matched controls were analysed between 9-12 months of age. All flow cytometry contour plots are representative of at least 2 experiments. Histograms depict medians, and values are indicated below each histogram. Statistical analysis was done using Kruskal-Wallis (¥p<0.05, ¥¥ p<0.01, ¥¥¥ p<0.001, ¥¥¥¥ p<0.0001).
mo./m (months of aged), PC (peritoneal cavity), Lymph. (lymphocytes), B-cells ($CD19^+$), B1a-like ($CD19^+$ $CD5^{hi}$ or $CD19^+$ $B220^{lo}$ $CD5^{hi}$), B2-like ($CD19^+$ $B220^{hi}$ $CD5^-$), B1b-like ($CD19^+$ $B220^{lo}$ $CD5^-$).

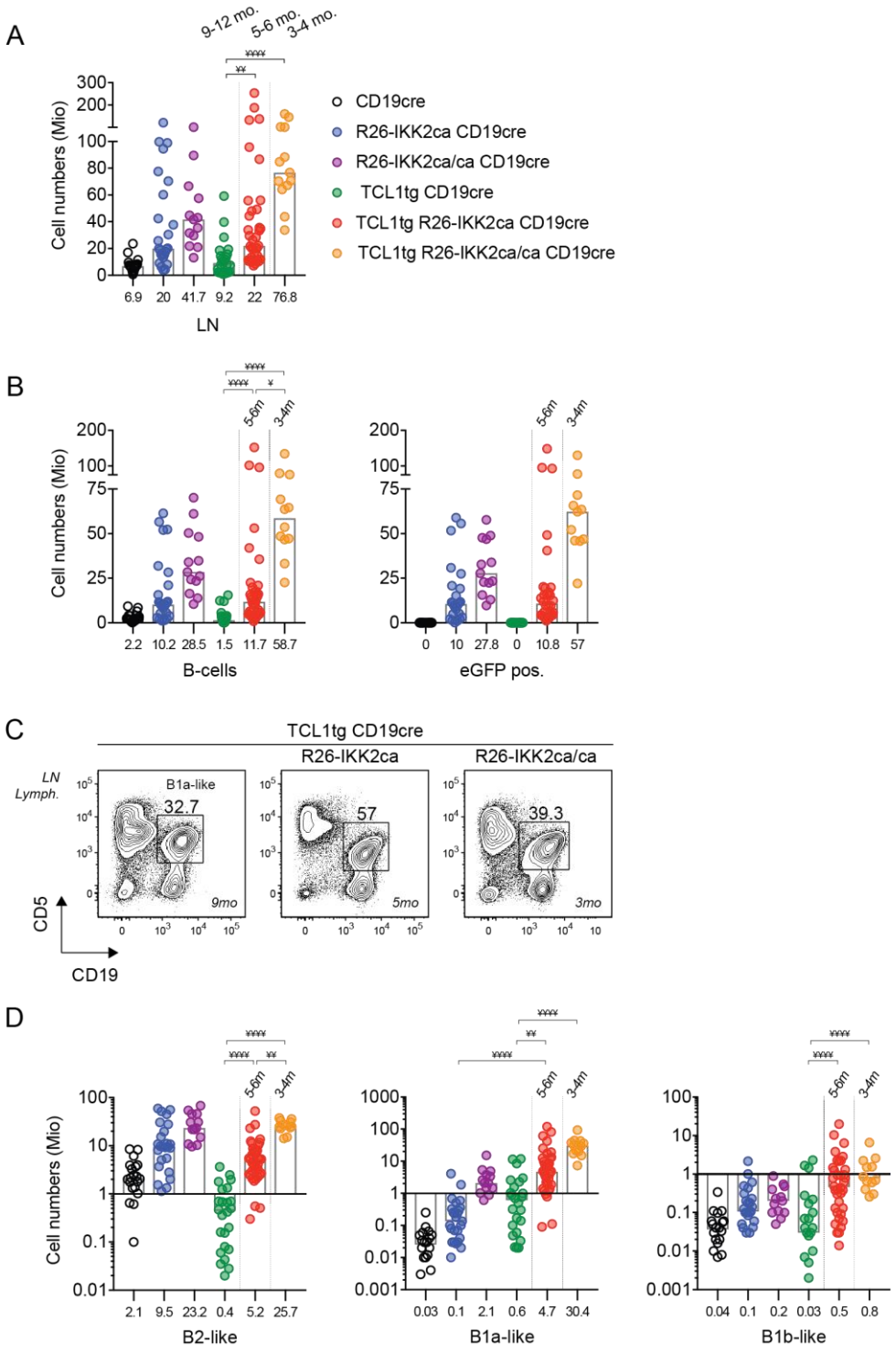


**Figure 32. Co-operation between IKK2ca and TCL1 in lymph node B-cells**

*Ex vivo* analysis of draining lymph nodes of burden mice using flow cytometry. Draining inguinal, axillary, and superficial cervical lymph nodes were pooled and analysed together. Bar chart shows (A) cell numbers, (B) B-cell and eGFP positive B-cell numbers for pooled draining lymph nodes. (C) Flow cytometry contour plots depict the percentage of B1a-like cells from lymphocytes in lymph nodes of sick mice. (D) Bar charts show B2-, B1a- and B1b-like cell numbers in lymph nodes of sick mice. As indicated, sick TCL1tg R26-IKK2ca CD19cre and TCL1tg R26-IKK2ca/ca CD19cre mice cohorts were analysed between 3-4 months and 5-6 months of age, respectively. TCL1tg CD19cre mice and aged matched controls were analysed between 9-12 months of age. All flow cytometry contour plots are representative of at least 2 experiments. Histograms depict medians, and values are indicated below

Figure 32 **(continued)** each histogram. Statistical analysis was done using Kruskal-Wallis (¥p<0.05, ¥¥ p<0.01, ¥¥¥¥ p<0.0001).
mo./m (months of aged), LN (lymph nodes), B-cells ($CD19^+$), eGFP pos. ($CD19^+$ $eGFP^+$), Lymph. (lymphocytes), B1a-like ($CD19^+$ $CD5^{hi}$ or $CD19^+$ $B220^{lo}$ $CD5^{hi}$), B2-like ($CD19^+$ $B220^{hi}$ $CD5^-$), B1b-like ($CD19^+$ $B220^{lo}$ $CD5^-$).

Notably, 3-4 months old TCL1tg CD19cre mice present with a small $CD5^+$ B1a-like population (median 2.9 million) in the spleen, which is two-fold bigger in the TCL1tg R26-IKK2ca CD19cre aged matched mice (Figure S 25E). While one additional copy of the IKK2ca knock-in transgene drastically tips the balance towards a CLL-like phenotype. Two months later, in 5-6 months old TCL1tg CD19cre mice, this $CD5^+$ B1a-like population has almost doubled in size (median 5.2 million), while it has massively expanded to 421 million in TCL1tg R26-IKK2ca CD19cre mice (Figure S 26E). The kinetics of $CD5^+$ B1a-like cell accumulation further points towards a strong cooperation between TCL1 and canonical NF-κB in the disease progression.

Therefore, the combination of constitutive canonical NF-κB activation and the expression of the TCL1tg oncogene strongly cooperate in the development of CLL-like disease in mice. There are several possible mechanisms of how canonical NF-κB could accelerate disease progression. It could be possible that a certain NF-κB activation threshold needs to be reached for the disease to take its course. Alternatively, strong canonical NF-κB activation could accelerate the proliferation of CLL-like cells, thus shortening the expected survival of the mice. Another hypothesis could be that the B1-cell hyperplasia generated by strong canonical NF-κB could increase the number of possible CLL precursor cells, thus shortening the survival of the mice.

### IV.2.3.2 Characterization of constitutive canonical NF-κB activation in the TCL1tg murine CLL model

The constitutive canonical NF-κB activation caused by two knock-in transgenes of IKK2ca in B-cells leads in age to the accumulation of $CD5^+$ B1a-like cells in lymphoid organs and to a median survival of 351 days. When constitutive canonical NF-κB activation is combined with the TCL1tg, both events cooperate in dramatically accelerating disease progression. The CLL-like disease developed in the TCL1tg mouse is characterized by a mono to oligoclonal expansion [229]. I therefore, wanted to assess whether constitutive activation of the canonical NF-κB pathway affects the clonality of

the disease. If by constitutive activation of the canonical NF-κB pathway increases the number of potential murine CLL precursors, there might be a higher chance that multiple independent events within the same animal would give rise to a clonal expansion, translating into a polyclonal disease.

#### IV.2.3.2.1 Constitutive canonical NF-κB activation leads to an oligoclonal CLL-like disease in the TCL1tg mouse model

In order to determine whether constitutive canonical NF-κB activation in B-cells has an effect on the clonality of the $CD5^+$ B1a-like expansion observed in the TCL1tg mice, I decided to take advantage of the BCR diversity analysing the VDJ recombination of the immunoglobulin heavy-(IgH) chain. In the C57BL/6 mouse line, a total of 152 VH-gene segments, 17-20 DH-gene segments and four JH-gene segments have been described (Figure 33A). Taking into account the random process of VDJ recombination and the amount of VH, DH and JH gene segments combinations possible, the probability that two B-cells share the same VDJ rearrangement is extremely small. Additionally, in the process of J and D joining, and DJ to V joining additional variation is added by the deletion and insertion of bases, giving rise to unique VDJ rearrangement. The particular region of the BCR where the V, D and J gene segments join forms coding determination region 3 (CDR3), which recognizes the antigen in the antibody and is the most variable part of the antibody.

##### IV.2.3.2.1.1 JH-gene segment usage analysis

As an initial step, a PCR was set up that would amplify the IgH VDJ rearrangements. One primer binds at the 3' end of the JH4-gene segment, thus amplifying rearrangements into all four JH-gene segments independent of which JH-gene segment was used. The other primer binds to the 5' end of the most commonly used V-gene segments in the murine genome. Therefore, amplicons of four different molecular sizes would be visible accounting for the rearrangements into the JH1 (1.6Kb), JH2 (1.3Kb), JH3 (1Kb) and JH4 (500bp) gene segments (Figure S 31A, lane 5).

Genomic DNA was extracted from splenocytes of wild type controls and burdened TCL1tg CD19cre, TCL1tg R26-IKK2ca CD19cre or TCL1tg R26-IKK2ca/ca CD19cre mice to amplify the IgH VDJ sequence. If after the PCR only one amplicon is detected, or one particular amplicon has a stronger intensity, a higher percentage of B-cells rearranged

into that specific JH-gene segment, one indication for clonal B-cell expansion. To illustrate this point, the PCR amplicons for one TCL1tg CD19cre, three TCL1tg R26-IKK2ca CD19cre and one CD19cre control sample where separated on an agarose gel (Figure S 31B). In lane 1 and 4, a band of 1.5Kp is visible in addition to bands of lower molecular weight and intensity; therefore the majority of B-cells in both of these samples will have a BCR that has rearranged into the JH2-gene segment. Similarly, in lane 2 and 3, a band of 500bp is visible in addition to bands of higher molecular weight. This means that both samples have a significant percentage of B-cells with BCRs that have rearranged into the JH4-gene segment.

## IgH VDJ cloning and sequencing of control samples

In order to assess VDJ rearrangements in more detail, I devised a cloning strategy (Figure 33C) described in detail in the Materials and methods section. Briefly, the VDJ rearrangements were amplified by PCR and homology cloned into vectors specific for each JH-gene segment. An adaptor sequence homologous to the cloning vector was introduced upstream of the VH-gene sequence, while a specific sequence homologous to a unique sequence within each JH-gene segments termed the catch sequence (CS), was cloned into the different JH cloning vectors. Therefore, only amplicons carrying the right CS would be cloned into the specific JH destination vectors [248].

The VDJ rearrangement of the immunoglobulin heavy-chain was cloned from B-cells from wild type controls (n=4) or terminally sick TCL1tg CD19cre (n=2), TCL1tg R26-IKK2ca CD19cre (n=6) or TCL1tg R26-IKK2ca/ca CD19cre (n=3) mice. Two PCR multiplex amplifications were designed for rearrangements into JH1 and JH4, as well as JH2 and JH3 (Figure S 32). Interestingly, rearrangement into JH2 and JH3 could also be detected with the JH1/JH4 PCR reaction (Figure S 32B). Similarly, the rearrangement into JH1 could also be amplified with the JH2/JH3 PCR reaction (Figure S 32C).

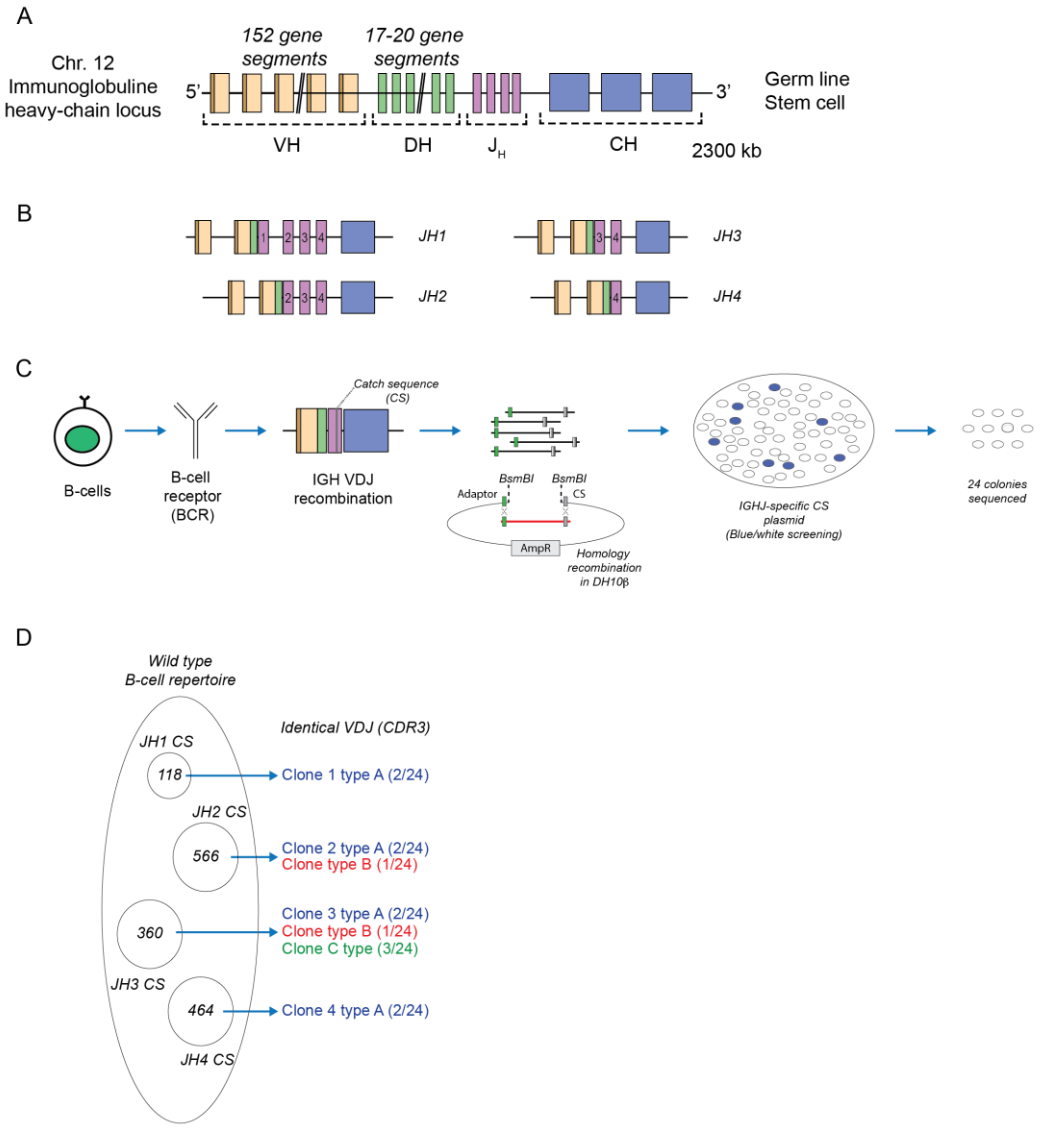


**Figure 33. Strategy for cloning the VDJ rearrangements of the immunoglobulin heavy-chain.**

(A) Germ line locus for the immunoglobulin heavy-chain (IgH) in the mouse C57BL/6 background. (B) The four possible VDJ rearrangements into the different joining-gene segments. (C) First, the genomic DNA is extracted from splenocytes containing B-cells. Second, the VDJ rearrangements of the IgH of the BCR repertoire are amplified by PCR. Third, the individual amplicons are cloned into JH specific plasmids using quick and clean cloning. Forth, blue and white screening is used to identify and quantify the number of JH specific colonies. Finally, colonies are picked and the cloned IgH VDJ sequenced. (D) Representation of cloned IgH VDJ repertoire in control wild type samples. Total number of white colonies obtained for each JH CS plasmid is indicated inside a circle. Blue arrow indicates major clones identified for each plasmid, clone type, number of clones with identical sequences and number of colonies sequenced (see Tables S1 and S6-S8). Three type of rearrangements were identified: sequence type A were unique, sequence type B were identified by different JH CS plasmids, and sequence type C were identified more than once within the same JH CS plasmid.
Figure 33 **(continued).** VH (variable, yellow), DH (diversity, green), JH (joining, pink), CH (constant, blue), Kb (kilo bases), bp (base pairs), PCR (polymerase chain reaction)

The analysis of VDJ rearrangements cloned from wild type B-cells showed that additionally to productive rearrangements, unproductive rearrangements could be detected (Table S 2, Table S 3, Table S 4 and Table S 5). These unproductive rearrangements represent the second heavy-chain allele of a B-cell with a productive rearrangement. In the four wild type samples used as controls, these unproductive rearrangements represented 27 (20/73 sequences in wild type sample 4) to 44% (21/44 sequences in wild type sample 2) of the clones identified. Moreover, rearranged sequences with different JH-gene segments located 5' from the plasmid specific JH catch sequences (CS) used could be additionally detected (see Materials and methods).

Interestingly, only in one of the four wild type samples analysed all the sequenced colonies had unique VDJ sequences (Table S 2). In the other three wild type samples several VDJ sequences found were not unique. In wild type control 3, nine VDJ sequences were identified at least twice in the analysis (n=9/80, Table S 4). Similarly, in wild type control 4, 13 VDJ sequences were identified at least a second time (n=15/73, Table S 6). Moreover, in wild type control 2 (Clone_01, n=4/12; Table S 3), wild type control 3 (Clone_058, n=3/24; Table S 4) and wild type control 4 (Clone_08, n=4/22; Clone_29 n=3/24; Table S 5) the VDJ rearrangement was identified more than twice in the picked colonies. Additionally, in wild type control 4, Clone_15 was identified with both with the J2 and the J3 CS plasmids, but belonged to the J1 rearranged samples (Table S 5). All other instances, the sequences identified a second time were cloned with the same JH CS plasmid. Interestingly, in wild type control 4 two different VDJ rearrangements produced the same CDR3 amino acid sequence (Clone_60 and Clone_61; Table S 5).

Finally, the IgH VDJ cloning provided information associated with the mutational status of each VDJ rearrangement. A 95% of sequence identity with the germ line sequence was set as the cut-off value. Any IgH VDJ sequence with an identity above 95% was defined as unmuted. However, if the IgH VDJ sequence had less than 95% identity with the germ line sequences, then that particular BCR was mutated. That mutational status could be used as an indicator of somatic hypermutation and transition through the germinal centre. Interestingly, for the majority of the rearrangements cloned the sequences had more than 95% identity with the germ line (Table S 2, Table S 3, Table S 4 and Table S 5). However, in every sample at least one mutated IgH VDJ sequence could be identified (Clones 05, 10 and 26 in wild type control 1, Table S 2; Clone_09 in wild type control 2, Table S 3; Clones 20, 28, 42 and 62 in wild type control 3, Table S 4; and

Clones 9 and 14 in wild type control 4, Table S 5). The low number of mutated IgH VDJ sequences identified is most likely due to the fact for the wild type controls the bulk of B-cells were used, therefore there is a reduced number of germinal centre experienced B-cells.

Given that in nature, the possibility for two independent B-cells to generate the same VDJ sequence is minimal, the fact that in the current VDJ rearrangement several rearrangements have been identified more than once is contradictory. It is likely that using genomic DNA as template for the amplifying and cloning the VDJ rearrangements in B-cells the same strand of DNA is amplified more and thus there is a higher probability for it to be cloned into the JH CS specific destination plasmids. Moreover, the identification of both IgH VJD productive and unproductive rearrangements points to the possibility of cloning both IgH alleles from the same B-cell with the methodology employed here.

### IgH VDJ cloning and sequencing of tumour samples

Given the IgH VDJ rearrangement diversity observed in the wild type control samples in the previous part, I decided that the further sequencing of at least eight colonies from each JH CS plasmid should be sufficient to determine the clonality of the TCL1tg derived lymphomas. Clonal VDJ rearrangements were identified by their higher frequency in the pool of sequenced colonies within each JH CS specific plasmid.

The analysis of the cloned VDJ rearrangements from burdened TCL1tg CD19cre mice revealed that the $CD5^+$ B1a-like tumours were oligoclonal (Figure 34A and Table 10). In the TCL1tg CD19cre sample CLL_00425 two productive and one unproductive clonal VDJ rearrangements were identified. As CLL-cells depend on a functional BCR for their survival, the identification of an unproductive VDJ clonal rearrangement represents the second IgH allele of a productive rearrangement, which is either detect at a similar frequency in the analysis or cannot be detected. Interestingly, the CLL_00425 Clone_01, containing a rearrangement involving the JH1-gene segment, was detected with both the JH2 and JH3 CS specific plasmids. In the case of the TCL1tg CD19cre sample CLL_32284 four clonal VDJ rearrangements were identified, three of them productive and one unproductive. It is likely that the unproductive VDJ rearrangement, Clone_04, corresponds to the second IgH allele of one of the other three clones with productive rearrangements. Therefore, in reality three main clones would be present in the TCL1tg

CD19cre sample CLL_32284. These results constitute further evidence of a reduced BCR repertoire in these samples.

Further enhanced constitutive activation of canonical NF-κB through expression of two copies of the IKK2ca transgene does not affect the oligoclonal nature of the CD5+ B1a-like tumours, as oligoclonal tumours were found in both TCL1tg R26-IKK2ca CD19cre (Table 11) and TCL1tg R26-IKK2ca/ca CD19cre burdened mice (Table 12). From the six TCL1tg R26-IKK2ca CD19cre samples analysed up to 5 clones were identified per sample, not taking into account the functionality of their heavy chain rearrangements (Table 11). Importantly, although no functional clonal VDJ rearrangement was identified for sample CLL_01140, two clonal unproductive rearrangements were detected. The fact that 100% of the sequenced colonies for the JH4 CS plasmid were identical (30/30 colonies, Figure 34B and Table 11) strongly supports the idea of an oligoclonal lymphoma where one clone is dominant.

**Table 10. Analysis of IgH VDJ rearrangements cloned from splenocytes of burdened TCL1tg CD19cre mice**

| Mouse ID | Major clones identified | | | | | | | | |
|---|---|---|---|---|---|---|---|---|---|
| CLL_32284 | JH1 CS plasmid | | | | | | | | |
| | Clone | Functionality | VH-gene | DH-gene | JH-gene | Identity (%) | CDR3 length | CDR3 amino acid sequence | Colonies§ |
| | Clone_03 | Productive | V14-4 | D1-1 | JH1 | 99.31 | 15 | CTTSYTTVVADWYFDVW | 2/8 |
| | JH2 CS plasmid | | | | | | | | |
| | Clone | Functionality | VH-gene | DH-gene | JH-gene | Identity (%) | CDR3 length | CDR3 amino acid sequence | Colonies§ |
| | Clone_01 | Productive | V5-2 | D1-1 | JH1 | 99.31 | 16 | CARPHYYGSSRNWYFDVW | 2/8 |
| | JH3 CS plasmid | | | | | | | | |
| | Clone | Functionality | VH-gene | DH-gene | JH-gene | Identity (%) | CDR3 length | CDR3 amino acid sequence | Colonies§ |
| | Clone_02 | Productive | V1-80 | D2-3 | JH3 | 98.96 | 8 | CATNDGFAYW | 3/8 |
| | Clone_04 | Unproductive | V1-67 | D1-2 | JH3 | 98.96 | X | CARTL##WFAYW | 2/8 |
| | JH4 CS plasmid | | | | | | | | |
| | Clone | Functionality | VH-gene | DH-gene | JH-gene | Identity (%) | CDR3 length | CDR3 amino acid sequence | Colonies§ |
| | All 7 sequences were unique. | | | | | | | | |
| CLL_00425 | JH1 CS plasmid | | | | | | | | |
| | Clone | Functionality | VH-gene | DH-gene | JH-gene | Identity (%) | CDR3 length | CDR3 amino acid sequence | Colonies§ |
| | Not done. | | | | | | | | |
| | JH2 CS plasmid | | | | | | | | |
| | Clone | Functionality | VH-gene | DH-gene | JH-gene | Identity (%) | CDR3 length | CDR3 amino acid sequence | Colonies§ |
| | Clone_01 | Productive | V1-39 | D6-3 | JH1 | 99.0 | 13 | CARTRPLWNWYFDVW | 16/30 |
| | Clone_03 | Unproductive | V1-67 P | D2-1 | JH2 | 99.3 | X | CARSTMV#YFDYW | 11/30 |
| | JH3 CS plasmid | | | | | | | | |
| | Clone | Functionality | VH-gene | DH-gene | JH-gene | Identity (%) | CDR3 length | CDR3 amino acid sequence | Colonies§ |
| | Clone_01 | Productive | V1-39 | D6-3 | JH1 | 99.0 | 13 | CARTRPLWNWYFDVW | 3/30 |
| | Clone_02 | Productive | V1-4 | D1-1 | JH3 | 99.0 | 12 | CARYYGSSYWFAYW | 24/30 |
| | Clone_03 | Unproductive | V1-67 P | D2-1 | JH2 | 99.3 | X | CARSTMV#YFDYW | 3/30 |
| | JH4 CS plasmid | | | | | | | | |
| | Clone | Functionality | VH-gene | DH-gene | JH-gene | Identity (%) | CDR3 length | CDR3 amino acid sequence | Colonies§ |
| | Not done. | | | | | | | | |

§ Number of colonies with identical sequence and total number of colonies sequenced, * Stop codon in CDR3 region, out-of-frame CDR3, # restored frameshift for out-of-frame junctions

**Table 11. Analysis of IgH VDJ rearrangements cloned from splenocytes of burdened TCL1tg R26-IK2ca CD19cre mice**

| Mouse ID | Major clones identified | | | | | | | | |
|---|---|---|---|---|---|---|---|---|---|
| CLL0_1140 | JH1 CS plasmid | | | | | | | | |
| | Clone | Functionality | VH-gene | DH-gene | JH-gene | Identity (%) | CDR3 length | CDR3 amino acid sequence | Colonies[§] |
| | Clone_01 | Unproductive | V1-67 P | D2-4 | JH4 | 99.0 | 16 | CARWLL*LRRRHYAMDYW | 1/6 |
| | Clone_02 | Unproductive | V1-67 P | | JH4 | 99.3 | X | CARWLL*LRRRHYAMDYWGHRD HGHLSRRSPTIFSAAMENRCSSF ILSRFSGCILKLILRTMLTTS | 4/6 |
| | JH2 CS plasmid | | | | | | | | |
| | Clone | Functionality | VH-gene | DH-gene | JH-gene | Identity (%) | CDR3 length | CDR3 amino acid sequence | Colonies[§] |
| | Not done. | | | | | | | | |
| | JH3 CS plasmid | | | | | | | | |
| | Clone | Functionality | VH-gene | DH-gene | JH-gene | Identity (%) | CDR3 length | CDR3 amino acid sequence | Colonies[§] |
| | Not done. | | | | | | | | |
| | JH4 CS plasmid | | | | | | | | |
| | Clone | Functionality | VH-gene | DH-gene | JH-gene | Identity (%) | CDR3 length | CDR3 amino acid sequence | Colonies[§] |
| | Clone_01 | Unproductive | V1-67 P | D2-4 | JH4 | 99.3 | 16 | CARWLL*LRRRHYAMDYW | 30/30 |
| CLL_32351 | JH1 CS plasmid | | | | | | | | |
| | Clone | Functionality | VH-gene | DH-gene | JH-gene | Identity (%) | CDR3 length | CDR3 amino acid sequence | Colonies[§] |
| | Clone_01 | Productive | V12-3 | D2-3 | JH1 | 98.61 | 12 | CAGDSDGYWYFDVW | 3/8 |
| | Clone_02 | Productive | V1-39 | D1-1 | JH4 | 98.96 | 12 | CAIDTTVVKAMDYW | 2/8 |
| | JH2 CS plasmid | | | | | | | | |
| | Clone | Functionality | VH-gene | DH-gene | JH-gene | Identity (%) | CDR3 length | CDR3 amino acid sequence | Colonies[§] |
| | Not done. | | | | | | | | |
| | JH3 CS plasmid | | | | | | | | |
| | Clone | Functionality | VH-gene | DH-gene | JH-gene | Identity (%) | CDR3 length | CDR3 amino acid sequence | Colonies[§] |
| | Not done. | | | | | | | | |
| | JH4 CS plasmid | | | | | | | | |
| | Clone | Functionality | VH-gene | DH-gene | JH-gene | Identity (%) | CDR3 length | CDR3 amino acid sequence | Colonies[§] |
| | Not done. | | | | | | | | |
| CLL_31937 | JH1 CS plasmid | | | | | | | | |
| | Clone | Functionality | VH-gene | DH-gene | JH-gene | Identity (%) | CDR3 length | CDR3 amino acid sequence | Colonies[§] |
| | Not done. | | | | | | | | |
| | JH2 CS plasmid | | | | | | | | |
| | Clone | Functionality | VH-gene | DH-gene | JH-gene | Identity (%) | CDR3 length | CDR3 amino acid sequence | Colonies[§] |
| | Clone_01 | Unproductive | V5-2 | D2-5 | JH2 | 99.3 | X | CARL*##FDYW | 8/8 |
| | JH3 CS plasmid | | | | | | | | |
| | Clone | Functionality | VH-gene | DH-gene | JH-gene | Identity (%) | CDR3 length | CDR3 amino acid sequence | Colonies[§] |
| | Not done. | | | | | | | | |
| | JH4 CS plasmid | | | | | | | | |
| | Clone | Functionality | VH-gene | DH-gene | JH-gene | Identity (%) | CDR3 length | CDR3 amino acid sequence | Colonies[§] |
| | Not done. | | | | | | | | |

[§] Number of colonies with identical sequence and total number of colonies sequenced, * Stop codon in CDR3 region, out-of-frame CDR3, # restored frameshift for out-of-frame junctions

**Table 11 (continued): Analysis of IgH VDJ rearrangements cloned from splenocytes of burdened TCL1tg R26-IK2ca CD19cre mice**

| Mouse ID | Major clones identified | | | | | | | | |
|---|---|---|---|---|---|---|---|---|---|
| CLL_32100 | JH1 CS plasmid | | | | | | | | |
| | Clone | Functionality | VH-gene | DH-gene | JH-gene | Identity (%) | CDR3 length | CDR3 amino acid sequence | Colonies[§] |
| | Clone_01 | Productive | V5-6 (or V5-6-1*01) | D1-1 | JH2 | 99.3 | 13 | CARHYYGSSYYFDYW | 1/10 |
| | Clone_02 | Productive | V11-2 | D2-1 | JH1 | 98.6 | 11 | CMRYGNYWYFDVW | 5/10 |
| | Clone_03 | Unknown | V1-18 | | JH1 | 99.0 | X | Rearranged sequence but no junction found | 4/10 |
| | JH2 CS plasmid | | | | | | | | |
| | Clone | Functionality | VH-gene | DH-gene | JH-gene | Identity (%) | CDR3 length | CDR3 amino acid sequence | Colonies[§] |
| | Clone_01 | Productive | V5-6 (or V5-6-1*01) | D1-1 | JH2 | 99.3 | 13 | CARHYYGSSYYFDYW | 5/8 |
| | Clone_02 | Productive | V11-2 | D2-1 | JH1 | 98.6 | 11 | CMRYGNYWYFDVW | 1/8 |
| | JH3 CS plasmid | | | | | | | | |
| | Clone | Functionality | VH-gene | DH-gene | JH-gene | Identity (%) | CDR3 length | CDR3 amino acid sequence | Colonies[§] |
| | Clone_01 | Productive | V5-6 (or V5-6-1*01) | D1-1 | JH2 | 99.3 | 13 | CARHYYGSSYYFDYW | 2/10 |
| | Clone_05 | Unproductive | V5-2 | D2-4 | JH3 | 99.3 | X | CARHYYDYDGA#WFAYW | 2/10 |
| | Clone_04 | Unproductive | V1-31 | D4-1 | JH3 | 99.3 | X | CARYWD#FAYW | 3/10 |
| | JH4 CS plasmid | | | | | | | | |
| | Clone | Functionality | VH-gene | DH-gene | JH-gene | Identity (%) | CDR3 length | CDR3 amino acid sequence | Colonies[§] |
| | Clone_01 | Productive | V5-6 (or V5-6-1*01) | D1-1 | JH2 | 99.3 | 13 | CARHYYGSSYYFDYW | 10/10 |
| CLL_32371 | JH1 CS plasmid | | | | | | | | |
| | Clone | Functionality | VH-gene | DH-gene | JH-gene | Identity (%) | CDR3 length | CDR3 amino acid sequence | Colonies[§] |
| | Clone_01 | Productive | V1-81 | D1-1 | JH1 | 98.96 | 14 | CAERFTTVVARYFDVW | 1/7 |
| | Clone_03.0 | Productive | V11-2 | D2-5 | JH1 | 98.61 | 11 | CMRYSNYWYFDVW | 6/7 |
| | JH2 CS plasmid | | | | | | | | |
| | Clone | Functionality | VH-gene | DH-gene | JH-gene | Identity (%) | CDR3 length | CDR3 amino acid sequence | Colonies[§] |
| | Clone_01 | Productive | V1-81 | D1-1 | JH1 | 98.96 | 14 | CAERFTTVVARYFDVW | 1/8 |
| | Clone_03.1 | Productive | V11-2 | D2-5 | JH1 | 98.61 | 11 | CMKYSNYWYFDVW | 1/8 |
| | Clone_03.0 | Productive | V11-2 | D2-5 | JH1 | 98.61 | 11 | CMRYSNYWYFDVW | 3/8 |
| | JH3 CS plasmid | | | | | | | | |
| | Clone | Functionality | VH-gene | DH-gene | JH-gene | Identity (%) | CDR3 length | CDR3 amino acid sequence | Colonies[§] |
| | Clone_03.0 | Productive | V11-2 | D2-5 | JH1 | 98.61 | 11 | CMRYSNYWYFDVW | 5/8 |
| | JH4 CS plasmid | | | | | | | | |
| | Clone | Functionality | VH-gene | DH-gene | JH-gene | Identity (%) | CDR3 length | CDR3 amino acid sequence | Colonies[§] |
| | Clone_02 | Productive | V1-82 | D1-1 | JH2 | 98.96 | 13 | CARSGYYGSSPLDYW | 2/8 |
| CLL_31938 | JH1 CS plasmid | | | | | | | | |
| | Clone | Functionality | VH-gene | DH-gene | JH-gene | Identity (%) | CDR3 length | CDR3 amino acid sequence | Colonies[§] |
| | Clone_01 | Productive | V1-62-2 (or V1-71) | D2-3 | JH1 | 98.96 | 17 | CARHEEEGYYGLGGYFDVW | 2/7 |
| | Clone_05 | Unproductive | V1-70 P | D1-1 | JH4 | 98.96 | X | CARTGGLLR**V#YYAMDYW | 2/7 |
| | JH2 CS plasmid | | | | | | | | |
| | Clone | Functionality | VH-gene | DH-gene | JH-gene | Identity (%) | CDR3 length | CDR3 amino acid sequence | Colonies[§] |
| | Clone_02 | Productive | V1-39 | D2-3 | JH1 | 98.96 | 12 | CARYDGNYGVFDVW | 2/7 |
| | Clone_03 | Productive | V1-67 | D2-3 | JH2 | 98.96 | 10 | CARDYDGYFDYW | 2/7 |
| | JH3 CS plasmid | | | | | | | | |
| | Clone | Functionality | VH-gene | DH-gene | JH-gene | Identity (%) | CDR3 length | CDR3 amino acid sequence | Colonies[§] |
| | Clone_04 | Unproductive | V1-82 | D4-1 | JH3 | 98.96 | X | CARSNW#AWFAYW | 3/6 |
| | JH4 CS plasmid | | | | | | | | |
| | Clone | Functionality | VH-gene | DH-gene | JH-gene | Identity (%) | CDR3 length | CDR3 amino acid sequence | Colonies[§] |
| | Clone_05 | Unproductive | V1-70 P | D1-1 | JH4 | 98.96 | X | CARTGGLLR**V#YYAMDYW | 7/8 |

[§] Number of colonies with identical sequence and total number of colonies sequenced, * Stop codon in CDR3 region, out-of-frame CDR3, # restored frameshift for out-of-frame junctions

**Table 12. Analysis of IgH VDJ rearrangements cloned from splenocytes of burdened TCL1tg R26-IK2ca/ca CD19cre mice**

| Mouse ID | Major clones identified | | | | | | | | |
|---|---|---|---|---|---|---|---|---|---|
| CLL_32299 | JH1 CS plasmid | | | | | | | | |
| | Clone | Functionality | VH-gene | DH-gene | JH-gene | Identity (%) | CDR3 length | CDR3 amino acid sequence | Colonies[§] |
| | Clone_02 | Unproductive | V1-67 | D2-3 | JH1 | 99.3 | X | CASMMVTTT#YFDVW | 2/10 |
| | Clone_03 | Unproductive | V1-21-1 P | | JH1 | 99.0 | X | SARLR**LLVLRCL | 3/10 |
| | JH2 CS plasmid | | | | | | | | |
| | Clone | Functionality | VH-gene | DH-gene | JH-gene | Identity (%) | CDR3 length | CDR3 amino acid sequence | Colonies[§] |
| | Clone_01 | Productive | V1-9 | | JH2 | 99.3 | 6 | CARWFDYW | 8/10 |
| | JH3 CS plasmid | | | | | | | | |
| | Clone | Functionality | VH-gene | DH-gene | JH-gene | Identity (%) | CDR3 length | CDR3 amino acid sequence | Colonies[§] |
| | All 10 sequences were unique, | | | | | | | | |
| | JH4 CS plasmid | | | | | | | | |
| | Clone | Functionality | VH-gene | DH-gene | JH-gene | Identity (%) | CDR3 length | CDR3 amino acid sequence | Colonies[§] |
| | Clone_01 | Productive | V1-9 | | JH2 | 99.3 | 6 | CARWFDYW | 2/10 |
| CLL_32274 | JH1 CS plasmid | | | | | | | | |
| | Clone | Functionality | VH-gene | DH-gene | JH-gene | Identity (%) | CDR3 length | CDR3 amino acid sequence | Colonies[§] |
| | Clone_04 | Productive | V1-47 | D4-1 | JH1 | 98.96 | 10 | CAVANWDYFDVW | 1/12 |
| | Clone_05 | Productive | V14-2 | D2-13 | JH1 | 99.31 | 10 | CAWGSFWYFDVW | 3/12 |
| | Clone_06 | Productive | V1-81 | D2-2 | JH1 | 98.96 | 11 | CAYGYGYWYFDVW | 3/12 |
| | Clone_08 | Unproductive | V5-17 | D1-1 | JH1 | 99.31 | X | CAITTVVA##YWYFDVW | 5/12 |
| | JH2 CS plasmid | | | | | | | | |
| | Clone | Functionality | VH-gene | DH-gene | JH-gene | Identity (%) | CDR3 length | CDR3 amino acid sequence | Colonies[§] |
| | Clone_04 | Productive | V1-47 | D4-1 | JH1 | 98.96 | 10 | CAVANWDYFDVW | 3/10 |
| | Clone_09 | Unproductive | V14-4 | D2-4 | JH2 | 99.31 | X | CTKGMITTGA#YYFDYW | 2/10 |
| | JH3 CS plasmid | | | | | | | | |
| | Clone | Functionality | VH-gene | DH-gene | JH-gene | Identity (%) | CDR3 length | CDR3 amino acid sequence | Colonies[§] |
| | Clone_01 | Productive | V1-19 | D3-1 | JH3 | 96.18 | 10 | CAREGGATLAYW | 2/10 |
| | Clone_03 | Productive | V5-6 (or V5-6-1) | D4-1 | JH3 | 99.31 | 7 | CARLTGAYW | 3/10 |
| | Clone_07 | Productive | V14-4 | D1-1 | JH3 | 99.31 | 12 | CTLFITTVVDLAYW | 3/10 |
| | JH4 CS plasmid | | | | | | | | |
| | Clone | Functionality | VH-gene | DH-gene | JH-gene | Identity (%) | CDR3 length | CDR3 amino acid sequence | Colonies[§] |
| | Clone_02 | Productive | V1-54 | D1-1 | JH3 | 98.96 | 14 | CARGIRTTVVEGFAYW | 3/7 |
| | Clone_03 | Productive | V5-6 (or V5-6-1) | D4-1 | JH3 | 99.31 | 7 | CARLTGAYW | 4/ |
| CLL_32987 | JH1 CS plasmid | | | | | | | | |
| | Clone | Functionality | VH-gene | DH-gene | JH-gene | Identity (%) | CDR3 length | CDR3 amino acid sequence | Colonies[§] |
| | Clone_01 | Productive | V12-3 | D2-3 | JH1 | 98.61 | 12 | CAGDYDGYWYFDVW | 2/11 |
| | Clone_02 | Productive | V1-75 | D2-12 | JH1 | 98.61 | 14 | CARGYYGYDVWYFDVW | 3/11 |
| | JH2 CS plasmid | | | | | | | | |
| | Clone | Functionality | VH-gene | DH-gene | JH-gene | Identity (%) | CDR3 length | CDR3 amino acid sequence | Colonies[§] |
| | Clone_03 | Unproductive | V5-2 | D2-3 | JH2 | 99.31 | X | CARLM#YFDYW | 10/12 |
| | JH3 CS plasmid | | | | | | | | |
| | Clone | Functionality | VH-gene | DH-gene | JH-gene | Identity (%) | CDR3 length | CDR3 amino acid sequence | Colonies[§] |
| | Clone_03 | Unproductive | V5-2 | D2-3 | JH2 | 99.31 | X | CARLM#YFDYW | 4/12 |
| | JH4 CS plasmid | | | | | | | | |
| | Clone | Functionality | VH-gene | DH-gene | JH-gene | Identity (%) | CDR3 length | CDR3 amino acid sequence | Colonies[§] |
| | Clone_03 | Unproductive | V5-2 | D2-3 | JH2 | 99.31 | X | CARLM#YFDYW | 7/11 |

[§] Number of colonies with identical sequence and total number of colonies sequenced, * Stop codon in CDR3 region, out-of-frame CDR3, # restored frameshift for out-of-frame junction

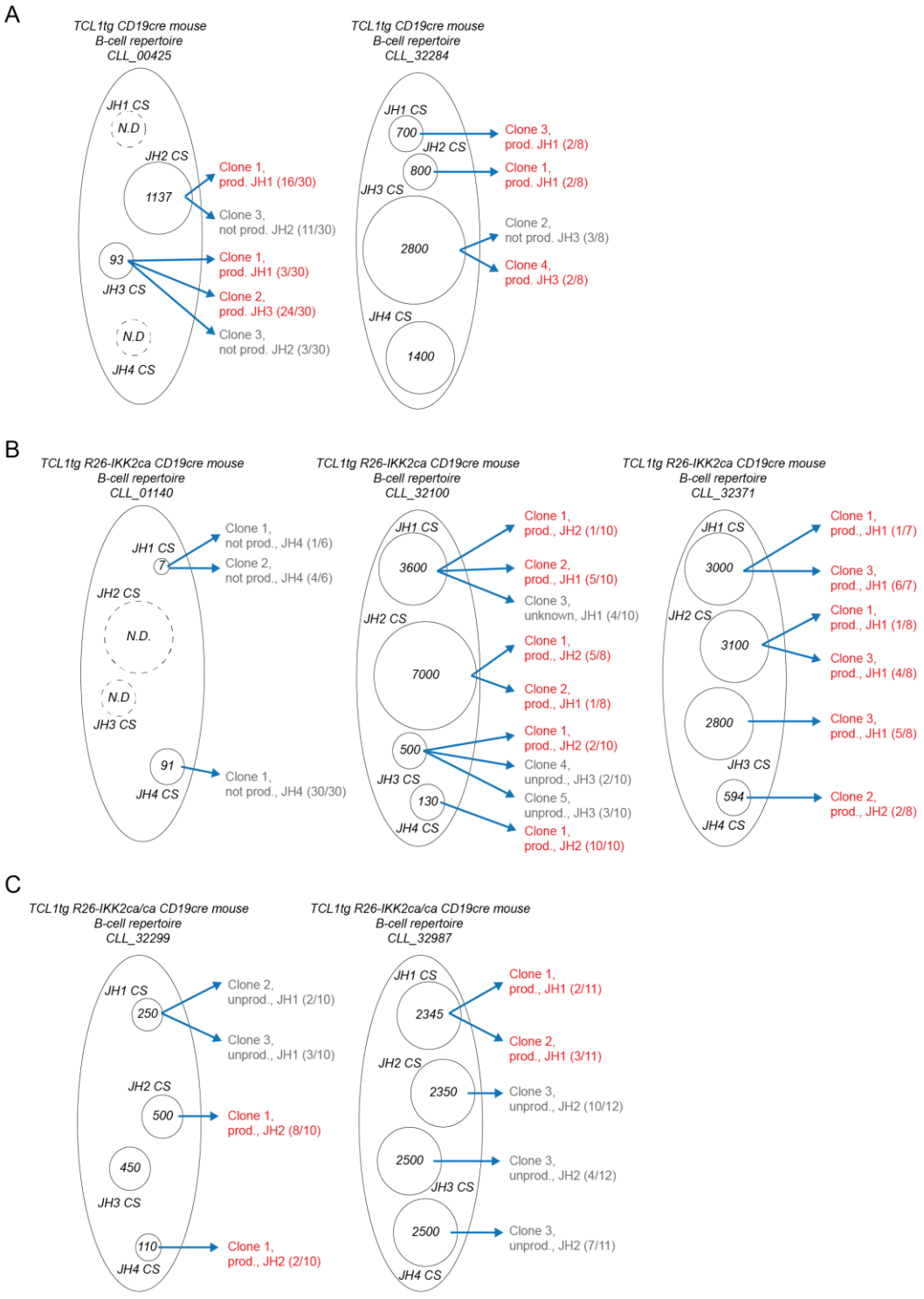


**Figure 34. Cloned IgH VDJ rearrangements point to oligoclonal lymphomas**

Clonality analysis of the BCR repertoire from splenocytes of burdened mice of the following genotypes: (A) TCL1tg CD19cre, (B) TCL1tg R26-IKK2ca CD19cre and (C) TCL1tg R26-IKK2ca/ca CD19cre burden mice. Total number of white colonies obtained for each JH CS plasmid is indicated inside a circle. Blue arrow indicates major clones identified for each sample, rearrangement productivity, JH-gene segment, number of clones with identical sequences and number of total colonies sequenced (see Tables S6-8).

Interestingly, for sample TCL1tg R26-IKK2ca CD19cre CLL_31937 only JH2-gene segment containing VDJ rearrangements were detected by PCR (Figure S 32B and C). Therefore, only the VDJ rearrangements into JH2-gene segment were cloned using the JH2 CS specific plasmid. Under these conditions, only one unproductive VDJ rearrangement was identified for this sample (Frequency 0.1, Table 11). Similarly, for sample CLL_32351 solely JH1-gene segments specific rearrangements were detected by PCR. Thus, JH1-gene segments were cloned using the JH1 CS specific plasmid. Two productive clonal VDJ rearrangements were detected, suggesting the presence of an oligoclonal CLL expansion in this sample.

In the remaining three TCL1tg R26-IKK2ca samples (CLL_32100, CLL_32371 and CLL_31938) two to three productive clonal VDJ rearrangements were identified in addition to up to two unproductive rearrangements (Table 11, Figure 34B). For instance, for the TCL1tg R26-IKK2ca CD19cre sample CLL_32371, out of the three clones identified, Clone_03 was the mostly prominent clone: being identified in 85% (6/7), 50% (4/8) and 62% (5/8) of the JH1 CS, JH2 CS and JH3 CS sequenced colonies, respectively (Table 11 and Figure 34B). On the other hand, Clone_01 was detected in 14% (1/7) and 12% (1/8) of the sequenced colonies for the JH1 and JH2 CS plasmids, respectively; while Clone_02 was detected in 25% (2/8 colonies) of sequenced colonies for the JH4 CS plasmid.

Finally, from the three TCL1tg R26-IKK2ca/ca CD19cre samples analysed up to nine major clones were identified per sample, independently of their functionality (Table 12). Sample CLL_32274 had the highest number of clonal VDJ rearrangements, out of which 7 were productive and 2 were unproductive. While in the remaining two samples, three clonal VDJ rearrangements were identified (Figure 34C). In sample CLL_3229 only one major clonal rearrangement was identified (Clone_01), in addition to two clonal unproductive rearrangements. In comparison, in sample CLL_32987 the major clonal rearrangement identified was unproductive (Clone_03), while the other two clonal productive rearrangements identified were present at a lower frequency.

In addition to the identification of clonal IgH VDJ rearrangements present in the lymphoma samples analysed, their sequencing also provided the mutational status of the VH-gene segments. In human CLL the $CD5^+$ B1a-like cells can be classified accordingly to their BCR mutational status: unmutated-CLL have a poor prognosis, while mutated-CLL is more indolent [215, 255]. In the TCL1tg-driven murine CLL the disease

has an unmutated-like status [256]. I could confirm that in the two TCL1tg CD19cre lymphoma samples analysed here, the clones identified had over 98% identity with the germ line VH-gene segment (Table 10). Further enhanced NF-κB activation did not affect the mutational status of the CLL-cells. Both TCL1tg R26-IKK2ca CD19cre (Table 11) and TCL1tg R26-IKK2ca/ca CD19cre clonal lymphomas (Table 12) had over 95% identity with the germ line VH-gene segments. Therefore, the mutational status of the disease is not altered by the combination of constitutive canonical NF-κB activation with TCL1.

The analysis of the IgH VDJ recombination in B-cells of control and burdened mice shows that the $CD5^+$ B1a-like cells in the TCL1tg compound mice have an unmutated IgH VDJ status and are at least oligoclonal, compared to the wild type controls where a much higher diversity of VDJ recombination was observed. Moreover, the analysis of a higher number of colonies renders a more accurate picture of the clonal dynamics and clone size for each lymphoma sample.

#### IV.2.3.2.2 *Ex vivo* immunophenotyping of burdened CLL/SLL mice

In human CLL, it is now accepted that the tissue microenvironment has a pathogenic or modulatory role on the disease. Herishanu et al. (2011) have proposed the lymph node as a particular pathogenic niche in CLL, where a transcriptional analysis points to activation of BCR- and canonical NF-κB of CLL-cells [141]. Therefore, constitutive activation of canonical NF-κB could mimic aspects of niche interactions. Thus, to gain a better understanding in the role of constitutive canonical NF-κB activation and the TCL1 oncogene in the development of CLL-like disease in mice, the *ex vivo* expression of several immunoreceptors, the CD69 cell surface receptor, chemokine associated receptors, regulators of apoptosis, the IRF4 transcription factor and CLL associated proteins were assessed by flow cytometry in the bone marrow, spleen, peritoneal cavity and draining lymph nodes from burdened and aged control mice. For the comparison, the *ex vivo* expression of each marker was assessed using flow cytometry and the MFI of each marker was normalized to the B2 CD19cre control subpopulation. Although in the mouse B1a-cells are a normal subset found mainly in the peritoneum and to a lesser extent in the spleen, for this particular comparison B1a-like populations in the bone marrow and lymph nodes were also included in the analysis of control mice.

### *Ex vivo* comparison of B1a-like cells in burdened mice

The comparison of B1a-like cells in burdened mice resulted in a significantly differential expression of the immunoreceptor MHC-II and the chemokine receptor CXCR4. Additionally, differential expression trends were also observed for the immunoreceptors CD25, CD40 and CD86; the cell surface receptor CD69; the anti-apoptotic protein BCL2; and the CLL-associated proteins Zap70 and PD1.

First, two different relative expression trends were observed for MHC-II. In the bone marrow, the relative expression of MHC-II increased in an IKK2ca dose dependent manner (Figure 35 and Figure S 33F). Additionally, there was a significant increase in the expression of MHC-II on B1a-like cells from burdened TCL1tg R26-IKK2ca CD19cre mice compared to R26-IKK2ca CD19cre mice, pointing to the potential role of TCL1 and canonical NF-κB cooperation in MHC-II expression in the bone marrow niche (Figure S 33F). Interestingly, the situation in the peritoneum was inverted; there was trend for lower relative MHC-II levels in an IKK2ca dose dependent manner (Figure 35 and Figure S 35F). Moreover, there was a significant decrease in MHC-II expression in the TCL1tg R26-IKK2ca CD19cre B1a-like cells compared to the CD19cre control mice. The trend of reduced MHC-II expression levels associated with NF-κB constitutive activation was also observed in B1a-like cells from the lymph nodes (Figure 38 and Figure S 36F) and was less evident in the spleen (Figure 36 and Figure S 34F) of burdened mice.

Furthermore, the comparison of burdened TCL1tg R26-IKK2ca CD19cre with aged matched controls (Figure S 37F) also showed increased expression levels MHC-II in the bone marrow in both B2- and B1a-like cells compared to CD19cre controls. On the other hand, an inverse trend was observed in B2-cells present in spleen, peritoneal cavity and lymph nodes, where the expression of IKK2ca and IKK2ca in combination with TCL1tg lowered the surface expression of MHC-II. This trend was also observed for and B1a-like cells in the peritoneal cavity and lymph nodes. Similar results were observed in the comparison of burdened TCL1tg R26-IKK2ca/ca CD19cre mice with aged matched controls (Figure S 38G).

Given the different relative expression trends observed between B-cells from the bone marrow and the other organs analysed (spleen, peritoneum and lymph nodes), it is possible that the niche has an additional influence in the collaboration between strong canonical NF-κB activation and the TCL1tg oncogene in modulating the MHC-II surface expression. Furthermore, the low MHC-II expression levels observed could indicate a

reduced ability of the CLL-like cell to elicit an immune response in these particular niches. The higher MHC-II expression observed in the bone marrow is puzzling. It could be possible that in the bone marrow niche the CLL-like cell might be generating an inflammatory phenotype. Alternatively, canonical NF-κB activation alone could affect the ubiquitination or the internalization and further degradation of MHC-II [257, 258], also the intracellular MHC-II expression remains to be investigated.

Second, the expression of the chemokine receptor CXCR4 showed a trend for reduced levels in B1a-like cells of burdened mice in an IKK2ca dose depended manner in the spleen (Figure 36 and Figure S 34I), peritoneum (Figure 37 and Figure S 35I) and the lymph nodes (Figure 38 and Figure S 36I), and to lesser extent in the bone marrow (Figure 35 and Figure S 33I). Furthermore, in the peritoneum there was a significant decrease in CXCR4 expression in R26-IKK2ca CD19cre B1a-like cells compared to CD19cre controls (Figure S 35I). Moreover, the analysis of burdened TCL1tg R26-IKK2ca CD19cre and aged matched control mice showed a significant reduction in CXCR4 relative levels in R26-IKK2ca CD19cre and TCL1tg R26-IKK2ca CD19cre compared to CD19cre B1a-like cells (Figure S 37H) in the peritoneum. A similar effect was observed for the other organs analysed and for the analysis of TCL1tg R26-IKK2ca/ca CD19cre burden mice and aged matched controls (Figure S 38I). Therefore, it is likely that the main negative regulator of CXCR4 expression is constitutive canonical NF-κB activation and that TCL1tg has negligible effects on its expression. This reduced CXCR4 expression could point to a higher mobility of IKK2ca+; TCL1+ CLL-like cells into the periphery compared to normal B1a-like cells or TCL1+ B1a-like cells. Additionally, the lower CXCR4 surface expression observed could make them more independent of the SDF1 producing stroma cells in the niche. Interestingly, Chen et al. have reported that BTK inhibition by ibrutinib directly reduced CXCR4 levels in CLL-like cells promoting their migration [259]. These results are contradictory to the observation of reduced CXCR4 expression in the B1a-like cells present in TCL1tg R26-IKK2ca compound mice that show an accelerated disease progression compared to the CD19cre TCL1tg mice.. Further analyses are necessary to address the role of reduced CXCR4 surface expression in TCL1tg R26-IKK2ca and its potential association to a more aggressive type of CLL.

Third, there was a trend for lower CD25 expression levels in B1a-like cells in the bone marrow of burdened mice when the TCL1tg was present (Figure S 33A). However, in the spleen and lymph nodes the reduced CD25 expression occurred in an IKK2ca dose dependent manner (Figure S 34A and Figure S 36A).

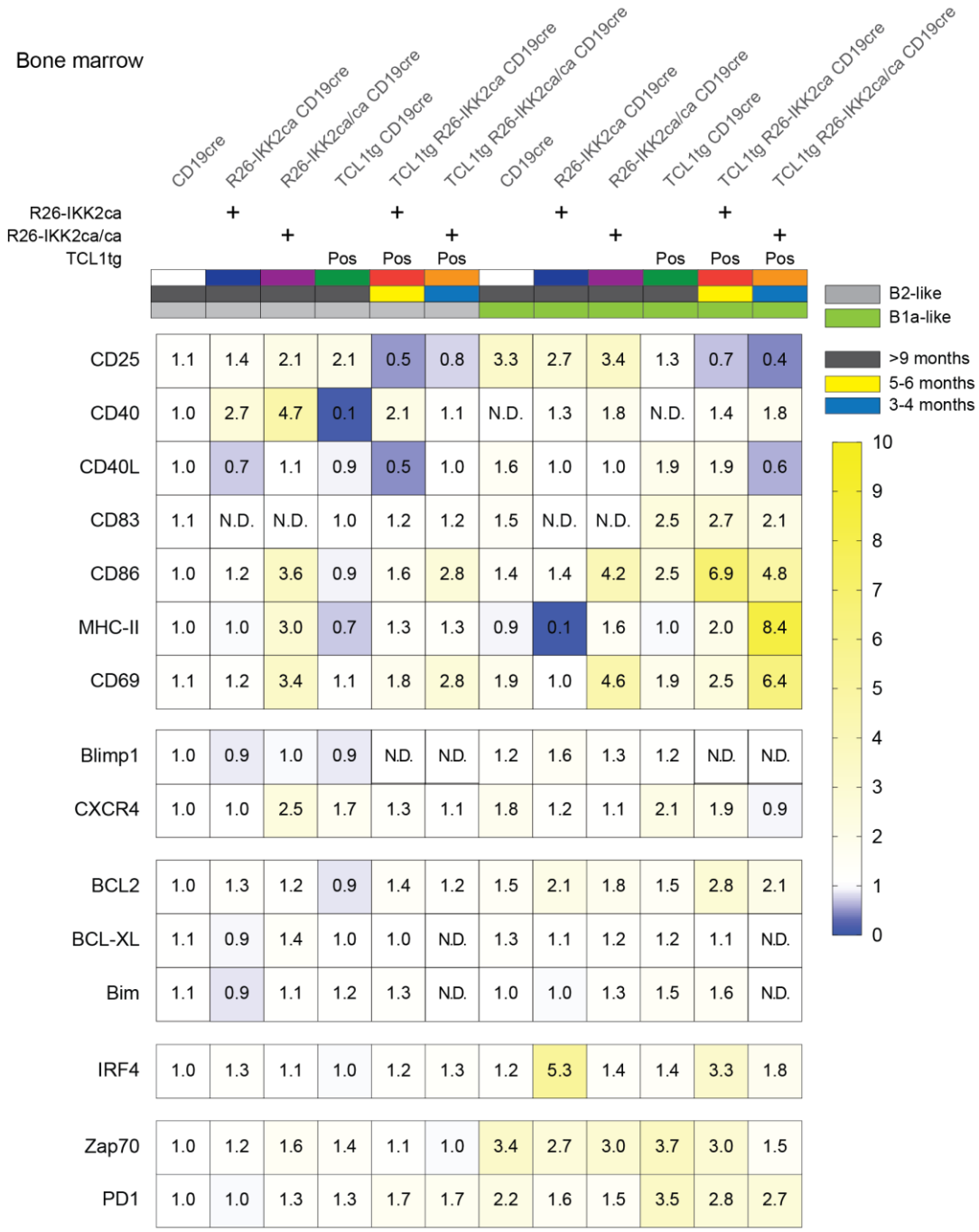


**Figure 35. Bone marrow B2- vs. B1a-like cells immunophenotyping**

*Ex vivo* immunophenotyping of B-cell subsets B2- and B1a-like in bone marrow from burden and control mice by flow cytometry. Heatmaps depicts geometric mean for the MFI each marker relative to B2 CD19cre controls. At least 2 (2-10) mice were analysed per genotype.
B2-like ($CD19^{+}$ $B220^{hi}$), B1a-like ($CD19^{+}$ $B220^{lo}$), N.D. (not done).

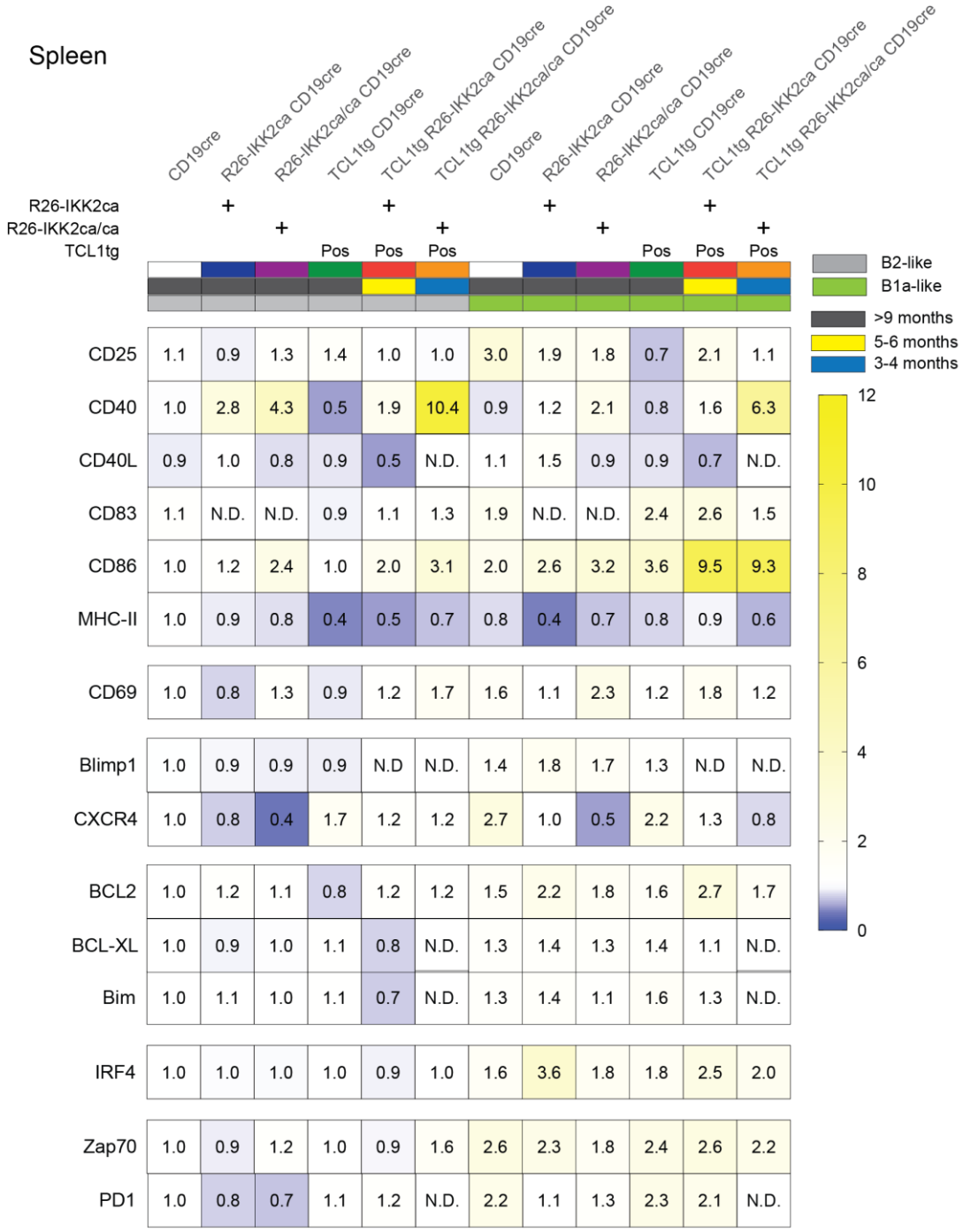


**Figure 36. Splenic B2- vs. B1a-like cells immunophenotyping**

*Ex vivo* immunophenotyping of B-cell subsets B2- and B1a-like in spleen from burden and control mice by flow cytometry. Heatmaps depicts geometric mean for the MFI each marker relative to B2 CD19cre controls. At least 2 (2-10) mice were analysed per genotype.
B2-like ($CD19^{+}$ $B220^{hi}$), B1a-like ($CD19^{+}$ $B220^{lo}$), N.D. (not done).

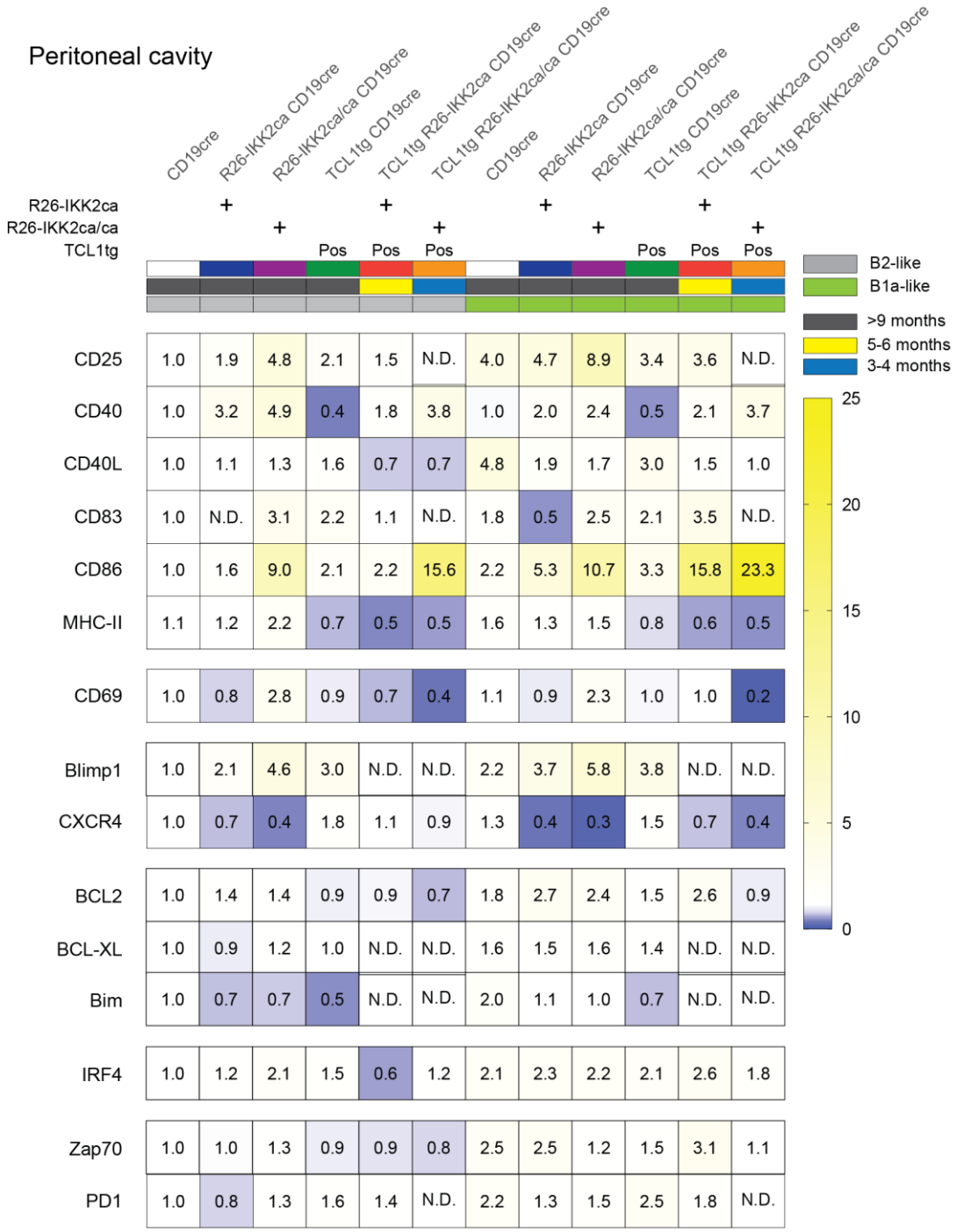


**Figure 37. Peritoneal cavity B2- vs. B1a- cells immunophenotyping**

*Ex vivo* immunophenotyping of B-cell subsets B2- and B1a-like in peritoneal cavity from burden and control mice by flow cytometry. Heatmaps depicts geometric mean for the MFI each marker relative to B2 CD19cre controls. At least 2 (2-10) mice were analysed per genotype.
B2-like ($CD19^{+}$ $B220^{hi}$), B1a-like ($CD19^{+}$ $B220^{lo}$), N.D. (not done).

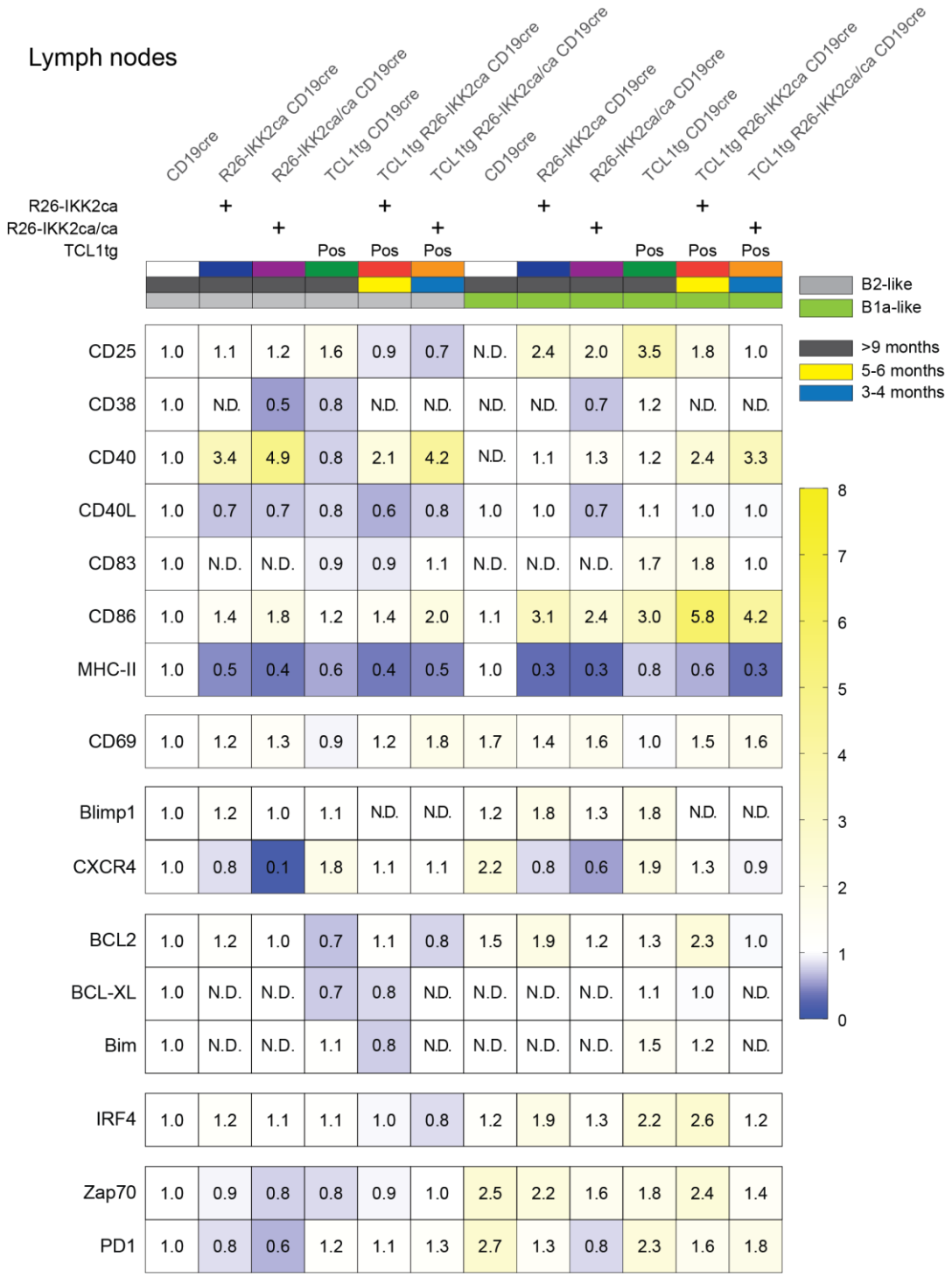


**Figure 38. Lymph node B2- vs. B1a-like cells immunophenotyping**

*Ex vivo* immunophenotyping of B-cell subsets B2- and B1a-like in draining lymph nodes from burden and control mice by flow cytometry. Heatmaps depicts geometric mean for the MFI each marker relative to B2 CD19cre controls. At least 2 (2-10) mice were analysed per genotype.
B2-like ($CD19^{+}$ $B220^{hi}$), B1a-like ($CD19^{+}$ $B220^{lo}$), N.D. (not done).

In comparison, CD40 presented a trend for higher expression levels in B1a-like cells from burden mice in an IKK2ca dose dependent manner (Figure S 33B, Figure S 34B, Figure S 35B and Figure S 36B). Moreover, the analysis of burdened TCL1tg R26-IKK2ca CD19cre and aged matched controls showed that TCL1tg R26-IKK2ca CD19cre B1a-like cells have a significantly higher expression than the CD19cre controls, while the R26-IKK2ca CD19cre B1a-like cells have an intermediate CD40 expression (Figure S 37B). A similar trend was observed in the TCL1tg R26-IKK2ca/ca CD19cre burden mice (Figure S 38C). Thus, it is likely that both canonical NF-κB and TCL1tg contribute to increase CD40 expression.

Similarly, CD86 presented a trend for higher expression in B1a-like cells in spleen (Figure S 34E), peritoneum (Figure S 35E) and lymph nodes (Figure S 36E) from burdened mice in an IKK2ca dose dependent manner and as well as the presence of TCL1tg. Moreover, in the lymph nodes the expression level in B1a-like cells of R26-IKK2ca/ca CD19cre and TCL1tg CD19cre cells is relatively similar, but the combination of both leads to a stronger relative CD86 expression. Furthermore, the comparison of burdened TCL1tg R26-IKK2ca CD19cre and their aged matched controls showed that, at least in young age (5-6 months of age), the significant increase in CD86 relative MFI levels is a result of TCL1tg expression (Figure S 37E).

Fourth, the expression levels of the cell surface receptor CD69 were affected by the presence of IKK2ca. There is a trend for higher relative CD69 MFI when the second allele of IKK2ca is present in B1a-like cells in bone marrow (Figure S 33G), spleen (Figure S 34G) and peritoneal cavity (Figure S 35G). While in the TCL1tg compound mice, the trend for higher CD69 expression occurs in an IKK2ca dose dependent manner in B1a-like cells from bone marrow and spleen. However, in the peritoneum the effect is the opposite resulting in a trend for reduced CD69 expression in both B2- and B1a-like cells. Surprisingly, there is a significant increase in the relative expression of CD69 in B1a-like cells from the peritoneum of TCL1tg R26-IKK2ca CD19cre burdened mice compared to B1a-cells in aged matched controls (Figure S 37G).

Fifth, the anti-apoptotic protein BCL2 has a very particular expression pattern. There is a trend for higher BCL2 expression in the R26-IKK2ca heterozygous B1a-like cells compared to the homozygous or wild type cells (Figure S 33J, Figure S 34J, Figure S 35J and Figure S 36J). Interestingly, the R26-IKK2ca/ca CD19cre and TCL1tg CD19cre B1a-like cells have similar BCL2 expression levels. The comparison of TCL1tg R26-IKK2ca

CD19cre burdened mice with aged matched controls, also points to a positive effect of hemizygous IKK2ca and additional effects of TCL1 in the expression of BCL2 in B1a-like cells (Figure S 37I).

Sixth, there is a trend for lower Zap70 expression in an IKK2ca dose dependent manner in the B1a-like cells in the absence of TCL1tg (Figure S 33N, Figure S 34N, Figure S 35N and Figure S 36N). This is also true for B1a-cells positive for TCL1tg in bone marrow and spleen. However, in the peritoneum and to a lesser extent in the lymph nodes, the combination of the TCL1tg with one allele of IKK2ca results in relative higher Zap70 levels. Notably, in 5-6 months old mice, at least in the peritoneum and the lymph nodes, the TCL1tg B1a-like cells have a relative lower expression of Zap70 compared to TCL1tg R26-IKK2ca CD19cre or R26-IKK2ca CD19cre mice (Figure S 37N).

Finally, the relative MFIs for PD1 appear to go down in an IKK2ca dose dependent manner in B1a-like cells from burdened mice (Figure S 33O, Figure S 34O, Figure S 35O and Figure S 36O). The highest level of expression is observed in the TCL1tg CD19cre B1a-like cells.

Therefore, constitutive canonical NF-κB activation as well as the TCL1tg alone or in combination with a particular microenvironment can modulate the expression of activation markers and other proteins.

### *Ex vivo* comparison of B2-cell subset in burdened mice

The B2 subset comparison from burdened mice shows a significantly differential expression of CD40, CD86, MHC-II and CXCR4. First, there is a significant increase in the relative expression of CD40 in B2-cells in an IKK2ca dose dependent manner in spleen (Figure S 34B), peritoneal cavity (Figure S 35B) and lymph nodes (Figure S 36B) that also affected TCL1tg positive B2-cells similarly. This trend for higher CD40 expression was also observed in bone marrow B2-like cells (Figure S 33B). The comparison of burdened TCL1tg R26-IKK2ca CD19cre mice had similar results (Figure S 37). There was a significantly higher expression of CD40 in B2-cells from R26-IKK2ca CD19cre controls and TCL1tg R26-IKK2ca CD19cre burdened mice compared to CD19cre aged matched controls.

Second, there is a trend for higher levels of the activation marker CD86 in an IKK2ca dose dependent manner in B2-cells from burdened mice (Figure S 33E, Figure S 34E, Figure S 35D and Figure S 36E). Moreover, the expression of CD86 was significantly increased in R26-IKK2ca/ca CD19cre and TCL1tg R26-IKK2ca/ca CD19cre B2-cells compared to CD19cre controls in the peritoneum (Figure S 35E).

Third, the relative expression of the immunoreceptor MHC-II was significantly reduced in TCL1tg CD19cre and TCL1tg R26-IKK2ca CD19cre B2-cells from burdened mice compared to the CD19cre controls in spleen (Figure S 34F) and lymph nodes (Figure S 36F). Similarly, the comparison of aged matched 3-4 (Figure S 38G) and 5-6 old (Figure S 37F) mice revealed a significant negative effect on the expression of MHC-II in eGFP+;IKK2ca+;TCL1+ B2-cells compared to CD19cre aged matched controls in the spleen and lymph nodes. It appears that the presence of TCL1tg negatively affects the expression of MHC-II in B-cells.

Finally, there was a significant lower expression of CXCR4 in R26-IKK2ca/ca CD19cre B2-cells compared to TCL1tg CD19cre B2-cells in the spleen of burden mice (Figure S 34I).

### *Ex vivo* comparison between B2- and B1a-like cells in burdened mice

The comparison of the B2- and B1a-cells subsets in spleen and peritoneal cavity from CD19cre controls showed that the relative expression of CD25 (Figure S 35A and Figure S 37A) and Zap70 (Figure S 35N, Figure S 34N and Figure S 37N) were significantly increased in the latter compared to the former. Therefore the differential expression of CD25 and Zap70 is likely to be B-cell type specific.

Additionally, in the analysis of 5-6 months old mice, the surface receptor CD69 was significantly higher in the B1a compared to B2-cells in the spleen; while the opposite was true for the peritoneum where the B1a-cells had a significantly lower CD69 expression than B2-cells (Figure S 37G). Moreover, the expression of CXCR4 was significantly higher in B1a-cells compared to their B2 counterpart in spleens of CD19cre and R26-IKK2ca CD19cre mice (Figure S 37H).

Meanwhile, the comparison between B1a-like and their B2 counterpart in burdened mice revealed a significant increase in the relative expression levels of activation

markers CD83 (Figure S 34D, Figure S 35D, Figure S 36D and Figure S 37D) and CD86 (Figure S 33E, Figure S 34E, Figure S 35E, Figure S 36E and Figure S 37E); the anti-apoptotic protein BCL2 (Figure S 33J, Figure S 34J, Figure S 35J and Figure S 36J), the transcription factor IRF4 (Figure S 33M, Figure S 34M, Figure S 35M and Figure S 36M) and the CLL-related signalling molecule Zap70 (Figure S 33N, Figure S 34N, Figure S 35N and Figure S 36N) in the TCL1tg R26-IKK2ca CD19cre mice. Additionally, there was a significant decrease in the relative MFI for the chemokine receptor CXCR4 (Figure S 35I).

Similarly, in burdened TCL1tg CD19cre mice, the B1a-like cells had a significantly higher expression of BCL2 in the spleen (Figure S 34J) and Zap70 in the draining lymph nodes (Figure S 36N) compared to their B2 counterparts.

It is likely that the higher Zap70 expression observed in both TCL1tg CD19cre mice as in the TCL1tg R26-IKK2ca CD19cre mice is cell-type related rather than TCL1tg or IKK2ca dependent. The relative expression of Zap70 in B1a-like cells in spleens of TCL1tg R26-IKK2ca CD19cre mice (geo. mean 2.6) is similar to that of CD19cre controls (geo. mean 2.6, Figure S 34N). Moreover, in both cases there is a 1.5-fold increase in the relative expression.

Furthermore, in 5-6 months old mice B1a-cells presents with higher IRF4 expression in B1a compared to B2-cells in spleen and peritoneum (Figure S 37L). Therefore, it is possible that the higher IRF4 relative MFI in B1a-like cells in the burdened TCL1tg R26-IKK2ca CD19cre mice might be rather a cell-type specific pattern, than the actual role of constitutive canonical NF-κB or TCL1tg expression.

#### IV.2.3.2.3 *In vitro* characterization

Constitutive canonical NF-κB activation in B-cells prolongs their survival *in vitro* and *in vivo* by replacing the requirement for BAFF [37]. Given that the TCL1tg CLL mouse model is accelerated in an IKK2ca dose dependent manner, I wanted to see if this accelerated disease progression was a result of either prolonged B-cell survival, a higher proliferation rate driven by canonical NF-κB or a cooperative effect between constitutive canonical NF-κB activation and TCL1tg.

### *In vitro* survival and proliferation

In order to determine whether the combination of the TCL1tg oncogene and the IKK2ca knock-in had an effect in B-cell survival, a pilot experiment was performed where either sorted B2- or $CD5^+$ B1a-like cells stained with cell trace were cultured *in vitro* for a period of nine days in the absence of any stimuli.

As it is to be expected, resting sorted B2-cells numbers were drastically reduced after 24 hours in culture (Figure S 39C). Interestingly, although both the CD19cre control and TCL1tg CD19cre B2-cells essentially all died by day two, there was a small population of B2-cells in the R26-IKK2ca CD19cre and TCL1tg R26-IKK2ca CD19cre cultures that survived until day nine in the absence of proliferation (Figure S 39). Therefore, at least *in vitro*, these results are in agreement with published results [37]. In this instance it was not possible to address the *in vitro* survival for R26-IKK2ca/ca CD19cre and R26-IKK2ca/ca TCL1tg CD19cre B2-cells. There were insufficient cell numbers obtained after the sort and cell trace staining.

Comparably to cultured B2-cells, the numbers of B1a-like cells were drastically reduced after 24 hours of culture (Figure 39C). The canonical NF-κB constitutive activation resulted in a reduced percentage of apoptotic cells at days two and three compared to culture TCL1tg CD19cre B1a-like cells. Moreover, combination of the IKK2ca knock-in allele reduced the percentage of apoptotic cells in both TCL1tg R26-IKK2ca CD19cre and TCL1tg R26-IKK2ca/ca CD19cre B1a-like cells in vitro comparable to their TCL1-controls (Figure 39A).

Surprisingly, at day three some of the cultured TCL1tg R26-IKK2ca CD19cre B1a-like cells were proliferating (Figure 39B). The observed proliferation phenotype was maintained at days six and nine. The proliferation index for the TCL1tg R26-IKK2ca CD19cre B1a-like cells increased from 1.18 in day three, to 1.97 in day six reaching a maximum of 2.21 at day nine (Table 13). Moreover, the percentage of apoptotic cells in the TCL1tg R26-IKK2ca CD19cre B1a-like cells remained constant, 20%, during the first three days of culture but increased at day six and nine (Figure 39A). Interestingly, balance between *in vitro* proliferation and apoptosis resulted in a constant absolute number of cells at day three, six and nine (Figure 39C). In other words, the rate at which cells were replicating was sufficient to compensate for the rate at which cells were dying *in vitro*.

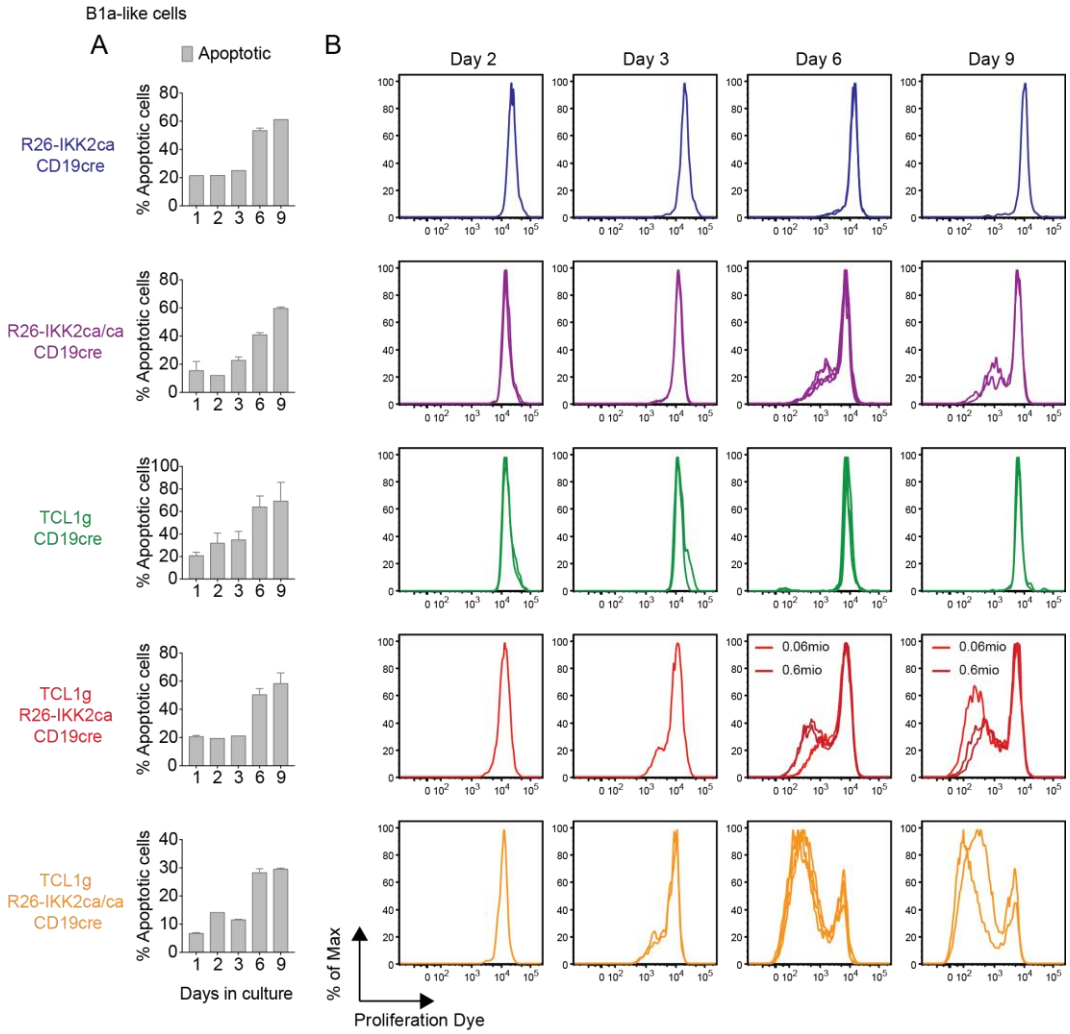


Cell numbers (x10³)

| Genotype | Day 1 | Day 3 | Day 6 | Day 9 |
|---|---|---|---|---|
| R26-IKK2ca CD19cre | 3 | 1.9 | 2.5 | 1.7 |
| R26-IKK2ca/ca CD19cre | 11.3 | 2 | 8.7 | 3.4 |
| TCL1tg CD19cre | 9.1 | 2.4 | 2.5 | 0.7 |
| TCL1tg R26-IKK2ca CD19cre | 2.1 | 1.3 | 1.4 | 1.1 |
| TCL1tg R26-IKK2ca/ca CD19cre | 7 | 8 | 30.6 | 51.5 |

**Figure 39. Effect of IKK2ca and TCL1tg in B1a-like cells *in vitro* proliferation**

Sorted B1a-like cells were cultured in B-cell media in resting conditions for 9 days and *in vitro* cell proliferation and cell survival was assessed by flow cytometry. (A) Bar charts show the percentage of apoptotic cells present in the culture as mean and SEM. (B) Histograms depict the *in vitro* proliferation of B1a-like cells. (C) Scatter plot and table show the absolute number of living B1a-cells in culture.
B1a ($CD19^+$ $B220^-$ $CD5^+$), Apoptotic cells (Annexin-V+ 7AAD-/Annexin-V+ 7AAD+) and Living cells (Annexin-V- 7AAD-).

**Table 13. B1a *in vitro* proliferation analysis**

| Days in culture | Genotype | Div. Index* | Pro. Index¥ | % Divided± |
|---|---|---|---|---|
| Day 3 | R26-IKK2ca CD19cre | 0 | 0 | 0 |
| | R26-IKK2ca/ca CD19cre | 0 | 0 | 0 |
| | TCL1tg CD19cre | 0 | 0 | 0 |
| | TCL1tg R26-IKK2ca CD19cre | 0.7 | 1.18 | 59.5 |
| | TCL1tg R26-IKK2ca/ca CD19cre | 0.35 | 1.425 | 24.7 |
| Day 6 | R26-IKK2ca CD19cre | 0 | 0 | 0 |
| | R26-IKK2ca/ca CD19cre | 0.29 | 1.72 | 16.8 |
| | TCL1tg CD19cre | 0 | 0 | 0 |
| | TCL1tg R26-IKK2ca CD19cre | 0.34 | 1.97 | 17.5 |
| | *TCL1tg R26-IKK2ca CD19cre, Conc.*⌘ | *0.27*⌘ | *1.77*⌘ | *15.35*⌘ |
| | TCL1tg R26-IKK2ca/ca CD19cre | 0.87 | 2.52 | 34.5 |
| Day 9 | R26-IKK2ca CD19cre | 0 | 0 | 0 |
| | R26-IKK2ca/ca CD19cre | 0.29 | 1.72 | 16.8 |
| | TCL1tg CD19cre | 0 | 0 | 0 |
| | TCL1tg R26-IKK2ca CD19cre | 0.465 | 2.21 | 21 |
| | *TCL1tg R26-IKK2ca CD19cre, Conc.*⌘ | *0.29*⌘ | *2.76*⌘ | *10.5*⌘ |
| | TCL1tg R26-IKK2ca/ca CD19cre | 0.87 | 2.52 | 34.5 |

* Division index, average number of divisions for all cells in the culture.
¥ Proliferation index, average number of divisions responding cells have undergone
± Percentage divided, percentage of cells that have undergone at least one round of cell division
⌘0.6 million cells were used for culture at day 0

An additional culture condition was used for the TCL1tg R26-IKK2ca CD19cre B1a-like cells where 10 times more cells, 0.6 million cells, were seeded at day zero. Although proliferation was not assessed at day three, it was evident at day six and nine (Figure 39B). Although both culture conditions displayed similar the proliferation Index values (1.97 vs. 1.77, Table 13) at day six, at day nine the concentrated culture had a proliferation index of 2.76 compared to 2.21 for the standard culture. Moreover, the stronger proliferation in combination with cell death resulted in an accumulation of absolute B1a-like cell numbers from day six to day nine (data not shown). This difference in proliferation indexes and proliferation behaviours could point to a density threshold that would push the proliferation forward. Although there is no evidence to suggest so, it is tempting to speculate that cell-to-cell contacts or paracrine signals potentiate the proliferative capacity of these cells *in vitro*.

Similarly, cultured TCL1tg R26-IKK2ca/ca CD19cre B1a-like cells also started proliferating at day three (Figure 39B). Thereafter, the resting TCL1tg R26-IKK2ca/ca CD19cre B1a-like cells displayed a more proliferative phenotype, reaching a maximum proliferation index of 2.5 at day six (Table 13). As a consequence, the absolute cell numbers increased exponentially with time (Figure 39C). Additionally, a fraction of the resting B1a-like R26-IKK2ca/ca CD19cre cells but not R26-IKK2ca CD19cre cells were

proliferating *in vitro* at day six (Figure 39B and Table 13). This proliferative phenotype was observed also at day nine, however the absolute number of cells was lower.

Even though no proliferation was observed in the sorted TCL1tg CD19cre and the R26-IKK2ca CD19cre B1a-like cells, the combination of the TCL1tg with one allele of IKK2ca resulted in proliferation at day three. Moreover, the combination of the TCL1 transgene with constitutive NF-κB activation resulted higher division index and proliferation index *in vitro* compared to the R26-IKK2ca/ca CD19cre B1a-like cells (Figure 39C). Interesting, the B1a-like TCL1tg R26-IKK2ca/ca CD19cre cells had a higher division and proliferation index than the TCL1tg R26-IKK2ca CD19cre cells. Although these results are preliminary, they point to a potential collaboration between constitutive canonical NF-κB activation and the TCL1tg oncogene in *in vitro* proliferation in B1a-like but not B2-cells. This *in vitro* proliferation could be translated *in vivo* to a proliferation advantage of IKK2ca+;TCL1+ B-cells thus explaining the accelerated disease onset observed in TCL1tg R26-IKK2ca compound mice.

## BCR stimulation

Given the potential role of BCR signals in driving NF-κB activation and promoting survival in CLL patients cell, an additional pilot experiment was set up to assess the role of BCR stimulation in proliferation of $CD5^+$ B1a-like cells.

As a reference control, B2-cells were stimulated *in vitro* with 15ug/ml of anti-IgM and cultured for three days. Already at 12 hours all samples showed a higher expression of the activation markers CD86 and MHC-II (Figure S 40A) indicating cross-linking of the BCR and activation of downstream signals. After three days of stimulation, B2-cells from all the genotypes analysed were proliferating (Figure S 40B). Interestingly, there was an increase in the proliferation index of TCL1tg CD19cre B2-cells in an IKK2ca dose dependent manner. Additionally, although the TCL1tg R26-IKK2ca/ca CD19cre B2-cells had the lowest division index and percentage of divided cells values, they also had the highest proliferation index value (Figure S 40C).

B1a-like cells were sorted from TCL1tg R26-IKK2ca/ca CD19cre or R26-IKK2ca/ca CD19cre mice, followed by cell trace staining. Finally, cells were stimulated with 2.5ug/ml or 5ug/ml dose of anti-IgM and cultured up to nine days. Although no proliferation was observed after 24 hours (Figure S 41A, Day 1), the B1a-like cells were

in an activated state (Figure S 41B). Both doses of anti-IgM stimuli resulted in increased MHC-II expression in R26-IKK2ca/ca CD19cre and TCL1tg R26-IKK2ca/ca CD19cre B1a-like cultured cells. Paradoxically, there was a population of cells that had reduced expression of the activation marker CD86.

*In vitro* proliferation after anti-IgM stimulation was assessed on days three and nine of culture. As mentioned previously, at day three the resting TCL1tg R26-IKK2ca/ca CD19cre B1a-like cells had started proliferating (Figure 39B). Interestingly, although at day three the resting TCL1tg R26-IKK2ca/ca CD19cre B1a-like cells had a higher division index compared to the cells stimulated with 5ug/mL of anti-IgM, they had a lower proliferation index (Figure S 41C). Indicating that compared to the resting TCL1tg R26-IKK2ca/ca CD19cre only a small fraction of stimulated cells was responsive (Figure S 41A). Moreover, at day nine the TCL1tg R26-IKK2ca/ca CD19cre B1a-like cells stimulated with a dose of 5ug/ml anti-IgM had both a higher division and proliferation index compared to the resting cells (Figure S 41C). Additionally, there was an increase in TCL1tg R26-IKK2ca/ca CD19cre B1a-like absolute cell numbers from day three to day nine, where a higher dose of stimuli led to a sharper increase (Figure S 41D).

Interestingly, although the control TCL1tg R26-IKK2ca/ca CD19cre resting B1a-like cells were proliferating at days three and nine, the absolute numbers decreased in that time frame (Figure S 41D). This could be explained to the increased apoptosis observed at day nine (data not shown).

In spite of the fact that these results are preliminary, it appears that BCR stimulation of either R26-IKK2ca/ca CD19cre or TCL1tg R26-IKK2ca/ca CD19cre $CD5^+$ B1a-like cells retards proliferation.

#### IV.2.3.2.4 Constitutive canonical NF-κB activation is insufficient to overcome the niche dependence of murine TCL1tg driven CLL

In human CLL, the NF-κB activation observed in patient biopsy samples is to a large extent a consequence of interactions of the CLL-cells with its surrounding environment. The contact of TCL1tg CLL-like cells with the niche microenvironment will drive a bi-directional remodelling to allow the TCL1tg CLL-cells to survive, proliferate, evade the immune system and potentially become resistant to chemotherapy. For instance, when the TCL1tg CLL-cells are in contact with the bone marrow-derived stromal cell

(BMDSC), the interaction induces the expression of the PCK-βII isotype in the BMDSC. In the absence of stromal PCK-β, the CLL-like cells are unable to remodel the niche and cannot survive [167]. Therefore, this bi-directional remodelling is fundamental for the development of CLL.

I wanted to address whether constitutive canonical NF-κB activation could overcome the dependence of external signals from the microenvironment for the survival of TCL1tg CLL-cells in mice. In order to do so, I set up transplant experiments where malignant cells were harvested from spleens of burdened TCL1tg CD19cre or TCL1tg R26-IKK2ca CD19cre mice (Figure 40A). Donor cells were enriched for TCL1tg CLL-like cells and transplanted into PKC-β knockout heterozygous (from now on referred to as PKC-β+/-) and homozygous (from now on referred to as PKC-β−/−KO) recipient mice [167, 245]. The transplanted mice were bled once a week and monitored for up to 6 months for the development of any symptoms.

The peripheral blood monitoring of the transplanted recipients revealed that only PKC-β+/- mice, but not homozygous knockout mice, developed a progressive accumulation of $CD5^+$ B1a-like cells in the blood independently of the genotype of the transplanted CLL-like cells (Figure 40C).

The median survival for both TCL1tg CD19cre and TCL1tg R26-IKK2ca CD19cre transplanted PKC-β+/- recipients was 8 weeks after the start of the transplant, and no cases showed development of CLL-like symptoms after 12 weeks from the start of the transplant (Figure 40B). Interestingly, not all of the recipient mice developed the CLL-like disease. Only four out of seven TCL1tg CD19cre CLL-like cell and 10 out of 15 TCL1g R26-IKK2ca CD19cre CLL-like cell transplanted mice developed CLL-like disease (Figure 40B). Moreover, only two out of three TCL1tg CD19Cre donors used were transplantable, while all three TCL1tg R26-IKK2ca CD19cre donors were transplantable (Figure 40C).

The *ex vivo* analysis of the burdened PKC-β+/- recipients revealed enlarged spleens with high cellularity and increased B-cell and B1a-like cell numbers (Figure 41A and B). The B1a-like cells comprised over 80% of B-cells present in the organ for both transplanted genotypes (Figure 41C). *Ex vivo* intracellular flow cytometry analysis of the B1a-like cells revealed that they were positive for the human TCL1 protein (data not shown). Moreover, the CLL-burdened mice transplanted with the TCL1tg R26-IKK2ca CD19cre

CLL-cells presented with eGFP positive B1a-like cells when analysed (data not shown). Therefore, the B1a-like cells expanded in the PKC-β+/- recipient mice had arisen from the transplanted donor CLL-like cells.

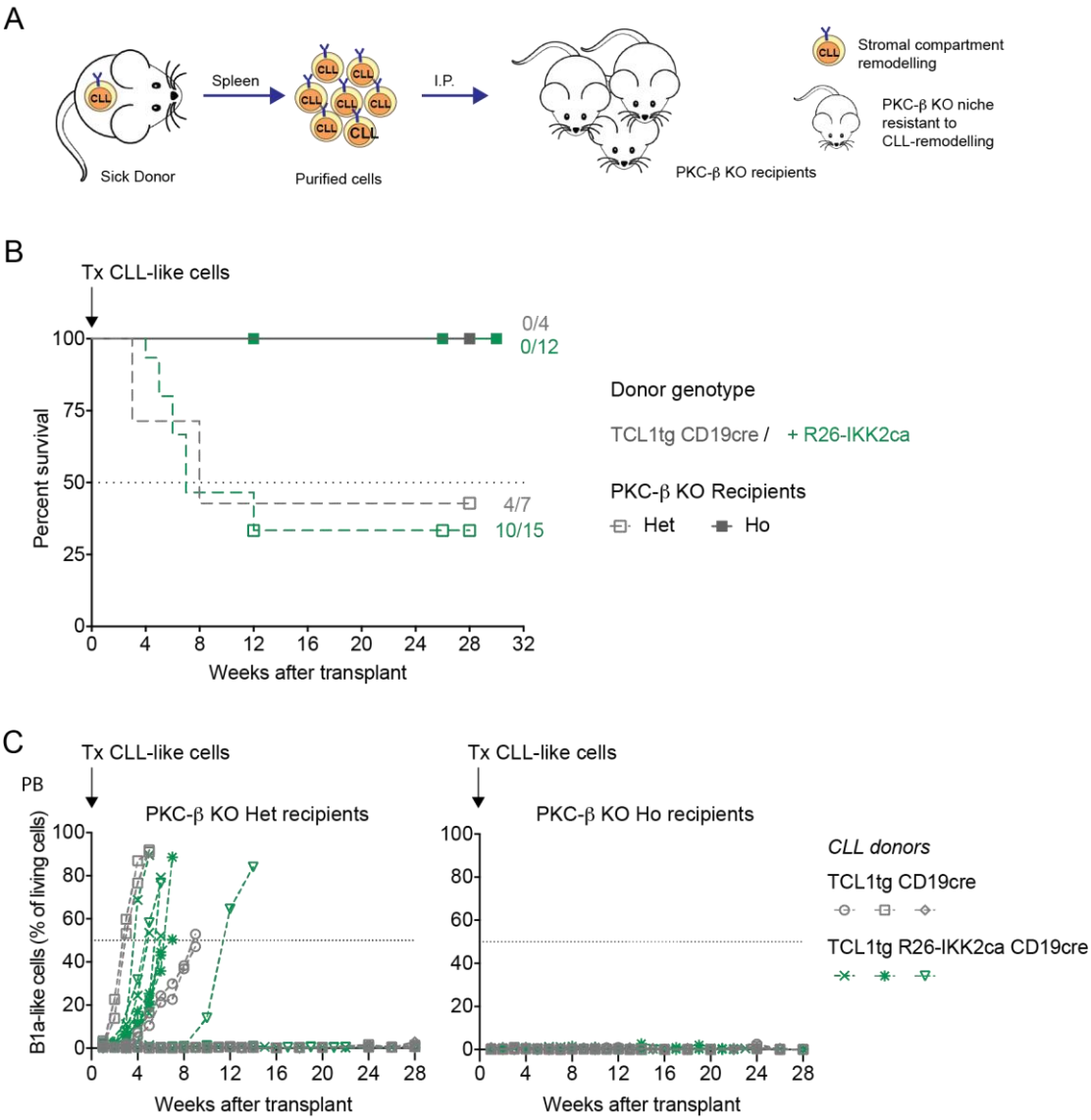


**Figure 40. IKK2ca expression does not compensate for niche survival signals**

Transplant of TCL1tg murine CLL-like cells into PKC-β KO recipients. (A) Scheme represents the experiment design. Briefly, splenocytes were harvested from sick mice; CLL-like cells were *ex vivo* enriched by MACS depletion of non B-cells; enriched CLL-like cells were intra-peritoneally injected into PKC-β+/– or KO recipients and followed up for 6 months for the development of CLL-like disease symptoms. (B) Kaplan-Meier survival curve analysis for PKC-β KO recipients transplanted with either TCL1tg R26-IKK2ca CD19cre or TCL1tg CD19cre control CLL-like cells. Number of recipients that developed CLL vs. total number of recipients transplanted is indicated. (C) Scatter plot shows the percentage of B1a-like cells present in peripheral blood after red blood cell lysis, over a period of 6 months after the transplant for PKC-β+/– and KO recipients of individual CLL-like lymphomas.
CLL (Chronic lymphocytic leukaemia), I.P. (intra peritoneal), Tx (transplant), Het (Heterozygous), Ho (Homozygous), PB (peripheral blood), B1a-like ($CD19^+$ $B220^-$ $CD5^+$)

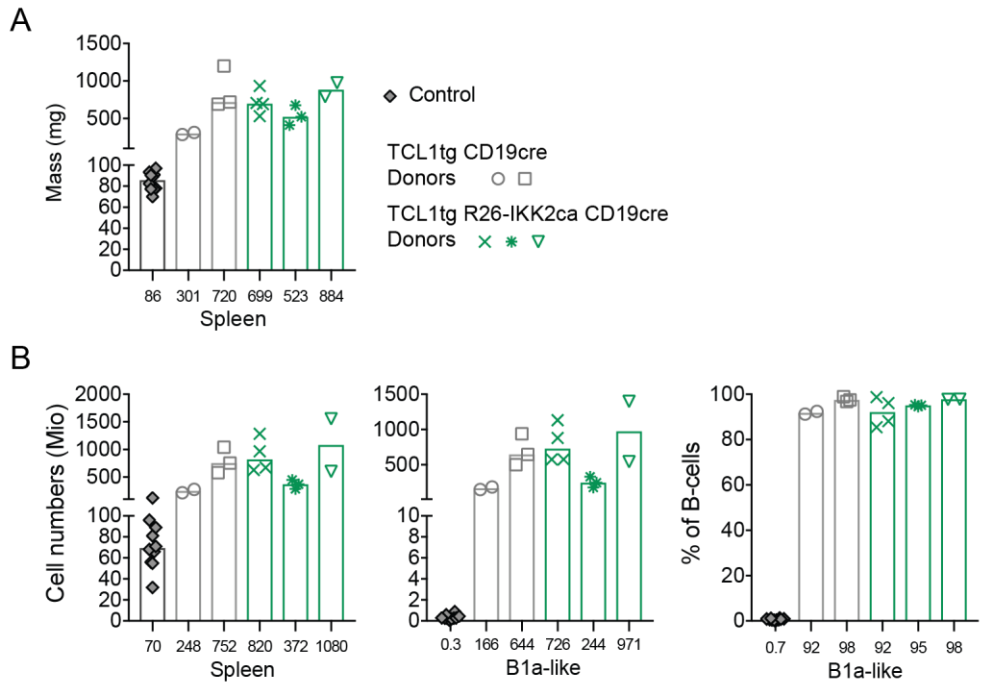


**Figure 41. B1a-like cells spleen infiltration in PKC-β+/- recipients**

*Ex vivo* analysis of spleens from CLL-burdened PKC-β+/- recipient mice using flow cytometry. Bar charts show (A) spleen mass, (B) splenocytes and B1a-like cell numbers, and (C) percentage of B1a-like cells from B-cells in PKC-β+/- recipients. Each bar represents a CLL-like lymphoma of the indicated genotype transplanted into multiple recipients.
B1a-like ($CD19^+$ $B220^{lo}$ $CD5^+$) and B-cells ($CD19^+$)

Additionally, the B1a-like cells were expanded in the peritoneum (Figure S 43A), and detected in the draining lymph nodes (Figure S 43B) and bone marrow (Figure S 43C) in the PKC-β+/- recipient mice. There was an increase from 20% B1a-cells in un-transplanted control PKC-β+/- mice to 80% B1a-like cells in the peritoneum of transplanted mice with either genotype of donor cells. There was a variable range infiltration of donor-derived B1a-like cells to the lymph nodes and bone marrow. There was a clear donor dependent variation, with some donors showing a more aggressive behaviour translating to an earlier disease onset and higher burden in lymph nodes and bone marrow.

In striking contrast, the PKC-β KO recipients were followed up to 6 months after the transplant without any signs of CLL-like symptoms. After the 6 months follow up period ended, the mice were analysed by flow cytometry. No B1a-like cells were detected in the spleens or other secondary lymphoid organs. Moreover, few B1a-like cells were present in the peritoneum of these animals. Finally, the B-cells of these animals were negative for the human TCL1 protein and also did not express the eGFP reporter gene of the R26-

IKK2ca allele. Therefore, the PKC-β KO homozygous mice were resistant to TCL1tg R26-IKK2ca CD19cre transplantation.

Together these results show that the cell intrinsic constitutive canonical NF-κB activation in the murine TCL1tg mouse model is not sufficient to overcome the PKC-β-dependent niche interaction required for long-term permanence and survival *in vivo*.

### IV.2.4 TOWARDS IDENTIFYING THE TCL1 PRECURSOR CELL IN MURINE CLL

In human CLL, to date there is no clear cell of origin for the disease. The current understanding is that different insults in either GC experienced B-cells or naïve B-cells lead to a disease with similar characteristics [192]. The TCL1 murine CLL model develops a disease with unmutated BCRs, reminiscent of a naïve non-GC B-cell precursor [256]. Similarly, the TCL1tg R26-IKK2ca compound mice also develop a disease with unmutated BCRs (Tables 6-9). By taking advantage of the accelerated disease progression in the TCL1tg R26-IKK2ca CD19cre mice, I wanted to investigate the precursor cell in the TCL1tg mouse model for CLL. For that purpose I used two different Cre mouse strains that express the Cre recombinase mainly in B-cells at the germinal centre stage: Cγ1cre [260] and AIDcre [244]. Given the unmutated BCR status of the TCL1tg R26-IKK2ca derived CLL-like cells, it was unlikely that the precursor cell was a post-GC B-cell in these mice. IKK2ca-expression reduces GCs in mice [164] but collaborates with TCL1 to dramatically expand the B1a-like cell pool. Therefore, it was of great interest to examine the consequences of TCL1 and IKK2ca co-expression mostly in GC B-cells in both the Cγ1cre and AIDcre mouse models.

#### IV.2.4.1 Cγ1cre-driven IKK2ca expression dramatically collaborates with TCL in murine CLL development

A small cohort of TCL1tg R26-IKK2ca Cγ1cre compound mice and controls were aged and monitored for the development of disease as in the CD19cre compound mice analysis (see above).

Surprisingly, TCL1tg R26-IKK2ca Cγ1cre mice have a median survival of 205 days (Figure 42A), only 19 days longer than the TCL1tg R26-IKK2ca CD19cre mice (Figure 29A). Additionally, the analysis of the peripheral blood showed the presence of $CD5^+$ B1a-like cells from 2-3 months of age onwards (Figure 42B). Interestingly, at 3 months

of age the majority of B1a-like cells in the peripheral blood are eGFP-negative;TCL1+ cells. While from 4 months onwards a small fraction of eGFP-negative cells remains, the progressively larger fraction is composed of eGFP+;IKK2ca+;TCL1+ cells. In 2 cases out of 3, eGFP+;IKK2ca+;TCL1+ B1a-like cells have expanded dramatically in absence of further eGFP-negative;TCL1+ cell expansion (Figure 42C). At this stage, it is not clear whether eGFP+;IKK2ca+;TCL1+ B1a-like cells have a competitive advantage over the eGFP-negative cells, or if the eGFP-negative cells over time recombine the STOP cassette and therefore start to express eGFP and IKK2ca. However, in the TCL1tg R26-CAR Cγ1cre control mice, although B1a-like cells can be also detected in the blood at 2-3 months of age, the expression of the CAR reporter gene, also knocked into the rosa26 locus [242], can only be observed in maximally 3% of living cells at 5 months of age in 2 out of 5 cases (Figure 42D). The absence of a progressive increase of CAR-expressing B1a-like cells in TCL1tg R26-CAR Cγ1cre mice strongly argues for a competitive advantage of eGFP+;IKK2ca+;TCL1+ B1a-like cells over eGFP-negative;TCL1+ B1a-like cells in the TCL1tg R26-IKK2ca Cγ1cre mice.

The *ex vivo* analysis of burdened TCL1tg R26-IKK2ca Cγ1cre mice shows enlarged spleens accompanied by a drastic increase in B-cell numbers compared to their aged matched controls (Figure S 44A and B); with the main B-cell population being B1a-like cells (Figure 42E). The conditional activation of the IKK2ca knock-in allele results in a 38-fold increase in B1a-like cell numbers compared to the TCL1tg Cγ1cre and TCL1tg R26-CAR Cγ1cre aged matched controls. Moreover, the expression of the reporter genes CAR or eGFP in these mice shows that 98% of the B1a-like cells in the spleen from TCL1tg R26-IKK2ca Cγ1cre are eGFP+, while there are less than 0.1% of CAR+ B1a-like cells in the TCL1tg R26-CAR Cγ1cre mice (Figure 42F). On the other hand, 33% of the B1a-like cells in the R26-IKK2ca Cγ1cre mice were eGFP+ (0.2 million eGFP+;IKK2ca+/0.6 million B1a-like cells, Figure 42E and F), while 10% were CAR+ in the R26-CAR Cγ1cre controls (0.1million CAR+/1 million B1a-like cells, Figure 42E and F). This differential expression of the CAR and eGFP reporter genes again points towards a competitive advantage of eGFP+;IKK2ca+;TCL1+ B1a-like cells over eGFP-negative;TCL1tg+ B1a-like cells.

The similar CLL-disease dynamics in the TCL1tg R26-IKK2ca Cγ1cre (Figure 42) and TCL1tg R26-IKK2ca CD19cre (Figure 29) is unexpected. As mentioned above, in the Cγ1cre strain the Cre recombinase is mainly expressed at the GC stage. However, there is

a 1% of B1-cells in the peritoneum of R26-YFP Cγ1cre that show Cre dependent recombination and expression of the enhanced yellow fluorescent protein (eYFP) reporter [243]. Given the role of constitutive canonical NF-κB activation in B1 cell development (Figure 27) and the fact that constitutive canonical NF-κB activation prevents GC formation (Figure S 48 and Figure S 49), the most reasonable explanation is that the population of 1% of Cγ1cre-dependent recombination in B1-cells is giving rise to the eGFP+;IKK2ca+;TCL1+ B1a-like cells and not their transition through the GC.

Indeed, six out of ten 1-year-old R26-IKK2ca Cγ1cre mice develop B1-cell hyperplasia in the peritoneum (Figure S 45B and Figure S 46C) compared to 1 out of 16 aged matched Cγ1cre controls (Figure S 46B). The B1-cell expansion observed in the 1-year-old R26-IKK2ca Cγ1cre mice affects either or both B1a and B1b subsets (Figure S 45 and Figure S 46). Moreover, Cre-mediated recombination in R26-CAR Cγ1cre 1-year-old mice results in 1.4% CAR+ B1a-cells and 6.6% CAR+ B1b-cells in the peritoneum (Figure S 46D, first column and Figure S 46A) compared to 60% eGFP+;IKK2ca+ B1a-cells and 39% of eGFP+;IKK2ca+ B1b-cells in R26-IKK2ca Cγ1cre 1-year-old mice (Figure S 45D, second column and Figure S 46A). In the cases with B1-cell hyperplasia, over 95% of the B1b- or B1a-cells are eGFP+ (Figure S 45D, third and fourth column correspondingly). Although these eGFP+;IKK2ca B1-cells only express IgM (Figure S 45C), I cannot exclude that they transitioned through the GC at some point. Interestingly, in 2-months-old R26-IKK2ca Cγ1cre mice only 5% of B1a- and B1b-cells in the peritoneum express eGFP (Figure S 47). Given that B1-cells possess self-replenishing capacities, the B1-cell expansion observed with age might not reflect the number of cells that have undergone Cre dependent recombination but might reflect the positive effect of constitutive canonical NF-κB activation on self-renewal/cellular expansion or a cumulative effect of recombination of eGFP-negative B1-cells in time.

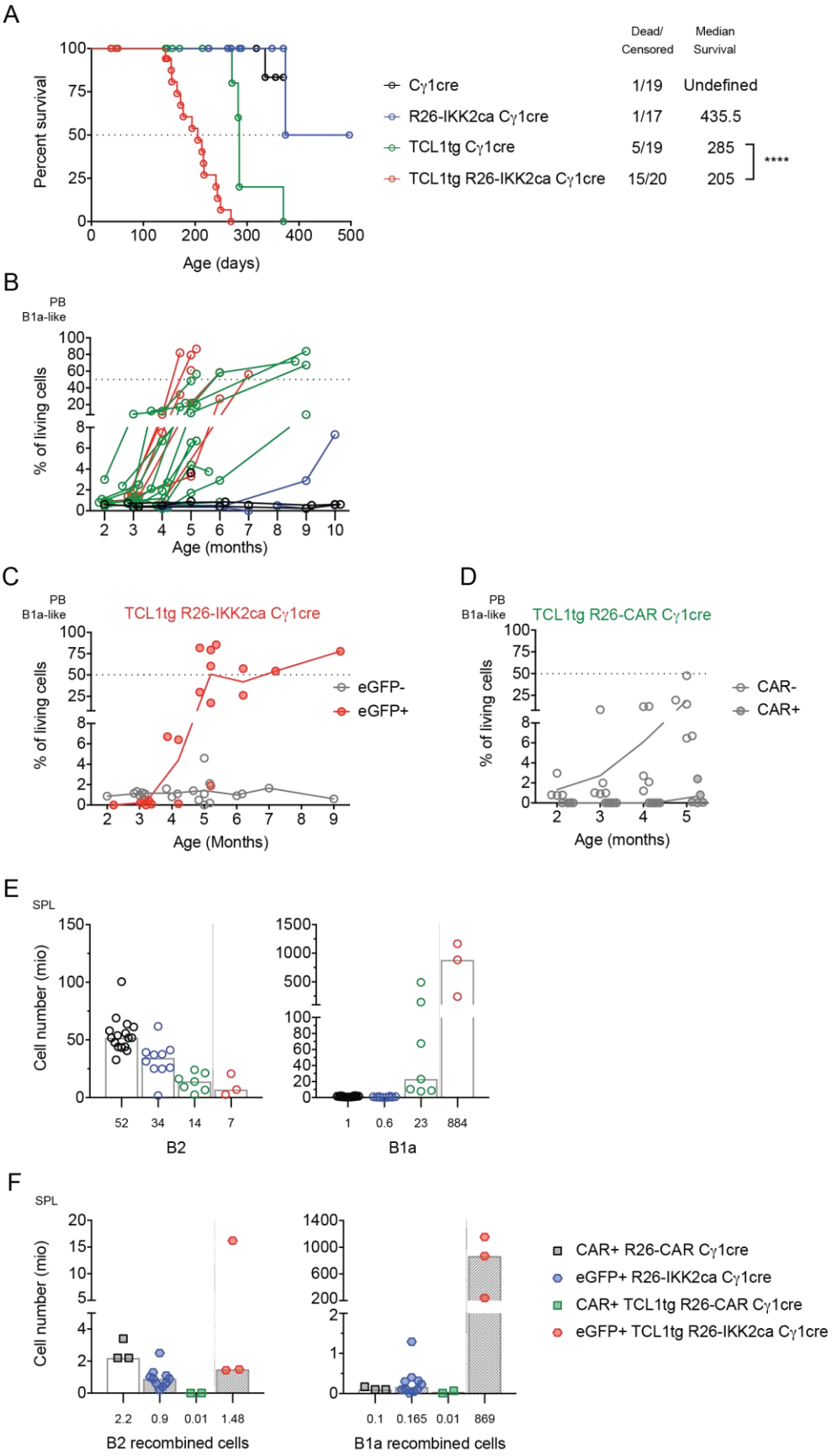


**Figure 42. Cγ1cre driven IKK2ca expression cooperates with TCL1 in murine CLL**

**Figure 42 (continued). Cγ1cre driven IKK2ca expression cooperates with TCL1 in murine CLL**

Monitoring of TCL1tg murine CLL development in the presence Cγ1cre-dependent canonical NF-κB activation. (A) Kaplan-Meier survival curve analysis for TCL1tg and R26-IKK2ca compound mice. Number of deceased and censored animals is indicated, as well as their median survival age in days. (B) Scatter plot shows the percentage of B1a-like cells present in peripheral blood after red blood cell lysis for each individual mouse, over a period of 10 months. (C) Scatter plot shows the percentage of eGFP- and eGFP+ B1a-like cells present in peripheral blood of the TCL1tg R26-IKK2ca Cγ1cre. (D) Scatter plot shows the percentage of CAR- and CAR+ B1a-like cells present in peripheral blood of the TCL1tg R26-CAR Cγ1cre. Bar charts show (E) total B2- and B1a-like cell numbers, and (F) number of CAR+ or eGFP+ expressing B2- and B1a-like cells in spleens of aged TCL1tg R26-IKK2ca Cγ1cre burdened mice and aged matched controls. The connecting lines in C and D represent means for each time point. Histograms in E and F depict medians, and values are indicated below each histogram.
PB (peripheral blood), SPL (spleen), B1a-like (B1a, $CD19^+$ $B220^-$ $CD5^+$) and B2 ($CD19^+$ $B220^+$).

Additionally, the analysis of the germinal centre reaction in 1-year-old R26-IKK2ca CD19cre (Figure S 48) and R26-IKK2ca Cγ1cre (Figure S 49) compound mice confirms the negative role of constitutive canonical NF-κB activation in the GC reaction. Briefly, the presence of the IKK2ca knock-in reduces the percentage of GC B-cells in the spleen of aged mice in both CD19cre (Figure S 48A) and Cγ1cre (Figure S 49A) compound mice. Moreover, in the CD19cre compound mice the percentage of eGFP+;IKK2ca+ GC B-cells in the spleen is extremely low (Figure S 48A and B). Similarly, in R26-IKK2ca Cγ1cre mice the percentage of eGFP+;IKK2ca+ GC B-cells is lower (10%) compared to the percentage of CAR+ GC B-cells in the aged matched R26-CAR Cγ1cre controls, were about 50% of all the GC B-cells express CAR (Figure S 49B and C).

Together, the eGFP+;IKK2ca+ B1-cell expansion and reduced eGFP+;IKK2ca+ GC B-cells in 1-year-old R26-IKK2ca Cγ1cre mice further support the role of constitutive canonical NF-κB activation in B1-cell expansion. It still remains unresolved whether the precursor cell in TCL1-derived CLL-like disease in mice has transiently entered the germinal centre reaction or not. In any case, it is remarkable that expression of IKK2ca in 1% of B1-cells in TCL1tg R26-IKKca Cγ1cre mice [243] leads to essentially the same dramatic acceleration in CLL progression compared to IKK2ca expression in over 90% of all B-cells in TCL1tg R26-IKKca CD19cre mice. This finding strongly argues to a cell-intrinsic co-operation between the TCL1 and IKK2ca oncogenes in CLL development.

### IV.2.4.2 AIDcre-driven IKK2ca expression dramatically collaborates with TCL1 in murine CLL development

To gain further understanding of the potential transition through the germinal centre of the CLL-precursor cell in the TCL1tg mouse model I used the AIDcre mouse strain[244]. This strain expresses the Cre recombinase under the promoter of the *Aicda* gene and the 1% of B1-cells recombined observed in the Cγ1cre[243] should not be present.

Unexpectedly, the median survival of the TCL1tg R26-IKK2ca AIDcre mice was 202 days (Figure 43A), similar to the TCL1tg R26-IKK2ca Cγ1cre (Figure 42A) and only 16 days longer than for TCL1tg R26-IKK2ca CD19cre mice (Figure 29A). Similarly as in the TCL1tg R26-IKK2ca Cγ1cre mice, at 3 months of age eGFP-negative;TCL1+ B1a-like cells can be detected in the peripheral blood of these mice, while two months later eGFP+;IKK2ca+;TCL1+ B1a-like cells have outcompeted them (Figure 43B and C). Moreover, there was a significant expansion of $CD5^+$ B1a-like cells in the spleens of TCL1tg R26-IKK2ca AIDcre mice compared to aged matched controls (Figure S 50A).

Interestingly, 90% of the B1a-like cells in the spleen express the eGFP reporter in the TCL1tg R26-IKK2ca AIDcre mice compared to 13% of B1a-cells in the R26-IKK2ca AIDcre aged matched control (Figure S 50B). Furthermore, the eGFP+;IKK2ca;TCL1+ B1a-like cells in the spleen of the TCL1tg R26-IKK2ca AIDcre mice are IgM+ IgD- pointing towards a non-GC origin.

Given the presence of eGFP+;IKK2ca+;TCL1+ B1a-like cells in the TCL1tg R26-IKK2ca AIDcre mice it remains unclear whether AID is or was expressed in these cells. Therefore, at this point I cannot conclude whether or not the CLL-precursor is actually a germinal centre experienced cell or whether CLL-like cells transition through the germinal centre or a GC-like state and whether this exposure is sufficient to drive AIDcre dependent recombination. Kaku *et al.* have reported expression of AID in CD25+ B1a-like cells [261]. Indeed, in AIDcre mice Cre-mediated recombination leads to conditional expression of genes not only in the germinal centre, but also in B1a and B1b subsets in the spleen and peritoneum ([262] and Figure S 51). Furthermore, in 7-months-old R26-IKK2ca AIDcre mice both B1a and B1b-cells in the peritoneum express eGFP (Figure S 52), supporting the idea of AID expression in the B1 subset.

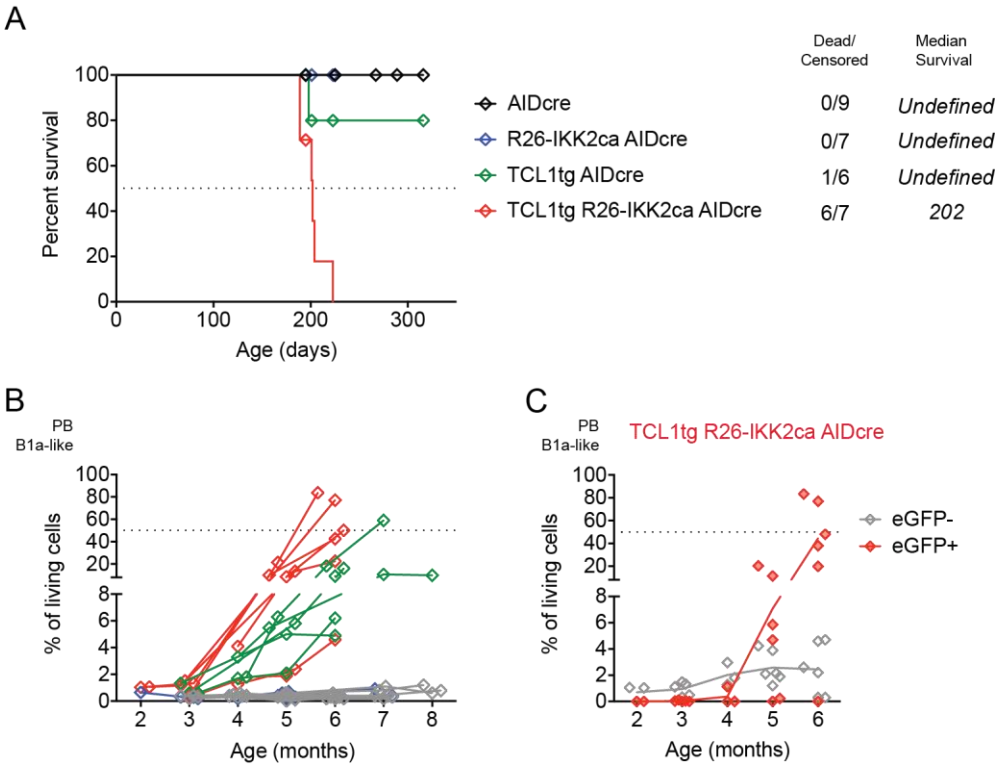


**Figure 43. AIDcre driven IKK2ca expression strongly cooperates with TCL1tg in murine CLL development.**

Monitoring TCL1tg murine CLL development in the presence AIDcre-dependent canonical NF-κB activation. (A) Kaplan-Meier survival curve analysis for TCL1tg and R26-IKK2ca compound mice. Number of deceased and censored animals is indicated, as well as the median survival age in days. (B) Scatter plot shows the percentage of B1a-like cells present in peripheral blood after red blood cell lysis for each individual mouse, over a period of 8 months. (C) Scatter plot shows the percentage of eGFP- and eGFP+ B1a-like cells present in peripheral blood of the TCL1tg R26-IKK2ca AIDcre. The connecting line represents the mean for each time point.
PB (peripheral blood), B1a-like ($CD19^+$ $B220^-$ $CD5^+$)

Taking these data into consideration, it is not surprising that the TCL1tg R26-IKK2ca AIDcre mice are burdened with eGFP+;IKK2ca;TCL1+ B1a-like CLL-cells and have a similar median survival as observed for the Cγ1cre compound mice. Nonetheless, the observed 7% recombination B1a-like cells in the spleen and 4% in the peritoneum of TCL1tg R26-IKK2ca AIDcre mice results in an ultimately lethal expansion of CLL-like cells with a strikingly similar kinetic as in the TCL1tg R26-IKK2ca CD19cre mice were recombination takes place in 95% of all B-cells. This constitutes compelling evidence for a strong cooperation of TCL1tg and constitutive canonical NF-κB activation at the single cell level in CLL-like development in mice.

Although the Cγ1cre and AIDcre conditional expression could not shed light into the precursor cell for TCL1tg-dependent CLL in mice, it further supports the strong co-operation of canonical NF-κB activation in CLL.

# V DISCUSSION

## V.1 LOSS OF A20 IN COMBINATION WITH ENHANCED EXPRESSION OF THE ALTERNATIVE NF-κB REGULATOR NIK IN B-CELL PHYSIOLOGY

The NF-κB family of transcription factors drive the expression of survival, proliferation, inflammation and differentiation in B-cells as well as in other cells of the immune system. The protein A20 acts as a negative regulator of the canonical NF-κB pathway, and in the absence of A20 canonical NF-κB signalling cannot be timely terminated [263, 264]. A major player in the activation of the alternative NF-κB pathway is the NF-κB inducing kinase NIK. Under steady state conditions the pathway is inactivated by the constant ubiquitination and consequent proteosomal degradation by TRAF2/3 and cIAP1/2 complex [265]. When the pathway is activated by external stimuli, NIK protein levels are stabilized by recruitment of the TRAF2/3 complex away from NIK, and NIK can activate the IKK1 kinase, and together they activate alternative NF-κB transcription factors [265].

Given the high prevalence of genetic lesions associated with A20, a negative regulator of the canonical NF-κB pathway as well as the alternative NF-κB pathway in B-cells in autoimmune disease and cancer, it is of high importance to gain further understanding of their role in disease development and progression. Genetic abnormalities in A20 and the alternative NF-κB arm TRAF3/NIK have been reported in patients with splenic marginal zone lymphoma (sMZL) [154, 179, 183]. Therefore, I wanted to address the question whether mutations in A20 and the cIAP2/3-TRAF2/3-NIK arm cooperate in sMZL development. My data provide evidence that hyper-activation of the alternative NF-κB pathway by expression of an additional allele of NIK in combination with inactivation of A20 do not cooperate in sMZL development in mice. Instead, homozygous loss of A20 combined with overexpression of NIK in B-cells resulted in an unexpected reduced mature B-cell pool. This impairment in mature B-cells homeostasis challenges the current understanding of NF-κB activation in B-cell development and homeostasis. Moreover, I also show that aberrant NF-κB activation resulted in an activated antigen presenting-like phenotype in mature B-cells that was accompanied by T-cell activation.

Convincing evidence documents the requirement of both canonical [37, 40, 61, 79, 266] and alternative [36, 89, 100, 103, 267-269] NF-κB activation in B-cell development and fitness. This is in line with my own observations where enhanced canonical NF-κB activation due to heterozygous loss of A20 combined with NIK overexpression driving alternative NF-κB activation cooperates in mature B-cell development. In striking contrast, I observe that bi-allelic loss of A20, instead of promoting marginal zone B-cell expansion, results in reduced mature B-cell numbers. Given the nature of NF-κB target genes, proliferation and survival, it is completely unexpected that NF-κB activation by integration of the canonical and alternative pathways leads to reduced mature B-cell numbers. There are several possible reasons that can cooperate in the development of the observed impaired B-cell homeostasis.

### ABERRANT NF-κB ACTIVATION MAY ALTER THE T1 TO T2 B-CELL STAGE TRANSITION

My data shows that activation of canonical NF-κB by loss of A20 in combination with activation of alternative NF-κB by expression of one additional allele of NIK in B-cells, which should provide a pro-survival and proliferation advantage, paradoxically results in reduced mature B-cell numbers in mice. Given the reduced mature B-cell numbers observed in A20F/F NIK-tg CD19cre mice, it is possible that aberrant activation of both canonical and alternative NF-κB pathway may alter normal B-cell development resulting in reduced mature B-cell numbers. My data shows that early B-cell development was largely unaffected by hyper-activation of either or both canonical and alternative NF-κB pathway in B-cells, however there was a small trend towards reduced immature T1 and increased T2 B-cell numbers (Figure 9 and Figure S 4) associated with the dual activation of the canonical and alternative NF-κB pathway by loss of A20 and gain of NIK expression, respectively. During normal B-cell development BAFF is a key player in the transition of T1 to T2 B-cells as well as in the generation and survival of mature B-cells [69, 270]. Binding of BAFF to its cognate receptor drives the induction of pro-survival genes and reduction of pro-apoptotic proteins via NF-κB in a NIK-dependent fashion [89, 271, 272]. Moreover, genetic studies in mice where transcription factors of the canonical and alternative NF-κB pathway were ablated in B-cells support the idea that pro-survival and proliferation signals downstream of both canonical and alternative NF-κB would are indispensable for the transition of T1 to T2 [36, 61, 268]. These studies showed that B-cells deficient of p50/p52 [61], RelB/c-Rel [36] and p52/RelB [268] suffer a developmental block a the T1 B-cell stage. Moreover, at least in p50/p52 mutant

mice c-Rel dependent expression of Bcl-xl and Cyclin-E are able to rescue the T1 developmental block [61]. On the other hand, overexpression of BAFF rescues self-reactive T2 cells from peripheral deletion [73]. Additionally, combined loss of IκBα, IκBε, c-Rel and TNF, which leads to B-cells with hyper-activated NF-κB, results in reduced T1 cell numbers as well as MZB-cell expansion [36]. On the other hand, loss of A20 in B-cells results in increased T2 cell numbers [79]. Taken together, all the previous evidence points to a requirement for both the canonical and alternative NF-κB pathways in the transition from T1 to T2 B-cells. This might explain why aberrant activation of both pathways results in a faster transition into the T2 developmental stage as shown here. Moreover, an accelerated B-cell development by a faster transition into the T2 B-cell developmental stage or a higher sensitivity to BAFF could affect the negative B-cell selection process and allow for the survival and further differentiation of auto-reactive B-cells.

Interestingly, my data also shows that the strong activation of the canonical and alternative NF-κB pathways in B-cells increased the expression CD21 and CD23 in A20-deficient NIK-tg B-cells (Figure S 3A and Figure S 4A). Both surface proteins are NF-κB target genes [252] and are used to phenotypically define the transitional B-cell stages according to their differential expression, in addition to surface IgM and surface IgD. Given that CD21 and CD23 had higher expression in the A20F/F NIK-tg CD19cre mice it would be important to confirm the proper identification of the T1 and T2 stages to have a better understanding on the role of dual activation of the canonical and alternative NF-κB pathways on the transition to the T2 stage. Histology sections depicting the spleen architecture could clarify if the T2 cells are at their proper location, or if the higher number of T2 cells actually corresponds to T1 cells with aberrant expression of CD21 and CD23. Moreover, transcriptional profiles of sorted T1 and T2 cells could provide further information to their actual biological state.

### ABERRANT NF-κB ACTIVATION IMPAIRS MATURE B-CELL HOMEOSTASIS

My data shows that homozygous loss of A20 in combination with expression of a knock-in NIK transgene in B-cells results in reduced B-cell numbers in mice affecting both follicular B-cells (FOB) and marginal zone B-cells (MZB). The aberrant NF-κB activation resulting from combining loss of A20 and overexpression of the NIK transgene could affect (1) the differentiation of B-cells into MZB-cells and (2) FOB-cells, (3) the

expression of integrins required for cell migration and proper localization, and (4) the cell survival and its sensitivity to cell death signals.

First, the finding that combination of heterozygous loss of A20 with overexpression of NIK leads to an expansion of mature B-cells affecting both FOB- and MZB-cells is in accordance with previous reports on the role the canonical as well as the alternative NF-κB pathway play in MZB- and FOB-cell development [36, 37, 73, 89, 184, 268]. In fact, genetic studies in mice provide evidence supporting the requirement of both the canonical and alternative NF-κB pathways in MZB development [36, 86, 268]. Although ablation of RelB or c-Rel is dispensable for B-cell development, the combined deletion of both NF-κB members drastically reduces the number of MZB-cells in young mice [36]. Moreover, the ablation of p52 and RelB further intensifies this phenotype [268]. In the case of A20, the evidence points to its requirement for proper MZB differentiation [79, 80]. $A20^{F/F}$ CD19cre mice have an accumulation of MZP and an improper localization of MZB-cell within the spleens [79]. In contrast, combined loss of IκBα, IκBε, c-Rel and TNF, which leads to B-cells with hyper-activated NF-κB, results in expansion of MZB-cells [36]. Similarly, constitutive activation of the canonical NF-κB pathway through expression of a constitutively active IKK2 in B-cells leads to increased MZB-cell numbers [37]. Moreover, ablation of the TRAF3 protein adaptor, a negative regulator of the alternative NF-κB pathway upstream of NIK, in B-cells leads to development of clonal sMZL or B1a-cell lymphomas in 18-months-old mice [184]. Paradoxically, my data shows that while heterozygous loss of A20 in combination with expression of the NIK transgene resulted in an expansion of MZB-cells, homozygous deletion of A20 in combination with the expression of the NIK transgene results in dramatically reduced MZB-cells numbers. Therefore, it seems plausible that a tight control of NF-κB activation is indispensable for proper MZB-cell development.

Second, reduced mature B-cell numbers in A20F/F NIK-tg CD19cre mice could be explained by altered B-cell differentiation to the FOB stage. Although loss of A20 has no apparent effect on FOB-cell development [79], constitutive canonical NF-κB signalling results in FOB-cell expansion in mice [37]. Likewise, NIK-tg overexpression in B-cells results in FOB-cell expansion [89]. Moreover, while $RelB^{-/-}$ and $c\text{-}Rel^{-/-}$ mice have normal FOB-cell numbers $RelB^{-/-}$ $c\text{-}Rel^{-/-}$ double knockout mice have reduced FOB-cell numbers [36]. Therefore, all the evidence points to the requirement of signals that activate both canonical and alternative NF-κB pathways for FOB-cell development and homeostasis.

Paradoxically, my data shows that the combination of loss of A20 and NIK-tg overexpression resulted in reduced FOB-cell numbers (Figure 8). This finding is contradictory with the requirement of both NF-κB activation pathways in FOB-cell differentiation. Therefore, it seems plausible that a tight control of NF-κB activation is indispensable for proper mature B-cell development in general.

Interestingly, the aberrant activation of NF-κB by loss of A20 and overexpression of NIK elevated the expression of CD1d, CD21 and reduced expression of CD23 in mature B-cells (Figure S 3A). However, there was an absence of $CD23^{low}$ $CD21^{high}$ $CD1d^{high}$ B-cells (Figure S 3). The absence of $CD23^{low}$ $CD21^{high}$ $CD1d^{high}$ B-cells points to the possibility that all MZB-cells identified in A20F/F NIK-tg CD19cre mice might actually be MZB-cell precursors or that FOB-cells might actually be closer to MZB-cell precursors than FOB-cells. The effects of strong NF-κB activation on the expression of these surface markers complicate the proper identification of MZB-cells and their precursors. The true identity of these cells remains to be resolved and further experiments are required to properly characterize the biological nature of these B-cells. Analysing the expression profile of FACS-purified eGFP positive $CD1d^{high}$ $CD21^{high}$ potential MZB-cells will bring light into their biological characteristics. Furthermore, *ex vivo* differentiation into plasma cells after a T-cell-independent stimulus such as LPS would further confirm their biological function. Taken together, my data suggests that activation of the NF-κB pathway over a particular threshold could lead to differentiation signals that drive cells into the MZB linage or alternatively to hyper-sensitive state that leads to a negative fitness of these cells.

Third, the reduced mature B-cell numbers in A20F/F NIK-tg CD19cre mice could be explained by the altered integrin expression affecting the migration and homing of mature B-cells. A20-deficient B-cells with overexpression of the NIK transgene have higher alpha-L/beta-2 integrin expression accompanied by a slightly increased beta-1 integrin expression (**Fehler! Verweisquelle konnte nicht gefunden werden.** and Figure S 7). These findings further support the role of alternative NF-κB signalling in integrin expression [182, 268]. For instance, DeSilva et al. (2016) have associated beta-2 integrin expression with alternative NF-κB activation. B-cells deficient for *relb/nfkb2* have a strong reduction in the expression of beta-2 integrin compared to controls [268]. Overexpression of BAFF promotes a higher expression of alpha-L, beta-2 and to a lesser extent beta-1 integrins mainly in MZB-cells, but also FOB-cells, in an p52-dependent fashion [182]. The LFA-1 complex, formed by alpha-L and beta-2 integrins, is important

for keeping B-cells in the marginal zone [75]. At the same time, it has been reported that alpha-4/beta-1 integrin dimers are also expressed in MZB-cells and play a role in their localization [75]. The current understanding of MZB-cell biology suggests that they are highly motile cells within the spleen, recirculating between the MZ and the follicle. FOB-cells can also migrate from the follicle to the MZ in the spleen, and their lower integrin expression in part prevents their retention and permits their passive flow into the red pulp [76]. It has been proposed that the reduced numbers of mature MZB-cells in the A20F/F CD19cre mice is due to aberrant migration. In fact, in these mice, the splenic marginal zone is nearly devoid of B-cells [79]. Interestingly, my data shows that A20F/F CD19cre B-cells had significantly lower surface expression of beta-2 integrins (**Fehler! Verweisquelle konnte nicht gefunden werden.** and Figure S 7B), which could explain their failure to localize to or be retained in the splenic marginal zone. Therefore, aberrant overexpression of LFA-1 and beta-1 integrins in FOB-cells could promote their retention to the marginal zone and alter the normal B-cell homeostasis. Additional histological studies providing evidence of the localization of the FOB- and MZB-cells within the splenic architecture will confirm if the aberrant integrin expression is associated with a migration and homing defect.

Furthermore, aberrant integrin expression caused by strong activation of NF-κB in B-cells could further enhance the retention of B-cells in the spleen niche [182] and affect the egress, migration or homing of B-cells to secondary lymphoid organs in the periphery. This could account for the reduced B-cell numbers observed in the non-splenic secondary lymphoid organs (Figure 5, Figure 6 and S1-2) and the reduced recirculating B-cells in the bone marrow (Figure 11 and Figure 12) of A20F/F NIK-tg CD19cre mice. Additional analysis of integrin expression in B-cells in the periphery and in B-cells that recirculate to the bone marrow could shed light into their association with the reduced B-cell numbers observed in the secondary lymphoid organs. Moreover, proper migration and homing of transplanted eGFP+;A20-/-;NIK+ B-cells could shed light into the role of integrins in the observed reduced B-cell numbers in secondary lymphoid organs. In addition, using integrin-neutralizing antibodies could assess the role of integrins in the retention of B-cells in the spleen and their reduced numbers in the secondary lymphoid organs.

Fourth, the unexpected reduced mature B-cell numbers in A20F/F NIK-tg CD19cre mice could be a result of higher cell death of mature B-cells. Although there is no evidence that hyper-activation of NF-κB leads to higher apoptosis in the A20F/F NIK-tg CD19cre

mice (Figure 13), it is known that A20 protects cells against cell death in various cell types in an NF-κB independent fashion [79, 254, 273, 274]. It is possible that external signals such as TNF-α [273], IFN-γ[275] and CD95L[276] are required to induce cell death in B-cells. Supporting this role of A20, Onizawa et al. (2015) reported that loss of A20 in CD4 T-cell results in Caspase-independent nectroptosis [274]. Paradoxically, Tavares et al. (2010) have shown that loss of A20 in B-cells results in reduced FASL-depended cell death [254]. Therefore, it is possible that in the current context of aberrant B-cell activation, A20 might also protect B-cells from a Caspase-independent cell death program. Interestingly, Boutaffala et al. (2015) reported a novel pro-apoptotic role for NIK that is independent of alternative NF-κB activation in response to TNFα [277]. In their paper, they show that in hepatocytes loss of cIAP1 and cIAP2 increases NIK protein levels that will in turn drive Caspase-8 activation in a RIP1-dependent manner. However, very high protein levels of NIK lacking a TRAF3 binding domain (NIKΔT3) in B-cells do not result in reduced but highly expanded B-cell numbers [89]. Therefore, high expression of NIK alone is insufficient to induce B-cell death. It is worth mentioning that these mice have high levels of TRAF2 and TRAF3 and thus may have increased levels of cIAP1 and cIAP2. The role of the absence of these proteins in the NIK-dependent cell death model is unclear. Thus, if the loss of A20 had a similar effect as loss of cIAP1 and cIAP2 in NIK+ B-cells, then external signals could trigger a NIK-dependent cell death program. It is therefore necessary to further investigate the role of NIK in cell death in the absence of A20.

Interestingly, my data also shows that B1-cells had a similar fate to mature B-cells in A20F/F NIK-tg CD19cre mice (Figure 7). Although B1-cells can also be produced from bone marrow HSCs, they are thought to mainly develop from foetal liver HSCs during embryonic development and are maintained in the adult due to their self-renewing ability [110, 278-280]. Loss of A20 on its own already has a negative effect on B1-cell numbers [79]. Additionally, the absence of NEMO or IKK2 results in reduced MZB- and B1-cells pools [40]. Taking into account overexpressing BCL2 in these scenarios is unable to rescue both B-cell subsets suggests that additional canonical NF-κB target genes are required for the long-term persistence of B1-cells [40]. The fact that aberrant activation of NF-κB by loss of A20 and overexpression of NIK dramatically reduces B1-cell numbers brings another level of complexity to the role of NF-κB in mature B-cell homeostasis. If the reduced cell numbers were a result of increased cell death, then these results would support the role of A20 in protecting B1-cells against cell death. Alternatively, the reduced B1-cell numbers could indicate differentiation into short-

lived plasmablast or plasma cells [281, 282]. Further experiments are required to determine how aberrant NF-κB activation affects B1-cell development. Competitive foetal liver derived chimeras as well as bone marrow derived chimeras could provide an insight into the potential role of NF-κB in B1-cell development. Identification of natural IgM and IgG3 antibodies in serum or deposits in organs could indicate an increased differentiation of B1-derived plasma cells and explain the reduced B1-cell numbers

My data shows that loss of A20 in combination with over expression of the NIK transgene resulted in reduced mature B-cell numbers. Four non-mutually exclusive cell intrinsic mechanisms could explain the reduced B-cell numbers observed here. First, defects in the development into mature MZB-cells, and second, FOB-cells stages could explain the reduced mature B-cell numbers. Although signals activating both canonical and NF-κB pathways are required for proper FOB- and MZB-cell development, the my data suggest that a specific activation threshold might be required for development and aberrant NF-κB activation may force B-cells into an abnormal MZB-like precursor phenotype that fails to terminally differentiate. Third, the higher expression of the LFA-1 complex and additional integrins may affect migration and homing of mature B-cells into their functional niches. Finally, loss of A20 in combination with over expression with NIK might result in a higher sensitivity to cell death that is NF-κB independent, thus making B-cells hyper-sensitive to death stimuli and reducing the mature B-cell pool.

### ABERRANT NF-κB ACTIVATION IN B-CELLS PROMOTES AN EXTRINSIC INFLAMMATORY PHENOTYPE

My data shows that aberrant activation of NF-κB by loss of A20 and overexpression of NIK results in T-cell hyperplasia in young and aged mice (Figure 18 and Figure 23, respectively). Given (1) the pre-activated antigen presenting-like phenotype in A20-deficient NIK+ B-cells, (2) the accumulation of effector-like CD4 and CD8 T-cells, (3) the higher proportion of ICOS and PD1 high T-cells, (4) the accumulation of regulatory T-cells, and (5) a myeloid expansion in old age; I suspect that the T-cell hyperplasia observed is a response to aberrantly pre-activated A20-deficient NIK+ B-cells with the potential to drive a chronic inflammation in these mice.

First, my data show that A20-deficient NIK+ B-cells have a pre-activated antigen presenting cell-like phenotype characterized by a higher expression of CD69, CD86, MHC-II and to a lesser extent CD80. This expression profile is characteristic of MZB-cells [251]. As such these B-cells have the potential to present antigens to T-cells and start an immune response. Moreover, evidence points to the role B-cells as APC in vitro and in vivo [283-286] further supporting this hypothesis. Second, my data shows that a considerable proportion of CD4 and CD8 T-cells have an activated effector-like phenotype, pointing to an on-going immune reaction in these mice. Interestingly, Chu et al. (2011) reported that loss of A20 in B-cells is sufficient to drive an expansion of effector-like T-cells [79]. Moreover, Afshar-Sterle et al. (2014) reported the role of CD8 T-cells in mediating immune surveillance against the spontaneous development of B-cell lymphoma [276]. They showed that in the absence of T-cells, abnormal cancerous B-cells could survive and develop into tumours. Consequently, if signals from pre-activated B-cells or the B-cells themselves are driving a T-cell expansion, then T-cells may also be involved in in clearing the pre-activated B-cells in these mice. Therefore, it is likely that A20-deficient NIK+ B-cells present antigens to T-cells in A20F/F NIK-tg CD19cre mice, and that as a result of that interaction T-cells become activated.

Third, my data show that a significant percentage of CD4 and CD8 T-cells express higher levels of ICOS and PD1, indicative of T-cell activation [287] and exhaustion [288-290]. Moreover, the increased numbers of $PD1^{high}$ CD8 T-cells positively correlate with the reduced B-cell numbers observed in the A20F/F NIK-tg CD19cre mice (Figure S 15). Given the increased numbers of effector-like T-cells and the expression of PD1, I speculate that a percentage of those T-cells are anergic or exhausted as a result of constant activation by pre-activated B-cells. Analysis of the expression of additional T-cell exhaustion markers such as Tim-3 is required to confirm this hypothesis.

Fourth, I show here that in A20F/F NIK-tg CD19cre mice have increased numbers of CD25+ regulatory CD4 T-cells and follicular helper T-cells. The cell numbers of CD25+ CD4 T-cells are indicators of the regulatory burden on the immune system [291]. The higher number of CD25+ CD4 T-cells could be represent a regulatory response to the immune activation present in A20F/F NIK-tg CD19cre mice. Moreover, a direct interaction between pre-activated B-cells and CD25+ CD4 regulatory T-cells could promote an expansion of the latter. Supporting this hypothesis, one report showed B-cell-dependent regulatory T-cell activation in retroviral infections via the glucocorticoid-induced receptor superfamily member 18 (GITR) ligand in mice [292]. If

the combination of A20 inactivation with overexpression of NIK resulted in higher GITR ligand levels, then direct contact between CD25+ CD4 regulatory T-cells may expand them. Another outcome from direct interaction between CD25+ CD4 regulatory T-cells and pre-activated B-cells could be a regulatory T-cell-dependent clearance of the B-cells. Supporting this hypothesis, Zhao et al (2006) show that regulatory T-cells kill antigen presenting B-cells preferentially *in vitro* [293]. Therefore, It is likely that CD25+ regulatory CD4 T-cells expansion is caused by the pre-activated B-cell phenotype in the A20F/F NIK-tg CD19cre mice, and the CD25+ CD4 T-cells may be involved in clearing mature B-cells in these mice.

Another interesting aspect of my data is the increased number of follicular helper T-cells ($T_{FH}$) in the absence of GCs (discussed below) in A20F/F NIK-tg CD19cre mice. Phenotypically, $T_{FH}$ are characterized by a higher expression of the surface makers PD1 and CXCR5, and elevated levels of the transcription factor BCL6. Although my preliminary data suggest that $PD1^{high}$ $CXCR5^{high}$ CD4 T-cells have higher BCL6 expression levels compared to their $PD1^{low}$ $CXCR5^{low}$ CD4 T-cells counterparts (Figure S 9), it is evident that they have clearly upregulated PD1 to a higher extent than CXCR5 (Figure 20) and could therefore be activated, exhausted CD4 T-cells (Figure 21). Further analysis of their BCL6 expression should resolve their identification

Nonetheless, one possible explanation for the $T_{FH}$ expansion is the higher expression of activation markers such as CD80 and CD86 in the eGFP+;A20-/-;NIK+ B-cells. B-cells with a higher expression of CD80 and CD86 could positively modulate the activation and expansion of $T_{FH}$. Genetic studies in mice showed the importance of B-cell CD80 expression on the development of $T_{FH}$ [294]. Moreover, it has been proposed that memory B-cells with high expression of CD80 can interact with $T_{FH}$ generating a positive feedback loop of CD28/CD80 that drives T-cell expansion [295, 296]. Therefore, higher expression of CD80 and CD86 in the pre-activated antigen presenting-like A20-deficient NIK+ B-cells, in addition to driving conventional T-cell activation, could promote $T_{FH}$ differentiation explaining the high $T_{FH}$s numbers observed in the absence of GCs in A20F/F NIK-tg CD19cre mice.

Another possible explanation for the $T_{FH}$ expansion observed in A20F/F NIK-tg CD19cre mice may be an inappropriate immunological synapse between the B-cell and its cognate $T_{FH}$-cell. Several reports point to the importance of ICOS-L expression in B-cells and MZB-cells, specifically, for the proper development of $T_{FH}$ [297, 298]. The observed

low ICOS-L protein levels in B-cells accompanied by increased number of $T_{FH}$s are therefore puzzling. Hu et al. (2011) showed that NIK is required in for the expression of ICOS-L in B-cells and this ICOS-L expression supports the development of $T_{FH}$ [299]. Paradoxically, RelB$^{-/-}$ NF-κB2$^{-/-}$ double knockout GC B-cells have a slight reduction, although not significant, of ICOS-L expression [101]. One explanation for the lower ICOS-L surface levels in B-cells would be a higher shedding of ICOS-L by ADAM10 [297]. I therefore speculate that if NIK+ A20-deficient B-cells were to have a higher expression or a higher activation level of ADAM10, the higher levels of ADAM10 activity would result in stronger ICOS-L shedding reducing its detection. This to be tested hypothesis would fit with the higher number of $T_{FH}$ observed.

Finally, my data show that with age A20F/F NIK-tg CD19cre mice develop an expansion of myeloid cells (Figure 25), in addition to the T-cell hyperplasia that is maintained in old age. It has been proposed that chronic inflammation by the release of cytokines such as IL6 can lead to the expansion of myeloid cells in aged animals [79, 254]. Therefore it is likely that similar mechanisms take place in the A20F/F NIK-tg CD19cre mice, where aberrant activation of the NF-κB pathways in B-cells results in a B-cell extrinsic inflammatory phenotype. A better understanding of the cytokine milieu present in these animals might enlighten the current understanding. ELISAs or flow cytometry analysis of IFNγ, TNFα, IL10 and IL6 cytokines would add to our understanding of the inflammatory scenario present in these mice.

In summary, the antigen presenting-like phenotype in A20-deficient NIK+ B-cells and the finding that both CD4 and CD8 T-cells have an effector-like phenotype suggest that the B-cells can present antigens to their cognate T-cells, thus activating them and starting an immune reaction. Moreover, the presence of ICOS and PD1 high expressing CD4 and CD8 T-cells points to a scenario with repetitive activation of T-cells resulting in anergy, supporting the notion of B-cell-driven inflammation. Furthermore, the increased number of regulatory T-cells suggests a need for regulating an inflammatory response under conditions where B-cells fail to become GC B-cells and only T-cells are activated. All of the above suggest that pre-activated B-cells have a role in the T-cell hyperplasia observed in the A20F/F NIK-tg CD19cre mice. Given the activation T-cell status that may even result in anergy in response to B-cell hyper-activation, it is likely that the T-cells are responsible for clearing hyper-activated B-cells and thus reduce mature B-cell numbers.

Further experiments are required to evaluate the actual role of T-cells in the homeostasis of aberrantly activated B-cells. To address the role of T-cells in the impairment of B-cell homeostasis observed here transplant experiments into T-cell deficient mice versus wild type or RAG KO mice could shed light into the specific involvement of T-cells in clearing B-cells. Furthermore, crosses to CD3$\varepsilon^{-/-}$ mice, which are devoid of T-cells, would be an ideal system to test the effect of T-cells in the observed phenotype. If the A20-/-;NIK+ B-cells cannot replenish the B-cell compartment then the aberrant NF-κB activation most likely plays a role in B-cell survival or proliferation. That would imply that the phenotype observed is cell intrinsic, and T-cell independent. However, if in this scenario the B-cell compartment is replenished by the transplant, most likely the effector T-cells would have a role in B-cell clearance. These experiments would add to my finding that T-cells are activated in A20F/F NIK-tg CD19cre mice and to the potential role of pre-activated B-cells in initiating an inflammatory response.

### ABERRANT NF-κB ACTIVATION NEGATIVELY AFFECTS THE GC REACTION AND THE DEVELOPMENT OF ADAPTIVE IMMUNITY

My data provides additional evidence on the previous hypothesis on the negative role of NIK in germinal centre B-cells. Here, I show that the majority of the GC B-cells in the NIK-tg compound mice are eGFP negative and therefore do not express NIK (Figure 14). Moreover, there are very few eGFP positive plasma cells (Figure 15). Therefore, my data supports the notion that strong alternative NF-κB signalling negatively affects the germinal centre reaction. Similarly to the results presented here, Zhang et al. (2015) found that constitutive activation of the alternative NF-κB pathway by overexpression of NIK-tg at the GC B-cell stage has a negative effect in the GC reaction [165].

One interesting finding in this study was that the combination of loss of A20 and NIK overexpression resulted in higher levels of IRF4 and BCL6 in mature B-cells compared to controls (Figure 16 and Figure S 6). It is possible that elevated levels of both transcription factors inhibit the progression of B-cells into GC reaction. Supporting this hypothesis, Zhang et al. (2015) associated NIK overexpression in GC B-cells with significantly higher IRF4 expression [165]. In the same publication, they showed that Cγ1cre IμBCL6 NIK-tg mice had lower percentage of GC B-cells compared to BCL6, NIK-tg or YFP-tg reporter controls. Moreover, reduced percentages of GC B-cells expressed

the eGFP reporter for the NIK-tg compound mice 21 days post immunization [165]. These observations further support the hypothesis that at least higher expression of BCL6 in combination with over expression of NIK negatively selects GC B-cells.

Moreover, in mature B-cells BCL6 mRNA is readily available, and once the cell enters the GC reaction its translation is initiated. However, the regulatory mechanism for the translation and expression of BCL6 in GC B-cells is not understood [300]. I speculate that if there is a higher BCL6 protein content in mature B-cells here, A20 and NIK could play a role influencing this unknown regulatory mechanism.

The role of alternative NF-κB activation in the GC reaction is complex. On the one hand, Zhang et al. (2015) have shown that NIK impairs the GC reaction [165]. On the other hand, De Silva et al. (2016) provide evidence for the requirement of both RelB and p52, members of alternative NF-κB family of transcription factors, for B-cells to progress to GC reaction [268]. They propose that loss of the alternative NF-κB pathway leads to reduced ability to enter the cell cycle, since e*x vivo* stimulated double knockout $RelB^{-/-}$ $p52^{-/-}$ B-cells show a proliferation defect [101]. Interestingly, Zhang et al. (2015) speculated that additional canonical NF-κB activating mutation may confer a survival advantage to NIK+ B-cells [165]. However my data shows that canonical NF-κB activation by heterozygous or homozygous loss of A20 in NIK+ B-cells did not rescue the GC B-cell phenotype. It is possible that a different mechanism for canonical NF-κB activation might result in a different outcome. Tavares et al. (2010) and Chu et al. [79] found that loss of A20 in B-cells resulted in increased GC B-cell numbers in vivo, which Tavares et al. attributed to reduced FASL-depended cell death due to increased Bcl-xL expression in the absence of A20 *in vitro* [254]. Loss of A20 and over expression of NIK could result in B-cell that is more sensitive to cell death [79, 277] (discussed previously). Taken together, all the evidence points to a dominant negative role of NIK in GC B-cells that cannot be rescued by loss of A20, that is NIK-dependent but may be independent of alternative NF-κB activation.

Finally, the lower levels of ICOS-L expression in the A20F/F NIK-tg B-cells point towards an improper B-T-cell synapse. In spite of the increased number of $T_{FH}$ observed in these mice (Figure 20), the reduced interaction with $T_{FH}$ might be insufficient for proper signals required for GC reaction.

There are many open questions regarding the role of strong NF-κB activation and the GC reaction. Is it likely that the pre-activated state of the mature B-cells in these mice renders them unresponsive to further stimuli? Would further signals from $T_{FH}$ be able to drive them into the GC reaction? Are these cells able to respond to antigen presentation, of have they become anergic? As a first step, *ex vivo* stimulation with T-cell independent and T-cell dependent stimuli will provide further information about their responsiveness and activation potential. Recently, the *in vitro* germinal centre B-cell culture has been used as a tool to further study aspects of the biology of GC B-cells [99]. Assessing the capability of NIK+ B-cells to establish GC B-cell cultures would be another means to assess the role of strong alternative NF-κB activation in the GC reaction. Moreover, immunization of mice with T-cell specific antigens could address the role of B-cells as APCs and GC B-cells.

To summarize, my data supports the notion that loss of A20 results not only in prolonged NF-κB activation but also makes B-cells more susceptible to cell death most likely driven by external stimuli [240, 254, 274, 275, 301-306]. This highlights the importance of A20 in protecting against cell death. The model I proposed here is that aberrant NF-κB activation in B-cells leads to an atypical B-cell phenotype and I speculate that this triggers a T-cell immune response. The release of cytokines and signals coming from the activated T-cells to the B-cells with hyperactive phenotype could drive the extrinsic cell death program in these cells. In the absence of the protective role of A20, death stimuli that under normal consequences would result in B-cell survival now result in B-cell death. Thus, without A20 driving the balance towards survival, the B-cells are no longer protected and become prone to cell death. Additionally, it still remains to be proven whether the novel pro-apoptotic role of NIK also plays a role in mature B-cell death observed here.

## V.2 ROLE OF CANONICAL NF-κB IN B-CELL TRANSFORMATION

The members of the family of NF-κB transcription factors regulate the expression of genes involved in survival, differentiation and inflammation that play a key role in the development of the immune system and particularly B-cells. Thus it is surprising that no direct evidence has linked deregulated canonical NF-κB signalling to spontaneous transformation in B-cells. Here, I show for the first time B-cell lymphomagenesis in mice as a direct consequence of constitutive canonical NF-κB activation. My data shows that constitutive canonical NF-κB activation in B-cells resulted in the expansion of the B1a subset in mice that with age developed into a disease with characteristics of human small cell lymphocytic lymphoma (SLL). Moreover, my data further supports the importance of canonical NF-κB activation in CLL, by using the TCL1tg chronic lymphocytic leukaemia (CLL) mouse model. And finally, my data provides compelling evidence for the requirement of additional activation signals other than canonical NF-κB activation in CLL-cells to overcome the dependence of the niche for prolonged survival.

### CANONICAL NF-κB ACTIVATION IN B1-CELL DEVELOPMENT

The B1 B-cell compartment is composed of B1a and B1b B-cells that play an important role in the innate immune response. B1-cells are of foetal liver origin and have self-replenishing ability [278]. However, it is clear from bone marrow chimera experiments that hematopoietic stem cells also have the ability to replenish the B1 compartment [110]. Additionally, there is consensus that strong BCR signals are required for B1a development [81, 282, 307].

This thesis provides direct evidence on role of canonical NF-κB signalling in B1a biology. My data shows that constitutive canonical NF-κB activation in B-cells by the conditional expression of a constitutive active IKK2 resulted in the expansion of the B1-cell compartment in mice, favouring the B1a subset. My results are in agreement with previous studies on the requirement of canonical NF-κB activation in B1a B-cell development [35, 78, 120, 308]. Furthermore, they demonstrate that uncontrolled enhanced canonical NF-κB activation results in B1a-cell expansion, in line with previous experimental indications in this direction [122]. Paradoxically, overexpression of BCL10 in B-cells, required for NF-κB activation, results in reduced B1a-cell numbers but increased B1b-cell numbers in the peritoneum [185]. Moreover, BCL10 overexpression

in B-cells resulted not only in c-Rel-dependent activation of the canonical NF-κB but also p52-dependent activation of alternative NF-κB pathway [185]. Therefore, the additional activation of the alternative NF-κB pathway could skew the development into the B1b lineage. Interestingly, although constitutive canonical NF-κB activation in B-cells preferentially expanded the B1a subset, I also observed expansion of B1b-cells in both R26-IKK2ca Cγ1cre mice and R26-IKK2ca CD19cre mice, suggesting that canonical NF-κB activation also plays a role in B1b-cells. Taken together, these findings demonstrate that canonical NF-κB activation critically dictates the output of normal B1-cell development.

As motioned above, my results prove the direct link between enhanced canonical NF-κB activation and B1a expansion in mice, suggested by previous reports. Previously, Ding et al. (2007) reported that Siglec-G controls the level of activation of canonical NF-κB in B1a-cells, and in its absence B1a-cells expanded as a result of enhanced canonical NF-κB activation [122]. Moreover, Hahn et al. (2017) showed that the overexpression of the short (s)CYLD isoform in mouse B-cells resulted in Bcl3 dominated NF-κB activation [309]. Mice that expressed sCYLD in B-cells developed B1a expansion in old age [310]. Therefore, these findings indicated that enhanced NF-κB-associated signalling can be associated with B1a-cell expansion suggesting that a tight control of NF-κB activation is required for the normal homeostasis of the B1a compartment.

Previous studies demonstrated that the development of the B1a compartment requires the expression of a functional BCR signalling complex [282]. Moreover, it has been proposed that strong BCR signalling is required for B1a activation [81, 112, 250, 282]. My preliminary results show that strong canonical NF-κB activation by expression of two copies of IKK2ca resulted in *in vitro* proliferation of resting B1a-cells, suggesting that canonical NF-κB activation modulates the proliferation of B1a-cells. Although it still remains to be confirmed whether constitutive canonical NF-κB activation results in higher B1a proliferation that translates into an expansion of B1a-cells, my preliminary results suggest that constitutive canonical NF-κB activation in B1a-cells could act as a surrogate for NF-κB activation downstream strong BCR signals during the positive selection in B1a development. Consistently, Morimoto et al. (2016) have suggested that the absence of B1a-cells in leucine-rich repeat kinase 1 (LRRK1)-deficient mice is due to the failure of strong BCR signalling to induce canonical NF-κB activation required for the positive selection and survival of these cells [308]. Interestingly, Sasaki et al. (2013)

reported that although NF-κB signalling downstream of the BCR is not affected in LUBAC mutant mice, they have reduced B1a-cell numbers [35], implying that although canonical NF-κB signalling is required for B1a development, NF-κB activation downstream of BCR signalling is not the main driving force. One limitation in both studies is that due to the absence of B1a-cells in these mutant mice, the NF-κB activation downstream of BCR signalling was assessed in B2-cells and the physiological response of B1a-cells to BCR crosslinking may differ from that of B2-cells. Therefore, they were not able to address the requirement of canonical NF-κB activation after BCR signalling in B1a-cells. As mentioned previously, loss of Siglec-G in B-cells resulted in expanded B1a population [121, 122]. Moreover, Hoffmann et al. (2007) have showed that loss of Siglec-G in B-cells results in higher calcium mobilization in B1a-cells after BCR stimulation, however it is associated with reduced proliferation [121]. They suggest that the higher BCR-mediated calcium signalling responses promote the expansion of B1a-cells most likely by increasing the cell life span [121]. Given that this study did not address the status of NF-κB activation, it cannot be ruled out that the higher calcium mobilization associated responses are related to the enhanced NF-κB activation seen by Ding et al. (2007). Also TRAF6 is indispensible for B1a-cell development [120] suggesting that additional signals independent of strong BCR signalling are required for normal B-cell development and associated with canonical NF-κB activation. Therefore, these findings imply that constitutive canonical NF-κB activation might replace the requirement of strong BCR signals in B1a development while enhanced canonical NF-κB activation might amplify downstream signals of weaker BCR activation strength. Taken together, these findings suggest that canonical NF-κB activation in B1a-cells plays a role in proliferation and survival.

Mouse genetic studies have proven the strict requirement of BAFF for the development and survival of follicular and marginal zone mature B-cells [72, 85]. On the other hand, BAFF and its main receptor BAFF-R are not required for peritoneal B1-cell development. Nevertheless, subsequent studies provided evidence for a role of enhanced BAFF and APRIL signalling also in B1-cell survival and development [236, 311, 312]. Mechanistically, amongst other studies, Almaden et al. (2016) demonstrated that BAFF activates both canonical and alternative NF-κB signals in B-cells [36]. Moreover, since constitutive active IKK2-mediated constitutive canonical NF-κB activation in B-cells replaces the cell-intrinsic requirements for BAFF signals [37], constitutive canonical NF-κB activation could also replace homeostatic requirements in B1a-cells. My results

provide preliminary evidence for the role of BAFF in conjunction with canonical NF-κB activation in B1a proliferation *in vitro*. Therefore, the B1a expansion observed by constitutive canonical NF-κB activation may also imply the involvement of BAFF/APRIL signals in B-cell survival and proliferation *in vivo*.

### CANONICAL NF-κB ACTIVATION IN B-CELL LYMPHOMA

Molecular studies in samples from patients with immune diseases as well as B-cell lymphomas have pointed to the importance of deregulated canonical NF-κB activation in disease pathogenesis [1, 5-8, 313]. Here, I show that constitutive activation of the canonical pathway by expression of constitutive active IKK2 in B-cells results in B-cell lymphoma with features reminiscent of human SLL or CLL. My results add to previous findings on the role of constitutive canonical NF-κB activation in B-cells driving mature B-cell hyperplasia [37] and plasma cell hyperplasia [164] building a more comprehensive understanding on the role of canonical NF-κB activation in B-cell biology.

My finding that enhanced constitutive canonical NF-κB activation in B-cells promotes the expansion of $CD5^{+}$ $B220^{lo}$ B-cell lymphoma in mice is in agreement with previous studies suggesting a role of canonical NF-κB activation in CLL pathogenesis [199, 200, 310]. Human CLL is a very heterogeneous disease where diverse genetic aberrations result in the expansion of $CD5^{+}$ $IgM^{+}$ small B-lymphocytes [193, 314-316]. Although few mutations related to NF-κB activation have been reported in CLL patients samples [193, 194, 317], previous reports demonstrated that in general samples from CLL patients contain higher NF-κB activation compared to B-cells from healthy donors [195, 318]. Canonical NF-κB activation in CLL samples could be due to stimulation of CLL-cells with extrinsic signals such as BCR crosslinking [207, 319], TNF-α [320], NOTCH [221, 321], APRIL and BAFF [203, 236, 237, 322]. Moreover, additional signals from the surrounding cells can activate canonical NF-κB in CLL-cells [197, 323]. Previously, a gene expression profile study by Herishanu et al. (2011) identified that CLL samples from the lymph nodes have a higher expression of NF-κB related genes compared to samples from other organs [141]. Additionally, the oncogene T-cell leukaemia 1 (TCL1), which is highly expressed in CLL patient samples [324-326] and whose overexpression causes a CLL-like disease in mice [229], has the ability to activate canonical NF-κB in B-cells [231, 233]. Therefore, several mechanisms for canonical NF-κB activation in CLL-

cells have been identified supporting the association between enhanced canonical NF-κB activation and human CLL development. Interestingly, the NF-κB subunits that dominated the enhanced canonical NF-κB activation detected in CLL-cells, RelA and p50 [198, 327, 328], are also predominantly activated by the expression of the IKK2 constitutive active mutant in B-cells [37]. This suggests that similar mechanism may be involved in the development of human CLL and the murine malignant CLL-like B1a-cell expansion caused by constitutive activation of canonical NF-κB. Finally, inactivating mutations in the NF-κB inhibitory protein IκBε that result in NF-κB activation have been identified in CLL patients samples [143]. Interestingly, Sasaki et al. (2006) reported that B-cells with constitutive canonical NF-κB activation caused by expression of the IKK2 constitutive active mutant have higher IκBε protein levels [37]. It is possible that the higher expression of IκBε in my current lymphoma model may interfere with additional NF-κB related pathogenicity observed in human CLL. Taken together, all the evidence presented here suggests that enhanced canonical NF-κB activation in B-cells in CLL plays an important role in disease pathogenesis. My results further demonstrate that constitutive canonical NF-κB activation in B-cells is sufficient to promote enhanced B-cell survival and proliferation that can eventually develop into a CLL-like disease in mice.

## CANONICAL NF-κB ACTIVATION COOPERATES WITH TCL1 IN MURINE CLL DISEASE PROGRESSION

My results demonstrate that constitutive canonical NF-κB activation dramatically cooperates with the TCL1 oncogene in CLL pathogenesis in mice, accelerating the disease progression in a dose dependent manner. Previous studies in the TCL1tg mouse model on the role of canonical NF-κB activation corroborate my findings [329, 330]. One major finding supporting the cell-intrinsic importance of enhanced canonical NF-κB activation in TCL1-driven CLL-like disease in mice was that mutant IKK2-mediated constitutive canonical NF-κB activation in a small percentage of B-cells defined by Cγ1cre and AIDcre had a similar disease course, with similar median survivals, as observed for the expression of IKK2ca in over 80% of the B-cells mediated by CD19cre. This suggests that canonical NF-κB activation in TCL1tg cells dramatically enhances their competitive fitness by either prolonged survival or higher proliferation compared to TCL1tg+ only CLL-cells. It is unlikely that the murine CLL-like cells identified in the experiments with Cγ1cre and AIDcre were products of the germinal centre reaction. I

rather believe that Cre-mediated recombination leads to induction of IKK2ca in a small subset of TCL1tg B-cells, most likely B1-cells. Accordingly, recent evidence suggests that the AID enzyme is expressed in a small percentage of CLL-cells in humans [331-333], supporting my finding that AIDcre recombination takes place in a small percentage of TCL1+ B-cells, most likely pre-leukemic. Additionally, it has been reported that AID is expressed in a fraction of B1a-cells in mice [261]. Casola et al. (2006) suggested that cytokines could induce expression of Cre in Cγ1-cre mice [243]. It has been reported that the cytokine IL-4 [46] and CD40 signalling can trigger the expression of the AID enzyme as well as the expression of the germline Cγ1 region of the BCR [99]. Furthermore, signalling through CD38 in B-cells induces expression of the cγ1 germline transcripts [334]. Since CD38 is a prognostic factor in CLL [335-337], signalling through CD38 might induce the expression of the cγ1 germline transcripts in CLL-cells as seen in normal B-cells. Therefore, any of the above-described mechanisms would explain the induction of IKK2ca through Cre-mediated recombination in a small percentage of Cγ1cre and AIDcre TCL1+ B-cells. My data suggests that in the murine TCL1 model there is pre-malignant TCL1+ B-cell in 3 months old mice. Taking these into consideration, I hypothesise that at this pre-leukemic stage, either by direct interaction with the niche or by bi-directional remodelling of both the niche and the pre-leukemic CLL, the microenvironment promotes AID and cγ1 germline expression in a small percentage of cells, most likely proliferating cells, that induces expression of Cre protein and ensuing expression of the IKK2 mutant and therefore constitutive canonical NF-κB activation. The constitutive canonical NF-κB activation in IKK2ca+;TCL1+ pre-leukemic B-cells confers a striking competitive advantage over TCL1+ pre-leukemic B-cells.

My findings that IKK2ca B-cells show higher *in vitro* survival and spontaneous proliferation, and additionally have a higher expression of BCL2 anti-apoptotic proteins suggests that constitutive canonical NF-κB activation in B1a-cells promotes both cell survival and proliferation. Human CLL is characterized by a slow accumulation of CD5+ B-cells that are resistant to apoptosis and have slow proliferation rates. Several results associate enhanced canonical NF-κB activation in human CLL with the expression of anti-apoptotic proteins BCL2, BCL-XL, MCL1 and the inhibitors of Caspase XIAP and cIAP [197, 313, 321, 323, 328]. My preliminary results of reduced *in vitro* apoptosis accompanied by a higher expression of the anti-apoptotic protein BCL2 in B1a-cells suggest that constitutive canonical NF-κB activation prolongs B-cell survival by protecting cells against cell death by apoptosis. Recent evidence suggest that CLL-cells

have a higher proliferative rate than previously thought [338, 339], bringing the question of whether canonical NF-κB activation in CLL-cells also provides proliferation advantage. Igawa et al (2011) reported that NF-κB activation supports the expression of Cyclin D2 in CLL-cells, which is required for their proliferation [127]. The preliminary evidence of *in vitro* proliferation of IKK2ca+ and IKK2ca+;TCL1tg+ B-cells, but not TCL1tg+ B1a-cells in the absence of stimuli suggest that enhanced NF-κB activation may drive the expression of genes related with proliferation. Consistently, Enzler et al. (2009) reported that in the TCL1tg CLL mouse model TCL1+ CLL-like cells display higher proliferative activity compared to non-leukemic TCL1+ B-cells but also show higher apoptosis rates [322]. They propose that this high cell turnover is the cause of the slow disease progression in the TCL1tg mouse model [322]. Moreover, they showed that BAFF could rescue the increased apoptosis and *in vitro* promote expression of BCL2 and Mcl1 in a RelB and RelA dependent mechanism, resulting in higher CLL burden and accelerated disease progression [322]. In a later study, they additionally showed that APRIL-tg TCL1tg double transgenic mice also presented with an earlier disease onset and a shorter life span [237]. Interestingly, my preliminary results that at least *in vitro* stimulation of B1-cells with BAFF resulted in increased proliferation suggest that BAFF and constitutive canonical NF-κB activation may cooperate in B1 cell proliferation. One study in human CLL samples reported the expression of BAFF and APRIL in CLL-cells suggesting an possible autocrine stimulation [340]. Given that B1a-cells with constitutive canonical NF-κB activation seem to proliferate *in vitro* in the absence of any stimuli and are responsive to BAFF, it would be interesting to assess whether constitutive canonical NF-κB activation in B-cells has a similar effect on BAFF and April production and if BAFF and APRIL neutralizing antibodies have an effect *in vitro*. Although my results are preliminary and need to be confirmed, the development of CLL-like disease in mice by constitutive canonical NF-κB activation and the additional shorter disease progression in TCL1tg mice could both be a result of enhanced B-cell proliferation and higher resistance to apoptosis. Additional studies assessing cell turn over by 5-bromo-2-deoxyuridine (Br-dU) incorporation *in vivo*, staining of the proliferation marker Ki-67 and assessing Caspase activation would complement my preliminary results regarding *in vitro* proliferation and survival and bring further understanding on the mechanism of NF-κB activation in CLL disease.

## CONSTITUTIVE CANONICAL NF-κB ACTIVATION IN TCL1TG CLL-LIKE CELLS DOES NOT REPLACE SURVIVAL SIGNALS FROM THE SUPPORTIVE NICHE

My results show that constitutive canonical NF-κB activation in the TCL1 CLL mouse model is not sufficient to overcome the absence of required survival signals from the microenvironment in PKC-β KO mice. Herishanu et al. (2011) reported that the microenvironment affects the expression of genes in human CLL [141], supporting the notion that the tumour microenvironment plays a role in the disease pathogenesis. It is now accepted that a bidirectional remodelling between the CLL-cell and its surrounding microenvironment takes place in CLL and is required for the disease development and progression. Lutzny et al. (2013) demonstrated that direct contact of the CLL-cell leads to expression of the PKC-βII splice isoform in the microenvironment, which is required for the supportive role of the microenvironment in the development of CLL [167]. In the absence of PKC-β, transplants of murine TCL1tg CLL-cells into PKC-β KO mice fail to develop into CLL [167]. Given the aggressive CLL characteristics observed in the lymph nodes [341], with the notion that proliferation takes place mainly in the lymph nodes [338] and that there is higher NF-κB activity in CLL-cells from the lymph nodes, it was suggested that canonical NF-κB activation driven by the microenvironment is required for the proliferation and survival of the CLL-cells [141, 323]. My findings that transplanted TCL1tg CLL-cells with constitutive canonical NF-κB activation fail to produce CLL in PKC-β KO mice suggests that additional supportive signals from the microenvironment other than canonical NF-κB activation are required for the survival and proliferation of CLL-cells in these mice.

In summary, I demonstrated that strong constitutive canonical NF-κB activation results in the aberrant expansion of B1a-cells that with age develop into a disease similar to human SLL/CLL in mice. My findings suggest a role for enhanced canonical NF-κB activation as a driver in CLL and demonstrate that canonical NF-κB accelerates disease progression of the established TCL1tg CLL mouse model in a dose dependent manner. Furthermore, my results provide further support for the hypothesis that canonical NF-κB activation is a potential therapeutic target in CLL. But they also suggest that CLL-cells receive strong pro-survival signals from their microenvironment that are not mediated through NF-κB activation and might represent attractive targets in future therapeutic approaches.

# SUPPLEMENTAL MATERIAL

# SUMPLEMENTARY FIGURES

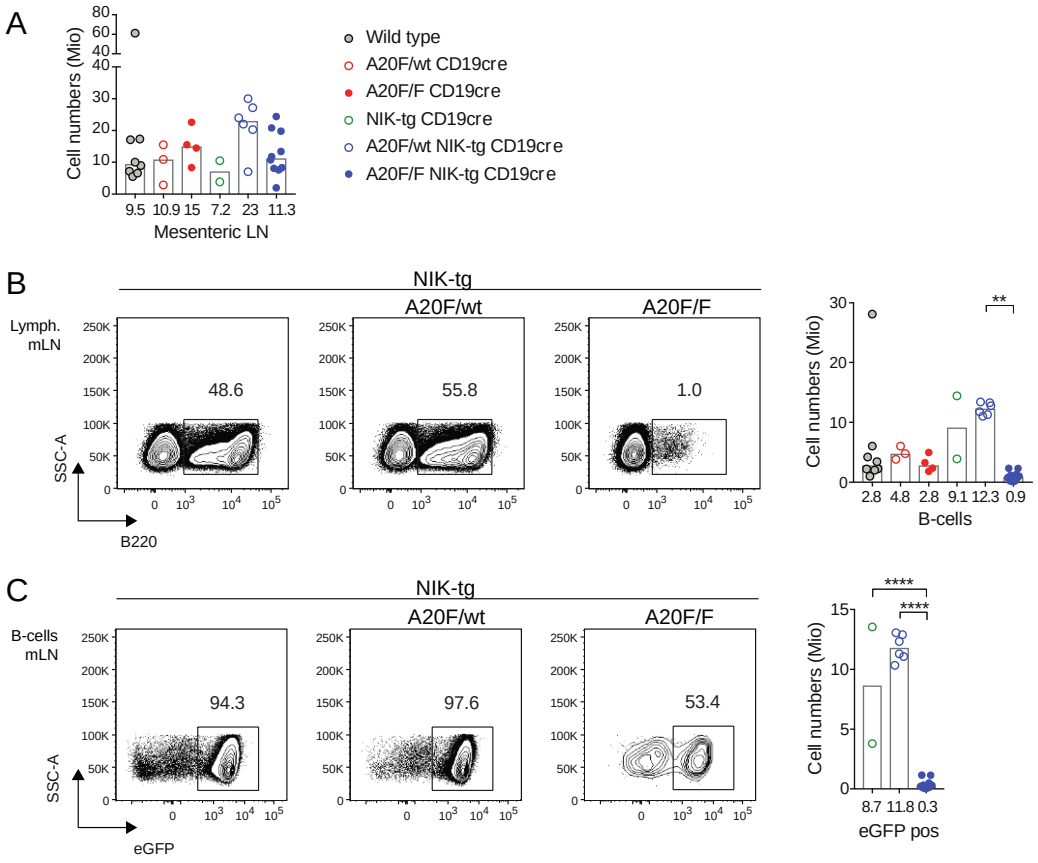


**Figure S 1. Reduced A20-/-;NIK+ B-cell numbers in mesenteric lymph nodes of young mice**

*Ex vivo* analysis of B-cells from mesenteric lymph nodes of young mice using flow cytometry. (A) Total mesenteric lymph nodes cell numbers. Contour plots depict percentages and bar charts indicate total cell numbers for (B) B-cells and (C) eGFP expressing B-cell. All flow cytometry contour plots are representative of at least 2 experiments. Bar charts represent medians and values are indicated below each histogram. Statistical analysis was done using One-way ANOVA (** $p<0.01$, **** $p<0.0001$).
LN (lymph node), mLN (mesenteric lymph nodes), eGFP (enhanced green fluorescent protein), pos (positive), B-cells ($B220^+$) and eGFP pos ($B220^+$ $eGFP^+$).

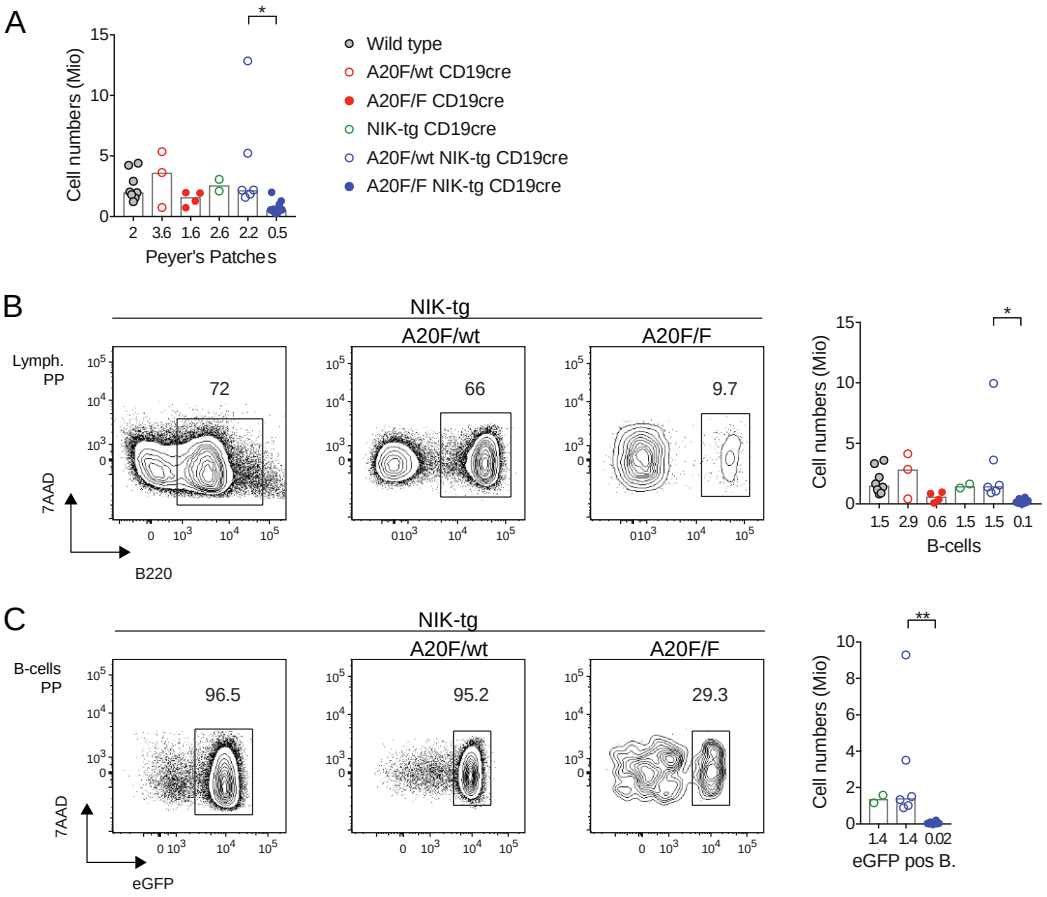


**Figure S 2. Reduced A20-/-;NIK+ B-cell numbers in Peyer's patches of young mice**

*Ex vivo* analysis of B-cells from Peyer's patches of young mice using flow cytometry. (A) Peyer's patches total cell numbers. Contour plots depict percentages and bar charts indicate total cell numbers for (B) B-cells and (C) eGFP expressing B-cells. All flow cytometry contour plots are representative of at least 2 experiments. Bar charts represent medians and values are indicated below each histogram. Statistical analysis was done using One-way ANOVA (* $p<0.05$, ** $p<0.01$).
PP (Peyer's patches), eGFP (enhanced green fluorescent protein), pos (positive), B-cells ($B220^+$) and eGFP pos ($B220^+$ $eGFP^+$).

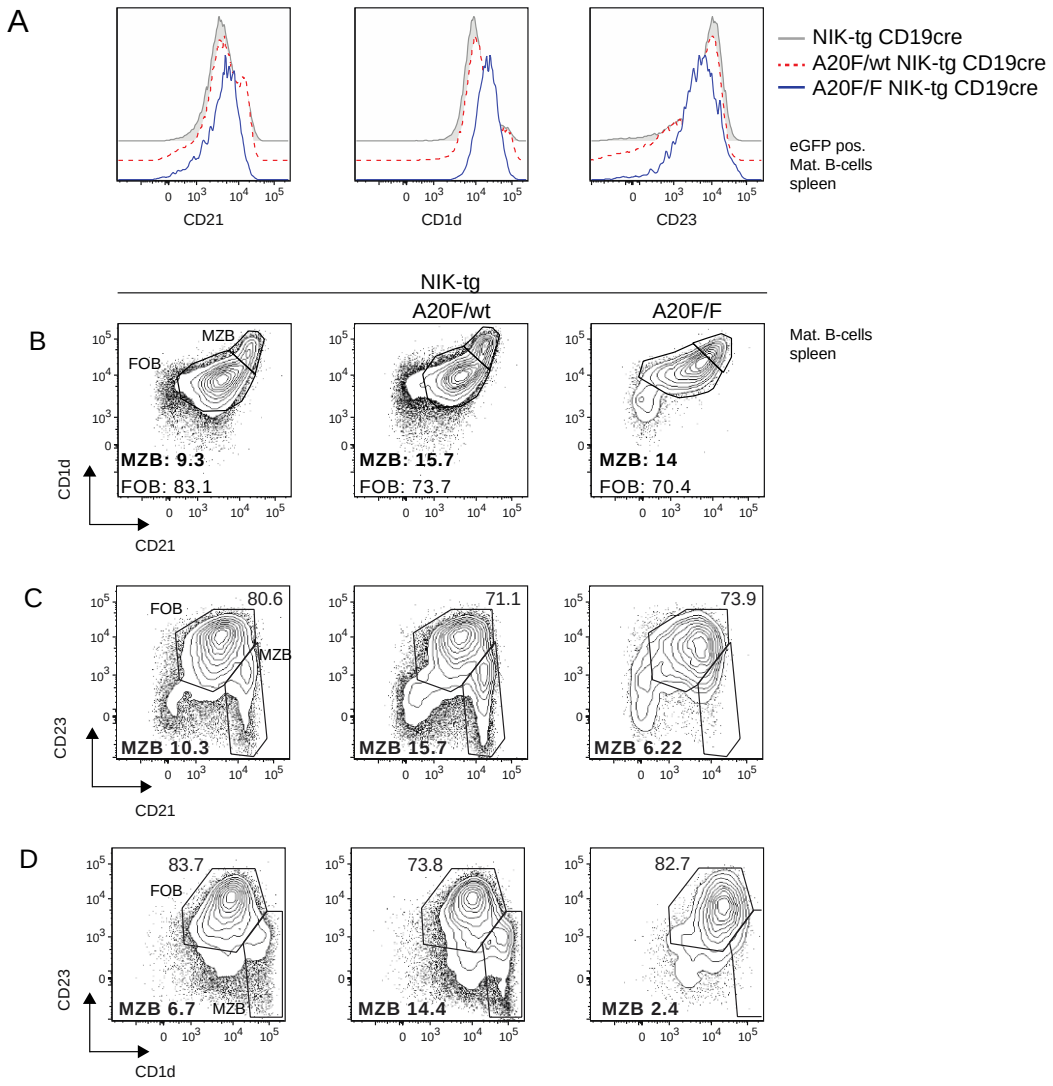


**Figure S 3. Abnormal marginal and follicular A20-/-;NIK+ B-cells**

*Ex vivo* analysis of mature B-cells from spleens of young mice using flow cytometry. (A) Histograms depict the expression of the surface markers CD21, CD1d and CD23 on mature eGFP positive B-cells. Contour plots depict 3 different gating strategies for marginal zone B-cells: (B) CD1d high CD21 high, (C) CD23 negative CD21 high or (D) CD23 negative CD1d high. All flow cytometry plots are representative of at least 2 experiments.
eGFP pos. Mat. B-cells ($B220^+$ $AA4.1^-$ $eGFP^+$), Mat. B-cells ($B220^+$ $AA4.1^-$), MZB (marginal zone B-cells) and FOB (follicular B-cells).

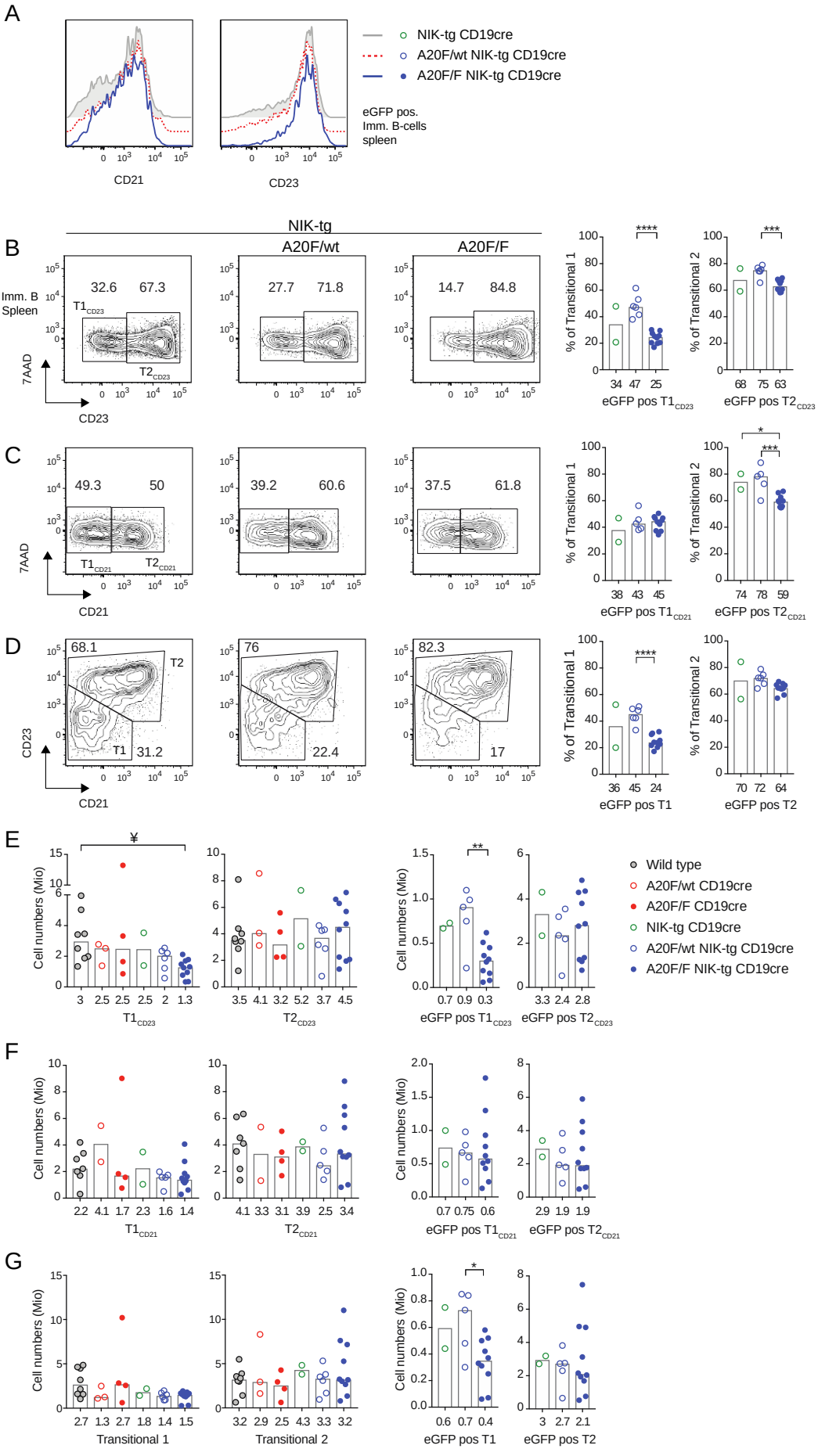
A
CD21
CD23
NIK-tg CD19cre
A20F/wt NIK-tg CD19cre
A20F/F NIK-tg CD19cre
eGFP pos.
Imm. B-cells
spleen
B
NIK-tg
A20F/wt
A20F/F
Imm. B
Spleen
32.6
67.3
27.7
71.8
14.7
84.8
7AAD
CD23
% of Transitional 1
% of Transitional 2
34 47 25
eGFP pos T1CD23
68 75 63
eGFP pos T2CD23
C
49.3
50
39.2
60.6
37.5
61.8
7AAD
CD21
38 43 45
eGFP pos T1CD21
74 78 59
eGFP pos T2CD21
D
68.1
T2
T1
31.2
76
22.4
82.3
17
CD23
CD21
36 45 24
eGFP pos T1
70 72 64
eGFP pos T2
E
Cell numbers (Mio)
3 2.5 2.5 2.5 2 1.3
T1CD23
3.5 4.1 3.2 5.2 3.7 4.5
T2CD23
0.7 0.9 0.3
eGFP pos T1CD23
3.3 2.4 2.8
eGFP pos T2CD23
Wild type
A20F/wt CD19cre
A20F/F CD19cre
NIK-tg CD19cre
A20F/wt NIK-tg CD19cre
A20F/F NIK-tg CD19cre
F
2.2 4.1 1.7 2.3 1.6 1.4
T1CD21
4.1 3.3 3.1 3.9 2.5 3.4
T2CD21
0.7 0.75 0.6
eGFP pos T1CD21
2.9 1.9 1.9
eGFP pos T2CD21
G
2.7 1.3 2.7 1.8 1.4 1.5
Transitional 1
3.2 2.9 2.5 4.3 3.3 3.2
Transitional 2
0.6 0.7 0.4
eGFP pos T1
3 2.7 2.1
eGFP pos T2

**Figure S 4. Transitional B-cells are not affected by combination of A20-deficiency and NIK overexpression**

*Ex vivo* analysis of immature B-cells from spleen of young mice using flow cytometry. (A) Histograms depict the expression of the surface markers CD21 and CD23 in eGFP positive immature B-cells. Contour plots depict the percentages and bar charts indicate percentages of eGFP positive cells and total cell numbers for (B, E) CD23 negative T1 and CD23 positive T2, (C, F) CD21 negative T1 and CD21 positive T2, and (D, G) CD23/CD21 low transitional 1 and CD23/CD21 h high transitional 2 B-cell subsets. All flow cytometry plots are representative of at least 2 experiments. Bar charts represent medians and values are indicated below each histogram. Statistical analysis was done using One-way ANOVA (* p<0.05, ** p<0.01, ***p<0.001, **** p<0.0001) or Kruskal-Wallis (¥ p<0.05).
eGFP (enhanced green fluorescent protein), eGFP pos. Imm. B-cells (eGFP positive immature B-cells, $B220^+$ $AA4.1^+$ $eGFP^+$), Imm. B (Immature B-cells, $B220^+$ $AA4.1^+$), $T1_{CD23}$ (CD23 negative T1, $B220^+$ $AA4.1^+$ $CD23^-$), $T2_{CD23}$ (CD23 positive T2, $B220^+$ $AA4.1^+$ $CD23^+$), $T1_{CD21}$ (CD21 negative T1, $B220^+$ $AA4.1^+$ $CD21^-$), $T2_{CD21}$ (CD21 positive T2, $B220^+$ $AA4.1^+$ $CD21^+$), T1 (Transitional 1, $B220^+$ $AA4.1^+$ $CD21^{lo}$ $CD23^{lo}$), T2 (Transitional 2, $B220^+$ $AA4.1^+$ $CD21^{hi}$ $CD23^{hi}$) and eGFP pos ($eGFP^+$).

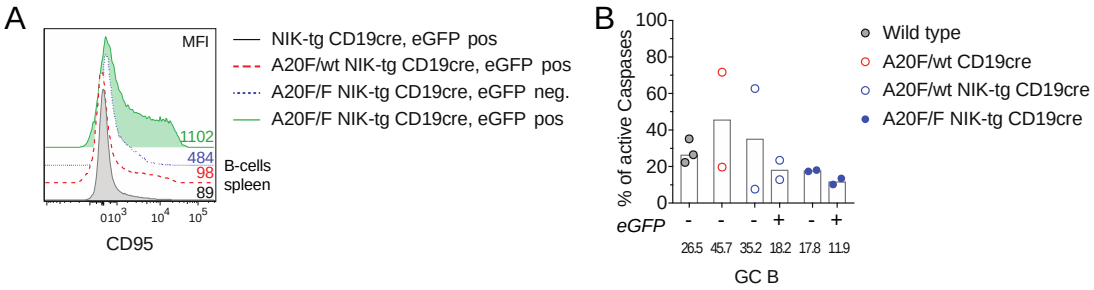


**Figure S 5. No increase in apoptosis observed in germinal centre A20-/-;NIK+ B-cells**

*Ex vivo* analysis of B-cells from spleen of young mice using flow cytometry. (A) Histograms depict CD95 expression in *ex vivo* B-cells, MFI are indicated for each population. (B) Bar chart shows the percentage of *ex vivo* active pan-Caspases GC B-cells in spleen. Bar charts represent medians and values are indicated below each histogram.
MFI (median fluorescence intensity), GC B (germinal centre B-cell, $B220^+$ $CD38^-$ $CD95^+$), eGFP (enhanced green fluorescent protein), activated pan-Caspases (Red-VAD-$FMK^+$ $7AAD^-$).

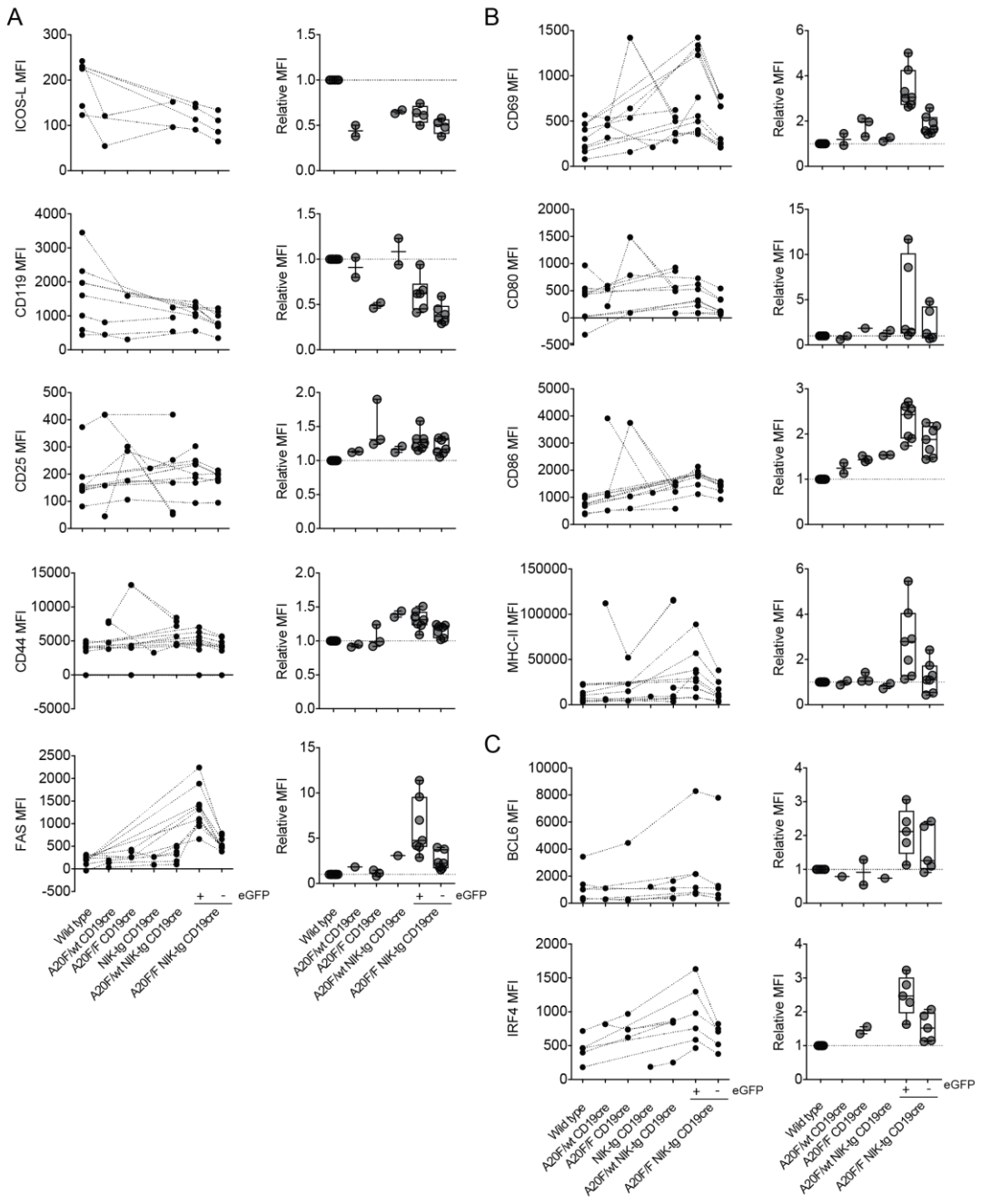


**Figure S 6. Aberrant pre-activated antigen presenting cell phenotype in eGFP+;A20-/-:NIK+ B-cells**

Expression of activation markers, receptors and transcription factors in B-cells from spleens of young mice. *Ex vivo* analysis of B-cells from spleen of young mice using flow cytometry. Scatter plots depict absolute MFIs and box plots show the MFI relative to wild type for (A) receptors and ligands: ICOS-L, CD119, CD25, CD44 and CD95/FAS; (B) B-cell activation markers: CD69, CD80, CD86 and MHC-II; and (C) transcription factors BCL6 and IRF4. In the box plots, the median is represented as a horizontal line, the box represents the 25$^{th}$ and 75$^{th}$ percentiles and the whiskers the minimum and maximum points. All individual values are plotted in the graph.
MFI (Median fluorescent Intensity), eGFP (enhanced green fluorescent protein), B-cells (B220$^{+}$).

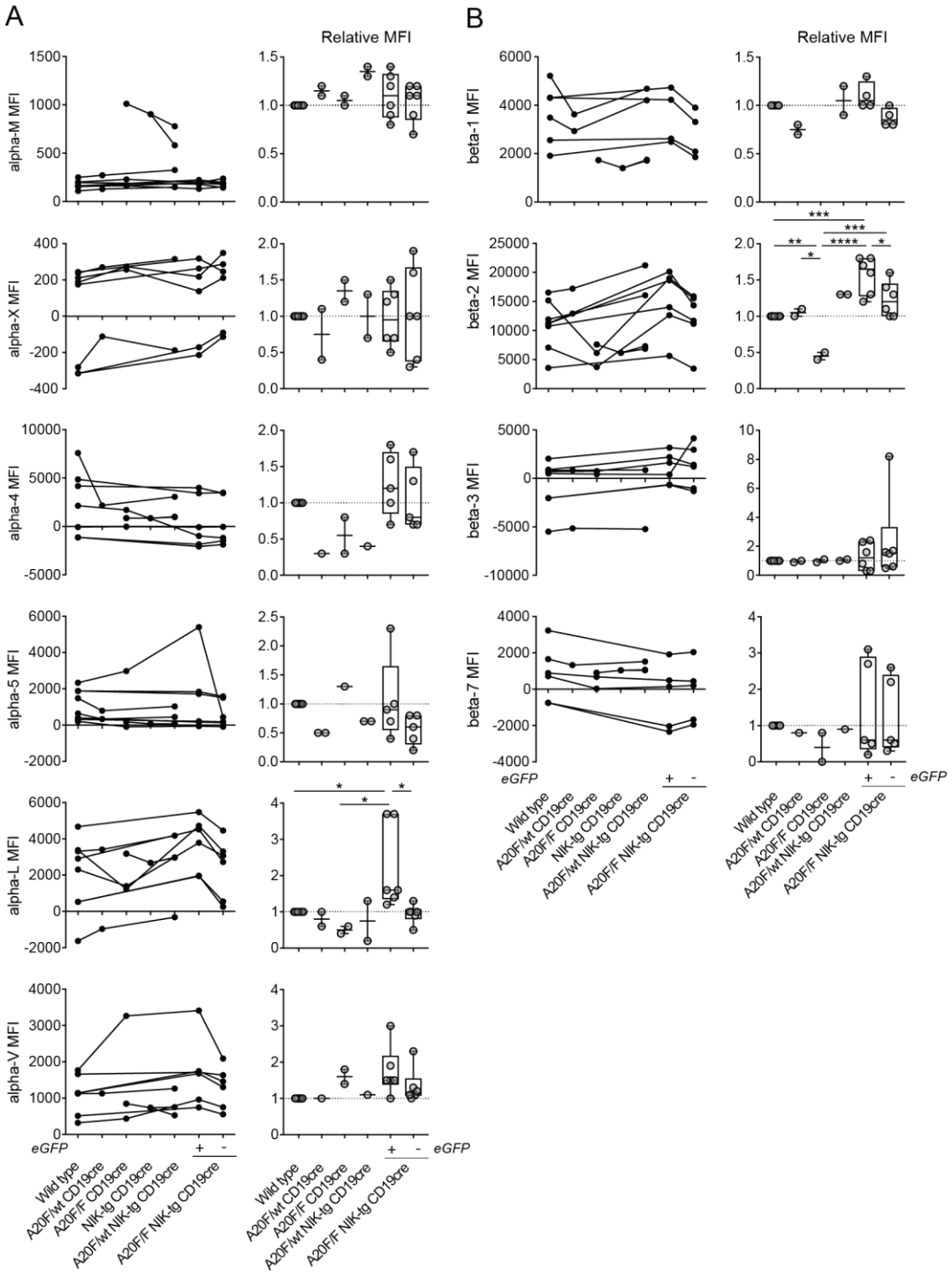


**Figure S 7. Aberrant alpha-L and beta-2 integrin expression in eGFP+:A20-/-;NIK+ B-cells**

*Ex vivo* analysis of integrin expression in B-cells from spleens of young mice using flow cytometry. (A) Scatter plots depict the absolute MFIs and box plots show the MFIs relative to wild type of (A) alpha-integrins: alpha-4, alpha-5, alpha-V, Alpha-L, alpha-M and alpha-X; and (B) beta-integrins: beta-1, beta-2, beta-3 and beta-7. In the box plots, the median is represented as a horizontal line, the box represents the 25$^{th}$ and 75$^{th}$ percentiles and the whiskers the minimum and maximum points. All individual values are plotted in the graph. Statistical analysis was done using One-way ANOVA (* p<0.05, ** p<0.01, *** p<0.001, **** p<0.0001).

MFI (Median fluorescent Intensity), eGFP (enhanced green fluorescent protein) and B-cells (B220$^{+}$).

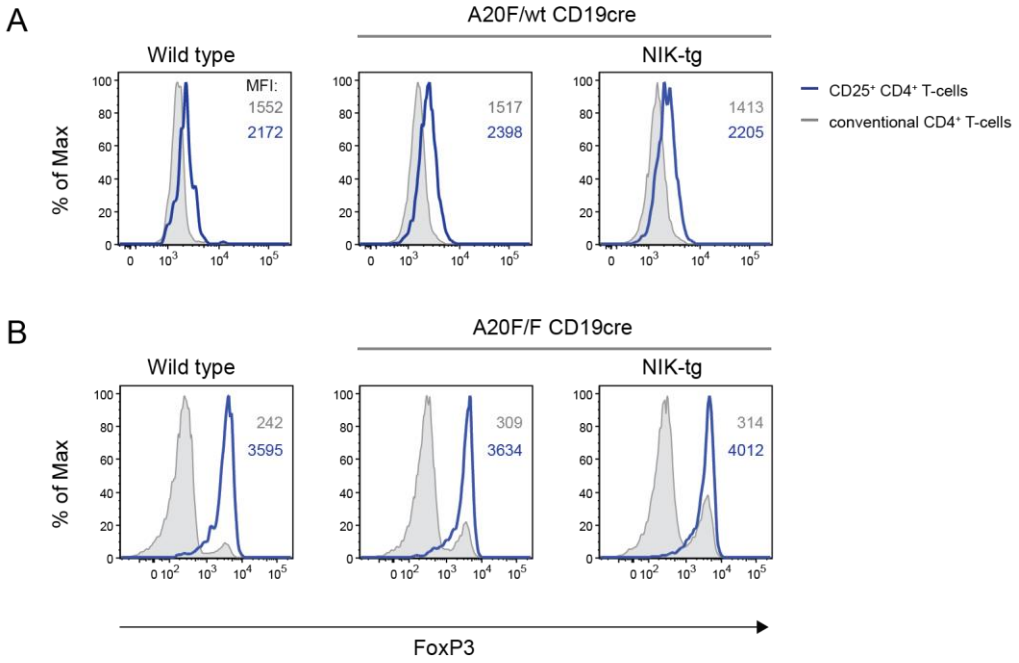


**Figure S 8. Expanded CD25$^+$ CD4$^+$ T-cells in A20-deficient NIK-tg CD19cre mice express the transcription factor FOXP3**

Ex vivo analysis of the expression of the transcription factor FoxP3 in splenic CD4 T-cells using flow cytometry. Flow cytometry histograms depict the intracellular expression of the FoxP3 transcription factor in CD25$^+$ CD4$^+$ T-cells (blue, open) and conventional CD4+ T-cells (grey, filled). Flow cytometry histograms in (B) are representative of at least 2 experiments, while in (A) represents a single experiment.

MFI (median fluorescence intensity), CD25$^+$ CD4 T (TCR$\beta^+$ CD4$^+$ CD25$^+$) and conventional CD4 T-cells (TCR$\beta^+$ CD4$^+$ CD25$^-$).

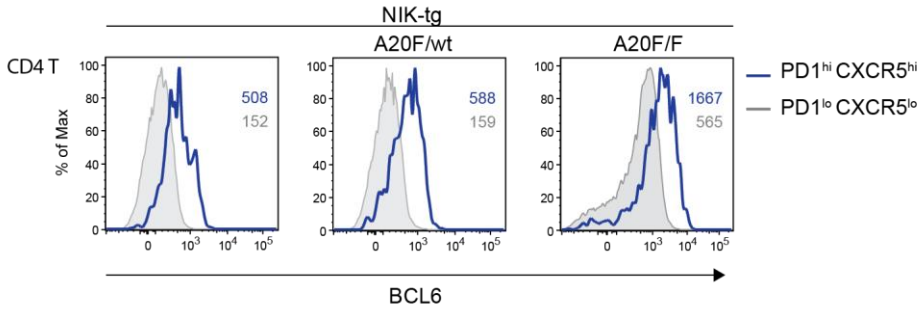


**Figure S 9. Expression of the transcription factor BCL6 in splenic PD1$^{high}$ CXCR5$^{high}$ CD4 T-cells**

Ex vivo analysis of the expression of the transcription factor BCL6 in splenic CD4 T-cells using flow cytometry. Flow cytometry histograms depict the intracellular expression of the BCL6 transcription factor in PD1$^{high}$ CXCR5$^{high}$ CD4$^+$ T-cells (blue, open) and PD1$^{lo}$ CXCR5$^{lo}$ CD4+ T-cells (grey, filled). Flow cytometry histograms are representative of single experiments, where the A20F/F NIK-tg CD19cre histogram belongs to a different experiment.

CD4 T (TCR$\beta^+$ CD4$^+$)

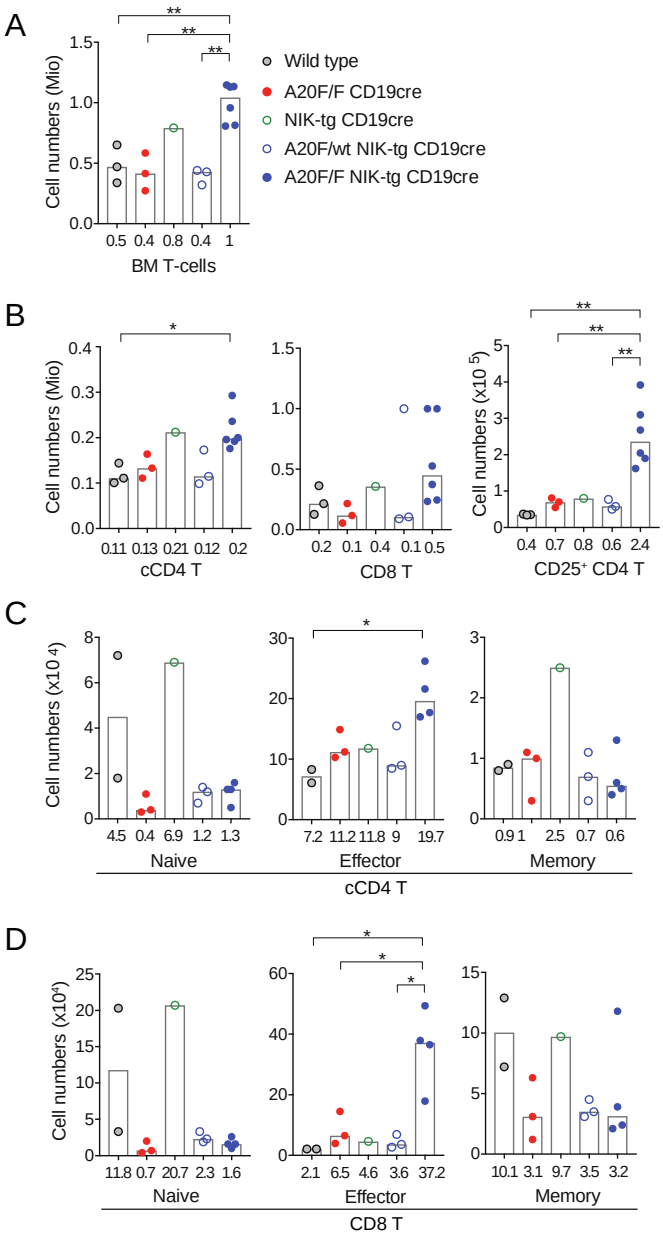


**Figure S 10. T-cell hyperplasia in bone marrow of A20F/F NIK-tg CD19cre young mice**

*Ex vivo* analysis of T-cells from bone marrow of young mice using flow cytometry, for one leg after red blood cell lysis. Bar charts indicate cell numbers for (A) T-cells, (B) T-cell subsets: conventional CD4, CD8, and CD25+ CD4 T-cells; and activation in (C) conventional CD4 and (D) CD8 T-cells. Bar charts represent medians and values are indicated below each histogram. Statistical analysis was done using One-way ANOVA (* $p<0.05$, ** $p<0.01$).

BM (bone marrow), T-cells ($TCR\beta^+$), cCD4 T (conventional CD4, $TCR\beta^+$ $CD4^+$ $CD8^-$ $CD25^-$), CD8 T ($TCR\beta^+$ $CD4^-$ $CD8^+$), $CD25^+$ CD4 T ($TCR\beta^+$ $CD4^+$ $CD25^+$), Naïve ($CD62L^+$ $CD44^-$), Effector ($CD62L^-$ $CD44^+$) and Memory ($CD62L^+$ $CD44^+$).

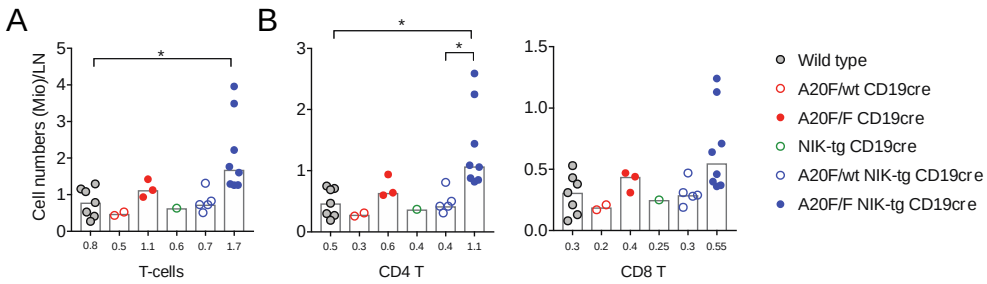


**Figure S 11. T-cell expansion in lymph nodes of A20F/F NIK-tg CD19cre young mice**

*Ex vivo* analysis of T-cells in lymph nodes of young mice using flow cytometry, normalized to one lymph node. Bar charts indicate cell numbers for (A) T-cells, and (B) T-cell subsets: CD4 and CD8. Bar charts represent medians and values are indicated below each histogram. Statistical analysis was done using One-way ANOVA (*p<0.05).
T-cells (TCRβ$^+$), CD4 T (TCRβ$^+$ CD4$^+$ CD8$^-$) and CD8 T (TCRβ$^+$ CD4$^-$ CD8$^+$).

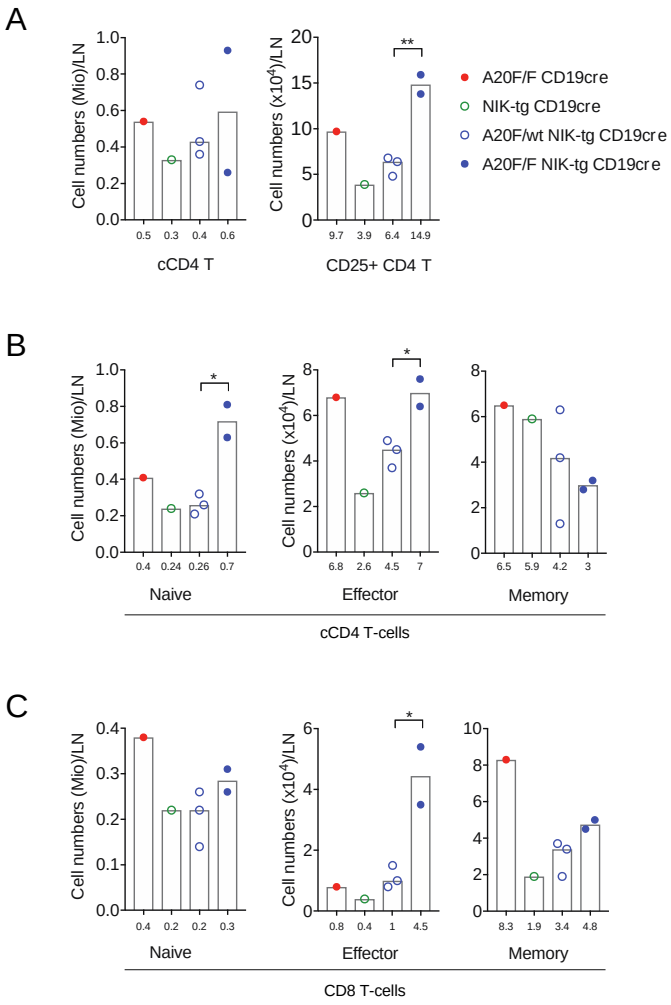


**Figure S 12. Expansion of CD25⁺ CD4, effector-like CD4 and effector like CD8 T-cells in lymph nodes of A20F/F NIK-tg CD19cre young mice**

*Ex vivo* analysis of T-cells in lymph nodes of young mice using flow cytometry, normalized to one lymph node. (A) Number of conventional CD4 T-cells and CD25⁺ CD4 T-cells. Cell numbers of naïve-, memory- and effector-like activation states for (B) cCD4 and (C) CD8 T-cells. Statistical analysis was done using T-test (* $p<0.05$).

cCD4 T (TCRβ⁺ CD4⁺ CD8⁻ CD25⁻), CD25+ CD4 T (TCRβ⁺ CD4⁺ CD8⁻ CD25⁺), CD8 T-cells (TCRβ⁺ CD4⁻ CD8⁺), Naïve (CD62L⁺ CD44⁻), Effector (CD62L⁻ CD44⁺) and Memory (CD62L⁺ CD44⁺).

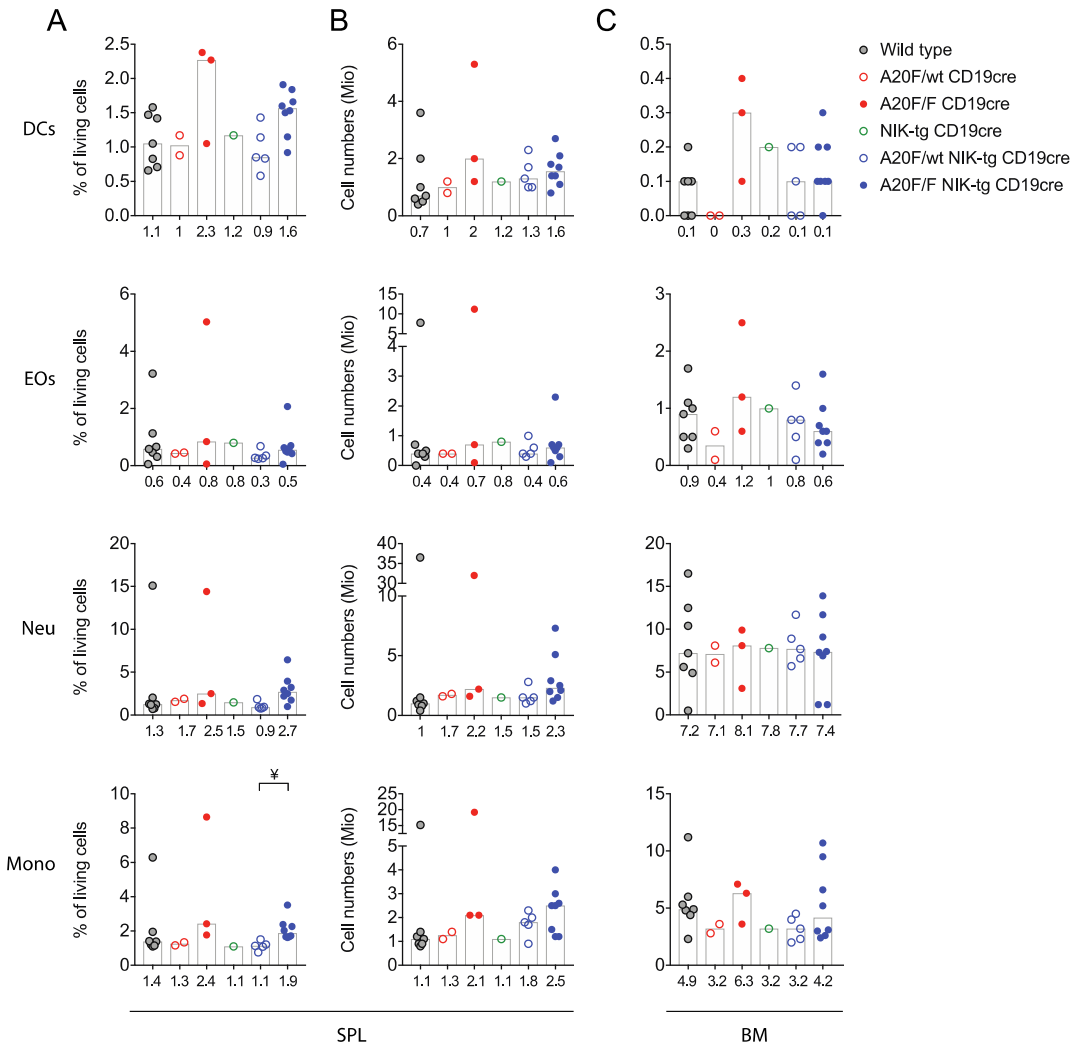


**Figure S 13. Myeloid cells are not affected by A20-/-;NIK+ B-cells in young mice**

*Ex vivo* analysis of myeloid cells in spleen and bone marrow from young mice using flow cytometry. (A) Percentage and (B) total cell number of myeloid cells in spleen of young mice. (C) Myeloid populations cell numbers in bone marrow, after red blood cell lysis for one leg. Bar charts depict medians and values are indicated below each histogram. Statistical analysis was done using Kruskal-Wallis test (¥ $p<0.05$). SPL (spleen), BM (bone marrow), DC (dendritic cells, $CD11c^+$), Eos (eosinophils, $CD11c^+$ $CD11b^+$ $SiglecF^{hi}$ $F4/80^{hi}$), Mono (monocytes, $CD11c^+$ $CD11b^+$ $SiglecF^{lo}$ $F4/80^{hi}$ $Gr1^{int}$) and Neu (neutrophils, $CD11c^+$ $CD11b^+$ $SiglecF^{lo}$ $F4/80^{lo}$ $Gr1^{hi}$).

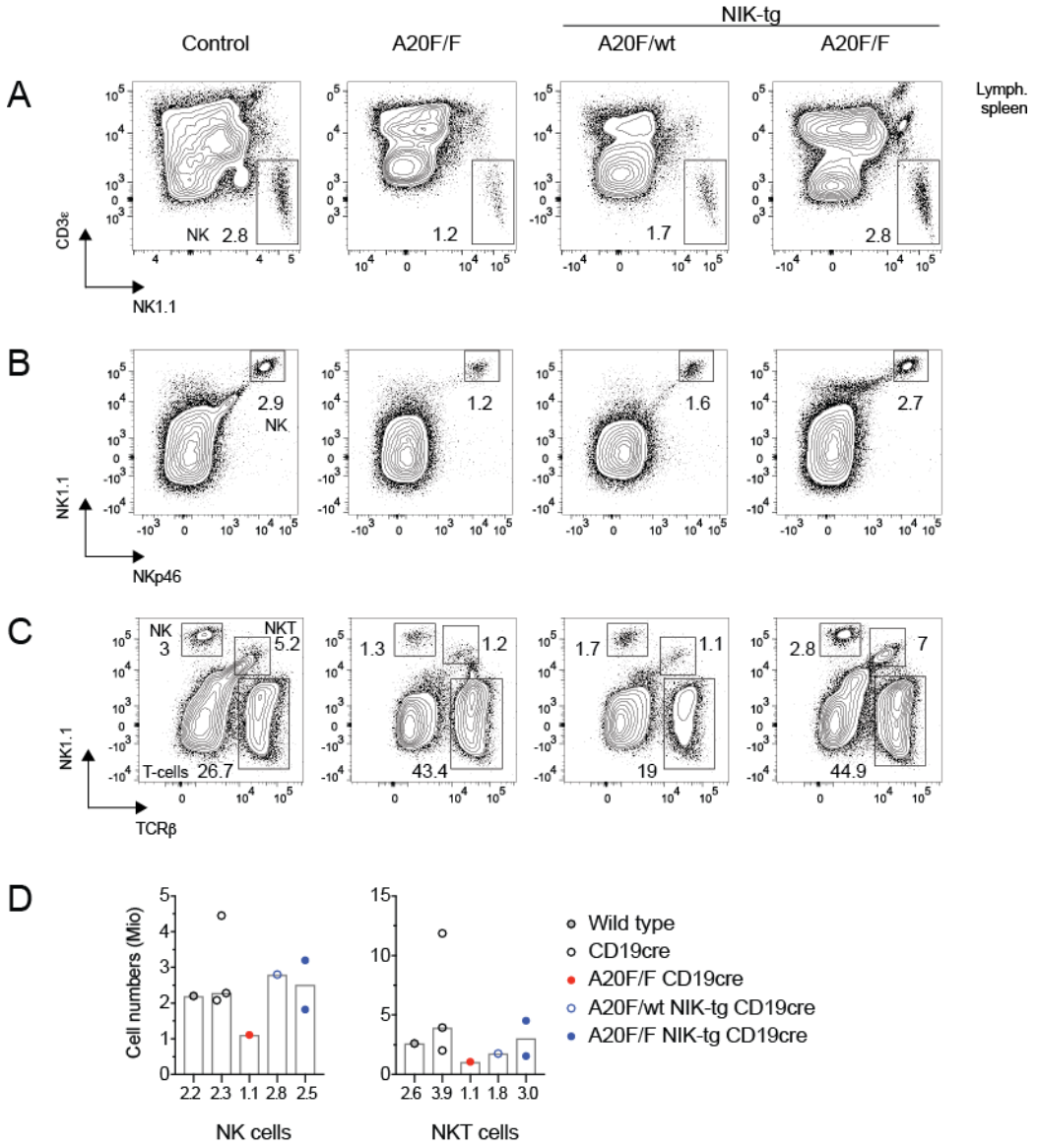


**Figure S 14. A20-/-;NIK+ B-cells do not elicit an natural killer or natural killer T-cell response**

Natural killer and natural killer T-cells in spleen of aged mice. Contour plots depict the percentage (A, B, C) natural killer cells and (C) natural killer T-cells. (D) Bar charts show natural killer and natural killer T-cell numbers. Bar charts depict medians and values are indicated below each histogram.
NK (natural killer cell, $CD3\varepsilon^-$ $NK1.1^+$, $NK1.1^+$ $NKp46^+$ or $TCR\beta^-$ $NK1.1^+$), T-cells ($TCR\beta^+$ $NK1.1^-$) and NKT (natural killer T-cell, $TCR\beta^+$ $NK1.1^+$).

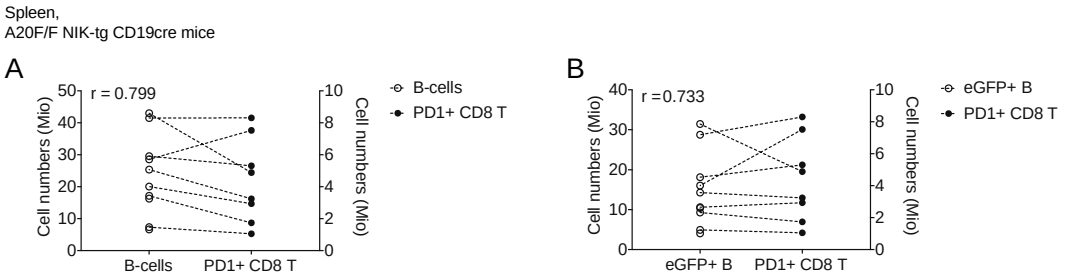


**Figure S 15. A20-/-;NIK+ B-cell numbers correlate with PD1 high CD8 T-cells**

Correlation between B-cell and PD1$^{high}$ CD8 T-cells in A20F/F NIK-tg CD19cre mice. Pearson correlation of (A) B-cell numbers (p=0.017) and (B) eGFP positive B-cell numbers (p=0.039) with number of PD1 positive CD8 T-cell numbers.
r (Pearson correlation), B-cells (B220$^{+}$), eGFP+ B (eGFP$^{+}$ B220$^{+}$) and PD1+ CD8 T (TCRβ$^{+}$ CD8$^{+}$ CD4$^{-}$ PD1$^{high}$).

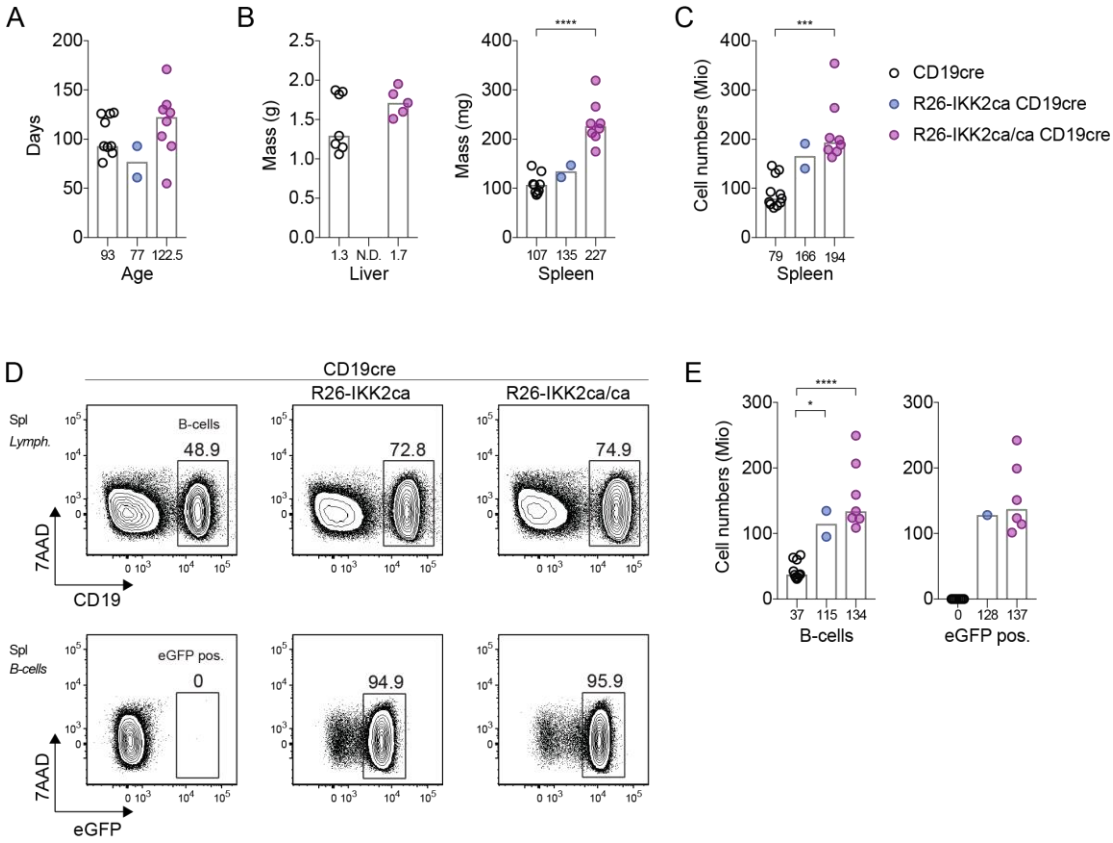


**Figure S 16. IKK2ca enhances B-cell numbers**

*Ex vivo* analysis of B-cells in spleens from 2-3-month-old mice using flow cytometry. Bar chars show (A) the age of the mice analysed, (B) the liver and spleen mass, and (C) the number of splenocytes. (D) Flow cytometry plots depict percentages and (E) bar charts show cell numbers for B-cells and eGFP positive B-cells. All flow cytometry contour plots are representative of at least 2 experiments. Histograms depict medians, and values are indicated below each histogram. Statistical analysis was done using One-way ANOVA (* p<0.05, *** p<0.001, **** p<0.0001).
N.D. (not done), Spl (spleen), Lymph. (lymphocytes), B-cells (CD19$^{+}$), and eGFP pos. (CD19$^{+}$ eGFP$^{+}$).

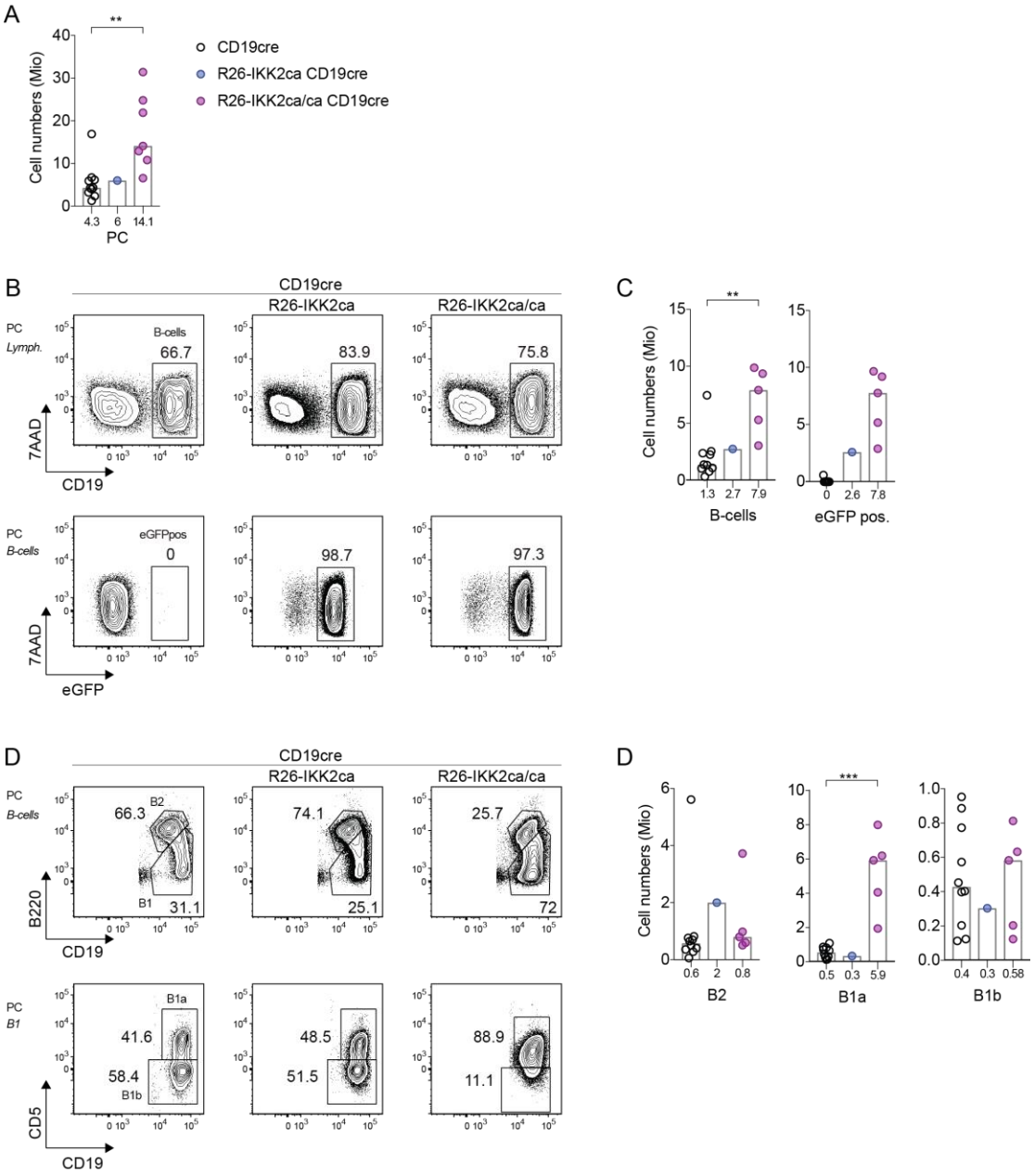


**Figure S 17. IKK2ca promotes B1 cell numbers in the peritoneal cavity**

*Ex vivo* analysis of B-cells in peritoneal cavity from 2/3-month-old mice using flow cytometry. (A) Bar chart shows total cell numbers after lavage. (B) Contour plots depict percentages and (C) bar chats show cell numbers for B-cells and eGFP positive B-cells in the peritoneal cavity after lavage. (D) Flow cytometry contour plots depict percentages for subsets B2, B1, B1a and B1b in the peritoneal cavity. (E) Bar charts show cell numbers for the B-cell subsets B2, B1a and B1b in the peritoneal cavity of young mice. All flow cytometry contour plots are representative of at least 2 experiments, except for the R26-IKK2ca CD19cre mice. Histograms depict medians, and values are indicated below each histogram. Statistical analysis was done using One-way ANOVA (** $p<0.01$, *** $p<0.001$).
PC (peritoneal cavity), Lymph. (lymphocytes), B-cells ($CD19^+$), eGFP pos. ($CD19^+$ $eGFP^+$), B2 ($CD19^+$ $B220^{hi}$), B1 ($CD19^+$ $B220^{lo}$), B1a ($CD19^+$ $B220^{lo}$ $CD5^{hi}$) and B1b ($CD19^+$ $B220^{lo}$ $CD5^-$).

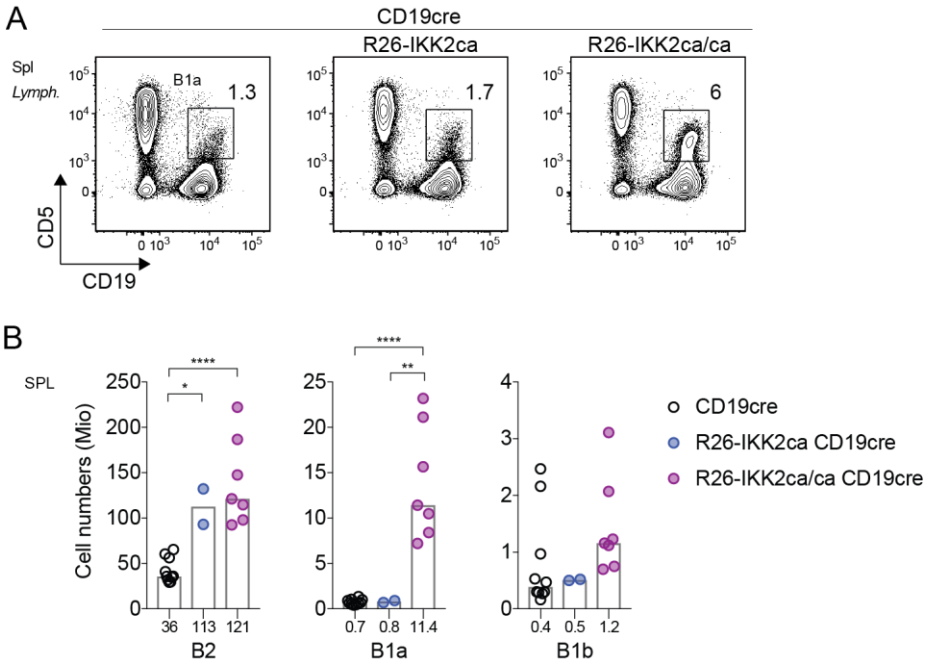


**Figure S 18. IKK2ca promotes B1 cell numbers in the spleen**

*Ex vivo* analysis of B-cell subsets in spleens from 2/3-month-old mice using flow cytometry. (A) Flow cytometry plots depict the percentage of B1a-cells in spleens. (B) Bar chats show cell numbers for the B-cell subsets B2, B1a and B1b in spleens of young mice. All flow cytometry contour plots are representative of at least 2 experiments. Histograms depict medians, and values are indicated below each histogram. Statistical analysis was done using One-way ANOVA (* $p<0.05$, ** $p<0.01$, **** $p<0.0001$).
Spl/SPL (spleen), Lymph. (lymphocytes), B2 ($CD19^+$ $B220^{hi}$), B1a ($CD19^+$ $CD5^{hi}$ or $CD19^+$ $B220^{lo}$ $CD5^{hi}$) and B1b ($CD19^+$ $B220^{lo}$ $CD5^-$).

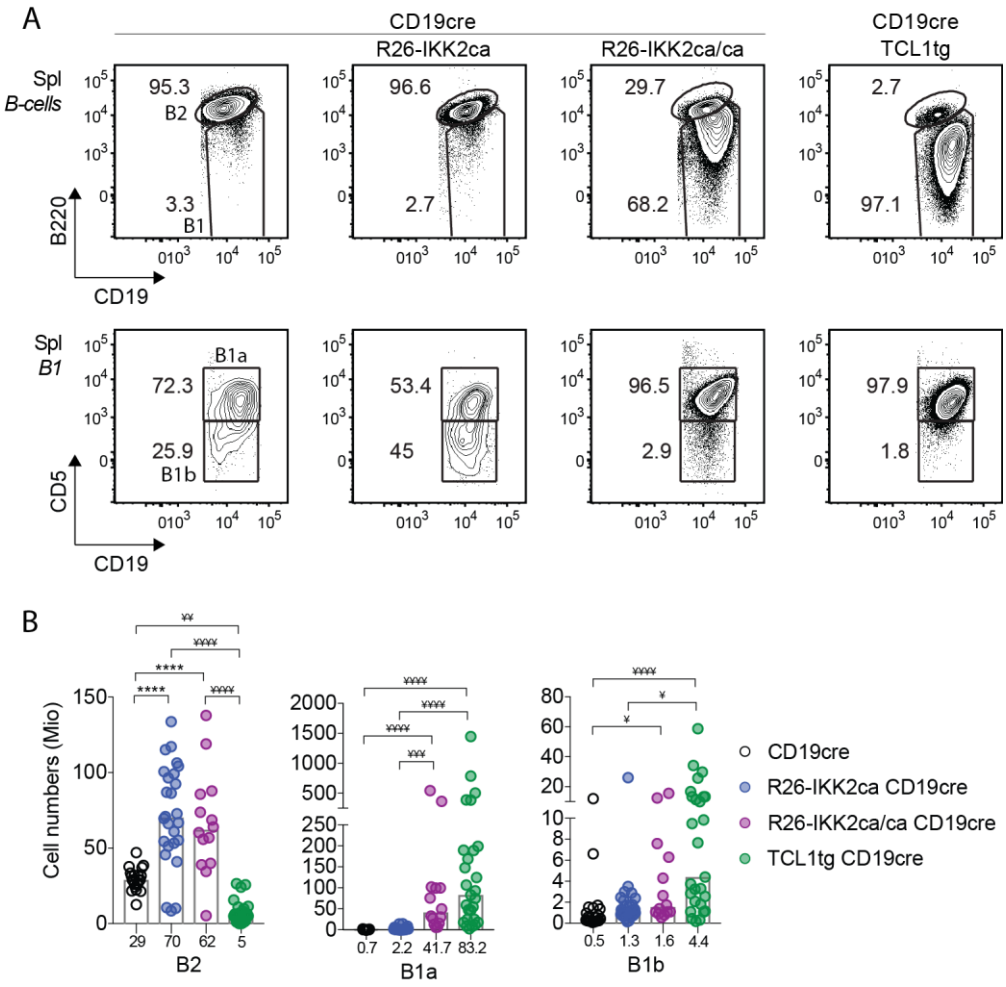


**Figure S 19. IKK2ca expression leads to B1a expansion in aged mice**

*Ex vivo* analysis of B-cell subsets in spleens from aged mice (> 9 months) using flow cytometry. (A) Flow cytometry contour plots depict percentages and (B) bar charts show cell numbers for the B-cell subsets B2, B1, B1a and B1b in spleen. All flow cytometry contour plots are representative of at least 2 experiments. Histograms depict medians, and values are indicated below each histogram. Statistical analysis was done using One-way ANOVA (**** p<0.0001) or Kruskal-Wallis (¥ p<0.05, ¥¥ p<0.01, ¥¥¥ p<0.001, ¥¥¥¥ p<0.0001).

Spl (spleen), B-cells ($CD19^+$), B2 ($CD19^+$ $B220^{hi}$), B1 ($CD19^+$ $B220^{lo}$), B1a ($CD19^+$ $B220^{lo}$ $CD5^{hi}$) and B1b ($CD19^+$ $B220^{lo}$ $CD5^-$).

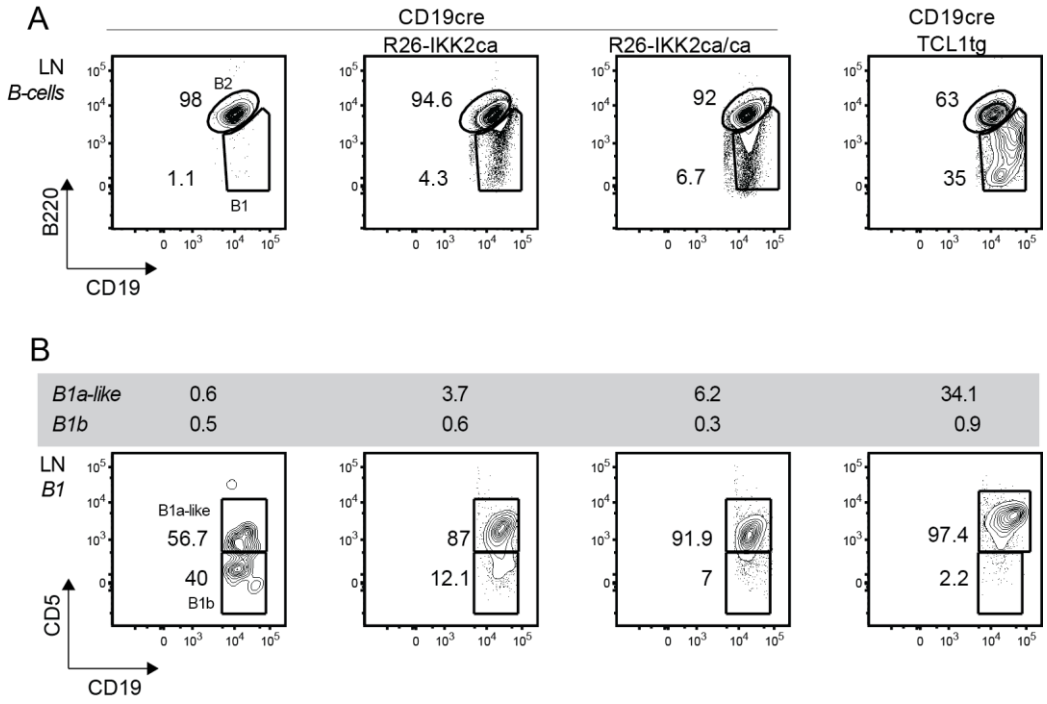


**Figure S 20. Effects on IKK2ca expression in lymph nodes**

*Ex vivo* analysis of B-cell subsets in draining lymph nodes from aged mice (> 9 months) using flow cytometry. Draining inguinal, axillary, and superficial cervical lymph nodes were pooled and analysed together. Flow cytometry contour plots depict percentage of (A) B2 and B1, and (B) B1a-like and B1b subsets. B1a-like and B1b as percentages of B-cells are indicated above the contour plots. All flow cytometry contour plots are representative of at least 2 experiments.
LN (lymph nodes), Lymph. (lymphocytes), B-cells ($CD19^{+}$), B2 ($CD19^{+}$ $B220^{hi}$), B1 ($CD19^{+}$ $B220^{lo}$), B1a-like ($CD19^{+}$ $B220^{lo}$ $CD5^{hi}$) and B1b ($CD19^{+}$ $B220^{lo}$ $CD5^{-}$).

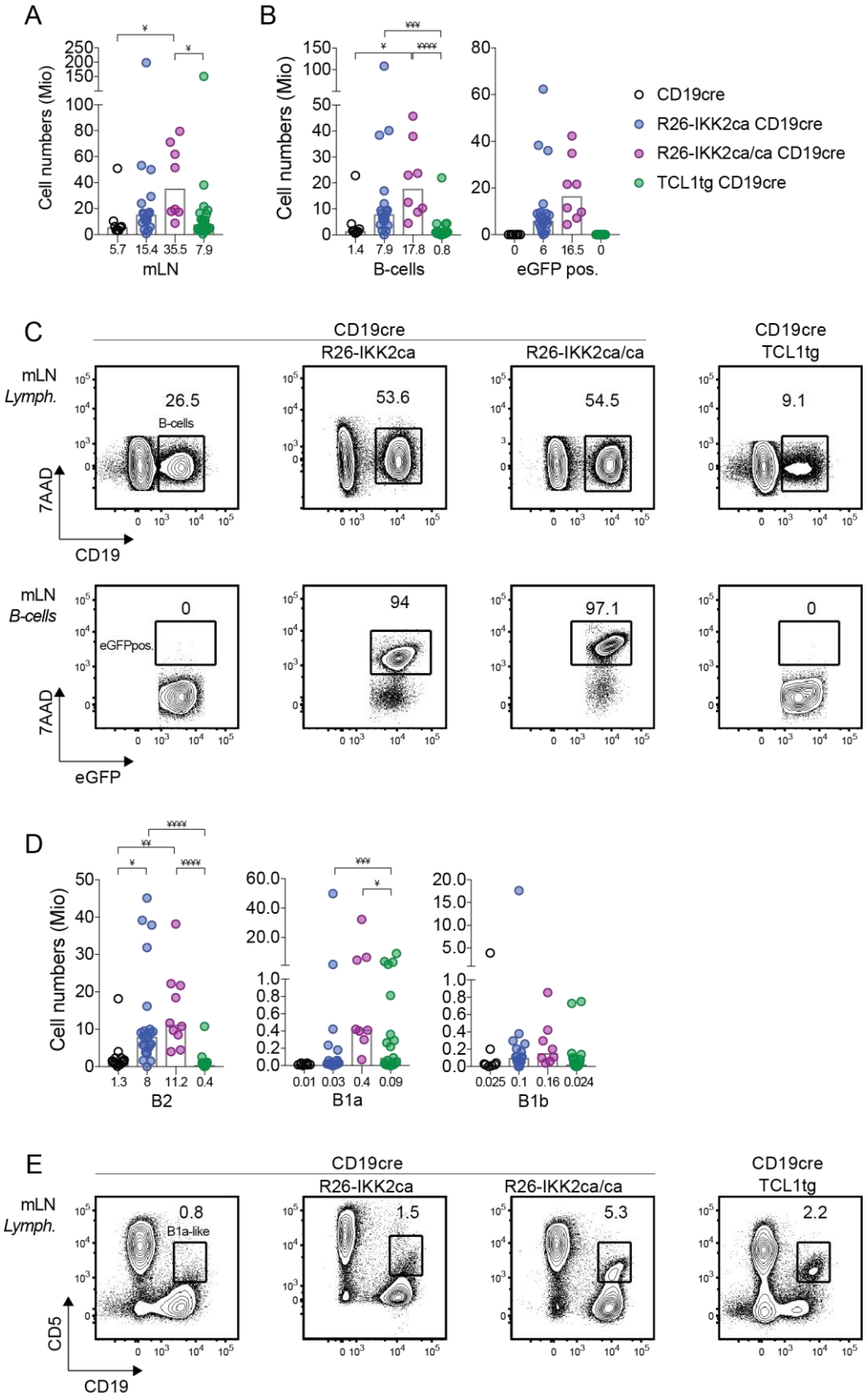


**Figure S 21. Effects of IKK2ca expression in mesenteric lymph nodes**

*Ex vivo* analysis of B-cells in mesenteric lymph nodes from aged mice (> 9 months) using flow cytometry. (A) Bar charts show total cell numbers. (B) Bar charts show cell numbers and (C) flow

cytometry contour plots depict percentages for B-cell and eGFP positive B-cells. (D) Bar charts show the number of B2, B1a and B1b subsets. (E) Flow cytometry contour plots depict percentage of B1a-like cells of lymphocytes. All flow cytometry contour plots are representative of at least 2 experiments. All contour plots for the R26-IKK2ca CD19cre mouse belong to a different experiment. Histograms depict medians, and values are indicated below each histogram. Statistical analysis was done using Kruskal-Wallis (¥p<0.05, ¥¥ p<0.01, ¥¥¥ p<0.001, ¥¥¥¥ p<0.0001).
mLN (mesenteric lymph nodes), Lymph. (lymphocytes), B-cells (CD19$^+$), eGFP pos. (CD19$^+$ eGFP$^+$), B2 (CD19$^+$ B220$^{hi}$), B1a (CD19$^+$ CD5$^{hi}$ or CD19$^+$ B220$^{lo}$ CD5$^{hi}$) and B1b (CD19$^+$ B220$^{lo}$ CD5$^-$).

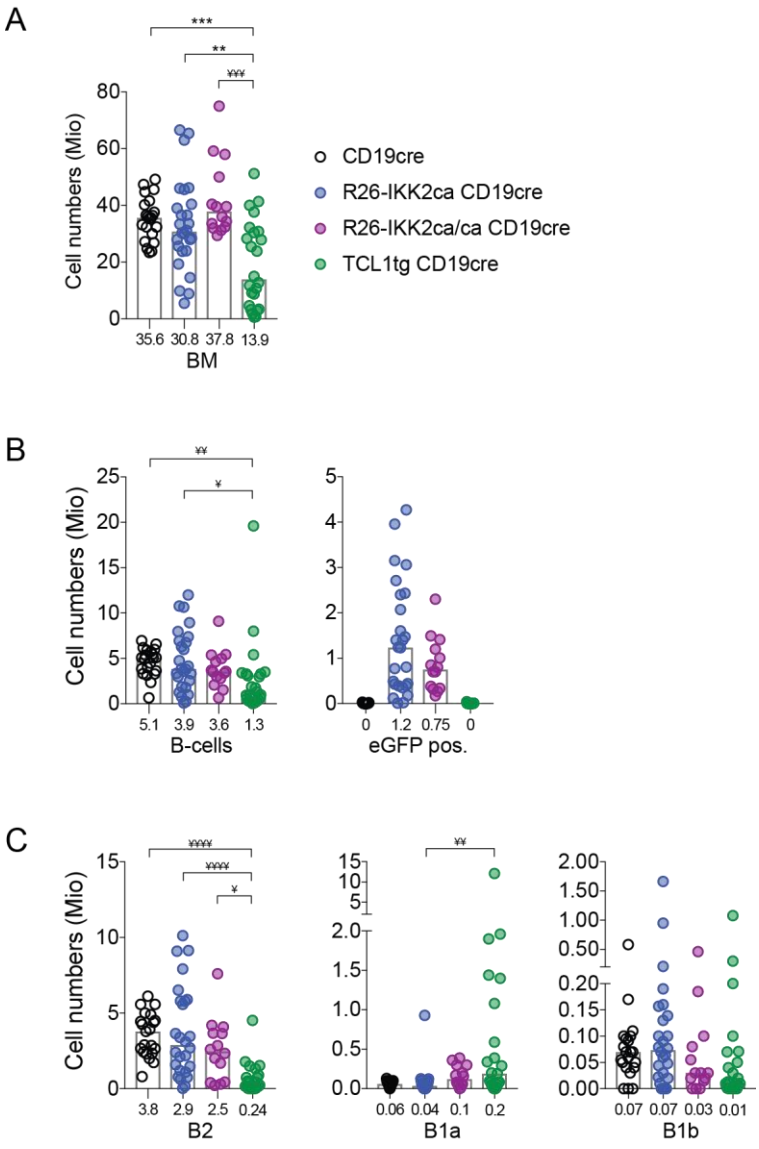


**Figure S 22. Effects of IKK2ca expression in the bone marrow**

*Ex vivo* analysis of B-cells in bone marrow from aged mice (> 9 months) using flow cytometry, for one leg after red blood cell lysis. Bar charts show (A) total cell numbers, (B) B-cells and eGFP positive B-cells numbers, and (C) B2, B1a and B1b subsets cell numbers. Histograms depict medians, and values are indicated below each histogram. Statistical analysis was done using One-Way ANOVA (** p<0.01, *** p<0.001) or Kruskal-Wallis (¥p<0.05, ¥¥ p<0.01, ¥¥¥ p<0.001, ¥¥¥¥ p<0.0001).
BM (bone marrow), B-cells (B220$^+$ CD19$^-$, B220$^+$ CD19$^+$ and B220$^-$ CD19$^+$), eGFP pos. (eGFP$^+$), B2 (CD19$^{hi}$ B220$^{hi}$), B1a (CD19$^+$ B220$^{lo}$ CD5$^{hi}$) and B1b (CD19$^+$ B220$^{lo}$ CD5$^-$).

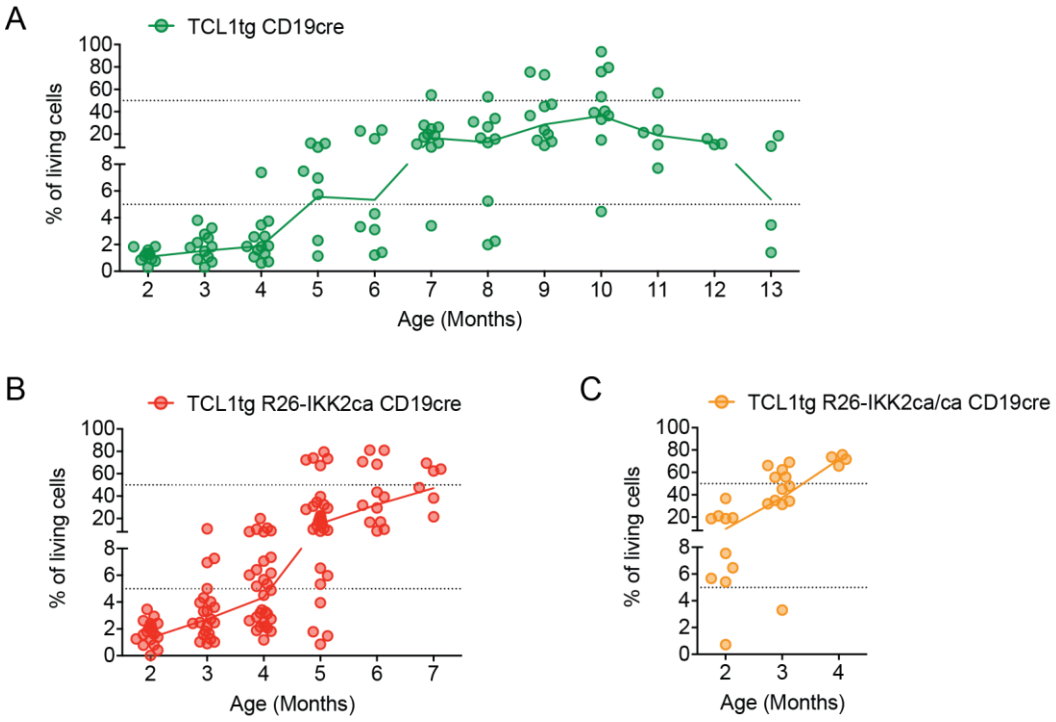


**Figure S 23. Co-operation between IKK2ca and TCL1 in CLL-like disease**

*Ex vivo* analysis of peripheral blood from TCL1tg compound mice using flow cytometry, after red blood cell lysis. Scatter plots show the percentage of $CD5^+$ B1a-like cells ($CD19^+$ $B220^{lo}$ $CD5^+$) in the peripheral blood of (A) TCL1tg CD19cre, (B) TCL1tg R26-IKK2ca CD19cre and (C) TCL1tg R26-IKK2ca/ca CD19cre mice. The connecting lines represent means for each time point.

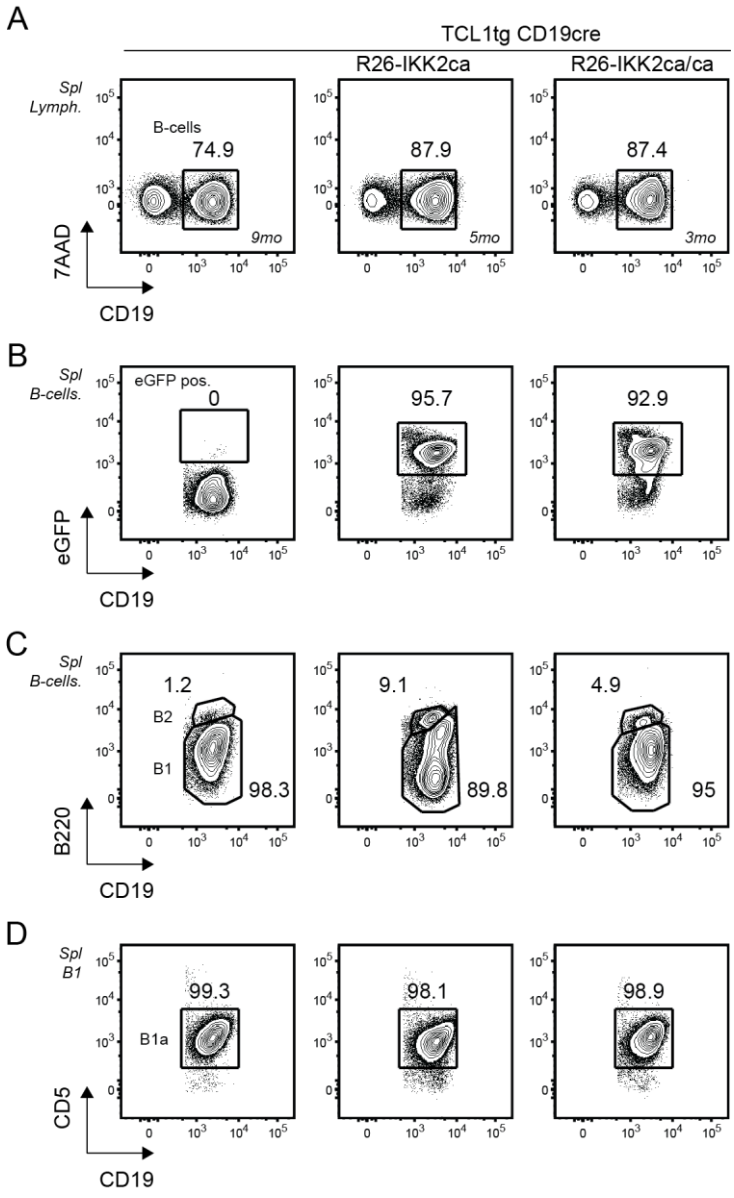


**Figure S 24. Co-operation between IKK2ca and TCL1 in splenic B-cells**

*Ex vivo* analysis of spleen from burdened TCL1tg compound mice using flow cytometry. Contour plots depict the percentage of (A) B-cells, (B) eGFP positive B-cells, (C) B2 and B1 subsets, and (D) $CD5^+$ B1a-like cells. All flow cytometry contour plots are representative of at least 2 experiments. The age of the mouse, in months, at the time of analysis is indicated in (A).
Spl. (spleen), Lymph. (lymphocytes), mo. (months), B-cells ($CD19^+$), eGFP pos. ($CD19^+$ $eGFP^+$), B2 ($CD19^+$ $B220^{hi}$), B1 ($CD19^+$ $B220^{lo}$) and B1a ($CD19^+$ $B220^{lo}$ $CD5^{hi}$).

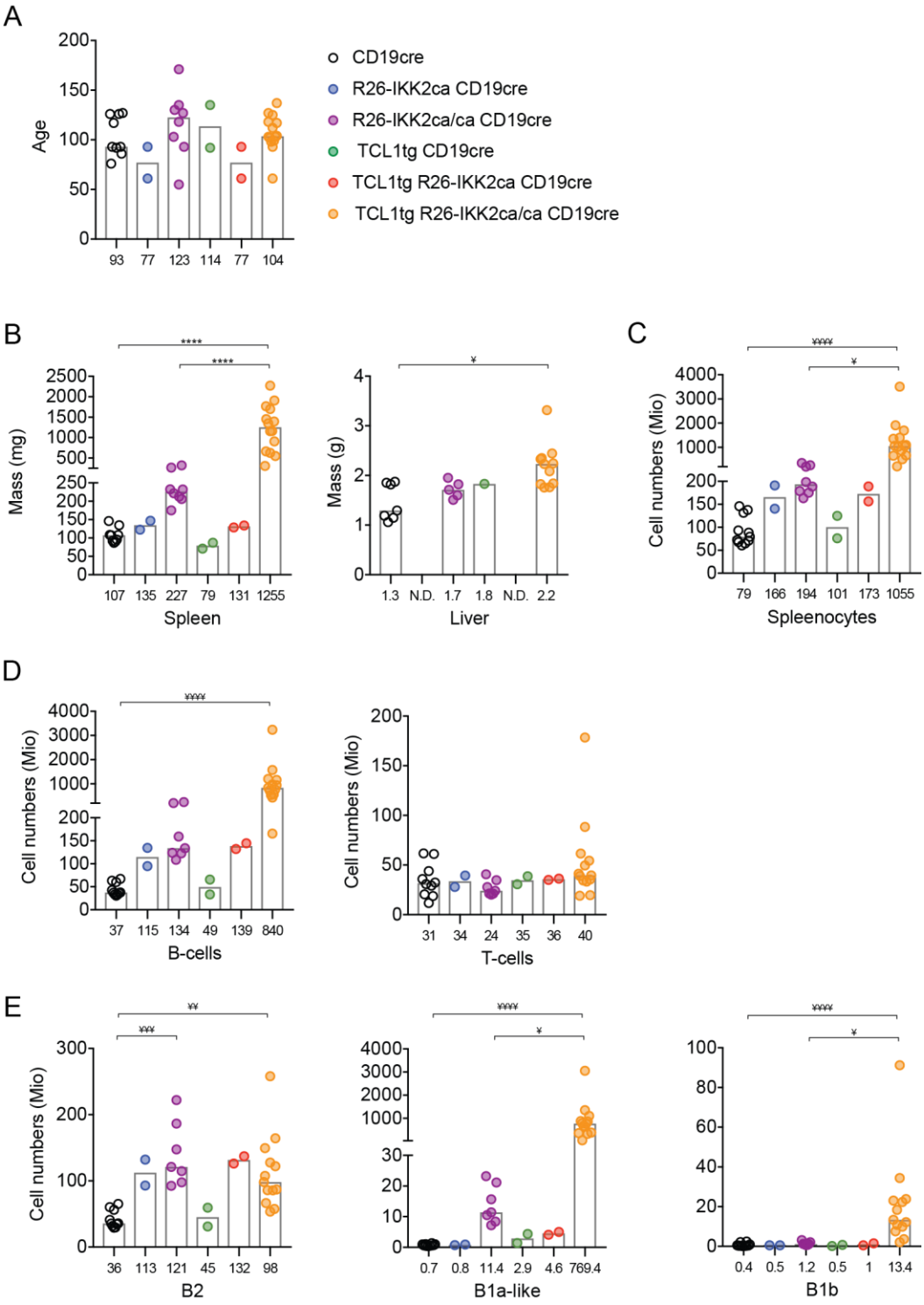


**Figure S 25. Co-operation between IKK2ca and TCL1 in splenic B-cells II**

*Ex vivo* analysis of spleen from burdened TCL1tg R26-IKK2ca/ca CD19cre and aged matched controls mice using flow cytometry. Bar charts indicate (A) age at the time of the analysis, (B) spleen and liver mass, (C) splenocytes cell numbers, (D) B- and T-cell numbers, and (E) B-cell subsets cell numbers. Histograms depict medians, and values are indicated below each histogram. Statistical analysis was done using One-Way ANOVA (**** p<0.0001) or Kruskal-Wallis (¥p<0.05, ¥¥ p<0.01, ¥¥¥ p<0.001, ¥¥¥¥ p<0.0001).

N.D. (not done), B-cells ($CD19^+$), T-cells ($CD19^-$ $CD5^+$), B2 ($CD19^+$ $B220^{hi}$), B1a-like ($CD19^+$ $B220^{lo}$ $CD5^{hi}$) and B1b ($CD19^+$ $B220^{lo}$ $CD5^{hi}$).

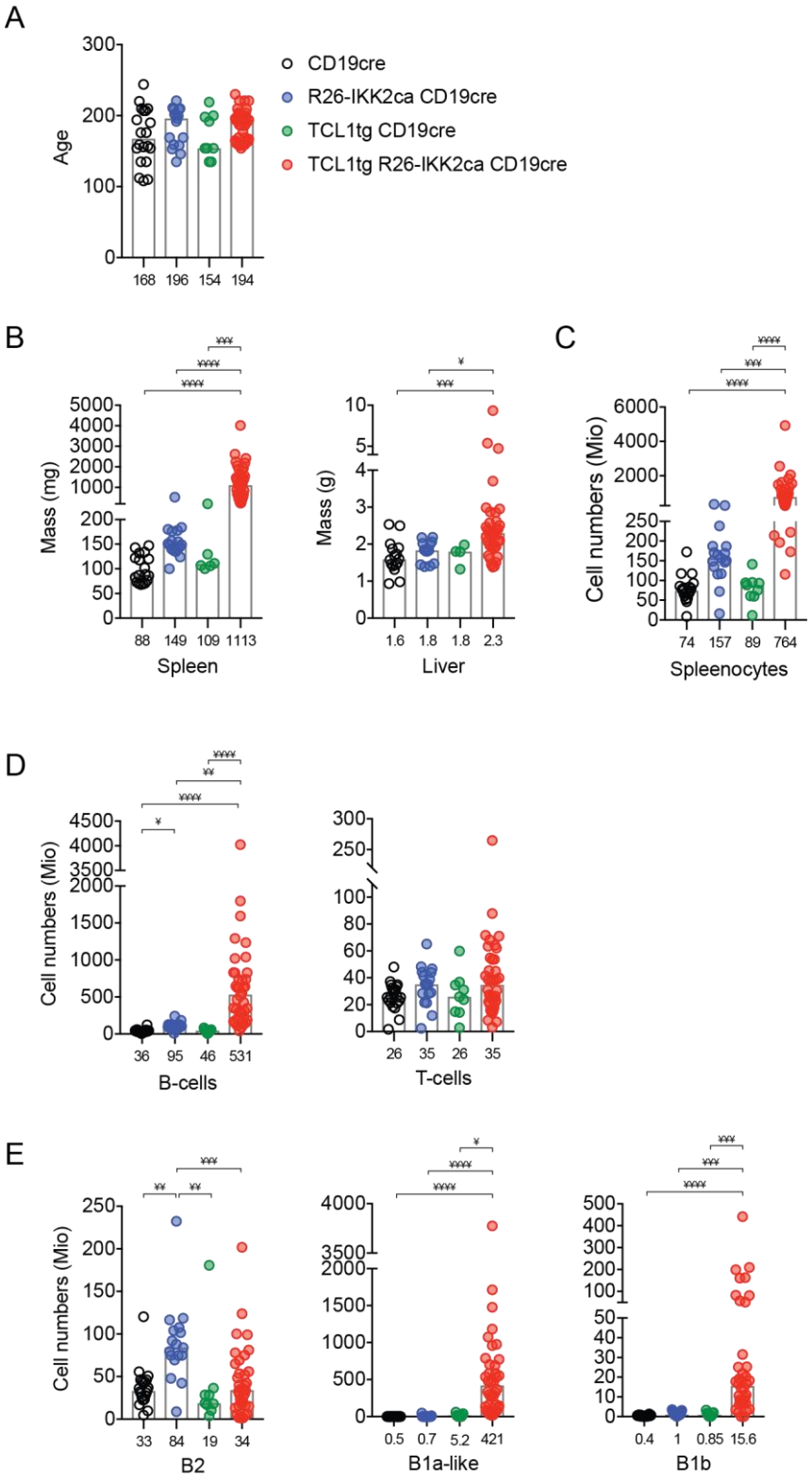


**Figure S 26. Co-operation between IKK2ca and TCL1 in splenic B-cells III**

*Ex vivo* analysis of spleen from burdened TCL1tg R26-IKK2ca CD19cre and aged matched controls mice using flow cytometry. Bar charts indicate (A) age at the time of the analysis, (B) spleen and liver mass, (C) splenocytes cell numbers, (D) B- and T-cell numbers, and (E) B-cell subsets cell numbers. Histograms depict medians, and values are indicated below each histogram. Statistical analysis was done using Kruskal-Wallis (¥p<0.05, ¥¥ p<0.01, ¥¥¥ p<0.001, ¥¥¥¥ p<0.0001).
B-cells ($CD19^+$), T-cells ($CD19^-$ $CD5^+$), B2 ($CD19^+$ $B220^{hi}$), B1a-like ($CD19^+$ $B220^{lo}$ $CD5^{hi}$) and B1b ($CD19^+$ $B220^{lo}$ $CD5^{hi}$).

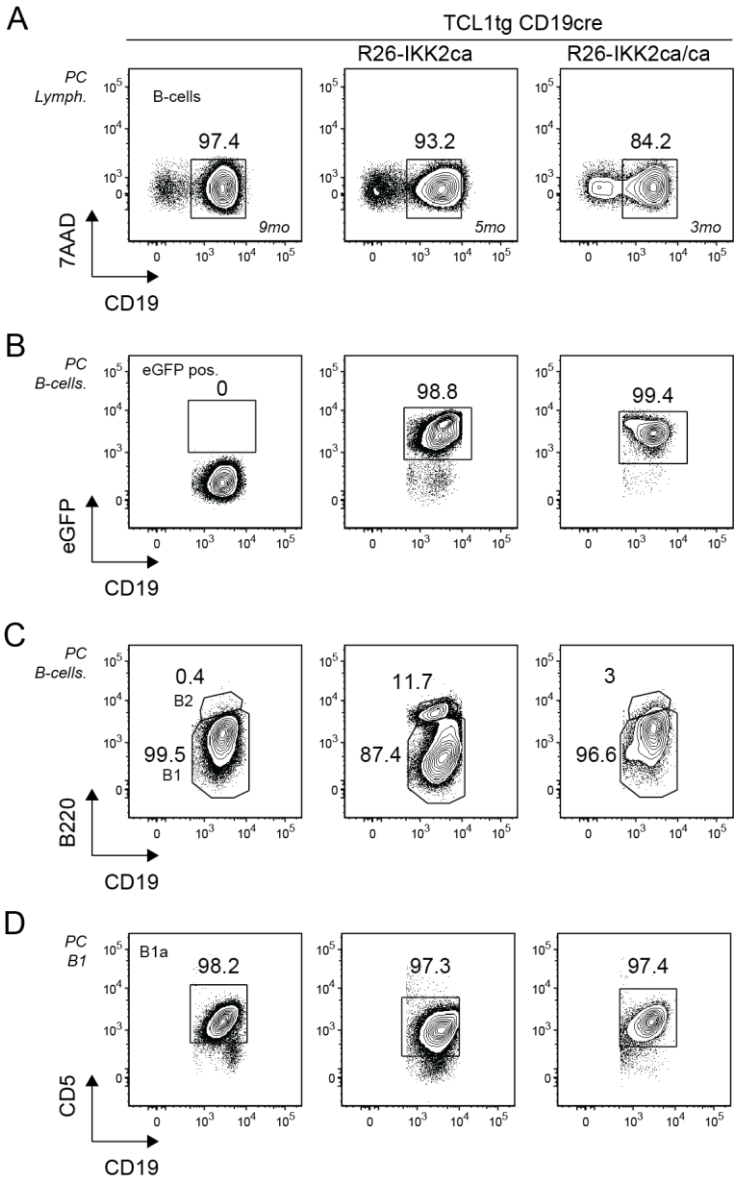


**Figure S 27. Co-operation between IKK2ca and TCL1 in peritoneal B-cells**

*Ex vivo* analysis of B-cells in the peritoneal cavity from burdened TCL1tg compound mice using flow cytometry. Flow cytometry contour plots depict the percentage of (A) B-cells, (B) eGFP positive B-cells, (C) B2 and B1 subsets, and (D) B1a-cells. All flow cytometry contour plots are representative of at least 2 experiments. The age of the mouse, in months, at the time of analysis is indicated in (A).
PC (peritoneal cavity), Lymph. (Lymphocytes), mo. (months), B-cells ($CD19^+$), eGFP pos. ($CD19^+$ $eGFP^+$), B2 ($CD19^+$ $B220^{hi}$), B1a ($CD19^+$ $B220^{lo}$ $CD5^{hi}$).

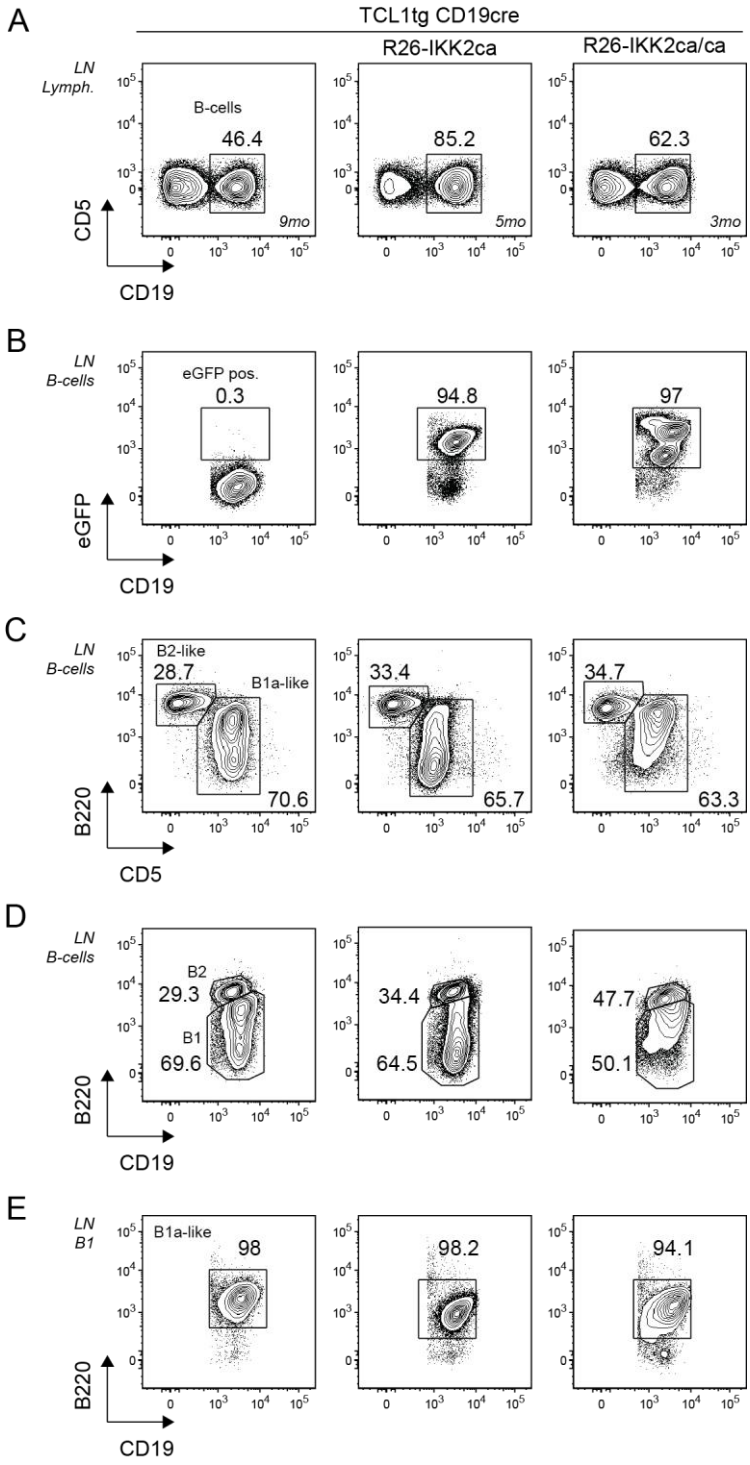


**Figure S 28. Co-operation between IKK2ca and TCL1 in lymph node B-cells**

*Ex vivo* analysis of B-cells in draining lymph nodes from burdened TCL1tg compound mice using flow cytometry. Draining inguinal, axillary, and superficial cervical lymph nodes were pooled and analysed together. Flow cytometry contour plots depict the percentage of (A) B-cells, (B) eGFP positive B-cells, (C) B2- and $CD5^+$ B1a-like cells, (D) B2 and B1 subsets, and (E) $CD5^+$ B1a-like cells. All flow cytometry contour plots are representative of at least 2 experiments. The age of the mouse, in months, at the time of analysis is indicated in (A).

LN (lymph nodes), Lymph. (lymphocytes), mo. (months), B-cells ($CD19^+$), eGFP pos. ($CD19^+$ $eGFP^+$), B2-like ($CD19^+$ $B220^{hi}$), B1a-like ($CD19^+$ $B220^{lo}$ $CD5^{hi}$), B2 ($CD19^+$ $B220^{hi}$), and B1 ($CD19^+$ $B220^{lo}$).

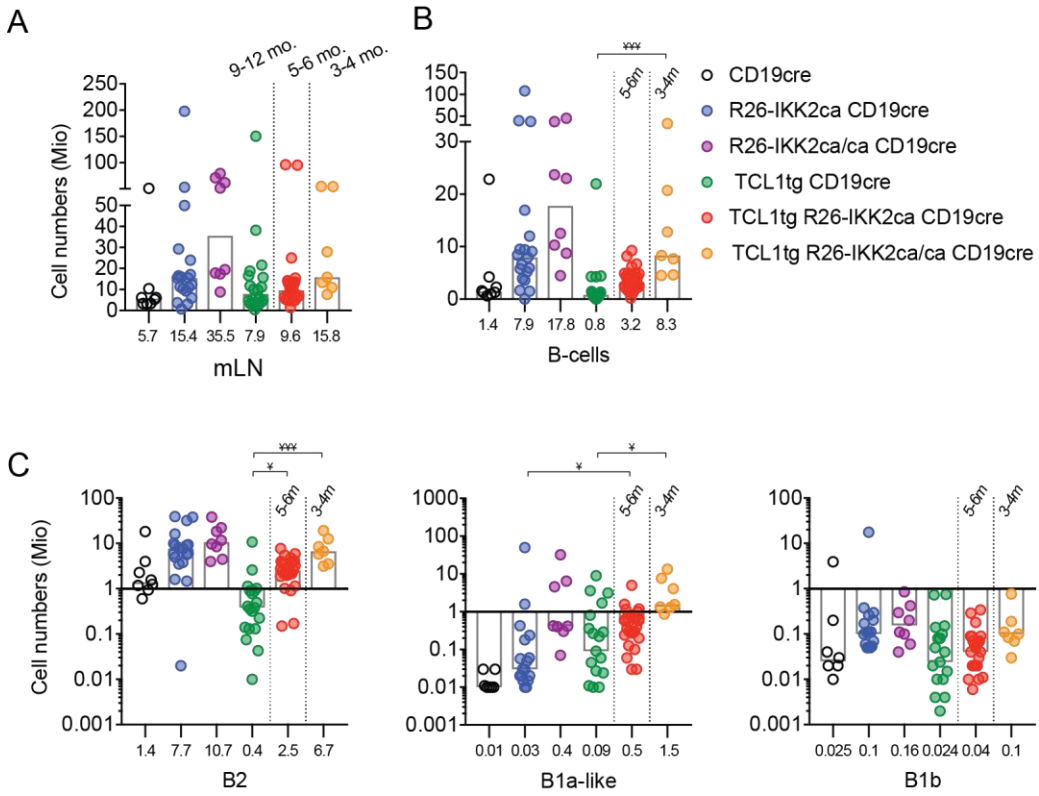


**Figure S 29. Co-operation between IKK2ca and TCL1 in mesenteric lymph node B-cells**

*Ex vivo* analysis of B-cells in mesenteric lymph nodes from burdened TCL1tg compound mice using flow cytometry. Bar chart shows (A) total, (B) B-cell, and (C) B-cell subsets cell numbers. Burdened TCL1tg R26-IKK2ca CD19cre and TCL1tg R26-IKK2ca/ca CD19cre mice cohorts were analysed at 3-4 months and 5-6 months of age, respectively. Burdened TCL1tg CD19cre mice and aged matched controls were analysed at 9-12 months of age. Histograms depict medians, and values are indicated below each histogram. Statistical analysis was done using Kruskal-Wallis (¥p<0.05, ¥¥¥ p<0.001).
mLN (mesenteric lymph nodes), m. (months), B-cells ($CD19^+$), B2 ($CD19^+$ $B220^{hi}$ $CD5^-$), B1a-like ($CD19^+$ $B220^{lo}$ $CD5^{hi}$) and B1b ($CD19^+$ $B220^{lo}$ $CD5^-$).

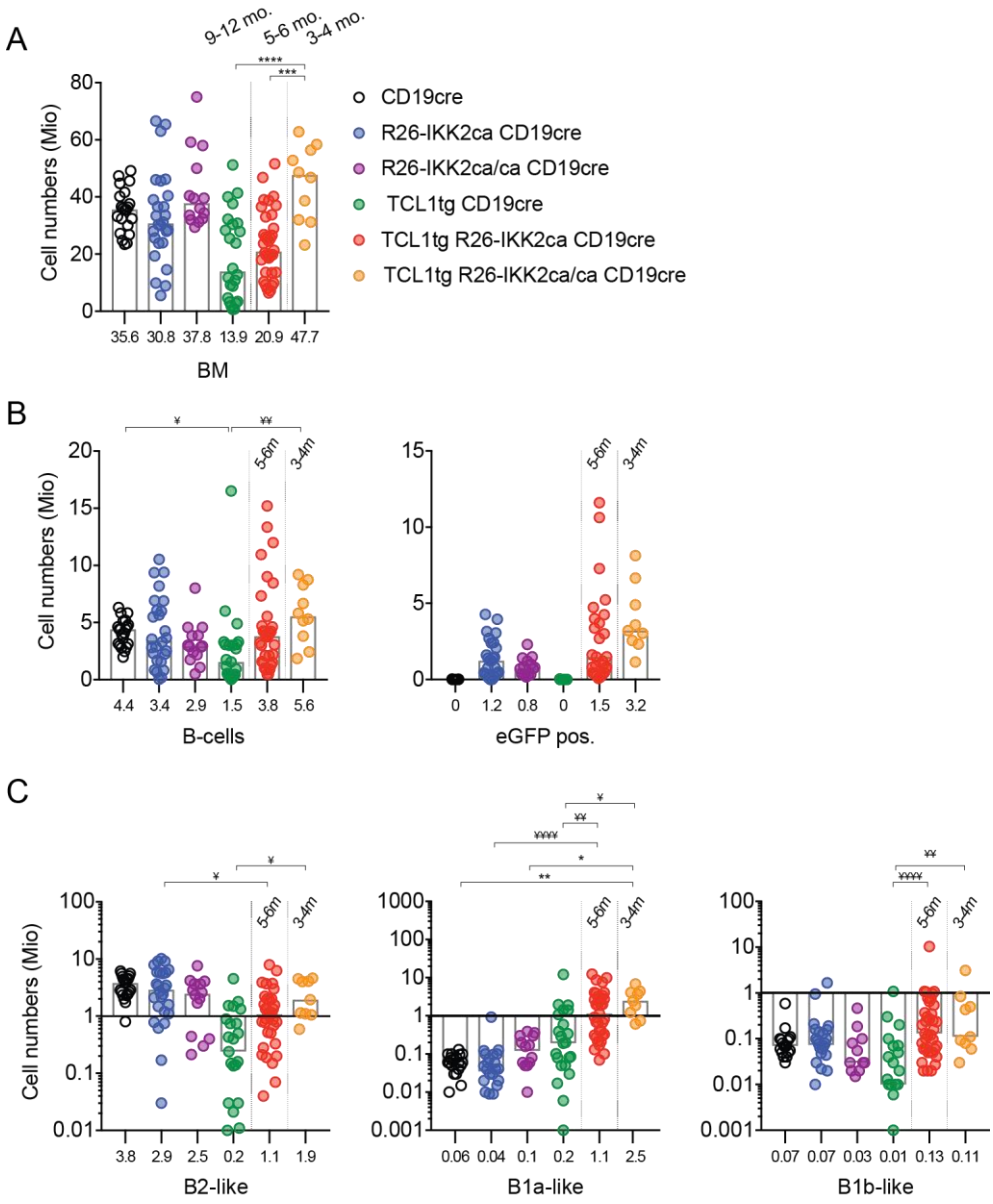


**Figure S 30.Co-operation between IKK2ca and TCL1 in bone marrow B-cells**

*Ex vivo* analysis of bone marrow in terminally sick mice using flow cytometry, for one leg after red blood cell lysis. Bar chart shows (A) total, (B) B-cell and eGFP positive B-cells, and (C) B-cell subsets cell numbers. As indicated, burdened TCL1tg R26-IKK2ca CD19cre and TCL1tg R26-IKK2ca/ca CD19cre mice cohorts were analysed between 3-4 months and 5-6 months of age, respectively. TCL1tg CD19cre mice and aged matched controls were analysed between 9-12 months of age. Histograms depict medians, and values are indicated below each histogram. Statistical analysis was done using One-Way ANOVA (* p<0.05, ** p<0.01, *** p<0.001, ****p<0.0001) or Kruskal-Wallis (¥p<0.05, ¥¥ p<0.01, ¥¥¥ p<0.001).

BM (bone marrow), B-cells ($B220^+$ $CD19^-$, $B220^-$ $CD19^+$, $B220^+$ $CD19^+$), eGFP pos. ($eGFP^+$), B2-like ($CD19^{hi}$ $B220^{hi}$ $CD5^-$), B1a-like ($CD19^+$ $B220^{lo}$ $CD5^{hi}$) and B1b-like ($CD19^+$ $B220^{lo}$ $CD5^-$).

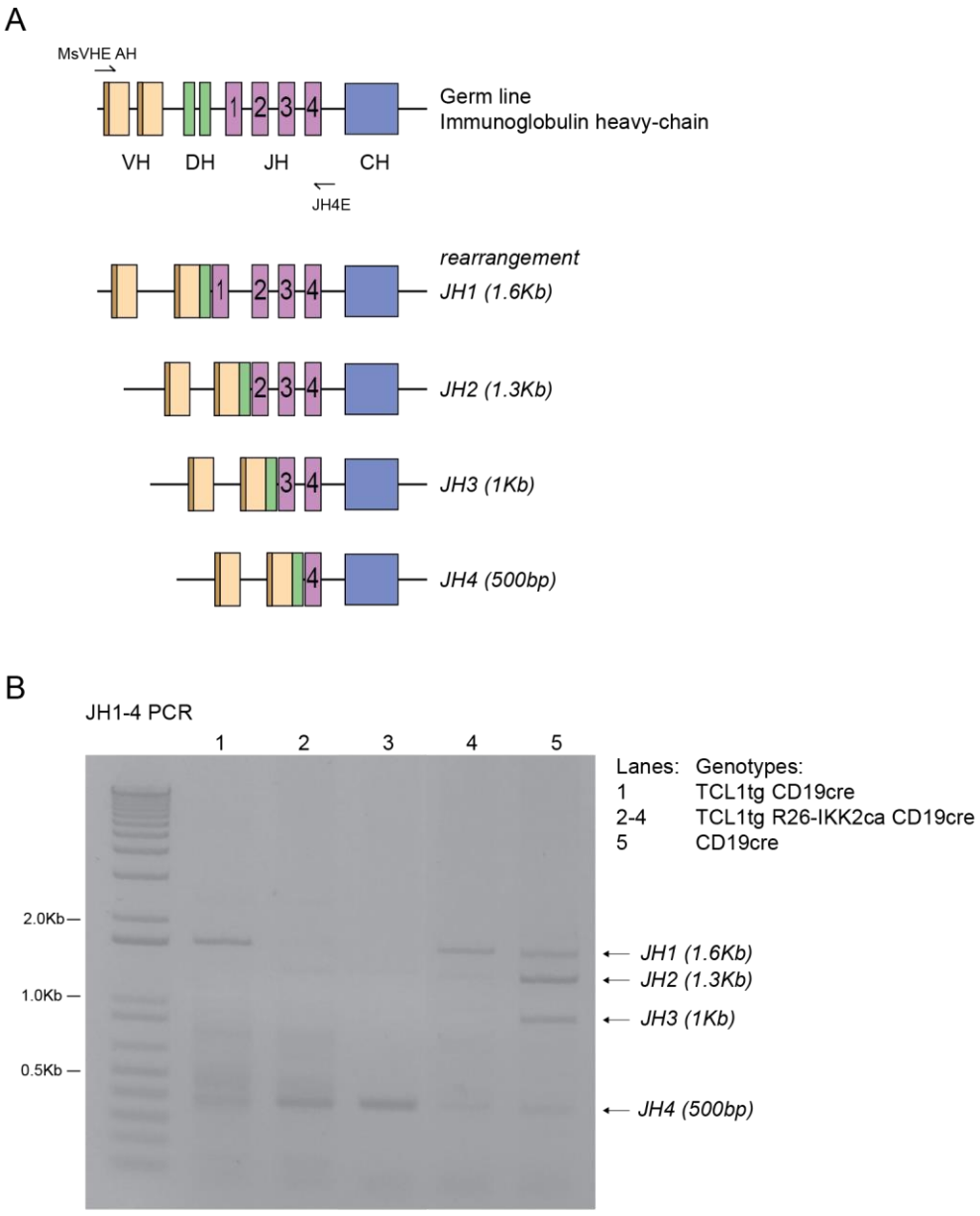


**Figure S 31. IgH VDJ rearrangement analysis by PCR**

Amplification of the VDJ rearrangements of the immunoglobulin heavy chain. (A) The scheme depicts the germ line locus for the IgH in the mouse C57BL/6 background and the four possible rearrangements into the different joining-gene segments. The rearrangements can be amplified by PCR using the primers MsVHE AH and JH4E that bind at the beginning of most commonly used VH-gene segments and at the end of the JH4-gene segment, respectively. The expected amplicon sizes for the rearrangements into the different JH-gene segments are indicated. (B) Visualization the VDJ rearrangements amplicons from tumour and control samples by separation in a 1.5% agarose electrophoresis.
VH (variable, yellow), DH (diversity, green), JH (joining, pink), CH (constant, blue), Kb (kilo bases), bp (base pairs) and PCR (polymerase chain reaction),

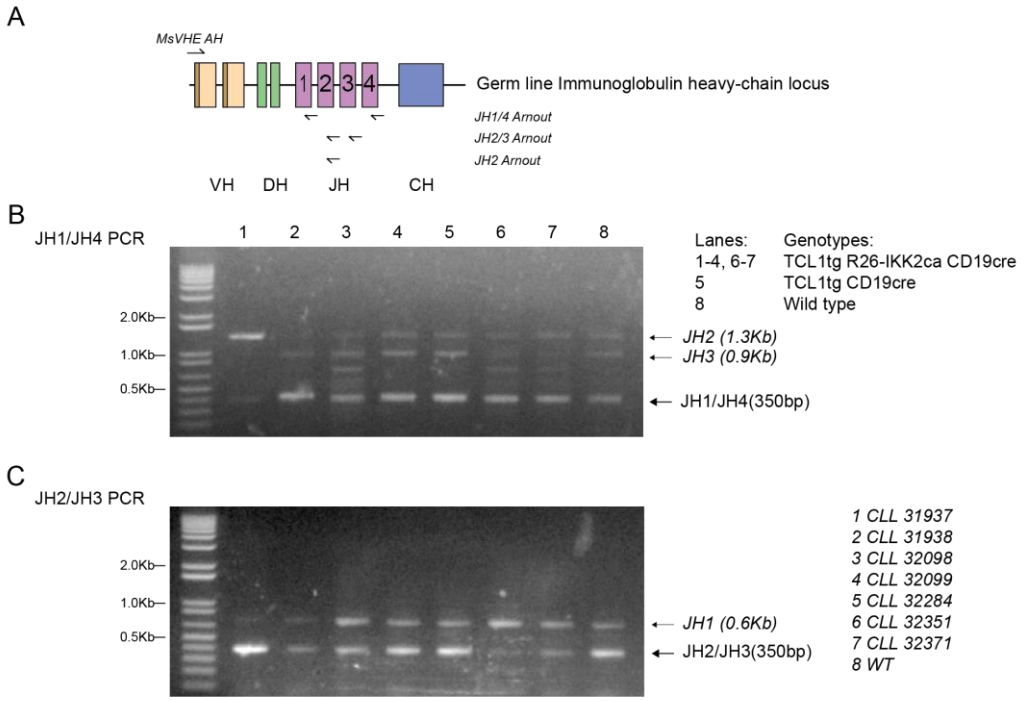


**Figure S 32. Cloning of IgH VDJ rearrangements**

Amplification of individual VDJ rearrangements of the immunoglobulin heavy chain. (A) The scheme depicts the germ line locus for the IgH in the mouse C57BL/6 background and the binding site of the primers used to amplify the individual rearrangements into the different JH-gene segments. (B and C) The amplicons were separated and visualizes in a 2% agarose electrophoresis. (B) The amplification of VDJ rearrangements into JH1 and JH4 produced amplicons of three different sizes: JH1 and JH4 amplicons have a size of 350bp; amplicons of 1.3Kb and 0.9Kb can also be observed, corresponding to JH2 and JH3 rearrangements, respectively. (C) The amplification of VDJ rearrangements into JH2 and JH3 produced amplicons of two different sizes: JH2 and JH3 amplicons have a size of 350bp; additionally an amplicons of 0.6Kb can be observed, corresponding to JH1 rearrangement.
VH (variable, yellow), DH (diversity, green), JH (joining, pink), CH (constant, blue), Kb (kilo bases), bp (base pairs) and PCR (polymerase chain reaction).

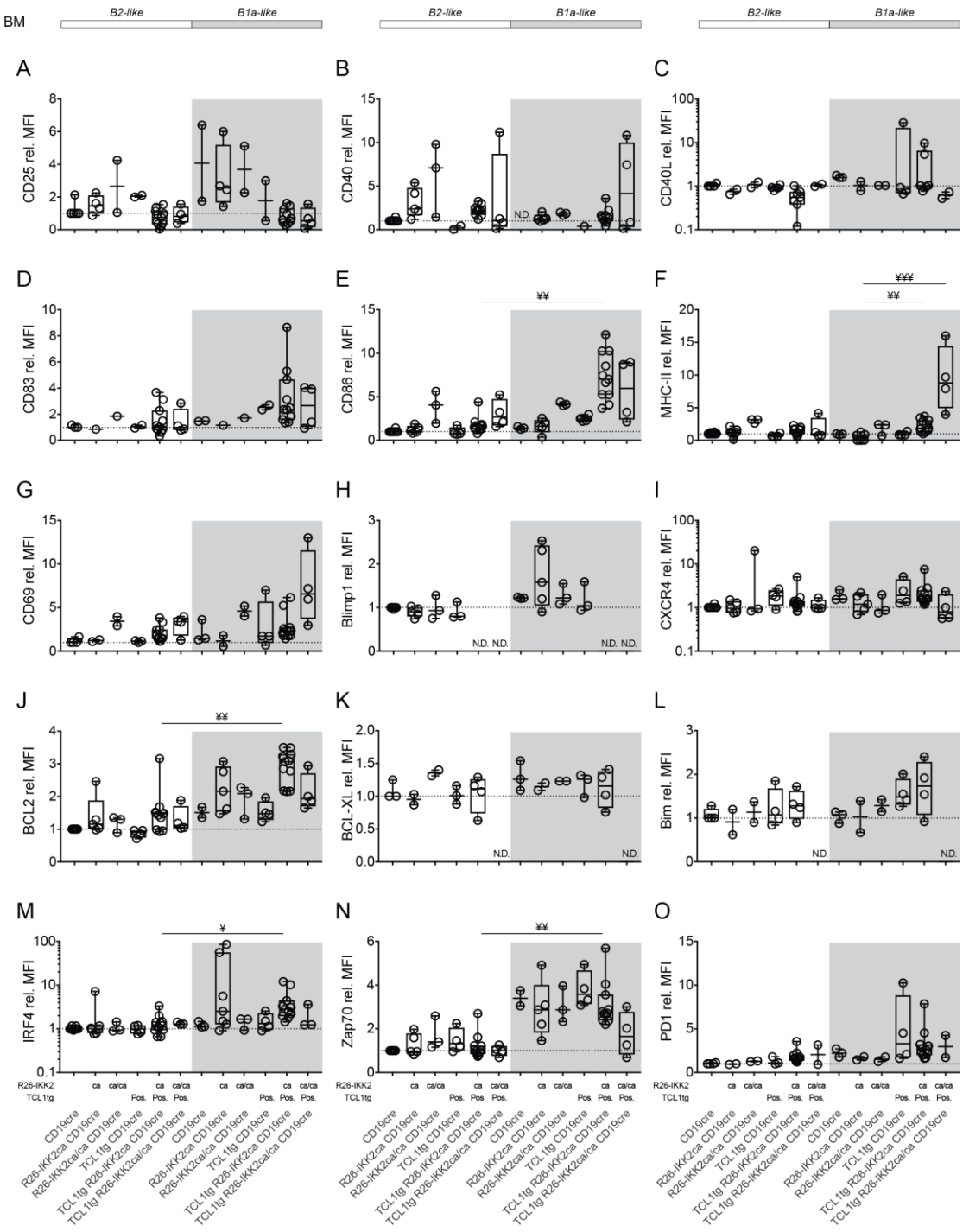


**Figure S 33. Immunophenotyping of bone marrow B2- and B1a-like cells in burdened mice**

Immunophenotyping of B-cells subsets B2- and B1a-like cells in bone marrow of burden mice using flow cytometry. Box plots show MFI relative to CD19cre B2-cells controls for (A-F) immune-receptors; (G) CD69 cell surface receptor, (H-I) chemokine associated receptors, (J-L) regulators of apoptosis, (M) IRF4 transcription factor and (N-O) CLL associated proteins. In the box plots, the median is represented as a horizontal line, the box represents the 25$^{th}$ and 75$^{th}$ percentiles and the whiskers the minimum and maximum points. All individual values are plotted in the graph. Statistical analysis was done using Kruskal-Wallis (¥ $p<0.05$, ¥¥ $p<0.01$, ¥¥¥ $p<0.001$).

BM (Bone marrow), B2-like (CD19$^{Hi}$ B220$^{Hi}$, white background), B1a-like (CD19$^{Hi}$ B220$^{Lo}$ CD5$^{+}$, grey background), N.D. (not done).

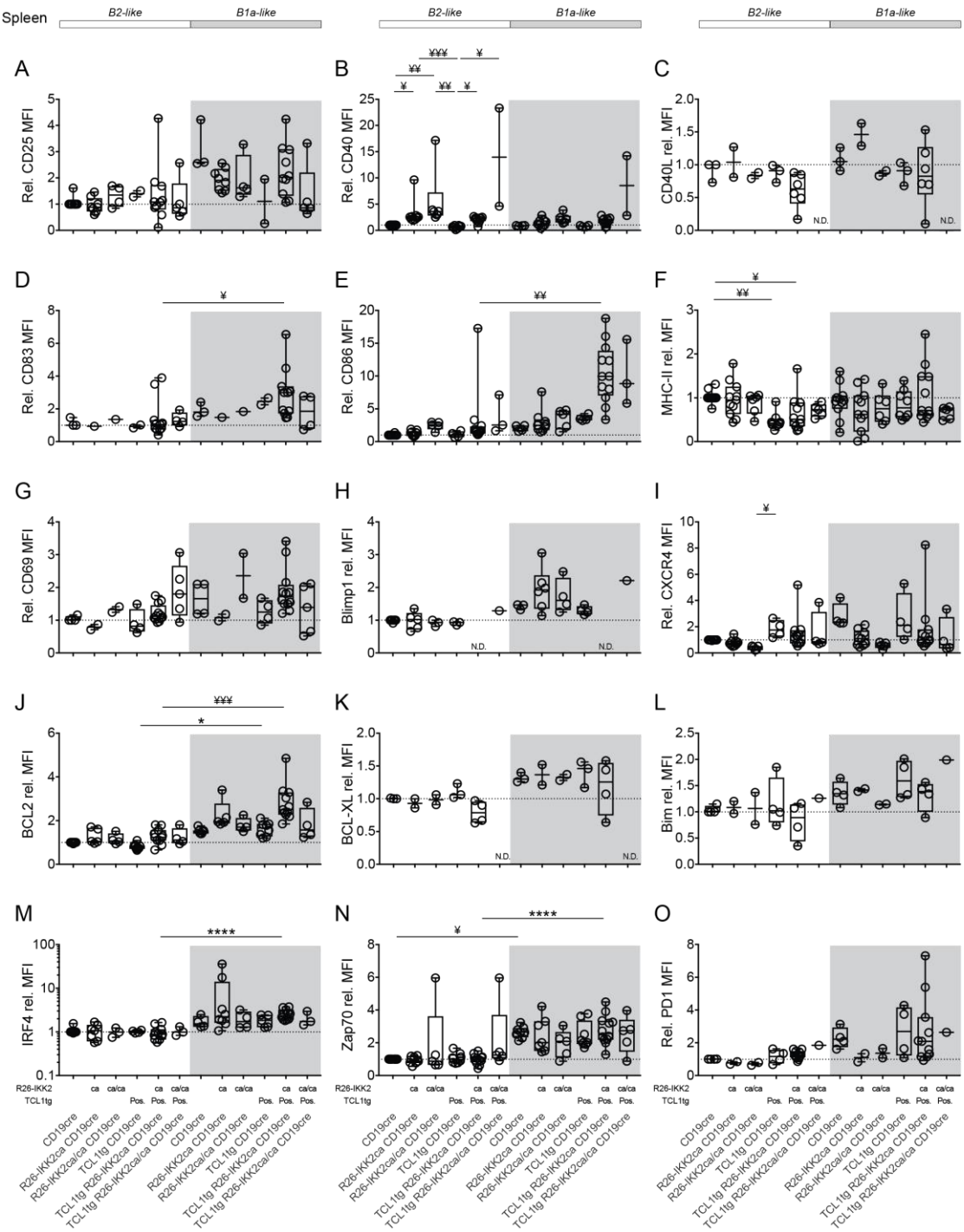


**Figure S 34. Immunophenotyping of splenic B2- and B1a-like cells in burdened mice**

*Ex vivo* immunophenotyping of B-cells subsets B2- and B1a-like cells in spleen of burden mice using flow cytometry. Box plots show MFI relative to CD19cre B2-cells controls for (A-F) immune-receptors; (G) CD69 cell surface receptor, (H-I) chemokine associated receptors, (J-L) regulators of apoptosis, (M) IRF4 transcription factor and (N-O) CLL associated proteins. In the box plots, the median is represented as a horizontal line, the box represents the 25$^{th}$ and 75$^{th}$ percentiles and the whiskers the minimum and maximum points. All individual values are plotted in the graph. Statistical analysis was done using One-Way ANOVA (* p<0.05) or Kruskal-Wallis (¥ p<0.05, ¥¥ p<0.01, ¥¥¥ p<0.001).
B2-like (CD19$^{+}$ B220$^{Hi}$, white background), B1a-like (CD19$^{+}$ B220$^{Lo}$ CD5$^{+}$, grey background), N.D. (not done).

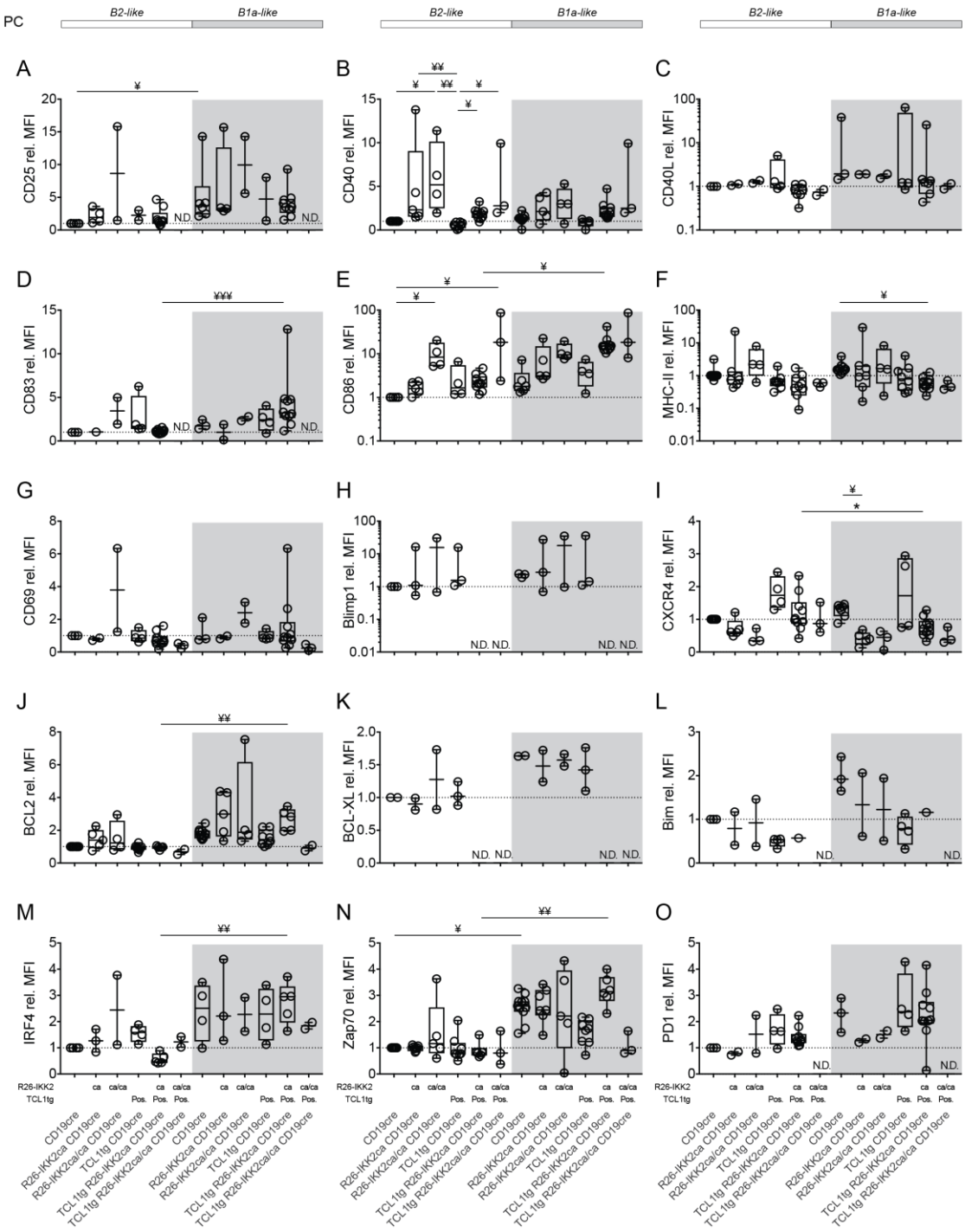


**Figure S 35. Immunophenotyping of peritoneal B2- and B1a-like cells in burdened mice**

*Ex vivo* immunophenotyping of B-cells subsets B2- and B1a-like cells in the peritoneal cavity of burden mice using flow cytometry. Box plots show MFI relative to CD19cre B2-cells controls for (A-F) immune-receptors; (G) CD69 cell surface receptor, (H-I) chemokine associated receptors, (J-L) regulators of apoptosis, (M) IRF4 transcription factor and (N-O) CLL associated proteins. In the box plots, the median is represented as a horizontal line, the box represents the 25$^{th}$ and 75$^{th}$ percentiles and the whiskers the minimum and maximum points. All individual values are plotted in the graph. Statistical analysis was done using Kruskal-Wallis (¥ $p<0.05$, ¥¥ $p<0.01$).

PC (Peritoneal cavity), B2-like (CD19$^{+}$ B220$^{Hi}$, white background), B1a-like (CD19$^{+}$ B220$^{Lo}$ CD5$^{+}$, grey background), N.D. (not done).

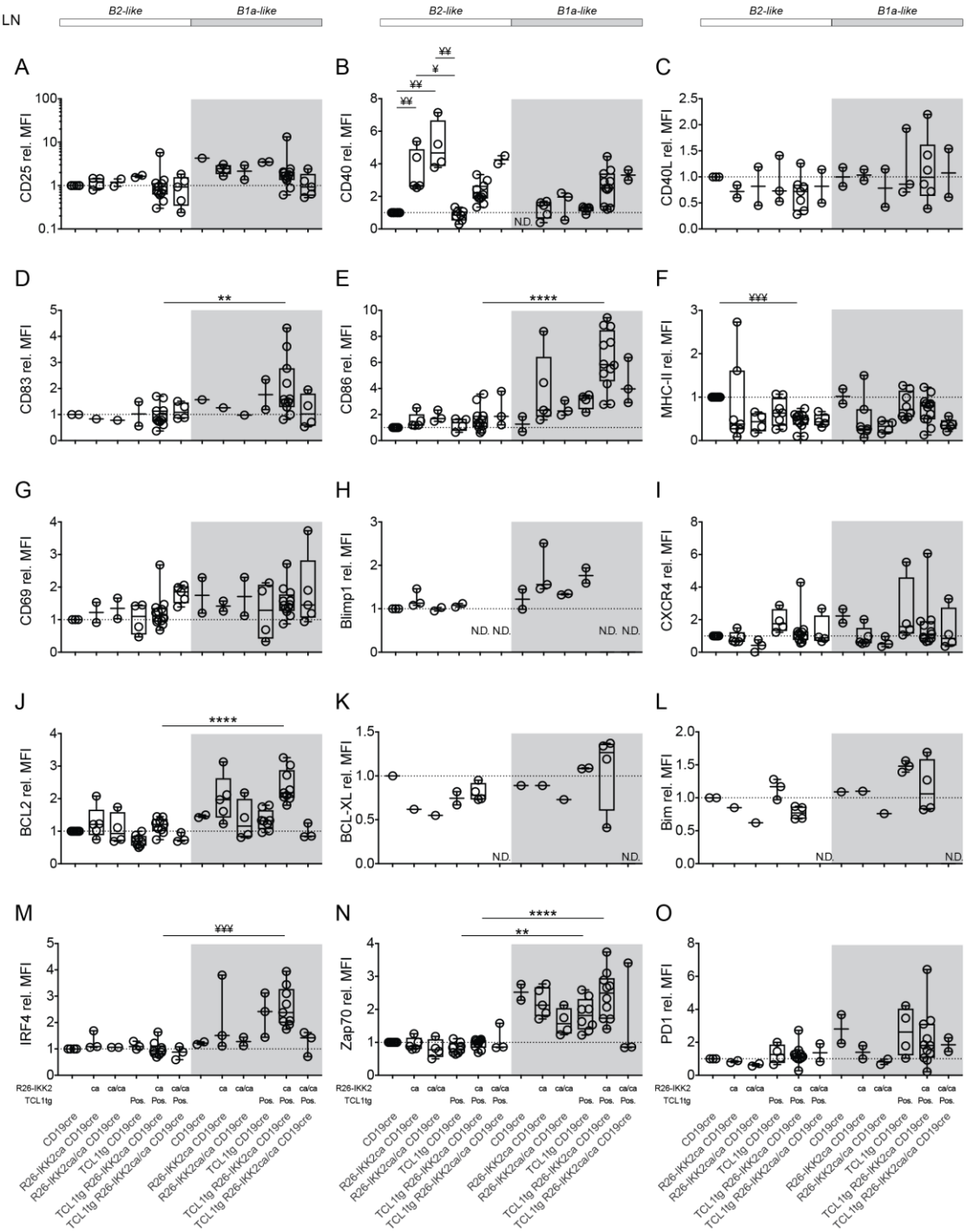


**Figure S 36. Immunophenotyping of lymph node B2- and B1a-like cells in burdened mice**

*Ex vivo* immunophenotyping of B-cells subsets B2- and B1a-like cells in draining lymph nodes of burden mice using flow cytometry. Draining inguinal, axillary and superficial cervical lymph nodes were pooled and analysed together. Box plots show MFI relative to CD19cre B2-cells controls for (A-F) immune-receptors; (G) CD69 cell surface receptor, (H-I) chemokine associated receptors, (J-L) regulators of apoptosis, (M) IRF4 transcription factor and (N-O) CLL associated proteins. In the box plots, the median is represented as a horizontal line, the box represents the 25$^{th}$ and 75$^{th}$ percentiles and the whiskers the minimum and maximum points. All individual values are plotted in the graph. Statistical analysis was done using One-Way ANOVA (** p<0.01, **** p<0.0001) or Kruskal-Wallis (¥ p<0.05, ¥¥ p<0.01, ¥¥¥ p<0.001).

LN (Lymph nodes), B2-like (CD19$^{+}$ B220$^{Hi}$, white background), B1a-like (CD19$^{+}$ B220$^{Lo}$ CD5$^{+}$, grey background), N.D. (not done).

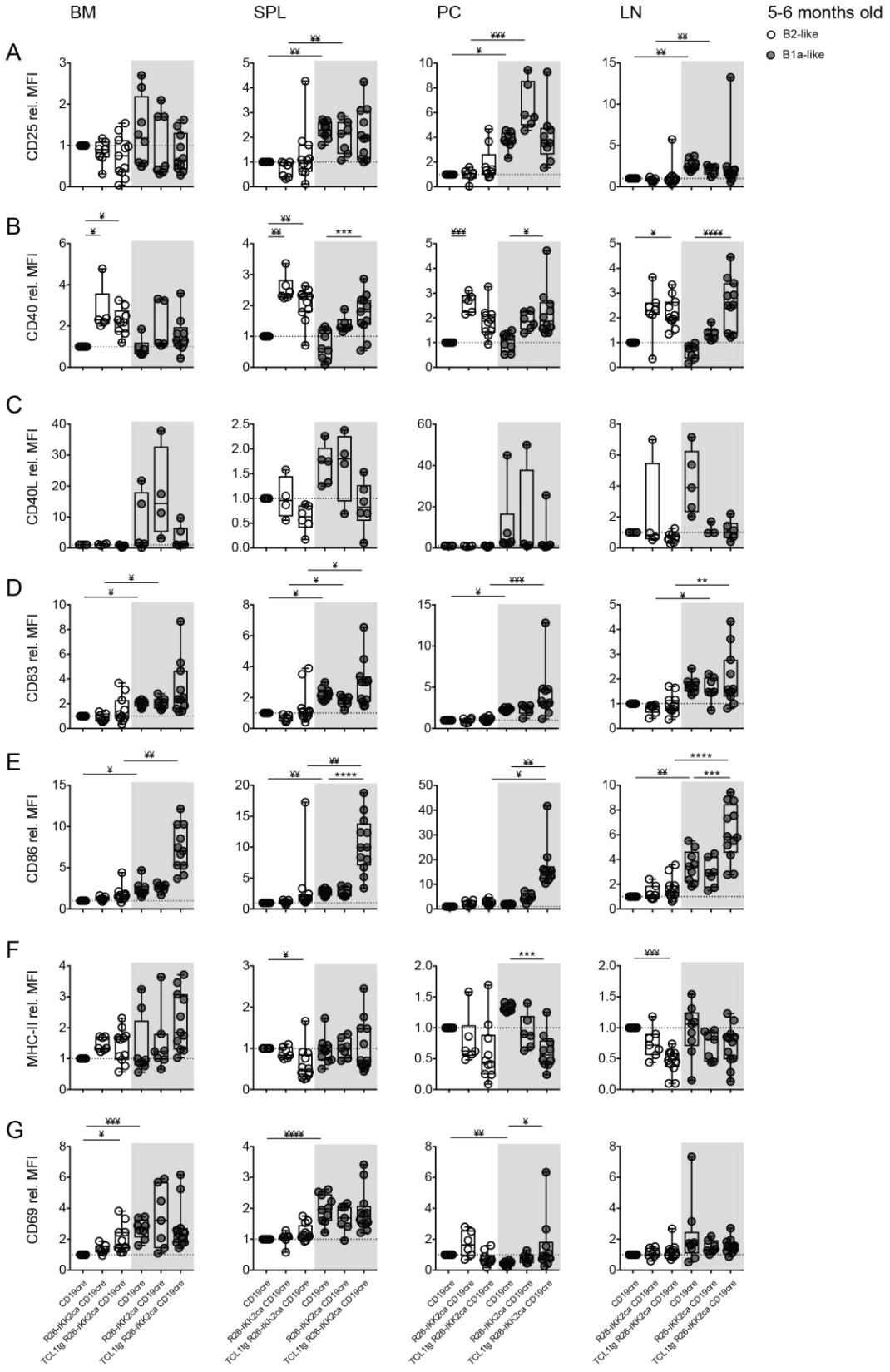


**Figure S 37. Immunophenotyping of B2- and B1a-like cells in 5/6-month-old mice**

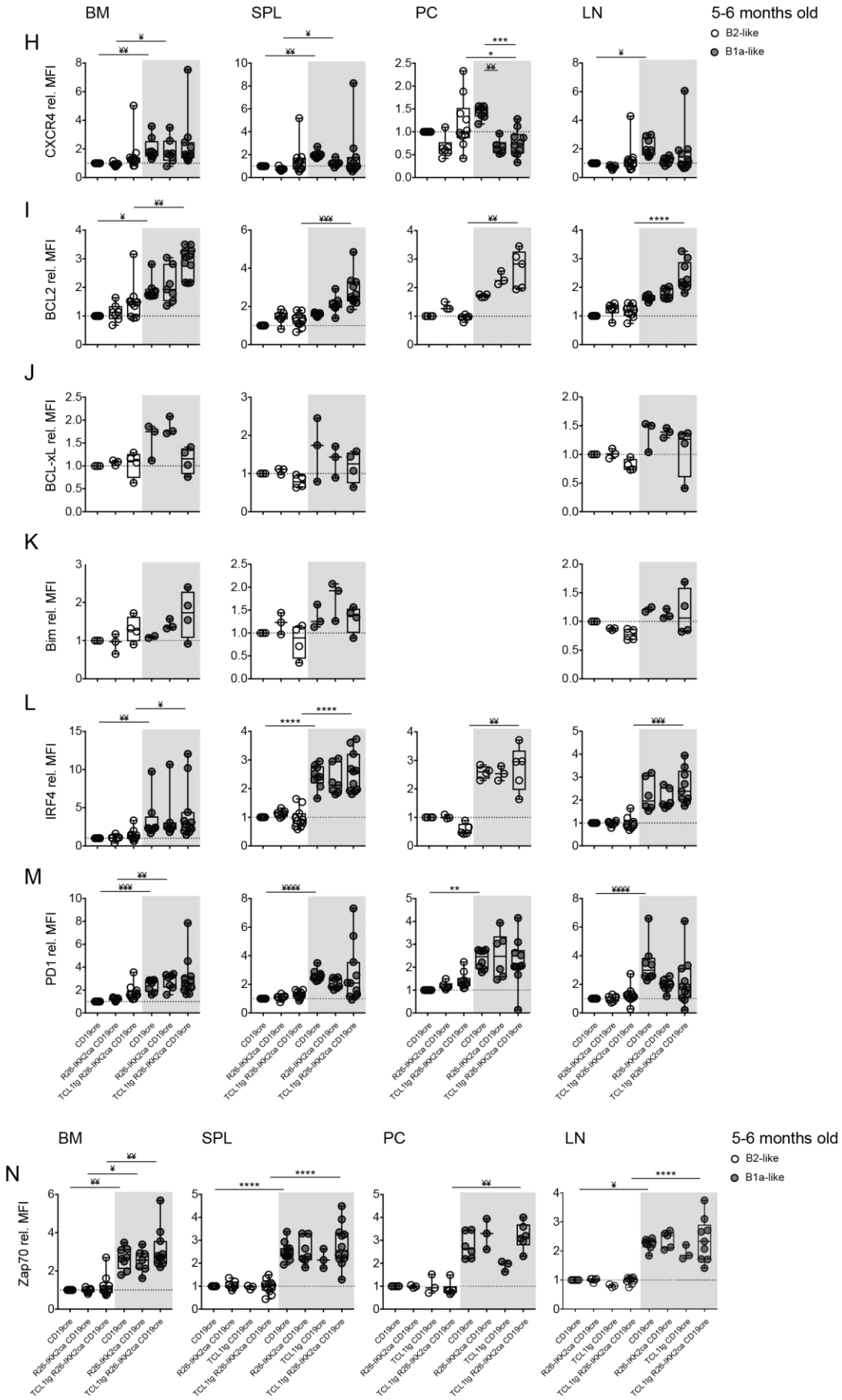
BM
SPL
PC
LN
5-6 months old
B2-like
B1a-like
H
CXCR4 rel. MFI
I
BCL2 rel. MFI
J
BCL-xL rel. MFI
K
Bim rel. MFI
L
IRF4 rel. MFI
M
PD1 rel. MFI
CD19cre
R26-IKK2ca CD19cre
TCL1tg R26-IKK2ca CD19cre
N
Zap70 rel. MFI
TCL1tg CD19cre

**Figure S 37 (continued): Immunophenotyping of B2- and B1a-like cells in 5/6-month-old mice**

*Ex vivo* immunophenotyping of subsets B2- and B1a-like in 5-6 months old burden TCL1tg R26-IKK2ca CD19cre and aged matched control mice, using flow cytometry. Box plots show MFI relative to CD19cre B2 controls for (A-F) immunoreceptors; (G) CD69 cell surface receptor, (H) CXCR4 chemokine receptor; (I-K) regulators of apoptosis, (L) IRF4 transcription factor and (M) CLL associated proteins, and (N) CLL associated proteins. In the box plots, the median is represented as a horizontal line, the box represents the $25^{th}$ and $75^{th}$ percentiles and the whiskers the minimum and maximum points. All individual values are plotted in the graph. Statistical analysis was done using One-Way ANOVA (** p<0.01, *** p<0.001, **** p<0.0001) or Kruskal-Wallis (¥ p<0.05, ¥¥ p<0.01, ¥¥¥ p<0.001, ¥¥¥¥ p<0.0001).
BM (Bone marrow), SPL (Spleen), PC (Peritoneal cavity), LN (Lymph nodes), B2-like ($CD19^{+}$ $B220^{Hi}$, white background), B1a-like ($CD19^{+}$ $B220^{Lo}$ $CD5^{+}$, grey background).

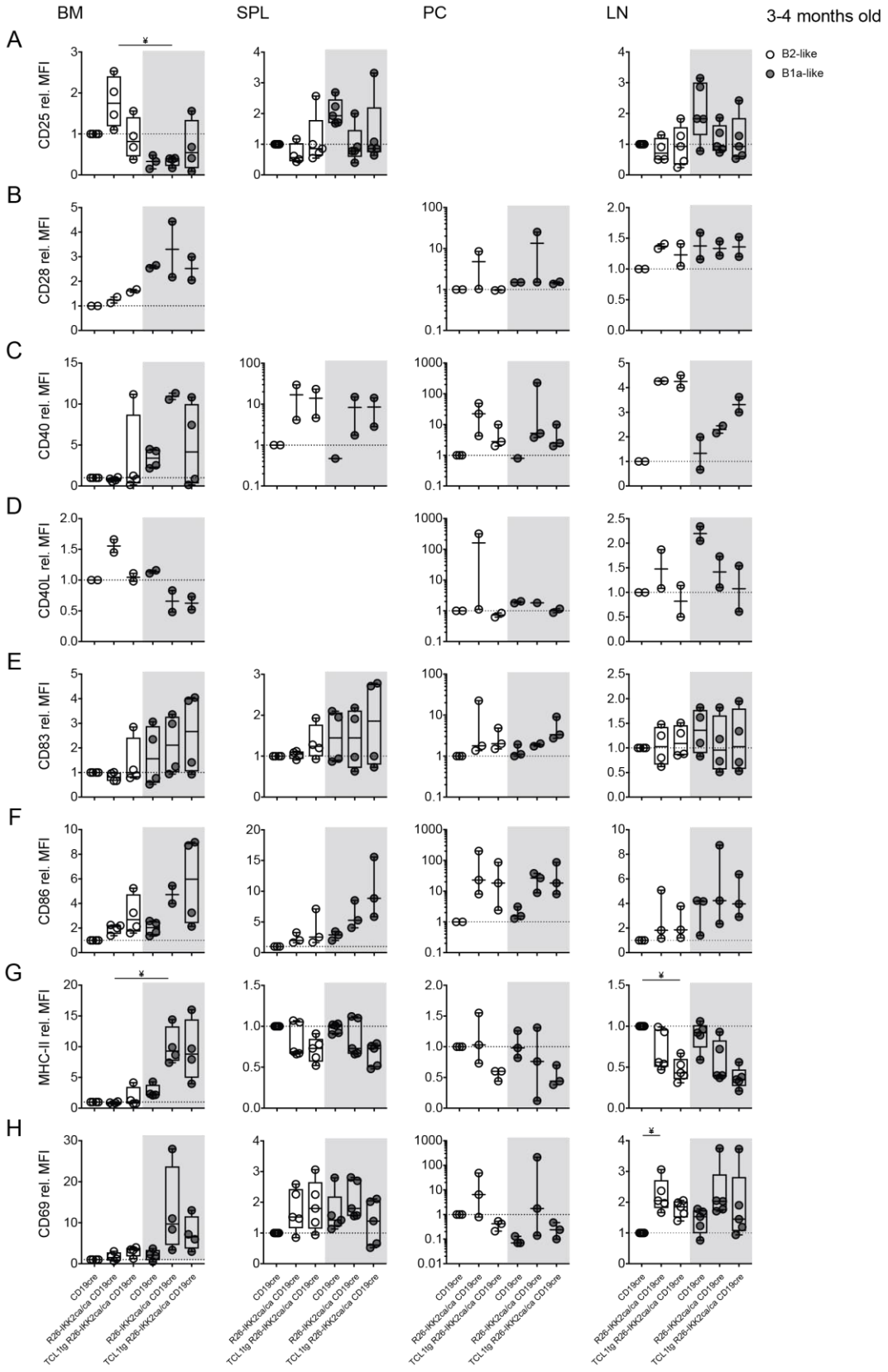


**Figure S 38. Immunophenotyping of B2- and B1a-like cells in 3/4-month-old mice**

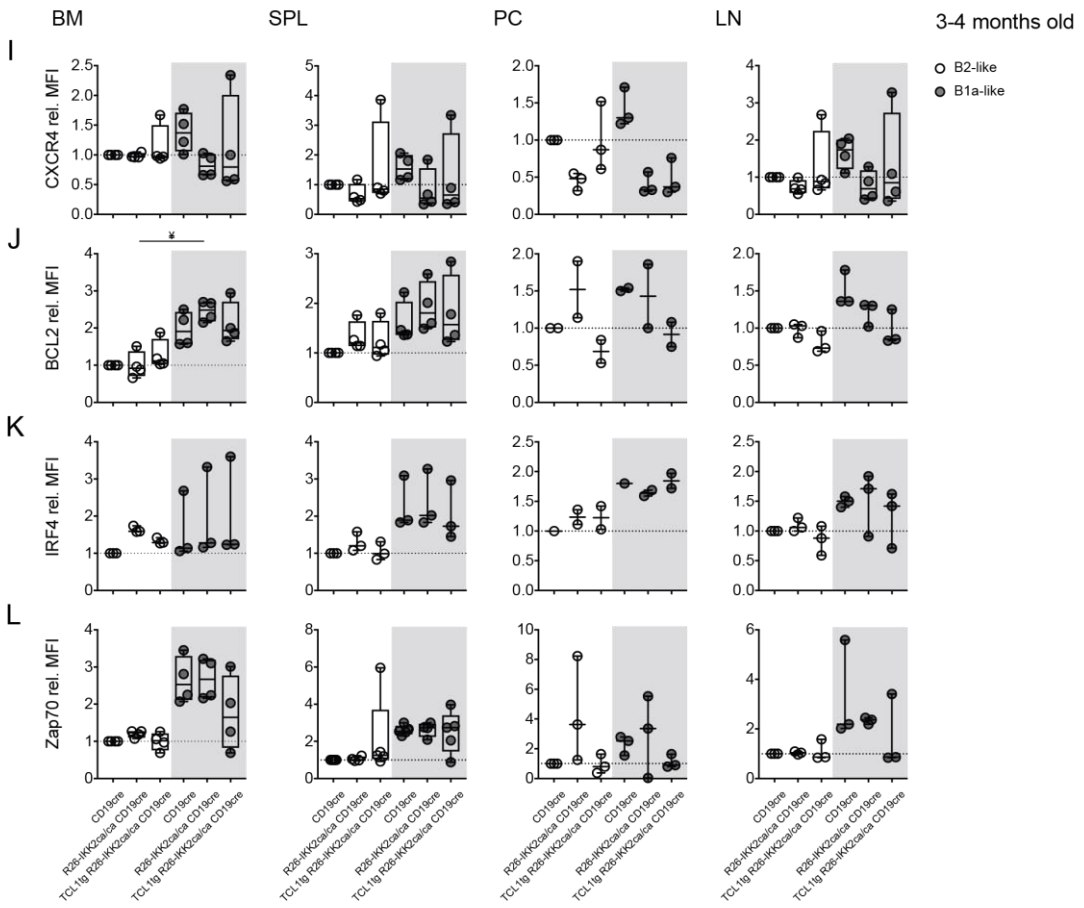


**Figure S 38 (continued): Immunophenotyping of B2- and B1a-like cells in 3/4-month-old mice**

*Ex vivo* immunophenotyping of subsets B2- and B1a-like in 3-4 months old burden TCL1tg R26-IKK2ca CD19cre and aged matched control mice, using flow cytometry. Box plots show MFI relative CD19cre B2-cells controls for (A-G) immunoreceptors; (H) CD69 cell surface receptor; (I) CXCR4 chemokine receptor; (J) regulator of apoptosis BCL2, (K) IRF4 transcription factor and (L) CLL associated protein Zap70. In the box plots, the median is represented as a horizontal line, the box represents the 25$^{th}$ and 75$^{th}$ percentiles and the whiskers the minimum and maximum points. All individual values are plotted in the graph. Statistical analysis was done using One-Way ANOVA (** p<0.01, *** p<0.001, **** p<0.0001) or Kruskal-Wallis (¥ p<0.05, ¥¥ p<0.01, ¥¥¥ p<0.001, ¥¥¥¥ p<0.0001).
BM (Bone marrow), SPL (Spleen), PC (Peritoneal cavity), LN (Lymph nodes), B2-like (CD19$^{+}$ B220$^{Hi}$, white background), B1a-like (CD19$^{+}$ B220$^{Lo}$ CD5$^{+}$, grey background).

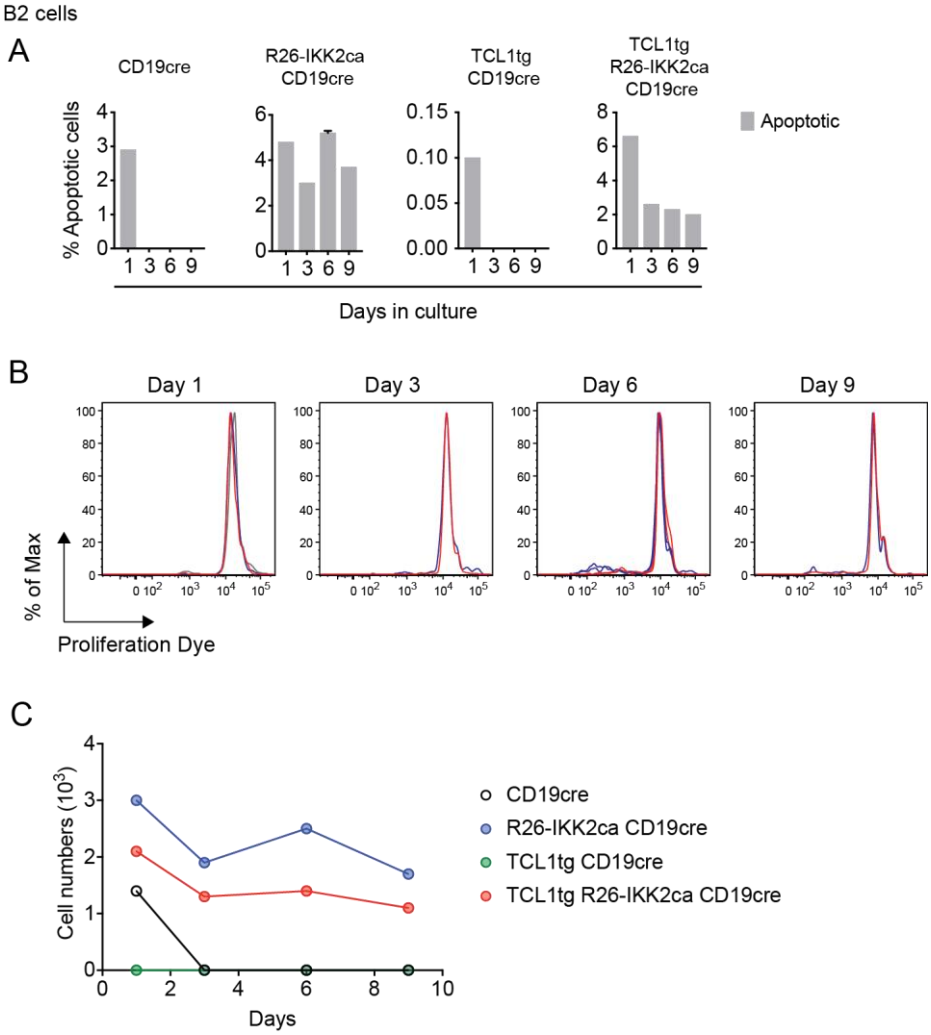


**Figure S 39. *In vitro* survival of resting B2-cells**

Sorted B2-cells were cultured in B-cell media in resting conditions for 9 days. *In vitro* cell proliferation and cell survival was assed by flow cytometry. (A) Bar charts show the percentage of apoptotic cells present in the culture as mean and SEM. (B) Histograms depict the *in vitro* proliferation of B2-cells. (C) Scatter plot shows the absolute number of living B2-cells in culture.
B2 ($CD19^+$ $B220^+$), Apoptotic cells (Annexin-V+ 7AAD-/Annexin-V+ 7AAD+) and Living cells (Annexin-V-7AAD-).

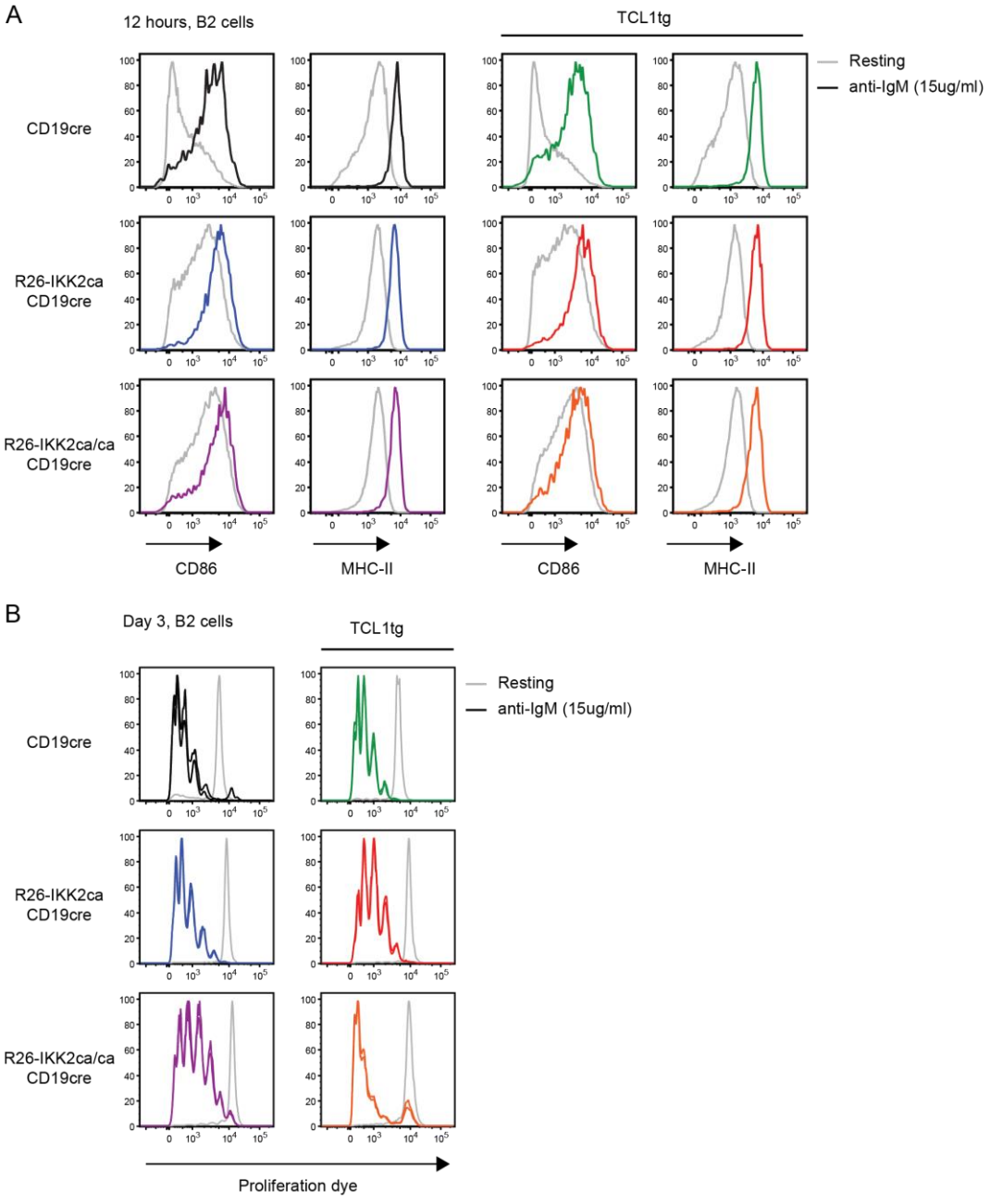


C

Day 3

| Genotype | Div. Index | Prol. Index | % Divided |
|---|---|---|---|
| CD19cre | 1.87 | 2.95 | 65.75 |
| R26-IKK2ca CD19cre | 2.61 | 2.77 | 94.3 |
| R26-IKK2ca/ca CD19cre | 2.11 | 2.68 | 73.75 |
| TCL1tg CD19cre | 2.19 | 2.59 | 84.6 |
| TCL1g R26-IKK2ca CD19cre | 2.67 | 2.85 | 93.75 |
| TCL1tg R26-IKK2ca/ca CD19cre | 1.25 | 3.2 | 37.5 |

**Figure S 40. B2-cells proliferate *in vitro* in response to B-cell receptor stimulation**

Purified B-cells from 3-months-old mice were stimulated *in vitro* with 15ug/ml anti-BCR and cultured for three days. (A) Histograms depict the expression of the activation markers CD86 and MHC-II after 12 hours of stimulation in B2-cells. (B) Histograms depict the *in vitro* proliferation of B2-cells, three days after stimulation. (C) Table shows the division index (Div. Index), proliferation index (Prol. Index) and percentage of divided cells (% Divided) values for B2-cells after three days of stimulation.

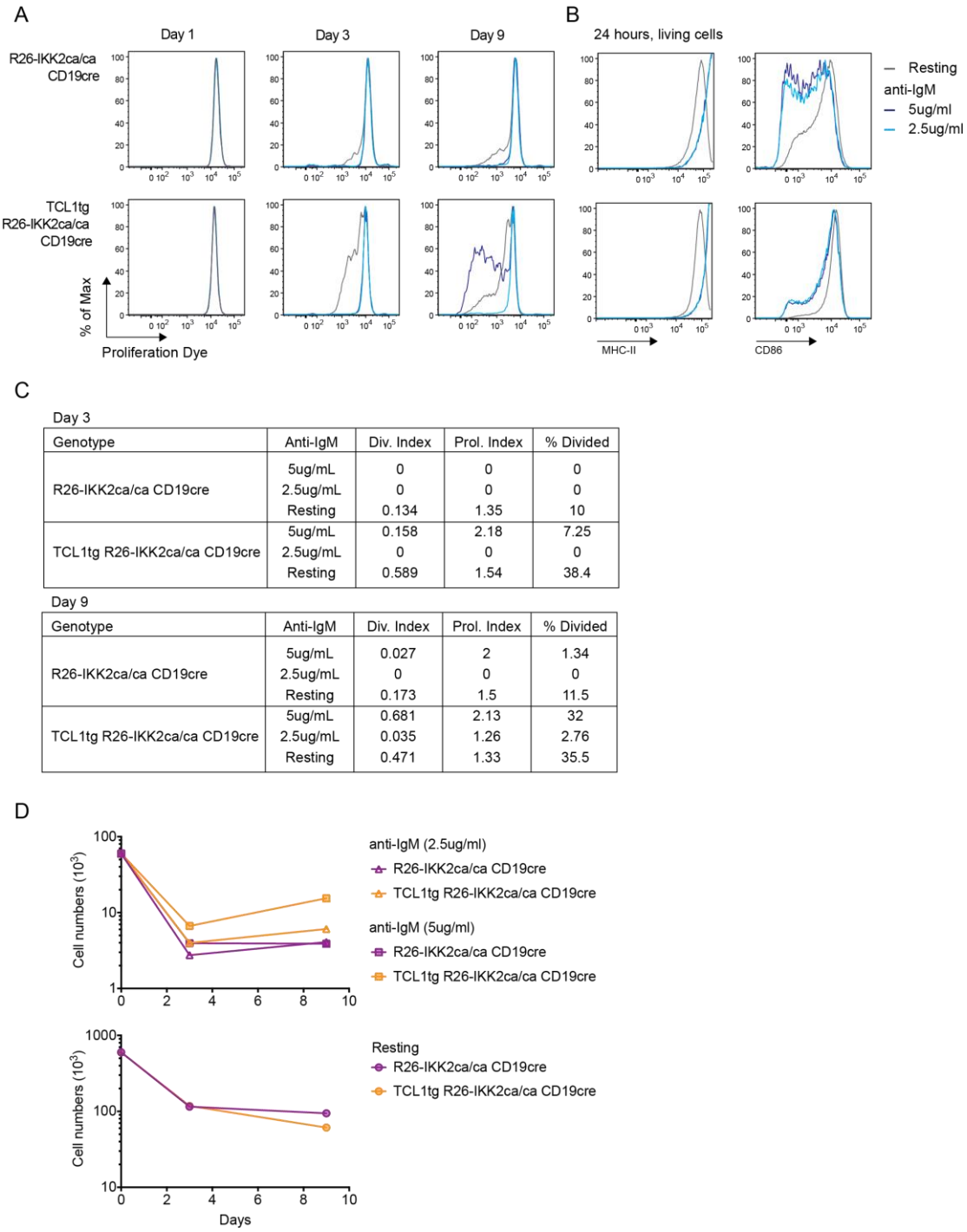


**Figure S 41. BCR crosslinking modulates B1a-like cells *in vitro* proliferation**

Sorted B1a-like cells were stimulated *in vitro* with either 2.5ug/ml or 5ug/ml anti-BCR and cultured for nine days. (A) Histograms depict the *in vitro* proliferation of B1a-like cells at days one, three and nine after stimulation. (B) Histograms depict the expression of the activation markers CD86 and MHC-II after 24 hours of stimulation in B1a-like cells. (C) Table shows the division index (Div. Index), proliferation index (Prol. Index) and percentage of divided cells (% Divided) values for B1a-like cells after three and nine days of stimulation. (D) Scatter plot depicts absolute numbers for living (Annexin-V$^-$ AAD$^-$) B1a-like cells.

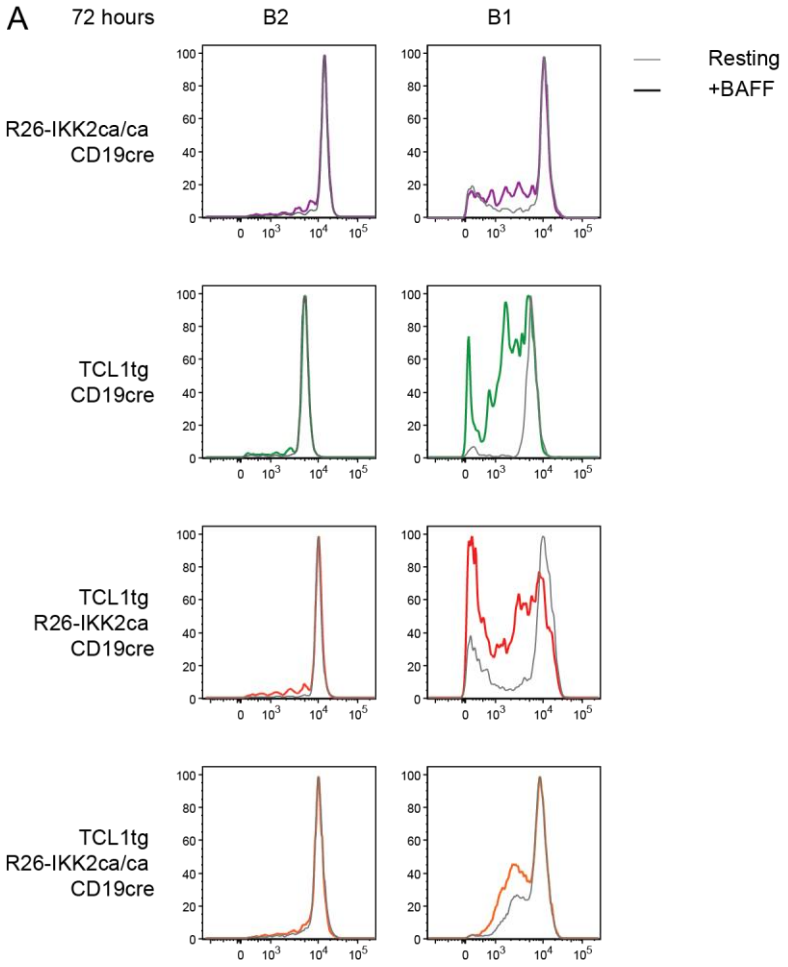


B

Day 3

| Genotype | Div. Index | Prol. Index | % Divided |
|---|---|---|---|
| Resting | | | |
| R26-IKK2ca/ca CD19cre | 0.141 | 2.02 | 7 |
| TCL1tg CD19cre | 0.151 | 1.9 | 7.9 |
| TCL1g R26-IKK2ca CD19cre | 0.19 | 1.93 | 9.8 |
| TCL1tg R26-IKK2ca/ca CD19cre | 0.201 | 1.88 | 10.7 |
| BAFF | | | |
| R26-IKK2ca/ca CD19cre | 0.31 | 1.87 | 16.4 |
| TCL1tg CD19cre | 0.7 | 1.74 | 40.1 |
| TCL1g R26-IKK2ca CD19cre | 0.7 | 1.73 | 40.4 |
| TCL1tg R26-IKK2ca/ca CD19cre | 0.34 | 2.33 | 14.6 |

**Figure S 42. BAFF *in vitro* stimulation promotes B1 cell proliferation**

Spleen purified B-cells were stimulated *in vitro* with 100ng/mL BAFF and cultured for three days. Histograms depict the *in vitro* proliferation of (A) B2-cells and (B) B1-cells 72 hours after stimulation. (C) Table shows the division index (Div. Index), proliferation index (Prol. Index) and percentage of divided cells (% Divided) values for B1-cells after 3 days of stimulation.
B2 ($CD19^+$ $B220^+$) and B1 ($CD19^+$ $B220^-$).

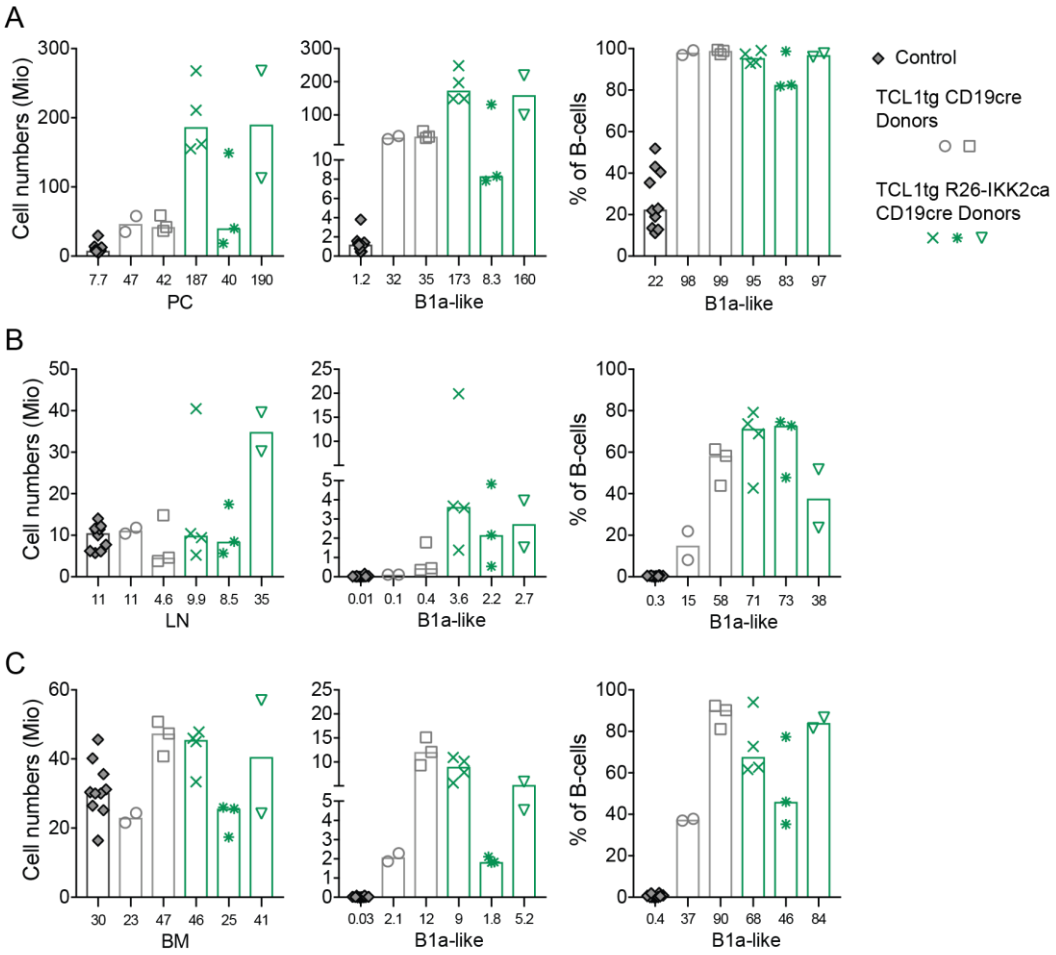


**Figure S 43. Transplanted TCL1tg CLL-cells infiltration and homing in PKC-β+/- recipients**

*Ex vivo* analysis of burdened CLL- transplanted PKC-β+/- recipient mice and aged matched controls using flow cytometry. Bar chart shows cell numbers, B1a-like cell numbers and B1a-like cells as percentages of B-cells for (A) peritoneal cavity; (B) draining lymph nodes and (C) bone marrow in PKC-β+/- mice. Histograms depict medians, and values are indicated below each histogram. Each bar represents a CLL-like lymphoma of the indicated genotype transplanted into multiple recipients.
PC (peritoneal cavity), LN (draining lymph nodes), BM (bone marrow), B1a-like ($CD19^+$ $B220^-$ $CD5^+$) and B-cells ($CD19^+$).

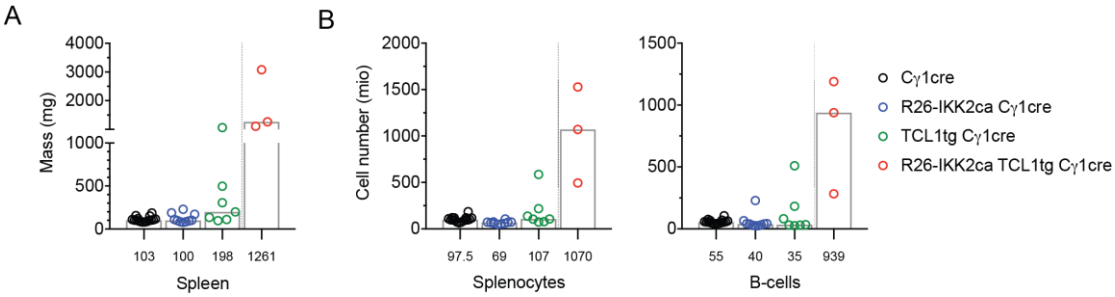


**Figure S 44. Conditional IKK2ca expression by Cγ1cre co-operates with TCL1 in splenic B-cells**

*Ex vivo* analysis of TCL1tg R26-IKK2ca Cγ1cre burdened mice and aged matched controls using flow cytometry. Bar chart show (A) spleen mass, and (B) total and B-cell numbers. Histograms depict medians, and values are indicated below each histogram.
B-cells ($CD19^+$).

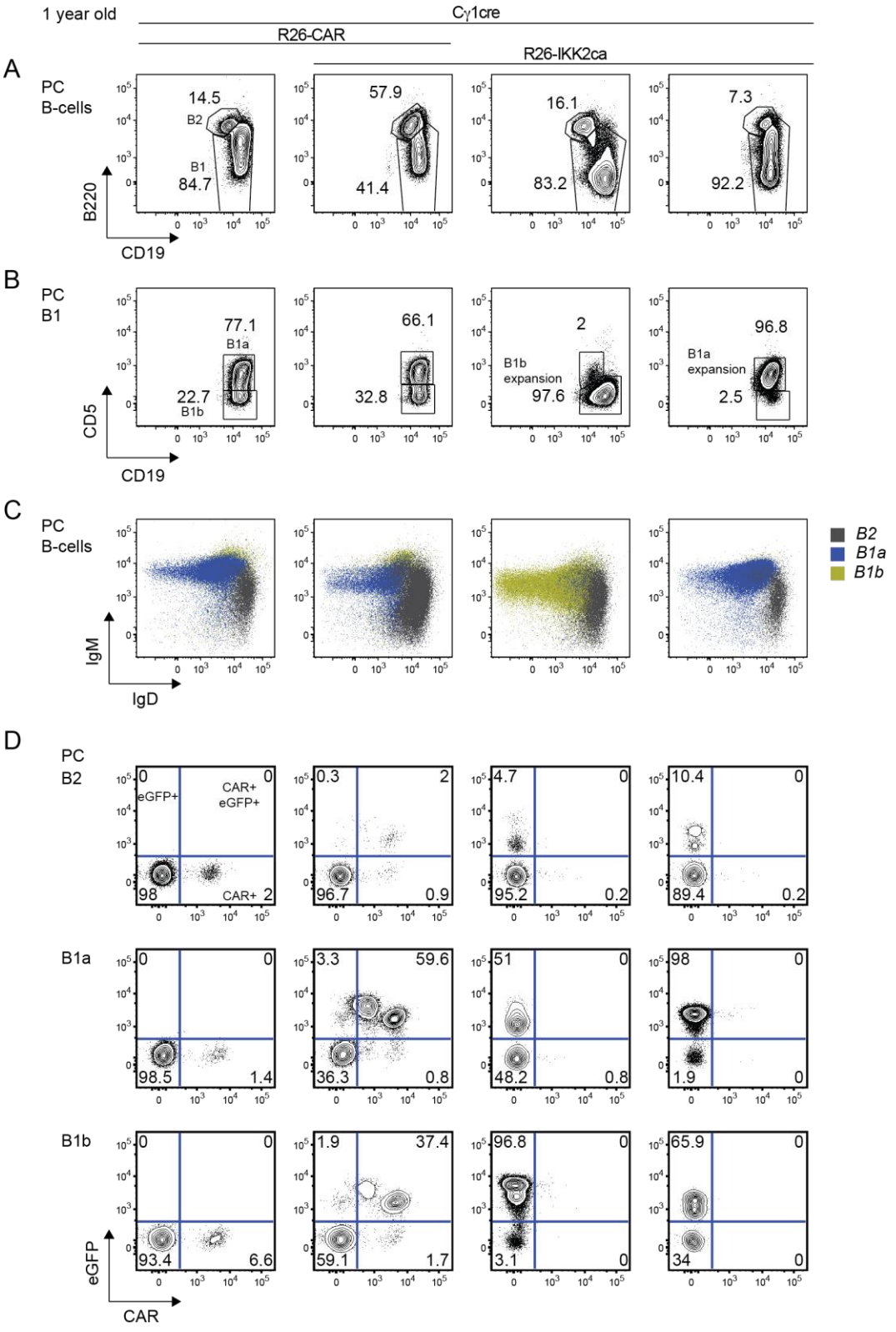


**Figure S 45. Conditional IKK2ca expression by Cγ1cre promotes B1 cell expansion in the peritoneal cavity with age**

*Ex vivo* analysis of 1-year-old R26-IKK2ca Cγ1cre and aged matched control mice using flow cytometry. Contour plots depict the percentage of (A) B2 and B1 subsets, and (B) B1a and B1b subsets in the peritoneum. (C) Dot plot depicts the expression of IgM and IgD in B2, B1a and B1B-cell subsets.

Figure S 45 **(continued).** (D) Contour plots depict the percentage of eGFP+, eGFP+;CAR+ and CAR+ expressing cells for the different B-cell subsets in the peritoneum. Flow cytometry plots are representative of at least 2 experiments.
PC (peritoneal cavity), B-cells ($CD19^+$), B2 ($CD19^+$ $B220^+$), B1 ($CD19^+$ $B220^{lo}$), B1a ($CD19^+$ $B220^{lo}$ $CD5^+$), B1b ($CD19^+$ $B220^{lo}$ $CD5^-$).

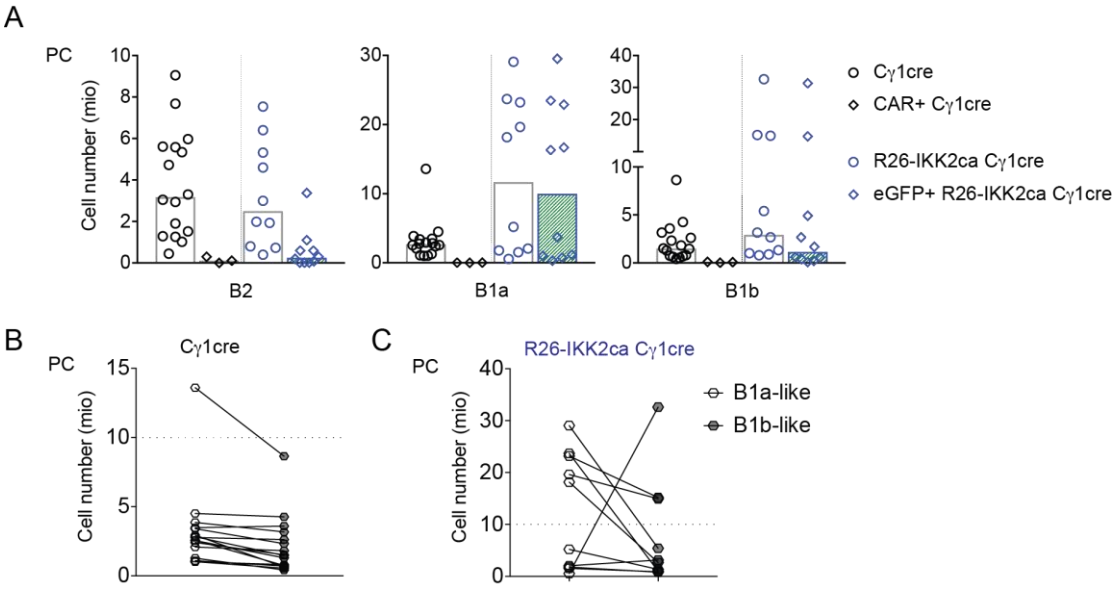


**Figure S 46. Conditional IKK2ca expression by Cγ1cre promotes B1 cell numbers in the peritoneal cavity of 1-year-old mice**

*Ex vivo* analysis of 1-year-old R26-IKK2ca Cγ1cre and aged matched control mice using flow cytometry. (A) Bar charts show B2, B1a and B1b total and CAR+/eGFP+ recombined cell numbers in the peritoneal cavity. Dot pots show the paired connected B1a- and B1b-like cell numbers for 1-year-old (B) Cγ1cre control mice and (C) R26-IKK2ca Cγ1cre mice. Histograms depict medians.
PC (peritoneal cavity), B2 ($CD19^+$ $B220^+$), B1a ($CD19^+$ $B220^{lo}$ $CD5^+$) and B1b ($CD19^+$ $B220^{lo}$ $CD5^-$).

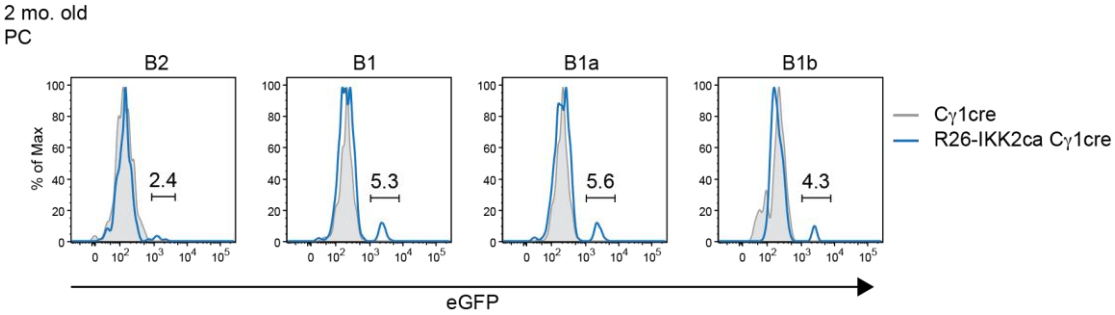


**Figure S 47. eGFP+;IKK2ca+ Cγ1cre-dependent expression in B1-cells in the peritoneal cavity of young mice**

*Ex vivo* analysis of 2-months-old R26-IKK2ca Cγ1cre and control mice using flow cytometry. Histograms depict the percentages of eGFP+;IKK2ca+ cells as a result of Cγ1cre-dependent recombination for the different B-cell subsets present in the peritoneal cavity. Flow cytometry plots are representative of at least 2 experiments.
PC (peritoneal cavity), mo. (months), B2 ($CD19^+$ $B220^+$), B1 ($CD19^+$ $B220^{lo}$), B1a ($CD19^+$ $B220^{lo}$ $CD5^+$) and B1b ($CD19^+$ $B220^{lo}$ $CD5^-$).

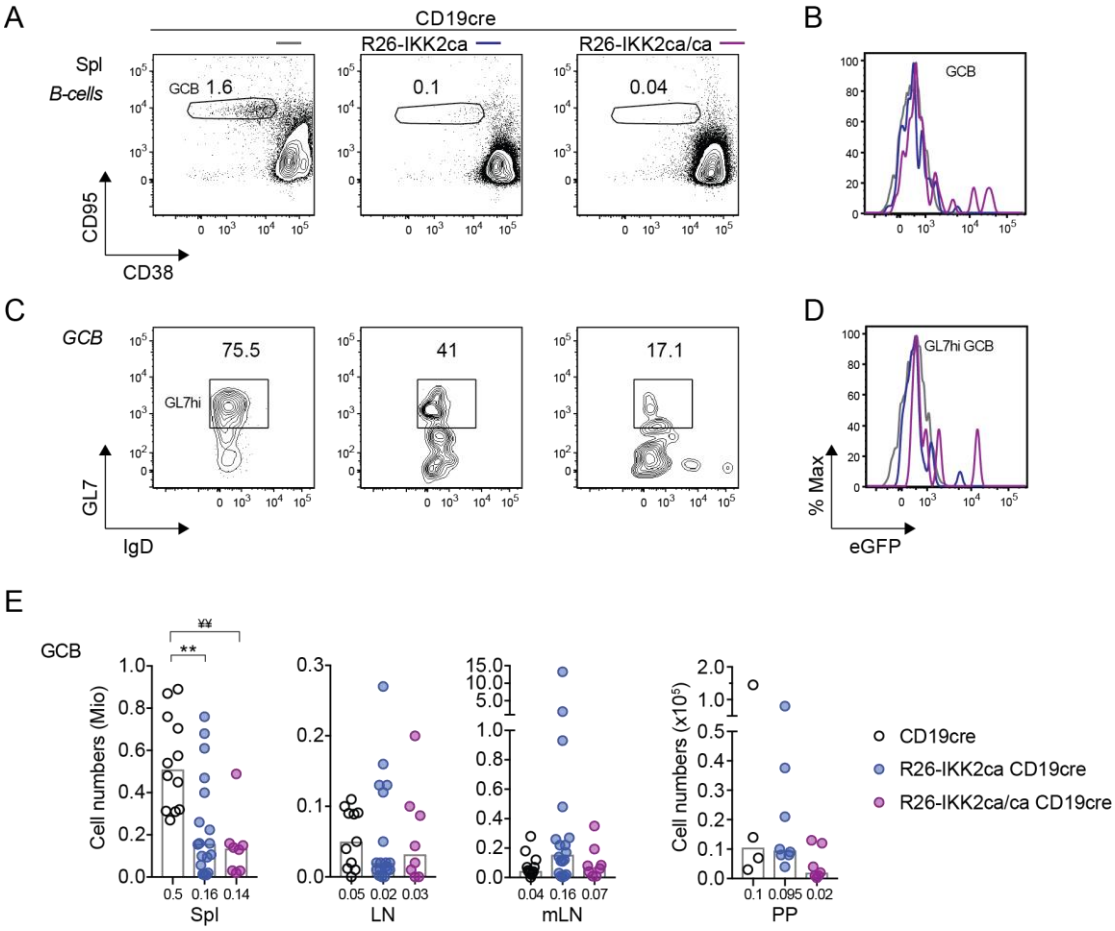


**Figure S 48. IKK2ca expression reduces GC B-cells in aged mice**

*Ex vivo* analysis of 1-year-old R26-IKK2ca CD19cre compound mice using flow cytometry. Contour plots depict the percentage of (A) germinal centre B-cells and (C) GL7hi germinal centre B-cells in spleen. Histograms depict the percentage of eGFP+;IKK2ca+ (B) germinal centre B-cells and (D) GL7hi germinal centre B-cells in spleen. (E) Bar charts show the number of total germinal centre B-cells in spleen, lymph nodes, mesenteric lymph nodes and Payer's patches. Flow cytometry plots are representative of at least 2 experiments. Histograms in bar charts depict medians, and values are indicated below each histogram. Statistical analysis was done using One-Way ANOVA (* $p<0.05$) or Kruskal-Wallis (¥¥ $p<0.01$).
Spl (spleen), LN (lymph nodes), mLN (mesenteric lymph nodes), PP (Payer's patches), B-cells ($CD19^+$), GCB (germinal centre B-cell, $CD19^+$ $CD95^+$ $CD38^-$), GL7hi ($CD19^+$ $CD95^+$ $CD38^-$ $GL7^{hi}$).

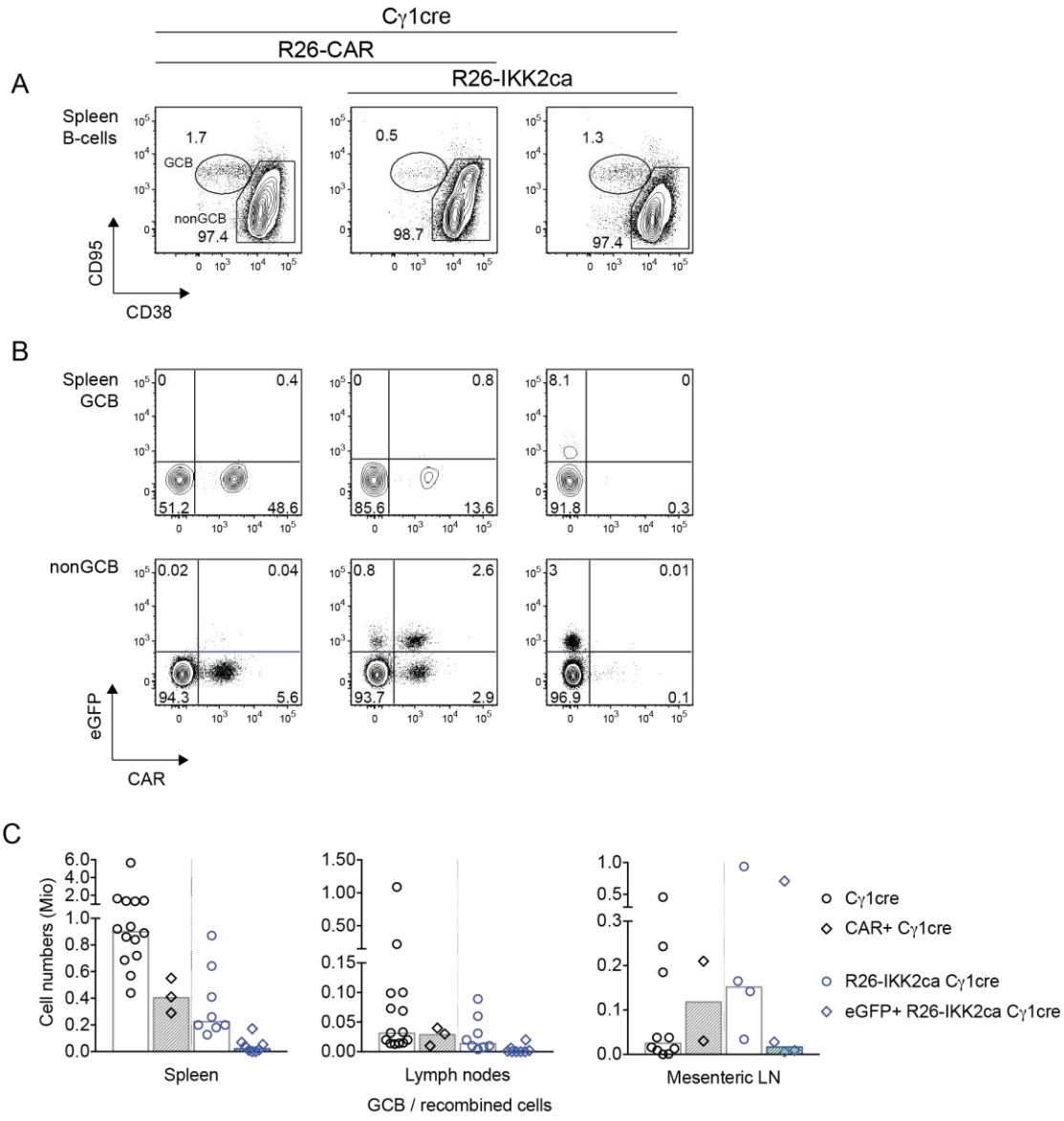


**Figure S 49. Conditional IKK2ca expression by Cγ1cre reduces GC B-cells**

*Ex vivo* analysis of 1-year-old R26-IKK2ca Cγ1cre and aged matched control mice using flow cytometry. (A) Contour plots depict the percentage of germinal centre B-cells in spleen. (B) Contour plots depict the percentage of eGFP+;IKK2ca+, CAR+;eGFP+;IKK2ca+ and CAR+ as a result of Cγ1cre-dependent recombination for germinal centre B-cells and non germinal centre B-cells. Flow cytometry plots are representative of at least 2 experiments. Histograms depict medians.
Spl (spleen), LN (lymph nodes), B-cells ($CD19^+$), GCB (germinal centre B-cell, $CD19^+$ $CD95^+$ $CD38^-$), nonGCB ($CD19^+$ $CD95^-$ $CD38^+$).

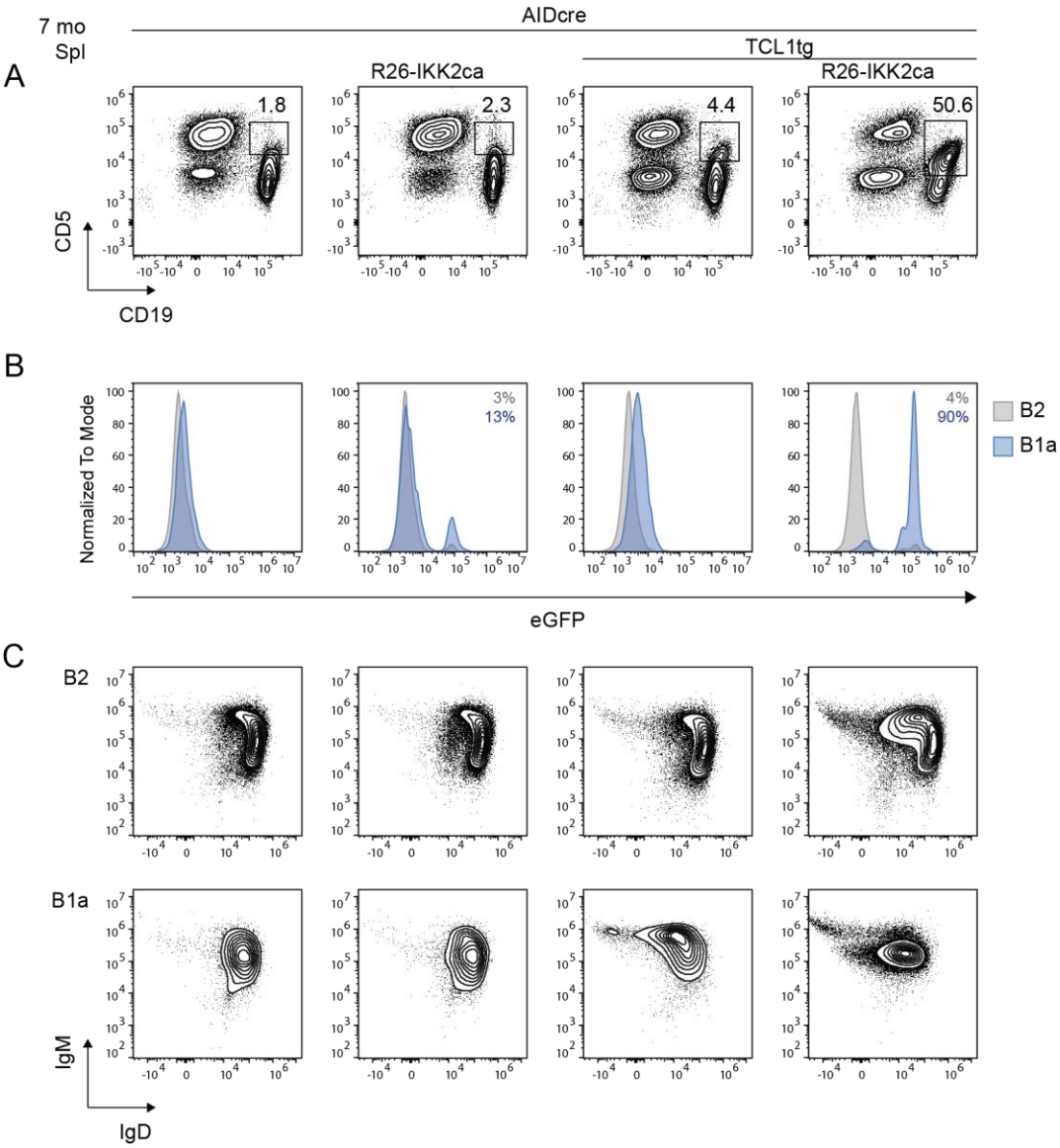


**Figure S 50. Conditional IKK2ca expression by AIDcre co-operates with TCL1tg in splenic B-cells**

*Ex vivo* analysis of TCL1tg R26-IKK2ca AIDcre burdened mice and aged matched controls using flow cytometry. (A) Contour plots depict the percentage of B1a-like cells in spleen. (B) Histograms depict the percentages of eGFP+;IKK2ca+ cells as a result of AIDcre-dependent recombination for B2- (grey) and B1a-like (blue) cells in spleen. (C) Contour plots depict the expression of IgM and IgD in B2- and B1a-like cells. Flow cytometry plots are representative of at least 2 experiments.
Spl (spleen), mo. (months), B2 ($CD19^+$ $B220^+$) and B1a ($CD19^+$ $B220^{lo}$ $CD5^+$).

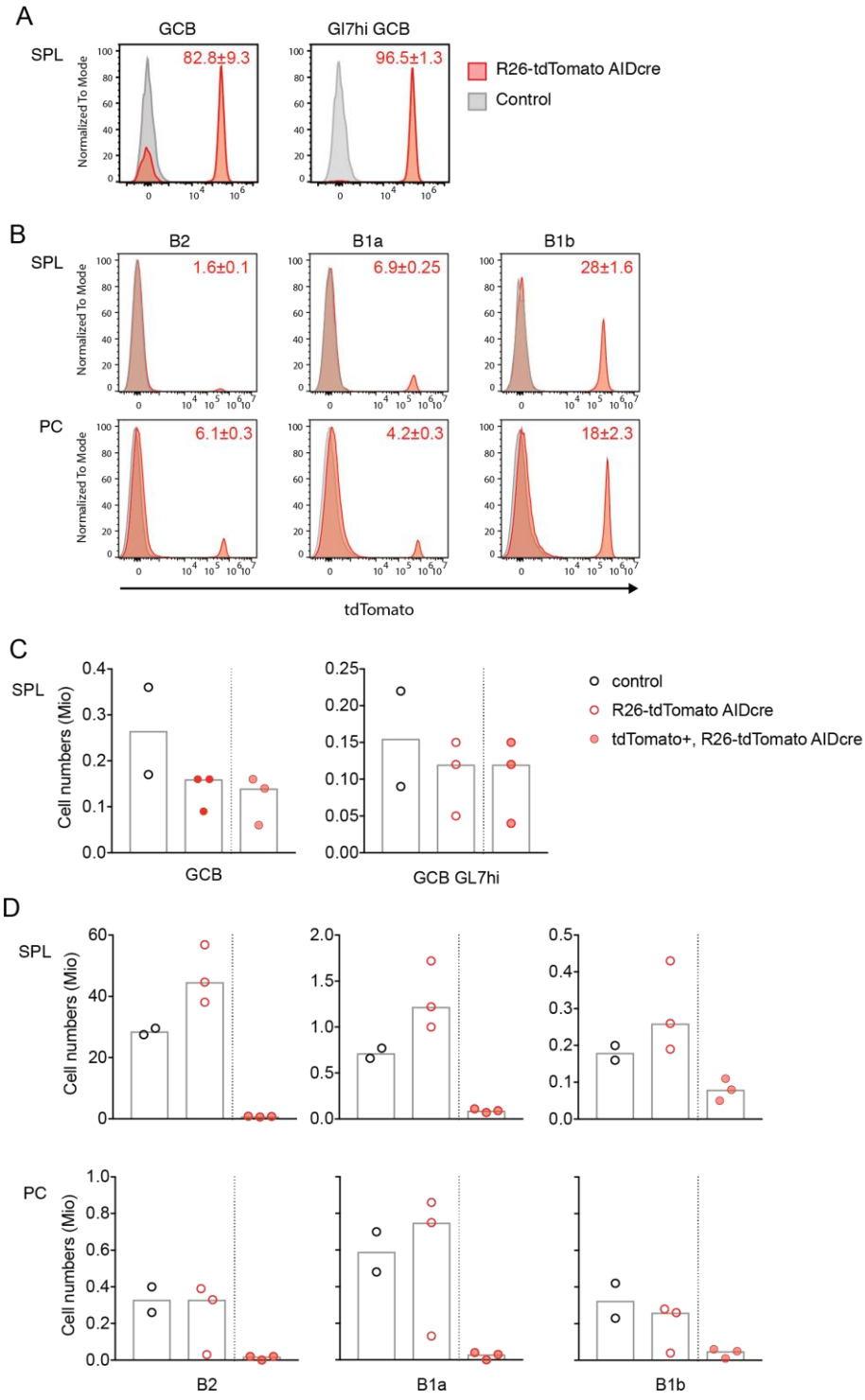


**Figure S 51. AIDcre-depended recombination in GC and B1-cells (Reproduced with permission of C. Steinecke)[262]**

*Ex vivo* analysis of 2-month-old R26-dtTomato AIDcre mice using flow cytometry. Histograms depict the percentages of dtTomato+ cells as a result of AIDcre-dependent recombination in (A) germinal centre cells and GL7hi germinal centre B-cells in the spleen; and (B) the different B-cell subsets in the spleen and peritoneal cavity. Bar charts show the total number and dtTomato+ cells numbers in (C) germinal centres in the spleen; and (D) B-cell subsets present in the spleen and peritoneal cavity. Flow cytometry histograms are representative of 3 biological replicates and data are represented as mean ± SEM. Histograms in bar charts depict medians.

Figure S 51 **(continued).** SPL (spleen), GCB (germinal centre B-cell, $CD19^+$ $CD95^+$ $CD38^-$), GL7hi ($CD19^+$ $CD95^+$ $CD38^-$ $GL7^{hi}$), PC (peritoneal cavity), B2 ($CD19^+$ $B220^+$), B1a ($CD19^+$ $B220^{lo}$ $CD5^+$) and B1b ($CD19^+$ $B220^{lo}$ $CD5^-$).

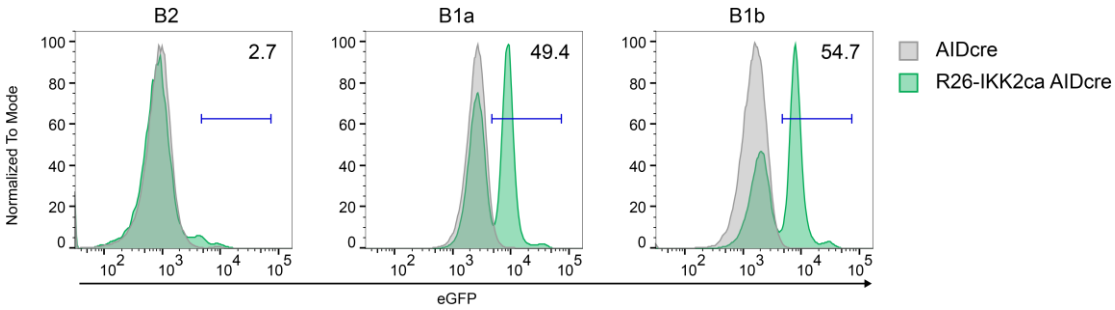


**Figure S 52. eGFP+;IKK2ca+ AIDcre-dependent expression in B1-cells in the peritoneal cavity**

*Ex vivo* analysis of 7-months-old R26-IKK2ca AIDcre and control mice using flow cytometry. Histograms depict the percentages of eGFP+;IKK2ca+ cells as a result of AIDcre-dependent recombination for the different B-cell subsets present in the peritoneal cavity.
B2 ($CD19^+$ $B220^+$), B1 ($CD19^+$ $B220^{lo}$), B1a ($CD19^+$ $B220^{lo}$ $CD5^+$) and B1b ($CD19^+$ $B220^{lo}$ $CD5^-$).

# SUPPLEMENTARY TABLES

**Table S 1. Colony numbers of IgH VDJ rearrangements cloning from wild type samples**

| Sample | Plasmid | Number of white colonies | | | | | |
|---|---|---|---|---|---|---|---|
| | | 10% plate | 90% plate | 100% plate | Total | Picked | Informative |
| 1 | JH1 CS | 300 | 2700 | N.D. | 3000 | 12 | 11 |
| | JH2 CS | 600 | 2300 | N.D. | 2900 | 12 | 12 |
| | JH3 CS | 500 | 2300 | N.D. | 3800 | 12 | 12 |
| | JH4 CS | 600 | 2300 | N.D. | 2900 | 12 | 12 |
| 2 | JH1 CS | 118 | 1000 | N.D. | 1118 | 12 | 12 |
| | JH2 CS | 52 | 349 | N.D. | 401 | 12 | 12 |
| | JH3 CS | 125 | 1000 | N.D. | 1125 | 12 | 11 |
| | JH4 CS | 52 | 450 | N.D. | 502 | 12 | 12 |
| 3 | JH1 CS | N.D. | N.D. | 133 | 133 | 24 | 24 |
| | JH2 CS | N.D. | N.D. | 838 | 838 | 24 | 23 |
| | JH3 CS | N.D. | N.D. | 1057 | 1057 | 24 | 24 |
| | JH4 CS | N.D. | N.D. | 280 | 280 | 24 | 21 |
| 4 | JH1 CS | N.D. | N.D. | 118 | 118 | 24 | 22 |
| | JH2 CS | N.D. | N.D. | 566 | 566 | 24 | 24 |
| | JH3 CS | N.D. | N.D. | 360 | 360 | 24 | 23 |
| | JH4 CS | N.D. | N.D. | 464 | 464 | 24 | 22 |

N.D. Not done

**Table S 2. Analysis of IgH VDJ rearrangements cloned from splenocytes of wild type mouse control 1**

| | Clone | Functionality | VH-gene | DH-gene | JH-gene | Identity (%) | CDR3 length | CDR3 amino acid sequence | Colonies[§] |
|---|---|---|---|---|---|---|---|---|---|
| JH1 CS plasmid | Clone_01 | Productive | V1-85 | D1-2 | JH1 | 98.96 | 14 | CAIITTGSGNWYFDVW | 1 |
| | Clone_02 | Productive | V5-17 | D2-12 | JH1 | 98.96 | 14 | CARHTHYSNPWYFDVW | 1 |
| | Clone_03 | Productive | V1-42 | D1-1 | JH1 | 99.31 | 16 | CARRPPNYYGSSMDFDVW | 1 |
| | Clone_04 | Productive | V1-85 | D2-2 | JH1 | 98.96 | 11 | CARVGYYGYFDVW | 1 |
| | Clone_05 | Productive | V1-54 | D4-1 | JH1 | 92.36 | 12 | CARYLTGTWYFDVW | 1 |
| | Clone_06 | Productive | V1-80 | D3-3 | JH1 | 98.96 | 11 | CASRELYWYFDVW | 1 |
| | Clone_07 | Productive | V5-17 | | JH1 | 99.31 | 7 | CATRYFDVW | 1 |
| | Clone_08 | Productive | V1-15 | D2-3 | JH1 | 98.61 | 13 | CTPIRGDGNWYFDVW | 1 |
| | Clone_09 | Unknown | V1-85 | | | 97.92 | X | | 1 |
| | Clone_10 | Unproductive | V1-85 | D1-1 | JH1 | 94.1 | X | CARGAYGSSYE#WYFDVW | 1 |
| | Clone_11 | Unproductive | V1-39 | D3-3 | JH1 | 98.96 | X | CARRGE*#YWYFDVW | 1 |
| JH2 CS plasmid | Clone_12 | Productive | V1-42 | D2-4 | JH1 | 99.31 | 12 | CARRDYDNWYFDVW | 1 |
| | Clone_13 | Productive | V1-82 | D1-1 | JH1 | 98.96 | 15 | CARSGYYYGSSWYFDVW | 1 |
| | Clone_14 | Unproductive | V1-83 | D1-1 | JH1 | 98.96 | X | CARTTVV#YWYFDVW | 1 |
| | Clone_15 | Unproductive | V5-2 | D1-1 | JH1 | 99.31 | X | CASPLMSSY#YFDVW | 1 |
| | Clone_16 | Productive | V1-81 | D2-2 | JH2 | 96.88 | 12 | CAIGLRRGYYFDYW | 1 |
| | Clone_17 | Productive | V1-81 | D1-1 | JH2 | 98.96 | 8 | CAPTVRGEKW | 1 |
| | Clone_18 | Productive | V1-84 | D2-3 | JH2 | 98.61 | 10 | CARAYDGYFDYW | 1 |
| | Clone_19 | Productive | V1-39 | D1-1 | JH2 | 98.96 | 11 | CARSSSLYYFDYW | 1 |
| | Clone_20 | Productive | V1-82 | D2-3 | JH2 | 98.96 | 9 | CARWLLREDYW | 1 |
| | Clone_21 | Unproductive | V5-2 | D2-5 | JH2 | 98.96 | X | CARRALL**LQLG##YFDYW | 1 |
| | Clone_22 | Unproductive | V5-2 | D1-1 | JH2 | 99.31 | X | CARRGVTTF#YFDYW | 1 |
| | Clone_23 | Unproductive | V1-9 | | JH2 | 98.96 | X | CASNYYGSSY | 1 |
| JH3 CS plasmid | Clone_24 | Productive | V1-82 | D2-5 | JH3 | 98.96 | 13 | CAISYSNYGAWFAYW | 1 |
| | Clone_25 | Productive | V1-4 | D2-4 | JH3 | 98.96 | 13 | CARCGGDYDEGFAYW | 1 |
| | Clone_26 | Productive | V1-26 | D3-3 | JH3 | 93.06 | 9 | CARGGREVAYW | 1 |
| | Clone_27 | Productive | V5-6 (V5-6-1) | D2-3 | JH3 | 99.31 | 15 | CARHRGYDGRHGGFAYW | 1 |
| | Clone_28 | Productive | V1-85 | D1-2 | JH3 | 98.96 | 10 | CATLLRGGFAYW | 1 |
| | Clone_29 | Productive | V10-1 | D3-3 | JH3 | 98.64 | 7 | CVRGDFAYW | 1 |
| | Clone_30 | Unproductive | V1-39 | D1-1 | JH3 | 98.96 | X | CARALYGSS#AWFAYW | 1 |
| | Clone_31 | Unproductive | V1-39 | D2-4 | JH3 | 98.96 | X | CARGDYDR#AWFAYW | 1 |
| | Clone_32 | Unproductive | V1-62-2 (or V1-71) | D1-1 | JH3 | 98.96 | X | CARHEEGFTTVVARG##WFAYW | 1 |
| | Clone_33 | Unproductive | V1-81 | D2-4 | JH3 | 98.96 | X | CARRGIT#AWFAYW | 1 |
| | Clone_34 | Unproductive | V1-67 P | D2-2 | JH3 | 98.96 | X | CARRGY#* | 1 |
| | Clone_35 | Unproductive | V14-4 | D1-1 | JH3 | 99.31 | X | CT*TLYYYG#FAYW | 1 |
| JH4 CS plasmid | Clone_36 | Unproductive | V1-42 | D2-1 | JH2 | 99.31 | X | CARWESLW*LRP#FDYW | 1 |
| | Clone_37 | Productive | V1-80 | D5-5 | JH3 | 97.92 | 10 | CARDDLSSLAYW | 1 |
| | Clone_38 | Productive | V1-80 | D2-4 | JH3 | 98.96 | 13 | CARSKDYDEAWFAYW | 1 |
| | Clone_39 | Unproductive | V1-37 | D2-3 | JH3 | 99.31 | X | CASMMVTTW#AYW | 1 |
| | Clone_40 | Productive | V1-80 | D1-1 | JH4 | 98.96 | 11 | CARGGRRNAMDYW | 1 |
| | Clone_41 | Productive | V1-62-2 (or V1-71) | D2-1 | JH4 | 98.96 | 12 | CARHGGNYRAMDYW | 1 |
| | Clone_42 | Productive | V1-31 | D1-1 | JH4 | 99.31 | 16 | CARSLYYYGSSNYAMDYW | 1 |
| | Clone_43 | Productive | V1-81 | D2-10 | JH4 | 98.96 | 17 | CARSRSSYGNYVLYAMDYW | 1 |
| | Clone_44 | Productive | V1-9 | D2-4 | JH4 | 98.96 | 15 | CARYDYDGGYYYAMDYW | 1 |
| | Clone_45 | Productive | V1-66 | D2-4 | JH4 | 97.22 | 12 | CARYYDYGGAMDYW | 1 |
| | Clone_46 | Productive | V1-66 | D2-3 | JH4 | 98.96 | 12 | CASDGYDGYAMDYW | 1 |
| | Clone_47 | Unproductive | V1-67 P | D2-5 | JH4 | 98.96 | X | CARRR**#YYAMDYW | 1 |

[§] Number of colonies with identical sequences, * Stop codon in CDR3 region, out-of-frame CDR3, # restored frameshift for out-of-frame junctions

**Table S 3. Analysis of IgH VDJ rearrangements cloned from splenocytes of wild type mouse control 2**

| | Clone | Functionality | VH-gene | DH-gene | JH-gene | Identity (%) | CDR3 length | CDR3 amino acid sequence | Colonies[§] |
|---|---|---|---|---|---|---|---|---|---|
| JH1 CS plasmid | Clone_01 | Productive | V1-39 | D2-2 | JH1 | 99.0 | 11 | CARGGYYWYFDVW | 3 |
| | Clone_02 | Productive | V1-80 | D2-3 | JH1 | 99.0 | 13 | CARSGDGYYRYFDVW | 1 |
| | Clone_03 | Productive | V1-42 | D1-1 | JH1 | 99.3 | 13 | CARYYYGRNWYFDVW | 1 |
| | Clone_04 | Productive | V1-80 | D1-1 | JH1 | 99.0 | 12 | CHYYGSSYWYFDVW | 1 |
| | Clone_05 | Unproductive | V5-2 | D2-3 | JH1 | 99.3 | X | CAR*WLLR#YFDVW | 1 |
| | Clone_06 | Unproductive | V1-4 | D1-1 | JH1 | 99.0 | X | CARDKDGYYGR##YFDVW | 1 |
| | Clone_07 | Unproductive | V1-67 P | D6-2 | JH1 | 99.0 | X | CASGL*##WYFDVW | 1 |
| | Clone_08 | Unproductive | V14-2 | | JH1 | 96.5 | 6 | GFRYFDVW | 1 |
| | Clone_09 | Unproductive | V1-27 P | D2-1 | JH1 | 92.3 | 11 | STRQSYYWYFDVW | 1 |
| JH2 CS plasmid | Clone_10 | Productive | V5-17 | D6-3 | JH1 | 99.3 | 11 | CARELPVRYFDVW | 1 |
| | Clone_11 | Unproductive | V3-8 | | JH1 | 99.3 | X | CAR##YFDVW | 1 |
| | Clone_12 | Productive | V1-39 | D2-5 | JH2 | 99.0 | 11 | CAREGYSNYVDYW | 1 |
| | Clone_13 | Productive | V1-42 | D1-1 | JH2 | 99.3 | 11 | CARLGSNYYFDYW | 1 |
| | Clone_14 | Productive | V1-7 | D3-3 | JH2 | 99.0 | 8 | CARSGPFDYW | 1 |
| | Clone_15 | Productive | V1-4 | D1-1 | JH2 | 99.0 | 15 | CARYPLLDYGKGYFDYW | 1 |
| | Clone_16 | Unproductive | V5-17 | | JH2 | 99.3 | X | CA#CGYW | 1 |
| | Clone_17 | Unproductive | V1-63 | D2-3 | JH2 | 95.8 | X | CARASSMMVT#YFDYW | 1 |
| | Clone_18 | Unproductive | V5-2 | | JH2 | 99.3 | X | CARH#YFDYW | 1 |
| | Clone_19 | Unproductive | V5-2 | D4-1 | JH2 | 99.0 | X | CARHGKG#YW | 1 |
| | Clone_20 | Unproductive | V1-9 | D2-2 | JH2 | 99.0 | X | CAYLLWLRRR#FAYW | 1 |
| | Clone_21 | Unproductive | V10-1 | D1-3 | JH2 | 98.6 | X | CVRHKI#FDYW | 1 |
| JH3 CS plasmid | Clone_22 | Productive | V1-39 | D2-4 | JH3 | 95.8 | 8 | CANDYGFAYW | 1 |
| | Clone_23 | Productive | V1-47 | D3-2 | JH3 | 99.0 | 9 | CARGGSWFAYW | 1 |
| | Clone_24 | Productive | V5-17 | D2-5 | JH3 | 99.3 | 12 | CARGYYSNYGFAYW | 1 |
| | Clone_25 | Productive | V1-80 | D1-1 | JH3 | 99.0 | 14 | CARLGYYGSSAWFAYW | 1 |
| | Clone_26 | Productive | V1-67 P | D3-3 | JH3 | 99.0 | 7 | CARRGFAYW | 1 |
| | Clone_27 | Productive | V10-3 | D2-4 | JH3 | 98.6 | 12 | CVRDNYDRTWFAYW | 1 |
| | Clone_28 | Unproductive | V1-67 P | D2-4 | JH3 | 99.0 | 12 | CARDLL*LRRFAYW | 1 |
| | Clone_29 | Unproductive | V4-2 | D2-12 | JH3 | 98.6 | X | CARQG**LL##WFAYW | 1 |
| | Clone_30 | Unproductive | V5-2 | D2-5 | JH3 | 99.3 | X | CARRFYSNY#FAYW | 1 |
| | Clone_31 | Unproductive | V5-2 | D2-2 | JH3 | 99.3 | X | CARRYYGYG#FAYW | 1 |
| | Clone_32 | Unproductive | V5-2 | D4-1 | JH3 | 99.3 | X | CASPPNWD##FAYW | 1 |
| JH4 CS plasmid | Clone_33 | Productive | V1-80 | D2-10 | JH3 | 99.0 | 11 | CAREGVWYPFAYW | 1 |
| | Clone_34 | Productive | V1-42 | D1-1 | JH4 | 99.3 | 13 | CANPGGRSLYAMDYW | 1 |
| | Clone_35 | Productive | V1-39 | D1-1 | JH4 | 99.0 | 13 | CAREDGSNYYAMDYW | 1 |
| | Clone_36 | Productive | V1-84 | D1-1 | JH4 | 98.6 | 16 | CAREGYYYGSSPYAMDYW | 1 |
| | Clone_37 | Productive | V1-47 | D1-1 | JH4 | 99.0 | 12 | CARGSSYYYAMDYW | 1 |
| | Clone_38 | Productive | V1-39 | D2-3 | JH4 | 99.0 | 10 | CARSHDGSMDYW | 1 |
| | Clone_39 | Productive | V1-80 | D2-4 | JH4 | 99.0 | 14 | CARYYDYDGYYAMDYW | 1 |
| | Clone_40 | Productive | V1-47 | D1-1 | JH4 | 99.0 | 14 | CATYGSSSYYYAMDYW | 1 |
| | Clone_41 | Unproductive | V5-2 | D1-1 | JH4 | 97.2 | X | CANLLW**R#AMDYW | 1 |
| | Clone_42 | Unproductive | V5-2 | D2-1 | JH4 | 99.3 | X | CANLLW*RR##AMDYW | 1 |
| | Clone_43 | Unproductive | V5-2 | D3-3 | JH4 | 99.3 | X | CAREEPS##YAMDYW | 1 |
| | Clone_44 | Unproductive | V5-2 | D2-5 | JH4 | 99.3 | 16 | CARHPLL**PHYYAMDYW | 1 |

[§] Number of colonies with identical sequences, * Stop codon in CDR3 region, out-of-frame CDR3, # restored frameshift for out-of-frame junctions

**Table S 4. Analysis of IgH VDJ rearrangements cloned from splenocytes of wild type mouse control 3**

| | Clone | Functionality | VH-gene | DH-gene | JH-gene | Identity (%) | CDR3 length | CDR3 amino acid sequence | Colonies[§] |
|---|---|---|---|---|---|---|---|---|---|
| JH1 CS plasmid | Clone_001 | Productive | V5-17 | D1-1 | JH1 | 99.3 | 15 | CAKVSSTVVEDWYFDVW | 1 |
| | Clone_002 | Productive | V1-7 | D2-1 | JH1 | 99.3 | 11 | CARDGNYWYFYVW | 1 |
| | Clone_003 | Productive | V5-4 | D1-1 | JH1 | 99.3 | 12 | CARDYGSSWYFDVW | 1 |
| | Clone_004 | Productive | V5-4 | D2-3 | JH1 | 99.3 | 13 | CAREGYDGNWYFDVW | 1 |
| | Clone_005 | Productive | V1-82 | D1-1 | JH1 | 99.3 | 15 | CARGDYYGSSYGYFDVW | 2 |
| | Clone_006 | Productive | V1-39 | D1-1 | JH1 | 99.0 | 17 | CARGHYYGSSYFYWYFDVW | 2 |
| | Clone_007 | Productive | V1-81 | D1-1 | JH1 | 99.3 | 10 | CARGRRWYFDVW | 2 |
| | Clone_008 | Productive | V1-82 | D1-1 | JH1 | 98.3 | 16 | CARPITTVVARFGYFDVW | 1 |
| | Clone_009 | Productive | V1-4 | D2-3 | JH1 | 99.0 | 14 | CARSGGYSSYWYFDVW | 1 |
| | Clone_010 | Productive | V1-83 | D1-1 | JH1 | 99.3 | 12 | CARTVATDWYFDVW | 1 |
| | Clone_011 | Productive | V14-2 | D1-1 | JH1 | 99.3 | 13 | CARYYGSSYWYFDVW | 1 |
| | Clone_012 | Productive | V1-22 | D1-1 | JH1 | 99.0 | 13 | CARYYYGSSRYFDVW | 1 |
| | Clone_013 | Productive | V5-17 | D5-7 | JH1 | 99.3 | 12 | CASQAGNYGYFDVW | 1 |
| | Clone_014 | Productive | V1-37 | D1-2 | JH1 | 99.0 | 13 | CGSVSLLRPWYFDVW | 2 |
| | Clone_015 | Productive | V14-4 | D1-3 | JH1 | 99.3 | 11 | CTTRGKYWYFDVW | 1 |
| | Clone_016 | Unproductive | V5-17 | D1-1 | JH1 | 99.3 | X | CAKALLR**##WYFDVW | 1 |
| | Clone_017 | Unproductive | V5-17 | D1-1 | JH1 | 99.3 | X | CARPKITTVVATP#WYFDVW | 1 |
| | Clone_018 | Unproductive | V5-2 | | JH1 | 99.3 | X | CARQ#YFDVW | 1 |
| | Clone_019 | Unproductive | V5-2 | D2-5 | JH1 | 99.3 | X | CASPPTIVT#YWYFDVW | 1 |
| | Clone_020 | Unproductive | V1-27 | D2-1 | JH1 | 92.6 | 17 | STR*RLW*LRGPYWYFDVW | 1 |
| JH2 CS plasmid | Clone_22 | Productive | V14-2 | D5-5 | JH1 | 99.3 | 10 | CARYYLWYFDVW | 1 |
| | Clone_23 | Unproductive | V5-17 | D1-1 | JH1 | 99.3 | X | CARGGTTVVATL##YFDVW | 1 |
| | Clone_24 | Unproductive | V14-2 | D1-1 | JH1 | 99.3 | X | CARGTTVVA#YWYFDVW | 1 |
| | Clone_25 | Unproductive | V1-37 | D2-4 | JH1 | 99.3 | 14 | CARRI*NDYFWYFDVW | 2 |
| | Clone_26 | Productive | V1-39 | D2-4 | JH2 | 99.0 | 15 | CAKEGDYDYDRDYFDYW | 1 |
| | Clone_27 | Productive | V14-1 | D3-2 | JH2 | 99.3 | 11 | CARDSSGFHFDYW | 1 |
| | Clone_28 | Productive | V1-54 | D1-1 | JH2 | 94.0 | 12 | CARNGGYYSYFDYW | 1 |
| | Clone_29 | Productive | V1-19 | D2-5 | JH2 | 99.0 | 15 | CARRGKLDSNSAYFDYW | 1 |
| | Clone_30 | Productive | V1-42 | D1-1 | JH2 | 97.5 | 11 | CARRYYGPLLDHW | 1 |
| | Clone_31 | Productive | V1-82 | D2-1 | JH2 | 98.3 | 11 | CARSPLGNYFDYW | 1 |
| | Clone_32 | Productive | V14-4 | D1-1 | JH2 | 99.3 | 11 | CTRRDYYGRGDYW | 1 |
| | Clone_33 | Productive | V14-4 | D2-1 | JH2 | 99.3 | 9 | CTTNYGNLDYW | 1 |
| | Clone_34 | Unproductive | V1-4 | D2-2 | JH2 | 99.3 | X | CAIKDT#YYFDYW | 1 |
| | Clone_35 | Unproductive | V5-6 (or V5-6-1) | D2-5 | JH2 | 99.3 | X | CARHLL**LR#YFDYW | 1 |
| | Clone_36 | Unproductive | V5-2 | D2-2 | JH2 | 99.0 | X | CARHWGGR#DYW | 1 |
| | Clone_37 | Unproductive | V5-17 | D2-3 | JH2 | 99.3 | X | CARKG*W##YFDYW | 1 |
| | Clone_38 | Unproductive | V5-2 | D2-2 | JH2 | 99.3 | X | CARLWLR##YYFDYW | 2 |
| | Clone_39 | Unproductive | V5-17 | D1-1 | JH2 | 99.3 | X | CARRGGLLR*G#YYFDYW | 1 |
| | Clone_40 | Unproductive | V1-9 | D1-1 | JH2 | 99.3 | X | CARRTTVVAT#FDYW | 1 |
| | Clone_41 | Unproductive | V5-6 (or V5-6-1) | D2-5 | JH2 | 99.3 | X | CARSYYSNT*#FDYW | 1 |
| | Clone_42 | Unproductive | V1-39 | D1-1 | JH2 | 91.5 | X | CPRSLTVVAR#FDCW | 1 |

[§] Number of colonies with identical sequences, * Stop codon in CDR3 region, out-of-frame CDR3, # restored frame shift for out-of-frame junctions

**Table S 4 (continued). Analysis of IgH VDJ rearrangements cloned from splenocytes of wild type mouse control 3**

| | Clone | Functionality | VH-gene | DH-gene | JH-gene | Identity (%) | CDR3 length | CDR3 amino acid sequence | Colonies[§] |
|---|---|---|---|---|---|---|---|---|---|
| JH3 CS plasmid | Clone_43 | Productive | V1-4 | D6-2 | JH1 | 97.2 | 12 | CARRTVVHWYFDVW | 1 |
| | Clone_44 | Productive | V1-81 | D1-1 | JH3 | 99.3 | 15 | CAREDYYYGSSSWFAYW | 2 |
| | Clone_45 | Productive | V1-62 (or V1-71) | D3-3 | JH3 | 99.3 | 10 | CAREGGPWFAYW | 1 |
| | Clone_46 | Productive | V1-9 | D2-5 | JH3 | 99.3 | 13 | CARGAYYSIPWFAYW | 1 |
| | Clone_47 | Productive | V5-17 | D1-1 | JH3 | 99.3 | 11 | CARGITTVVVGYW | 1 |
| | Clone_48 | Productive | V1-62 (or V1-71) | D1-1 | JH3 | 99.3 | 17 | CARHEETYYGSSYAWFAYW | 1 |
| | Clone_49 | Productive | V1-81 | D1-1 | JH3 | 99.3 | 16 | CARRWSFTTVVAPYFDYW | 2 |
| | Clone_50 | Productive | V1-9 | D1-1 | JH3 | 99.3 | 13 | CARYYYGSSYVFDYW | 1 |
| | Clone_51 | Productive | V1-85 | D3-1 | JH3 | 99.3 | 8 | CASLGGFAYW | 1 |
| | Clone_52 | Productive | V14-4 | D1-1 | JH3 | 99.3 | 12 | CTIRYYGSSYEDYW | 1 |
| | Clone_53 | Productive | V14-4 | D1-1 | JH3 | 99.3 | 12 | CTTNYYGSSWFAYW | 1 |
| | Clone_54 | Productive | V14-4 | D1-1 | JH3 | 99.3 | 13 | CTTPYYGSSYWFAYW | 1 |
| | Clone_55 | Unproductive | V1-9 | D2-3 | JH3 | 99.3 | X | CANDGYYV#FAYW | 1 |
| | Clone_56 | Unproductive | V5-2 | D2-5 | JH3 | 99.0 | X | CARL**#FDYW | 1 |
| | Clone_57 | Unproductive | V5-2 | D5-7 | JH3 | 99.3 | X | CARLLYSA#FAYW | 1 |
| | Clone_58 | Unproductive | V5-17 | D3-2 | JH3 | 99.3 | X | CAST##AYW | 3 |
| | Clone_59 | Unproductive | V14-4 | D1-1 | JH3 | 99.3 | X | CTT*LLR**LQ#WFAYW | 1 |
| | Clone_60 | Unproductive | V10-1 | D3-2 | JH3 | 98.6 | X | CVRRHY#AWFAYW | 1 |
| JH4 CS plasmid | Clone_061 | Productive | V1-9 | D2-1 | JH2 | 99.3 | 10 | CARTIDYGPDYW | 1 |
| | Clone_062 | Productive | V1S26 | | JH3 | 94.7 | 11 | CAREGYSNYFAYW[=] | 1 |
| | Clone_063 | Productive | V1-85 | D2-1 | JH3 | 99.3 | 12 | CARVDLLRAWFAYW | 1 |
| | Clone_064 | Unproductive | V14-1 | D2-2 | JH3 | 99.0 | X | CIILLWLRR#FAYW | 1 |
| | Clone_065 | Productive | V1-81 | D5-7 | JH4 | 99.3 | 10 | CAGPIYSAADSW | 1 |
| | Clone_066 | Productive | V1-82 | D1-1 | JH4 | 99.3 | 11 | CARGSYLYAMDYW | 1 |
| | Clone_067 | Productive | V1-39 | D1-1 | JH4 | 99.0 | 14 | CARIYYGSSYDGMDYW | 1 |
| | Clone_068 | Productive | V1-85 | D1-1 | JH4 | 99.3 | 9 | CARKVVSMDYW | 1 |
| | Clone_069 | Productive | V1-7 | D1-2 | JH4 | 99.3 | 12 | CARLLGLYYAMDYW | 1 |
| | Clone_070 | Productive | V1-82 | D2-1 | JH4 | 99.3 | 14 | CARRDGNPFYYAMDYW | 1 |
| | Clone_071 | Productive | V14-2 | D1-1 | JH4 | 99.3 | 14 | CARRDYYGSYYAMDYW | 1 |
| | Clone_072 | Productive | V1-54 | D2-4 | JH4 | 99.3 | 17 | CARREPIYYDSYYYAMDYW | 1 |
| | Clone_073 | Productive | V1-69 | D1-2 | JH4 | 98.3 | 11 | CARRLRYYAMDYW | 1 |
| | Clone_074 | Productive | V1-39 | D2-12 | JH4 | 99.3 | 10 | CARRSFTSMDYW | 1 |
| | Clone_075 | Productive | V1-39 | D2-3 | JH4 | 97.9 | 12 | CARSPDGYSAMDYW[¶] | 2 |
| | Clone_076 | Productive | V1-7 | D2-3 | JH4 | 99.3 | 9 | CASNERAMDYW | 1 |
| | Clone_077 | Unproductive | V5-6 (or V5-6-1) | | JH4 | 99.3 | X | CAK#YW | 1 |
| | Clone_078 | Unproductive | V5-2 | D2-2 | JH4 | 99.3 | X | CARGATMVTTG#YYYAMDYW | 1 |
| | Clone_079 | Unproductive | V1-67 | | JH4 | 99.3 | X | CARK#AMDYW | 1 |
| | Clone_080 | Unproductive | V5-2 | D4-1 | JH4 | 99.3 | X | CARPPTGT#YYAMDYW | 1 |

[§] Number of colonies with identical sequences, * Stop codon in CDR3 region, out-of-frame CDR3, # restored frame shift for out-of-frame junctions,
[=] IMGT/Junction Analysis gives no results for this JUNCTION, [¶] Same CDR3 AA sequence, VH-gene gDNA sequence differs in 3 bases (99% identical)

**Table S 5. Analysis of IgH VDJ rearrangements cloned from splenocytes of wild type mouse control 4**

| | Clone | Functionality | VH-gene | DH-gene | JH-gene | Identity (%) | CDR3 length | CDR3 amino acid sequence | Colonies[§] |
|---|---|---|---|---|---|---|---|---|---|
| JH1 CS plasmid | Clone_01 | Productive | V3-8 | D2-4 | JH1 | 99.3 | 11 | CARFDYHWYFDVW | 1 |
| | Clone_02 | Productive | V1-62-2 (or V1-71) | D1-1 | JH1 | 98.96 | 14 | CARHEAGSSLWYFDVW | 1 |
| | Clone_03 | Productive | V1-62-2 (or V1-71) | D2-4 | JH1 | 98.96 | 14 | CARHEGYDYDGYFDVW | 1 |
| | Clone_04 | Productive | V1-62-2 (or V1-71) | D2-4 | JH1 | 98.95 | 17 | CARHEQGPLYDYDWYFDVW | 1 |
| | Clone_05 | Productive | V1-9 | D1-1 | JH1 | 98.96 | 15 | CARPYYYGSTNWYFDVW | 2 |
| | Clone_06 | Productive | V5-17 | D2-3 | JH1 | 99.31 | 16 | CARRGIYDGYYDWYFDVW | 2 |
| | Clone_07 | Productive | V1-85 | D2-2 | JH1 | 98.26 | 14 | CARRGKWLPYWYFDVW[¶] | 2 |
| | Clone_08 | Productive | V1-20 (or V1-39) | D2-10 | JH1 | 53.78[+] | 12 | CARSDDGDWYFDVW[+] | 4 |
| | Clone_09 | Productive | V1-39 (or V1S135) | D2-10 | JH1 | 94.44 | 13 | CARSSYGNYWYFDVW | 2 |
| | Clone_10 | Productive | V5-2 | D1-1 | JH1 | 99.31 | 12 | CARTGSSYWYFDVW | 1 |
| | Clone_11 | Productive | V14-1 | D2-14 | JH1 | 99.31 | 9 | CTTVGTDFDVW | 2 |
| | Clone_12 | Unproductive | V2-9 | D1-1 | JH1 | 94.39 | 17 | CARNPLLLLR**LRYFDVW | 1 |
| | Clone_13 | Unproductive | V5-2 | D2-2 | JH1 | 99.31 | 16 | CARQRGLLW*GGWYFDVW | 1 |
| | Clone_14 | Unproductive | V1-27 P | D2-3 | JH1 | 92.33 | X | STRFGGYYV#WYFDVW | 1 |
| JH2 CS plasmid | Clone_15 | Productive | V1-81 | D1-1 | JH1 | 98.96 | 15 | CARDYYGSSWGWYFDVW | 1 |
| | Clone_16 | Productive | V1-67 | D1-1 | JH1 | 98.96 | 14 | CARFYYGSSYWYFDVW | 1 |
| | Clone_17 | Unproductive | V1-66 | D2-5 | JH1 | 98.96 | X | CAR*GSIVTT#YWYFDVW | 1 |
| | Clone_18 | Productive | V1-42 | D1-1 | JH2 | 99.3 | 11 | CAILITTVVAPLW | 1 |
| | Clone_19 | Productive | V1-9 | D2-4 | JH2 | 98.96 | 15 | CALYYDYDEGFYYFDYW | 1 |
| | Clone_20 | Productive | V1-9 | D1-1 | JH2 | 98.96 | 11 | CAREDYYGSSHYW | 1 |
| | Clone_21 | Productive | V1-9 | D2-5 | JH2 | 98.96 | 12 | CARGGYSKYYFDYW | 2 |
| | Clone_22 | Productive | V1-62-2 (or V1-71) | D2-14 | JH2 | 98.96 | 13 | CARHEDRSRGAFDYW | 1 |
| | Clone_23 | Productive | V1-62-2 (or V1-71) | D1-1 | JH2 | 98.96 | 16 | CARHEEGYYGSSSYFDYW | 1 |
| | Clone_24 | Productive | V5-17 | D1-1 | JH2 | 99.31 | 10 | CARPTTVGFDYW | 1 |
| | Clone_25 | Productive | V1-9 | D2-5 | JH2 | 98.96 | 15 | CARRGYSNYGGYYFDYW | 1 |
| | Clone_26 | Productive | V5-6 (or V5-6-1) | | JH2 | 99.31 | 7 | CARRVFDYW | 1 |
| | Clone_27 | Productive | V1-80 | D3-3 | JH2 | 98.96 | 12 | CARSGPSKRYFDYW | 1 |
| | Clone_28 | Productive | V1S34 | | JH2 | 100 | 9 | CARSRGNPDYW[=] | 1 |
| | Clone_29 | Productive | V14-4 | D2-5 | JH2 | 99.31 | 12 | CTTSPYSNYEGYYW | 3 |
| | Clone_30 | Productive | V14-4 | D3-3 | JH2 | 99.31 | 11 | CTTWEIEGYFDYW | 2 |
| | Clone_31 | Unproductive | V3-8 | D2-5 | JH2 | 99.3 | X | CARDYSNP#YFDYW | 1 |
| | Clone_32 | Unproductive | V5-2 | D2-3 | JH2 | 99.31 | 11 | CARS*WLLLFDYW | 1 |
| | Clone_33 | Unproductive | V5-6 (or V5-6-1) | D1-1 | JH2 | 97.21 | X | PGP#FDYW[∞] | 2 |

[§] Number of colonies with identical sequences, * Stop codon in CDR3 region, out-of-frame CDR3, # restored frame shift for out-of-frame junctions, [¶] Same CDR3 AA sequence, VH-gene gDNA sequence differs in 3 bases (99% identical), [+] Insert had only 85 bp, Identical genomic DNA sequence and CDR3 amino acid sequence, but different CS plasmid, [=] IMGT/Junction Analysis gives no results for this JUNCTION, [∞] Sequence difference, one base deletion/insertion

**Table S 5 (continued). Analysis of IgH VDJ rearrangements cloned from splenocytes of wild type mouse control 4**

| | Clone | Functionality | VH-gene | DH-gene | JH-gene | Identity (%) | CDR3 length | CDR3 amino acid sequence | Colonies[§] |
|---|---|---|---|---|---|---|---|---|---|
| JH3 CS plasmid | Clone_15 | Productive | V1-81 | D1-1 | JH1 | 98.96 | 15 | CARDYYGSSWGWYFDVW | 1 |
| | Clone_34 | Productive | V1-47 | D3-1 | JH2 | 98.96 | 11 | CARREYSYYFDYW | 1 |
| | Clone_35 | Productive | V1-80 | D2-4 | JH3 | 98.96 | 10 | CAGGLRRGFDYW | 1 |
| | Clone_36 | Productive | V14-2 | D3-2 | JH3 | 99.31 | 12 | CARDTAQATRFAYW | 1 |
| | Clone_37 | Productive | V1-62-2 (or V1-71) | D2-2 | JH3 | 98.96 | 20 | CARHEEEGIYYGYDEEAWFAYW | 2 |
| | Clone_38 | Productive | V14-2 | D2-3 | JH3 | 99.31 | 11 | CARLDGYYEFAYW | 1 |
| | Clone_39 | Productive | V1-42 | D3-3 | JH3 | 99.31 | 7 | CARRGFAYW | 1 |
| | Clone_40 | Productive | V1-7 | D1-1 | JH3 | 98.96 | 17 | CARSGDYYGSSYPAWFAYW | 1 |
| | Clone_41 | Productive | V1-82 | D1-1 | JH3 | 98.96 | 11 | CARSRDYGSSPYW | 1 |
| | Clone_42 | Productive | V1-67 | D1-2 | JH3 | 98.96 | 8 | CARWGLGYYW | 1 |
| | Clone_43 | Productive | V14-4 | D3-2 | JH3 | 99.31 | 10 | CTTPQATGFAYW | 1 |
| | Clone_44 | Productive | V14-4 | D2-1 | JH3 | 98.96 | 13 | CTTYSYGKGVWFAYW | 1 |
| | Clone_45 | Unproductive | V5-2 | D2-13 | JH3 | 99.31 | X | CAGYYGGY#YW | 2 |
| | Clone_46 | Unproductive | V1-4 | D4-1 | JH3 | 98.96 | X | CAPAGTL#WFAYW | 1 |
| | Clone_47 | Unproductive | V1-37 | D1-1 | JH3 | 99.31 | 8 | CARGGG*NYW | 1 |
| | Clone_48 | Unproductive | V5-2 | D2-2 | JH3 | 99.31 | X | CARPLLLWLRS#AWFAYW | 1 |
| | Clone_49 | Unproductive | V5-6 (or V5-6-1) | D2-2 | JH3 | 99.31 | X | CARQSTMVTT#VAYW | 2 |
| | Clone_50 | Unproductive | V5-2 | D1-1 | JH3 | 99.31 | X | CARRGVTTR#YW | 1 |
| | Clone_51 | Unproductive | V2-6 (or V2-6-8) | D1-1 | JH3 | 99.3 | X | CARVLLR**L#FAYW | 1 |
| | Clone_52 | Unproductive | V14-1 | D1-1 | JH3 | 99.31 | X | CT*LLLLR**L*#YW | 1 |
| JH4 CS plasmid | Clone_53 | Productive | V1-7 | D2-5 | JH3 | 98.96 | 15 | CARPNYSNYVRTWFAYW | 1 |
| | Clone_54 | Productive | V1-82 | D2-2 | JH3 | 98.96 | 10 | CASGTGSWFAYW | 1 |
| | Clone_55 | Productive | V1-67 | D1-1 | JH4 | 97.92 | 5 | CAIYFYW | 1 |
| | Clone_56 | Productive | V2-9 | D1-1 | JH4 | 98.95 | 16 | CAKHHYYGSSYGYAMDYW | 1 |
| | Clone_57 | Productive | V1-85 | D2-4 | JH4 | 98.96 | 13 | CAREITTRYYAMDYW | 1 |
| | Clone_58 | Productive | V1-63 | D1-1 | JH4 | 98.96 | 12 | CARGGGYYYAMDYW | 1 |
| | Clone_59 | Productive | V1-20 | D1-1 | JH4 | 98.96 | 10 | CARGGNYAMDYW | 1 |
| | Clone_60 | Productive | V1-5 | D2-10 | JH4 | 97.57 | 12 | CARGGYGNYAMDYW[$] | 1 |
| | Clone_61 | Productive | V1-81 | D2-10 | JH4 | 98.96 | 12 | CARGGYGNYAMDYW[$] | 1 |
| | Clone_62 | Productive | V14-2 | D1-1 | JH4 | 99.31 | 12 | CARGGYYGYAMDYW | 1 |
| | Clone_63 | Productive | V1-54 | D3-3 | JH4 | 98.96 | 11 | CARGLANYAMDYW | 1 |
| | Clone_64 | Productive | V1-9 | D4-1 | JH4 | 96.88 | 11 | CARYWDVYAMDYW | 1 |
| | Clone_65 | Productive | V14-2 | D6-2 P | JH4 | 99.31 | 11 | CASAYSLYAMDYW | 2 |
| | Clone_66 | Productive | V1-36 | D1-2 | JH4 | 96.18 | 10 | CASNDGGAMDYW | 1 |
| | Clone_67 | Productive | V1-83 | D3-1 | JH4 | 97.57 | 10 | CASPGYYAMDYW | 1 |
| | Clone_68 | Productive | V1-14 | D4-1 | JH4 | 98.61 | 9 | CATTGDAMDYW | 1 |
| | Clone_69 | Unproductive | V1-9 | D1-1 | JH4 | 98.96 | X | CAIGYYYGSSP#YAMDYW | 1 |
| | Clone_70 | Unproductive | V5-2 | D2-1 | JH4 | 99.31 | 14 | CARHG*LHTYYAMDYW | 1 |
| | Clone_71 | Unproductive | V5-6 (or V5-6-1) | D2-5 | JH4 | 99.31 | X | CARPSNG#AMDYW | 1 |
| | Clone_72 | Unproductive | V1-47 | D2-5 | JH4 | 98.96 | X | CPYSNYE#YYAMDYW | 1 |
| | Clone_73 | Unproductive | V1-63 | D2-1 | JH4 | 97.57 | 12 | ST**LPHYYAMDYW | 1 |

[§] Number of colonies with identical sequences, * Stop codon in CDR3 region, out-of-frame CDR3, # restored frame shift for out-of-frame junctions, Identical CDR3 and genomic DNA sequence, but different Vector, [$] Same CDR3 amino acid sequence, but different VH-gene,

**Table S 6. Colony numbers of IgH VDJ rearrangements cloning from splenocytes of TCL1tg CD19cre burdened mice**

| Mouse ID | Plasmid | Number of white colonies | | | | |
|---|---|---|---|---|---|---|
| | | 10% plate | 90% plate | Total | Picked | Informative |
| CLL_32284 | JH1 CS | N.D. | N.D. | 700 | 8 | 8 |
| | JH2 CS | N.D. | N.D. | 800 | 8 | 8 |
| | JH3 CS | N.D. | N.D. | 2800 | 8 | 8 |
| | JH4 CS | N.D. | N.D. | 1400 | 8 | 7 |
| CLL_00425 | JH1 CS | N.D. | N.D. | N.D. | N.D. | N.D. |
| | JH2 CS | N.D. | N.D. | 1137 | 30 | 30 |
| | JH3 CS | N.D. | N.D. | 93 | 30 | 30 |
| | JH4 CS | N.D. | N.D. | N.D. | N.D. | N.D. |

N.D. Not done

**Table S 7. Colony numbers of IgH VDJ rearrangements cloning from splenocytes of TCL1tg R26-IKK2ca CD19cre burdened mice**

| Mouse ID | Plasmid | Number of white colonies | | | | |
|---|---|---|---|---|---|---|
| | | 10% plate | 90% plate | Total | Picked | Informative |
| CLL_01140 | JH1 CS | N.D. | N.D. | 7 | 6 | 6 |
| | JH2 CS | N.D. | N.D. | N.D. | N.D. | N.D. |
| | JH3 CS | N.D. | N.D. | N.D. | N.D. | N.D. |
| | JH4 CS | N.D. | N.D. | 91 | 30 | 30 |
| CLL_32100 | JH1 CS | N.D. | N.D. | 3600 | 10 | 10 |
| | JH2 CS | N.D. | N.D. | 7000 | 10 | 8 |
| | JH3 CS | N.D. | N.D. | 500 | 10 | 10 |
| | JH4 CS | N.D. | N.D. | 130 | 10 | 10 |
| CLL_32351 | JH1 CS | N.D. | N.D. | 800 | 8 | 8 |
| | JH2 CS | N.D. | N.D. | N.D. | N.D. | N.D. |
| | JH3 CS | N.D. | N.D. | N.D. | N.D. | N.D. |
| | JH4 CS | N.D. | N.D. | N.D. | N.D. | N.D. |
| CLL_31937 | JH1 CS | N.D. | N.D. | N.D. | N.D. | N.D. |
| | JH2 CS | N.D. | N.D. | 5000 | 8 | 8 |
| | JH3 CS | N.D. | N.D. | 500 | N.D. | N.D. |
| | JH4 CS | N.D. | N.D. | N.D. | N.D. | N.D. |
| CLL_32371 | JH1 CS | 500 | 2500 | 3000 | 8 | 7 |
| | JH2 CS | 600 | 2500 | 3100 | 8 | 8 |
| | JH3 CS | 300 | 2500 | 2800 | 8 | 8 |
| | JH4 CS | 144 | 450 | 594 | 8 | 8 |
| CLL_31938 | JH1 CS | N.D. | N.D. | 400 | 8 | 7 |
| | JH2 CS | N.D. | N.D. | 900 | 8 | 7 |
| | JH3 CS | N.D. | N.D. | 2600 | 8 | 7 |
| | JH4 CS | N.D. | N.D. | 200 | 8 | 8 |

N.D. Not done

**Table S 8. Colony numbers of IgH VDJ rearrangements cloning from splenocytes of TCL1tg R26-IKK2ca/ca CD19cre burdened mice**

| Mouse ID | Plasmid | Number of white colonies | | | | |
|---|---|---|---|---|---|---|
| | | 10% plate | 90% plate | Total | Picked | Informative |
| CLL_32299 | JH1 CS | N.D. | N.D. | 250 | 10 | 10 |
| | JH2 CS | N.D. | N.D. | 500 | 10 | 10 |
| | JH3 CS | N.D. | N.D. | 450 | 10 | 10 |
| | JH4 CS | N.D. | N.D. | 110 | 10 | 10 |
| CLL_32274 | JH1 CS | N.D. | N.D. | 115 | 12 | 12 |
| | JH2 CS | N.D. | N.D. | 22 | 12 | 10 |
| | JH3 CS | N.D. | N.D. | 14 | 12 | 10 |
| | JH4 CS | N.D. | N.D. | 19 | 12 | 7 |
| CLL_32987 | JH1 CS | 345 | 2000 | 2345 | 12 | 11 |
| | JH2 CS | 350 | 2900 | 3250 | 12 | 12 |
| | JH3 CS | 500 | 2000 | 2500 | 12 | 12 |
| | JH4 CS | 400 | 2100 | 2500 | 12 | 11 |

N.D. Not done

# SUPPLEMENTAL METHODS

Genotyping PCR for CD19cre

The PCR reaction was done using homemade Taq, the 10X PCR Buffer with 15mM $MgCl_2$ (Metabion), 0.4mM dNTPs (Invitrogen, US), 1mM $MgCl_2$, 0.08μM of each primer, Ampuwa water and 1μL of genomic DNA. Thermal cycling conditions were:

| | | |
|---|---|---|
| Initial denaturation | 95° C x 3min | |
| Denaturation | 95° C x 30s | |
| Annealing | ***60° C x 30s*** | X 35 cycles |
| Extension | 72° C x 50s | |
| Final extension | 72° C x 2min | |
| | 10° C hold | |

Genotyping PCR for Cγ1cre PCR

The PCR reaction was done using Metabion Taq (Metabion), the 10X PCR Buffer with 1.5mM $MgCl_2$ (Metabion), 0.2mM dNTPs (Takara, US), 1mM $MgCl_2$, 0.08μM of each primer, Ampuwa water and 1μL of genomic DNA. Thermal cycling conditions were:

| | | |
|---|---|---|
| Initial denaturation | 94° C x 2 min | |
| Denaturation | 94° C x 60 s | |
| Annealing | ***65° C x 60 s*** | X 35 cycles |
| Extension | 72° C x 30 s | |
| Final extension | 72° C x 15min | |
| | 10° c hold | |

Genotyping PCR for Rosa26-Knock-in

The PCR reaction was done using homemade Taq, the 10X PCR Buffer with 1.5mM $MgCl_2$ (Metabion), 0.2mM dNTPs (Takara, US), 1mM $MgCl_2$, 0.08μM of each primer, Ampuwa water and 1μL of genomic DNA. Thermal cycling conditions were:

| | | | |
|---|---|---|---|
| Initial denaturation | 95° C x 3 min | | |
| Denaturation | 95° C x 30 s | | |
| Annealing | ***68° C x 30 s*** | -1º C/step | X 12 cycles |
| Extension | 72° C x 30 s | | |
| Denaturation | 95° C x 30 s | | |
| Annealing | ***56° C x 30 s*** | | X 20 cycles |
| Extension | 72° C x 20 s | | |
| Final extension | 72° C x 5min | | |
| | 10° c hold | | |

Genotyping PCR for R26-CAR:

The PCR reaction was done using homemade Taq, the 10X PCR Buffer with 1.5mM $MgCl_2$ (Metabion), 0.2mM dNTPs (Takara, US), 1mM $MgCl_2$, 0.08µM of each primer, Ampuwa water and 1µL of genomic DNA. Thermal cycling conditions were:

| | | | |
|---|---|---|---|
| Initial denaturation | 95° C x 3 min | | |
| Denaturation | 95° C x 30 s | | |
| Annealing | ***69° C x 30 s*** | -1º C/step | X 10 cycles |
| Extension | 72° C x 60 s | | |
| Denaturation | 95° C x 30 s | | |
| Annealing | ***59° C x 30 s*** | | X 20 cycles |
| Extension | 72° C x 20 s | | |
| Final extension | 72° C x 5min | | |
| | 10° c hold | | |

Genotyping PCR for TCL1tg:

The PCR reaction was done using homemade Taq, the 10X PCR Buffer with 1.5mM $MgCl_2$ (Metabion), 0.2mM dNTPs (Takara, US), 1mM $MgCl_2$, 0.08µM of each primer, Ampuwa water and 1µL of genomic DNA. Thermal cycling conditions were:

| | | |
|---|---|---|
| Initial denaturation | 95° C x 5 min | |
| Denaturation | 95° C x 45 s | |
| Annealing | ***54° C x 45 s*** | X 35 cycles |
| Extension | 72° C x 60 s | |
| Final extension | 72° C x 5 min | |
| | 10° c hold | |

Genotyping A20 PCR

The PCR reaction was done using homemade Taq, the 10X PCR Buffer with 1.5mM $MgCl_2$ (Metabion), 04mM dNTPs (Invitrogen, US), 0.08µM of each primer, Ampuwa water and 1ul of genomic DNA. Thermal cycling conditions were:

| | | |
|---|---|---|
| Initial denaturation | 95° C x 3 min | |
| Denaturation | 95° C x 30 s | |
| Annealing | ***65° C x 30 s*** | X 10 cycles |
| Extension | 72° C x 60 s | |
| Denaturation | 95° C x 30 s | |
| Annealing | ***55° C x 30 s*** | X 20 cycles |
| Extension | 72° C x 60 s | |
| Final extension | 72° C x 5min | |
| | 10° C hold | |

Genotyping PCR for PKCβ-KO

The PCR reaction was done using homemade Taq, the 10X PCR Buffer with 1.5mM $MgCl_2$ (Metabion), 04mM dNTPs (Invitrogen, US), 0.08μM of each primer, Ampuwa water and 1ul of genomic DNA. Thermal cycling conditions were:

| | | |
|---|---|---|
| Initial denaturation | 94° C x 5 min | |
| Denaturation | 94° C x 30 s | |
| Annealing | ***58° C x 30 s*** | X 40 cycles |
| Extension | 72° C x 60 s | |
| Final extension | 72° C x 10min | |
| | 10° c hold | |

Plasmids used for Quick and Clean (QC) cloning

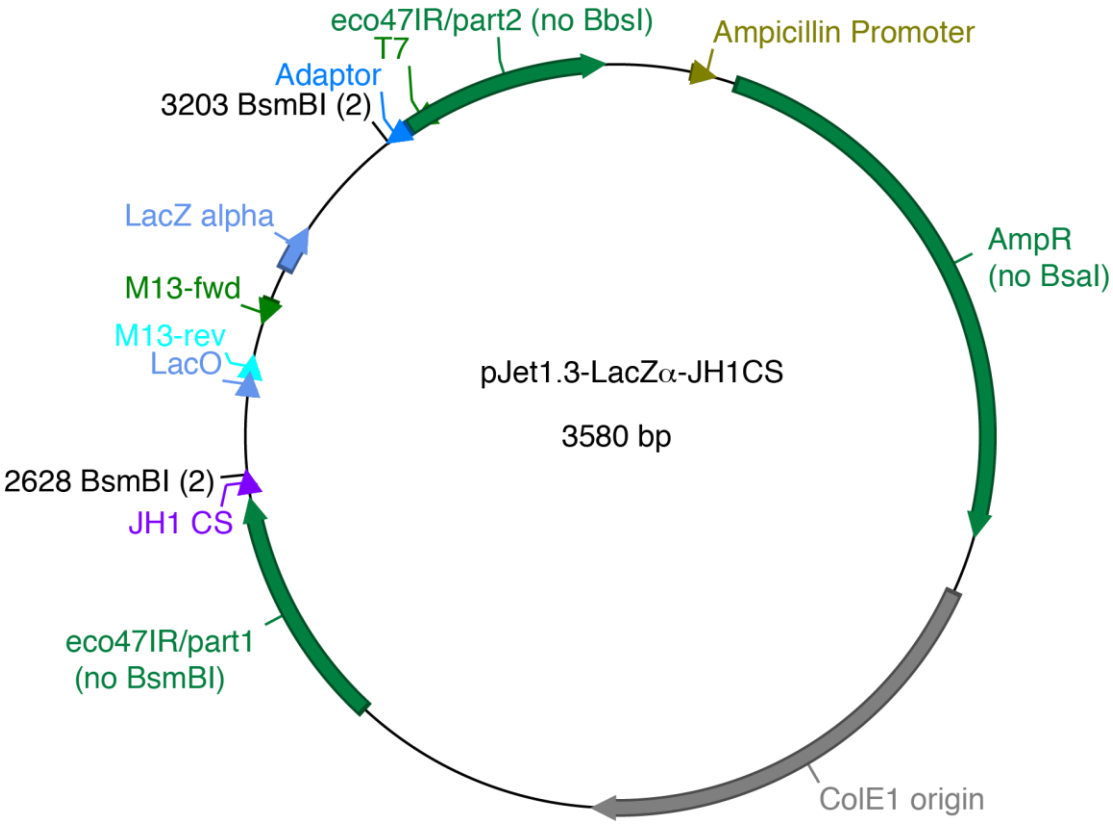


> pJet1.3-LacZα-JH1CS

ggcctcgtgatacgcctatttttataggttaatgtcatgataataatggtttcttagacgtcaggtggcacttttcggggaaatgtgcgcggaacccctatttgtttatttttctaa
atacattcaaatatgtatccgctcatgagacaataaccctgataaatgcttcaataatattgaaaaaggaagagtatgagtattcaacatttccgtgtcgcccttattcccctt
ttttgcggcattttgccttcctgtttttgctcacccagaaacgctggtgaaagtaaaagatgctgaagatcagttgggtgcacgagtgggttacatcgaactggatctcaac
agcggtaagatccttgagagttttcgccccgaagaacgttttccaatgatgagcacttttaaagttctgctatgtggcgcggtattatcccgtattgacgccgggcaagag
caactcggtcgccgcatacactattctcagaatgacttggttgagtactcaccagtcacagaaaagcatcttacggatggcatgacagtaagagaattatgcagtgct
gccataaccatgagtgataacactgcggccaacttacttctgacaacgatcggaggaccgaaggagctaaccgctttttgcacaacatgggggatcatgtaactcg
ccttgatcgttgggaaccggagctgaatgaagccataccaaacgacgagcgtgacaccacgatgcctgtagcaatggcaacaacgttgcgcaaactattaactgg
cgaactacttactctagcttcccggcaacaattaatagactggatggaggcggataaagttgcaggaccacttctgcgctcggcccttccggctggctggtttattgctg
ataaatctggagccggtgagcgtggttctcgcggtatcattgcagcactggggccagatggtaagccctcccgtatcgtagttatctacacgacggggagtcaggca
actatggatgaacgaaatagacagatcgctgagataggtgcctcactgattaagcattggtaactgtcagaccaagtttactcatatatactttagattgatttaaaacttc
atttttaatttaaaaggatctaggtgaagatccttttgataatctcatgaccaaaatcccttaacgtgagttttcgttccactgagcgtcagaccccgtagaaaagatcaaa
ggatcttcttgagatcctttttttctgcgcgtaatctgctgcttgcaaacaaaaaaaccaccgctaccagcggtggtttgtttgccggatcaagagctaccaactcttttccg
aaggtaactggcttcagcagagcgcagataccaaatactgtccttctagtgtagccgtagttaggccaccacttcaagaactctgtagcaccgcctacatacctcgctc
tgctaatcctgttaccagtggctgctgccagtggcgataagtcgtgtcttaccgggttggactcaagacgatagttaccggataaggcgcagcggtcgggctgaacgg
ggggttcgtgcacacagcccagcttggagcgaacgacctacaccgaactgagatacctacagcgtgagctatgagaaagcgccacgcttcccgaagggagaaa
ggcggacaggtatccggtaagcggcagggtcggaacaggagagcgcacgagggagcttccagggggaaacgcctggtatctttatagtcctgtcgggtttcgcca
cctctgacttgagcgtcgatttttgtgatgctcgtcaggggggcggagcctatggaaaaacgccagcaacgcggcctttttacggttcctggccttttgctggccttttgctc
acatgttctttcctgcgttatcccctgattctgtggataaccgtattaccgcctttgagtgagctgataccgctcgccgcagccgaacgaccgagcgcagcgagtcagtg
agcgaggaagcggaagagcgcccaatacgcaaaccgcctctccccgcgcgttggccgattcattaatgcagctggcacgacaggtttcccgactggaaagcaatt
ggcagtgagcgcaacgcaattaatgtgagttagctcactcattaggcaccccaggctttacactttatgcttccggctcgtataatgtgtggaattatgagcggataataa
tttcacacaggaggtttaaactttaaacatgtcaaaagaaacgtcttttgttaagaatgctgaggaacttgcaaagcaaaaaatggatgctattaaccctgaactttcttc
aaaatttaaatttttaataaaattcctgtctcagtttcctgaagcttgctctaaacctcgttcaaaaaaaatgcagaataaagttggtcaagaggaacatattgaatatttag
ctcgtagttttcatgagagtcgattgccaagaaaacccacgccacctacaacggttcctgatgaggtggttagcatagttcttaatataagttttaatatacagcctgaaa
atcttgagagaataaaagaagaacatcgattttccatggcagctgagaatattgtaggagatcttctagaaagatgaccgtggtccctgtgccccagatgagacgctg
gcacgacaggtttcccgactggaaagcgggcagtgagcgcaacgcaattaatgtgagttagctcactcattaggcaccccaggctttacactttatgcttccggctcgt
atgttgtgtggaattgtgagcggataacaatttcacacaggaaacagctatgaccatgattacgccaagcttgcatgcctgcaggtcgactctagaggatccccgggt
accgagctcgaattcactggccgtcgttttacaacgtcgtgactgggaaaaccctggcgttacccaacttaatcgccttgcagcacatccccctttcgccagctggcgta
atagcgaagaggcccgcaccgatcgcccttcccaacagttgcgcagcctgaatggcgaatggcgcctgatgcggtattttctccttacgcatctgtgcggtatttcaca
ccgcatatggtgcactctcagtacaatctgctctgatgccgcatagttaagccagccccgacacccgccaacacccgctgacgcgccctgacgggcttgtctgctccc
ggcatccgcttacagacaagctcgtctcaatcttgctgaaaaactcgagccatccggaagatctggcggccgctctccctatagtgagtcgtattacgccggatggat
atggtgttcaggcacaagtgttaaagcagttgattttattcactatgatgaaaaaaacaatgaatggaacctgctccaagttaaaaatagagataatacccgaaaactc
atcgagtagtaagattagagataatacaacaataaaaaaatggtttagaacttactcacagcgtgatgctactaattgggacaattttccagatgaagtatcatctaag
aatttaaatgaagaggacttcagagcttttgttaaaaattatttggcaaaaataatataattcggctgcaggggc

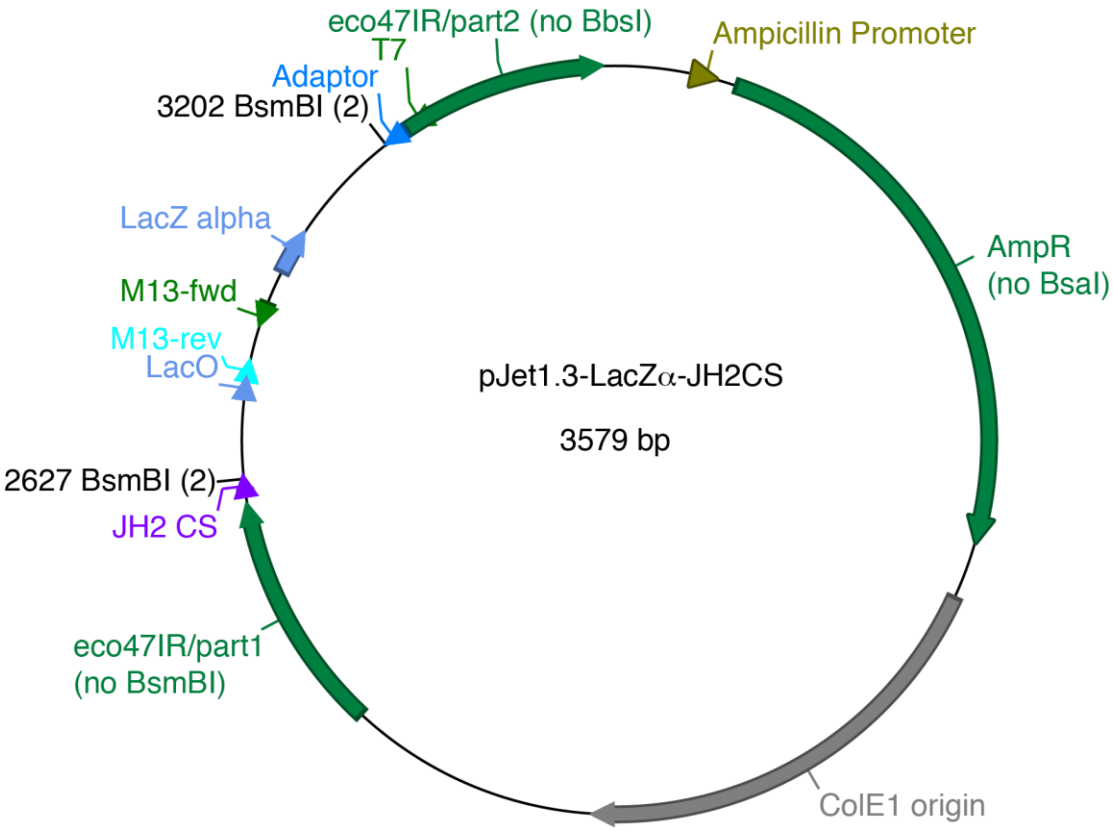


> pJet1.3-LacZα-JH2CS

ggcctcgtgatacgcctatttttataggttaatgtcatgataataatggtttcttagacgtcaggtggcacttttcggggaaatgtgcgcggaacccctatttgtttatttttctaa
atacattcaaatatgtatccgctcatgagacaataaccctgataaatgcttcaataatattgaaaaaggaagagtatgagtattcaacatttccgtgtcgcccttattccctt
ttttgcggcattttgccttcctgtttttgctcacccagaaacgctggtgaaagtaaaagatgctgaagatcagttgggtgcacgagtgggttacatcgaactggatctcaac
agcggtaagatccttgagagttttcgccccgaagaacgttttccaatgatgagcacttttaaagttctgctatgtggcgcggtattatcccgtattgacgccgggcaagag
caactcggtcgccgcatacactattctcagaatgacttggttgagtactcaccagtcacagaaaagcatcttacggatggcatgacagtaagagaattatgcagtgct
gccataaccatgagtgataacactgcggccaacttacttctgacaacgatcggaggaccgaaggagctaaccgcttttttgcacaacatgggggatcatgtaactcg
ccttgatcgttgggaaccggagctgaatgaagccataccaaacgacgagcgtgacaccacgatgcctgtagcaatggcaacaacgttgcgcaaactattaactgg
cgaactacttactctagcttcccggcaacaattaatagactggatggaggcggataaagttgcaggaccacttctgcgctcggcccttccggctggctggtttattgctg
ataaatctggagccggtgagcgtggttctcgcggtatcattgcagcactggggccagatggtaagccctcccgtatcgtagttatctacacgacggggagtcaggca
actatggatgaacgaaatagacagatcgctgagataggtgcctcactgattaagcattggtaactgtcagaccaagtttactcatatatactttagattgatttaaaacttc
atttttaatttaaaaggatctaggtgaagatccttttgataatctcatgaccaaaatcccttaacgtgagttttcgttccactgagcgtcagaccccgtagaaaagatcaaa
ggatcttcttgagatcctttttttctgcgcgtaatctgctgcttgcaaacaaaaaaaccaccgctaccagcggtggtttgtttgccggatcaagagctaccaactcttttccg
aaggtaactggcttcagcagagcgcagataccaaatactgtccttctagtgtagccgtagttaggccaccacttcaagaactctgtagcaccgcctacatacctcgctc
tgctaatcctgttaccagtggctgctgccagtggcgataagtcgtgtcttaccgggttggactcaagacgatagttaccggataaggcgcagcggtcgggctgaacgg
ggggttcgtgcacacagcccagcttggagcgaacgacctacaccgaactgagatacctacagcgtgagctatgagaaagcgccacgcttcccgaagggagaaa
ggcggacaggtatccggtaagcggcagggtcggaacaggagagcgcacgagggagcttccagggggaaacgcctggtatctttatagtcctgtcgggtttcgcca
cctctgacttgagcgtcgatttttgtgatgctcgtcaggggggcggagcctatggaaaaacgccagcaacgcggcctttttacggttcctggccttttgctggccttttgctc
acatgttctttcctgcgttatcccctgattctgtggataaccgtattaccgcctttgagtgagctgataccgctcgccgcagccgaacgaccgagcgcagcgagtcagtg
agcgaggaagcggaagagcgcccaatacgcaaaccgcctctccccgcgcgttggccgattcattaatgcagctggcacgacaggtttcccgactggaaagcaatt
ggcagtgagcgcaacgcaattaatgtgagttagctcactcattaggcaccccaggctttacactttatgcttccggctcgtataatgtgtggaattatgagcggataataa
tttcacacaggaggtttaaacttaaacatgtcaaaagaaacgtcttttgttaagaatgctgaggaacttgcaaagcaaaaaatggatgctattaaccctgaacttttcttc
aaaatttaaatttttaataaaattcctgtctcagtttcctgaagcttgctctaaacctcgttcaaaaaaaatgcagaataaagttggtcaagaggaacatattgaatatttag
ctcgtagttttcatgagagtcgattgccaagaaaacccacgccacctacaacggttcctgatgaggtggttagcatagttcttaatataagttttaatatacagcctgaaa
atcttgagagaataaaagaagaacatcgattttccatggcagctgagaatattgtaggagatcttctagaaagatgacgtgagagtggtgccttggctgagacgctgg
cacgacaggtttcccgactggaaagcgggcagtgagcgcaacgcaattaatgtgagttagctcactcattaggcaccccaggctttacacttttatgcttccggctcgta
tgttgtgtggaattgtgagcggataacaatttcacacaggaaacagctatgaccatgattacgccaagcttgcatgcctgcaggtcgactctagaggatccccgggta
ccgagctcgaattcactggccgtcgttttacaacgtcgtgactgggaaaaccctggcgttacccaacttaatcgccttgcagcacatccccctttcgccagctggcgtaa
tagcgaagaggcccgcaccgatcgcccttcccaacagttgcgcagcctgaatggcgaatggcgcctgatgcggtattttctccttacgcatctgtgcggtatttcacac
cgcatatggtgcactctcagtacaatctgctctgatgccgcatagttaagccagccccgacacccgccaacacccgctgacgcgccctgacgggcttgtctgctcccg
gcatccgcttacagacaagctcgtctcaatcttgctgaaaaactcgagccatccggaagatctggcggccgctctccctatagtgagtcgtattacgccggatggatat
ggtgttcaggcacaagtgttaaagcagttgattttattcactatgatgaaaaaaacaatgaatggaacctgctccaagttaaaaatagagataataccgaaaactcatc
gagtagtaagattagagataatacaacaataaaaaaatggtttagaacttactcacagcgtgatgctactaattgggacaattttccagatgaagtatcatctaagaatt
taaatgaagaggacttcagagcttttgttaaaaattatttggcaaaaataatataattcggctgcaggggc

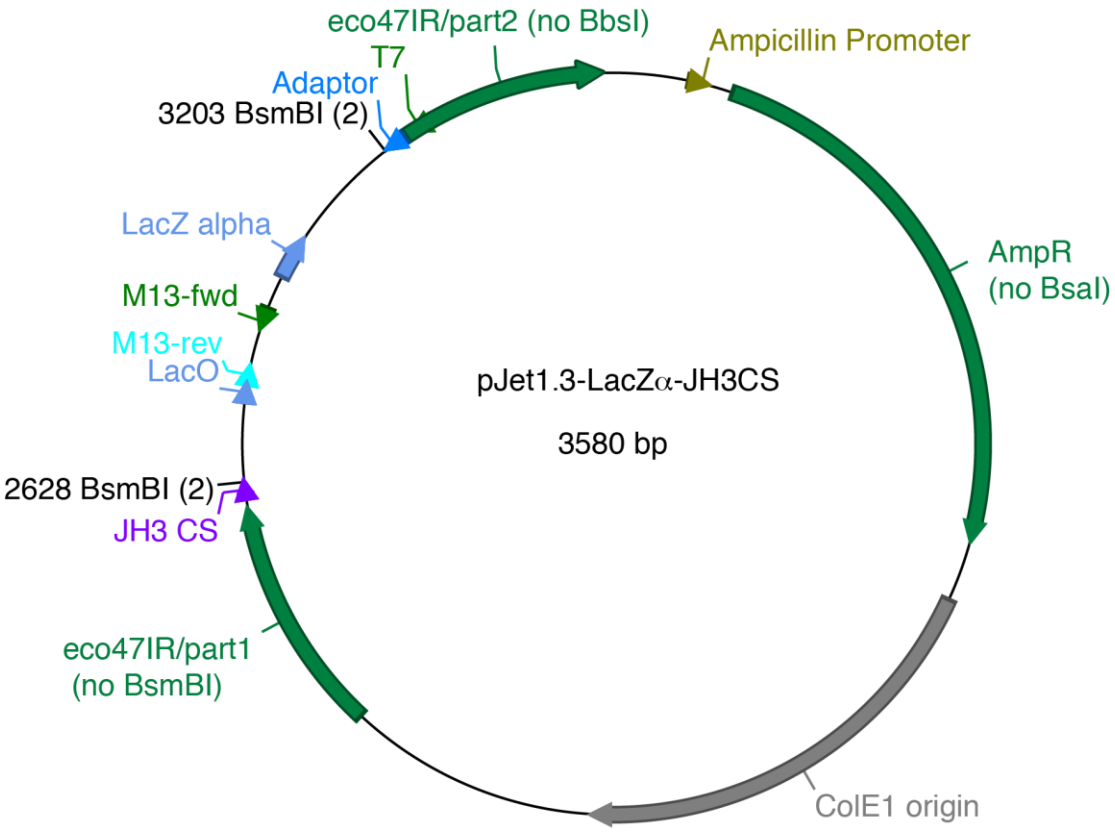


> pJet1.3-LacZα-JH3CS

ggcctcgtgatacgcctatttttataggttaatgtcatgataataatggtttcttagacgtcaggtggcacttttcggggaaatgtgcgcggaacccctatttgtttatttttctaa
atacattcaaatatgtatccgctcatgagacaataaccctgataaatgcttcaataatattgaaaaaggaagagtatgagtattcaacatttccgtgtcgcccttattccctt
ttttgcggcattttgccttcctgtttttgctcacccagaaacgctggtgaaagtaaaagatgctgaagatcagttgggtgcacgagtgggttacatcgaactggatctcaac
agcggtaagatccttgagagttttcgccccgaagaacgttttccaatgatgagcacttttaaagttctgctatgtggcgcggtattatcccgtattgacgccgggcaagag
caactcggtcgccgcatacactattctcagaatgacttggttgagtactcaccagtcacagaaaagcatcttacggatggcatgacagtaagagaattatgcagtgct
gccataaccatgagtgataacactgcggccaacttacttctgacaacgatcggaggaccgaaggagctaaccgcttttttgcacaacatgggggatcatgtaactcg
ccttgatcgttgggaaccggagctgaatgaagccataccaaacgacgagcgtgacaccacgatgcctgtagcaatggcaacaacgttgcgcaaactattaactgg
cgaactacttactctagcttcccggcaacaattaatagactggatggaggcggataaagttgcaggaccacttctgcgctcggcccttccggctggctggtttattgctg
ataaatctggagccggtgagcgtggttctcgcggtatcattgcagcactggggccagatggtaagccctcccgtatcgtagttatctacacgacggggagtcaggca
actatggatgaacgaaatagacagatcgctgagataggtgcctcactgattaagcattggtaactgtcagaccaagtttactcatatatactttagattgatttaaaacttc
atttttaatttaaaaggatctaggtgaagatccttttgataatctcatgaccaaaatcccttaacgtgagttttcgttccactgagcgtcagaccccgtagaaaagatcaaa
ggatcttcttgagatcctttttttctgcgcgtaatctgctgcttgcaaacaaaaaaaccaccgctaccagcggtggtttgtttgccggatcaagagctaccaactctttttccg
aaggtaactggcttcagcagagcgcagataccaaatactgtccttctagtgtagccgtagttaggccaccacttcaagaactctgtagcaccgcctacatacctcgctc
tgctaatcctgttaccagtggctgctgccagtggcgataagtcgtgtcttaccgggttggactcaagacgatagttaccggataaggcgcagcggtcgggctgaacgg
ggggttcgtgcacacagcccagcttggagcgaacgacctacaccgaactgagatacctacagcgtgagctatgagaaagcgccacgcttcccgaagggagaaa
ggcggacaggtatccggtaagcggcagggtcggaacaggagagcgcacgagggagcttccagggggaaacgcctggtatctttatagtcctgtcgggtttcgcca
cctctgacttgagcgtcgatttttgtgatgctcgtcaggggggcggagcctatggaaaaacgccagcaacgcggcctttttacggttcctggccttttgctggccttttgctc
acatgttctttcctgcgttatcccctgattctgtggataaccgtattaccgcctttgagtgagctgataccgctcgccgcagccgaacgaccgagcgcagcgagtcagtg
agcgaggaagcggaagagcgcccaatacgcaaaccgcctctccccgcgcgttggccgattcattaatgcagctggcacgacaggtttcccgactggaaagcaatt
ggcagtgagcgcaacgcaattaatgtgagttagctcactcattaggcaccccaggctttacactttatgcttccggctcgtataatgtgtggaattatgagcggataataa
tttcacacaggaggtttaaactttaaacatgtcaaaagaaacgtcttttgttaagaatgctgaggaacttgcaaagcaaaaaatggatgctattaaccctgaactttcttc
aaaatttaaatttttaataaaattcctgtctcagtttcctgaagcttgctctaaacctcgttcaaaaaaaatgcagaataaagttggtcaagaggaacatattgaatatttag
ctcgtagttttcatgagagtcgattgccaagaaaacccacgccacctacaacggttcctgatgaggtggttagcatagttcttaatataagttttaatatacagcctgaaa
atcttgagagaataaaagaagaacatcgattttccatggcagctgagaatattgtaggagatcttctagaaagatgacagtgaccagagtcccttggctgagacgctg
gcacgacaggtttcccgactggaaagcgggcagtgagcgcaacgcaattaatgtgagttagctcactcattaggcaccccaggctttacactttatgcttccggctcgt
atgttgtgtggaattgtgagcggataacaatttcacacaggaaacagctatgaccatgattacgccaagcttgcatgcctgcaggtcgactctagaggatccccgggt
accgagctcgaattcactggccgtcgttttacaacgtcgtgactgggaaaaccctggcgttacccaacttaatcgccttgcagcacatccccctttcgccagctggcgta
atagcgaagaggcccgcaccgatcgcccttcccaacagttgcgcagcctgaatggcgaatggcgcctgatgcggtattttctccttacgcatctgtgcggtatttcaca
ccgcatatggtgcactctcagtacaatctgctctgatgccgcatagttaagccagccccgacacccgccaacacccgctgacgcgccctgacgggcttgtctgctccc
ggcatccgcttacagacaagctcgtctcaatcttgctgaaaaactcgagccatccggaagatctggcggccgctctccctatagtgagtcgtattacgccggatggat
atggtgttcaggcacaagtgttaaagcagttgattttattcactatgatgaaaaaaacaatgaatggaacctgctccaagttaaaaatagagataatacccgaaaactc
atcgagtagtaagattagagataatacaacaataaaaaaatggtttagaacttactcacagcgtgatgctactaattgggacaattttccagatgaagtatcatctaag
aatttaaatgaagaggacttcagagcttttgttaaaaattatttggcaaaaataatataattcggctgcaggggc

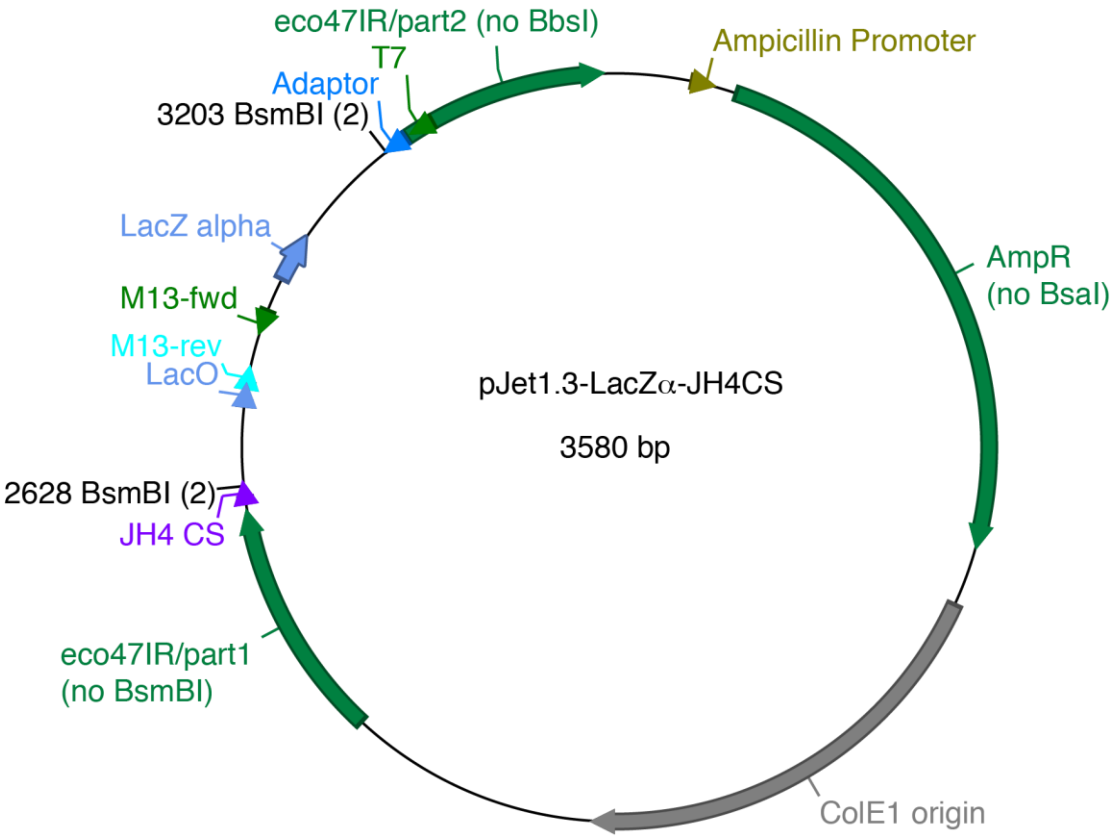


> pJet1.3-LacZα-JH4CS

ggcctcgtgatacgcctatttttataggttaatgtcatgataataatggtttcttagacgtcaggtggcacttttcggggaaatgtgcgcggaacccctatttgtttatttttctaa
atacattcaaatatgtatccgctcatgagacaataaccctgataaatgcttcaataatattgaaaaaggaagagtatgagtattcaacatttccgtgtcgcccttattccctt
ttttgcggcattttgccttcctgtttttgctcacccagaaacgctggtgaaagtaaaagatgctgaagatcagttgggtgcacgagtgggttacatcgaactggatctcaac
agcggtaagatccttgagagttttcgccccgaagaacgttttccaatgatgagcacttttaaagttctgctatgtggcgcggtattatcccgtattgacgccgggcaagag
caactcggtcgccgcatacactattctcagaatgacttggttgagtactcaccagtcacagaaaagcatcttacggatggcatgacagtaagagaattatgcagtgct
gccataaccatgagtgataacactgcggccaacttacttctgacaacgatcggaggaccgaaggagctaaccgcttttttgcacaacatgggggatcatgtaactcg
ccttgatcgttgggaaccggagctgaatgaagccataccaaacgacgagcgtgacaccacgatgcctgtagcaatggcaacaacgttgcgcaaactattaactgg
cgaactacttactctagcttcccggcaacaattaatagactggatggaggcggataaagttgcaggaccacttctgcgctcggcccttccggctggctggtttattgctg
ataaatctggagccggtgagcgtggttctcgcggtatcattgcagcactggggccagatggtaagccctcccgtatcgtagttatctacacgacggggagtcaggca
actatggatgaacgaaatagacagatcgctgagataggtgcctcactgattaagcattggtaactgtcagaccaagtttactcatatatactttagattgatttaaaacttc
atttttaatttaaaaggatctaggtgaagatccttttgataatctcatgaccaaaatcccttaacgtgagttttcgttccactgagcgtcagaccccgtagaaaagatcaaa
ggatcttcttgagatcctttttttctgcgcgtaatctgctgcttgcaaacaaaaaaaccaccgctaccagcggtggtttgtttgccggatcaagagctaccaactctttttccg
aaggtaactggcttcagcagagcgcagataccaaatactgtccttctagtgtagccgtagttaggccaccacttcaagaactctgtagcaccgcctacatacctcgctc
tgctaatcctgttaccagtggctgctgccagtggcgataagtcgtgtcttaccgggttggactcaagacgatagttaccggataaggcgcagcggtcgggctgaacgg
ggggttcgtgcacacagcccagcttggagcgaacgacctacaccgaactgagatacctacagcgtgagctatgagaaagcgccacgcttcccgaagggagaaa
ggcggacaggtatccggtaagcggcagggtcggaacaggagagcgcacgagggagcttccagggggaaacgcctggtatctttatagtcctgtcgggtttcgcca
cctctgacttgagcgtcgatttttgtgatgctcgtcaggggggcggagcctatggaaaaacgccagcaacgcggcctttttacggttcctggccttttgctggccttttgctc
acatgttctttcctgcgttatcccctgattctgtggataaccgtattaccgcctttgagtgagctgataccgctcgccgcagccgaacgaccgagcgcagcgagtcagtg
agcgaggaagcggaagagcgcccaatacgcaaaccgcctctccccgcgcgttggccgattcattaatgcagctggcacgacaggtttcccgactggaaagcaatt
ggcagtgagcgcaacgcaattaatgtgagttagctcactcattaggcaccccaggctttacactttatgcttccggctcgtataatgtgtggaattatgagcggataataa
tttcacacaggaggtttaaactttaaacatgtcaaaagaaacgtcttttgttaagaatgctgaggaacttgcaaagcaaaaaatggatgctattaaccctgaactttcttc
aaaatttaaatttttaataaaattcctgtctcagtttcctgaagcttgctctaaacctcgttcaaaaaaaatgcagaataaagttggtcaagaggaacatattgaatatttag
ctcgtagttttcatgagagtcgattgccaagaaaacccacgccacctacaacggttcctgatgaggtggttagcatagttcttaatataagttttaatatacagcctgaaa
atcttgagagaataaaagaagaacatcgattttccatggcagctgagaatattgtaggagatcttctagaaagatgactgaggttccttgaccccagttgagacgctgg
cacgacaggtttcccgactggaaagcgggcagtgagcgcaacgcaattaatgtgagttagctcactcattaggcaccccaggctttacacttttatgcttccggctcgta
tgttgtgtggaattgtgagcggataacaatttcacacaggaaacagctatgaccatgattacgccaagcttgcatgcctgcaggtcgactctagaggatccccgggta
ccgagctcgaattcactggccgtcgttttacaacgtcgtgactgggaaaaccctggcgttacccaacttaatcgccttgcagcacatccccctttcgccagctggcgtaa
tagcgaagaggcccgcaccgatcgcccttcccaacagttgcgcagcctgaatggcgaatggcgcctgatgcggtattttctccttacgcatctgtgcggtatttcacac
cgcatatggtgcactctcagtacaatctgctctgatgccgcatagttaagccagccccgacacccgccaacacccgctgacgcgccctgacgggcttgtctgctcccg
gcatccgcttacagacaagctcgtctcaatcttgctgaaaaactcgagccatccggaagatctggcggccgctctccctatagtgagtcgtattacgccggatggatat
ggtgttcaggcacaagtgttaaagcagttgattttattcactatgatgaaaaaaacaatgaatggaacctgctccaagttaaaaatagagataataccgaaaactcatc
gagtagtaagattagagataatacaacaataaaaaaatggtttagaacttactcacagcgtgatgctactaattgggacaattttccagatgaagtatcatctaagaatt
taaatgaagaggacttcagagcttttgttaaaaattatttggcaaaaataatataattcggctgcaggggc

# References


1. Saba, N. S., Liu, D., Herman, S. E. M., Underbayev, C., Tian, X., Behrend, D., et al. (2016). Pathogenic role of B-cell receptor signaling and canonical NF-κB activation in mantle cell lymphoma. *Blood*, *128*(1), 82–92. doi:10.1182/blood-2015-11-681460
2. Zhang, M., Xu-Monette, Z. Y., Li, L., Manyam, G. C., Visco, C., Tzankov, A., et al. (2016). RelA NF-κB subunit activation as a therapeutic target in diffuse large B-cell lymphoma. *Aging*, *8*(12), 3321–3340. doi:10.18632/aging.101121
3. Balaji, S., Ahmed, M., Lorence, E., Yan, F., Nomie, K., & Wang, M. (2018). NF-κB signaling and its relevance to the treatment of mantle cell lymphoma. *Journal of hematology & oncology*, *11*(1), 87–11. doi:10.1186/s13045-018-0621-5
4. Harhaj, E. W., & Giam, C.-Z. (2018). NF-κB signaling mechanisms in HTLV-1-induced adult T-cell leukemia/lymphoma. *The FEBS Journal*, *3*, 388–13. doi:10.1111/febs.14492
5. Paula Grondona, Philip Bucher, Klaus Schulze-Osthoff, Stephan Hailfinger, Anja Schmitt. (2018). NF-κB Activation in Lymphoid Malignancies: Genetics, Signaling, and Targeted Therapy. *Biomedicines*, *6*(2), 38–30. doi:10.3390/biomedicines6020038
6. Compagno, M., Lim, W. K., Grunn, A., Nandula, von, S., Brahmachary, M., Shen, Q., et al. (2009). Mutations of multiple genes cause deregulation of NF-κB in diffuse large B-cell lymphoma. *Nature*, *459*(7247), 717–721. doi:10.1038/nature07968
7. Roy, P., Sarkar, U., & Basak, S. (2018). The NF-κB Activating Pathways in Multiple Myeloma. *Biomedicines*, *6*(2), 59–19. doi:10.3390/biomedicines6020059
8. Véronique Imbert, Jean-François Peyron. (2017). NF-κB in Hematological Malignancies. *Biomedicines*, *5*(4), 27–16. doi:10.3390/biomedicines5020027
9. Staudt, L. M. (2010). Oncogenic Activation of NF- B. *Cold Spring Harbor Perspectives in Biology*, *2*(6), a000109–a000109. doi:10.1101/cshperspect.a000109
10. Vallabhapurapu, S., & Karin, M. (2009). Regulation and Function of NF-κB Transcription Factors in the Immune System. *Annual Review of Immunology*, *27*(1), 693–733. doi:10.1146/annurev.immunol.021908.132641
11. Harhaj, E. W., & Dixit, V. M. (2012). Regulation of NF-κB by deubiquitinases. *Immunological reviews*, *246*(1), 107–124. doi:10.1111/j.1600-065X.2012.01100.x
12. Hayden, M. S., & Ghosh, S. (2014). Regulation of NF-κB by TNF family cytokines. *Seminars in Immunology*, *26*(3), 253–266. doi:10.1016/j.smim.2014.05.004
13. Sun, S.-C. (2017). The non-canonical NF-κB pathway in immunity and inflammation. *Nature Reviews Immunology*, *17*(9), 545–558. doi:10.1038/nri.2017.52
14. Hayden, M. S., & Ghosh, S. (2011). NF-κB in immunobiology. *Cell Research*, *21*(2), 223–244. doi:10.1038/cr.2011.13
15. Haas, A. L. (2009). Linear polyubiquitylation: the missing link in NF-kappaB signalling. *Nature cell biology*, *11*(2), 116–118. doi:10.1038/ncb0209-116
16. Wajant, H., & Scheurich, P. (2011). TNFR1-induced activation of the classical NF-κB pathway. *FEBS Journal*, *278*(6), 862–876. doi:10.1111/j.1742-4658.2011.08015.x
17. Conze, D. B., Wu, C. J., Thomas, J. A., Landstrom, A., & Ashwell, J. D. (2008). Lys63-Linked Polyubiquitination of IRAK-1 Is Required for Interleukin-1 Receptor- and Toll-Like Receptor-Mediated NF- B Activation. *Molecular and Cellular Biology*, *28*(10), 3538–3547. doi:10.1128/MCB.02098-07
18. Chen, Z. J. (2012). Ubiquitination in signaling to and activation of IKK. *Immunological reviews*, *246*(1), 95–106. doi:10.1111/j.1600-065X.2012.01108.x

19. Niiro, H., & Clark, E. A. (2002). Decision making in the immune system: Regulation of B-cell fate by antigen-receptor signals. *Nature Reviews Immunology*, *2*(12), 945–956. doi:10.1038/nri955
20. Rickert, R. C. (2013). New insights into pre-BCR and BCR signalling with relevance to B cell malignancies. *Nature Reviews Immunology*, *13*(8), 578–591. doi:10.1038/nri3487
21. Seda, V., & Mraz, M. (2014). B-cell receptor signalling and its crosstalk with other pathways in normal and malignant cells. *European journal of haematology*, *94*(3), 193–205. doi:10.1111/ejh.12427
22. Baba, Y., & Kurosaki, T. (2011). Impact of Ca2+ signaling on B cell function. *Trends in Immunology*, *32*(12), 589–594. doi:10.1016/j.it.2011.09.004
23. Kurosaki, T., Shinohara, H., & Baba, Y. (2010). B Cell Signaling and Fate Decision. *Annual Review of Immunology*, *28*(1), 21–55. doi:10.1146/annurev.immunol.021908.132541
24. David, L., Li, Y., Ma, J., Garner, E., Zhang, X., & Wu, H. (2018). Assembly mechanism of the CARMA1–BCL10–MALT1–TRAF6 signalosome. *Proceedings of the National Academy of Sciences of the United States of America*, *115*(7), 1499–1504. doi:10.1073/pnas.1721967115
25. Zarnegar, B. J., Wang, Y., Mahoney, D. J., Dempsey, P. W., Cheung, H. H., He, J., et al. (2008). Noncanonical NF-κB activation requires coordinated assembly of a regulatory complex of the adaptors cIAP1, cIAP2, TRAF2 and TRAF3 and the kinase NIK. *Nature Immunology*, *9*(12), 1371–1378. doi:10.1038/ni.1676
26. Werner, S. L., Kearns, J. D., Zadorozhnaya, V., Lynch, C., O'Dea, E., Boldin, M. P., et al. (2008). Encoding NF- B temporal control in response to TNF: distinct roles for the negative regulators I B and A20. *Genes & development*, *22*(15), 2093–2101. doi:10.1101/gad.1680708
27. Wertz, I. E., O'Rourke, K. M., Zhou, H., Eby, M., Aravind, L., Seshagiri, S., et al. (2004). De-ubiquitination and ubiquitin ligase domains of A20 downregulate NF-kappaB signalling. *Nature*, *430*(7000), 694–699. doi:10.1038/nature02794
28. Garg, A. V., Ahmed, M., Vallejo, A. N., Ma, A., & Gaffen, S. L. (2013). The Deubiquitinase A20 Mediates Feedback Inhibition of Interleukin-17 Receptor Signaling. *Science Signaling*, *6*(278), ra44–ra44. doi:10.1126/scisignal.2003699
29. Shembade, N., Ma, A., & Harhaj, E. W. (2010). Inhibition of NF- B Signaling by A20 Through Disruption of Ubiquitin Enzyme Complexes. *Science*, *327*(5969), 1135–1139. doi:10.1126/science.1182364
30. Skaug, B., Chen, J., Du, F., He, J., Ma, A., & Chen, Z. J. (2011). Direct, Noncatalytic Mechanism of IKK Inhibition by A20. *Molecular Cell*, *44*(4), 559–571. doi:10.1016/j.molcel.2011.09.015
31. Pelzer, C., & Thome, M. (2011). IKKα takes control of canonical NF-κB activation. *Nature Immunology*, *12*(9), 815–816. doi:10.1038/ni.2082
32. Verstrepen, L., Verhelst, K., Carpentier, I., & Beyaert, R. (2011). TAX1BP1, a ubiquitin-binding adaptor protein in innate immunity and beyond. *Trends in Biochemical Sciences*. doi:10.1016/j.tibs.2011.03.004
33. Chen, F. (2004). Endogenous inhibitors of nuclear factor-kappaB, an opportunity for cancer control. *Cancer research*, *64*(22), 8135–8138. doi:10.1158/0008-5472.CAN-04-2096
34. Chu, Y., Soberon, V., Glockner, L., Beyaert, R., Massoumi, R., van Loo, G., et al. (2012). A20 and CYLD Do Not Share Significant Overlapping Functions during B Cell Development and Activation. *The Journal of Immunology*. doi:10.4049/jimmunol.1200396
35. Sasaki, Y., Sano, S., Nakahara, M., Murata, S., Kometani, K., Aiba, Y., et al. (2013).

Defective immune responses in mice lacking LUBAC-mediated linear ubiquitination in B cells. *The EMBO journal*, *32*(18), 2463–2476. doi:10.1038/emboj.2013.184

36. Almaden, J. V., Liu, Y. C., Yang, E., Otero, D. C., Birnbaum, H., Davis-Turak, J., et al. (2016). B-cell survival and development controlled by the coordination of NF-κB family members RelB and cRel. *Blood*, *127*(10), 1276–1286. doi:10.1182/blood-2014-10-606988
37. Sasaki, Y., Derudder, E., Hobeika, E., Pelanda, R., Reth, M., Rajewsky, K., & Schmidt-Supprian, M. (2006). Canonical NF-κB Activity, Dispensable for B Cell Development, Replaces BAFF-Receptor Signals and Promotes B Cell Proliferation upon Activation. *Immunity*, *24*(6), 729–739. doi:10.1016/j.immuni.2006.04.005
38. Stadanlick, J. E., Kaileh, M., Karnell, F. G., Scholz, J. L., Miller, J. P., Quinn, W. J., et al. (2008). Tonic B cell antigen receptor signals supply an NF-kappaB substrate for prosurvival BLyS signaling. *Nature Immunology*, *9*(12), 1379–1387. doi:10.1038/ni.1666
39. Tao, Z., Fusco, A., Huang, D.-B., Gupta, K., Young Kim, D., Ware, C. F., et al. (2014). p100/IκBδ sequesters and inhibits NF-κB through kappaBsome formation. *Proceedings of the National Academy of Sciences of the United States of America*, *111*(45), 15946–15951. doi:10.1073/pnas.1408552111
40. Derudder, E., Herzog, S., Labi, V., Yasuda, T., Köchert, K., Janz, M., et al. (2016). Canonical NF-κB signaling is uniquely required for the long-term persistence of functional mature B cells. *Proceedings of the National Academy of Sciences*, *113*(18), 5065–5070. doi:10.1073/pnas.1604529113
41. Zarnegar, B., He, J. Q., Oganesyan, G., Hoffmann, A., Baltimore, D., & Cheng, G. (2004). Unique CD40-mediated biological program in B cell activation requires both type 1 and type 2 NF-kappaB activation pathways. *Proceedings of the National Academy of Sciences of the United States of America*, *101*(21), 8108–8113. doi:10.1073/pnas.0402629101
42. Zarnegar, B., Yamazaki, S., He, J. Q., & Cheng, G. (2008). Control of canonical NF-kappaB activation through the NIK-IKK complex pathway. *Proceedings of the National Academy of Sciences*, *105*(9), 3503–3508. doi:10.1073/pnas.0707959105
43. Gray, C. M., Remouchamps, C., McCorkell, K. A., Solt, L. A., Dejardin, E., Orange, J. S., & May, M. J. (2014). Noncanonical NF-κB signaling is limited by classical NF-κB activity. *Science Signaling*, *7*(311), ra13–ra13. doi:10.1126/scisignal.2004557
44. Litman, G. W., Anderson, M. K., & Rast, J. P. (1999). Evolution of antigen binding receptors. *Annual Review of Immunology*, *17*(1), 109–147. doi:10.1146/annurev.immunol.17.1.109
45. Flajnik, M. F. (2002). Comparative analyses of immunoglobulin genes: surprises and portents. *Nature Reviews Immunology*, *2*(9), 688–698. doi:10.1038/nri889
46. Zotos, D., & Tarlinton, D. M. (2012). Determining germinal centre B cell fate. *Trends in Immunology*, *33*(6), 281–288. doi:10.1016/j.it.2012.04.003
47. Klein, U., & Dalla-Favera, R. (2008). Germinal centres: role in B-cell physiology and malignancy. *Nature Reviews Immunology*, *8*(1), 22–33. doi:10.1038/nri2217
48. ALLMAN, D., & Pillai, S. (2008). Peripheral B cell subsets. *Current Opinion in Immunology*, *20*(2), 149–157. doi:10.1016/j.coi.2008.03.014
49. Melchers, F. (2015). Checkpoints that control B cell development. *Journal of Clinical Investigation*, *125*(6), 2203–2210. doi:10.1172/JCI78083
50. Hardy, R. R., & Hayakawa, K. (2001). B cell development pathways. *Annual Review of Immunology*, *19*, 595–621. doi:10.1146/annurev.immunol.19.1.595
51. Matthias, P., & Rolink, A. G. (2005). Transcriptional networks in developing and mature B cells. *Nature Reviews Immunology*, *5*(6), 497–508. doi:10.1038/nri1633
52. Jung, D., & Alt, F. W. (2004). Unraveling V(D)J recombination; insights into gene

regulation. *Cell*, *116*(2), 299–311.

53. Nemazee, D. (2017). Mechanisms of central tolerance for B cells. *Nature Reviews Immunology*, *17*(5), 281–294. doi:10.1038/nri.2017.19
54. Nechanitzky, R., Akbas, D., Scherer, S., Györy, I., Hoyler, T., Ramamoorthy, S., et al. (2013). Transcription factor EBF1 is essential for the maintenance of B cell identity and prevention of alternative fates in committed cells. *Nature Immunology*, *14*(8), 867–875. doi:10.1038/ni.2641
55. Dudley, D. D., Chaudhuri, J., Bassing, C. H., & Alt, F. W. (2005). Mechanism and control of V(D)J recombination versus class switch recombination: similarities and differences. *Advances in immunology*, *86*, 43–112. doi:10.1016/S0065-2776(04)86002-4
56. Schatz, D. G., Oettinger, M. A., & Schlissel, M. S. (1992). V(D)J recombination: molecular biology and regulation. *Annual Review of Immunology*, *10*(1), 359–383. doi:10.1146/annurev.iy.10.040192.002043
57. Bassing, C. H., Swat, W., & Alt, F. W. (2002). The mechanism and regulation of chromosomal V(D)J recombination. *Cell*, *109 Suppl*, S45–55.
58. Rumfelt, L. L., Zhou, Y., Rowley, B. M., Shinton, S. A., & Hardy, R. R. (2006). Lineage specification and plasticity in CD19- early B cell precursors. *The Journal of experimental medicine*, *203*(3), 675–687. doi:10.1084/jem.20052444
59. Alves-Pereira, C. F., de Freitas, R., Lopes, T., Gardner, R., Marta, F., Vieira, P., & Barreto, V. M. (2014). Independent recruitment of Igh alleles in V(D)J recombination. *Nature Communications*, *5*(1), 547–15. doi:10.1038/ncomms6623
60. Feng, B., Cheng, S., Pear, W. S., & Liou, H.-C. (2004). NF-kB inhibitor blocks B cell development at two checkpoints. *Medical immunology (London, England)*, *3*(1), 1. doi:10.1186/1476-9433-3-1
61. Feng, B., Cheng, S., Hsia, C. Y., King, L. B., Monroe, J. G., & Liou, H.-C. (2004). NF-κB inducible genes BCL-X and cyclin E promote immature B-cell proliferation and survival. *Cellular Immunology*, *232*(1-2), 9–20. doi:10.1016/j.cellimm.2005.01.006
62. Jung, D., Giallourakis, C., Mostoslavsky, R., & Alt, F. W. (2006). MECHANISM AND CONTROL OF V(D)J RECOMBINATION AT THE IMMUNOGLOBULIN HEAVY CHAIN LOCUS. *Annual Review of Immunology*, *24*(1), 541–570. doi:10.1146/annurev.immunol.23.021704.115830
63. Derudder, E., Cadera, E. J., Vahl, J. C., Wang, J., Fox, C. J., Zha, S., et al. (2009). Development of immunoglobulin λ-chain–positive B cells, but not editing of immunoglobulin κ-chain, depends on NF-κB signals. *Nature Immunology*, *10*(6), 647–654. doi:10.1038/ni.1732
64. Gellert, M. (2002). V(D)J R ECOMBINATION: RAG P ROTEINS, R EPAIRF ACTORS, ANDR EGULATION*. *Annual Review of Biochemistry*, *71*(1), 101–132. doi:10.1146/annurev.biochem.71.090501.150203
65. Chung, J. B., Silverman, M., & Monroe, J. G. (2003). Transitional B cells: step by step towards immune competence. *Trends in Immunology*, *24*(6), 342–348. doi:10.1016/S1471-4906(03)00119-4
66. Mackay, F., & Schneider, P. (2009). Cracking the BAFF code. *Nature Reviews Immunology*, *9*(7), 491–502. doi:10.1038/nri2572
67. Gerondakis, S., & Siebenlist, U. (2010). Roles of the NF- B Pathway in Lymphocyte Development and Function. *Cold Spring Harbor Perspectives in Biology*, *2*(5), a000182–a000182. doi:10.1101/cshperspect.a000182
68. Yan, M., Brady, J. R., Chan, B., Lee, W. P., Hsu, B., Harless, S., et al. (2001). Identification of a novel receptor for B lymphocyte stimulator that is mutated in a mouse strain with severe B cell deficiency. *Current biology : CB*, *11*(19), 1547–1552.

69. Schiemann, B., Gommerman, J. L., Vora, K., Cachero, T. G., Shulga-Morskaya, S., Dobles, M., et al. (2001). An essential role for BAFF in the normal development of B cells through a BCMA-independent pathway. *Science*, *293*(5537), 2111–2114. doi:10.1126/science.1061964

70. Amanna, I. J., Dingwall, J. P., & Hayes, C. E. (2003). Enforced bcl-xL gene expression restored splenic B lymphocyte development in BAFF-R mutant mice. *Journal of immunology (Baltimore, Md. : 1950)*, *170*(9), 4593–4600.

71. Woess, C., Tuzlak, S., Labi, V., Drach, M., Bertele, D., Schneider, P., & Villunger, A. (2015). Combined loss of the BH3-only proteins Bim and Bmf restores B-cell development and function in TACI-Ig transgenic mice. *Cell Death and Differentiation*, *22*(9), 1477–1488. doi:10.1038/cdd.2015.8

72. Ng, L. G., Mackay, C. R., & Mackay, F. (2005). The BAFF/APRIL system: life beyond B lymphocytes. *Molecular Immunology*, *42*(7), 763–772. doi:10.1016/j.molimm.2004.06.041

73. Thien, M., Phan, T. G., Gardam, S., Amesbury, M., Basten, A., Mackay, F., & Brink, R. (2004). Excess BAFF rescues self-reactive B cells from peripheral deletion and allows them to enter forbidden follicular and marginal zone niches. *Immunity*, *20*(6), 785–798. doi:10.1016/j.immuni.2004.05.010

74. Pillai, S., & Cariappa, A. (2009). The follicular versus marginal zone B lymphocyte cell fate decision. *Nature Reviews Immunology*, *9*(11), 767–777. doi:10.1038/nri2656

75. Lu, T. T., & Cyster, J. G. (2002). Integrin-mediated long-term B cell retention in the splenic marginal zone. *Science*, *297*(5580), 409–412. doi:10.1126/science.1071632

76. Arnon, T. I., Horton, R. M., Grigorova, I. L., & Cyster, J. G. (2012). Visualization of splenic marginal zone B-cell shuttling and follicular B-cell egress. *Nature*, *493*(7434), 684–688. doi:10.1038/nature11738

77. Cinamon, G., Zachariah, M. A., Lam, O. M., Foss, F. W., & Cyster, J. G. (2007). Follicular shuttling of marginal zone B cells facilitates antigen transport. *Nature Immunology*, *9*(1), 54–62. doi:10.1038/ni1542

78. Pohl, T., Gugasyan, R., Grumont, R. J., Strasser, A., Metcalf, D., Tarlinton, D., et al. (2002). The combined absence of NF-kappa B1 and c-Rel reveals that overlapping roles for these transcription factors in the B cell lineage are restricted to the activation and function of mature cells. *Proceedings of the National Academy of Sciences of the United States of America*, *99*(7), 4514–4519. doi:10.1073/pnas.072071599

79. Chu, Y., Vahl, J. C., Kumar, D., Heger, K., Bertossi, A., Wójtowicz, E., et al. (2011). B cells lacking the tumor suppressor TNFAIP3/A20 display impaired differentiation and hyperactivation and cause inflammation and autoimmunity in aged mice. *Blood*, *117*(7), 2227–2236. doi:10.1182/blood-2010-09-306019

80. Hövelmeyer, N., Reissig, S., Xuan, N. T., Adams-Quack, P., Lukas, D., Nikolaev, A., et al. (2011). A20 deficiency in B cells enhances B-cell proliferation and results in the development of autoantibodies. *European journal of immunology*, *41*(3), 595–601. doi:10.1002/eji.201041313

81. Casola, S., Otipoby, K. L., Alimzhanov, M., Humme, S., Uyttersprot, N., Kutok, J. L., et al. (2004). B cell receptor signal strength determines B cell fate. *Nature Immunology*, *5*(3), 317–327. doi:10.1038/ni1036

82. Cariappa, A., Tang, M., Parng, C., Nebelitskiy, E., Carroll, M., Georgopoulos, K., & Pillai, S. (2001). The follicular versus marginal zone B lymphocyte cell fate decision is regulated by Aiolos, Btk, and CD21. *Immunity*, *14*(5), 603–615.

83. Xue, L., Morris, S. W., Orihuela, C., Tuomanen, E., Cui, X., Wen, R., & Wang, D. (2003). Defective development and function of Bcl10-deficient follicular, marginal zone

and B1 B cells. *Nature Immunology*, *4*(9), 857–865. doi:10.1038/ni963

84. Shinohara, H., & Kurosaki, T. (2016). Negative role of TAK1 in marginal zone B-cell development incidental to NF-κB noncanonical pathway activation. *Immunology and Cell Biology*, *94*(9), 821–829. doi:10.1038/icb.2016.44
85. Rauch, M., Tussiwand, R., Bosco, N., & Rolink, A. G. (2009). Crucial Role for BAFF-BAFF-R Signaling in the Survival and Maintenance of Mature B Cells. *PLoS ONE*, *4*(5), e5456–12. doi:10.1371/journal.pone.0005456
86. Cariappa, A., Liou, H. C., Horwitz, B. H., & Pillai, S. (2000). Nuclear factor kappa B is required for the development of marginal zone B lymphocytes. *The Journal of experimental medicine*, *192*(8), 1175–1182.
87. Ferguson, A. R., & Corley, R. B. (2005). Accumulation of marginal zone B cells and accelerated loss of follicular dendritic cells in NF-kappaB p50-deficient mice. *BMC immunology*, *6*, 8. doi:10.1186/1471-2172-6-8
88. Zapata, J. M., Llobet, D., Krajewska, M., Lefebvre, S., Kress, C. L., & Reed, J. C. (2009). Lymphocyte-specific TRAF3 transgenic mice have enhanced humoral responses and develop plasmacytosis, autoimmunity, inflammation, and cancer. *Blood*, *113*(19), 4595–4603. doi:10.1182/blood-2008-07-165456
89. Sasaki, Y., Calado, D. P., Derudder, E., Zhang, B., Shimizu, Y., Mackay, F., et al. (2008). NIK overexpression amplifies, whereas ablation of its TRAF3-binding domain replaces BAFF:BAFF-R-mediated survival signals in B cells. *Proceedings of the National Academy of Sciences*, *105*(31), 10883–10888. doi:10.1073/pnas.0805186105
90. Hampel, F., Ehrenberg, S., Hojer, C., Draeseke, A., Marschall-Schroter, G., Kuhn, R., et al. (2011). CD19-independent instruction of murine marginal zone B-cell development by constitutive Notch2 signaling. *Blood*, *118*(24), 6321–6331. doi:10.1182/blood-2010-12-325944
91. Takemori, T., Kaji, T., Takahashi, Y., Shimoda, M., & Rajewsky, K. (2014). Generation of memory B cells inside and outside germinal centers. *European journal of immunology*, *44*(5), 1258–1264. doi:10.1002/eji.201343716
92. Zhang, Y., Garcia-Ibanez, L., & Toellner, K.-M. (2016). Regulation of germinal center B-cell differentiation. *Immunological reviews*, *270*(1), 8–19. doi:10.1111/imr.12396
93. Ye, B. H., Cattoretti, G., Shen, Q., Zhang, J., Hawe, N., de Waard, R., et al. (1997). The BCL-6 proto-oncogene controls germinal-centre formation and Th2-type inflammation. *Nature genetics*, *16*(2), 161–170. doi:10.1038/ng0697-161
94. Willis, S. N., Good-Jacobson, K. L., Curtis, J., Light, A., Tellier, J., Shi, W., et al. (2014). Transcription factor IRF4 regulates germinal center cell formation through a B cell-intrinsic mechanism. *The Journal of Immunology*, *192*(7), 3200–3206. doi:10.4049/jimmunol.1303216
95. Ochiai, K., Maienschein-Cline, M., Simonetti, G., Chen, J., Rosenthal, R., Brink, R., et al. (2013). Transcriptional Regulation of Germinal Center B and Plasma Cell Fates by Dynamical Control of IRF4. *Immunity*, *38*(5), 918–929. doi:10.1016/j.immuni.2013.04.009
96. De Silva, N. S., Simonetti, G., Heise, N., & Klein, U. (2012). The diverse roles of IRF4 in late germinal center B-cell differentiation. *Immunological reviews*, *247*(1), 73–92. doi:10.1111/j.1600-065X.2012.01113.x
97. Phan, R. T., & Dalla-Favera, R. (2004). The BCL6 proto-oncogene suppresses p53 expression in germinal-centre B cells. *Nature*, *432*(7017), 635–639. doi:10.1038/nature03147
98. Nutt, S. L., Hodgkin, P. D., Tarlinton, D. M., & Corcoran, L. M. (2015). The generation of antibody-secreting plasma cells. *Nature Reviews Immunology*, *15*(3), 160–171. doi:10.1038/nri3795

99. Nojima, T., Haniuda, K., Moutai, T., Matsudaira, M., Mizokawa, S., Shiratori, I., et al. (2011). In-vitro derived germinal centre B cells differentially generate memory B or plasma cells in vivo. *Nature Communications*, *2*, 465. doi:10.1038/ncomms1475

100. Heise, N., De Silva, N. S., Silva, K., Carette, A., Simonetti, G., Pasparakis, M., & Klein, U. (2014). Germinal center B cell maintenance and differentiation are controlled by distinct NF-κB transcription factor subunits. *The Journal of experimental medicine*, *211*(10), 2103–2118. doi:10.1084/jem.20132613

101. De Silva, N. S., Anderson, M. M., Carette, A., Silva, K., Heise, N., Bhagat, G., & Klein, U. (2016). Transcription factors of the alternative NF-κB pathway are required for germinal center B-cell development. *Proceedings of the National Academy of Sciences of the United States of America*, *113*(32), 9063–9068. doi:10.1073/pnas.1602728113

102. Brightbill, H. D., Jackman, J. K., Suto, E., Kennedy, H., Jones, C., III, Chalasani, S., et al. (2015). Conditional Deletion of NF-κB–Inducing Kinase (NIK) in Adult Mice Disrupts Mature B Cell Survival and Activation. *Journal of immunology (Baltimore, Md. : 1950)*, *195*(3), 953–964. doi:10.4049/jimmunol.1401514

103. Mills, D. M., Bonizzi, G., Karin, M., & Rickert, R. C. (2007). Regulation of late B cell differentiation by intrinsic IKKalpha-dependent signals. *Proceedings of the National Academy of Sciences of the United States of America*, *104*(15), 6359–6364. doi:10.1073/pnas.0700296104

104. Baumgarth, N. (2010). The double life of a B-1 cell: self-reactivity selects for protective effector functions. *Nature Reviews Immunology*, *11*(1), 34–46. doi:10.1038/nri2901

105. Berland, R., & Wortis, H. H. (2002). Origins and functions of B-1 cells with notes on the role of CD5. *Annual Review of Immunology*, *20*, 253–300. doi:10.1146/annurev.immunol.20.100301.064833

106. Tung, J. W., Mrazek, M. D., Yang, Y., Herzenberg, L. A., & Herzenberg, L. A. (2006). Phenotypically distinct B cell development pathways map to the three B cell lineages in the mouse. *Proceedings of the National Academy of Sciences of the United States of America*, *103*(16), 6293–6298. doi:10.1073/pnas.0511305103

107. Holodick, N. E., Tumang, J. R., & Rothstein, T. L. (2010). Immunoglobulin secretion by B1 cells: Differential intensity and IRF4-dependence of spontaneous IgM secretion by peritoneal and splenic B1 cells. *European journal of immunology*, *40*(11), 3007–3016. doi:10.1002/eji.201040545

108. Sindhava, V. J., & Bondada, S. (2012). Multiple Regulatory Mechanisms Control B-1 B Cell Activation. *Frontiers in Immunology*, *3*, 1–6. doi:10.3389/fimmu.2012.00372

109. Griffin, D. O., & Rothstein, T. L. (2012). Human B1 Cell Frequency: Isolation and Analysis of Human B1 Cells. *Frontiers in Immunology*, *3*. doi:10.3389/fimmu.2012.00122

110. Esplin, B. L., Welner, R. S., Zhang, Q., Borghesi, L. A., & Kincade, P. W. (2009). A differentiation pathway for B1 cells in adult bone marrow. *Proceedings of the National Academy of Sciences*, *106*(14), 5773–5778. doi:10.1073/pnas.0811632106

111. Rajewsky, K. (2015). The Herzenberg lecture: how to make a B-1 cell? *Annals of the New York Academy of Sciences*, *1362*(1), 6–7. doi:10.1111/nyas.12767

112. Fagarasan, S., Watanabe, N., & Honjo, T. (2000). Generation, expansion, migration and activation of mouse B1 cells. *Immunological reviews*, *176*, 205–215.

113. Rickert, R. C., Rajewsky, K., & Roes, J. (1995). Impairment of T-cell-dependent B-cell responses and B-1 cell development in CD19-deficient mice. *Nature*, *376*(6538), 352–355. doi:10.1038/376352a0

114. Pao, L. I., Lam, K. P., Henderson, J. M., Kutok, J. L., Alimzhanov, M., Nitschke, L., et al. (2007). B cell-specific deletion of protein-tyrosine phosphatase Shp1 promotes B-

1a cell development and causes systemic autoimmunity. *Immunity*, *27*(1), 35–48. doi:10.1016/j.immuni.2007.04.016

115. Alsadeq, A., Hobeika, E., Medgyesi, D., Kläsener, K., & Reth, M. (2014). The role of the Syk/Shp-1 kinase-phosphatase equilibrium in B cell development and signaling. *The Journal of Immunology*, *193*(1), 268–276. doi:10.4049/jimmunol.1203040
116. Duan, B., & Morel, L. (2006). Role of B-1a cells in autoimmunity. *Autoimmunity Reviews*, *5*(6), 403–408. doi:10.1016/j.autrev.2005.10.007
117. Alugupalli, K. R., Leong, J. M., Woodland, R. T., Muramatsu, M., Honjo, T., & Gerstein, R. M. (2004). B1b lymphocytes confer T cell-independent long-lasting immunity. *Immunity*, *21*(3), 379–390. doi:10.1016/j.immuni.2004.06.019
118. Wong, S. C. (2002). Peritoneal CD5+ B-1 Cells Have Signaling Properties Similar to Tolerant B Cells. *Journal of Biological Chemistry*, *277*(34), 30707–30715. doi:10.1074/jbc.M202460200
119. Popi, A. F., Longo-Maugéri, I. M., & Mariano, M. (2016). An Overview of B-1 Cells as Antigen-Presenting Cells. *Frontiers in Immunology*, *7*(1), 253–6. doi:10.3389/fimmu.2016.00138
120. Kobayashi, T., Kim, T. S., Jacob, A., Walsh, M. C., Kadono, Y., Fuentes-Pananá, E., et al. (2009). TRAF6 Is Required for Generation of the B-1a B Cell Compartment as well as T Cell-Dependent and -Independent Humoral Immune Responses. *PLoS ONE*, *4*(3), e4736–12. doi:10.1371/journal.pone.0004736
121. Hoffmann, A., Kerr, S., Jellusova, J., Zhang, J., Weisel, F., Wellmann, U., et al. (2007). Siglec-G is a B1 cell–inhibitory receptor that controls expansion and calcium signaling of the B1 cell population. *Nature Immunology*, *8*(7), 695–704. doi:10.1038/ni1480
122. Ding, C., Liu, Y., Wang, Y., Park, B. K., Wang, C.-Y., Zheng, P., & Liu, Y. (2007). Siglecg Limits the Size of B1a B Cell Lineage by Down-Regulating NFκB Activation. *PLoS ONE*, *2*(10), e997–10. doi:10.1371/journal.pone.0000997
123. Nitschke, L. (2009). CD22 and Siglec-G: B-cell inhibitory receptors with distinct functions. *Immunological reviews*, *230*(1), 128–143. doi:10.1111/j.1600-065X.2009.00801.x
124. Deng, J., Wang, X., Chen, Q., Sun, X., Xiao, F., Ko, K.-H., et al. (2016). B1a cells play a pathogenic role in the development of autoimmune arthritis. *Oncotarget*, *7*(15), 19299–19311. doi:10.18632/oncotarget.8244
125. Bertoni, F., Rossi, D., & Zucca, E. (2018). Recent advances in understanding the biology of marginal zone lymphoma. *F1000Research*, *7*, 406. doi:10.12688/f1000research.13826.1
126. Teixeira Mendes, L. S., Peters, N., Attygalle, A. D., & Wotherspoon, A. (2017). Cyclin D1 overexpression in proliferation centres of small lymphocytic lymphoma/chronic lymphocytic leukaemia. *Journal of Clinical Pathology*, *70*(10), 899–902. doi:10.1136/jclinpath-2017-204364
127. Igawa, T., Sato, Y., Takata, K., Fushimi, S., Tamura, M., Nakamura, N., et al. (2011). Cyclin D2 is overexpressed in proliferation centers of chronic lymphocytic leukemia/small lymphocytic lymphoma. *Cancer Science*, *102*(11), 2103–2107. doi:10.1111/j.1349-7006.2011.02046.x
128. Metcalf, R. A., Zhao, S., Anderson, M. W., Lu, Z. S., Galperin, I., Marinelli, R. J., et al. (2010). Characterization of D-cyclin proteins in hematolymphoid neoplasms: lack of specificity of cyclin-D2 and D3 expression in lymphoma subtypes. *Modern Pathology*, *23*(3), 420–433. doi:10.1038/modpathol.2009.173
129. Scarfò, L., & Ghia, P. (2013). Reprogramming cell death: BCL2 family inhibition in hematological malignancies. *Immunology Letters*. doi:10.1016/j.imlet.2013.09.015

130. Gibson, S. E., Leeman-Neill, R. J., Jain, S., Piao, W., Cieply, K. M., & Swerdlow, S. H. (2016). Proliferation centres of chronic lymphocytic leukaemia/small lymphocytic lymphoma have enhanced expression of MYC protein, which does not result from rearrangement or gain of the MYC gene. *British Journal of Haematology*, *175*(1), 173–175. doi:10.1111/bjh.13844

131. Puente, X. S., Pinyol, M., Quesada, V., Conde, L., Ordóñez, G. R., Villamor, N., et al. (2011). Whole-genome sequencing identifies recurrent mutations in chronic lymphocytic leukaemia. *Nature*, *475*(7354), 101–105. doi:10.1038/nature10113

132. Kato, M., Sanada, M., Kato, I., Sato, Y., Takita, J., Takeuchi, K., et al. (2009). Frequent inactivation of A20 in B-cell lymphomas. *Nature*, *459*(7247), 712–716. doi:10.1038/nature07969

133. Zhang, J., Grubor, V., Love, C. L., Banerjee, A., Richards, K. L., Mieczkowski, P. A., et al. (2013). Genetic heterogeneity of diffuse large B-cell lymphoma. *Proceedings of the National Academy of Sciences*. doi:10.1073/pnas.1205299110

134. Kraan, W., Horlings, H. M., van Keimpema, M., Schilder-Tol, E. J. M., Oud, M. E. C. M., Scheepstra, C., et al. (2013). High prevalence of oncogenic MYD88 and CD79B mutations in diffuse large B-cell lymphomas presenting at immune-privileged sites. *Blood Cancer Journal*, *3*(9), e139. doi:10.1038/bcj.2013.28

135. Chapuy, B., Stewart, C., Dunford, A. J., Kim, J., Kamburov, A., Redd, R. A., et al. (2018). Molecular subtypes of diffuse large B cell lymphoma are associated with distinct pathogenic mechanisms and outcomes. *Nature Medicine*, *24*(5), 679–690. doi:10.1038/s41591-018-0016-8

136. Kawamata, N., Ogawa, S., Gueller, S., Ross, S. H., Huynh, T., Chen, J., et al. (2009). Identified hidden genomic changes in mantle cell lymphoma using high-resolution single nucleotide polymorphism genomic array. *Experimental Hematology*, *37*(8), 937–946. doi:10.1016/j.exphem.2009.04.012

137. Pasqualucci, L., Khiabanian, H., Fangazio, M., Vasishtha, M., Messina, M., Holmes, A. B., et al. (2014). Genetics of Follicular Lymphoma Transformation. *Cell Reports*, *6*(1), 130–140. doi:10.1016/j.celrep.2013.12.027

138. Pasqualucci, L., Trifonov, V., Fabbri, G., Ma, J., Rossi, D., Chiarenza, A., et al. (2011). Analysis of the coding genome of diffuse large B-cell lymphoma. *Nature genetics*, *43*(9), 830–837. doi:10.1038/ng.892

139. Steidl, C., & Gascoyne, R. D. (2011). The molecular pathogenesis of primary mediastinal large B-cell lymphoma. *Blood*, *118*(10), 2659–2669. doi:10.1182/blood-2011-05-326538

140. Chanudet, E., Huang, Y., Ichimura, K., Dong, G., Hamoudi, R. A., Radford, J., et al. (2009). A20 is targeted by promoter methylation, deletion and inactivating mutation in MALT lymphoma. *Leukemia : official journal of the Leukemia Society of America, Leukemia Research Fund, U.K*, *24*(2), 483–487. doi:10.1038/leu.2009.234

141. Herishanu, Y., Perez-Galan, P., Liu, D., Biancotto, A., Pittaluga, S., Vire, B., et al. (2011). The lymph node microenvironment promotes B-cell receptor signaling, NF- B activation, and tumor proliferation in chronic lymphocytic leukemia. *Blood*, *117*(2), 563–574. doi:10.1182/blood-2010-05-284984

142. Benedetti, D., Tissino, E., Pozzo, F., Bittolo, T., Caldana, C., Perini, C., et al. (2017). NOTCH1 mutations are associated with high CD49d expression in chronic lymphocytic leukemia: link between the NOTCH1 and the NF-κB pathways. *Leukemia : official journal of the Leukemia Society of America, Leukemia Research Fund, U.K*, *32*(3), 654–662. doi:10.1038/leu.2017.296

143. Mansouri, L., Sutton, L.-A., Ljungström, V., Bondza, S., Arngården, L., Bhoi, S., et al. (2015). Functional loss of IκBε leads to NF-κB deregulation in aggressive chronic lymphocytic leukemia. *Journal of Experimental Medicine*, *212*(6), 833–843.

doi:10.1084/jem.20142009

144. Meissner, B., Kridel, R., Lim, R. S., Rogic, S., Tse, K., Scott, D. W., et al. (2013). The E3 ubiquitin ligase UBR5 is recurrently mutated in mantle cell lymphoma. *Blood*, *121*(16), 3161–3164. doi:10.1182/blood-2013-01-478834

145. Pham, L. V., Fu, L., Tamayo, A. T., Bueso-Ramos, C., Drakos, E., Vega, F., et al. (2011). Constitutive BR3 receptor signaling in diffuse, large B-cell lymphomas stabilizes nuclear factor- B-inducing kinase while activating both canonical and alternative nuclear factor- B pathways. *Blood*, *117*(1), 200–210. doi:10.1182/blood-2010-06-290437

146. Ibrahim, H. A., Amen, F., Reid, A. G., & Naresh, K. N. (2011). BCL3 translocation, amplification and expression in diffuse large B-cell lymphoma. *European journal of haematology*. doi:10.1111/j.1600-0609.2011.01684.x

147. Mansouri, L., Noerenberg, D., Young, E., Mylonas, E., Abdulla, M., Frick, M., et al. (2016). Frequent NFKBIE deletions are associated with poor outcome in primary mediastinal B-cell lymphoma. *Blood*, *128*(23), 2666–2670. doi:10.1182/blood-2016-03-704528

148. Küppers, R. (2009). Molecular biology of Hodgkin lymphoma. *Hematology / the Education Program of the American Society of Hematology. American Society of Hematology. Education Program*, 491–496. doi:10.1182/asheducation-2009.1.491

149. Ranuncolo, S. M., Pittaluga, S., Evbuomwan, M. O., Jaffe, E. S., & Lewis, B. A. (2012). Hodgkin lymphoma requires stabilized NIK and constitutive RelB expression for survival. *Blood*, *120*(18), 3756–3763. doi:10.1182/blood-2012-01-405951

150. Otto, C., Giefing, M., Massow, A., Vater, I., Gesk, S., Schlesner, M., et al. (2012). Genetic lesions of the TRAF3 and MAP3K14 genes in classical Hodgkin lymphoma. *British Journal of Haematology*, *157*(6), 702–708. doi:10.1111/j.1365-2141.2012.09113.x

151. Demchenko, Y. N., Glebov, O. K., Zingone, A., Keats, J. J., Bergsagel, P. L., & Kuehl, W. M. (2010). Classical and/or alternative NF-kappaB pathway activation in multiple myeloma. *Blood*, *115*(17), 3541–3552. doi:10.1182/blood-2009-09-243535

152. Troppan, K., Hofer, S., Wenzl, K., Lassnig, M., Pursche, B., Steinbauer, E., et al. (2015). Frequent Down Regulation of the Tumor Suppressor Gene A20 in Multiple Myeloma. *PLoS ONE*, *10*(4), e0123922–12. doi:10.1371/journal.pone.0123922

153. Kasama, Y., Mizukami, T., Kusunoki, H., Peveling-Oberhag, J., Nishito, Y., Ozawa, M., et al. (2014). B-Cell-Intrinsic Hepatitis C Virus Expression Leads to B-Cell-Lymphomagenesis and Induction of NF-κB Signalling. *PLoS ONE*, *9*(3), e91373–11. doi:10.1371/journal.pone.0091373

154. Novak, U., Rinaldi, A., Kwee, I., Nandula, S. V., Rancoita, P. M. V., Compagno, M., et al. (2009). The NF- B negative regulator TNFAIP3 (A20) is inactivated by somatic mutations and genomic deletions in marginal zone lymphomas. *Blood*, *113*(20), 4918–4921. doi:10.1182/blood-2008-08-174110

155. Honma, K., Tsuzuki, S., Nakagawa, M., Karnan, S., Aizawa, Y., Kim, W. S., et al. (2008). TNFAIP3is the target gene of chromosome band 6q23.3-q24.1 loss in ocular adnexal marginal zone B cell lymphoma. *Genes, Chromosomes and Cancer*, *47*(1), 1–7. doi:10.1002/gcc.20499

156. Kim, W. S., Honma, K., Karnan, S., Tagawa, H., Kim, Y. D., Oh, Y. L., et al. (2007). Genome-wide array-based comparative genomic hybridization of ocular marginal zone B cell lymphoma: comparison with pulmonary and nodal marginal zone B cell lymphoma. *Genes, Chromosomes and Cancer*, *46*(8), 776–783. doi:10.1002/gcc.20463

157. Bi, Y., Zeng, N., Chanudet, E., Huang, Y., Hamoudi, R. A., Liu, H., et al. (2012). A20 inactivation in ocular adnexal MALT lymphoma. *Haematologica*, *97*(6), 926–930.

doi:10.3324/haematol.2010.036798

158. Honma, K., Tsuzuki, S., Nakagawa, M., Tagawa, H., Nakamura, S., Morishima, Y., & Seto, M. (2009). TNFAIP3/A20 functions as a novel tumor suppressor gene in several subtypes of non-Hodgkin lymphomas. *Blood*, *114*(12), 2467–2475. doi:10.1182/blood-2008-12-194852

159. Chanudet, E., Ye, H., Ferry, J., Bacon, C., Adam, P., Müller-Hermelink, H., et al. (2009). A20deletion is associated with copy number gain at the TNFA/B/Clocus and occurs preferentially in translocation-negative MALT lymphoma of the ocular adnexa and salivary glands. *The Journal of Pathology*, *217*(3), 420–430. doi:10.1002/path.2466

160. Schmitz, R., Hansmann, M. L., Bohle, V., Martin-Subero, J. I., Hartmann, S., Mechtersheimer, G., et al. (2009). TNFAIP3 (A20) is a tumor suppressor gene in Hodgkin lymphoma and primary mediastinal B cell lymphoma. *Journal of Experimental Medicine*, *206*(5), 981–989. doi:10.1084/jem.20090528

161. Nomoto, J., Hiramoto, N., Kato, M., Sanada, M., Maeshima, A. M., Taniguchi, H., et al. (2012). Deletion of the TNFAIP3/A20 gene detected by FICTION analysis in classical Hodgkin lymphoma. *BMC Cancer*, *12*(1), 457. doi:10.1186/1471-2407-12-457

162. Paik, J. H., Go, H., Nam, S. J., Kim, T. M., Heo, D. S., Kim, C.-W., & Jeon, Y. K. (2013). Clinicopathologic implication of A20/TNFAIP3 deletion in diffuse large B-cell lymphoma: an analysis according to immunohistochemical subgroups and rituximab treatment. *Leukemia & lymphoma*, 1–8. doi:10.3109/10428194.2012.762511

163. Philipp, C., Edelmann, J., Bühler, A., Winkler, D., Stilgenbauer, S., & Küppers, R. (2010). Mutation analysis of the TNFAIP3 (A20) tumor suppressor gene in CLL. *International journal of cancer. Journal international du cancer*, *128*(7), 1747–1750. doi:10.1002/ijc.25497

164. Calado, D. P., Zhang, B., Srinivasan, L., Sasaki, Y., Seagal, J., Unitt, C., et al. (2010). Constitutive Canonical NF-κB Activation Cooperates with Disruption of BLIMP1 in the Pathogenesis of Activated B Cell-like Diffuse Large Cell Lymphoma. *Cancer Cell*, *18*(6), 580–589. doi:10.1016/j.ccr.2010.11.024

165. Zhang, B., Calado, D. P., Wang, Z., Fröhler, S., Köchert, K., Qian, Y., et al. (2015). An oncogenic role for alternative NF-κB signaling in DLBCL revealed upon deregulated BCL6 expression. *Cell Reports*, *11*(5), 715–726. doi:10.1016/j.celrep.2015.03.059

166. Schuh, K., Avots, A., Tony, H. P., Serfling, E., & Kneitz, C. (1996). Nuclear NF-ATp is a hallmark of unstimulated B cells from B-CLL patients. *Leukemia & lymphoma*, *23*(5-6), 583–592. doi:10.3109/10428199609054868

167. Lutzny, G., Kocher, T., Schmidt-Supprian, M., Rudelius, M., Klein-Hitpass, L., Finch, A. J., et al. (2013). Protein Kinase C-β-Dependent Activation of NF-κB in Stromal Cells Is Indispensable for the Survival of Chronic Lymphocytic Leukemia B Cells In Vivo. *Cancer Cell*, *23*(1), 77–92. doi:10.1016/j.ccr.2012.12.003

168. Patten, C. L., & Cutucache, C. E. (2016). Murine Models of Splenic Marginal Zone Lymphoma: A Role for Cav1? *Frontiers in Oncology*, *6*(7), 487–7. doi:10.3389/fonc.2016.00258

169. Piris, M. A., Onaindía, A., & Mollejo, M. (2017). Splenic marginal zone lymphoma. *Best Practice & Research Clinical Haematology*, *30*(1-2), 56–64. doi:10.1016/j.beha.2016.09.005

170. Bikos, V., Darzentas, N., Hadzidimitriou, A., Davis, Z., Hockley, S., Traverse-Glehen, A., et al. (2012). Over 30% of patients with splenic marginal zone lymphoma express the same immunoglobulin heavy variable gene: ontogenetic implications. *Leukemia : official journal of the Leukemia Society of America, Leukemia Research Fund, U.K*. doi:10.1038/leu.2012.3

171. Yan, Q., Huang, Y., Watkins, A. J., Kocialkowski, S., Zeng, N., Hamoudi, R. A., et al. (2012). BCR and TLR signaling pathways are recurrently targeted by genetic changes in splenic marginal zone lymphomas. *Haematologica*, *97*(4), 595–598. doi:10.3324/haematol.2011.054080

172. Peveling-Oberhag, J., Crisman, G., Schmidt, A., Döring, C., Lucioni, M., Arcaini, L., et al. (2012). Dysregulation of global microRNA expression in splenic marginal zone lymphoma and influence of chronic hepatitis C virus infection. *Leukemia : official journal of the Leukemia Society of America, Leukemia Research Fund, U.K*, –. doi:10.1038/leu.2012.29

173. Arcaini, L., & Rossi, D. (2012). Nuclear factor- B dysregulation in splenic marginal zone lymphoma: new therapeutic opportunities. *Haematologica*, *97*(5), 638–640. doi:10.3324/haematol.2011.058362

174. Rossi, D., & Gaidano, G. (2012). Molecular genetics of high-risk chronic lymphocytic leukemia. *Expert Review of Hematology*, *5*(6), 593–602. doi:10.1586/ehm.12.58

175. Gaidano, G., Foà, R., & Dalla-Favera, R. (2012). Molecular pathogenesis of chronic lymphocytic leukemia. *Journal of Clinical Investigation*, *122*(10), 3432–3438. doi:10.1172/JCI64101

176. Arribas, A. J., Gómez-Abad, C., Sánchez-Beato, M., Martínez, N., DiLisio, L., Casado, F., et al. (2013). Splenic marginal zone lymphoma: comprehensive analysis of gene expression and miRNA profiling. *Modern Pathology*, *26*(7), 889–901. doi:10.1038/modpathol.2012.220

177. Clipson, A., Wang, M., de Leval, L., Ashton-Key, M., Wotherspoon, A., Vassiliou, G., et al. (2014). KLF2 mutation is the most frequent somatic change in splenic marginal zone lymphoma and identifies a subset with distinct genotype. *Leukemia : official journal of the Leukemia Society of America, Leukemia Research Fund, U.K*, *29*(5), 1177–1185. doi:10.1038/leu.2014.330

178. Kiel, M. J., Velusamy, T., Betz, B. L., Zhao, L., Weigelin, H. G., Chiang, M. Y., et al. (2012). Whole-genome sequencing identifies recurrent somatic NOTCH2mutations in splenic marginal zone lymphoma. *The Journal of experimental medicine*, *209*(9), 1553–1565. doi:10.1084/jem.20120910

179. Rossi, D., Trifonov, V., Fangazio, M., Bruscaggin, A., Rasi, S., Spina, V., et al. (2012). The coding genome of splenic marginal zone lymphoma: activation of NOTCH2 and other pathways regulating marginal zone development. *Journal of Experimental Medicine*, *209*(9), 1537–1551. doi:10.1084/jem.20120904

180. Peveling-Oberhag, J., Wolters, F., Döring, C., Walter, D., Sellmann, L., Scholtysik, R., et al. (2015). Whole exome sequencing of microdissected splenic marginal zone lymphoma: a study to discover novel tumor-specific mutations. *BMC Cancer*, *15*(1), 540–10. doi:10.1186/s12885-015-1766-z

181. Campos-Martín, Y., Martínez, N., Martínez-López, A., Cereceda, L., Casado, F., Algara, P., et al. (2017). Clinical and diagnostic relevance of NOTCH2-and KLF2-mutations in splenic marginal zone lymphoma. *Haematologica*, *102*(8), e310–e312. doi:10.3324/haematol.2016.161711

182. Enzler, T., Bonizzi, G., Silverman, G. J., Otero, D. C., Widhopf, G. F., Anzelon-Mills, A., et al. (2006). Alternative and Classical NF-κB Signaling Retain Autoreactive B Cells in the Splenic Marginal Zone and Result in Lupus-like Disease. *Immunity*, *25*(3), 403–415. doi:10.1016/j.immuni.2006.07.010

183. Rossi, D., Deaglio, S., Dominguez-Sola, D., Rasi, S., Vaisitti, T., Agostinelli, C., et al. (2011). Alteration of BIRC3 and multiple other NF- B pathway genes in splenic marginal zone lymphoma. *Blood*, *118*(18), 4930–4934. doi:10.1182/blood-2011-06-359166

184. Moore, C. R., Liu, Y., Shao, C., Covey, L. R., Morse, H. C., & Xie, P. (2011). Specific

deletion of TRAF3 in B lymphocytes leads to B-lymphoma development in mice. *Leukemia : official journal of the Leukemia Society of America, Leukemia Research Fund, U.K*, *26*(5), 1122–1127. doi:10.1038/leu.2011.309

185. Li, Z., Wang, H., Xue, L., Shin, D. M., Roopenian, D., Xu, W., et al. (2009). E -BCL10 mice exhibit constitutive activation of both canonical and noncanonical NF- B pathways generating marginal zone (MZ) B-cell expansion as a precursor to splenic MZ lymphoma. *Blood*, *114*(19), 4158–4168. doi:10.1182/blood-2008-12-192583
186. Hart, G. T., Wang, X., Hogquist, K. A., & Jameson, S. C. (2011). Kruppel-like factor 2 (KLF2) regulates B-cell reactivity, subset differentiation, and trafficking molecule expression. *Proceedings of the National Academy of Sciences of the United States of America*, *108*(2), 716–721. doi:10.1073/pnas.1013168108
187. Jha, P., & Das, H. (2017). KLF2 in Regulation of NF-κB-Mediated Immune Cell Function and Inflammation. *International Journal of Molecular Sciences*, *18*(11), 2383–18. doi:10.3390/ijms18112383
188. Landau, D. A., Carter, S. L., Stojanov, P., McKenna, A., Stevenson, K., Lawrence, M. S., et al. (2013). Evolution and Impact of Subclonal Mutations in Chronic Lymphocytic Leukemia. *Cell*, *152*(4), 714–726. doi:10.1016/j.cell.2013.01.019
189. López, C., Delgado, J., Costa, D., Villamor, N., Navarro, A., Cazorla, M., et al. (2013). Clonal evolution in chronic lymphocytic leukemia: Analysis of correlations with IGHVmutational status, NOTCH1mutations and clinical significance. *Genes, Chromosomes and Cancer*, n/a–n/a. doi:10.1002/gcc.22087
190. Fabbri, G., Khiabanian, H., Holmes, A. B., Wang, J., Messina, M., Mullighan, C. G., et al. (2013). Genetic lesions associated with chronic lymphocytic leukemia transformation to Richter syndrome. *Journal of Experimental Medicine*, *12*(2), 115. doi:10.1016/S0092-8674(00)81401-4
191. Rossi, D., Ciardullo, C., Spina, V., & Gaidano, G. (2013). Molecular bases of chronic lymphocytic leukemia in light of new treatments. *Immunology Letters*. doi:10.1016/j.imlet.2013.09.010
192. Seifert, M., Sellmann, L., Bloehdorn, J., Wein, F., Stilgenbauer, S., Dürig, J., & Küppers, R. (2012). Cellular origin and pathophysiology of chronic lymphocytic leukemia. *Journal of Experimental Medicine*, *209*(12), 2183–2198. doi:10.1084/jem.20120833
193. Landau, D. A., & Wu, C. J. (2013). Chronic lymphocytic leukemia: molecular heterogeneity revealed by high-throughput genomics. *Genome medicine*, *5*(5), 47. doi:10.1186/gm451
194. Damm, F., Mylonas, E., Cosson, A., Yoshida, K., Valle, Della, V., Mouly, E., et al. (2014). Acquired Initiating Mutations in Early Hematopoietic Cells of CLL Patients. *Cancer Discovery*, *4*(9), 1088–1101. doi:10.1158/2159-8290.CD-14-0104
195. Furman, R. R., Asgary, Z., Mascarenhas, J. O., Liou, H. C., & Schattner, E. J. (2000). Modulation of NF-kappa B activity and apoptosis in chronic lymphocytic leukemia B cells. *Journal of immunology (Baltimore, Md. : 1950)*, *164*(4), 2200–2206.
196. Herreros, B., Rodríguez-Pinilla, S. M., Pajares, R., Martínez-Gónzalez, M. Á., Ramos, R., Munoz, I., et al. (2010). Proliferation centers in chronic lymphocytic leukemia: the niche where NF-κB activation takes place. *Leukemia : official journal of the Leukemia Society of America, Leukemia Research Fund, U.K*, *24*(4), 872–876. doi:10.1038/leu.2009.285
197. Cuní, S., Pérez-Aciego, P., Pérez-Chacón, G., Vargas, J. A., Sánchez, A., Martín-Saavedra, F. M., et al. (2004). A sustained activation of PI3K/NF-κB pathway is critical for the survival of chronic lymphocytic leukemia B cells. *Leukemia : official journal of the Leukemia Society of America, Leukemia Research Fund, U.K*, *18*(8), 1391–1400. doi:10.1038/sj.leu.2403398
198. Hewamana, S., Alghazal, S., Lin, T. T., Clement, M., Jenkins, C., Guzman, M. L., et al.

(2008). The NF-kappaB subunit Rel A is associated with in vitro survival and clinical disease progression in chronic lymphocytic leukemia and represents a promising therapeutic target. *Blood*, *111*(9), 4681–4689. doi:10.1182/blood-2007-11-125278

199. Pepper, C., Hewamana, S., Brennan, P., & Fegan, C. (2009). NF-κB as a prognostic marker and therapeutic target in chronic lymphocytic leukemia. *Future Oncology*, *5*(7), 1027–1037. doi:10.2217/fon.09.72

200. López-Guerra, M., & Colomer, D. (2010). NF-κB as a therapeutic target in chronic lymphocytic leukemia. *Expert Opinion on Therapeutic Targets*, *14*(3), 275–288. doi:10.1517/14728221003598930

201. Tromp, J. M., Tonino, S. H., Elias, J. A., Jaspers, A., Luijks, D. M., Kater, A. P., et al. (2010). Dichotomy in NF-κB signaling and chemoresistance in immunoglobulin variable heavy-chain-mutated versus unmutated CLL cells upon CD40/TLR9 triggering. *Oncogene*, *29*(36), 5071–5082. doi:10.1038/onc.2010.248

202. Nakaima, Y., Watanabe, K., Koyama, T., Miura, O., & Fukuda, T. (2013). CD137 Is Induced by the CD40 Signal on Chronic Lymphocytic Leukemia B Cells and Transduces the Survival Signal via NF-κB Activation. *PLoS ONE*, *8*(5), e64425. doi:10.1371/journal.pone.0064425.s002

203. Endo, T., Nishio, M., Enzler, T., Cottam, H. B., Fukuda, T., James, D. F., et al. (2007). BAFF and APRIL support chronic lymphocytic leukemia B-cell survival through activation of the canonical NF-kappaB pathway. *Blood*, *109*(2), 703–710. doi:10.1182/blood-2006-06-027755

204. Rozovski, U., Harris, D. M., Li, P., Liu, Z., Jain, P., Veletic, I., et al. (2017). Activation of the B-cell receptor successively activates NF-κB and STAT3 in chronic lymphocytic leukemia cells. *International journal of cancer. Journal international du cancer*, *141*(10), 2076–2081. doi:10.1002/ijc.30892

205. Ponader, S., Chen, S.-S., Buggy, J. J., Balakrishnan, K., Gandhi, V., Wierda, W. G., et al. (2012). The Bruton tyrosine kinase inhibitor PCI-32765 thwarts chronic lymphocytic leukemia cell survival and tissue homing in vitro and in vivo. *Blood*, *119*(5), 1182–1189. doi:10.1182/blood-2011-10-386417

206. Woyach, J. A., Bojnik, E., Ruppert, A. S., Stefanovski, M. R., Goettl, V. M., Smucker, K. A., et al. (2014). Bruton's tyrosine kinase (BTK) function is important to the development and expansion of chronic lymphocytic leukemia (CLL). *Blood*, *123*(8), 1207–1213. doi:10.1182/blood-2013-07-515361

207. Herman, S. E. M., Mustafa, R. Z., Gyamfi, J. A., Pittaluga, S., Chang, S., Chang, B., et al. (2014). Ibrutinib inhibits BCR and NF-κB signaling and reduces tumor proliferation in tissue-resident cells of patients with CLL. *Blood*, *123*(21), 3286–3295. doi:10.1182/blood-2014-02-548610

208. Colombo, M., Cutrona, G., Reverberi, D., Fabris, S., Neri, A., Fabbi, M., et al. (2011). Intraclonal cell expansion and selection driven by B cell receptor in chronic lymphocytic leukemia. *Molecular medicine (Cambridge, Mass.)*, *17*(7-8), 834–839. doi:10.2119/molmed.2011.00047

209. Sellmann, L., Scholtysik, R., Kreuz, M., Cyrull, S., Tiacci, E., Stanelle, J., et al. (2010). Gene dosage effects in chronic lymphocytic leukemia. *Cancer Genetics and Cytogenetics*, *203*(2), 149–160. doi:10.1016/j.cancergencyto.2010.09.002

210. Garding, A., Bhattacharya, N., Claus, R., Ruppel, M., Tschuch, C., Filarsky, K., et al. (2013). Epigenetic Upregulation of lncRNAs at 13q14.3 in Leukemia Is Linked to the In Cis Downregulation of a Gene Cluster That Targets NF-kB. *PLoS Genetics*, *9*(4), e1003373. doi:10.1371/journal.pgen.1003373.s012

211. Edelmann, J., Holzmann, K., Miller, F., Winkler, D., Buhler, A., Zenz, T., et al. (2012). High-resolution genomic profiling of chronic lymphocytic leukemia reveals new

recurrent genomic alterations. *Blood*, *120*(24), 4783–4794. doi:10.1182/blood-2012-04-423517

212. Rossi, D., Rasi, S., Spina, V., Bruscaggin, A., Monti, S., Ciardullo, C., et al. (2013). Integrated mutational and cytogenetic analysis identifies new prognostic subgroups in chronic lymphocytic leukemia. *Blood*, *121*(8), 1403–1412. doi:10.1182/blood-2012-09-458265

213. Landau, D. A., Carter, S. L., Getz, G., & Wu, C. J. (2013). Clonal evolution in hematological malignancies and therapeutic implications. *Leukemia : official journal of the Leukemia Society of America, Leukemia Research Fund, U.K*, *28*(1), 34–43. doi:10.1038/leu.2013.248

214. Jimenez-Zepeda, V. H., Chng, W. J., Schop, R. F. J., Braggio, E., Leis, J. F., Kay, N., & Fonseca, R. (2013). Recurrent Chromosome Abnormalities Define Nonoverlapping Unique Subgroups of Tumors in Patients With Chronic Lymphocytic Leukemia and Known Karyotypic Abnormalities. *Clinical Lymphoma Myeloma and Leukemia*, *13*(4), 467–476. doi:10.1016/j.clml.2013.05.003

215. Delgado, J., Salaverria, I., Baumann, T., Martínez-Trillos, A., Lee, E., Jiménez, L., et al. (2014). Genomic complexity and IGHV mutational status are key predictors of outcome of chronic lymphocytic leukemia patients with TP53 disruption. *Haematologica*, *99*(11), e231–4. doi:10.3324/haematol.2014.108365

216. Schnaiter, A., Paschka, P., Rossi, M., Zenz, T., Buhler, A., Winkler, D., et al. (2013). NOTCH1, SF3B1 and TP53 mutations in fludarabine-refractory CLL patients treated with alemtuzumab: results from the CLL2H trial of the GCLLSG. *Blood*. doi:10.1182/blood-2013-03-488197

217. Di Bernardo, M. C., Crowther-Swanepoel, D., Broderick, P., Webb, E., Sellick, G., Wild, R., et al. (2008). A genome-wide association study identifies six susceptibility loci for chronic lymphocytic leukemia. *Nature genetics*, *40*(10), 1204–1210. doi:10.1038/ng.219

218. Quesada, V., Conde, L., Villamor, N., Ordóñez, G. R., Jares, P., Bassaganyas, L., et al. (2011). Exome sequencing identifies recurrent mutations of the splicing factor SF3B1 gene in chronic lymphocytic leukemia. *Nature genetics*, *44*(1), 47–52. doi:10.1038/ng.1032

219. Strefford, J. C., Sutton, L.-A., Baliakas, P., Agathangelidis, A., Malčíková, J., Plevova, K., et al. (2013). Distinct patterns of novel gene mutations in poor-prognostic stereotyped subsets of chronic lymphocytic leukemia: the case of SF3B1 and subset #2. *Leukemia : official journal of the Leukemia Society of America, Leukemia Research Fund, U.K*. doi:10.1038/leu.2013.98

220. Dreger, P., Schnaiter, A., Zenz, T., Bottcher, S., Rossi, M., Paschka, P., et al. (2013). TP53, SF3B1, and NOTCH1 mutations and outcome of allotransplantation for chronic lymphocytic leukemia: six-year follow-up of the GCLLSG CLL3X trial. *Blood*, *121*(16), 3284–3288. doi:10.1182/blood-2012-11-469627

221. Fabbri, G., Rasi, S., Rossi, D., Trifonov, V., Khiabanian, H., Ma, J., et al. (2011). Analysis of the chronic lymphocytic leukemia coding genome: role of NOTCH1 mutational activation. *Journal of Experimental Medicine*, *208*(7), 1389–1401. doi:10.1016/j.ccr.2005.04.012

222. Rossi, D., Rasi, S., Fabbri, G., Spina, V., Fangazio, M., Forconi, F., et al. (2012). Mutations of NOTCH1 are an independent predictor of survival in chronic lymphocytic leukemia. *Blood*, *119*(2), 521–529. doi:10.1182/blood-2011-09-379966

223. Willander, K., Dutta, R. K., Ungerbäck, J., Gunnarsson, R., Juliusson, G., Fredrikson, M., et al. (2013). NOTCH1 mutations influence survival in chronic lymphocytic leukemia patients. *BMC Cancer*, *13*(1), 274. doi:10.1186/1471-2407-13-274

224. Ramsay, A. J., Quesada, V., Foronda, M., Conde, L., Martínez-Trillos, A., Villamor, N., et al. (2013). POT1 mutations cause telomere dysfunction in chronic lymphocytic leukemia. *Nature genetics*. doi:10.1038/ng.2584

225. Havelange, V., PEKARSKY, Y., Nakamura, T., Palamarchuk, A., Alder, H., Rassenti, L., et al. (2011). IRF4 mutations in chronic lymphocytic leukemia. *Blood*, *118*(10), 2827–2829. doi:10.1182/blood-2011-04-350579

226. Wu, W., Zhu, H., Fu, Y., Shen, W., Xu, J., Miao, K., et al. (2013). Clinical significance of down-regulated cylindromatosis gene (CYLD) in chronic lymphocytic leukemia. *Leukemia & lymphoma*, 1–18. doi:10.3109/10428194.2013.809077

227. Baer, C., Oakes, C. C., Ruppert, A. S., Claus, R., Kim-Wanner, S.-Z., Mertens, D., et al. (2015). Epigenetic silencing of miR-708 enhances NF-κB signaling in chronic lymphocytic leukemia. *International journal of cancer. Journal international du cancer*, *137*(6), 1352–1361. doi:10.1002/ijc.29491

228. Simonetti, G., Bertilaccio, M. T. S., Ghia, P., & Klein, U. (2014). Mouse models in the study of chronic lymphocytic leukemia pathogenesis and therapy. *Blood*, *124*(7), 1010–1019. doi:10.1182/blood-2014-05-577122

229. Bichi, R., Shinton, S. A., Martin, E. S., Koval, A., Calin, G. A., Cesari, R., et al. (2002). Human chronic lymphocytic leukemia modeled in mouse by targeted TCL1 expression. *Proceedings of the National Academy of Sciences of the United States of America*, *99*(10), 6955–6960. doi:10.1073/pnas.102181599

230. PEKARSKY, Y., Koval, A., Hallas, C., Bichi, R., Tresini, M., Malstrom, S., et al. (2000). Tcl1 enhances Akt kinase activity and mediates its nuclear translocation. *Proceedings of the National Academy of Sciences of the United States of America*, *97*(7), 3028–3033. doi:10.1073/pnas.040557697

231. Pekarsky, Y., Palamarchuk, A., Maximov, V., Efanov, A., Nazaryan, N., Santanam, U., et al. (2008). Tcl1 functions as a transcriptional regulator and is directly involved in the pathogenesis of CLL. *Proceedings of the National Academy of Sciences*, *105*(50), 19643–19648. doi:10.1073/pnas.0810965105

232. Gaudio, E., Spizzo, R., Paduano, F., Luo, Z., Efanov, A., Palamarchuk, A., et al. (2012). Tcl1 interacts with Atm and enhances NF- B activation in hematologic malignancies. *Blood*, *119*(1), 180–187. doi:10.1182/blood-2011-08-374561

233. Chen, S.-S., Raval, A., Johnson, A. J., Hertlein, E., Liu, T.-H., Jin, V. X., et al. (2009). Epigenetic changes during disease progression in a murine model of human chronic lymphocytic leukemia. *Proceedings of the National Academy of Sciences*, *106*(32), 13433–13438. doi:10.1073/pnas.0906455106

234. Klein, U., Lia, M., Crespo, M., Siegel, R., Shen, Q., Mo, T., et al. (2010). The DLEU2/miR-15a/16-1 Cluster Controls B Cell Proliferation and Its Deletion Leads to Chronic Lymphocytic Leukemia. *Cancer Cell*, *17*(1), 28–40. doi:10.1016/j.ccr.2009.11.019

235. Lia, M., Carette, A., Tang, H., Shen, Q., Mo, T., Bhagat, G., et al. (2012). Functional dissection of the chromosome 13q14 tumor-suppressor locus using transgenic mouse lines. *Blood*, *119*(13), 2981–2990. doi:10.1182/blood-2011-09-381814

236. Planelles, L., Carvalho-Pinto, C. E., Hardenberg, G., Smaniotto, S., Savino, W., Gómez-Caro, R., et al. (2004). APRIL promotes B-1 cell-associated neoplasm. *Cancer Cell*, *6*(4), 399–408. doi:10.1016/j.ccr.2004.08.033

237. Lascano, V., Guadagnoli, M., Schot, J. G., Luijks, D. M., Guikema, J. E. J., Cameron, K., et al. (2013). Chronic lymphocytic leukemia disease progression is accelerated by APRIL / TACI interaction in the TCL1 transgenic mouse model. *Blood*. doi:10.1182/blood-2013-04-497693

238. Kil, L. P., de Bruijn, M. J., van Hulst, J. A., Langerak, A. W., Yuvaraj, S., & Hendriks, R. W. (2013). Bruton's tyrosine kinase mediated signaling enhances leukemogenesis

in a mouse model for chronic lymphocytic leukemia. *American journal of blood research*, *3*(1), 71–83.

239. Vereecke, L., Beyaert, R., & van Loo, G. (2009). The ubiquitin-editing enzyme A20 (TNFAIP3) is a central regulator of immunopathology. *Trends in Immunology*, *30*(8), 383–391. doi:10.1016/j.it.2009.05.007

240. Vereecke, L., Sze, M., Guire, C. M., Rogiers, B., Chu, Y., Schmidt-Supprian, M., et al. (2010). Enterocyte-specific A20 deficiency sensitizes to tumor necrosis factor-induced toxicity and experimental colitis. *Journal of Experimental Medicine*, *207*(7), 1513–1523. doi:10.1084/jem.20092474

241. Rickert, R. C., Roes, J., & Rajewsky, K. (1997). B lymphocyte-specific, Cre-mediated mutagenesis in mice. *Nucleic Acids Research*, *25*(6), 1317–1318. doi:10.1038/onc.2014.450

242. Heger, K., Kober, M., Rieß, D., Drees, C., de Vries, I., Bertossi, A., et al. (2015). A novel Cre recombinase reporter mouse strain facilitates selective and efficient infection of primary immune cells with adenoviral vectors. *European journal of immunology*, *45*(6), 1614–1620. doi:10.1002/eji.201545457

243. Casola, S., Cattoretti, G., Uyttersprot, N., Koralov, S. B., Seagal, J., Segal, J., et al. (2006). Tracking germinal center B cells expressing germ-line immunoglobulin gamma1 transcripts by conditional gene targeting. *Proceedings of the National Academy of Sciences of the United States of America*, *103*(19), 7396–7401. doi:10.1073/pnas.0602353103

244. Robbiani, D. F., Bothmer, A., Callen, E., Reina-San-Martin, B., Dorsett, Y., Difilippantonio, S., et al. (2008). AID Is Required for the Chromosomal Breaks in c-myc that Lead to c-myc/IgH Translocations. *Cell*, *135*(6), 1028–1038. doi:10.1016/j.cell.2008.09.062

245. Leitges, M., Schmedt, C., Guinamard, R., Davoust, J., Schaal, S., Stabel, S., & Tarakhovsky, A. (1996). Immunodeficiency in protein kinase cbeta-deficient mice. *Science*, *273*(5276), 788–791.

246. Arnaout, R., Lee, W., Cahill, P., Honan, T., Sparrow, T., Weiand, M., et al. (2011). High-Resolution Description of Antibody Heavy-Chain Repertoires in Humans. *PLoS ONE*, *6*(8), e22365–8. doi:10.1371/journal.pone.0022365

247. Dechow, T., Steidle, S., Götze, K. S., Rudelius, M., Behnke, K., Pechloff, K., et al. (2014). GP130 activation induces myeloma and collaborates with MYC. *Journal of Clinical Investigation*, *124*(12), 5263–5274. doi:10.1172/JCI69094

248. Thieme, F., Engler, C., Kandzia, R., & Marillonnet, S. (2011). Quick and clean cloning: a ligation-independent cloning strategy for selective cloning of specific PCR products from non-specific mixes. *PLoS ONE*, *6*(6), e20556. doi:10.1371/journal.pone.0020556

249. Alamyar, E., Giudicelli, V., Li, S., Duroux, P., & Lefranc, M.-P. (2014, July 28). IMGT/HIGHV-QUEST: THE IMGT WEB PORTAL FOR IMMUNOGLOBULIN (IG) OR ANTIBODY AND T CELL RECEPTOR (TR) ANALYSIS FROM NGS HIGH THROUGHPUT AND DEEP SEQUENCING
. *Immunome Research*. Retrieved July 28, 2014, from www.immunome-research.net

250. Martin, F., & Kearney, J. F. (2000). B-cell subsets and the mature preimmune repertoire. Marginal zone and B1 B cells as part of a "natural immune memory". *Immunological reviews*, *175*, 70–79.

251. Pillai, S., Cariappa, A., & Moran, S. T. (2005). MARGINAL ZONE B CELLS. *Annual Review of Immunology*, *23*(1), 161–196. doi:10.1146/annurev.immunol.23.021704.115728

252. Debnath, I., Roundy, K. M., Weis, J. J., & Weis, J. H. (2007). Defining In Vivo Transcription Factor Complexes of the Murine CD21 and CD23 Genes. *Journal of*

*immunology (Baltimore, Md. : 1950)*, *178*(11), 7139–7150. doi:10.4049/jimmunol.178.11.7139

253. Speiser, D. E., Utzschneider, D. T., Oberle, S. G., Münz, C., Romero, P., & Zehn, D. (2014). T cell differentiation in chronic infection and cancer: functional adaptation or exhaustion? *Nature Reviews Immunology*, *14*(11), 768–774. doi:10.1038/nri3740

254. Tavares, R. M., Turer, E. E., Liu, C. L., Advincula, R., Scapini, P., Rhee, L., et al. (2010). The Ubiquitin Modifying Enzyme A20 Restricts B Cell Survival and Prevents Autoimmunity. *Immunity*, *33*(2), 181–191. doi:10.1016/j.immuni.2010.07.017

255. Packham, G., Krysov, S., Allen, A., Savelyeva, N., Steele, A. J., Forconi, F., & Stevenson, F. K. (2014). The outcome of B-cell receptor signaling in chronic lymphocytic leukemia: proliferation or anergy. *Haematologica*, *99*(7), 1138–1148. doi:10.3324/haematol.2013.098384

256. Yan, X.-J., Albesiano, E., Zanesi, N., Yancopoulos, S., Sawyer, A., Romano, E., et al. (2006). B cell receptors in TCL1 transgenic mice resemble those of aggressive, treatment-resistant human chronic lymphocytic leukemia. *Proceedings of the National Academy of Sciences of the United States of America*, *103*(31), 11713–11718. doi:10.1073/pnas.0604564103

257. Ma, J. K., Platt, M. Y., Eastham-Anderson, J., Shin, J. S., & Mellman, I. (2012). MHC class II distribution in dendritic cells and B cells is determined by ubiquitin chain length. *Proceedings of the National Academy of Sciences of the United States of America*, *109*(23), 8820–8827. doi:10.1073/pnas.1202977109

258. Matsuki, Y., Ohmura-Hoshino, M., Goto, E., Aoki, M., Mito-Yoshida, M., Uematsu, M., et al. (2007). Novel regulation of MHC class II function in B cells. *The EMBO journal*, *26*(3), 846–854. doi:10.1038/sj.emboj.7601556

259. Chen, S. S., Chang, B. Y., Chang, S., Tong, T., Ham, S., Sherry, B., et al. (2015). BTK inhibition results in impaired CXCR4 chemokine receptor surface expression, signaling and function in chronic lymphocytic leukemia. *Leukemia : official journal of the Leukemia Society of America, Leukemia Research Fund, U.K*, *30*(4), 833–843. doi:10.1038/leu.2015.316

260. CASOLA, S. (2007). Control of peripheral B-cell development. *Current Opinion in Immunology*, *19*(2), 143–149. doi:10.1016/j.coi.2007.02.010

261. Kaku, H., Holodick, N. E., Tumang, J. R., & Rothstein, T. L. (2017). CD25+ B-1a Cells Express Aicda. *Frontiers in Immunology*, *8*, 97–6. doi:10.3389/fimmu.2017.00672

262. Steinecke, C., & Schmidt-Supprian, M. (2018, January 31). dt-Tomato ADIcre dependent expression in GCB and B1 cells.

263. Heyninck, K., de Valck, D., Vanden Berghe, W., van Criekinge, W., Contreras, R., Fiers, W., et al. (1999). The zinc finger protein A20 inhibits TNF-induced NF-kappaB-dependent gene expression by interfering with an RIP- or TRAF2-mediated transactivation signal and directly binds to a novel NF-kappaB-inhibiting protein ABIN. *The Journal of cell biology*, *145*(7), 1471–1482.

264. Boone, D. L., Turer, E. E., Lee, E. G., Ahmad, R.-C., Wheeler, M. T., Tsui, C., et al. (2004). The ubiquitin-modifying enzyme A20 is required for termination of Toll-like receptor responses. *Nature Immunology*, *5*(10), 1052–1060. doi:10.1038/ni1110

265. Sun, S.-C. (2010). Non-canonical NF-κB signaling pathway. *Cell Research*, *21*(1), 71–85. doi:10.1038/cr.2010.177

266. Bendall, H. H., Sikes, M. L., Ballard, D. W., & Oltz, E. M. (1999). An intact NF-kappa B signaling pathway is required for maintenance of mature B cell subsets. *Molecular Immunology*, *36*(3), 187–195.

267. Hahn, M., Macht, A., Waisman, A., & Hövelmeyer, N. (2015). NF-κB-inducing kinase

is essential for B-cell maintenance in mice. *European journal of immunology*, *46*(3), 732–741. doi:10.1002/eji.201546081

268. De Silva, N. S., Silva, K., Anderson, M. M., Bhagat, G., & Klein, U. (2016). Impairment of Mature B Cell Maintenance upon Combined Deletion of the Alternative NF-κB Transcription Factors RELB and NF-κB2 in B Cells. *Journal of immunology (Baltimore, Md. : 1950)*, *196*(6), 2591–2601. doi:10.4049/jimmunol.1501120
269. Fagarasan, S., Shinkura, R., Kamata, T., Nogaki, F., Ikuta, K., Tashiro, K., & Honjo, T. (2000). Alymphoplasia (aly)-type nuclear factor kappaB-inducing kinase (NIK) causes defects in secondary lymphoid tissue chemokine receptor signaling and homing of peritoneal cells to the gut-associated lymphatic tissue system. *The Journal of experimental medicine*, *191*(9), 1477–1486.
270. Mackay, F., & Browning, J. L. (2002). BAFF: A fundamental survival factor for B cells. *Nature Reviews Immunology*, *2*(7), 465–475. doi:10.1038/nri844
271. Kayagaki, N., Yan, M., Seshasayee, D., Wang, H., Lee, W., French, D. M., et al. (2002). BAFF/BLyS receptor 3 binds the B cell survival factor BAFF ligand through a discrete surface loop and promotes processing of NF-kappaB2. *Immunity*, *17*(4), 515–524.
272. Otipoby, K. L., Sasaki, Y., Schmidt-Supprian, M., Patke, A., Gareus, R., Pasparakis, M., et al. (2008). BAFF activates Akt and Erk through BAFF-R in an IKK1-dependent manner in primary mouse B cells. *Proceedings of the National Academy of Sciences*, *105*(34), 12435–12438. doi:10.1073/pnas.0805460105
273. Lee, E. G. (2000). Failure to Regulate TNF-Induced NF-kappa B and Cell Death Responses in A20-Deficient Mice. *Science*, *289*(5488), 2350–2354. doi:10.1126/science.289.5488.2350
274. Onizawa, M., Oshima, S., Schulze-Topphoff, U., Oses-Prieto, J. A., Lu, T., Tavares, R., et al. (2015). The ubiquitin-modifying enzyme A20 restricts ubiquitination of the kinase RIPK3 and protects cells from necroptosis. *Nature Immunology*, *16*(6), 618–627. doi:10.1038/ni.3172
275. Yin, L., Fang, Z., Shen, N.-J., Qiu, Y.-H., Li, A.-J., & Zhang, Y.-J. (2017). Downregulation of A20 increases the cytotoxicity of IFN-γ in hepatocellular carcinoma cells. *Drug design, development and therapy*, *11*, 2841–2850. doi:10.2147/DDDT.S135993
276. Afshar-Sterle, S., Zotos, D., Bernard, N. J., Scherger, A. K., Rödling, L., Alsop, A. E., et al. (2014). Fas ligand–mediated immune surveillance by T cells is essential for the control of spontaneous B cell lymphomas. *Nature Medicine*, *20*(3), 283–290. doi:10.1038/nm.3442
277. Boutaffala, L., Bertrand, M. J. M., Remouchamps, C., Seleznik, G., Reisinger, F., Janas, M., et al. (2015). NIK promotes tissue destruction independently of the alternative NF-κB pathway through TNFR1/RIP1-induced apoptosis. *Cell Death and Differentiation*, *22*(12), 2020–2033. doi:10.1038/cdd.2015.69
278. Li, Y.-S., Zhou, Y., Tang, L., Shinton, S. A., Hayakawa, K., & Hardy, R. R. (2015). A developmental switch between fetal and adult B lymphopoiesis. *Annals of the New York Academy of Sciences*, *1362*(1), 8–15. doi:10.1111/nyas.12769
279. Hardy, R. R. (2006). B-1 B cell development. *Journal of immunology (Baltimore, Md. : 1950)*, *177*(5), 2749–2754.
280. Hardy, R. R., & Hayakawa, K. (2015). Perspectives on fetal derived CD5 +B1 B cells. *European journal of immunology*, *45*(11), 2978–2984. doi:10.1002/eji.201445146
281. Savage, H. P., Yenson, V. M., Sawhney, S. S., Mousseau, B. J., Lund, F. E., & Baumgarth, N. (2017). Blimp-1–dependent and –independent natural antibody production by B-1 and B-1–derived plasma cells. *The Journal of experimental medicine*, *214*(9), 2777–2794. doi:10.1084/jem.20161122
282. Hardy, R. R. (2006). B-1 B cells: development, selection, natural autoantibody and

leukemia. *Current Opinion in Immunology*, *18*(5), 547–555. doi:10.1016/j.coi.2006.07.010

283. Rodríguez-Pinto, D., & Moreno, J. (2005). B cells can prime naive CD4 +T cells in vivoin the absence of other professional antigen-presenting cells in a CD154-CD40-dependent manner. *European journal of immunology*, *35*(4), 1097–1105. doi:10.1002/eji.200425732

284. Rossetti, R. A. M., Lorenzi, N. P. C., Yokochi, K., Rosa, M. B. S. de F., Benevides, L., Margarido, P. F. R., et al. (2018). B lymphocytes can be activated to act as antigen presenting cells to promote anti-tumor responses. *PLoS ONE*, *13*(7), e0199034–18. doi:10.1371/journal.pone.0199034

285. Ahmadi, T., Flies, A., Efebera, Y., & Sherr, D. H. (2008). CD40 Ligand-activated, antigen-specific B cells are comparable to mature dendritic cells in presenting protein antigens and major histocompatibility complex class I- and class II-binding peptides. *Immunology*, *124*(1), 129–140. doi:10.1111/j.1365-2567.2007.02749.x

286. Lapointe, R., Bellemare-Pelletier, A., Housseau, F., Thibodeau, J., & Hwu, P. (2003). CD40-stimulated B lymphocytes pulsed with tumor antigens are effective antigen-presenting cells that can generate specific T cells. *Cancer research*, *63*(11), 2836–2843.

287. Dong, C., Juedes, A. E., Temann, U. A., Shresta, S., Allison, J. P., Ruddle, N. H., & Flavell, R. A. (2001). ICOS co-stimulatory receptor is essential for T-cell activation and function. *Nature*, *409*(6816), 97–101. doi:10.1038/35051100

288. Sharpe, A. H., & Pauken, K. E. (2017). The diverse functions of the PD1 inhibitory pathway. *Nature Reviews Immunology*, *65*, 1089–15. doi:10.1038/nri.2017.108

289. Im, S. J., Hashimoto, M., Gerner, M. Y., Lee, J., Kissick, H. T., Burger, M. C., et al. (2016). Defining CD8+ T cells that provide the proliferative burst after PD-1 therapy. *Nature*, *537*(7620), 417–421. doi:10.1038/nature19330

290. Wei, F., Zhong, S., Ma, Z., Kong, H., Medvec, A., Ahmed, R., et al. (2013). Strength of PD-1 signaling differentially affects T-cell effector functions. *Proceedings of the National Academy of Sciences of the United States of America*, *110*(27), E2480–E2489. doi:10.1073/pnas.1305394110

291. Liston, A., & Gray, D. H. D. (2014). Homeostatic control of regulatory T cell diversity. *Nature Reviews Immunology*, *14*(3), 154–165. doi:10.1038/nri3605

292. Moore, T. C., Gonzaga, L. M., Mather, J. M., Messer, R. J., & Hasenkrug, K. J. (2017). B Cell Requirement for Robust Regulatory T Cell Responses to Friend Retrovirus Infection. *mBio*, *8*(4), e01122–17. doi:10.1128/mBio.01122-17

293. Zhao, D.-M., Thornton, A. M., DiPaolo, R. J., & Shevach, E. M. (2006). Activated CD4+CD25+ T cells selectively kill B lymphocytes. *Blood*, *107*(10), 3925–3932. doi:10.1182/blood-2005-11-4502

294. Good-Jacobson, K. L., Song, E., Anderson, S., Sharpe, A. H., & Shlomchik, M. J. (2012). CD80 expression on B cells regulates murine T follicular helper development, germinal center B cell survival, and plasma cell generation. *The Journal of Immunology*, *188*(9), 4217–4225. doi:10.4049/jimmunol.1102885

295. Hao, Z., Duncan, G. S., Seagal, J., Su, Y.-W., Hong, C., Haight, J., et al. (2008). Fas Receptor Expression in Germinal-Center B Cells Is Essential for T and B Lymphocyte Homeostasis. *Immunity*, *29*(4), 615–627. doi:10.1016/j.immuni.2008.07.016

296. Wang, C. J., Heuts, F., Ovcinnikovs, V., Wardzinski, L., Bowers, C., Schmidt, E. M., et al. (2015). CTLA-4 controls follicular helper T-cell differentiation by regulating the strength of CD28 engagement. *Proceedings of the National Academy of Sciences of the United States of America*, *112*(2), 524–529. doi:10.1073/pnas.1414576112

297. Lownik, J. C., Luker, A. J., Damle, S. R., Cooley, L. F., Sayed, El, R., Hutloff, A., et al.

(2017). ADAM10-Mediated ICOS Ligand Shedding on B Cells Is Necessary for Proper T Cell ICOS Regulation and T Follicular Helper Responses. *Journal of immunology (Baltimore, Md. : 1950)*, *199*(7), 2305–2315. doi:10.4049/jimmunol.1700833

298. Nus, M., Sage, A. P., Lu, Y., Masters, L., Lam, B. Y. H., Newland, S., et al. (2017). Marginal zone B cells control the response of follicular helper T cells to a high-cholesterol diet. *Nature Medicine*, *23*(5), 601–610. doi:10.1038/nm.4315

299. Hu, H., Wu, X., Jin, W., Chang, M., Cheng, X., & Sun, S. C. (2011). Noncanonical NF- B regulates inducible costimulator (ICOS) ligand expression and T follicular helper cell development. *Proceedings of the National Academy of Sciences of the United States of America*, *108*(31), 12827–12832. doi:10.1073/pnas.1105774108

300. Basso, K., & Dalla-Favera, R. (2012). Roles of BCL6 in normal and transformed germinal center B cells. *Immunological reviews*, *247*(1), 172–183. doi:10.1111/j.1600-065X.2012.01112.x

301. Yang, J. (2012). Zinc finger protein A20 protects rats against chronic liver allograft dysfunction. *World Journal of Gastroenterology*, *18*(27), 3537. doi:10.3748/wjg.v18.i27.3537

302. Kattah, M. G., Shao, L., Rosli, Y. Y., Shimizu, H., Whang, M. I., Advincula, R., et al. (2018). A20 and ABIN-1 synergistically preserve intestinal epithelial cell survival. *The Journal of experimental medicine*, *265*, jem.20180198–15. doi:10.1084/jem.20180198

303. Xuan, N. T., Wang, X., Nishanth, G., Waisman, A., Borucki, K., Isermann, B., et al. (2014). A20 expression in dendritic cells protects mice from LPS-induced mortality. *European journal of immunology*, *45*(3), 818–828. doi:10.1002/eji.201444795

304. Sun, J., Sun, L., Zhang, N., Lu, X., & Zhang, H. (2012). A20 is up-regulated in primary mouse hepatocytes subjected to hypoxia and reperfusion. *Cell Biochemistry and Function*, *30*(8), 683–686. doi:10.1002/cbf.2850

305. Lim, M. C. C., Maubach, G., Sokolova, O., Feige, M. H., Diezko, R., Buchbinder, J., et al. (2017). Pathogen-induced ubiquitin-editing enzyme A20 bifunctionally shuts off NF-κB and caspase-8-dependent apoptotic cell death. *Cell Death and Differentiation*, *24*(9), 1621–1631. doi:10.1038/cdd.2017.89

306. Zhang, P., Wang, P.-X., Zhao, L.-P., Zhang, X., Ji, Y.-X., Zhang, X.-J., et al. (2018). The deubiquitinating enzyme TNFAIP3 mediates inactivation of hepatic ASK1 and ameliorates nonalcoholic steatohepatitis. *Nature Medicine*, *24*(1), 84–94. doi:10.1038/nm.4453

307. Pillai, S., Cariappa, A., & Moran, S. T. (2004). Positive selection and lineage commitment during peripheral B-lymphocyte development. *Immunological reviews*, *197*, 206–218.

308. Morimoto, K., Baba, Y., Shinohara, H., Kang, S., Nojima, S., Kimura, T., et al. (2016). LRRK1 is critical in the regulation of B-cell responses and CARMA1-dependent NF-κB activation. *Scientific Reports*, *6*(1), 21–13. doi:10.1038/srep25738

309. Hövelmeyer, N., Wunderlich, F. T., Massoumi, R., Jakobsen, C. G., Song, J., Wörns, M. A., et al. (2007). Regulation of B cell homeostasis and activation by the tumor suppressor gene CYLD. *The Journal of experimental medicine*, *204*(11), 2615–2627. doi:10.1084/jem.20070318

310. Hahn, M., Bürckert, J.-P., Luttenberger, C. A., Klebow, S., Hess, M., Al-Maarri, M., et al. (2017). Aberrant splicing of the tumor suppressor CYLD promotes the development of chronic lymphocytic leukemia via sustained NF-κB signaling. *Leukemia : official journal of the Leukemia Society of America, Leukemia Research Fund, U.K*, *32*(1), 72–82. doi:10.1038/leu.2017.168

311. Dillon, S. R., Gross, J. A., Ansell, S. M., & Novak, A. J. (2006). An APRIL to remember: novel TNF ligands as therapeutic targets. *Nature Reviews Drug Discovery*, *5*(3), 235–246. doi:10.1038/nrd1982

312. Amezcua Vesely, M. C., Schwartz, M., Bermejo, D. A., Montes, C. L., Cautivo, K. M., Kalergis, A. M., et al. (2012). FcγRIIb and BAFF differentially regulate peritoneal B1 cell survival. *The Journal of Immunology*, *188*(10), 4792–4800. doi:10.4049/jimmunol.1102070

313. Kai, X., Chellappa, V., Donado, C., Reyon, D., Sekigami, Y., Ataca, D., et al. (2014). IκB Kinase β ( IKBKB) Mutations in Lymphomas That Constitutively Activate Canonical Nuclear Factor κB (NFκB) Signaling. *The Journal of biological chemistry*, *289*(39), 26960–26972. doi:10.1074/jbc.M114.598763

314. Rodríguez-Vicente, A. E., Díaz, M. G., & Hernández-Rivas, J. M. (2013). Chronic lymphocytic leukemia: a clinical and molecular heterogenous disease, *206*(3), 49–62. doi:10.1016/j.cancergen.2013.01.003

315. Quesada, V., Ramsay, A. J., Rodríguez, D., Puente, X. S., Campo, E., & López-Otín, C. (2013). The genomic landscape of chronic lymphocytic leukemia: clinical implications. *BMC medicine*, *11*(1), 124. doi:10.1186/1741-7015-11-124

316. Ouillette, P., Saiya-Cork, K., Seymour, E. K., Li, C., Shedden, K., & Malek, S. N. (2013). Clonal evolution, genomic drivers and effects of therapy in chronic lymphocytic leukemia. *Clinical Cancer Research*. doi:10.1158/1078-0432.CCR-13-0138

317. Patel, M. N., Bernard, W. G., Milev, N. B., Cawthorn, W. P., Figg, N., Hart, D., et al. (2015). Hematopoietic IKBKE limits the chronicity of inflammasome priming and metaflammation. *Proceedings of the National Academy of Sciences of the United States of America*, *112*(2), 506–511. doi:10.1073/pnas.1414536112

318. Zaninoni, A., Imperiali, F. G., Pasquini, C., Zanella, A., & Barcellini, W. (2003). Cytokine modulation of nuclear factor-κB activity in B-chronic lymphocytic leukemia. *Experimental Hematology*, *31*(3), 185–190. doi:10.1016/S0301-472X(02)01046-9

319. Minden, M. D.-V., Übelhart, R., Schneider, D., Wossning, T., Bach, M. P., Buchner, M., et al. (2012). Chronic lymphocytic leukaemia is driven by antigen-independent cell-autonomous signalling. *Nature*, *489*(7415), 309–312. doi:10.1038/nature11309

320. Krenn, P. W., Hofbauer, S. W., Pucher, S., Hutterer, E., Hinterseer, E., Denk, U., et al. (2016). ILK Induction in Lymphoid Organs by a TNFα-NF-κB-Regulated Pathway Promotes the Development of Chronic Lymphocytic Leukemia. *Cancer research*, *76*(8), 2186–2196. doi:10.1158/0008-5472.CAN-15-3379

321. Rosati, E., Sabatini, R., Rampino, G., Tabilio, A., Di Ianni, M., Fettucciari, K., et al. (2009). Constitutively activated Notch signaling is involved in survival and apoptosis resistance of B-CLL cells. *Blood*, *113*(4), 856–865. doi:10.1182/blood-2008-02-139725

322. Enzler, T., Kater, A. P., Zhang, W., Widhopf, G. F., Chuang, H. Y., Lee, J., et al. (2009). Chronic lymphocytic leukemia of E -TCL1 transgenic mice undergoes rapid cell turnover that can be offset by extrinsic CD257 to accelerate disease progression. *Blood*, *114*(20), 4469–4476. doi:10.1182/blood-2009-06-230169

323. Buggins, A. G. S., Pepper, C., Patten, P. E. M., Hewamana, S., Gohil, S., Moorhead, J., et al. (2010). Interaction with Vascular Endothelium Enhances Survival in Primary Chronic Lymphocytic Leukemia Cells via NF- B Activation and De novo Gene Transcription. *Cancer research*, *70*(19), 7523–7533. doi:10.1158/0008-5472.CAN-10-1634

324. Herling, M., Patel, K. A., Khalili, J., Schlette, E., Kobayashi, R., Medeiros, L. J., & Jones, D. (2005). TCL1 shows a regulated expression pattern in chronic lymphocytic leukemia that correlates with molecular subtypes and proliferative state. *Leukemia*

*: official journal of the Leukemia Society of America, Leukemia Research Fund, U.K*, *20*(2), 280–285. doi:10.1038/sj.leu.2404017

325. Hoyer, K. K., French, S. W., Turner, D. E., Nguyen, M. T. N., Renard, M., Malone, C. S., et al. (2002). Dysregulated TCL1 promotes multiple classes of mature B cell lymphoma. *Proceedings of the National Academy of Sciences of the United States of America*, *99*(22), 14392–14397. doi:10.1073/pnas.212410199
326. Herling, M., Patel, K. A., Weit, N., Lilienthal, N., Hallek, M., Keating, M. J., & Jones, D. (2009). High TCL1 levels are a marker of B-cell receptor pathway responsiveness and adverse outcome in chronic lymphocytic leukemia. *Blood*, *114*(21), 4675–4686. doi:10.1182/blood-2009-03-208256
327. Hewamana, S., Lin, T. T., Rowntree, C., Karunanithi, K., Pratt, G., Hills, R., et al. (2009). Rel A Is an Independent Biomarker of Clinical Outcome in Chronic Lymphocytic Leukemia. *Journal of Clinical Oncology*, *27*(5), 763–769. doi:10.1200/JCO.2008.19.1114
328. Lopez-Guerra, M., Roue, G., Perez-Galan, P., Alonso, R., Villamor, N., Montserrat, E., et al. (2009). p65 Activity and ZAP-70 Status Predict the Sensitivity of Chronic Lymphocytic Leukemia Cells to the Selective I B Kinase Inhibitor BMS-345541. *Clinical Cancer Research*, *15*(8), 2767–2776. doi:10.1158/1078-0432.CCR-08-2382
329. ZANESI, N., Balatti, V., Riordan, J., Burch, A., Rizzotto, L., Palamarchuk, A., et al. (2013). A Sleeping Beauty screen reveals NF-kB activation in CLL mouse model. *Blood*, *121*(21), 4355–4358. doi:10.1182/blood-2013-02-486035
330. Chen, T. L., Tran, M., Lakshmanan, A., Harrington, B. K., Gupta, N., Goettl, V. M., et al. (2017). NF-κB p50 (nfkb1) contributes to pathogenesis in the Eμ-TCL1 mouse model of chronic lymphocytic leukemia. *Blood*, *130*(3), 376–379. doi:10.1182/blood-2017-01-761130
331. Patten, P. E. M., Chu, C. C., Albesiano, E., Damle, R. N., Yan, X. J., Kim, D., et al. (2012). IGHV-unmutated and IGHV-mutated chronic lymphocytic leukemia cells produce activation-induced deaminase protein with a full range of biologic functions. *Blood*, *120*(24), 4802–4811. doi:10.1182/blood-2012-08-449744
332. Huemer, M., Rebhandl, S., Zaborsky, N., Gassner, F. J., Hainzl, S., Weiss, L., et al. (2014). AID induces intraclonal diversity and genomic damage in CD86 +chronic lymphocytic leukemia cells. *European journal of immunology*, *44*(12), 3747–3757. doi:10.1002/eji.201344421
333. Kasar, S., Kim, J., Improgo, R., Tiao, G., Polak, P., Haradhvala, N., et al. (2015). Whole-genome sequencing reveals activation-induced cytidine deaminase signatures during indolent chronic lymphocytic leukaemia evolution. *Nature Communications*, *6*(1), 5446–12. doi:10.1038/ncomms9866
334. Kaku, H., Horikawa, K., Obata, Y., Kato, I., Okamoto, H., Sakaguchi, N., et al. (2002). NF-kappaB is required for CD38-mediated induction of C(gamma)1 germline transcripts in murine B lymphocytes. *International immunology*, *14*(9), 1055–1064.
335. Patten, P. E. M., Buggins, A. G. S., Richards, J., Wotherspoon, A., Salisbury, J., Mufti, G. J., et al. (2008). CD38 expression in chronic lymphocytic leukemia is regulated by the tumor microenvironment. *Blood*, *111*(10), 5173–5181. doi:10.1182/blood-2007-08-108605
336. Deaglio, S., Vaisitti, T., Zucchetto, A., Gattei, V., & Malavasi, F. (2010). CD38 as a molecular compass guiding topographical decisions of chronic lymphocytic leukemia cells. *Seminars in cancer biology*, *20*(6), 416–423. doi:10.1016/j.semcancer.2010.08.003
337. Bagnara, D., Kaufman, M. S., Calissano, C., Marsilio, S., Patten, P. E. M., Simone, R., et al. (2011). A novel adoptive transfer model of chronic lymphocytic leukemia suggests a key role for T lymphocytes in the disease. *Blood*, *117*(20), 5463–5472.

doi:10.1182/blood-2010-12-324210

338. Herndon, T. M., Chen, S. S., Saba, N. S., Valdez, J., Emson, C., Gatmaitan, M., et al. (2017). Direct in vivo evidence for increased proliferation of CLL cells in lymph nodes compared to bone marrow and peripheral blood. *Leukemia : official journal of the Leukemia Society of America, Leukemia Research Fund, U.K*, *31*(6), 1340–1347. doi:10.1038/leu.2017.11

339. Messmer, B. T., Messmer, D., Allen, S. L., Kolitz, J. E., Kudalkar, P., Cesar, D., et al. (2005). In vivo measurements document the dynamic cellular kinetics of chronic lymphocytic leukemia B cells. *Journal of Clinical Investigation*, *115*(3), 755–764. doi:10.1172/JCI23409

340. Bojarska-Junak, A., Hus, I., Chocholska, S., Wąsik-Szczepanek, E., Sieklucka, M., Dmoszyńska, A., & Roliński, J. (2009). BAFF and APRIL expression in B-cell chronic lymphocytic leukemia: Correlation with biological and clinical features. *Leukemia Research*, *33*(10), 1319–1327. doi:10.1016/j.leukres.2009.03.030

341. Mittal, A. K., Chaturvedi, N. K., Rai, K. J., Gilling-Cutucache, C. E., Nordgren, T. M., Moragues, M., et al. (2014). Chronic lymphocytic leukemia cells in a lymph node microenvironment depict molecular signature associated with an aggressive disease. *Molecular medicine (Cambridge, Mass.)*, *20*, 290–301. doi:10.2119/molmed.2012.00303

# ABBREVIATIONS

| | |
|---|---|
| ABC-DLBCL | activated B-cell diffuse large B-cell lymphoma |
| ABIN | A20 binding inhibitor of NF-κB1 |
| AID | Activation-induced deaminase |
| APC | antigen presenting cell |
| BAFF | B-cell activation factor |
| BAFFR | B-cell activating factor (BAFF) receptor |
| BCL | B-cell lymphoma |
| BCMA | B-cell maturation antigen |
| BCR | B-cell receptor |
| BL | Burkitt's lymphoma |
| Blimp1 | B lymphocyte-induced maturation protein 1 |
| BMDSC | bone marrow-derived stromal cell |
| Br-dU | 5-bromo-2-deoxyuridine |
| BTK | Burton's tyrosine kinase |
| CBM | CARD11-BCL10-MATL1 complex |
| cCD4 | conventional CD4 T-cell |
| CD40L | CD40-ligand |
| CDR | constant determining regions |
| CLL | chronic lymphocytic leukaemia |
| CLP | common lymphoid progenitor |
| CS | catch sequence |
| CSR | class switch recombination |
| CYLD | cylindromatosis |
| DAG | diacylglycerol |
| DCs | dendritic cells |
| DH | immunoglobulin heavy-chain diversity gene segment |
| DLBCL | diffuse-large B-cell lymphomas |
| DUB | deubiquitinase |
| DZ | dark zone |
| eGFP | enhanced green fluorescent protein |
| ELP | early lymphoid progenitors |
| eYFP | yellow fluorescent protein |
| $T_{FH}$ | follicular helper T-cells |
| FL | follicular lymphoma |
| FOB | follicular B-cells |
| FSB | foetal bovine serum |
| GALT | gut-associated lymphoid tissue |
| GC | germinal centres |
| GCB | germinal centre B-cell |
| GITR | glucocorticoid-induced receptor superfamily member 18 |
| HEL | hen egg lysozyme |
| I- κB | inhibitory of κ-B |

IAP Inhibitor of apoptosis protein
ICOS Inducible T-cell co-stimulator
IFN-γ interferon- γ
IgD Immunoglobulin D
IgH immunoglobulin heavy-chain
Igκ immunoglobulin kappa
Igλ immunoglobulin lambda
IGL immunoglobulin light-chain
IgM immunoglobulin M
IKK I-κB kinase complex
IKK2ca IKK2 constitutive active mutant
IL-1β Interleukin- β1
IL- β1R1 interleukin- β1 receptor 1
IL2-Rα IL-2 receptor α
IL7-Rα IL-7 receptor α
$IP_3$ inositol-1,4,5-triphospate
IRAK IL-1 receptor-associated kinase
IRES internal ribosomal entry site
IRF4 Interferon regulatory factor 4
JH immunoglobulin heavy-chain joining gene segment
JL immunoglobulin light-chain joining gene segment
K48 Lysine-48-linked polyubiquitin chains
K63 Lysine-63-linked polyubiquitin chains
KLF2 Kruppel-like factor 2
LD1 Ligand Delta1
LFA-1 leukocyte function-associated antigen 1
LN lymph nodes
LPS lipopolysaccharides
LRRK1 leucine-rich repeat kinase 1
LT-α/β lymphotoxin- α/β
LUBAC Linear ubiquitin chain assembly complex
LZ light zone
MACS Magnetic assorted cell sorting
MALT mucosa-associated lymphoid tissue
MAPK mitogen activated protein kinases
MCL mantel cell lymphoma
MDR minimal deleted region
MHC-II major histocompatibility complex class-II
mIgM membrane-bound IgM
mLN mesenteric lymph nodes
MMP multipotent myeloid/lymphoid progenitors
MyD88 Myeloid differentiation factor 88
MZB marginal zone B-cell
MZP marginal zone precursor
NEMO NF-κB essential modulator
NEMO-ID NEMO immunodeficiency

NF-κB nuclear factor kappa-light-chain-enhancer of activated B-cells
NF-κB nuclear factor-κB
NFAT nuclear factor of activated T-cells
NIK NF-κB inducing kinase
nMZL nodal marginal zone lymphoma
OTD Ovarian Tumour domain
PALS periarteriolar lymphoid sheath
PBS phosphate buffered saline
PCR polymerase chain reaction
PD1 Programmed cell death 1
PFA paraformaldehyde
pHSC pluripotent hematopoietic stem cell
PI3K phosphoinositide-3-kinease
$PIP_2$ phosphatidyl-inositol-4,5-biphosphate
$PIP_3$ phosphatidyl-inositol-3,4,5-triphosphate
PKC-β Protein kinase C-β
PLCγ2 phospholipase Cγ2
PMA phorbol myristate acetate
PMBL primary mediastinal B-cell lymphoma
PNA peanut agglutinin
PP Peyer's patches
pre-BCR pre B-cell receptor
RAG recombination-activating-genes
RANKL receptor activator of NF-κB ligand
RHD Rel homology domain
RIP Receptor-interacting protein 1
RS Richter syndrome
SCID severe combined immune deficiency
sCYLD short CYLD
SHM somatic hyper mutation
SLC surrogate light chain
SLL Small lymphocytic Lymphoma
sMZL splenic marginal zone lymphoma
SPF specific pathogen-free
Syk Spleen tyrosine kinase
T1 Transitional 1 B-cell
T2 Transitional 2 B-cell
T3 Transitional 3 B-cell
TACI transmembrane activator and calcium modulator and cyclophilin ligand interactor
TAD transcription activation domain
TAK1 Transforming growth factor-β activated protein kinase 1
TCL1 T-cell leukaemia 1
TD T-cell dependent
TdT terminal deoxynucleotidyl transferase
tg transgene

TGF-β transforming growth factor-β
TI T-cell independent
TIR Toll/IL-1R
TLR Toll-like receptor
TNF-α Tumour necrosis factor-α
TNFAIP3 tumour necrosis factor-α-inducible gene
TNFR tumour necrosis factor receptor
TRADD TNFR1-associated DEATH domain protein
TRAF TNFR associated factor
TWEAK TNF related weak inducer of apoptosis
UBD ubiquitin-binding domains
VH immunoglobulin heavy-chain variable gene segment
VL immunoglobulin light-chain variable gene segment
WES whole exome sequencing
WGS whole genome sequencing
ZnF Zinc finger

## Acknowledgments

First and foremost I would like to thank Prof. Marc Schmidt-Supprian, for giving me the opportunity to come to Munich, Germany, and develop my scientific skills working in his laboratory. I am so grateful to have worked with him these years. His eagerness to understand the many open scientific questions, his vast knowledge in the field, his constant encouragement and his humility together have made working with him an amazing experience. Moreover, his guidance and support have been fundamental during my PhD.

I would like to thank Prof. Matthias Mann for being my "Doktorvater" and a mentor in many different ways. I have truly enjoyed our discussions and I am very grateful for the time he has invested in me. I would also like to thank Dr. Ingo Ringshausen for being a member of my Thesis Advisory Committee, his encouragement and providing me with the Emu-TCL1tg mouse. I am grateful for his suggestions and input regarding the CLL project. Additionally, I would additionally like to thank PD Dr. Ursula Zimber-Strobl, PD Dr. Fabiana Perocchi, Prof. Karl-Peter Hopfner and Prof. Martin Biel for taking the time to review my thesis and being members of PhD examination board. Particularly to Ursula for the time and effort she dedicated to read the manuscript of my thesis and make suggestions for future publications.

I would like to thank all members of the Schmidt-Supprian laboratory for the amenable times spent at the bench, the stimulating scientific discussions, and the positive working environment. It has been a pleasure to work side by side with them. I would like to thank Arianna Bertossi, Paola Sansonetti, Klaus Heger and Dilib Kumar for their help during my first years of the PhD. In particular I would like to thank Yuanyuan Chu and Christoph Vahl. They were both incredible teachers and colleagues, who were always willing to take the time to discuss experiments and protocols. I specially would like to thank Maike Kober and David Riess, with whom I got to experience my PhD journey on the bench, the desk, and beyond the laboratory. I will be forever thankful for their support, scientific contribution and the time spent together during their stay at the Schmidt-Supprian laboratory. I have special thanks to Christoph Dress, Sabrina Bortoluzzi, Mayur Bakshi, Madlen Olsen, Hyunju Oh-Strauss and Nyambayar Dashtsoodol for their contribution to having an encouraging working environment. I

would particularly like to thank Seren Baygüm, Carina Steinecke and Tim Ammon for their suggestions while planning experiments, and for the lively scientific discussions. I would like to thank the former master student in the lab Mayra Lorenz, who I had the pleasure to supervise. Her attitude in the laboratory was a breath of fresh air. I would also like to thank Leonie Kohlhammer, and her successor Gene Swinerd, for their interest in continuing investigating the role of constitutive canonical NF-κB activation in B-cell lymphomagenesis. Furthermore, I would like to thank Julia Knogler, Claudia Mugler and Barbara Habermehl for their technical assistance during my PhD. The work presented here would not have been possible without their assistance. I would like to thank particularly Julia Knogler for all her help with the mouse experiments.

I would like to thank Dr. Ulrich Keller for his collaboration with the adoptive transplant of murine CLL-line cells into PKC-β knockout mice. Moreover, I would like to thank Prof. Reihard Fässler for his generosity while we (the Schmidt-Supprian laboratory) were a part of his department at the Max Planck Institute of Biochemistry and to the Fässler laboratory members for their positive attitude and companionship during the first years of my PhD. I particularly like to thank Rafael Ruppert, Christoph Vahl and David Riess, for all their help with the FACS ARIA at the Max Planck Institute of Biochemistry. Additionally I would like to thank Markus Utzt for his help with the sorter at the Klinikum rechts der Isar. Furthermore, I would like to thank the animal caretakers from the Max Planck Institute and from the “Zentrum für Präklinische Forschung” at the Klinikum rechts der Isar.

I would like to thank the International Max Planck Research School for their support, and in particular to Hans-Joerg Schäffer, Maximiliane Reif and Ingrid Wolf for the incredible organization they do. Additionally, I would like to thank the International Research Training Group 1243 for their support, in particular to Elisabeth Schröder-Reiter and Elke Hammerbacher.

Finally, I would like to thank my family and friends for their unconditional support, patience and positive energies. I am extremely grateful to my dad, my sensei in life, for his objective way of thinking and the great discussions on every aspect of life, and to my mom for her constant belief in my abilities. They were invaluable. Particularly I would like to thank Johanna McCarter for reading part of the manuscript and her insightful comments; Franzika Kundrat and Mariana Reategui for their constant motivation; and to Tim for his constant support and companionship during the final steps.